QUANTUM OPTICS FOR ENGINEERS

Quantum Entanglement

SECOND EDITION

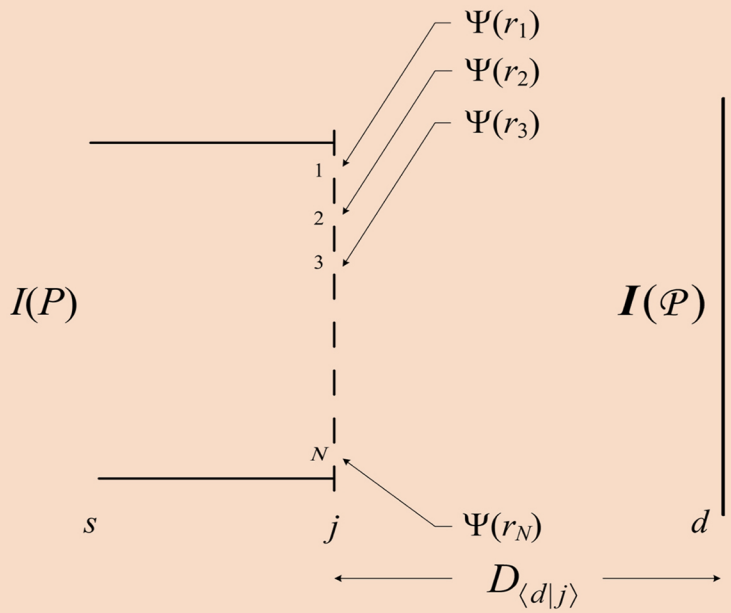

F. J. Duarte

CRC Press
Taylor & Francis Group

Quantum Optics for Engineers

The second edition of *Quantum Optics for Engineers: Quantum Entanglement* is an updated and extended version of its first edition. New features include a transparent interferometric derivation of the physics for quantum entanglement devoid of mysteries and paradoxes. It also provides a utilitarian matrix version of quantum entanglement apt for engineering applications.

Features:

- Introduces quantum entanglement via the Dirac–Feynman interferometric principle, free of paradoxes.
- Provides a practical matrix version of quantum entanglement which is highly utilitarian and useful for engineers.
- Focuses on the physics relevant to quantum entanglement and is coherently and consistently presented via Dirac's notation.
- Illustrates the interferometric quantum origin of fundamental optical principles such as diffraction, refraction, and reflection.
- Emphasizes mathematical transparency and extends on a pragmatic interpretation of quantum mechanics.

This book is written for advanced physics and engineering students, practicing engineers, and scientists seeking a workable-practical introduction to quantum optics and quantum entanglement.

Quantum Optics for Engineers

Quantum Entanglement

Second Edition

F. J. Duarte

CRC Press
Taylor & Francis Group
Boca Raton London New York

CRC Press is an imprint of the
Taylor & Francis Group, an **informa** business

Designed cover image: F. J. Duarte

Second edition published 2024
by CRC Press
2385 NW Executive Center Drive, Suite 320, Boca Raton FL 33431

and by CRC Press
4 Park Square, Milton Park, Abingdon, Oxon, OX14 4RN

CRC Press is an imprint of Taylor & Francis Group, LLC

First edition published by CRC Press 2014

Library of Congress Cataloging-in-Publication Data
Names: Duarte, F. J. (Frank J.), author.
Title: Quantum optics for engineers : quantum entanglement / F. J. Duarte.
Description: Second edition. | Boca Raton : CRC Press, [2024] |
Includes bibliographical references and index. |
Summary: "The second edition of Quantum Optics for Engineers: Quantum Entanglement is an updated, and extended version of its first edition. New features include a transparent interferometric derivation of the physics for quantum entanglement devoid of mysteries and paradoxes. It also provides a utilitarian matrix version of quantum entanglement apt for engineering applications. Features: introduces quantum entanglement via the Dirac-Feynman interferometric principle, free of paradoxes, provides a practical matrix version of quantum entanglement which is highly utilitarian and useful for engineers, focuses on the physics relevant to quantum entanglement and is coherently and consistently presented via Dirac's notation, illustrates the interferometric quantum origin of fundamental optical principles such as diffraction, refraction, and reflection, and emphasizes mathematical transparency and extends on a pragmatic interpretation of quantum mechanics. The book is written for advanced physics and engineering students, practicing engineers and scientists seeking a workable-practical introduction to quantum optics and quantum entanglement"— Provided by publisher.
Identifiers: LCCN 2023038810 (print) | LCCN 2023038811 (ebook)
| ISBN 9781032499345 (hbk) | ISBN 9781032504858 (pbk) | ISBN 9781003398707 (ebk)
Subjects: LCSH: Quantum optics.
Classification: LCC QC446.2 .D83 2024 (print) | LCC QC446.2 (ebook) |
DDC 535/.15—dc23/eng/20231222
LC record available at https://lccn.loc.gov/2023038810
LC ebook record available at https://lccn.loc.gov/2023038811

ISBN: 9781032499345 (hbk)
ISBN: 9781032504858 (pbk)
ISBN: 9781003398707 (ebk)

DOI: 10.1201/9781003398707

Typeset in Times
by codeMantra

In memory of my father: Luis Enrique Duarte (1921–2011)

Contents

Preface

Optics plays a crucial role in the success of today's science and technology. It does so from the vast spaces of astronomy to nanotechnology. Within optics, *quantum optics* is the dominant asset. The aim of this book is to make available the principles of quantum optics directly to engineers, engineering students, and scientists in general. This is done by presenting the subject, and associated elements of coherent optics, from a pragmatic and forthright perspective using Dirac's notation. This second edition entitled *Quantum Optics for Engineers: Quantum Entanglement* retains all the main features included in the original first edition while expanding substantially the coverage of quantum entanglement. In addition to presenting quantum entanglement via its interferometric physics origin, the mechanics itself is explained via a practical matrix formalism particularly apt for engineering applications. It is indeed a pleasure to offer, to the scientific and engineering communities, this second edition of *Quantum Optics for Engineers: Quantum Entanglement*.

F. J. Duarte
Jonesborough, Tennessee.
July, 2023.

Author's Biography

F. J. Duarte is a Chilean-born laser physicist, quantum physicist, inventor, and author. He has been residing in the United States since 1983. Duarte studied mathematics and physics at Macquarie University (Sydney, Australia) where he was a student of the quantum physicist John C. Ward. At Macquarie, in 1978, he was the first to be awarded a First Class Honors in physics for his thesis on the *Excitation Processes in Continuous Wave Rare Gas-Metal Halide Vapour Lasers*. Also at Macquarie, he completed his PhD research, on optically-pumped molecular lasers, in 1981, under the guidance of James A. Piper. The same year he became a Postdoctoral Fellow at the University of New South Wales, where he designed and built UV tunable lasers for high-resolution IR-UV double-resonance spectroscopy. Duarte has worked and contributed professionally in the academic, industrial, and defense sectors and has practiced physics in Australia, the Americas, and Europe. Notable in his career is his tenure at the Eastman Kodak Company's Imaging Research Laboratories (1985–2006) where he led the Imaging and Spectral Measurements Laboratory. He is the author of numerous refereed papers and US patents.

Duarte is the editor/author of some 17 scholarly books including *Dye Laser Principles* (1990), *High-Power Dye Lasers* (1991), *Tunable Lasers Handbook* (1995), *Tunable Laser Applications* (1995, 2009, 2016), and *Organic Lasers and Organic Photonics* (2018). He is the co-author of *Quantum Entanglement Engineering and Applications* (2021) and the sole author of *Tunable Laser Optics* (2003, 2015), *Fundamentals of Quantum Entanglement* (2019, 2022), and *Quantum Optics for Engineers* (2014, 2024). Duarte has made original contributions in the fields of coherent imaging, directed energy, extremely-expanded laser beams (up to 3000:1), heat conduction, high-power tunable lasers, laser metrology, liquid and polymer-nanoparticle organic gain media, narrow-linewidth tunable laser oscillators, *N*-slit quantum interferometry, electrically-pumped organic semiconductor coherent emission, quantum entanglement, and space-to-space interferometric communications. He is also the author of the generalized multiple-prism grating dispersion theory and has pioneered the use of Dirac's quantum notation in interferometry and classical optics.

Duarte's contributions have found applications in atomic physics, astronomy, chemistry, coherence, cytology, electrophoresis, femtosecond laser microscopy, geodesics, geophysics, gravitational lensing, heat transfer, imaging, laser isotope

separation, laser medicine, laser pulse compression, laser spectroscopy, mathematical transforms, nanoengineering, nanophotonics, nonlinear optics, optofluidics, organic semiconductor lasers, phase imaging, polarization rotation, quantum computing, quantum entanglement, quantum fluctuations, quantum philosophy, quantum thermodynamics, space exploration, and tunable diode laser design.

Duarte was elected Fellow of the Australian Institute of Physics in 1987 and Fellow of the Optical Society of America (OSA) in 1993. He has received the *Engineering Excellence Award* (1995) for the invention of the *N*-slit laser interferometer, and the *David Richardson Medal* (2016) 'for seminal contributions to the physics and technology of multiple-prism arrays for narrow-linewidth tunable laser oscillators and laser pulse compression' from the Optical Society (now *Optica*).

1 Introduction

1.1 INTRODUCTION

Perhaps no other subject in the history of physics has captured the human imagination more than quantum mechanics has. This captivation has extended beyond physics, and science, and well into the realm of popular culture. This is because quantum mechanics, also known as quantum physics, correctly describes the micro world and the sub-nano world in a mathematical way that appears to be mysterious and ineffable to the inhabitants of the classical world.

A most succinct description of quantum mechanics has been given by the well-known quantum and particle physicist John Clive Ward: *The inner mysteries of quantum mechanics require a willingness to extend one's mental processes into a strange world of phantom possibilities, endlessly branching into more and more abstruse chains of coupled logical networks, endlessly extending themselves forward and even backwards in time*' (Ward, 2004).

In *Quantum Optics for Engineers*, second edition, we explore fascinating aspects of quantum optics from the perspective of quantum interference and quantum entanglement. The presentation of the physics, via direct and transparent mathematics, neutralizes mysteries and paradoxes often associated with quantum entanglement and quantum mechanics.

1.2 BRIEF HISTORICAL PERSPECTIVE

Quantum mechanics came to light via the work of Max Planck, published in 1901. In that contribution, Planck used concepts of thermodynamics to explain the energy distribution of light sources as a function of wavelength (Planck, 1901). In doing so, he introduced, without derivation, an equation in which the energy of the emission was a function of frequency ν, that is,

$$E = h\,\nu \tag{1.1}$$

where the units of the energy E is Joule (J), the units of the frequency ν is Hz, and h is known as Planck's constant ($h = 6.62607015 \times 10^{-34}$ Js). That was the birth of quantum mechanics. It was born from the experiment, and it was a macroscopic empirical birth.

Another experimental observation relevant to the development of quantum mechanics was the photoelectric effect (Hertz, 1887). This effect of fundamental significance to modern photomultipliers, and photodetectors in general, means that when a surface comprised of charged particles is irradiated with light of frequency ν, there is a probability that electrons will be emitted from that surface. An explanation to the photoelectric effect was provided by Einstein (1905) via the relationship

DOI: 10.1201/9781003398707-1

$$E = \hbar\omega - W \tag{1.2}$$

where W is defined as the work function or energy required to emit an electron from the irradiated surface. Einstein also proposed that light behaves as a stream of energy units that he called *lightquanta*.

A few years later, Bohr (1913) postulated that electrons in an atom can only populate well-defined orbits at discrete energies W_n. When the electron jumps from one orbit of energy W_n to another one at W_{n+1}, it does so by emitting radiation at a frequency ν, so that (Bohr, 1913)

$$W_n - W_{n+1} = h\nu \tag{1.3}$$

The developments introduced above were the preamble to the 1925–1927 revolution that yielded the *quantum mechanics* we know today. Heisenberg (1925), Born and Jordan (1925), and Born et al. (1926) introduced quantum mechanics in matrix form. Schrödinger (1926) introduced his quantum wave equation. Dirac (1925) first established that there was a correspondence between Heisenberg's non-commuting dynamical variables and the Poisson bracket. Then he discovered that there was an equivalence between the Born–Jordan formulation and the Schrödinger equation (Dirac, 1926). Further, he demonstrated that there was a direct correspondence between the Heisenberg–Dirac quantum mechanics and Schrödinger's wave mechanics (Dirac, 1927).

In addition to the three formulations just mentioned, Dirac (1939) further introduced his *bra ket* notation, also known as *Dirac's notation*, which is the preferred formulation of quantum mechanics used in this book.

Further approaches to quantum mechanics include the Feynman formulation via *integral paths* (Feynman and Hibbs, 1965) and the phase-space formulation (Moyal, 1949). There are also other lesser-known formulations.

Post–quantum mechanical developments include *quantum electrodynamics* (Tomonaga, 1946; Schwinger, 1948; Feynman, 1949; Dyson, 1949), *renormalization theory* (Ward, 1950), *Feynman diagrams* (Feynman, 1949), and the *standard model* of particle physics (Salam and Ward, 1959, 1964; Glashow, 1961; Weinberg, 1967). Figure 1.1 provides an approximate time line of key developments in the quantum era.

1.3 THE PRINCIPLES OF QUANTUM MECHANICS

The Principles of Quantum Mechanics is a landmark book written by one of the creators of quantum mechanics, Paul Adrien Maurice Dirac. The first edition of this masterpiece was published in 1930. The second edition was published in 1935 and the third edition in 1947. The fourth edition, used by us as a reference throughout this work, was published in 1958, and it is this edition that gives origin to the 1978 version, its ninth revised printing.

An interesting aspect for this book is that Dirac's *bra ket* notation was introduced in its third edition (1947). This is explained by the Australian particle physicist R. H. Dalitz (known of the *Dalitz plot* and the *Dalitz pair*), who in 1947 was taking lectures from Dirac in Cambridge (Dalitz, 1987).

The Principles of Quantum Mechanics, third and fourth editions, are the vehicles by which Dirac's notation was introduced to physicists although Dirac first disclosed

1901: $E=h\nu$

1901-1924: Early quantum concepts

1925-1927: Formulation of quantum mechanics

1939: Dirac's notation

1946-1949: Quantum electrodynamics

1949: Feynman's diagrams

1950: Renormalization theory

1959-1967: Formulation of the Standard Model

1964: Prediction of the Higgs boson

2012: Discovery of the Higgs boson

FIGURE 1.1 Timeline depicting important developments in the quantum era.

the notation in a paper entitled *A New Notation for Quantum Mechanics* (Dirac, 1939). This paper, in a fairly mechanistic style, limits itself to introducing the new notation and providing a correspondence between it and the 'old notation.' The paper does not explain how Dirac discovered or created the new notation. Nor does he explain it in the book. At one time, I did ask Dick Dalitz if Dirac had explained in his lectures how he created, or discovered, his *bra ket* notation, and his reply was… 'no' (Duarte, 2014). *The Principles of Quantum Mechanics* used by us as a reference throughout this work is the fourth edition (Dirac, 1958).

The most relevant chapters to our immediate interest from *The Principles of Quantum Mechanics* are as follows:

- The principle of superposition
- Dynamical variables and observables
- Representations
- The quantum conditions
- The equations of motion
- Perturbation theory
- Systems containing several similar particles
- Theory of radiation

Throughout the book, he does use his *bra ket* notation extensively albeit it is not the only type of notation he utilizes.

Besides issues of notation, Dirac's book is remarkable in that it provides probably the very first discussion of optics in a quantum context. It does so via a brilliant and prophetic discussion of interferometry. He begins by considering a beam of 'roughly monochromatic light' and continues by referring to this beam of light as 'consisting

of a large number of photons.' The beam is then 'split up into two components of equal intensity' (Dirac, 1958). In today's terminology, Dirac's discussion applies perfectly to an *ensemble of indistinguishable photons* as in a high-power narrow-linewidth laser beam undergoing interference in a Mach–Zehnder interferometer (Duarte, 1998).

This discussion qualifies Dirac as the father of quantum optics and the father of laser optics (Duarte, 2003).

It is also apparent that *The Principles of Quantum Mechanics* served as inspiration to Feynman for his lectures on physics not only on the central topic of Dirac's notation but also on the fundamental ideas on interference and various other mathematical formalisms.

1.4 THE FEYNMAN LECTURES ON PHYSICS

Volume III of *The Feynman Lectures on Physics* (Feynman et al., 1965) offers a brilliant discussion of quantum mechanics via Dirac's notation. From a fascinating discussion of the two-slit interference thought experiments, using electrons, to practical applications of two-state systems, and beyond, this book is a physics treasure. At a basic level, *The Feynman Lectures on Physics*, Volume III, is a brilliant introduction to the use and practice of Dirac's notation in quantum mechanics.

At this stage, it is also instructive to mention that in his 1965 book on the path integral approach to quantum mechanics, Feynman applies quantum mechanics directly to the classical macroscopic problem of diffraction (Feynman and Hibbs, 1965). It is necessary to make this explicit observation for the benefit of some practitioners who insist on imposing the use of classical tools to describe macroscopic diffraction and interference.

1.5 THE PHOTON

In this section, first we explore the opinion on this subject given by a few luminaries of quantum physics: Dirac, Feynman, Haken, and Lamb. Then, our own opinion on the subject is offered.

Dirac (1958): 'The essential point is the association of each of the translational states of a photon with one of the wave functions of ordinary wave optics… the wave function gives information about the probability of one photon being in a particular place and not the probable number of photons in that place.'

Feynman (1965): 'Newton thought that light was made up of particles, but then it was discovered that it behaves like a wave… We say: It is like *neither*.'

Haken (1981): 'In quantum mechanics we attribute an infinite extended wave to a freely moving particle with momentum p so that $\lambda = h/p$. The wave must be of infinite extent, otherwise it would not have a definite wavelength.'

Lamb (1995): 'Photons cannot be localized in any meaningful manner, and they do not behave at all like particles, whether described by a wave function or not.'

Indeed, the *nonlocality* of the photon is intuitive to experimentalists experienced in optics: 'All the indistinguishable photons illuminate the array of N slits, or grating, simultaneously. If only one photon propagates, at any given time, then that individual photon illuminates the whole array of N slits simultaneously' (Duarte, 2003). The nonlocality of the photon is central to the physics of this book.

Those are some written thoughts on a photon. As can be observed, there is no complete conceptual convergence on the meaning of a photon. Here, rather than offering yet another language-based concept of the photon, we shall examine in a pragmatic approach what we know about the basic features of the photon:

1. A single photon moves, in vacuum, at the speed of light c.
2. A single photon has a wavelength λ, which is related to its frequency ν by

$$\lambda = \frac{c}{\nu} \tag{1.4}$$

3. A single photon exhibits a quantum energy of

$$E = h\nu \tag{1.5}$$

   or $E = \hbar\omega$.

4. A single photon exhibits a quantum momentum of

$$p = \hbar k = \frac{h}{\lambda} \tag{1.6}$$

5. A single photon is associated with complex wave functions of the form

$$\psi(x,t) = \psi_0 e^{-i(\omega t - kx)} \tag{1.7}$$

6. Photons are non-local and can exhibit *enormous coherence lengths*

$$\Delta x \approx \frac{c}{\Delta \nu} \tag{1.8}$$

   Under these premises, we can attempt a conceptual description of a photon as a unique physical entity that can be mathematically described using complex wave functions while exhibiting a quantum energy $E = h\nu$. Hence, the photon can be outlined as a coherent non-local form of energy (Duarte, 2022). As of now, limitations in the existing language prevent us from a more definite description other than this approximate outline. Besides issues of ineffability, here we refer to the photon, or quantum, as a unique form of coherent non-local energy.

Notice that in the case of emission resulting in the generation of an ensemble of coherent photons, as in the case of a narrow-linewidth laser, a refinement on the wave description of Haken (1981) should refer to a *near-infinite* wave since the wavelength, in practice, would always exhibit a measurable linewidth; in other words, the wavelength is $\lambda \pm \Delta\lambda$ and not just λ.

Quantum mechanically, indistinguishable photons *are the same photon*. In other words, two photons coming from different narrow-linewidth lasers with energies $E = h\nu_1$ and $E = h\nu_1$ are the same photon and will interfere precisely as described by Dirac (1958) even though they originate from different sources. Thus, a seventh item to be added to the list above becomes:

7. Ensembles of indistinguishable photons exhibiting very narrow linewidth $\Delta\nu$ originating from monochromatic sources, such as narrow-linewidth lasers, approximate the behavior of a single photon. This means that single photons and ensembles of indistinguishable photons can be described mathematically via identical superposition probability amplitudes.

1.6 QUANTUM OPTICS

As described previously, the first known discussion of quantum optics was provided by Dirac. He did so via interference. Furthermore, and very importantly, he did so considering a macroscopic interferometric experiment involving a beam of 'roughly monochromatic light' and continues by referring to this beam of light as 'consisting of a large number of photons.' The beam is then 'split up into two components of equal intensity' (Dirac, 1958). In other words, Dirac applies his quantum concepts directly to a *macroscopic interferometric experiment* involving ensembles of indistinguishable photons.

When Dirac says 'split up into two components of equal intensity,' he means *equal probability*. In turn, this means that initially the photon, or ensemble of indistinguishable photons, had a probability amplitude to propagate into each path of the interferometer.

The use of quantum physics in macroscopic optics is not unique to Dirac. In 1965, Feynman used his path integrals to describe divergence and diffraction resulting from the passage through a Gaussian slit (Feynman and Hibbs, 1965). Even further, Feynman in his *Feynman Lectures on Physics* (problem book to Feynman et al., 1965) gives credit to Hanbury Brown and Twiss (1956) as performing an early experiment in quantum optics. Hanbury Brown and Twiss collected light from the star Sirius in two separate detectors; the signals from these detectors are then made to interfere. Building on Feynman's description of double-slit electron interference, Dirac's quantum notation was applied to *N*-slit photon interference (Duarte, 1991).

In addition to applications to macroscopic interference, a clear and intrinsic quantum physics development was the derivation of probability amplitude equations associated with counter-propagating photons with entangled polarizations (Pryce and Ward, 1947; Ward, 1949):

$$|\psi\rangle = 2^{-1/2}\left(|x\rangle_1|y\rangle_2 - |y\rangle_1|x\rangle_2\right) \tag{1.9}$$

1930: Dirac's pair theory

1947: Dirac's two-beam interference

1947-1950: γ-Ray quantum polarization entanglement

1956: Hanbury Brown-Twiss effect

1964: Bell's inequalities

1965: Path integral description of beam divergence

1965: Double-slit thought experiments via Dirac's notation

1982: Optical polarization entanglement experiments

1987-1991: *N*-slit interference via Dirac's notation

1984-1991: Quantum cryptography

1993-1997: Quantum teleportation

FIGURE 1.2 Timeline depicting important developments in quantum optics while emphasizing the application of Dirac's notation.

and the subsequent experimental confirmation provided via the measurements of polarization correlations by Wu and Shaknov (1950). A development directly related to photon entanglement was the introduction of Bell's inequality (1964). All-optical experiments on polarization entanglement were reported by Aspect (1982).

A further development in quantum optics was the introduction of quantum cryptography (Bennett and Brassard, 1984; Ekert, 1991). An advance directly related to the physics of entanglement is quantum teleportation (Bennett et al., 1993; Bouwmeester et al., 1997). Figure 1.2 highlights the timeline of key developments in quantum optics while emphasizing the application of Dirac's notation.

1.7 QUANTUM OPTICS FOR ENGINEERS

Quantum Optics for Engineers is designed as a textbook, primarily utilizing Dirac's quantum notation, to describe optics in a unified and cohesive approach. The emphasis is pragmatic. This approach uses a minimum of mathematical sophistication. In other words, the reader should be able to use the tools provided primarily with the knowledge of first-year courses in calculus and algebra.

The subject matter is contained in Chapters 1–23, while a set of companion Appendices (A–K) provide additional necessary information relevant to the chapter material and quantum optics in general. The concept here is to offer the student a self-contained book, thus minimizing the need to refer to additional texts except for those who would like to expand their knowledge of a particular subject.

The reader will also notice that some of the equations, and figures, in this book, are reproduced in several of the chapters. In other words, they are repeated. This has been done quite deliberately to avoid having to go back in the text to find a particular

equation and then forward again to continue the work. Besides highlighting the importance of some concepts, this approach should facilitate remembering those equations and easing the lecture process. Hopefully, this will enhance the learning process according to the old Roman saying: *repetitio est mater studiorum* (approximately translated as 'repetition is the mother of learning').

1.7.1 Quantum Optics for Engineers: Quantum Entanglement, Second Edition

The second edition of *Quantum Optics for Engineers: Quantum Entanglement* differs from the first edition in the following:

1. It has a new chapter entitled *Bell's Theorem* (Chapter 14).
2. It has a new chapter entitled *Quantum Entanglement Probability Amplitudes for* $n = N = 2$ (Chapter 15).
3. It has a new chapter entitled *Quantum Entanglement Probability Amplitudes for* $n = N = 2^1, 2^2, 2^3, \ldots 2^r$ (Chapter 16).
4. It has a new chapter entitled *Quantum Entanglement Probability Amplitudes for* $n = N = 3, 6$ (Chapter 17).
5. It has a new chapter entitled *Quantum Entanglement in Matrix Notation* (Chapter 18).
6. It has a new chapter entitled *Quantum Computing in Matrix Notation* (Chapter 19).
7. It has a new chapter entitled *Quantum Principles and the Probability Amplitude* (Chapter 22).
8. The chapter on quantum interpretations has been rewritten and is now entitled *On the Interpretation of Quantum Mechanics* (Chapter 23).
9. Previous chapters on *Laser Excitation*, *Laser Resonators and Laser Cavities via Dirac's Notation*, and *Generalized Multiple-Prism Dispersion Theory*, have been moved to the Appendix.
10. All chapters and appendices from the first edition have been revised, updated, and some, such as the chapters on *Interferometry via Dirac's Notation* (Chapter 7) and *Matrix Notation in Quantum Mechanics* (Chapter 9), have been updated and expanded.

When necessary and appropriate, the first edition (Duarte, 2014) is cited. This is particularly relevant to some physics and statements revealed for the first time in the first edition.

REFERENCES

Aspect, A., Grangier, P., and Roger, G. (1982). Experimental test of Bell's inequalities using time-varying analyzers. *Phys. Rev. Lett.* 49, 1804–1807.

Bell, J. S. (1964). On the Einstein-Podolsky-Rosen paradox. *Physics* 1, 195–200.

Bennett, C. H., and Brassard, G. (1984). Quantum cryptography: public key distribution and coin tossing. *Proceedings of IEEE International Conference on Computers Systems and Signal Processing*, Bangalore, India.

Bennett, C. H., Brassard, G., Crépeau, C., Jozsa, R., Peres, A., and Wootters, W. K. (1993). Teleporting an unknown quantum state via dual classical and Einstein-Podolsky-Rosen channels, *Phys. Rev. Lett.* 70, 1895–1899.

Bohr, N. (1913). On the constitution of atoms and molecules. *Phil. Mag.* 26, 857–875.

Born, M., and Jordan, P. (1925). Zur quantenmechanik. *Z. Phys.* 34, 858–888.

Born, M., Heisenberg, W., and Jordan, P. (1926). Zur quantenmechanik II. *Z. Phys.* 35, 557–617.

Bouwmeester, D., Pan, J-W., Mattle, K., Eibl, M., Weinfurter, H., and Zeilinger, A. (1997). Experimental quantum teleportation. *Nature* 390, 575–579.

Dalitz, R. H. (1987). Another side to *Paul Dirac. In Paul Adrien Maurice Dirac* (Kursunoglo, B. N., and Wigner E. P., eds.). Cambridge University, Cambridge, Chapter 10.

Dirac, P. A. M. (1925). The fundamental equations of quantum mechanics. *Proc. Roy. Soc. London A* 109, 642–653.

Dirac, P. A. M. (1926). On the theory of quantum mechanics. *Proc. Roy. Soc. London A* 112, 661–677.

Dirac, P. A. M. (1927). The physical interpretation of the quantum dynamics. *Proc. R. Soc. London A* 113, 621–641.

Dirac, P. A. M. (1939). A new notation for quantum mechanics. *Math. Proc. Cambridge Phil. Soc*. 35, 416–418.

Dirac, P. A. M. (1958). *The Principles of Quantum Mechanics*, 4th ed. Oxford University, Oxford, U.K.

Duarte, F. J. (1991). Dispersive dye lasers. In *High Power Dye Lasers* (Duarte, F. J., ed.). Springer-Verlag, Berlin, pp. 7–43.

Duarte, F. J. (1998). Interference of two independent sources. *Am. J. Phys.* 66, 662–663.

Duarte, F. J. (2003). *Tunable Laser Optics*, Elsevier-Academic, New York.

Duarte, F. J. (2014). *Quantum Optics for Engineers*, 1st ed. CRC, Boca Raton, FL.

Duarte, F. J. (2022). *Fundamentals of Quantum Entanglement*, 2nd ed. Institute of Physics, Bristol.

Dyson, F. J. (1949). The S matrix in quantum electrodynamics. *Phys. Rev.* 75, 1736–1755.

Einstein, A. (1905). Uber einen erzeugung und verwandlung des lichtes betreffenden. *Ann. Phys.* 17, 132–148.

Ekert, A. K. (1991) Quantum cryptography based on Bell's theorem. *Phys. Rev. Lett*. 67, 661–663.

Feynman, R. P. (1949). Space-time approach to quantum electrodynamics. *Phys. Rev.* 76, 769–789.

Feynman, R. P., and Hibbs, A. R. (1965). *Quantum Mechanics and Path Integrals*, McGraw-Hill, New York.

Feynman, R. P., Leighton, R. B., and Sands, M. (1965). *The Feynman Lectures on Physics*, Vol. III, Addison-Wesley, Reading, MA.

Glashow, S. L. (1961). Partial-symmetries of weak interactions. *Nucl. Phys.* 22, 579–588.

Haken, H. (1981). *Light*, North-Holland, Amsterdam.

Hanbury Brown, R., and Twiss, R. Q. (1956), A test of a new type of stellar interferometer on Sirius, *Nature* 178, 1046–1048.

Heisenberg, W. (1925). Uber quantenthoretische umdeutung kinematischer und mechanischer beziehungen. *Z. Phys.* 33, 879–893.

Hertz, H. (1887). Uber einen einfluss des ultravioletten lichtes auf die elektrische entladung. *Ann. Phys.* 31, 983–1000.

Lamb, W. E. (1995). Anti-photon, *Appl. Phys.* B 60, 77–84.

Moyal, J. E. (1949). Quantum mechanics as a statistical theory. *Proc. Cambridge Phil. Soc.* 45, 99–124.

Planck, M (1901). Ueber das gesetz der energieverteilung im normalspectrum, *Ann. Phys.* 309 (3), 553–563.

Pryce, M. H. L., and Ward, J. C. (1947). Angular correlation effects with annihilation radiation. *Nature* 160, 435.
Salam, A., and Ward, J. C. (1959). Weak and electromagnetic interactions, *Nuovo Cimento* 11, 568–577.
Salam, A., and Ward, J. C. (1964). Electromagnetic and weak interactions, *Phys. Lett.* 13, 168–171.
Schrödinger, E. (1926). An undulatory theory of the mechanics of atoms and molecules. *Phys. Rev.* 28, 1049–1070.
Schwinger, J. (1948). On quantum-electrodynamics and the magnetic moment of the electron. *Phys. Rev.* 73, 416–417.
Snyder, H. S., Pasternack, S., and Hornbostel, J. (1948). Angular correlation of scattered annihilation radiation. *Phys. Rev.* 73, 440–448.
Tomonaga, S. (1946). On a relativistically invariant formulation of the quantum theory of wave fields. *Prog. Theo. Phys.* 1, 27–42.
Ward, J. C. (1949). *Some Properties of the Elementary Particles*. D. Phil Thesis, Oxford University, Oxford.
Ward, J. C. (1950). An identity in quantum electrodynamics. *Phys. Rev.* 78, 182.
Ward, J. C. (2004). *Memoirs of a theoretical physicist*. *Optics Journal*, Rochester, NY.
Weinberg, S. (1967). A model of leptons. *Phys. Rev. Lett.* 19, 1264–1266.
Wu, C. S., and Shaknov, I. (1950). The angular correlation of scattered annihilation radiation. *Phys. Rev.* 77, 136.

2 Planck's Quantum Energy Equation

2.1 INTRODUCTION

In his work on light sources and black body radiation, Max Planck, around 1900, was confronted with experimental data that could not be explained with the prevailing theoretical concepts of the time. The problem was to express the energy distribution of light emission as a function of wavelength.

His approach to solve this problem is outlined here using Planck's notation: the number of electromagnetic modes per unit volume can expressed as (Planck, 1901)

$$u = \frac{8\pi\nu^2}{c^3}U \tag{2.1}$$

where ν is the frequency of the emission, in Hz or cycles per second, and c is the speed of light ($c = 2.99792458$ m/s). The question then becomes how to define the energy distribution U. Planck approaches this problem using thermodynamic arguments related to the entropy. However, immediately before doing that, he takes a crucial step of introducing, without any derivation whatsoever, the energy expression (Planck, 1901)

$$E = h\,\nu \tag{2.2}$$

Prior to this equation, he writes that the 'energy is proportional to the frequency ν.' Once he unveils this enormous discovery, Planck proceeds with his thermodynamics argument providing an explicit expression for the entropy of the system

$$S = k\left(\left(1+\frac{U}{h\nu}\right)\ln\left(1+\frac{U}{h\nu}\right)-\frac{U}{h\nu}\ln\left(\frac{U}{h\nu}\right)\right) \tag{2.3}$$

and then using $(1/T) = dS/dU$, he proceeds to differentiate Equation (2.3) and arrives at

$$U = h\nu(e^{h\nu/kT}-1)^{-1} \tag{2.4}$$

which, using Equation (2.1), leads directly to Planck's distribution (Planck, 1901)

$$u = \frac{8\pi h\nu^3}{c^3}(e^{h\nu/kT}-1)^{-1} \tag{2.5}$$

DOI: 10.1201/9781003398707-2

In the previous equations, $k = 1.380649 \times 10^{-23}$ J/K is Boltzmann's constant, T is the absolute temperature, and $h = 6.62607015 \times 10^{-34}$ Js is of course Planck's constant.

Planck's quantum equation, also known as Planck's relation, $E = h\nu$, is one of the most fundamental principles of quantum mechanics and one of the most important equations in physics. The fact that the energy of the emission depends on the frequency of the emission ν, according to the elegant relation $E = h\nu$, is a fundamental quantum law that was arrived to from *macroscopic observations* performed on a *classical experiment*. Planck's contribution represents one of the greatest triumphs of a physicist's intuition in the history of physics. Around 1900, when Planck discovered this empirical law, the physics world was classical and entirely macroscopic.

2.2 PLANCK'S EQUATION AND WAVE OPTICS

From Planck's quantum energy equation

$$E = h\nu$$

one can use special relativity's $E = mc^2$ to arrive at (de Broglie, 1923)

$$p = h\,\frac{\nu}{c} \tag{2.6}$$

which, using $\lambda = c/\nu$, leads directly to

$$p = \hbar k \tag{2.7}$$

where $k = 2\pi/\lambda$ is known as the wavenumber. This momentum expression in wave form, $p = \hbar k$, is known as de Broglie's equation and plays a significant role in developing further concepts in quantum optics.

In Chapter 3, Heisenberg's uncertainty principle (Heisenberg, 1927; Feynman et al., 1965; Dirac, 1958) is developed from transparent physics. The approach is based on interferometry principles that lead to the *interferometric identity* (Duarte, 2003)

$$\Delta\lambda\, \Delta x \approx \lambda^2 \tag{2.8}$$

which can also be expressed as

$$\Delta\nu\, \Delta x \approx c \tag{2.9}$$

Using the expression for momentum $p = \hbar k$, which is based on $E = h\nu$, one arrives directly to Heisenberg's uncertainty principle

$$\Delta p\, \Delta x \approx h \tag{2.10}$$

This simple exercise is useful in exposing the order of fundamental concepts in quantum mechanics. This order places $E = h\nu$, and interferometric principles, at the very foundations of quantum physics.

2.3 PLANCK'S CONSTANT *h*

Planck's constant h is one of the most important constants in physics and certainly the most important constant in quantum mechanics. Indeed, it can be said that in quantum mechanics and quantum optics, h is everywhere. In other words, h is synonymous with quantum.

As noted by Duarte (2022), there appears to be no straightforward and transparent 'independent derivation' of $E = h\nu$, via quantum physics, since this expression and h are deeply engrained in the very foundations of the theory.

Since Dirac's probability amplitudes, such as $\langle d|j\rangle$, originally depend only on wave functions of the form

$$\Psi(x,t) = \Psi_0 e^{-i(\omega t - kx)} \tag{2.11}$$

perhaps a careful re-derivation of transition and emission probabilities might open a path forward to find an expression for $E = h\nu$ in the absence of *ad hoc* assumptions.

In his experiment, Planck arrived at $h = 6.55 \times 10^{-34}$ Js. In this book, the current National Institute of Standards and Technology (NIST) value of $h = 6.62607015 \times 10^{-34}$ Js is used (see Table K.1 for values of fundamental constants). A review of the history and methodology of measurements for h is given by Steiner (2013).

Planck's constant is directly related to another extraordinarily important constant, the *fine structure constant* α (Dirac, 1938)

$$\alpha = \left(\frac{e^2}{4\pi\varepsilon_0 c\hbar} \right) \tag{2.12}$$

which can be rearranged to yield

$$h = \alpha^{-1} \left(\frac{e^2}{2c\varepsilon_0} \right) \tag{2.13}$$

Measurements in quantum electrodynamics yield $\alpha^{-1} = 137.035999084$ (Hanneke et al., 2008). Feynman referred to the number 1/137 as the 'mysterious number' (Feynman et al., 1963). At present, there is no theory that predicts α. A theory that would predict α was Dirac's focus of attention for a long time (Dirac, 1938; Kursunoglu, 1987).

2.3.1 BACK TO $E = h\nu$

From experimental evidence, Planck knew that energy E and frequency ν were related so that $E = h\nu$ was a very good guess. Is it possible to arrive at an equation of the form of $E = h\nu$ from first principles independent of Plank's experimental evidence? A simple heuristic approach to the $E = h\nu$ question is as following: $E = mc^2$ can also be written as

$$E = pc \tag{2.14}$$

$$E = \left(\frac{pc}{\nu}\right) \cdot \nu \tag{2.15}$$

And thus,

$$E = \eta\nu \tag{2.16}$$

where $\eta = (pc/\nu)$ a quantity with units of energy × time, or Js, that is, the same units as h. This heuristic approach provides a direct relation between E and ν which is dimensionally correct without *ad hoc* assumptions. Perhaps Planck did consider such an approach and did not bother to disclose it.

PROBLEMS

2.1 Use Equation (2.4) into Equation (2.1) to arrive at Equation (2.5).
2.1 Use Equation (2.8) and $p = \hbar k$ to arrive at $\Delta p\, \Delta x \approx h$.
2.2 Show that Equation (2.8) can be expressed as Equation (2.9).
2.3 Show that Equation (2.12) can be rearranged to yield Equation (2.13).
2.4 Using the constant values given in Table K.1, verify that Equation (2.12) leads to the numerical value of $\alpha^{-1} \approx 137.035999$.

REFERENCES

de Broglie, L. (1923). Waves and quanta. *Nature* 112, 540.
Dirac, P. A. M. (1958). *The Principles of Quantum Mechanics*, 4th ed. Oxford University, Oxford, U.K.
Duarte, F. J. (2003). *Tunable Laser Optics*, 1st ed. Elsevier-Academic, New York.
Duarte, F. J. (2022). *Fundamentals of Quantum Entanglement*, 2nd ed. Institute of Physics, Bristol, U.K.
Feynman, R. P., Leighton, R. B., and Sands, M. (1963). *The Feynman Lectures on Physics*, Vol. I, Addison-Wesley, Reading, MA.
Feynman, R. P., Leighton, R. B., and Sands, M. (1965). *The Feynman Lectures on Physics*, Vol. III, Addison-Wesley, Reading, MA.
Hanneke, D., Fogwell, S., and Gabrielse, G. (2008). New measurement of the electron magnetic moment and the fine structure constant. *Phys. Rev. Lett.* **100**, 120801.
Heisenberg, W. (1927). Uber den anschaulichen inhalt der quantentheoretischen kinematic und mechanic, *Z. Phys.* **43**, 172–198.
Kursunoglu, B. N. (1987). Dirac's influence on quantum field theory. In *Paul Adrien Maurice Dirac* (Kursunoglu, B. N. and Wigner, E. P. eds.). Cambridge University, Cambridge, U.K., Chapter 23, 276–291.
Planck, M. (1901). Ueber das gesetz der energieverteilung im normalspectrum. *Ann. Phys.* **309** (3), 553–563.
Steiner, R. (2013). History and progress on accurate measurements of the Planck Constant. *Rep. Prog. Phys.* **76**, 016101.

3 The Uncertainty Principle

3.1 HEISENBERG'S UNCERTAINTY PRINCIPLE

Perhaps no other topic in physics is surrounded with more awe and mystique as Heisenberg's succinct and beautiful uncertainty principle. Besides its beauty, the uncertainty principle is central to the most successful physical theory ever discovered by mankind: quantum mechanics. Richard Feynman, by far, the most successful communicator of physics, said, 'The uncertainty principle protects quantum mechanics' (Feynman et al., 1965).

Heisenberg (1927) introduced his famed *uncertainty principle* as

$$p_1 \, q_1 \sim h \tag{3.1}$$

where p_1 refers to the momentum uncertainty, q_1 refers to the position uncertainty, and $h = 6.62607015 \times 10^{-34}$ Js is Planck's constant, one of the most fundamental constants in the whole of nature. Dirac in his book expresses the Heisenberg uncertainty principle as (Dirac, 1958)

$$\Delta q \; \Delta p \approx h \tag{3.2}$$

Similarly, Feynman et al. (1965) describe the uncertainty relation as

$$\Delta y \; \Delta p_y \approx h \tag{3.3}$$

In general, for the three space coordinates, we have

$$\Delta x \; \Delta p_x \approx h, \;\; \Delta y \; \Delta p_y \approx h, \;\; \Delta z \; \Delta p_z \approx h \tag{3.4}$$

Considering the uncertainty principle relevant to the x coordinate

$$\Delta x \; \Delta p_x \approx h \tag{3.5}$$

it should be mentioned that the uncertainties in x and p_x are intimately related. In other words, a series of measurements on these quantities yield $(x \pm \Delta x)$ and $(p_x \pm \Delta p_x)$ with Δx and Δp_x directly related via $\Delta x \; \Delta p_x \approx h$. The larger the value of Δx, the smaller the value of Δp_x. In other words, the more accurately we can measure the position of a particle, the less accurately we can determine its momentum, and *vice versa*. In quantum physics, x and p_x are said to be non-commuting observables (Dirac, 1958). Uncertainty and errors are essential to physical measurements and have been part of physics since the dawn of physics. Newton in his *Principia* (Newton, 1687) has already dealt with measurement errors and uncertainties. In this regard, a measurement of x with $\Delta x = 0$

DOI: 10.1201/9781003398707-3

is not possible in physics. Similarly, a measurement of p_x with $\Delta p_x = 0$ is physically impossible. There is always an uncertainty, no matter how small, no matter how infinitesimal. A similar observation was made, in the quantum context, by Dirac in 1930 (Dirac, 1958), and as we shall see later, this observation is crucial to interpretational issues of quantum mechanics (see Chapter 23).

In his lectures, Feynman also relates the uncertainty principle to the double-slit experiment and hence to interferometry. He did so conceptually, in reference to the impossibility of determining the path of the electron without disturbing the interference pattern (Feynman et al., 1965). In this chapter, we offer further elucidation on the link between the uncertainty principle and *N*-slit interferometry. In fact, we show that it is possible to obtain the original uncertainty principle from interferometric principles, thus indicating that interferometry is of fundamental importance to quantum mechanics—even more fundamental than the Heisenberg's uncertainty principle itself.

The approach to Heisenberg's uncertainty principle, disclosed here, is from a physics perspective while avoiding the use of unnecessary mathematics, or preestablished analytical techniques, which might obscure the essence of physics.

3.2 THE WAVE-PARTICLE DUALITY

The quantum energy of a wave, of frequency v, is given by Planck's quantum energy equation

$$E = hv \tag{3.6}$$

Equating this to the relativistic energy of a particle $E = mc^2$ and using the identity $\lambda = c/v$, an expression for the momentum is given as

$$p = \frac{h}{\lambda} \tag{3.7}$$

which, using the identity

$$k = \frac{2\pi}{\lambda} \tag{3.8}$$

can also be expressed as

$$p = \hbar\, k \tag{3.9}$$

This momentum equation was applied to particles, such as electrons, by de Broglie (Haken, 1981). Thus, wave properties such as frequency and wavelength were attributed to the motion of particles. Notice that the momentum expression can be rewritten as

$$p\ \lambda = h \tag{3.10}$$

which already embodies the *dimensionality* described in Heisenberg's uncertainty principle. As will be seen in the exposition given next, this expression is crucial in the approximate derivation of the uncertainty principle.

Note: the particle-duality concept applies perfectly to known particles as the electron.

However, the photon is not a particle (Lamb, 1995): 'All the indistinguishable photons illuminate the array of N slits, or grating, simultaneously. If only one photon propagates, at any given time, then that individual photon illuminates the whole array of N slits simultaneously' (Duarte, 2003). The best way to describe a photon is as a form of a field or as 'nonlocal coherent energy' (Duarte, 2022). Many of the difficulties associated with the interpretation of quantum mechanics arise from the unnecessary representation of the photon as a particle. This is important since this book is about photons and quanta.

3.3 THE FEYNMAN APPROXIMATION

In his book on *Quantum Mechanics and Path Integrals*, Feynman makes use of the two-slit experiment to provide an approximate description of the physics behind the uncertainty principle (Feynman and Hibbs, 1965). Here, Feynman's description is outlined using a slightly different notation. Feynman observes that in the two-slit experiment (see Figure 3.1), the separation of the center of the slits, a, divided by the intra-interferometric distance (distance from the slits to the interferometric plane) D, that is, a/D is approximately equal to the ratio of the wavelength λ to the distance from the central maxima to the first secondary maxima at the interferometric plane Δx. In other words,

$$\frac{a}{D} \approx \frac{\lambda}{\Delta x} \tag{3.11}$$

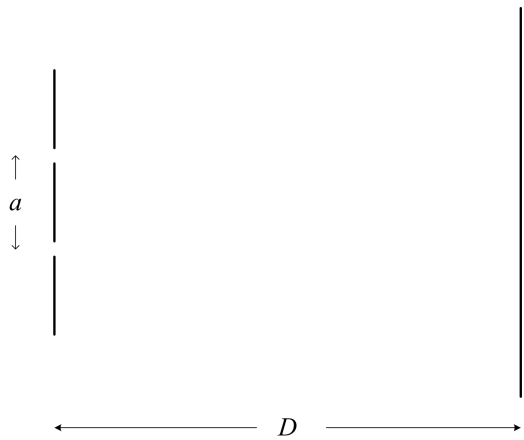

FIGURE 3.1 Two-slit interferometer used in the Feynman approximation. The separation between the center of the slits is a, while the intra-interferometric distance from the slits to the interferometric plane is D.

It should be noted that this geometrical identity can be either obtained directly from experimental results or by using the interferometric equation (Duarte, 1993) described in the next section. Then, using the same two-slit experiment for electrons, Feynman postulates that the passage through the slits induces a change in momentum and that the ratio $(\Delta p/p)$ is approximately equal to a/D, so that

$$\frac{\Delta p}{p} \approx \frac{a}{D} \tag{3.12}$$

and then, using $p\lambda = h$, we get

$$\Delta x \ \Delta p \approx h \tag{3.13}$$

3.1.1 Example

In Figure 3.1, the basic geometry of a two-slit interferometer is illustrated. The separation of the center of the slits is a, the intra-interferometric distance from the slits to the interferometric plane is D. For two 570 μm slits, separated by 570 μm, $a \approx 1140$ μm. Thus, for $D \approx 7.235$ m, the ratio $(a/D) \approx 1.58 \times 10^{-4}$. The corresponding two-slit interferogram for He–Ne laser illumination at $\lambda \approx 632.82$ nm is shown in Figure 3.2. From this interferogram, given that each pixel is ~20 μm wide, we get $(\lambda/\Delta x) \approx 1.62 \times 10^{-4}$, thus corroborating Feynman's approximation $(a/D) \approx (\lambda/\Delta x)$. The slight difference between the two ratios is well within the experimental uncertainties involved, which are not included here to keep the exposition simple.

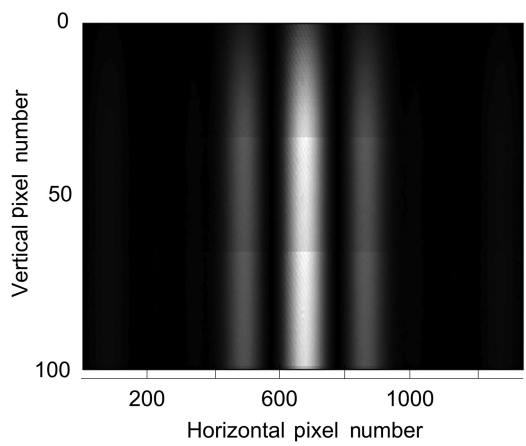

FIGURE 3.2 Measured double-slit interferogram generated by two slits of 570 μm separated by 570 μm. The intra-interferometric distance (from the slits to the interferometric plane) is $D \approx 7.235$ m, and the laser wavelength from the He–Ne laser is $\lambda \approx 632.8$ nm.

3.4 THE INTERFEROMETRIC APPROXIMATION

As mentioned at the instruction, Feynman relates the uncertainty principle to the double-slit electron experiment and hence to interferometry. Here, the link between the uncertainty principle and generalized *N*-slit interferometry is described in detail. The following exposition is based on the approach given in Duarte (2003).

The generalized one-dimensional interferometric equation derived using Dirac's notation is given by (Duarte, 1991, 1993)

$$\langle d|s\rangle\ \langle d|s\rangle^{*} = \sum_{j=1}^{N} \Psi(r_j)^2 + 2\sum_{j=1}^{N} \Psi(r_j)\left(\sum_{m=j+1}^{N} \Psi(r_m)\cos(\Omega_m - \Omega_j) \right) \tag{3.14}$$

The interference term in this equation, $\cos(\Omega_m - \Omega_j)$, can be expressed as (Duarte, 1997)

$$\cos\big((\theta_m - \theta_j) \pm (\varphi_m - \varphi_j)\big) = \cos\big(|l_m - l_{m-1}|k_1 \pm |L_m - L_{m-1}|k_2\big) \tag{3.15}$$

and from this equation, the diffraction grating equation can be obtained (see Chapter 5)

$$d_m(\sin\Theta_m \pm \sin\Phi_m) = m\lambda \tag{3.16}$$

where $m = 0,\ \pm1,\ \pm2,\ \pm3....$ For a grating utilized in the reflection domain, in Littrow configuration, $\Theta_m = \Phi_m = \Theta$, so that the grating equation reduces to

$$2d\sin\Theta = m\lambda \tag{3.17}$$

Using Equation (3.17) and considering an expanded light beam incident on a reflection grating, as illustrated in Figure 3.3, and allowing for an infinitesimal change in wavelength

$$\lambda_1 = \frac{2d}{m}\left(\frac{\Delta x_1}{l}\right) \tag{3.18}$$

$$\lambda_2 = \frac{2d}{m}\left(\frac{\Delta x_2}{l}\right) \tag{3.19}$$

where l is the grating length and Δx is the path difference. From the geometry,

$$\sin\Theta = \frac{\Delta x}{l} \tag{3.20}$$

and subtracting Equation (3.18) from (3.19), it follows that

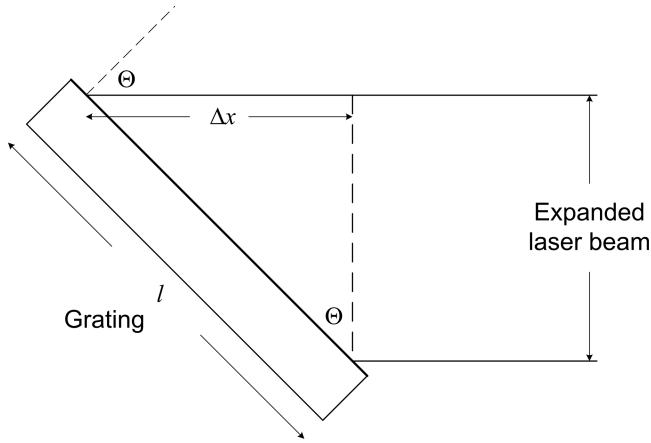

FIGURE 3.3 Path differences in a diffraction grating of the reflective class in Littrow configuration. From the geometry, $\sin\Theta = (\Delta x/l)$.

$$\Delta\lambda = \frac{l\lambda}{\Delta x}\left(\frac{\Delta x_1 - \Delta x_2}{l}\right) \tag{3.21}$$

To distinguish between a maximum and a minimum, the *difference* in path differences should be equal to a single wavelength, so that

$$(\Delta x_1 - \Delta x_2) \approx \lambda \tag{3.22}$$

Hence, Equation (3.21) reduces to the well-known and important diffraction identity

$$\Delta\lambda \approx \frac{\lambda^2}{\Delta x} \tag{3.23}$$

Considering $p\lambda = h$ for two slightly different wavelengths

$$p_1 - p_2 = h\frac{(\lambda_1 - \lambda_2)}{\lambda_1\lambda_2} \tag{3.24}$$

and since the difference between λ_1 and λ_2 is infinitesimal, then we have

$$\Delta p \approx h\ \frac{\Delta\lambda}{\lambda^2} \tag{3.25}$$

Substitution of Equation (3.23) into (3.25) leads directly to

$$\Delta p\ \Delta x \approx h \tag{3.26}$$

which is known as *Heisenberg's uncertainty principle* (Dirac, 1958). This approach describes the interferometric foundation of the uncertainty principle and hints toward interference as a more fundamental principle.

It should be noted that the 'interferometric approximation' toward the uncertainty principle is perfectly sufficient since the uncertainty principle is the essence of *indeterminancy*, a concept crucial to quantum mechanics (Born, 1949). Researchers have also found the interferometric approach to the uncertainty principle compatible with a quantum fluctuations approach to the subject (Madrid, 2020).

3.5 THE MINIMUM UNCERTAINTY PRINCIPLE

The paths described here have used approximate optical and interferometric methods to arrive at the uncertainty principle

$$\Delta p\ \Delta x \approx h$$

where Δx and Δp are outlined as the *uncertainties* in displacement x and momentum p, respectively. From a physics perspective, this is quite alright since an 'exact' derivation of the uncertainty principle appears to be a contradiction.

An alternative, more restrictive, version of the uncertainty principle is given by Feynman as

$$\Delta p\ \Delta x \approx \frac{\hbar}{2} \tag{3.27}$$

Feynman arrives at this expression using a probability density approach and states 'for any other form of a distribution in x or p, the product $\Delta p\ \Delta x$ cannot be smaller than the one we have found here' (Feynman et al., 1965). Thus, we call this the minimum uncertainty principle.

The literature offers several approaches to this definition. Here, we briefly describe the approach of Landau and Lifshitz (1976). These authors begin by defining the uncertainties via the standard of deviation

$$(\delta x)^2 = (x - \bar{x})^2 \tag{3.28}$$

$$(\delta p_x)^2 = (p_x - \bar{p_x})^2 \tag{3.29}$$

and then, they consider the inequality

$$\int_{-\infty}^{\infty} \left|\alpha x\psi + (d\psi/dx)\right|^2 dx \geq 0 \tag{3.30}$$

where α is an arbitrary real constant and ψ is an ordinary wave function. Evaluation of this integral leads to

$$\delta x \ \delta p_x \geq \frac{\hbar}{2} \tag{3.31}$$

which is known as the least possible value of the $\delta x \delta p_x$ product or as the *minimum uncertainty product*. Thus, the minimum product is 4π smaller than the approximate expression derived from the physics. Landau and Lifshitz (1976) write that 'the least possible value' of the uncertainty product is $(\hbar/2)$.

3.6 THE GENERALIZED UNCERTAINTY PRINCIPLE

In this chapter, we mainly refer to a generalization of Heisenberg's uncertainty principle provided by Robertson in 1929. In that short paper, Roberson states, 'This principle, as formulated by Heisenberg for two conjugate quantum-mechanical variables states that the accuracy with which two such variables can be measured simultaneously is subject to the restriction that the product of the uncertainties in the two measurements is at least of order h' (Robertson, 1929). He then explains the desirability to extend the principle to two variables that are not conjugate.

To this effect, Robertson defines a mean value (A_0) of a Hermitian operator A (see Chapter 11), in a system described by the wave function ψ, as

$$A_0 = \int \psi^* A \psi \ d\tau \tag{3.32}$$

The uncertainty in A , that is ΔA , is defined 'in accordance with statistical usage' as (Robertson, 1929)

$$(\Delta A)^2 = \int \psi^* (A - A_0)^2 \psi \ d\tau \tag{3.33}$$

likewise, we can write

$$(\Delta B)^2 = \int \psi^* (B - B_0)^2 \psi \ d\tau \tag{3.34}$$

Then, Robertson introduces the Schwarzian inequality

$$\left[\int (f_1 f_1^* + f_2 f_2^*) d\tau\right] \left[\int (g_1 g_1^* + g_2 g_2^*) d\tau\right] \geq \left|\int (f_1 g_1 + f_2 g_2) d\tau\right|^2 \tag{3.35}$$

and defines

$$f_1^* = (A - A_0)\psi = f_2 \tag{3.36}$$

$$g_1 = (B - B_0)\psi = -g_2^* \tag{3.37}$$

Using these definitions, it follows that

$$f_1 = (A - A_0)\psi^* = f_2^* \tag{3.38}$$

$$g_1^* = (B - B_0)\psi^* = -g_2 \tag{3.39}$$

substituting into the left-hand side of Equation (3.35), we get

$$\left[2\int \psi^*(A - A_0)^2\psi \; d\tau\right]\left[2\int \psi^*(B - B_0)^2\psi \; d\tau\right] \geq \left|\int (f_1 g_1 + f_2 g_2)\, d\tau\right|^2 \tag{3.40}$$

Next, reducing the $(f_1 g_1 + f_2 g_2)$ term, within the integral on the right-hand side of Equation (3.35), and using Equations (3.33) and (3.34) (on the left-hand side), leads to Robertson's result

$$4\ (\Delta A)^2(\Delta B)^2 \geq \left|\int \psi^*(AB - BA)\psi \; d\tau\right|^2 \tag{3.41}$$

$$\Delta A\ \Delta B \geq \frac{1}{2}\left|\int \psi^*(AB - BA)\psi \; d\tau\right| \tag{3.42}$$

This result is also reproduced in the recent literature as (Erhart et al., 2012)

$$\sigma(A)\sigma(B) \geq \frac{1}{2}\left|\langle\psi|[A,B]|\psi\rangle\right| \tag{3.43}$$

where

$$[A,B] = AB - BA \tag{3.44}$$

Revisiting the Robertson result here teaches us that this generalization flows mainly from a mathematical technique, that is, the application of the Schwarz inequality.

Recent work has led to further generalized formulations of Heisenberg's uncertainty principle. This work has been carried out motivated by concerns that the original Heisenberg version of the uncertainty principle only applies to a limited array of measurement apparatuses (Ozawa, 2004). Very briefly, and without further discussion, a generalized version of the uncertainty principle has been put forward for a measurable A and an observable B (Erhart et al., 2012)

$$\left(e(A)\eta(B) + e(A)\sigma(B) + \sigma(A)\eta(B)\right) \geq \frac{1}{2}\left|\langle\psi|[A,B]|\psi\rangle\right| \tag{3.45}$$

where $e(A)$ is the root mean square deviation of an output operator O_A, while the disturbance $\eta(B)$ is defined as the root mean square of the change in the observable B during the measurement. The second and third terms, of the left-hand side, flow from the non-commutability of A and B (Ozawa, 2004).

Notice that the right-hand side of the inequality is the same as Robertson's, and it is on the right-hand side that the physics resides. It should be mentioned here

that in Chapter 15, on the subject of entanglement, an analogous expression to $[A, B] = AB - BA$ is developed in the form of $\left(|x\rangle|y\rangle - |y\rangle|x\rangle\right)$.

3.7 EQUIVALENT VERSIONS OF HEISENBERG'S UNCERTAINTY PRINCIPLE

Heisenberg's uncertainty principle, $\Delta x\ \Delta p \approx h$, can be expressed in several useful versions. Assuming an independent derivation of $\Delta p\ \Delta x \approx h$, and using $p = \hbar k$, it can be expressed in its wavelength-spatial form

$$\Delta\lambda \approx \frac{\lambda^2}{\Delta x} \tag{3.46}$$

This is a widely used identity in interferometry utilized to express linewidth in wavelength units (m). We also know that the interferometric identity given in Equation (3.46) can be expressed in its frequency-spatial version

$$\Delta\nu \approx \frac{c}{\Delta x} \tag{3.47}$$

which is also widely used in interferometry to express linewidth in frequency units (Hz).

Using $E = mc^2$, the uncertainty principle can also be expressed in its energy–time form

$$\Delta E\ \Delta t \approx h \tag{3.48}$$

which, using the quantum energy $E = h\nu$, can be transformed into its frequency–time version

$$\Delta\nu\ \Delta t \approx 1 \tag{3.49}$$

This succinct and beautiful expression is a crucial result for the field of pulsed lasers and in particular for femtosecond (fs) and attosecond (at) lasers. In fact, $\Delta\nu\ \Delta t \approx 1$ means that, for a laser working optimally at the limit established by the uncertainty principle, the time duration of the pulses Δt can be determined from its spectral profile.

From Equation (3.49), we can write directly an expression for the time segment

$$\Delta t \approx \frac{1}{\Delta\nu} \tag{3.50}$$

which is also known as the *coherence time*. From this time, the *coherence length* can be defined as

$$\Delta x \approx \frac{c}{\Delta\nu} \tag{3.51}$$

which is an alternative form of Equation (3.47).

One final observation: the highly practical identities $\Delta\lambda \approx \lambda^2/\Delta x$ and $\Delta\nu \approx c/\Delta x$ are routinely applied in the field of interferometry to express measured linewidths either in frequency or wavelength units (Duarte, 2003). Note that all these expressions are simply based on $\Delta x\ \Delta p \approx h$ and not in its more restrictive minimum product version.

3.7.1 Example

An optimized multiple-prism grating solid-state organic dye laser (Duarte, 1999) yields kW pulses tunable in the $565 \leq \lambda \leq 603$ nm range. Its smooth temporal pulse is indicative of single-longitudinal-mode oscillation and is shown in Figure 3.4. The duration of this pulse at full-width-half-maximum (FWHM) is $\Delta t \approx 3$ ns. The corresponding Fabry–Perot interferogram from this single-longitudinal-mode emission is shown in Figure 3.5. The half-width of the rings is measured to be $\Delta\nu \approx 350$ MHz. Thus, it can be directly established that the product $\Delta\nu\ \Delta t \approx 1.06$ for this narrow-linewidth pulsed laser emission which is near the limit established frequency–time version of the Heisenberg uncertainty principle $\Delta\nu\ \Delta t \approx 1$.

3.8 APPLICATIONS OF THE UNCERTAINTY PRINCIPLE IN OPTICS

The uncertainty principle is widely applied in optics. It applies to interferometry, linewidth measurements, and beam divergence measurements. Here we focus on the uncertainty principle and beam divergence. Applications of these concepts to astronomy are also mentioned.

3.8.1 Beam Divergence

Heisenberg's uncertainty principle can be used to derive some useful identities in optics and interferometry. Starting from

$$\Delta p\ \Delta x \approx h$$

and substituting for Δp using $p = \hbar k$, yields

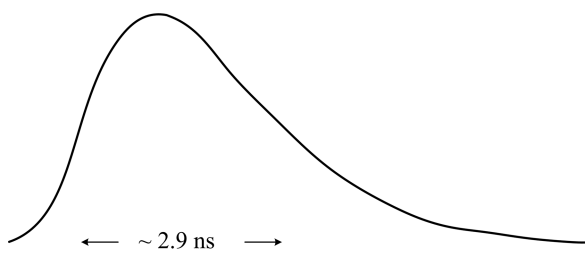

FIGURE 3.4 Temporal profile of a laser pulse from an optimized multiple-prism grating solid-state dye laser. The temporal scale is 1 ns/div (Reproduced from Duarte, F. J., *Appl. Opt.* **38**, 6347–6349, 1999, with permission from Optica).

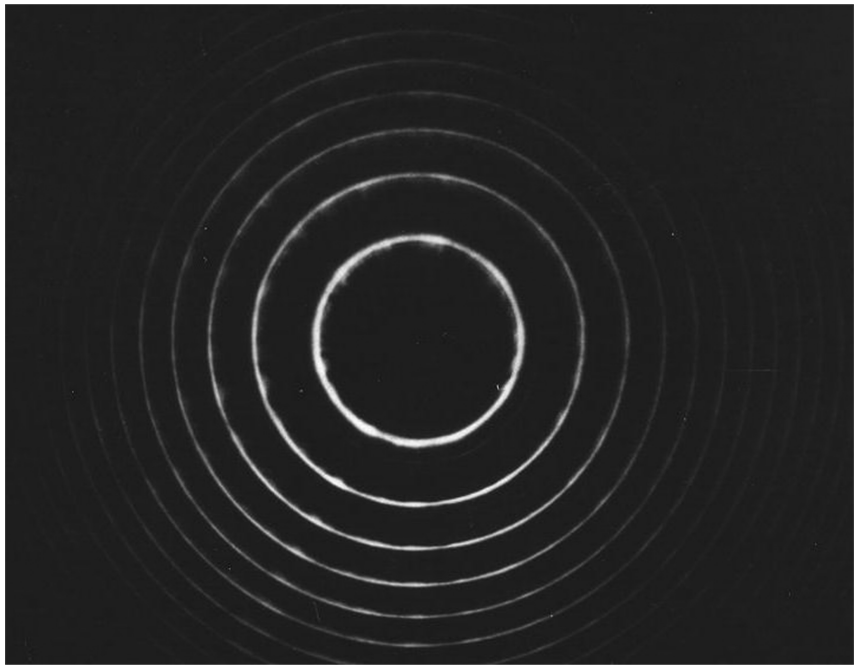

FIGURE 3.5 Corresponding Fabry–Perot interferogram of the single-longitudinal-mode oscillation from the optimized multiple-prism grating solid-state dye laser (Reproduced from Duarte, F. J., *Appl. Opt.* **38**, 6347–6349, 1999, with permission from Optica).

$$\Delta k\ \Delta x \approx 2\pi \tag{3.52}$$

which leads to

$$\Delta\lambda\ \approx \frac{\lambda^2}{\Delta x}$$

For a diffraction-limited beam traveling in the z direction $k_x = k \sin\theta$. Thus, for a very small angle θ

$$k_x \approx k\theta \tag{3.53}$$

so that

$$\Delta k_x \approx k\ \Delta\theta \tag{3.54}$$

Using $\Delta k_x\ \Delta x \approx 2\pi$ and Equation (3.54), it is readily seen that the beam has an angular divergence given by

$$\Delta\theta \approx \frac{\lambda}{\Delta x} \tag{3.55}$$

which is a succinct equation for angular beam divergence, and in essence an additional manifestation of the uncertainty principle. Equation (3.55) indicates that the angular spread of a propagating beam of wavelength λ is inversely proportional to its original width. The narrower the beam, the larger its divergence. This equation also states that light of shorter wavelength experiences less beam divergence, which is a well-known experimental fact in laser physics. This implies that the beam divergence can be controlled using geometrical (Δx) as well as physical means (λ).

Equation (3.55) has the same form as the return-pass beam divergence equation derived from classical principles (Duarte, 1990), namely,

$$\Delta\theta = \frac{\lambda}{\pi w}\left(1+\left(\frac{L_{\mathcal{R}}}{B}\right)^2+\left(\frac{A\,L_{\mathcal{R}}}{B}\right)^2\right)^{1/2} \tag{3.56}$$

where w is the beam waist, $L_{\mathcal{R}} = (\pi w^2/\lambda)$ is known as the Rayleigh length, and A and B are geometrical–spatial matrix propagation parameters defined in Duarte (2003, 2015) and explained in Appendix F. For an optimized design,

$$\left(1+\left(\frac{L_{\mathcal{R}}}{B}\right)^2+\left(\frac{A\,L_{\mathcal{R}}}{B}\right)^2\right)^{1/2} \approx 1 \tag{3.57}$$

and Equation (3.56) reduces to

$$\Delta\theta \approx \frac{\lambda}{\pi w} \tag{3.58}$$

This minimized beam divergence is known as the *diffraction limit*. The equivalence of Equations (3.55) and (3.58) is self-evident.

In summary, the generalized interference equation, that is Equation (3.14), leads to the interferometric identity $\Delta\lambda \approx \lambda^2/\Delta x$ which, in conjunction with the uncertainty principle $\Delta p\,\Delta x \approx h$, leads to the expression of the diffraction-limited beam divergence $\Delta\theta \approx \lambda/\Delta x$.

3.8.2 Beam Divergence in Astronomy

An important application of the uncertainty principle manifests itself in calculations of the angular resolution limit of telescopes used in astronomical observations. Reflection telescopes such as the Newtonian and Cassegrain telescopes are depicted in Figure 3.6 and discussed further in Duarte (2003). The angular resolution that can be achieved with these telescopes, under ideal conditions, is approximately quantified by the diffraction limit of the beam divergence given in Equation (3.55), that is, the smallest angular discrimination, or resolution limit, of a telescope with a diameter $D = 2w$ is given by

$$\Delta\theta \approx \frac{2\lambda}{\pi D} \tag{3.59}$$

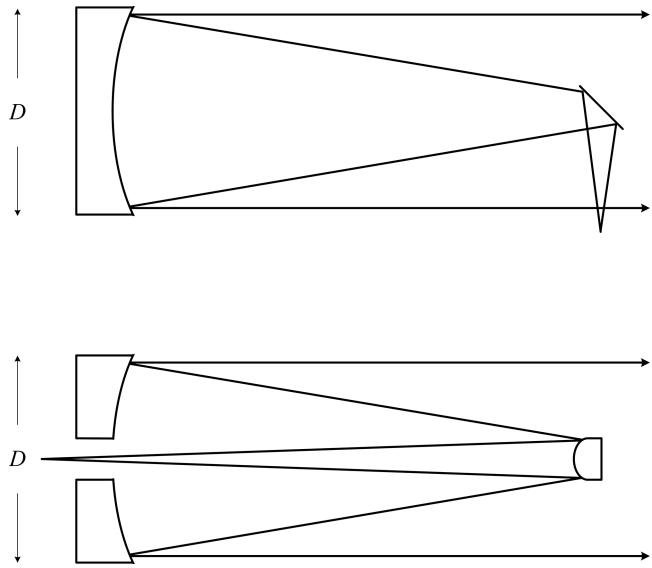

FIGURE 3.6 Reflection telescopes used in astronomical observations. (a) Newtonian telescope. (b) Cassegrain telescope. The diameter D of the main mirror determines the angular resolution of the telescope.

This equation teaches us that the two alternatives to improve the angular resolution of a telescope are either to observe at shorter wavelengths (λ) or to increase the diameter (D) of the telescope. This equation explains the quest toward the building of large, very large, and extremely large terrestrial telescopes. Previously, we estimated the angular resolution for telescope diameters of 10 m and 100 m Duarte (2003). For $\lambda = 500\,\text{nm}$, the angular resolutions for large and very large telescopes, at various diameters, are listed in Table 3.1. In addition to better angular resolutions, large aperture telescopes provide increased signal since the area of collection increases substantially. The construction of very large telescopes, with diameters greater than 50 m, should be feasible in the future via the use of very light segmented mirrors.

The James Webb Space Telescope is of Cassegrain type with a segmented primary mirror with a diameter $D \approx 6.5$ m optimized for the infrared. At $\lambda \approx 13$ μm, $\Delta\theta \approx (4/\pi)\times 10^{-6}$ rad.

TABLE 3.1
Angular Resolutions for Newtonian and Cassegrain Telescopes

Diameter (m)	Area (m^2)	$\Delta\theta$ (rad)
10	25π	$(1/\pi)\times 10^{-7}$
50	625π	$(2/\pi)\times 10^{-8}$
100	2500π	$(1/\pi)\times 10^{-8}$
$1000/\pi$	$(25/\pi)\times 10^{4}$	10^{-9}

The subject of laser beam divergence for *laser guide star* in astronomy, using narrow-linewidth oscillators emitting at $\lambda \approx 589$ nm, is discussed by Duarte (2003, 2015).

3.8.3 The Uncertainty Principle and the Cavity Linewidth Equation

In this section, the nexus between the uncertainty principle and the single-pass cavity linewidth equation is outlined: the generalized one-dimensional interferometric equation (Duarte, 1991, 1992)

$$\langle d|s\rangle\langle d|s\rangle^{*} = \sum_{j=1}^{N} \Psi(r_j)^2 + 2\sum_{j=1}^{N} \Psi(r_j)\left(\sum_{m=j+1}^{N} \Psi(r_m)\cos(\Omega_m - \Omega_j) \right)$$

is used in Appendix B to derive the cavity linewidth equation (Duarte, 1992)

$$\Delta\lambda \approx \Delta\theta \left(\frac{\partial\theta}{\partial\lambda} \right)^{-1} \tag{3.60}$$

which is also expressed as

$$\Delta\lambda \approx \Delta\theta(\nabla_{\lambda}\theta)^{-1} \tag{3.61}$$

where $\nabla_{\lambda}\theta = (\partial\theta/\partial\lambda)$. This equation is used extensively to determine the emission linewidth in high-gain pulsed narrow-linewidth dispersive laser oscillators (Duarte, 1990). As indicated, this equation originates from the generalized *N*-slit interference equation and incorporates the beam divergence expression $\Delta\theta$ whose diffraction-limited value

$$\Delta\theta \approx \frac{\lambda}{\Delta x}$$

can be derived from the uncertainty principle $\Delta p\ \Delta x \approx h$, as previously illustrated.

In addition to the explicit equations for beam divergence given here, it is also important to indicate that the beam profile can be generated directly from the generalized *N*-slit interferometric equation, Equation (3.14), and the beam divergence calculated from the history of the beam profiles. In other words, the interferometric equation inherently contains the correct information on beam divergence, which is not surprising since it can also be used to derive the uncertainty principle as we have just seen.

Equation (3.60) also has a geometrical origin (Robertson, 1955), thus illustrating, once again, the synergy between classical and quantum physics.

3.8.4 Tuning Laser Microcavities

A fine-tuning technique applicable to microelectromechanical systems (MEMS)–driven miniature laser cavities consists simply in changing the cavity length as illustrated in Figure 3.7. This approach exploits the very fact that the free spectral range (FSR) of the cavity is a function of Δx. Here, we examine this approach to wavelength tuning, following the approach of Duarte (2003, 2009). Going back to the interferometric identity

$$\delta\lambda \approx \frac{\lambda^2}{\Delta x} \tag{3.62}$$

one can write for an initial wavelength λ_1

$$\delta\lambda_1 \approx \frac{\lambda_1^2}{2L} \tag{3.63}$$

and for a subsequent wavelength λ_2

$$\delta\lambda_2 \approx \frac{\lambda_2^2}{2(L \pm \Delta L)} \tag{3.64}$$

Moreover, it is convenient to define the number of longitudinal modes in each case as

$$N_1 = \frac{\Delta\lambda_1}{\delta\lambda_1} \tag{3.65}$$

and

$$N_2 = \frac{\Delta\lambda_2}{\delta\lambda_2} \tag{3.66}$$

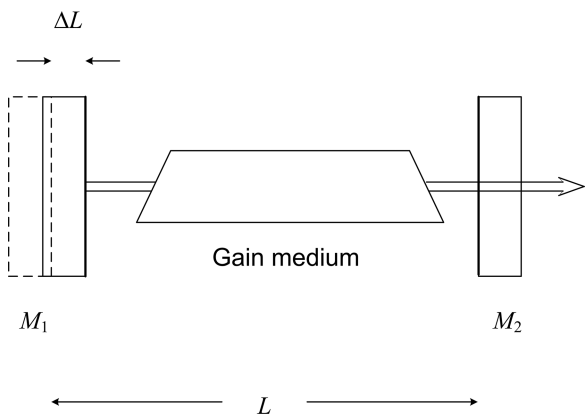

FIGURE 3.7 Wavelength tuning by changing the length of the cavity L. This is accomplished via the displacement of one of the mirrors of the resonator.

where $\Delta\lambda_1$ and $\Delta\lambda_1$ are the corresponding laser linewidths. If the laser linewidth, during this ΔL change, is maintained so that $\Delta\lambda_1 \approx \Delta\lambda_2$, then taking the ratio of Equations (3.63) and (3.64) leads to (Duarte, 2003)

$$\lambda_2 \approx \lambda_1 \left(\frac{N_1}{N_2} \right)^{1/2} \left(1 \pm \frac{\Delta L}{L} \right)^{1/2} \tag{3.67}$$

For $N_1 \approx N_2$, or single-longitudinal-mode oscillation, this equation reduces to Duarte (2003)

$$\lambda_2 \approx \lambda_1 \left(1 \pm \frac{\Delta L}{L} \right)^{1/2} \tag{3.68}$$

Uenishi et al. (1996) report on experiments using the $\Delta L/L$ method to perform wavelength tuning in a MEMS driven semiconductor laser cavity. In that experiment, they observed wavelength tuning, in the absence of mode-hoping, as long as the change in wavelength did not exceed $\lambda_2 - \lambda_1 \approx 1$ nm. Using their graphical data for the scan initiated at $\lambda_1 \approx 1547$ nm, it is established that $\Delta L \approx 0.4$ μm, and using $L \approx 305$ μm, Equation (3.65) yields $\lambda_1 \approx 1549$ nm, which approximately agrees with the authors' observations (Uenishi et al., 1996). In this regard, it should be mentioned that Equation (3.65) was implicitly derived with the assumption of a wavelength scan obeying the condition $\delta\lambda_1 \approx \delta\lambda_2$. Albeit here we use the term microcavity, this approach should also apply to cavities in the sub-micrometer regime or nanocavities.

3.8.5 Nanocavities

The longitudinal-mode spacing in a cavity of length $L = \Delta x/2$ is known as the *FSR* of the cavity and can be designated as

$$\delta\lambda \approx \frac{\lambda^2}{2L} \tag{3.69}$$

or

$$\delta\nu \approx \frac{c}{2L} \tag{3.70}$$

For very short cavities, with cavity lengths in the sub-micrometer range, or the nanometer range, the longitudinal-mode spacing becomes rather large. For example, for $L \approx 300$ nm at $\lambda \approx 540$ nm, the longitudinal-mode spacing becomes $\delta\lambda \approx 486$ nm, which is an enormous separation. This means that a measured linewidth in the tens of nm easily meets the criteria for single-longitudinal-mode emission. Thus, the challenge with nanocavities lies in restricting the emission to a single-transverse mode since, as established by Equation (3.14), a very short cavity length requires an infinitesimal aperture size.

Nanocavities are of interest not only because of their size but also because they exhibit some interesting characteristics such as lasing with extremely low thresholds (De Martini and Jakobovitz, 1980). High spatial and spectral coherent emission, with a measured visibility of $v \approx 0.90$, from an electrically driven laser dye-doped organic semiconductor nanocavity ($L \approx 300$ nm), in the pulsed regime, has been reported by Duarte et al. (2005, 2008). A directional beam with a near-Gaussian spatial distribution was obtained by using an extra-cavity double-interferometric filter configuration. More recently, the coherence of this emission has been described as intrinsic quantum coherence (Duarte and Taylor, 2022).

PROBLEMS

3.1 Show that $\Delta x\, \Delta p \approx h$ can be expressed as $\Delta\lambda \approx \lambda^2/\Delta x$.
3.2 Show that $\Delta x\, \Delta p \approx h$ can be expressed as $\Delta\nu \approx c/\Delta x$.
3.3 Show that $\Delta x\, \Delta p \approx h$ can be expressed as $\Delta\nu\ \Delta t \approx 1$.
3.4 Show that $\Delta\nu \approx c/\Delta x$ follows from $\Delta\lambda \approx \lambda^2/\Delta x$.
3.5 Show that $(f_1 g_1 + f_2 g_2) = \psi^*(AB - BA)\psi$.
3.6 Calculate the diffraction-limited beam divergence, at FWHM, for (a) a laser beam with a 150 μm radius at $\lambda = 590$ nm, and (b) a laser beam with a 500 μm radius at $\lambda = 590$ nm.
3.7 Repeat the calculations of the first problem for the excimer laser (XeCl) wavelength $\lambda = 308$ nm. Comment.
3.8 Calculate the dispersive cavity linewidth for a high-power tunable laser yielding a diffraction-limited beam divergence, 150 μm in radius, at $\lambda = 590$ nm. Assume that an appropriate beam expander illuminates a 3300 l/mm grating deployed in the first order. The grating has a 50 mm length perpendicular to the grooves.
3.9 (a) For a pulsed laser delivering a 350 MHz laser linewidth, at the limit established by Heisenberg's uncertainty principle, estimate its shortest possible pulse width. (b) For a laser emitting 1 fs pulses estimate its broadest possible spectral width in nanometers centered around $\lambda = 500$ nm.
3.10 For a cavity with a length $L = 100$ μm, calculate the change in wavelength for $\Delta L = 1.0$ μm, given that the initial wavelength is $\lambda = 1500$ nm.

REFERENCES

De Martini, F., and Jakobovitz, J. R. (1980). Anomalous spontaneous-emission-decay phase transition and zero-threshold laser action in a microscopic cavity, *Phys. Rev. Lett.* 60, 1711–1714.

Dirac, P. A. M. (1958). *The Principles of Quantum Mechanics*, 4th ed. Oxford University, Oxford, U.K.

Duarte, F. J. (1990). Narrow-linewidth pulsed dye laser oscillators. In *Dye Laser Principles* (Duarte, F. J., and Hillman, L. W., eds.). Academic, New York, Chapter 4, pp. 133–183.

Duarte, F. J. (1991). Dispersive dye lasers. In *High Power Dye Lasers* (Duarte, F. J., ed.). Springer-Verlag, Berlin, Chapter 2, pp. 7–43.

Duarte, F. J. (1992). Cavity dispersion equation $\approx (\partial/\partial)^{-}1$: a note on its origin. *Appl. Opt.* 31, 6979–6982.
Duarte, F. J. (1993). On a generalized interference equation and interferometric measurements. *Opt. Commun.* 103, 8–14.
Duarte, F. J. (1997). Interference, diffraction, and refraction, via Dirac's notation. *Am. J. Phys.* 65, 637–640.
Duarte, F. J. (1999). Multiple-prism grating solid-state dye laser oscillator: optimized architecture. *Appl. Opt.* 38, 6347–6349.
Duarte, F. J. (2003). *Tunable Laser Optics*, 1st ed. Elsevier-Academic, New York.
Duarte, F. J. (2008). Coherent electrically excited semiconductors: coherent or laser emission? *Appl. Phys. B.* 90, 101–108.
Duarte, F. J. (2015). *Tunable Laser Optics*, 2nd ed. CRC, Boca Raton, FL.
Duarte, F. J. (2022). *Fundamentals of Quantum Entanglement*, 2nd ed. Institute of Physics, Bristol, U.K.
Duarte, F. J., Liao, L. S., and Vaeth, K. M. (2005). Coherent characteristics of electrically excited tandem organic light emitting diodes. *Opt. Lett.* 30, 3072–3074.
Duarte, F. J., and Taylor, T. S. (2022). Quantum coherent in electrically-pumped organic interferometric emitters, *Appl. Phys. B*. 128, 11.
Erhart, J., Sponar, S., Suluok, G., Badurek, G., Ozawa, M., and Hasegawa, Y. (2012). Experimental demonstration of a universally valid error-disturbance uncertainty relation in spin measurements. *Nature Phys.* 8, 185–189.
Feynman, R. P., and Hibbs, A. R. (1965). *Quantum Mechanics and Path Integrals*, McGraw-Hill, New York.
Feynman, R. P., Leighton, R. B., and Sands, M. (1965). *The Feynman Lectures on Physics*, Vol. III, Addison-Wesley, MA.
Haken, H. (1981). *Light*, North Holland, Amsterdam.
Heisenberg, W. (1927). Uber den anschaulichen inhalt der quantentheoretischen kinematic und mechanic. *Z. Phys.* 43, 172–198.
Lamb, W. E. (1995). Anti-photon. *Appl. Phys. B*. 60, 77–84.
Landau, L. D. and Lifshitz, E. M. (1976). *Quantum Mechanics*, Pergamon, New York.
Madrid, J., Giné, J., and Chemisana, D. (2020). Quantum fluctuations and the N-slit interference. *Int. J. Theor. Phys.* 60, 1–9.
Newton, I. (1687). *Principia Mathematica*, Royal Society, London, U.K.
Ozawa, M. (2004). Uncertainty relations for noise and disturbance in generalized quantum measurements. *Ann. Phys.* 311, 350–416.
Robertson, H. P. (1929). The uncertainty principle. *Phys. Rev.* 34, 163–164.
Robertson, J. K. (1955). *Introduction to Optics: Geometrical and Physical*, Van Nostrand, New York.
Uenishi, Y., Honna, K., and Nagaola, S. (1996). Tunable laser diode using a nickel micromachined external mirror. *Electron. Lett.* 32, 1207–1208.

4 The Dirac–Feynman Quantum Interferometric Principle

4.1 DIRAC'S NOTATION IN OPTICS

Dirac's notation is one of the mathematical avenues that can be used to describe nature quantum mechanically. This mathematical notation was invented, or discovered, by Dirac in 1939 and is particularly well suited to describe quantum optics. In this chapter, we introduce the basics of Dirac's notation and apply the notation to the generalized description of the fundamental phenomenon of interference that, as it will be seen, is crucial to quantum physics itself. This description is based on topics and elements of a review given by Duarte (2003).

In *The Principles of Quantum Mechanics*, first published in 1930, Dirac discusses the essence of interference as a one-photon phenomenon. Albeit his discussion is qualitative, it is also profound. In 1965, Feynman discussed electron interference via a double-slit thought experiment using probability amplitudes and Dirac's notation as a tool (Feynman et al., 1965). In 1987, inspired by Feynman's discussion, Dirac's notation was applied to the propagation of coherent light, or ensembles of indistinguishable photons, in an *N*-slit interferometer (Duarte and Paine, 1989, 1991, 1993).

The ideas of the notation invented by Dirac (1939) can be explained by considering the propagation of a photon from plane *s* to plane *d*, as illustrated in Figure 4.1.

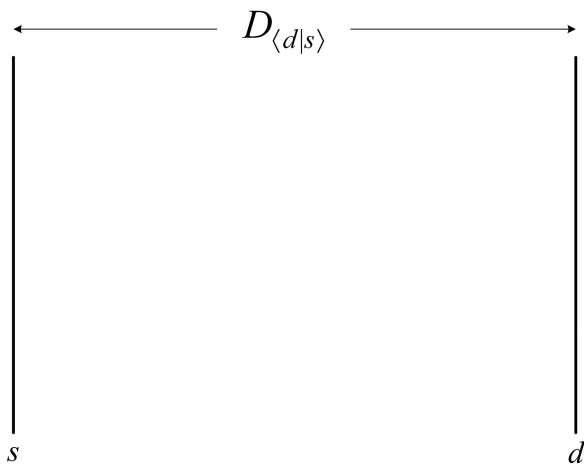

FIGURE 4.1 Propagation from *s* to the interferometric plane *d* is expressed as the probability amplitude $\langle d|s\rangle$. $D_{\langle d|s\rangle}$ is the physical distance between the two planes.

DOI: 10.1201/9781003398707-4

According to the Dirac's concept, there is a probability amplitude, denoted by $\langle d|s\rangle$, that quantifies such propagation. Historically, Dirac introduced the nomenclature of *ket vectors*, denoted by $|\ \rangle$, and *bra vectors*, denoted by $\langle\ |$, which are mirror images of each other. Thus, the probability amplitude is described by the *braket* $\langle d|s\rangle$, which is a *complex number.*

In Dirac's notation, the propagation from s to d is expressed in reverse order by $\langle d|s\rangle$. In other words, the *starting* position is at the *right* and the *final* position is at the *left*. If the propagation of the photon is not directly from plane s to plane d, but it involves the passage through an intermediate plane j, as illustrated in Figure 4.2, then the probability amplitude describing such propagation becomes

$$\langle d|s\rangle = \langle d|j\rangle\langle j|s\rangle \tag{4.1}$$

If the photon from s must also propagate through planes j and k in its trajectory to d, that is $s \to j \to k \to d$, as illustrated in Figure 4.3, then the probability amplitude is given by

$$\langle d|s\rangle = \langle d|k\rangle\langle k|j\rangle\langle j|s\rangle \tag{4.2}$$

If an additional intermediate plane l is added, so that the propagation, from plane to plane proceeds as $s \to j \to k \to l \to d$, then the probability amplitude is given by

$$\langle d|s\rangle = \langle d|l\rangle\langle l|k\rangle\langle k|j\rangle\langle j|s\rangle \tag{4.3}$$

When at the intermediate plane, in Figure 4.2, a number of N alternatives are available to the passage of the photon, as depicted in Figure 4.4, then the overall probability amplitude must consider *every possible alternative*, which is expressed mathematically by a summation over j in the form of

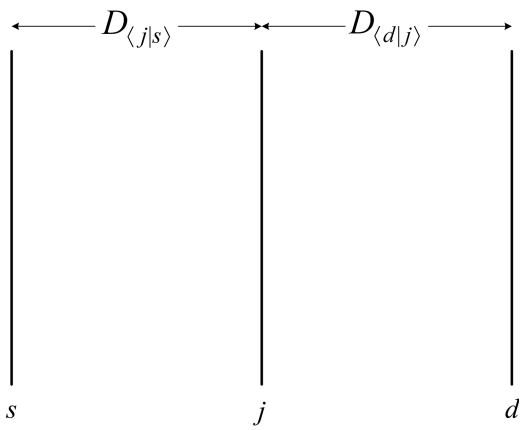

FIGURE 4.2 Propagation from s to the interferometric plane d via an intermediate plane j is expressed as the probability amplitude $\langle d|s\rangle = \langle d|j\rangle\langle j|s\rangle$. $D_{\langle j|s\rangle}$ and $D_{\langle d|j\rangle}$ are the distances between the designated planes.

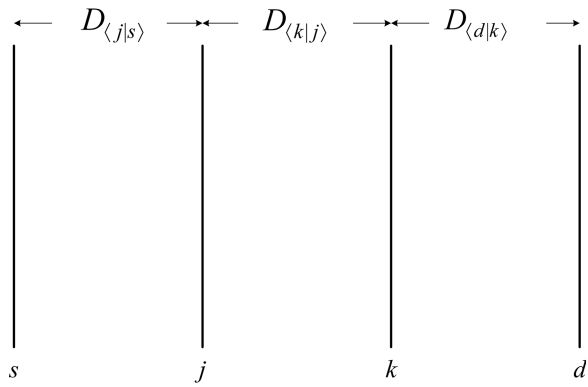

FIGURE 4.3 Propagation from s to the interferometric plane d via two intermediate planes j and k is expressed as the probability amplitude $\langle d|s\rangle = \langle d|k\rangle\ \langle k|j\rangle\ \langle j|s\rangle$. $D_{\langle j|s\rangle}$, $D_{\langle k|j\rangle}$, and $D_{\langle d|k\rangle}$ are the distances between the designated planes.

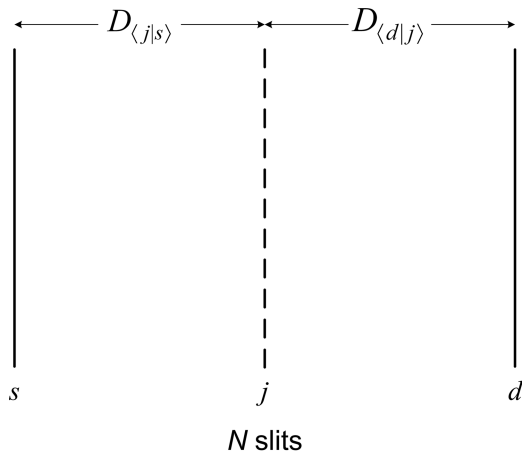

FIGURE 4.4 Propagation from s to the interferometric plane d via an array of N slits positioned at the intermediate plane j. $D_{\langle d|j\rangle}$ is the distance between the N-slit array and the d plane.

$$\langle d|s\rangle = \sum_{j=1}^{N} \langle d|j\rangle\langle j|s\rangle \tag{4.4}$$

Consideration of *every possible alternative* N in the computation of probability amplitude, as described in Equation (4.4), is an essential and crucial quantum feature.

For the case of an additional intermediate plane with N alternatives, as illustrated in Figure 4.5, the probability amplitude is written as

$$\langle d|s\rangle = \sum_{k=1}^{N}\sum_{j=1}^{N} \langle d|k\rangle\langle k|j\rangle\langle j|s\rangle \tag{4.5}$$

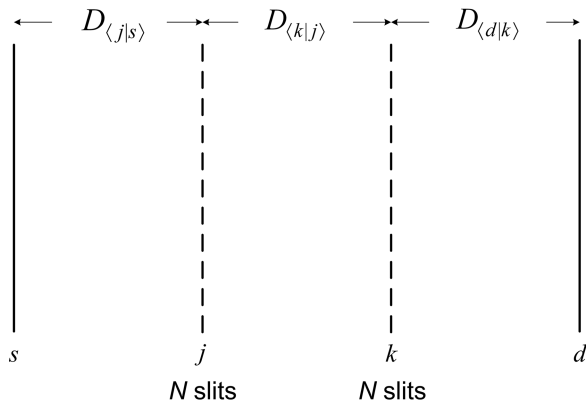

FIGURE 4.5 Propagation from s to the interferometric plane d via an array of N slits positioned at the intermediate plane j and via an additional array of N slits positioned at k. $D_{\langle k|j\rangle}$ is the distance between the N-slit arrays.

Moreover, for the case including three intermediate N-slit arrays, the probability amplitude becomes

$$\langle d|s\rangle = \sum_{l=1}^{N}\sum_{k=1}^{N}\sum_{j=1}^{N}\langle d|l\rangle\langle l|k\rangle\langle k|j\rangle\langle j|s\rangle \tag{4.6}$$

The addition of further intermediate planes, with N alternatives, can then be systematically incorporated into the notation. The Dirac notation albeit originally applied to the propagation of single particles (Dirac, 1958; Feynman et al., 1965) also applies to describe the propagation of ensembles of coherent, or indistinguishable, photons (Duarte, 1991, 1993, 2004).

4.2 THE DIRAC–FEYNMAN INTERFEROMETRIC PRINCIPLE

Any state, such as $|\psi\rangle$, can be described in terms of a set, or superposition, of *base states* (Dirac, 1958; Feynman et al., 1965). The amplitude to transition from any state to another state is written as a sum of products, such as

$$\langle d|s\rangle = \sum_{i=1}^{N}\langle d|i\rangle\langle i|s\rangle \tag{4.7}$$

This is inherently well suited to describe N-slit interferometry as already described in the previous section. Later, in Chapter 15, it will be shown that this fundamental interferometric principle is also the basis to derive the superposition probability amplitude for quantum entanglement (Duarte 2013, 2022).

The Dirac–Feynman interferometric principle applies to either single-photon illumination or to illumination via an ensemble of indistinguishable photons as available

from narrow-linewidth tunable lasers (Duarte, 1993). In this regard, 'All the indistinguishable photons illuminate the array of *N* slits, or grating, simultaneously. If only one photon propagates, at any given time, then that individual photon illuminates the whole array of *N* slits simultaneously' (Duarte, 2003).

The base states are orthogonal.

$$\langle i|j\rangle = \delta_{ij} \tag{4.8}$$

Furthermore, the amplitude to get from one state to another directly is the complex conjugate of the reverse

$$\langle d|s\rangle^{*} = \langle s|d\rangle \tag{4.9}$$

Albeit implicitly intuitive, it should be made explicit that a probability amplitude of the form $\langle d|s\rangle$ inherently incorporates the concepts of *space* and *time* in it since the photon propagates in space from *s* to *d* at the speed of light *c*.

As a matter of formality, it should be mentioned that the space of *bra ket* vectors, when the vectors are restricted to a finite length and finite scalar products, is called a *Hilbert space* (Dirac, 1958). However, Dirac himself points out that *bra ket* vectors form a more general space than a Hilbert space. (Note: a Hilbert space is a generalized Euclidean space.)

4.3 INTERFERENCE AND THE INTERFEROMETRIC PROBABILITY EQUATION

Dirac's notation offers a natural avenue to describe the propagation of quanta from a source to a detection plane, via a pair of slits. This was done by Feynman in a thought experiment using electrons and two slits. The Feynman approach was extended to the description of indistinguishable *photon propagation* from a source *s* to an interferometric plane *d*, via a transmission grating *j* comprised of *N* slits, as illustrated in Figure 4.6, by Duarte (1989, 1991).

In the interferometric architecture of Figure 4.6, an expanded laser beam, from a single-transverse-mode, narrow-linewidth laser, becomes the radiation source (*s*) and illuminates an array of *N* slits, or transmission grating (*j*). The interaction of the coherent radiation with the *N*-slit array (*j*) produces an interference signal at *d*. A crucial point here is that 'all the indistinguishable photons illuminate the array of *N* slits, or grating, simultaneously. If only one photon propagates, at any given time, then that individual photon illuminates the whole array of *N* slits simultaneously' (Duarte, 2003).

The probability amplitude that describes the propagation from the source (*s*) to the detection plane (*d*), via the array of *N* slits (*j*), is given by (Duarte, 1991, 1993)

$$\langle d|s\rangle = \sum_{j=1}^{N} \langle d|j\rangle\langle j|s\rangle$$

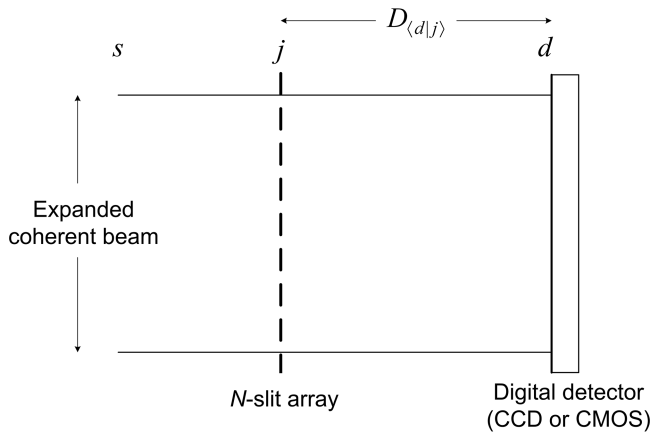

FIGURE 4.6 *N*-slit laser interferometer: a near-Gaussian beam from a single-transverse-mode (TEM_{00}), narrow-linewidth laser is pre-expanded in a two-dimensional telescope and then expanded in one dimension (parallel to the plane of incidence) by a multiple-prism beam expander (Duarte, 1987). This expanded beam can be further transformed into a nearly uniform illumination source (*s*) (Duarte, 2003). Then, uniform light source (*s*) illuminates an array of *N* slits at *j*. Interaction of the coherent emission with the slit array produces interference at the interferometric plane *d* (Duarte, 1993).

According to Dirac (1958), the probability amplitudes can be represented by *wave functions of ordinary wave optics*. Thus, following Feynman et al. (1965)

$$\langle j|s\rangle = \Psi(r_{j,s})e^{-i\theta_j} \tag{4.10}$$

$$\langle d|j\rangle = \Psi(r_{x,j})e^{-i\phi_j} \tag{4.11}$$

where θ_j and ϕ_j are the phase terms associated with the incidence and diffraction waves, respectively. Using Equations (4.10) and (4.11), for the probability amplitudes, the propagation probability amplitude

$$\langle d|s\rangle = \sum_{j=1}^{N} \langle d|j\rangle\langle j|s\rangle$$

can be written as

$$\langle d|s\rangle = \sum_{j=1}^{N} \Psi(r_j)e^{-i\Omega_j} \tag{4.12}$$

where

$$\Psi(r_j) = \Psi(r_{x,j})\Psi(r_{j,s}) \tag{4.13}$$

and

$$\Omega_j = (\theta_j + \phi_j) \tag{4.14}$$

Next, the propagation probability is obtained by expanding Equation (4.12) and multiplying the expansion by its complex conjugate (Born, 1926)

$$\left|\langle d|s\rangle\right|^2 = \langle d|s\rangle\langle d|s\rangle^* \tag{4.15}$$

Expansion of the probability amplitude and multiplication with its complex conjugate, following some algebra, leads to

$$\langle d|s\rangle\langle d|s\rangle^* = \sum_{j=1}^{N}\Psi(r_j)\sum_{m=1}^{N}\Psi(r_m)e^{i(\Omega_m-\Omega_j)} \tag{4.16}$$

Expanding Equation (4.16) and using the identity

$$2\cos(\Omega_m - \Omega_j) = e^{-i(\Omega_m-\Omega_j)} + e^{i(\Omega_m-\Omega_j)} \tag{4.17}$$

lead to the explicit form of the generalized propagation probability in one dimension (Duarte and Paine, 1989; Duarte, 1991)

$$\left|\langle d|s\rangle\right|^2 = \sum_{j=1}^{N}\Psi(r_j)^2 + 2\sum_{j=1}^{N}\Psi(r_j)\left(\sum_{m=j+1}^{N}\Psi(r_m)\cos(\Omega_m-\Omega_j)\right) \tag{4.18}$$

This equation is the one-dimensional generalized interferometric equation. The reader should keep in mind that it is completely equivalent to Equation (4.16).

4.3.1 Examples: Double-, Triple-, Quadruple-, and Quintuple-Slit Interference

Expanding Equation (4.16) for two slits ($N = 2$), as applicable to double-slit interference, we get

$$\left|\langle d|s\rangle\right|^2 = \Psi(r_1)\left(\Psi(r_1)e^{i(\Omega_1-\Omega_1)} + \Psi(r_2)e^{i(\Omega_2-\Omega_1)}\right) + \Psi(r_2)\left(\Psi(r_1)e^{i(\Omega_1-\Omega_2)} + \Psi(r_2)e^{i(\Omega_2-\Omega_2)}\right)$$

$$\left|\langle d|s\rangle\right|^2 = \Psi(r_1)\left(\Psi(r_1) + \Psi(r_2)e^{i(\Omega_2-\Omega_1)}\right) + \Psi(r_2)\left(\Psi(r_1)e^{i(\Omega_1-\Omega_2)} + \Psi(r_2)\right)$$

$$\left|\langle d|s\rangle\right|^2 = \Psi(r_1)^2 + \Psi(r_2)^2 + \left(\Psi(r_1)\Psi(r_2)e^{i(\Omega_2-\Omega_1)} + \Psi(r_1)\Psi(r_2)e^{i(\Omega_1-\Omega_2)}\right)$$

$$\left|\langle d|s\rangle\right|^2 = \Psi(r_1)^2 + \Psi(r_2)^2 + \left(\Psi(r_1)\Psi(r_2)e^{i(\Omega_2-\Omega_1)} + \Psi(r_1)\Psi(r_2)e^{-i(\Omega_2-\Omega_1)}\right)$$

$$\left|\langle d|s\rangle\right|^2 = \Psi(r_1)^2 + \Psi(r_2)^2 + 2\Psi(r_1)\Psi(r_2)\cos(\Omega_2 - \Omega_1) \tag{4.19}$$

Expanding Equation (4.18) for three slits ($N = 3$), applicable to triple slit interference, we get

$$\begin{aligned}\left|\langle d|s\rangle\right|^2 = {} & \Psi(r_1)^2 + \Psi(r_2)^2 + \Psi(r_3)^2 + 2\big(\Psi(r_1)\Psi(r_2)\cos(\Omega_2 - \Omega_1) \\ & + \Psi(r_1)\Psi(r_3)\cos(\Omega_3 - \Omega_1) + \Psi(r_2)\Psi(r_3)\cos(\Omega_3 - \Omega_2)\big)\end{aligned} \tag{4.20}$$

Expanding Equation (4.18) for four slits ($N = 4$), applicable to quadruple slit interference, we get

$$\begin{aligned}\left|\langle d|s\rangle\right|^2 = {} & \Psi(r_1)^2 + \Psi(r_2)^2 + \Psi(r_3)^2 + \Psi(r_4)^2 + 2\big(\Psi(r_1)\Psi(r_2)\cos(\Omega_2 - \Omega_1) \\ & + \Psi(r_1)\Psi(r_3)\cos(\Omega_3 - \Omega_1) + \Psi(r_1)\Psi(r_4)\cos(\Omega_4 - \Omega_1) \\ & + \Psi(r_2)\Psi(r_3)\cos(\Omega_3 - \Omega_2) + \Psi(r_2)\Psi(r_4)\cos(\Omega_4 - \Omega_2) \\ & + \Psi(r_3)\Psi(r_4)\cos(\Omega_4 - \Omega_3)\big)\end{aligned} \tag{4.21}$$

Expanding Equation (4.18) for five slits ($N = 5$), applicable to quintuple-slit interference, we get

$$\begin{aligned}\left|\langle d|s\rangle\right|^2 = {} & \Psi(r_1)^2 + \Psi(r_2)^2 + \Psi(r_3)^2 + \Psi(r_4)^2 + \Psi(r_5)^2 \\ & + 2\big(\Psi(r_1)\Psi(r_2)\cos(\Omega_2 - \Omega_1) + \Psi(r_1)\Psi(r_3)\cos(\Omega_3 - \Omega_1) + \Psi(r_1)\Psi(r_4)\cos(\Omega_4 - \Omega_1) \\ & + \Psi(r_1)\Psi(r_5)\cos(\Omega_5 - \Omega_1) + \Psi(r_2)\Psi(r_3)\cos(\Omega_3 - \Omega_2) + \Psi(r_2)\Psi(r_4)\cos(\Omega_4 - \Omega_2) \\ & + \Psi(r_2)\Psi(r_5)\cos(\Omega_5 - \Omega_2) + \Psi(r_3)\Psi(r_4)\cos(\Omega_4 - \Omega_3) + \Psi(r_3)\Psi(r_5)\cos(\Omega_5 - \Omega_3) \\ & + \Psi(r_4)\Psi(r_5)\cos(\Omega_5 - \Omega_4)\big)\end{aligned} \tag{4.22}$$

and so on. Besides the explicit interferometric expressions for $N = 2$, $N = 3$, $N = 4$, and $N = 5$, Equation (4.18) can be programmed to include sextuple ($N = 6$), septuple ($N = 7$), octuple ($N = 8$), nonuple ($N = 9$), or any number of slits and in practice, it has been used to do calculations, and comparisons with measurements, in the $2 \le N \le 2000$ range (Duarte, 1993, 2009).

4.3.2 Geometry of the *N*-Slit Quantum Interferometer

The relevant geometry, and geometrical parameters, at the transmission grating (j) and the plane of interference (d) is illustrated in Figures 4.6–4.8. According to the

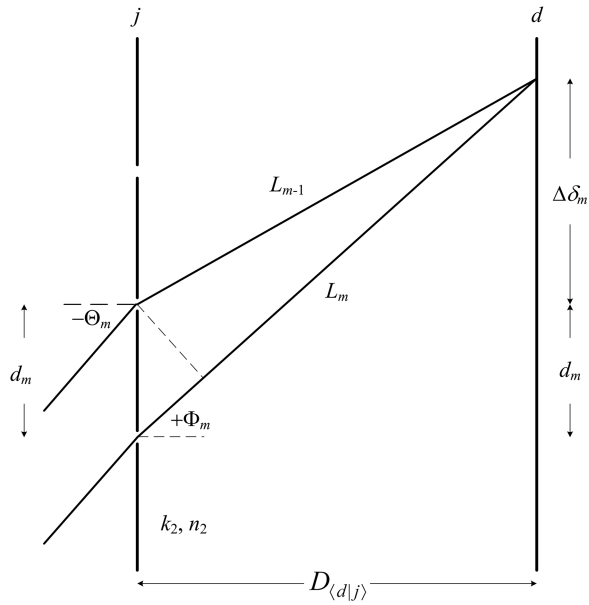

FIGURE 4.7 The *N*-slit array, or transmission grating, plane (*j*) and the interferometric plane (*d*) (not to scale) illustrating the path difference and the various parameters involved in the exact description of the geometry.

geometry, the phase difference term in Equations (4.16) and (4.18) can be expressed as (Duarte, 1997)

$$\cos\Big((\theta_m - \theta_j) \pm (\phi_m - \phi_j)\Big) = \cos\Big(|l_m - l_{m-1}|k_1 \pm |L_m - L_{m-1}|k_2\Big) \tag{4.23}$$

where

$$k_1 = \frac{2\pi n_1}{\lambda_v} \tag{4.24}$$

and

$$k_2 = \frac{2\pi n_2}{\lambda_v} \tag{4.25}$$

are the wavenumbers of the two optical regions are defined in Figure 4.8. Here, $\lambda_1 = \lambda_v/n_1$ and $\lambda_2 = \lambda_v/n_2$ where λ_v is the vacuum wavelength, while n_1 and n_2 are the corresponding indexes of refraction (Wallenstein and Hänsch, 1974; Born and Wolf, 1999). The phase differences are expressed via direct geometrical equations of the form (Duarte, 1993)

$$|L_m - L_{m-1}| = \frac{d_m(\Delta\delta_m + d_m)}{|L_m|} \tag{4.26}$$

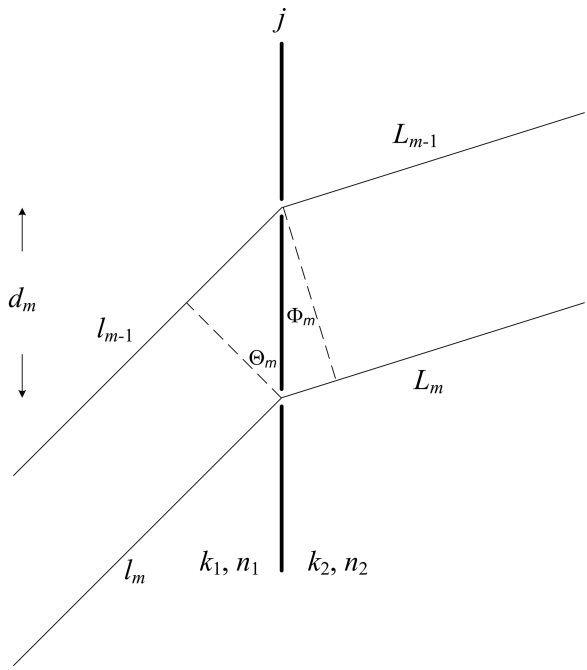

FIGURE 4.8 Close-up of the *N*-slit array, or transmission grating, plane (j) illustrating the path length difference and the angles of incidence (Θ_m) and diffraction (Φ_m) for the condition $D_{\langle d|j\rangle} >> d_m$ (Reproduced from Duarte, F. J., *Am. J. Phys.* **65**, 637-640, 1997, with permission of the American Association of Physics Teachers).

$$L_m^2 = D_{\langle d|j\rangle}^2 + (\Delta\delta_m + d_m) \tag{4.27}$$

$$L_{m-1}^2 = D_{\langle d|j\rangle}^2 + \Delta\delta_m^2 \tag{4.28}$$

In this notation, $\Delta\delta_m$ is the lateral displacement on the d plane, and $D_{\langle d|j\rangle}$ is the intra-interferometric distance from the j plane to the d plane. Accurate representation of the geometry is important when writing software to generate numerical interferograms based on Equation (4.18). The geometry is discussed further in Appendix E.

4.3.3 The Diffraction Grating Equation

In the phase term equation

$$\cos\left((\theta_m - \theta_j) \pm (\phi_m - \phi_j)\right) = \cos\left(|l_m - l_{m-1}|k_1 \pm |L_m - L_{m-1}|k_2\right)$$

the corresponding path differences are $|l_m - l_{m-1}|$ and $|L_m - L_{m-1}|$. Since *maxima* occur at

$$\left(|l_m - l_{m-1}|n_1 \pm |L_m - L_{m-1}|n_2\right)\frac{2\pi}{\lambda_v} = M\pi \tag{4.29}$$

where $M = 0,\ \pm 2,\ \pm 4,\ \pm 6...$, it can be shown that

$$d_m\left(n_1 \sin\Theta_m \pm n_2 \sin\Phi_m\right)\frac{2\pi}{\lambda_v} = M\pi \tag{4.30}$$

which, for $n_1 = n_2 = 1$ and $\lambda = \lambda_v$, reduces to

$$d_m(\sin\Theta_m \pm \sin\Phi_m)k = M\pi \tag{4.31}$$

that can be expressed as the well-known grating equation

$$d_m(\sin\Theta_m \pm \sin\Phi_m) = m\lambda \tag{4.32}$$

where $m = 0,\ \pm 1,\ \pm 2,\ \pm 3...$ For a grating utilized in the reflection domain, in *Littrow configuration*, $\Theta_m = \Phi_m = \Theta$ so that the grating equation reduces to

$$2d\sin\Theta = m\lambda \tag{4.33}$$

These diffraction equations are reconsidered, in a more general form, with an extra sign alternative, in Chapter 5.

4.3.4 *N*-Slit Interferometer Experiment

The *N*-slit interferometer is illustrated in Figure 4.9. In practice, this interferometer can be configured with a variety of lasers including tunable lasers. However, one requirement is that the laser to be utilized must emit in the narrow-linewidth regime and in a single-transverse-mode (TEM_{00}) with a near-Gaussian profile. Ideally, the

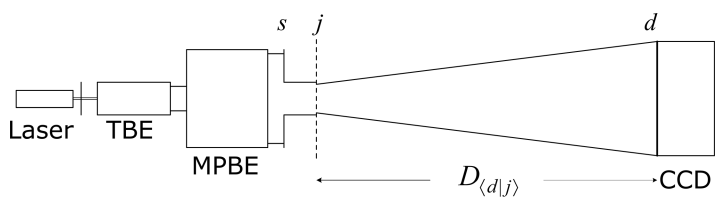

FIGURE 4.9 Top view schematics of the *N*-slit interferometer. A neutral density filter follows the TEM_{00} narrow-linewidth. The laser beam is then magnified in two dimensions by a telescope beam expander (TBE). The magnified beam is then expanded in one dimension by a multiple-prism beam expander (MPBE). A wide aperture then selects the central part of the expanded beam to illuminate the *N*-slit array (*j*). The interferogram then propagates via the intra-interferometric path $D_{\langle d|j\rangle}$ on its way toward the interference plane *d*. Detection of the interferogram at *d* can either be performed by a silver halide film or a digital array such as a CCD or CMOS detector.

source should be a single-longitudinal-mode laser. The reason for this requirement is that narrow-linewidth lasers yield sharp, well-defined interference patterns close to those predicted theoretically for a single wavelength.

One particular configuration of the *N*-slit laser interferometer (NSLI), described by Duarte (1993), utilizes a TEM_{00} He–Ne laser ($\lambda \approx 632.82$ nm) with a beam 0.5 mm in diameter, as the illumination source. This class of laser yields a smooth near-Gaussian beam profile and narrow-linewidth emission ($\Delta\nu \approx 1$ GHz). The laser beam is then magnified, in two dimensions, by a Galilean telescope. Following the telescopic expansion, the beam is further expanded, in one dimension, by a multiple-prism beam expander. This class of optical architecture can yield an expanded smooth near-Gaussian beam approximately 50 mm wide. An option is to insert a convex lens prior to the multiple-prism expander, thus producing an extremely elongated near-Gaussian beam (Duarte, 1987, 1993). The beam propagation through this system can be accurately characterized using ray transfer matrices as discussed in Duarte (2003). Also, as an option, at the exit of the multiple-prism beam expander an aperture, a few mm wide, can be deployed.

The beam profile thus produced can be neatly reproduced by the interferometric equation as illustrated later in this chapter. Thus, the source *s* can be either the exit prism of the multiple-prism beam expander or the wide aperture. For the results discussed in this chapter, on the detection side, the interference screen at *d* is a digital detector comprised of a photodiode array with individual pixels each 25 μm in width.

Now, we consider a series of cases that demonstrate the measurement capability of the NSLI and the ability of the generalized interferometric equation to either predict or reproduce the measurement. The first case considered is the well-known double-slit experiment also known as Young's interference experiment. For ($N = 2$) with slits 50 μm in width, separated by 50 μm, the elongated Gaussian beam provides a nearly plane illumination. That is also approximately the case even if a larger number of slits, of these dimensions, are illuminated. For the particular case of a two-slit experiment involving 50 μm slits separated by 50 μm and a grating to screen distance $D_{\langle d|j\rangle} = 10$ cm, the interference signal is displayed in Figure 4.10a. The calculated interference, using Equation (4.18), and assuming plane wave illumination is given in Figure 4.10b.

For an array of $N = 23$ slits, each 100 μm in width and separated by 100 μm, the measured and calculated interferograms are shown in Figure 4.11. Here the grating to digital detector distance is $D_{\langle d|j\rangle} = 1.5$ cm. This is a *near-field* result and corresponds entirely to the interferometric regime.

For an array of $N = 100$ slits, each 30 μm in width and separated by 30 μm, the measured and calculated interferograms are shown in Figure 4.12. Here the grating to digital detector distance is $D_{\langle d|j\rangle} = 75$ cm. In Figure 4.12, the ±1 diffraction orders are present.

In practice, the transmission gratings are not perfect and offer an uncertainty in the dimension of the slits. The uncertainty in the slit dimensions of the grating, incorporating the 30 μm slits, used in this experiments was measured to be $\leq 2\%$. The theoretical interferogram for the grating comprised of $N = 100$ slits, each 30.0 ± 0.6 μm wide and separated by 30.0 ± 0.6 μm, is given in Figure 4.13. Notice the symmetry deterioration.

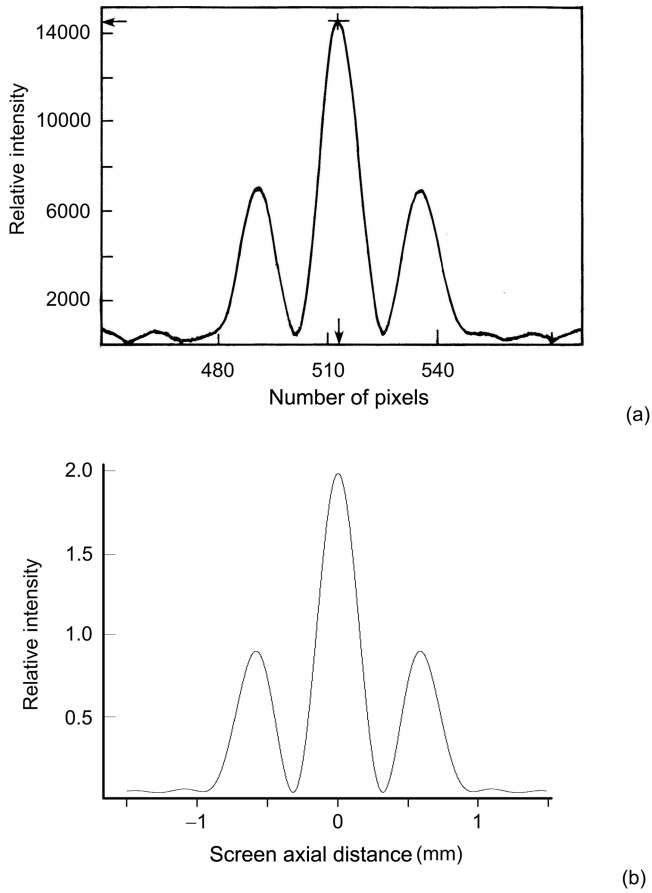

FIGURE 4.10 (a) Measured interferogram resulting from the interaction of coherent laser emission at $\lambda = 632.82$ nm and two slits ($N = 2$) 50 μm wide, separated by 50 μm. The j to d distance is $D_{\langle d|j\rangle} = 10$ cm. Each pixel is 25 μm wide. (b) Corresponding theoretical interferogram from Equation (4.18).

When a wide slit is used to select the central portion of the elongated Gaussian beam, the interaction of the coherent laser beam with the slit results in diffraction prior to the illumination of the transmission grating. The interferometric Equation (4.18) can be used to characterize this diffraction. This is done by dividing the wide slit in hundreds of smaller slits. As an example, a 4 mm wide aperture is divided into 800 slits, each 4 μm wide and separated by a 1 μm interslit distance (Duarte, 1993). The calculated near-field diffraction pattern, for a distance of $D_{\langle d|j\rangle} = 10$ cm, is shown in Figure 4.14.

Using this as the radiation source to illuminate the $N = 100$ slit grating, comprised of 30 μm slits with an interslit distance of 30 μm (for $D_{\langle d|j\rangle} = 75$ cm), yields the theoretical interferogram displayed in Figure 4.15. This is a *cascade interferometric*

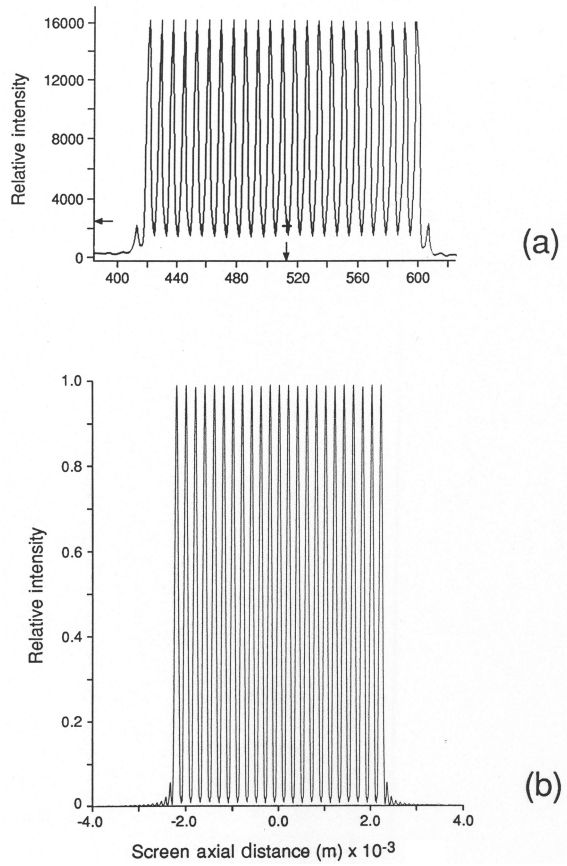

FIGURE 4.11 (a) Measured interferogram, in the near field, resulting from the interaction of coherent laser emission at $\lambda = 632.82$ nm and $N = 23$ slits, 100 μm wide, separated by 100 μm. Here, $D_{\langle d|j\rangle} = 1.5$cm. (b) Corresponding near-field theoretical interferogram from Equation (4.18) (Reproduced from Duarte, F. J., *Opt. Commun.* **103**, 8–14, 1993, with permission from Elsevier).

technique in which the interferometric distribution in one plane is used to illuminate an *N*-slit array in the immediately following plane and is applied further in Chapter 22.

4.4 COHERENT AND SEMI-COHERENT INTERFEROGRAMS

The interferometric equation

$$\left|\langle d|s\rangle\right|_{\lambda}^{2} = \sum_{j=1}^{N} \Psi(r_j)_{\lambda}^{2} + 2\sum_{j=1}^{N} \Psi(r_j)_{\lambda} \left(\sum_{m=j+1}^{N} \Psi(r_m)_{\lambda} \cos(\Omega_m - \Omega_j) \right) \tag{4.34}$$

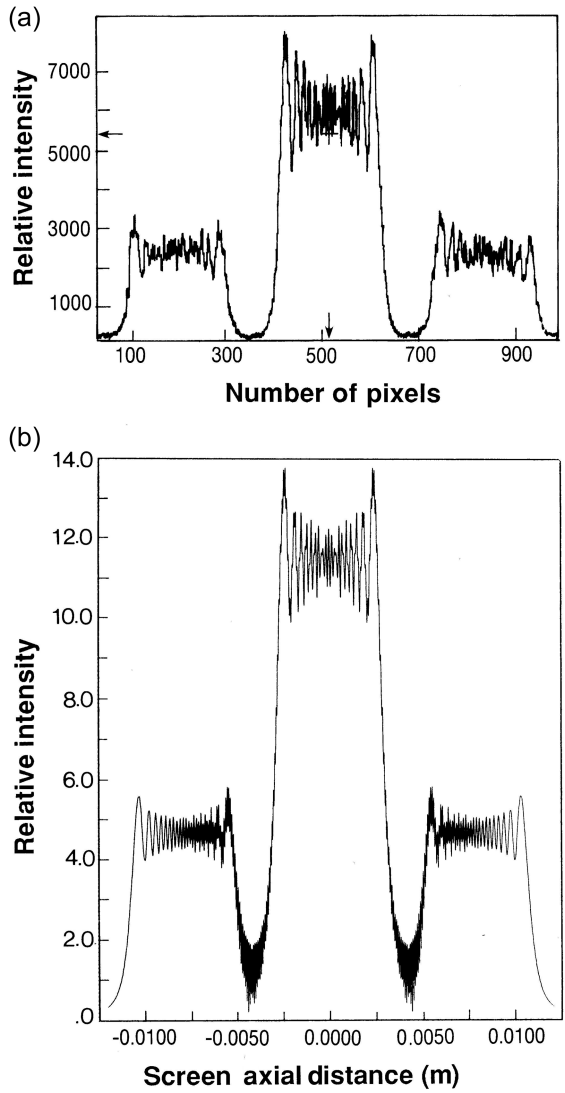

FIGURE 4.12 (a) Measured interferogram resulting from the interaction of coherent laser emission at $\lambda = 632.82$ nm and $N = 100$, slits 30 μm wide, separated by 30 μm. Here, $D_{\langle d|j\rangle} = 75$cm. (b) Corresponding theoretical interferogram from Equation (4.18) (Reproduced from Duarte, F. J., *Opt. Commun.* **103**, 8–14, 1993, with permission from Elsevier).

was originally derived to account for single-photon propagation only (Duarte, 1993, 2004). This is illustrated by adding a single-wavelength subscript to Equation (4.18), as made explicit now in Equation (4.33). Thus, this equation is intrinsically related to monochromatic and/or highly-coherent emission. In practice, it has also been found that it accounts for the propagation of ensembles of indistinguishable photons or

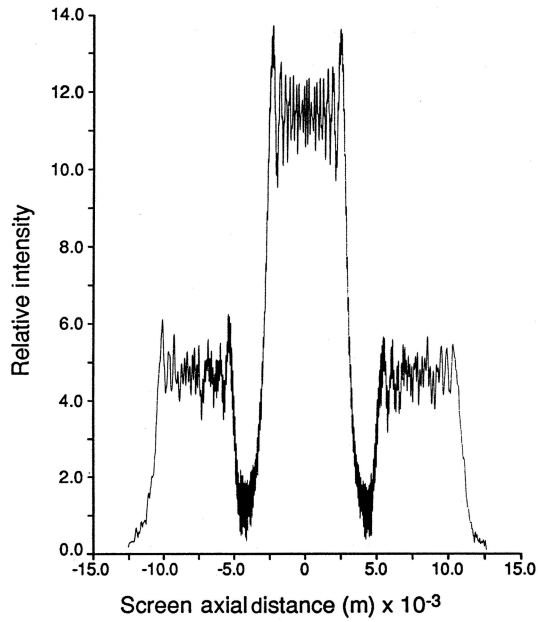

FIGURE 4.13 Theoretical interferometric/diffraction distribution using a $\leq 2\%$ uncertainty in the dimensions of the 30 μm slits. In this calculation $N = 100$ and $D_{\langle d|j\rangle} = 75$cm. A deterioration in the spatial symmetry of the distribution is evident (Reproduced from Duarte, F. J., *Opt. Commun.* **103**, 8–14, 1993, with permission from Elsevier).

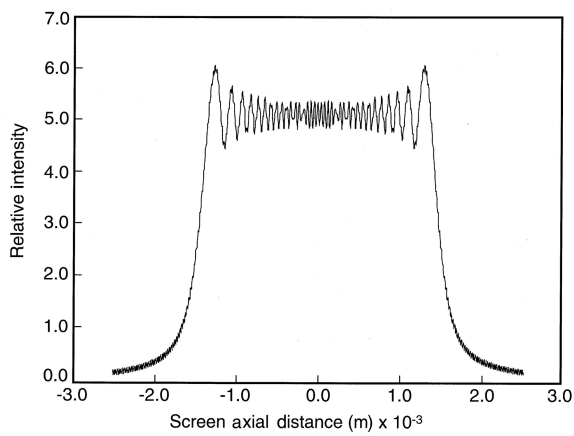

FIGURE 4.14 Theoretical near-field diffraction distribution produced by a 4 mm aperture illuminated at $\lambda = 632.82$ nm, and $D_{\langle d|j\rangle} = 10$ cm (Reproduced from Duarte, F. J., *Opt. Commun.* **103**, 8–14, 1993, with permission from Elsevier).

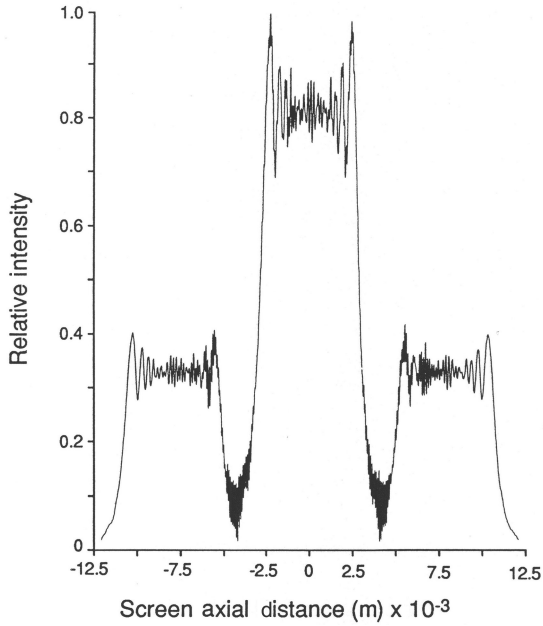

FIGURE 4.15 Theoretical interferometric distribution incorporating diffraction-edge effects in the illumination. In this calculation, the width of the slits in the array is 30 μm, separated by 30 μm, $N = 100$ and $D_{\langle d|j\rangle} = 75$ cm. The aperture-grating distance is 10 cm (Reproduced from Duarte, F. J., *Opt. Commun.* **103**, 8–14, 1993, with permission from Elsevier).

narrow-linewidth emission as available from narrow-linewidth laser sources (Duarte, 1993, 2003). The question then arises on the applicability of Equation (4.34) to the case of semi-coherent, partially-coherent, or broadband emission.

Equation (4.34) provides an interferogram for a single wavelength and in practice for an ensemble of indistinguishable photons. These interferograms are narrow, spatially sharp, and well defined. For broadband emission, or semi-coherent emission, the sharpness of the interferogram diminishes and the interferometric pattern becomes broad and less defined. This is how this occurs: each wavelength has a unique interferometric signature defined by Equation (4.34). A detector registers that signature. If the emission is broadband or semi-coherent, a multitude of different interferograms are generated and the detector (either digital or a photographic plaque) provides an integrated picture of a composite interferogram produced by the array of wavelengths involved in the emission.

Thus, for broadband emission, Equation (4.34) is modified to include a sum over the wavelength range involved, so that

$$\sum_{\lambda=\lambda_1}^{\lambda_n} \left|\langle d|s\rangle\right|_{\lambda}^{2} = \sum_{\lambda=\lambda_1}^{\lambda_n} \left(\sum_{j=1}^{N} \Psi(r_j)_{\lambda}^{2} + 2 \sum_{j=1}^{N} \Psi(r_j)_{\lambda} \left(\sum_{m=j+1}^{N} \Psi(r_m)_{\lambda} \cos(\Omega_m - \Omega_j) \right) \right) \quad (4.35)$$

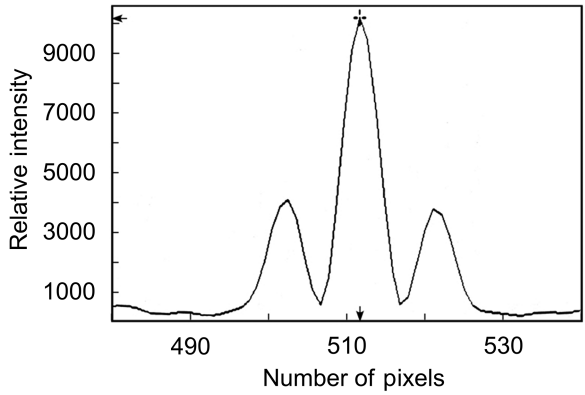

FIGURE 4.16 Measured double-slit interferogram generated with He–Ne laser emission from the $3s_2 - 2p_{10}$ transition at $\lambda \approx 543.3$nm. Here, $N = 2$ for a slit width of 50 μm. The intra-interferometric distance is $D_{\langle d|j\rangle} = 10$ cm (Reproduced from Duarte, F. J., *Opt. Lett.* **32**, 412–414, 2007, with permission from Optica).

The concept just described has been previously outlined by Duarte (2007, 2008) and is further illustrated next. In Figure 4.16, the double-slit interferogram produced with narrow-linewidth emission from the $3s_2 - 2p_{10}$ transition of a He–Ne laser, at $\lambda \approx 543.3$ nm, is displayed. The visibility of this interferogram is calculated using (Michelson, 1927)

$$\mathcal{V} = \frac{I_1 - I_2}{I_1 + I_2} \tag{4.36}$$

to be $\mathcal{V} \approx 0.95$. In Figure 4.17, the double-slit interferogram produced, under identical geometrical conditions, but with the emission from an electrically excited coherent

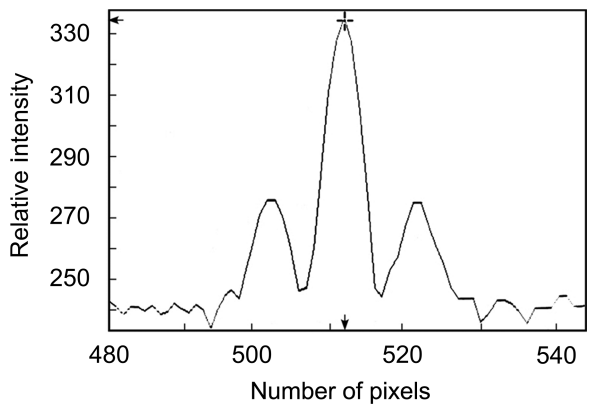

FIGURE 4.17 Measured double-slit interferogram generated with emission from an organic semiconductor interferometric emitter at $\lambda \approx 540$ nm. Here, $N = 2$ for a slit width of 50 μm. The intra-interferometric distance is $D_{\langle d|j\rangle} = 10$ cm (Reproduced from Duarte, F. J., *Opt. Lett.* **32**, 412–414, 2007, with permission from Optica).

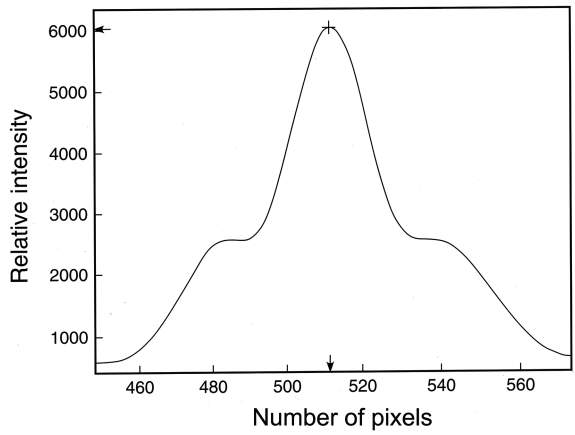

FIGURE 4.18 Measured double-slit interferometer generated via a broadband visible source. Here, $N = 2$ for a slit width of 50 μm. The intra-interferometric distance is $D_{\langle d|j\rangle} = 10$ cm (Reproduced from Duarte, F. J., *Tunable Laser Optics*, 2nd ed. CRC, Boca Raton, 2015).

organic semiconductor interferometric emitter, at $\lambda \approx 540$ nm, is displayed. Here the visibility is slightly lower – $\mathcal{V} \approx 0.90$.

A double-slit interferogram produced, under identical geometrical conditions, but with the emission from a broadband source, centered around $\lambda \approx 540$ nm, is depicted in Figure 4.18. The corresponding visibility is $\mathcal{V} \approx 0.44$. A survey of measured double-slit interferograms visibilities from relevant semi-coherent, or partially-coherent, sources reveals a visibility range of $0.4 \leq \mathcal{V} \leq 0.65$. On the other hand, the visibility range for double-slit interferograms originating from various laser sources is $0.85 \leq \mathcal{V} \leq 0.99$ (Duarte, 2008).

4.5 THE INTERFEROMETRIC PROBABILITY EQUATION IN TWO AND THREE DIMENSIONS

The two-dimensional interferometric case can be described considering a diffractive grid, or two-dimensional *N*-slit array, as depicted in Figure 4.19. Photon propagation takes place from *s* to the interferometric plane *d* via a two-dimensional transmission grating j_{xy}, that is, *j* is replaced by a grid comprised of *j* components in the *y* direction and *j* components in the *x* direction. Note that in the one-dimensional case, only the *y* component of *j* is present which is written simply as *j*. The plane configured by the j_{xy} grid is orthogonal to the plane of propagation. Hence, for photon propagation from *s* to *d*, via j_{xy}, the probability amplitude is given by (Duarte, 1995)

$$\langle d|s\rangle = \sum_{j_x=1}^{N} \sum_{j_y=1}^{N} \langle d|j_{xy}\rangle \langle j_{xy}|s\rangle \tag{4.37}$$

Now, if the *j* is abstracted from j_{xy}, then Equation (4.37) can be expressed as

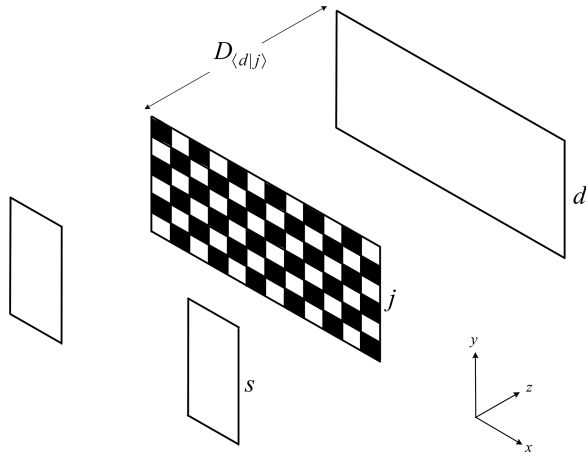

FIGURE 4.19 Two-dimensional depiction of the interferometric system $\langle d|j\rangle\langle j|s\rangle$ (Adapted from Duarte, F. J., Interferometric imaging, In: *Tunable Laser Applications*, Duarte, F. J. (ed.), Marcel Dekker, New York, 1995).

$$\langle d|s\rangle = \sum_{x=1}^{N}\sum_{y=1}^{N}\Psi(r_{xy})e^{-i\Omega_{xy}} \tag{4.38}$$

and the corresponding probability is given by (Duarte, 1995)

$$\left|\langle d|s\rangle\right|^2 = \sum_{x=1}^{N}\sum_{y=1}^{N}\Psi(r_{xy})\sum_{q=1}^{N}\sum_{p=1}^{N}\Psi(r_{pq})e^{i(\Omega_{qp}-\Omega_{xy})} \tag{4.39}$$

For a three-dimensional transmission grating, it can be shown that

$$\left|\langle d|s\rangle\right|^2 = \sum_{x=1}^{N}\sum_{y=1}^{N}\sum_{z=1}^{N}\Psi(r_{xyz})\sum_{q=1}^{N}\sum_{p=1}^{N}\sum_{r=1}^{N}\Psi(r_{qpr})e^{i(\Omega_{qpr}-\Omega_{xyz})} \tag{4.40}$$

These equations apply either to the propagation of single photons or to the propagation of ensembles of *coherent*, *indistinguishable*, or *monochromatic* photons.

For broadband emission, as described in the previous section, an interferometric summation over the emission spectrum is necessary.

The application of quantum principles to the description of propagation of a large number of monochromatic, or indistinguishable, photons was already advanced by Dirac in his discussion of interference (Dirac, 1958; Duarte, 1998).

4.6 CLASSICAL AND QUANTUM ALTERNATIVES

Increasingly, the field of optics has seen a transition from a classical to a quantum description. Some phenomena are purely quantum and cannot be described classically.

Other phenomena, such as polarization and interference, can be described either classically or quantum mechanically. In the case of interference, and diffraction, the beauty is that the quantum mechanical description also applies to the description of ensembles of indistinguishable photons. Moreover, when we describe interference and diffraction using quantum mechanical tools, all we are doing is following the steps of giants such as Dirac (1958) and Feynman (Feynman and Hibbs, 1965).

As we shall see in Chapter 5, there is another powerful reason to describe interference quantum mechanically: this description provides a unified avenue to the whole of optics in a succinct hierarchy that goes

INTERFERENCE → DIFFRACTION → REFRACTION → REFLECTION

(Duarte, 1997). By contrast, the situation from a traditional classical perspective is rather disjointed as can be observed by perusing any good book on classical optics. There, the description goes like reflection, refraction, diffraction, and interference in a non-cohesive manner. Classically, there is no mathematical coherence in the description.

Furthermore, in our quantum description, a single equation is used to describe interference, and interference–diffraction phenomena, in the near and the far field in a unified manner (Duarte, 1993, 1997).

PROBLEMS

4.1 Show that substitution of Equations (4.10) and (4.11) into Equation (4.9) leads to Equation (4.11).

4.2 Show that Equation (4.16) can be expressed as Equation (4.18).

4.3 From the geometry of Figure 4.7 derive Equations (4.26) to (4.28).

4.4 Write an equation for $\left|\langle d|s\rangle\right|^2$ in the case relevant to $N = 3$ staring from Equation (4.16).

4.5 Write an equation for $\left|\langle d|s\rangle\right|^2$ in the probability amplitude given in Equation (4.5).

REFERENCES

Born, M. (1926). Zur quantenmechanik der stoßvorgänge. *Z. Phys.* 37, 863–827.

Born, M., and Wolf, E. (1999). *Principles of Optics*, 7th ed. Cambridge University, Cambridge, U.K.

Dirac, P. A. M. (1939). A new notation for quantum mechanics. *Math. Proc. Cam. Phil. Soc.* 35, 416–418.

Dirac, P. A. M. (1958). *The Principles of Quantum Mechanics*, 4th ed. Oxford University, Oxford, U.K.

Duarte, F. J. (1987). Beam shaping with telescopes and multiple-prism beam expanders. *J. Opt. Soc. Am. A*. 4, P30.

Duarte, F. J. (1991). Dispersive dye lasers. In *High Power Dye Lasers* (Duarte, F. J., ed.). Springer-Verlag, Berlin, Chapter 2, pp. 7–43.

Duarte, F. J. (1993). On a generalized interference equation and interferometric measurements. *Opt. Commun.* 103, 8–14.

Duarte, F. J. (1995). Interferometric imaging. In *Tunable Laser Applications* (Duarte, F. J., ed.). Marcel Dekker, New York, Chapter 5, pp. 153–178.
Duarte, F. J. (1997). Interference, diffraction, and refraction, via Dirac's notation. *Am. J. Phys.* 65, 637–640.
Duarte, F. J. (1998). Interference of two independent sources. *Am. J. Phys*. **66**, 662–663.
Duarte, F. J. (2003). *Tunable Laser Optics*, 1st ed. Elsevier-Academic, New York.
Duarte, F. J. (2004). Comment on 'reflection, refraction and multislit interference'. *Eur. J. Phys.* 25, L57–L58.
Duarte, F. J. (2007). Coherent electrically-excited organic semiconductors: visibility of interferograms and emission linewidth, *Opt. Lett.* 32, 412–414.
Duarte, F. J. (2008). Coherent electrically excited organic semiconductors: coherent or laser emission? *Appl. Phys.* B 90, 101–108.
Duarte, F. J. (2009). Interferometric imaging. In *Tunable Laser Applications*, 2nd ed. (Duarte, F. J., ed.). CRC, New York, Chapter 12, pp. 341–373.
Duarte, F. J. (2013). The probability amplitude for entangled polarizations. *J. Mod. Opt*. **60**, 1585–1587.
Duarte, F. J. (2015). *Tunable Laser Optics*, 2nd ed. CRC, Boca Raton, FL.
Duarte, F. J. (2022). *Fundamentals of Quantum Entanglement*, 2nd ed. Institute of Physics, Bristol.
Duarte, F. J., and Paine, D. J. (1989). Quantum mechanical description of N-slit interference phenomena. In *Proceedings of the International Conference on Lasers'89* (Harris, D. G. and Shay, T. M., eds.). STS Press, McLean, VA, pp. 42–47.
Feynman . R. P., and Hibbs, A. R. (1965). *Quantum Mechanics and Path Integrals*, Mc Graw-Hill, New York.
Feynman, R. P., Leighton, R. B., and Sands, M. (1965). *The Feynman Lectures on Physics*, Vol. III, Addison-Wesley, Reading, MA.
Michelson, A. A. (1927). *Studies in Optics*, University of Chicago, Chicago, IL.
Wallenstein, R., and Hänsch, T. W. (1974). Linear pressure tuning of a multielement dye laser spectrometer. *Appl. Opt.* 13, 1625–1628.

5 Interference, Diffraction, Refraction, and Reflection via Dirac's Notation

5.1 INTRODUCTION

In this chapter, we use the generalized one-dimensional interferometric equation to introduce the concepts of diffraction, refraction, and reflection, cohesively and unified.

In this regard, we have an equation derived using the probabilistic concept of single-photon propagation, via Dirac's quantum notation, explaining in a unified manner the major concepts of classical optics.

In the original exposition of this united and cohesive approach to optics (Duarte, 1997, 2003), only positive refraction was considered. Here, both, *positive* and *negative refractions* (Veselago, 1968) are incorporated (Duarte, 2006). Subsequently, the brief exposition of generalized prismatic dispersion also encompasses the positive and negative alternatives.

5.2 INTERFERENCE AND DIFFRACTION

Feynman, in his usual style, stated that '*no one has ever been able to define the difference between interference and diffraction satisfactorily*' (Feynman et al., 1965).

In the discussion related to Figure 5.1, and its variants, reference was only made to interference. However, what we really have is interference in three diffraction orders. That is, the 0th, or central order, and the ±1, or secondary orders. In other words, there is an interference pattern associated with each diffraction order. Physically, however, it is part of the same phenomenon. The interaction of coherent light with a set of slits, in the near field, gives rise to an interference pattern. As the intra-interferometric distance $D_{\langle d|j \rangle}$ increases, the central interference pattern begins to provide origin to secondary patterns, which gradually separate from the central order at lower intensities. These are the ±1 diffraction orders. This physical phenomenon, as one goes from the near to the far field, is clearly illustrated in Figures 5.2–5.5. One of the beauties of the Dirac description of optics is the ability to continuously describe the evolution of the interferometric distribution, as it moves from the *near* to the *far* field, with a single mathematical equation.

DOI: 10.1201/9781003398707-5

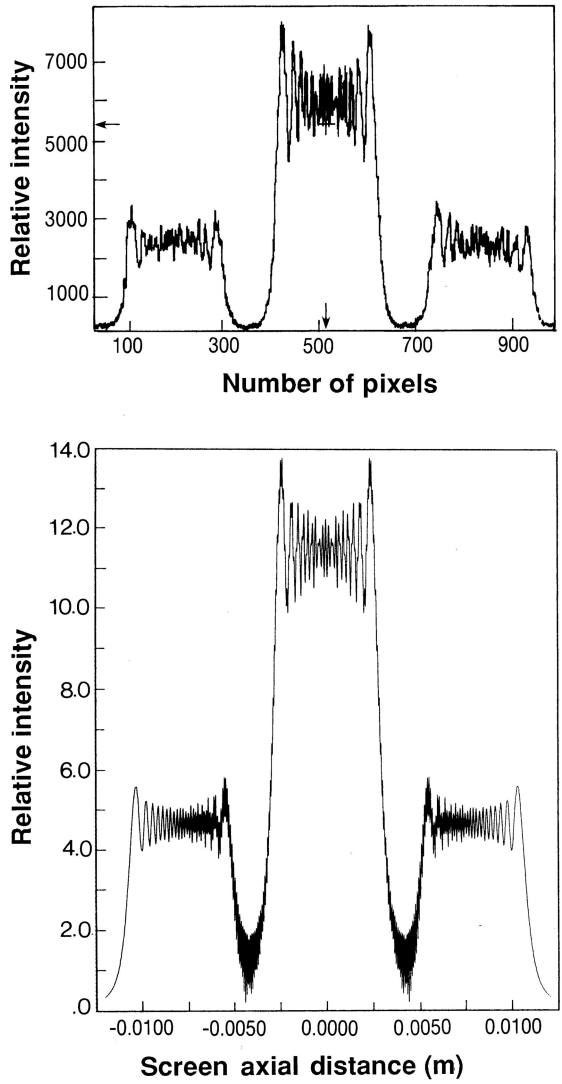

FIGURE 5.1 (a) Measured interferogram resulting from the interaction of coherent laser emission at $\lambda = 632.82\,\text{nm}$ and 100 slits 30 μm wide, separated by 30 μm and $D_{\langle d|j\rangle} = 75$ cm. (b) Corresponding theoretical interferogram from Equation (5.1) (Reproduced from Duarte, F. J., *Opt. Commun.* **103**, 8–14, 1993, with permission from Elsevier).

The second interference-diffraction entanglement refers to the fact that our generalized interference equation can be naturally applied to describe a diffraction pattern produced by a single wide slit as shown in Figure 5.6. Under those circumstances, the wide slit is mathematically represented by a multitude of subslits.

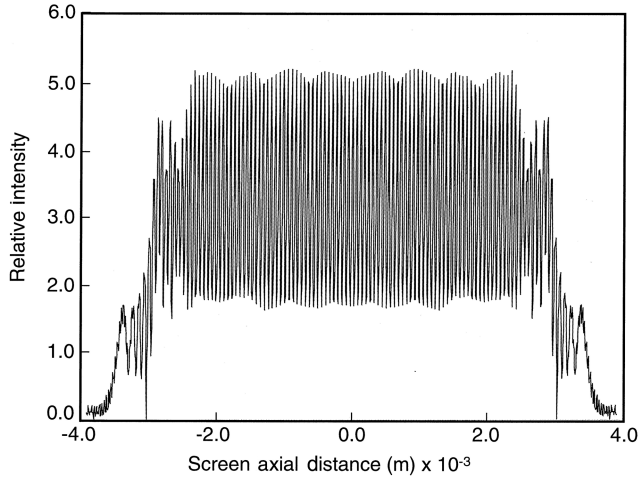

FIGURE 5.2 Interferogram at a grating to screen distance of $D_{\langle d|j\rangle} = 5$ cm. The interferometric distribution, in the *near field*, is mainly part of a single order. At the boundaries, there is an incipient indication of emerging orders. Slit width is 30 μm and slits are separated by 30 μm, $N = 100$, and $\lambda = 632.82$ nm (Reproduced from Duarte, F. J., *Tunable Laser Optics*, 2nd ed. CRC, Boca Raton, FL, 2015).

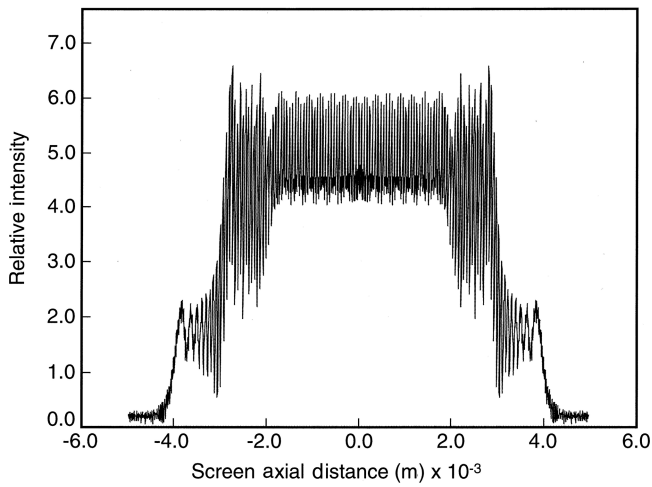

FIGURE 5.3 Interferogram at a grating to screen distance of $D_{\langle d|j\rangle} = 10$ cm. The presence of the emerging (±1) orders is more visible. Slit width is 30 μm and slits are separated by 30 μm, $N = 100$, and $\lambda = 632.82$ nm (Reproduced from Duarte, F. J., *Tunable Laser Optics*, 2nd ed. CRC, Boca Raton, FL, 2015).

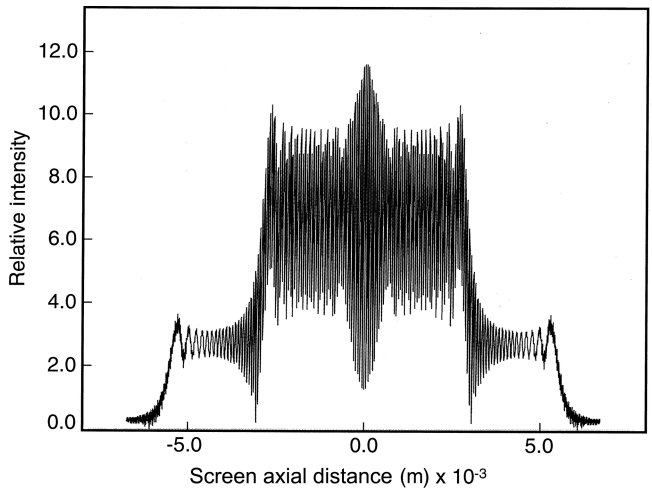

FIGURE 5.4 Interferogram at a grating to screen distance of $D_{\langle d|j\rangle} = 25$ cm. The emerging (± 1) orders give rise to an overall distribution with clear 'shoulders.' Slit width is 30 μm and slits are separated by 30 μm, $N = 100$, and $\lambda = 632.82$ nm (Reproduced from Duarte, F. J., *Tunable Laser Optics*, 2nd ed. CRC, Boca Raton, FL, 2015).

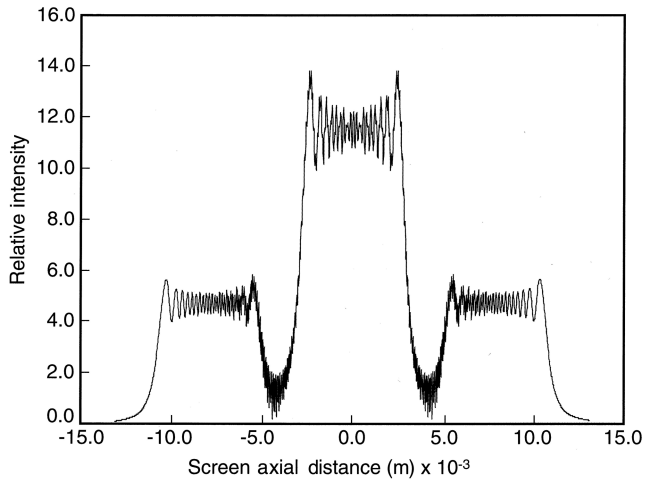

FIGURE 5.5 Interferogram at a grating to screen distance of $D_{\langle d|j\rangle} = 75$ cm. The -1, 0, and $+1$ diffraction orders are clearly established. Notice the increase in the width of the distribution as the j to d distance increases from 5 to 75 cm. Slit width is 30 μm and slits are separated by 30 μm, $N = 100$, and $\lambda = 632.82$ nm (Reproduced from Duarte, F. J., *Tunable Laser Optics*, 2nd ed. CRC, Boca Raton, FL, 2015).

5.2.1 Generalized Diffraction

The intimate relation between interference and diffraction has its origin in the interferometric equation itself (Duarte, 2003):

$$\left|\langle d|s\rangle\right|^2 = \sum_{j=1}^{N} \Psi(r_j)^2 + 2\sum_{j=1}^{N} \Psi(r_j) \left(\sum_{m=j+1}^{N} \Psi(r_m) \cos(\Omega_m - \Omega_j) \right) \tag{5.1}$$

for, it is the $\cos(\Omega_m - \Omega_j)$ term, that gives rise to the different diffraction orders.

Here, we revisit the geometry at the *N*-slit plane *j* and illustrate what is obviously seen in Figures 5.1–5.5: up on arrival to a slit, diffraction occurs symmetrically toward both sides as illustrated in Figures 5.7–5.10. Figure 5.7 depicts the usual description associated with incidence below the normal (−) and diffraction above the normal (+). Figure 5.8 illustrates incidence above the normal (+) and diffraction above the normal (+) (Duarte, 2006). For completeness, we also include the case of incidence below the normal (−) followed by diffraction below the normal (−) and incidence above the normal (+) followed by diffraction below the normal (−) (Figures 5.9 and 5.10).

Thus, the equations describing the geometry (Duarte, 1997) are slightly modified to account for all the ± alternatives

$$\cos\left(\pm(\theta_m - \theta_j) \pm (\phi_m - \phi_j)\right) = \cos\left(\pm|l_m - l_{m-1}|\, k_1 \pm |L_m - L_{m-1}|\, k_2\right) \tag{5.2}$$

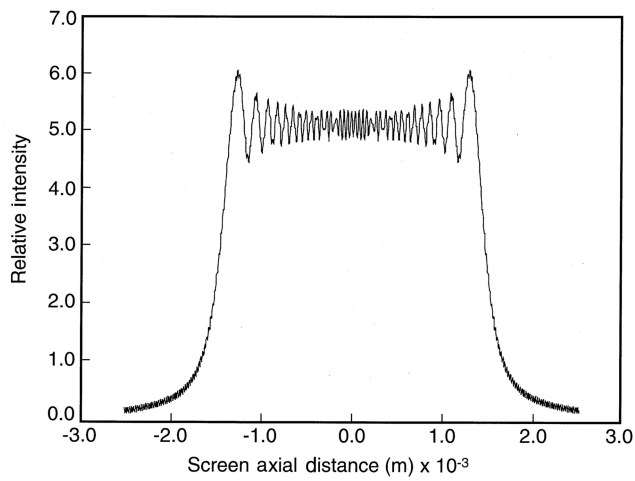

FIGURE 5.6 Theoretical near field diffraction distribution produced by a 4 mm aperture illuminated at $\lambda = 632.82$ nm. Here, $D_{\langle d|j\rangle} = 10$ cm (Reproduced from Duarte, F. J., *Opt. Commun.* **103**, 8–14, 1993, with permission from Elsevier).

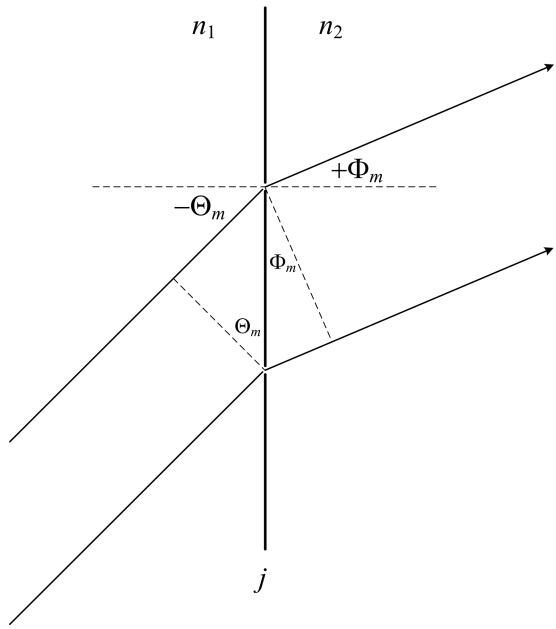

FIGURE 5.7 Outline of the j plane in a transmission grating showing incidence below the normal (−) and diffraction above the normal (+) consistent with the convention leading to positive refraction (Reproduced from Duarte, F. J., *Appl. Phys. B.* **82**, 35–38, 2006, with permission from Springer Nature).

where

$$k_1 = \frac{2\pi n_1}{\lambda_v} \tag{5.3}$$

and

$$k_2 = \frac{2\pi n_2}{\lambda_v} \tag{5.4}$$

are the wavenumbers of the two optical regions defined in Figures 5.7–5.10. Here, as we saw previously, $\lambda_1 = \lambda_v/n_1$ and $\lambda_2 = \lambda_v/n_2$, where λ_v is the vacuum wavelength and n_1 and n_2 are the corresponding indexes of refraction.

As previously explained in Chapter 4, the phase differences can be expressed via geometrical expressions of the form (Duarte, 1993)

$$\left|L_m - L_{m-1}\right| = \frac{d_m(\Delta\delta_m + d_m)}{\left|L_m\right|} \tag{5.5}$$

$$L_m^2 = D_{\langle d|j\rangle}^2 + \Delta\delta_m^2 \tag{5.6}$$

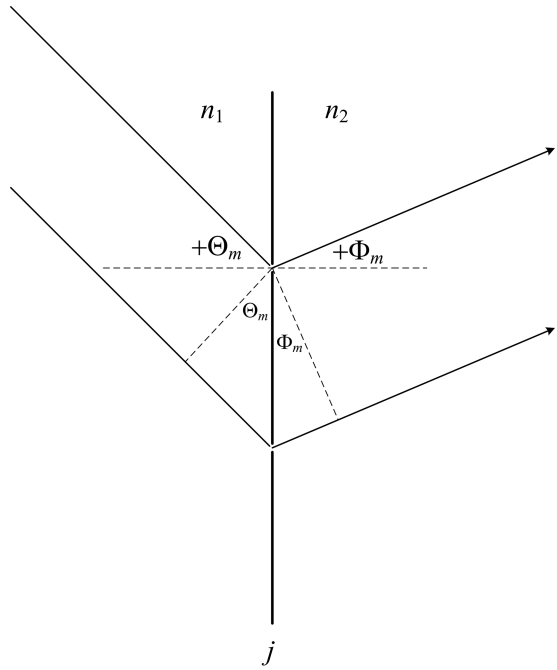

FIGURE 5.8 Outline of the *j* plane in a transmission grating showing incidence above the normal (+) and diffraction above the normal (+) consistent with the convention leading to negative refraction (Reproduced from Duarte, F. J., *Appl. Phys. B.* **82**, 35–38, 2006, with permission from Springer Nature).

$$L_{m-1}^2 = D_{\langle d|j\rangle}^2 + \left(\Delta d_m - \delta\right)^2 \tag{5.7}$$

From the geometry of Figure 5.11

$$\sin\Phi_m = \frac{\left|L_m - L_{m-1}\right|}{d_m} \tag{5.8}$$

and

$$\left|L_m - L_{m-1}\right| \approx d_m \sin\Phi_m \tag{5.9}$$

$$\left|l_m - l_{m-1}\right| \approx d_m \sin\Theta_m \tag{5.10}$$

where Θ_m and Φ_m are the angles of incidence and diffraction, respectively. Given that maxima occur at

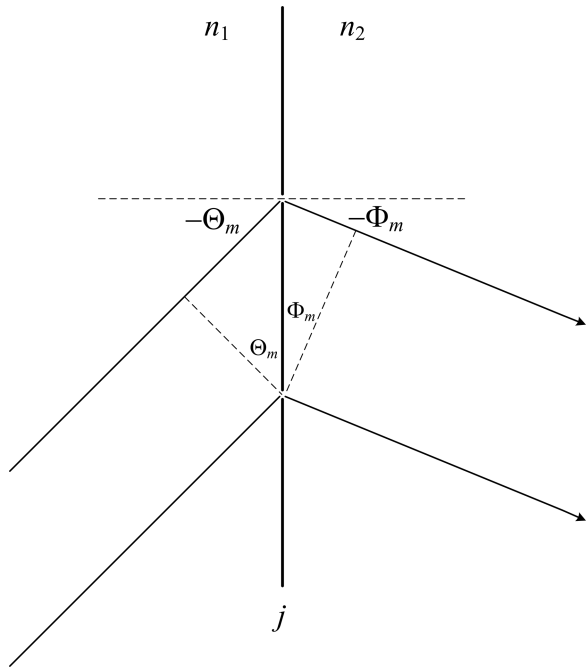

FIGURE 5.9 Outline of the *j* plane in a transmission grating showing incidence below the normal (−) and diffraction below the normal (−) consistent with the convention leading to negative refraction.

$$\left(\pm|l_m - l_{m-1}|n_1 \pm |L_m - L_{m-1}|n_2\right)\frac{2\pi}{\lambda_v} = M\pi \tag{5.11}$$

then using Equations (5.9) and (5.10)

$$d_m\left(\pm n_1 \sin\Theta_m \pm n_2 \sin\Phi_m\right)\frac{2\pi}{\lambda_v} = M\pi \tag{5.12}$$

where $M = 0, 2, 4, 6,...$ For $n_1 = n_2$, we have $\lambda = \lambda_v$, and this equation reduces to the *generalized diffraction grating equation*

$$d_m\left(\pm \sin\Theta_m \pm \sin\Phi_m\right) = m\lambda \tag{5.13}$$

where $m = 0, 1, 2, 3,...$ are the various *diffraction orders.*

An observation is due here: in our discussion on the interferometric equations, we have made explicit reference to the exact geometrical equations (Equations (5.5)–(5.7)).

However, in the derivation of Equations (5.12) and (5.13), we have used the approximation $D_{(d|j)} >> d_m$. Are we being consistent? The answer is yes! Equations (5.5)

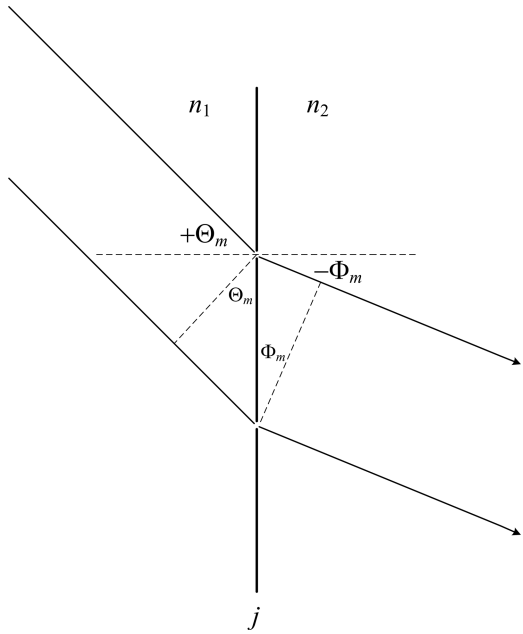

FIGURE 5.10 Outline of the j plane in a transmission grating showing incidence above the normal (+) and diffraction below the normal (−) consistent with the convention leading to positive refraction

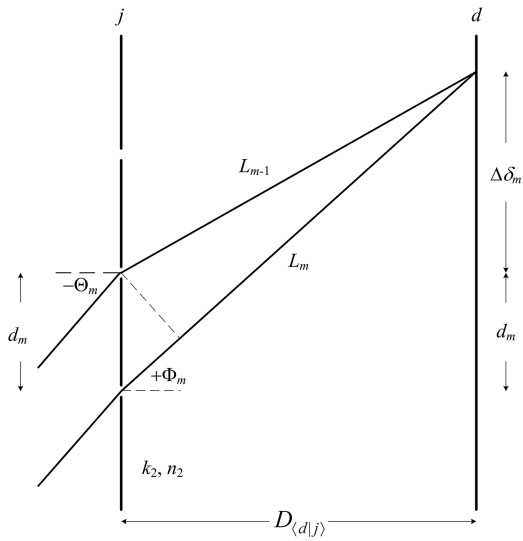

FIGURE 5.11 Close-up of the N-slit array, or transmission grating, plane (j) illustrating the path length difference and the angles of incidence ($-\Theta_m$) and diffraction ($+\Phi_m$) for the condition $D_{\langle d|j\rangle} >> d_m$.

to (5.7) are used in the generalized interferometric equation (Equation (5.1)), while the approximation $D_{\langle d|j\rangle} >> d_m$ has been applied in the derivation of the generalized diffraction equation

$$d_m\left(\pm\sin\Theta_m \pm \sin\Phi_m\right) = m\lambda$$

that manifests itself in the *far field* as beautifully illustrated in Figures 5.2–5.5. From this equation, it is clear that beyond the zeroth order, m can take a series of ± values, that is $m = \pm 1,\ \pm 2,\ \pm 3...$

Note: the parameter d_m depicts a fractional distance on the j plane and should be labeled as Δj_m. However, here we use d_m to be consistent with tradition in the published literature.

5.2.2 Positive Diffraction

From the generalized diffraction equation (Equation (5.13)) including both ± alternatives, the usual traditional equation can be stated as

$$d_m\left(\sin\Theta_m \pm \sin\Phi_m\right) = m\lambda \tag{5.14}$$

which was previously derived starting from (Duarte, 1997)

$$\cos\left((\theta_m - \theta_j) \pm (\phi_m - \phi_j)\right) = \cos\left(|l_m - l_{m-1}|\,k_1 \pm |L_m - L_{m-1}|\,k_2\right) \tag{5.15}$$

From Equation (5.14), setting $\Theta_m = \Phi_m = \Theta$, the diffraction grating equation for Littrow configuration emerges the well-known grating equation

$$m\lambda = 2d_m \sin\Theta \tag{5.16}$$

5.3 POSITIVE AND NEGATIVE REFRACTION

So far, we have discussed interference and diffraction and have seen how diffraction manifests itself as the interferometric distribution propagates toward the far field. An additional fundamental phenomenon in optics is *refraction*.

Refraction is the change in the geometrical path, of a beam of light, due to transmission from the original medium of propagation to a second medium with a different refractive index. For example, refraction is the bending of a ray of light caused due to propagation in a glass, or crystalline, prism.

If in the diffraction grating equation, d_m is made very small relative to a given λ, diffraction ceases to occur, and the only solution can be found for $m = 0$ (Duarte, 1997). That is, under these conditions, a grating made of grooves coated on a transparent substrate, such as optical glass, does not diffract and exhibits the refraction properties of the glass. For example, since the maximum value of $(\pm\sin\Theta_m \pm \sin\Phi_m)$ is 2, for a 5000 lines/mm transmission grating, let us say, no diffraction can be observed for the visible spectrum. Hence, for the condition $d_m << \lambda$, the diffraction grating equation can only be solved for

$$d_m\left(\pm n_1 \sin\Theta_m \pm n_2 \sin\Phi_m\right)\frac{2\pi}{\lambda_v} = 0 \tag{5.17}$$

which leads to

$$\left(\pm n_1 \sin\Theta_m \pm n_2 \sin\Phi_m\right) = 0 \tag{5.18}$$

For the case of incidence below the normal (−) and refraction above the normal (+) (Figure 5.7)

$$-n_1 \sin\Theta_m + n_2 \sin\Phi_m = 0 \tag{5.19}$$

so that

$$n_1 \sin\Theta_m = n_2 \sin\Phi_m \tag{5.20}$$

which is the well-known *equation of refraction*, also known as *Snell's la*w. Under the present physical conditions, Θ_m is the angle of incidence and Φ_m becomes the *angle of refraction*. The same outcome is obtained for incidence above the normal (+) and refraction below the normal (−) (Figure 5.10). In textbooks, Equation (5.20) is usually expressed as

$$n = \frac{\sin\Theta_m}{\sin\Phi_m} \tag{5.21}$$

Snell's law is sometimes also written as $(\sin\Theta_m / \sin\Phi_m) = n = (c/\upsilon)$, which is referred to as Maxwell's formula (Born and Wolf, 1999).

For the case of incidence above the normal (+) and refraction above the normal (+) (Figure 5.8)

$$+n_1 \sin\Theta_m + n_2 \sin\Phi_m = 0 \tag{5.22}$$

so that

$$n_1 \sin\Theta_m = -n_2 \sin\Phi_m \tag{5.23}$$

which is Snell's law for *negative refraction*. The same outcome is obtained for incidence below the normal (−) and diffraction below the normal (−) (Figure 5.9).

5.3.1 Focusing

Once the law of refraction is introduced, focusing is the next logical and natural step. This is because focusing naturally flows from the law of refraction, or Snell's law, acting on a curved surface. The relationships between surface radius of curvature, refractive index, and focal length for various lens types is discussed in detail in classical optics books such as *Fundamental of Optics* (Jenkins and White, 1957).

For completeness, in Appendix F, we provide an extensive table with focusing parameters for various lenses of interest using the *ABCD* propagation matrix formalism (Siegman, 1986; Duarte, 2003).

5.4 REFLECTION

The discussion on interference, up to now, has involved an *N*-slit array or a transmission grating. It should be indicated that the arguments and physics apply equally well to a reflection interferometer (Duarte, 2003). That is, to an interferometer incorporating a reflection, rather than a transmission, grating. Explicitly, if a mirror is placed at an infinitesimal distance immediately behind the *N*-slit array, as illustrated in Figure 5.12, then the transmission interferometer becomes a reflection interferometer. Under those circumstances, the equations

$$d_m\left(\pm n_1 \sin\Theta_m \pm n_2 \sin\Phi_m\right)\frac{2\pi}{\lambda_v} = M\pi$$

and

$$d_m\left(\pm \sin\Theta_m \pm \sin\Phi_m\right) = m\lambda$$

apply in the reflection domain, with Θ_m being the incidence angle and Φ_m the diffraction angle in the *reflection* domain. For the case of $d_m << \lambda$ and $n_1 = n_2$, we then have

$$\left(\pm \sin\Theta_m \pm \sin\Phi_m\right) = 0 \tag{5.24}$$

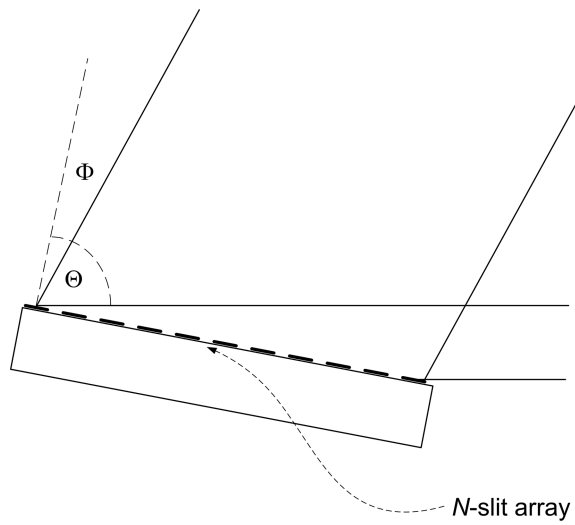

FIGURE 5.12 Approaching a mirror, at an infinitesimal distance, to an *N*-slit array, is used to configure a reflection diffraction grating. The incidence angle is Θ, and the diffraction angle is Φ.

For incidence above the normal (+) and reflection below the normal (−)

$$+\sin\Theta_m - \sin\Phi_m = 0 \tag{5.25}$$

which means

$$\Theta_m = \Phi_m \tag{5.26}$$

where Θ_m is the angle of incidence and Φ_m is the angle of reflection. This is known as the *law of reflection*.

5.5 SUCCINCT DESCRIPTION OF OPTICS

A summary of fundamental optical principles can now be given. Starting from the Dirac quantum principle (Dirac, 1939, 1958)

$$\langle d|s\rangle = \sum_{j=1}^{N} \langle d|j\rangle\langle j|s\rangle$$

the generalized one-dimensional interferometric probability equation is derived (Duarte, 1989, 1991)

$$\left|\langle d|s\rangle\right|^2 = \sum_{j=1}^{N} \Psi(r_j)^2 + 2\sum_{j=1}^{N} \Psi(r_j)\left(\sum_{m=j+1}^{N} \Psi(r_m)\cos(\Omega_m - \Omega_j)\right)$$

From the phase term of this equation, the generalized diffraction equation

$$d_m\left(\pm n_1 \sin\Theta_m \pm n_2 \sin\Phi_m\right)\frac{2\pi}{\lambda_v} = M\pi$$

can be obtained, from which the generalized diffraction grating equation

$$d_m\left(\pm\sin\Theta_m \pm \sin\Phi_m\right) = m\lambda$$

can be arrived to. From the generalized diffraction equation and applying the condition $d_m << \lambda$, the generalized refraction equation

$$(\pm n_1 \sin\Theta_m \pm n_2 \sin\Phi_m) = 0$$

is obtained. From this equation, one can arrive at the law of reflection

$$\Theta_m = \Phi_m$$

Most other important optical phenomena, such as focusing and dispersion, can be explained from the principles outlined here. This hierarchical, orderly, and unified description of optics: *interference* → *diffraction* → *refraction* → *reflection*

(Duarte, 1997, 2003) illustrates that quantum principles are perfectly compatible with classical empirical phenomena. The phenomenon of multiple-prism dispersion originates from the derivatives of refraction and is treated in Appendix C.

Going back to the Feynman statement, on interference and diffraction, we can confidently state that this whole phenomenon is succinctly and beautifully described by the interferometric probability equation

$$\left|\langle d|s\rangle\right|^2 = \sum_{j=1}^{N} \Psi(r_j)^2 + 2\sum_{j=1}^{N} \Psi(r_j)\left(\sum_{m=j+1}^{N} \Psi(r_m)\cos(\Omega_m - \Omega_j)\right)$$

Indeed, in reference to the interferometric progression illustrated in Figures 5.2–5.5, we see that the basic phenomenon is interference. Pure interference dominates in the near field. However, as the propagation distance increases toward the far field, diffraction orders ($m = \pm 1, \pm 2, \pm 3...$) do appear. This appearance of diffraction orders is analogous to a quantization of the interferometric distribution.

5.6 QUANTUM INTERFERENCE AND CLASSICAL INTERFERENCE

The following is a summary following a discussion on the distinctions between quantum and classical interference provided by Duarte (2022).

In classical interference

$$\text{Maxwell equations} \rightarrow \sum_{n=1}^{N} I_n + 2\sum_{n=1}^{N} I_n^{\frac{1}{2}}\left(\sum_{m=n+1}^{N} I_m^{\frac{1}{2}}\cos\delta\right) \tag{5.27}$$

where I_n are *intensities* so that Equation (5.27) is a mathematical expression describing the interference of classical intensities.

In quantum interference

$$\sum_{j=1}^{N}\langle d|j\rangle\langle j|s\rangle \rightarrow \sum_{j=1}^{N}\Psi(r_j)\sum_{m=1}^{N}\Psi(r_m)e^{i(\Omega_m-\Omega_j)} \tag{5.28}$$

the origin is a superposition of probability amplitudes. The single-photon quantum *probability* is obtained via the use of Born's rule leading to

$$\langle d|s\rangle\langle d|s\rangle^* = \left(\sum_{j=1}^{N}\langle d|j\rangle\langle j|s\rangle\right)\left(\sum_{j=1}^{N}\langle d|j\rangle\langle j|s\rangle\right)^* \tag{5.29}$$

and its corresponding intensity is[1]

$$I(\nu) = K\,h\nu\,\langle d|s\rangle\langle d|s\rangle^* \tag{5.30}$$

Here, Equation (5.29) is a *quantum probability* equation, while Equation (5.30) is a quantum intensity equation whose spatial distribution depends on the dimensionless probability given in (5.29).

For *r indistinguishable quanta*, the corresponding intensity becomes

$$I(\nu)_r = r\,\mathrm{K}\,h\nu\,\langle d|s\rangle\,\langle d|s\rangle^* \tag{5.31}$$

Here, it should be emphasized that $\langle d|s\rangle\,\langle d|s\rangle^*$, $I(\nu)$, and $I(\nu)_r$ are *purely quantum*.

In the classical domain, where intensities are measured, a transition is allowed, or an equivalence is permitted, for r indistinguishable quanta (Duarte and Taylor, 2021), that is

$$I(\nu)_r \to I_n \tag{5.32}$$

thus allowing the interference of $I_1, I_2, I_3 \ldots I_n$ via the classical N-slit interference equation

$$I = \sum_{n=1}^{N} I_n + 2\sum_{n=1}^{N} I_n^{\frac{1}{2}} \left(\sum_{m=n+1}^{N} I_m^{\frac{1}{2}} \cos\delta \right)$$

Note: the quantum-classical $I(\nu)_r \to I_n$ transition occurs here via diffraction at each of the slits in the classical array as described in Chapter 4 and Section 5.2. In other words, each of the slits in the classical array is subdivided into N-subslits, each of which gives rise to a diffractive light source I_n that then interferes via Equation (5.27).

PROBLEMS

5.1 Show that the geometry depicted in Figure 5.11 leads to Equation (5.12).

5.2 Substitute Equations (5.9) and (5.10) into Equation (5.11) to obtain Equation (5.13).

5.3 Show that from the geometry outlined in Figure 5.6, Equation (5.20) follows.

5.4 Show that from the geometry outlined in Figure 5.8, Equation (5.23) follows.

REFERENCES

Born, M., and Wolf, E. (1999). *Principles of Optics*, 7th ed. Cambridge, New York.

Dirac, P. A. M. (1939). A new notation for quantum mechanics. *Math. Proc. Cam. Phil. Soc.* 35, 416–418.

Dirac, P. A. M. (1958). *The Principles of Quantum Mechanics*, 4th ed. Oxford University, Oxford, U.K.

Duarte, F. J. (1991). Dispersive dye lasers. In *High Power Dye Lasers* (Duarte, F. J., ed.). Springer-Verlag, Berlin, Chapter 2, pp. 7–43.

Duarte, F. J. (1993). On a generalized interference equation and interferometric measurements. *Opt. Commun.* 103, 8–14.

Duarte, F. J. (1997). Interference, diffraction, and refraction, via Dirac's notation. *Am. J. Phys.* 65, 637–640.

Duarte, F. J. (2003). *Tunable Laser Optics*, 1st ed. Elsevier-Academic, New York.

Duarte, F. J. (2006). Multiple-prism dispersion equations for positive and negative refraction, *Appl. Phys. B*. 82, 35–38.

Duarte, F. J. (2015). *Tunable Laser Optics*, 2nd ed. CRC, Boca Raton, FL.

Duarte, F. J. (2022). *Fundamentals of Quantum Entanglement*, 2nd ed. Institute of Physics, Bristol, U.K.

Duarte, F. J., and Paine, D. J. (1989). Quantum mechanical description of N-slit interference phenomena. In *Proceedings of the International Conference on Lasers'89* (Harris, D. G. and Shay, T. M., eds.). STS Press, McLean, VA, pp. 42–47.

Duarte, F. J. and Taylor, T. S. (2021). *Quantum Entanglement Engineerings and Applications*, Institute of Physics, Bristol, U.K.

Feynman, R. P., Leighton, R. B., and Sands, M. (1965). *The Feynman Lectures on Physics*, Vol. I, Addison-Wesley, Reading, MA.

Jenkins, F. A., and White, H. E. (1957). *Fundamentals of Optics*, McGraw-Hill, New York.

Siegman, A. E. (1986). *Lasers*, University Science Books, Mill Valley, CA.

Veselago, V. G. (1968). The electrodynamics of substances with simultaneously negative values of ε and μ. *Sov. Phys. Usp.* 10, 509–514.

6 Dirac's Notation Identities

6.1 USEFUL IDENTITIES

Dirac's quantum *bra ket* notation was introduced by Dirac (1939) in the absence of a written explanation on its origin. This remarkable occurrence has since remained a mystery other than to assume that to Dirac, the *bra ket* avenue was a natural way to represent and discuss probability amplitudes in time and space. Dalitz (2000) who took many lectures from Dirac, when asked, responded that he did not observe Dirac discussing the origin of his brilliant notation. In this regard, Dirac only acknowledged his desire to improve the existing quantum notation. It should be added that 'good notation' was very important to Dirac (Dirac, 1939; Kragh, 1990).

As described by Dirac (1958) and Feynman et al. (1965), Dirac's notation includes various mathematical properties and allows for abstractions and permutations. Here, a few useful set of identities and properties of the notation are described.

First, the complex conjugate of $\langle\phi|\psi\rangle$ is defined as

$$\langle\phi|\psi\rangle = \langle\psi|\phi\rangle^* \tag{6.1}$$

Also, the probability amplitude

$$\langle\phi|\psi\rangle = \langle\phi|j\rangle\langle j|\psi\rangle \tag{6.2}$$

can be expressed in abstract form as

$$|\psi\rangle = |j\rangle\langle j|\psi\rangle \tag{6.3}$$

An additional form of abstract notation is

$$\langle\chi|A|\phi\rangle = \langle\chi|i\rangle\langle i|A|j\rangle\langle j|\phi\rangle \tag{6.4}$$

where A is

$$A = |i\rangle\langle j|A|j\rangle\langle j| \tag{6.5}$$

Another abstraction is illustrated by

$$A|\phi\rangle = |i\rangle\langle i|A|j\rangle\langle j|\phi\rangle \tag{6.6}$$

Further, A can be multiplied by B so that

DOI: 10.1201/9781003398707-6

$$\langle \chi | BA | \phi \rangle = \langle \chi | i \rangle \langle i | B | j \rangle \langle j | A | k \rangle \langle k \phi \rangle \tag{6.7}$$

To express

$$\langle \chi | A | \phi \rangle = \langle \chi | i \rangle \langle i | A | j \rangle \langle j | \phi \rangle \tag{6.8}$$

in the abstract form

$$\langle \chi | \psi \rangle = \langle \chi | i \rangle \langle i | \psi \rangle \tag{6.9}$$

it is necessary that

$$\langle i | \psi \rangle = \langle i | A | j \rangle \langle j | \phi \rangle = \langle i | A | \phi \rangle \tag{6.10}$$

which means that

$$\langle \chi | \psi \rangle = \langle \chi | A | \phi \rangle \tag{6.11}$$

Further abstracting leads to

$$| \psi \rangle = | A | \phi \rangle \tag{6.12}$$

Other examples of abstractions include

$$\langle i | \phi \rangle = C_i \tag{6.13}$$

$$\langle i | \chi \rangle = D_i \tag{6.14}$$

$$| \phi \rangle = \sum_i | i \rangle C_i \tag{6.15}$$

$$| \chi \rangle = \sum_i | i \rangle D_i \tag{6.16}$$

$$\langle \chi | = \sum_i D_i^* \langle i | \tag{6.17}$$

which is the abstracted version of

$$\langle \chi | \phi \rangle = \sum_{ij} D_j^* \langle j | i \rangle C_i \tag{6.18}$$

and since $\langle j | i \rangle = \delta_{ij}$

$$\langle \chi | \phi \rangle = \sum_i D_i^* C_i \tag{6.19}$$

Finally, using the ultimate abstraction suggested by Dirac (Feynman et al., 1965), Equation (6.19) can be expressed as

$$| = \sum_i |i\rangle\langle i| \tag{6.20}$$

In practice, to keep a clear track of the physics, it is advisable to use abstractions only when necessary.

6.1.1 Example

The probability amplitude describing interference in a Mach–Zehnder interferometer can be described as (Duarte, 2003)

$$\langle d | s \rangle = \sum_{kj} \langle d | k \rangle \langle k | j \rangle \langle j | s \rangle \tag{6.21}$$

Defining

$$\langle j | s \rangle = C_j \tag{6.22}$$

$$\langle k | d \rangle = D_k \tag{6.23}$$

$$\langle d | s \rangle = \sum_{kj} D_k^* \langle k | j \rangle C_j \tag{6.24}$$

and using $\langle k | j \rangle = \delta_{kj}$, we get

$$\langle d | s \rangle = \sum_j D_j^* C_j \tag{6.25}$$

6.2 LINEAR OPERATIONS

Dirac (1958) describes various mathematical properties related to his *ket* vectors. First, if c_1 and c_2 are complex numbers, *ket* vectors can be multiplied by these complex numbers and added to produce a new *ket* vector

$$c_1 |\phi\rangle + c_2 |\psi\rangle = |\theta\rangle \tag{6.26}$$

Superposition of a state, with itself, yields the original state

$$c_1 |\phi\rangle + c_2 |\phi\rangle = (c_1 + c_2) |\phi\rangle \tag{6.27}$$

Additional sum and product conditions are illustrated by

$$\langle\phi|\big(|\psi\rangle+|\chi\rangle\big)=\langle\phi|\psi\rangle+\langle\phi|\chi\rangle \tag{6.28}$$

$$\Big\langle\phi\Big|\big(c|\psi\big)\Big\rangle=c\langle\phi|\psi\rangle \tag{6.29}$$

and

$$\big(\langle\phi|+\langle\chi|\big)|\psi\rangle=\langle\phi|\psi\rangle+\langle\chi|\psi\rangle \tag{6.30}$$

$$\big(c\langle\phi|\big)|\psi\rangle=c\langle\phi|\psi\rangle \tag{6.31}$$

If α is a linear operator, then

$$|\vartheta\rangle=\alpha|\psi\rangle \tag{6.32}$$

and

$$\alpha\big(|\psi\rangle+|\chi\rangle\big)=\alpha|\psi\rangle+\alpha|\chi\rangle \tag{6.33}$$

$$\alpha\big(c|\psi\rangle\big)=c\alpha|\psi\rangle \tag{6.34}$$

$$(\alpha+\beta)|\psi\rangle=\alpha|\psi\rangle+\beta|\psi\rangle \tag{6.35}$$

$$(\alpha\beta)|\psi\rangle=\alpha\big(\beta|\psi\rangle\big) \tag{6.36}$$

$$\big(\langle\phi|\alpha\big)|\psi\rangle=\langle\phi|\big(\alpha|\psi\rangle\big) \tag{6.37}$$

Further useful identities introduced by Dirac (1958) are

$$|\phi\rangle|\psi\rangle=|\psi\rangle|\phi\rangle \tag{6.38}$$

$$|\phi\rangle|\psi\rangle=|\psi\rangle|\phi\rangle=|\phi\psi\rangle \tag{6.39}$$

$$|\phi\rangle|\psi\rangle|\chi\rangle\ldots=|\phi\psi\chi\ldots\rangle \tag{6.40}$$

Also, for indistinguishable quanta, Dirax (1958) expresses the *ket* for the assembly as

$$|a_1 b_2 c_3 \ldots g_n\rangle = |a_1\rangle|b_2\rangle|c_3\rangle\ldots|g_n\rangle \tag{6.41}$$

which can be rewritten as (Duarte, 2019)

$$|a_1\rangle|b_2\rangle|c_3\rangle\ldots|g_n\rangle = |a\rangle_1|b\rangle_2|c\rangle_3\ldots|g\rangle_n \tag{6.42}$$

and ultimately as

$$|X\rangle = |a\rangle_1|b\rangle_2|c\rangle_3\ldots|g\rangle_n \tag{6.43}$$

This combined state identity is crucial to the interferometric derivation of superposition probability amplitude for quantum entanglement (Duarte, 2013, 2014).

6.2.1 Example

The Pryce–Ward probability amplitude (Pryce and Ward, 1947; Ward, 1949), prior to normalization, for entangled photons, with polarizations x and y, traveling in opposite directions 1 and 2, is given by (see Chapter 15)

$$|\psi\rangle = \left(|x\rangle_1|y\rangle_2 - |y\rangle_1|x\rangle_2\right) \tag{6.44}$$

which can also be expressed as

$$|\psi\rangle = \left(|x, y\rangle - |y, x\rangle\right) \tag{6.45}$$

6.3 EXTENSION TO INDISTINGUISHABLE QUANTA ENSEMBLES

Identity (6.43) can also be expressed as

$$|x\rangle_I = |x\rangle_1|x\rangle_2|x\rangle_3\ldots|x\rangle_g\ldots \tag{6.46}$$

$$|y\rangle_{II} = |y\rangle_1|y\rangle_2|y\rangle_3\ldots|y\rangle_g\ldots \tag{6.47}$$

which can be applied to explain the origin of coherent emission from electrically-pumped organic semiconductors (Duarte and Taylor, 2022). Here, $|x\rangle_I$ represents an ensemble of indistinguishable quanta in the $|x\rangle$ state of polarization, while $|y\rangle_{II}$ represents an ensemble of indistinguishable quanta in the $|y\rangle$ state of polarization (see Chapter 22).

Using Equations (6.46) and (6.47), the quantum entanglement state $|\psi\rangle_-$ becomes

$$|\psi\rangle_- = 2^{-1/2}\left(|x\rangle_I|y\rangle_{II} - |y\rangle_I|x\rangle_{II}\right) \tag{6.48}$$

where the entanglement refers to the entanglement of *ensembles* of indistinguishable states such as $|x\rangle_I$ and $|y\rangle_{II}$ (Duarte and Taylor, 2022).

PROBLEMS

6.1 Write in abstract form the probability amplitude corresponding to a Sagnac interferometer given by (Duarte, 2003)

$$\langle d|s\rangle = \sum_{kj} \langle d|k\rangle \langle k|j\rangle \langle j|s\rangle$$

assuming that $\langle k|j\rangle = 1$ (see Chapter 7).

6.2 The probability amplitude for a multiple beam interferometer, see Chapter 7, can be expressed as Duarte (2003)

$$\langle d|s\rangle = \langle d|m\rangle \langle m|l\rangle \langle l|k\rangle \langle k|j\rangle \langle j|s\rangle$$

Use the various abstract identities, given in this chapter, to efficiently abstract this probability amplitude.

6.3 Show that using $\langle k|j\rangle = \delta_{kj}$ Equation (6.24) can be written as Equation (6.25).

REFERENCES

Dalitz, R. H. (2000). Private communication.

Dirac, P. A. M. (1939). A new notation for quantum mechanics. *Math. Proc. Cam. Phil. Soc.* 35, 416–418.

Dirac, P. A. M. (1958). *The Principles of Quantum Mechanics*, 4th ed. Oxford, London, U.K.

Duarte, F. J. (2003). *Tunable Laser Optics*, Elsevier-Academic, New York.

Duarte, F. J. (2013). The probability amplitude for entangled polarizations: an interferometric approach. *J. Mod. Opt.* 60, 1585–1587.

Duarte, F. J. (2014). *Quantum Optics for Engineers*, 1st ed. CRC, Boca Raton, FL.

Duarte, F. J. (2019). *Fundamentals of Quantum Entanglement*, 1st ed. Institute of Physics, Bristol, U.K.

Duarte, F. J., and Taylor, T. S. (2022). Quantum coherence in electrically pumped organic interferometric emitters. *Appl. Phys. B.* 128, 11.

Feynman, R. P., Leighton, R. B., and Sands, M. (1965). *The Feynman Lectures on Physics*, Vol. III, Addison-Wesley, Reading, MA.

Kragh, H. S. (1990). *Dirac*, Cambridge University, Cambridge, U.K.

Pryce, M. L. H. and Ward, J. C. (1947). Angular correlation effects with annihilation radiation, *Nature* 160, 435.

Ward, J. C. (1949). *Some Properties of the Elementary Particles*, Oxford University, Oxford, U.K.

7 Interferometry via Dirac's Notation

7.1 INTERFERENCE *À LA* DIRAC

The genesis of quantum optics can be found in Dirac's discussion on interference as disclosed in *The Principles of Quantum Mechanics* (Dirac, 1958). This is a masterful, and prophetic discussion, that begins by considering a '*roughly monochromatic light*' source. The discussion continues by considering '*a beam of light consisting of a large number of photons*.' In other words, Dirac is considering a beam of light with a definite spectral linewidth and high power, a beam of light as available from narrow-linewidth high-power lasers (Duarte, 1998, 2003). For the discussion at hand, the term *monochromatic* is reserved for single-photon emission, while quasi-monochromatic, semi-monochromatic, or nearly monochromatic relates to spectrally narrow emission as available from narrow-linewidth high-power lasers. These narrow-linewidth lasers provide populations of indistinguishable photons. The narrower the laser linewidth, the more indistinguishable the photons are. In the case of optimized pulsed laser oscillators, the emission linewidth can be as narrow as allowed by Heisenberg's uncertainty principle, that is, $\Delta\nu \approx 350$ MHz (or $\Delta\lambda \approx 0.0004$ nm at $\lambda \approx 590$ nm) $\Delta t\ \Delta\nu \approx 1.05$ (Duarte, 1999).

Thus, in Dirac's discussion on interference, we are dealing with a population, or ensemble, of indistinguishable photons. He then goes on to associate '*the translational state of a photon with one of the wave functions of ordinary wave optics*' (Dirac, 1958).

He argues that the association is only statistical and that the wave function provides information '*about the probability of our finding the photon in any particular place*.' This idea is reinforced with a similar sentence stating that the wave function gives us information about '*one photon being in a particular place*' (Dirac, 1958). He then considers a beam of light with a large number of nearly monochromatic, that is, indistinguishable photons and divides it into two beams of equal intensity, and the two subbeams are made to interfere. In this regard, Dirac's thought experiment applies directly to a high-power laser beam (of linewidth $\Delta\nu$) made to interfere in a Mach–Zehnder interferometer. Dirac explains that each photon travels partly into the two interfering subbeams: '*each photon then interferes with itself*' (Dirac, 1958). This statement is directly applicable to the experiment at hand in which a large number of indistinguishable photons is divided into two subbeams. Under these circumstances, each individual photon in that ensemble of indistinguishable photons travels partly into each beam (given that they have a large coherent length defined by $\Delta x \approx c/\Delta\nu$) and interferes with itself. Now, mathematically, what interferes are the probability amplitudes associated with each photon.

DOI: 10.1201/9781003398707-7

At this stage, three explanations are necessary. First, as Dirac himself explains, when the beam is divided into two sub-components, this means that a single photon partially propagate into subbeams. *The photon is nonlocal*. It is not a particle (Lamb, 1995).

Second, under Dirac's description, interference between two beams from different lasers emitting at the same frequency is perfectly allowed since the photons are indistinguishable and therefore *the same*. In other words, interference from two laser sources, of the exact same frequency, and linewidth, appears the same as if the beam of one of the lasers were divided and then allowed to interfere.

Third, as explained elsewhere in this book, the equation for *N*-slit interference is derived for a single photon. However, it applies equally well to a population or *ensemble of indistinguishable photons*. If light from a narrow-linewidth laser is used (that would be a nearly perfect population of indistinguishable photons), the interferograms are perfectly sharp and exhibit a visibility (Michelson, 1927)

$$\mathcal{V} = \frac{I_1 - I_2}{I_1 + I_2} \tag{7.1}$$

with $\mathcal{V} \approx 1$. If, on the other hand, broadband emission is used, the interference equation becomes part of an interferometric distribution, including the interferograms corresponding to all the different wavelengths used. Thus, the interferograms become broad, with decreased spatial definition and decreased visibility (Duarte, 2008). This effect is explained in detail in Chapter 4.

Emphasizing the nonlocality of the photon: 'All the indistinguishable photons illuminate the array of *N* slits, or grating, simultaneously. If only one photon propagates, at any given time, then that individual photon illuminates the whole array of *N* slits simultaneously' (Duarte, 2003).

Dirac (1958) provided the genesis for quantum interferometry. Useful references on classical interferometry include Steel (1967), Meaburn (1976), and Born and Wolf (1999).

7.2 THE *N*-SLIT INTERFEROMETER

The *N*-slit laser interferometer (*N*SLI) is depicted in Figure 7.1. The coherent light is expanded via a multiple-prism beam expander to illuminate the *N*-slit array. The single-photon source, or the source of the ensemble of indistinguishable photons, is labeled as *s*.

The *N*-silt array is *j* and the interferometric plane, or detector, *d*. The intra-interferometric distance from *j* to *d* is $D_{\langle d|j\rangle}$. Utilizing the Dirac–Feynman principle, the probability amplitude for single-photon propagation from *s* to *d* is given by

$$\langle d|s\rangle = \sum_{j=1}^{N} \langle d|j\rangle\langle j|s\rangle \tag{7.2}$$

Using Born's rule, the propagation probability becomes (Duarte, 1993)

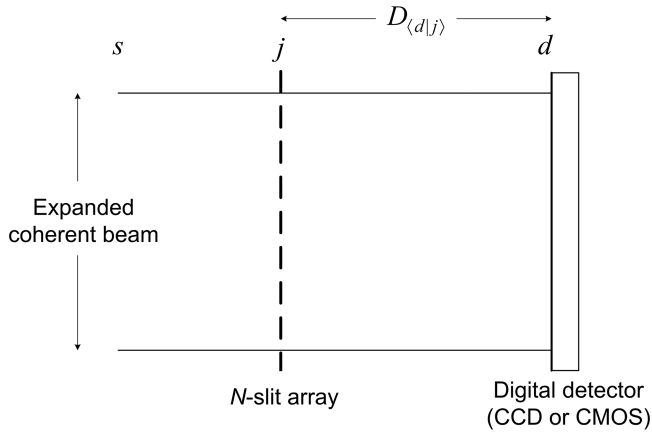

FIGURE 7.1 *N*-slit coherent interferometer. Illumination (*s*) is delivered via a multiple-prism beam expander to illuminate the *N*-slit array (*j*). The intra-interferometric distance is $D_{\langle d|j\rangle}$.

$$\langle d|s\rangle\langle d|s\rangle^{*} = \sum_{j=1}^{N}\Psi(r_j)\sum_{m=1}^{N}\Psi(r_m)e^{i(\Omega_m-\Omega_j)} \tag{7.3}$$

which is equivalent to

$$\langle d|s\rangle\langle d|s\rangle^{*} = \sum_{j=1}^{N}\Psi(r_j)^2 + 2\sum_{j=1}^{N}\Psi(r_j)\left(\sum_{m=j+1}^{N}\Psi(r_m)\cos(\Omega_m-\Omega_j)\right) \tag{7.4}$$

it can be shown that for $N = 2$, or a double-slit interferometer, the superposition probability becomes (Duarte 1993)

$$\langle d|s\rangle\langle d|s\rangle^{*} = \Psi(r_1)^2 + \Psi(r_2)^2 + 2\Psi(r_1)\Psi(r_2)\cos(\Omega_2-\Omega_1) \tag{7.5}$$

It can also be shown that for $N = 7$, the interferometric probability becomes

$$\begin{aligned}\left|\langle d|s\rangle\right|^2 &= \Psi(r_1)^2+\Psi(r_2)^2+\Psi(r_3)^2+\Psi(r_4)^2+\Psi(r_5)^2+\Psi(r_6)^2+\Psi(r_7)^2\\ &+2\big(\Psi(r_1)\Psi(r_2)\cos(\Omega_2-\Omega_1)+\Psi(r_1)\Psi(r_3)\cos(\Omega_3-\Omega_1)+\Psi(r_1)\Psi(r_4)\cos(\Omega_4-\Omega_1)\\ &+\Psi(r_1)\Psi(r_5)\cos(\Omega_5-\Omega_1)+\Psi(r_1)\Psi(r_6)\cos(\Omega_6-\Omega_1)+\Psi(r_1)\Psi(r_7)\cos(\Omega_7-\Omega_1)\\ &+\Psi(r_2)\Psi(r_3)\cos(\Omega_3-\Omega_2)+\Psi(r_2)\Psi(r_4)\cos(\Omega_4-\Omega_2)+\Psi(r_2)\Psi(r_5)\cos(\Omega_5-\Omega_2)\\ &+\Psi(r_2)\Psi(r_6)\cos(\Omega_6-\Omega_2)+\Psi(r_2)\Psi(r_7)\cos(\Omega_7-\Omega_2)+\Psi(r_3)\Psi(r_4)\cos(\Omega_4-\Omega_3)\\ &+\Psi(r_3)\Psi(r_5)\cos(\Omega_5-\Omega_3)+\Psi(r_3)\Psi(r_6)\cos(\Omega_6-\Omega_3)+\Psi(r_3)\Psi(r_7)\cos(\Omega_7-\Omega_3)\\ &+\Psi(r_4)\Psi(r_5)\cos(\Omega_5-\Omega_4)+\Psi(r_4)\Psi(r_6)\cos(\Omega_6-\Omega_4)+\Psi(r_4)\Psi(r_7)\cos(\Omega_7-\Omega_4)\\ &+\Psi(r_5)\Psi(r_6)\cos(\Omega_6-\Omega_5)+\Psi(r_5)\Psi(r_7)\cos(\Omega_7-\Omega_5)+\Psi(r_6)\Psi(r_7)\cos(\Omega_7-\Omega_6)\big)\end{aligned} \tag{7.6}$$

In Figures 7.2 and 7.3, two calculated interferograms, using Equation (7.4), for the N-slit interferometer, with $N = 50$, and $D_{\langle d|j\rangle} = 25$ cm, are shown for $\lambda_1 = 589$ nm and $\lambda_2 = 590$ nm, respectively.

Careful scrutiny of the spatial profile of the calculated probabilities reveals discernible differences. The wavelength sensitivity of multiple-beam interferometry has

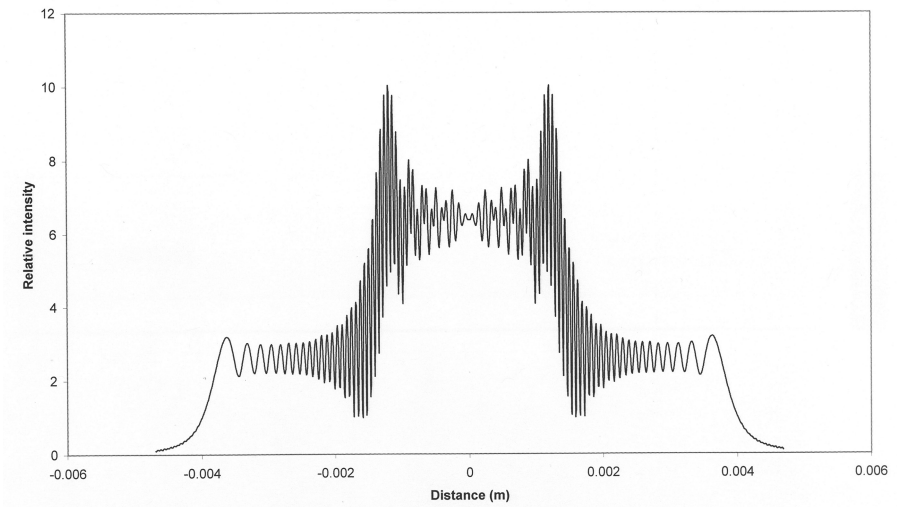

FIGURE 7.2 Interferogram at $\lambda_1 = 589$ nm. These calculations are for slits 30 μm wide, separated by 30 μm, and $N = 50$. The j to d distance is $D_{\langle d|j\rangle} = 25$ cm.

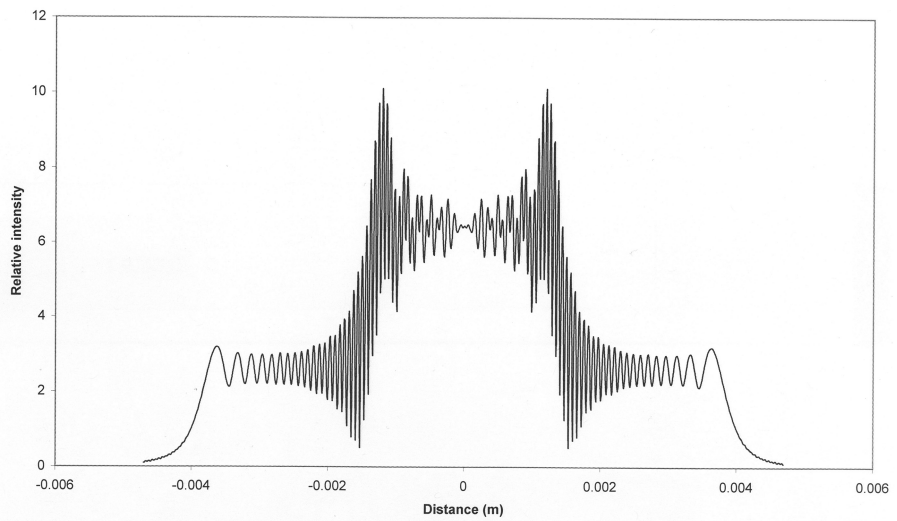

FIGURE 7.3 Interferogram at $\lambda_2 = 590$ nm. These calculations are for slits 30 μm wide, separated by 30 μm, and $N = 50$. The j to d distance is $D_{\langle d|j\rangle} = 25$ cm.

its origin in the phase information of the equations describing the behavior of the interferometric signal. In the case of the *N*-slit interferometer the interferometric profile is characterized by the interferometric Equation (7.3) or its equivalent Equation (7.4). This equation includes a phase difference term that, as explained in Chapter 4, can be expressed as

$$\cos\left((\theta_m - \theta_j) \pm (\phi_m - \phi_j)\right) = \cos\left(|l_m - l_{m-1}|\, k_1 \pm |L_m - L_{m-1}|\, k_2\right) \tag{7.7}$$

where

$$k_1 = \frac{2\pi n_1}{\lambda_v} \tag{7.8}$$

and

$$k_2 = \frac{2\pi n_2}{\lambda_v} \tag{7.9}$$

Here, $\lambda_1 = \lambda_v / n_1$ and $\lambda_1 = \lambda_v / n_2$ where λ_v is the vacuum wavelength and n_1 and n_2 are the corresponding indexes of refraction (Wallenstein and Hänsch, 1974; Born and Wolf, 1999). Hence, it is easy to see that different wavelengths will produce different interferograms. Hence, one of the applications of the *N*-slit interferometer is as a wavelength meter. For a given set of geometrical parameters measured interferograms can be matched, in an iterative process, with theoretical interference patterns to determine the wavelength of the radiation. Again, resolution depends on the optical path length between the slit array and the digital detector, the size of the pixels, and the linearity of the detector. In this regard, increased resolution in CCD and CMOS detectors should improve significantly the wavelength resolution achievable with the *N*-slit interferometer. This, coupled with the simplicity of the optics, should enhance *considerably the application perspectives of this interferometer as a wavelength meter*. For a review in the subject of wavelength meters, the reader should refer to Demtröder (2003).

Further applications of the *N*SLI are described by Duarte (2016) and include interferometric imaging, microdensitometry, microscopy, and secure optical communications (see Chapter 8).

7.3 THE HANBURY BROWN–TWISS INTERFEROMETER

The Hanbury Brown–Twiss effect originates in interferometric measurements performed by an 'intensity interferometer' used for astronomical observations (Hanbury Brown and Twiss, 1956). A diagram of the stellar intensity interferometer used to determine the diameter of stars is depicted in Figure 7.4. Feynman in one of his exercises to the *Feynman Lectures in Physics* (Feynman et al., 1965) explains that the electrical currents from the two detectors are mixed in a coincidence circuit in which the currents become indistinguishable. Feynman then asks to show that the coincidence counting rate, in the Hanbury Brown–Twiss configuration, is proportional to an expression of the form

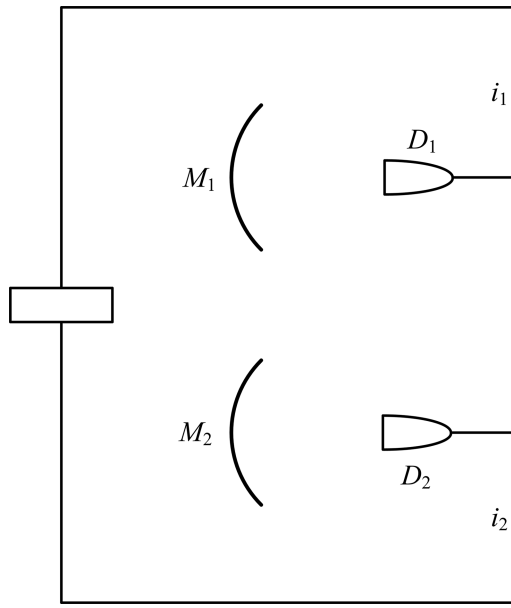

FIGURE 7.4 The Hanbury Brown and Twist interferometer. The light, from an astronomical source, is collected at mirrors M_1 and M_2, and focused onto detectors D_1 and D_2. The current generated at these detectors, i_1 and i_2, interfere with the electronics to produce an interference signal characterized by an equation of the form of Equation (7.13).

$$2 + 2\cos k(R_2 - R_1) \tag{7.10}$$

where R_1 and R_2 are the distances from detectors 1 and 2 to the source. Using the N-slit interferometric equation (Duarte, 1991, 1993)

$$\left|\langle d|s\rangle\right|^2 = \sum_{j=1}^{N} \Psi(r_j)^2 + 2\sum_{j=1}^{N} \Psi(r_j)\left(\sum_{m=j+1}^{N} \Psi(r_m)\cos(\Omega_m - \Omega_j)\right) \tag{7.11}$$

with $N = 2$ one immediately arrives at

$$\left|\langle d|s\rangle\right|^2 = \Psi(r_1)^2 + \Psi(r_2)^2 + 2\Psi(r_1)\Psi(r_2)\cos(\Omega_2 - \Omega_1)$$

and setting $\Psi(r_1) = \Psi(r_2) = 1$

$$\left|\langle d|s\rangle\right|^2 = 2 + 2\cos(\Omega_2 - \Omega_1) \tag{7.12}$$

Now, using (as suggested by Feynman) $\Omega_1 = kR_1$ and $\Omega_2 = kR_2$

$$\left|\langle d|s\rangle\right|^2 = 2 + 2\cos k(R_2 - R_1) \tag{7.13}$$

From the measured signal distribution, and these equations, the angular spread of the emission can be determined, and knowing the distance from the source to the detector, it becomes possible to estimate the diameter of the aperture at the emission; in other words, the diameter of the star under observation.

The Hanbury Brown–Twiss interferometric argument was not easily accepted by the physics community at the time given that many physicists erroneously thought of visible photons as uncorrelated particles arriving either at detector 1 or detector 2. In other words, many had not accepted the Dirac description of interference and did not understand the concept of coherent length. Feynman was very keen on the Hanbury Brown–Twiss interferometer and he thought of it as a pioneering experiment in quantum optics.

7.4 BEAM-SPLITTER INTERFEROMETERS

Two-beam interferometers are optical devices that divide and then recombine to form a light beam. It is on recombination of the beams that interference occurs. The most well-known two-beam interferometers are the Mach–Zehnder interferometer, the Michelson interferometer, the Sagnac interferometer, and the HOM interferometer.

For a highly coherent light beam, such as the beam from a narrow-linewidth laser, the coherence length

$$\Delta x \approx \frac{c}{\Delta \nu} \tag{7.14}$$

can be rather large, thus demanding a relatively large optical path length in the two-beam interferometer of choice. This relation provides an avenue to accurately determine the linewidth of a laser.

The following discussion on interferometry is based on the original chapter of the first edition plus material from reviews by Duarte (2003, 2022).

7.4.1 The Mach–Zehnder Interferometer

The Mach–Zehnder interferometer is illustrated in Figure 7.5. In this interferometer, the incident light beam is divided into two subbeams by a beam splitter. The reflected beam, on the incidence beam splitter, is then sent into a path defined by the reflection on M_1 toward the exit beam splitter. The transmitted beam, on the incidence beam splitter, is sent into a path defined by the reflection on M_2 toward the exit beam splitter.

Both counter-propagating beams are recombined at the exit beam splitter. The interference mechanics of the counter-propagating beams can be described using Dirac's notation via the superposition probability amplitude

$$\langle d|s\rangle = \langle d|k'\rangle\langle d|k'\rangle\langle k'|M_1\rangle\langle M_1|j\rangle\langle j|s\rangle + \langle d|k\rangle\langle k|M_2\rangle\langle M_2|j'\rangle\langle j'|s\rangle \tag{7.15}$$

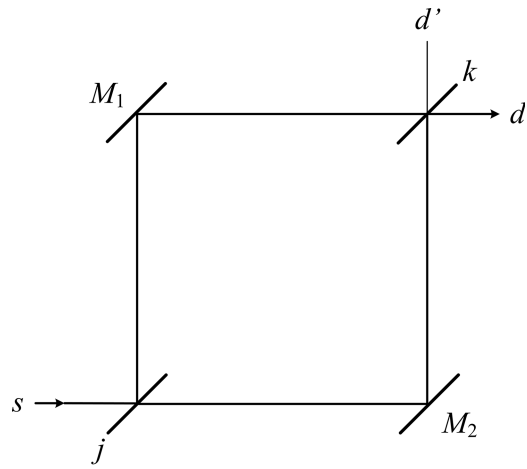

FIGURE 7.5 Mach–Zehnder interferometer configured with entrance (j) and exit (k) beam splitters and internal mirrors M_1 and M_2. In the schematics, d' represents a weak secondary output.

where j and k refer to the beam splitters in the reflective mode, while j' and k' refer to the beam splitters in the transmission mode. Assuming perfect reflectivity at the M_1 and M_2 mirrors, Equation (7.15) is equivalent to (Duarte 2003, 2014)

$$\langle d|s\rangle = \langle d|k'\rangle\langle k'|j\rangle\langle j|s\rangle + \langle d|k\rangle\langle k|j'\rangle\langle j'|s\rangle \tag{7.18}$$

Using the Dirac identity $|\phi\rangle = |j\rangle\langle j|\phi\rangle$, Equation (7.18) reduces to

$$\langle d|s\rangle = \langle d|k'\rangle\langle k'|C\rangle + \langle d|k\rangle\langle k|D\rangle \tag{7.19}$$

where

$$|C\rangle = |j\rangle\langle j|s\rangle \tag{7.20}$$

and

$$|D\rangle = |j'\rangle\langle j'|s\rangle \tag{7.21}$$

then, abstracting the $\langle d$ and normalizing, Equation (7.19) reduces to

$$|s\rangle = 2^{-1/2}\left(|E\rangle + |F\rangle\right) \tag{7.22}$$

where

$$|E\rangle = |k'\rangle\langle k'|C\rangle \tag{7.23}$$

and

$$|F\rangle = |k\rangle\langle k|D\rangle \tag{7.24}$$

and once its linear combination is considered, the overall probability amplitude becomes

$$|s\rangle = 2^{-1/2}\left(|E\rangle \pm |F\rangle\right) \tag{7.25}$$

For the d' detector

$$\langle d'|s\rangle = \langle d'|k\rangle\langle k|M_1\rangle\langle M_1|j\rangle\langle j|s\rangle + \langle d'|k'\rangle\langle k'|M_2\rangle\langle M_2|j'\rangle\langle j'|s\rangle \tag{7.26}$$

$$\langle d'|s\rangle = \langle d'|k\rangle\langle k|j\rangle\langle j|s\rangle + \langle d'|k'\rangle\langle k'|j'\rangle\langle j'|s\rangle \tag{7.27}$$

$$\langle d'|s\rangle = \langle d'|k\rangle\langle k|C\rangle + \langle d'|k'\rangle\langle k'|D\rangle \tag{7.28}$$

and ultimately to an equation of the form of (7.25). It should be noticed that if the mirrors M_1 and M_2 are not abstracted, the final result is still given by Equation (7.25).

Equation (7.25) is the probability amplitudes that describe single-photon propagation, or the propagation of an ensemble of indistinguishable photons, in Mach–Zehnder interferometers.

One final observation is that Equation (7.25) can be directly derived from the generalized Dirac–Feynman superposition probability amplitude

$$\langle d|s\rangle = \sum_{j=1}^{N=2}\langle d|j\rangle\langle j|s\rangle \tag{7.29}$$

for $N = 2$, which is applicable to the double-slit interferometer (see Chapter 4). However, physically speaking a Mach–Zehnder interferometer is very different to a double-slit interferometer. In the double-slit interferometer the single photon, or the ensemble of indistinguishable photons, undergoes violent diffraction at the slits. This diffraction makes the physics between the two interferometers quite different. The only similarity between the two interferometers is that they are both two-path interferometers, that is, $N = 2$. However, while the Mach–Zehnder interferometer is a *two-beam* interferometer the double-slit, two-slit, or Young, interferometer is a *parallel diffraction* interferometer (Duarte, 2019).

A prismatic Mach–Zehnder interferometer is illustrated in Figure 7.6. In this prismatic version of the Mach–Zehnder, there is asymmetry in regard to the intra-interferometric beam dimensions. The $P_1 - M_2 - P_2$ beam is expanded relatively to the $P_1 - M_1 - P_2$ beam. Moreover, in this particular example (based on a prism with a magnification of $k_{1,1} \approx 5$, see Chapter 12), there is also a power asymmetry since the unexpanded beam propagating in the $P_1 - M_1 - P_2$ arm has about 30% of the incident power, while the expanded beam $P_1 - M_2 - P_2$ carries the remaining 70% of the

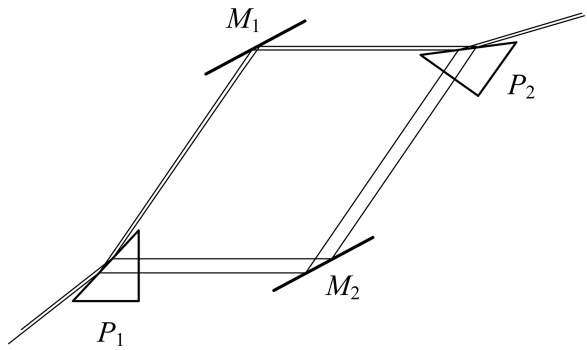

FIGURE 7.6 Prismatic Mach–Zehnder interferometer configured with $P_1 \rightarrow j$, M_1, and exit prism $P_2 \rightarrow k$.

incident power, for light polarized parallel to the plane of incidence. In this regard, it should be possible to design a prismatic Mach–Zehnder where the power density (W/m^2) in each arm is balanced. Applications for this type of interferometer include imaging and microscopy. Additional Mach–Zehnder interferometric configurations include transmission gratings as beam splitters (Steel, 1967).

7.4.2 The Michelson Interferometer

The Michelson interferometer (Michelson, 1927) is illustrated in Figure 7.7. In this interferometer, the incident light beam is divided into two subbeams by a beam splitter that serves both as input and output elements. The reflected beam, on the incidence beam splitter, is then sent into a path defined by the reflection on M_1 and back toward the exit beam splitter. The transmitted beam, on the incidence beam splitter,

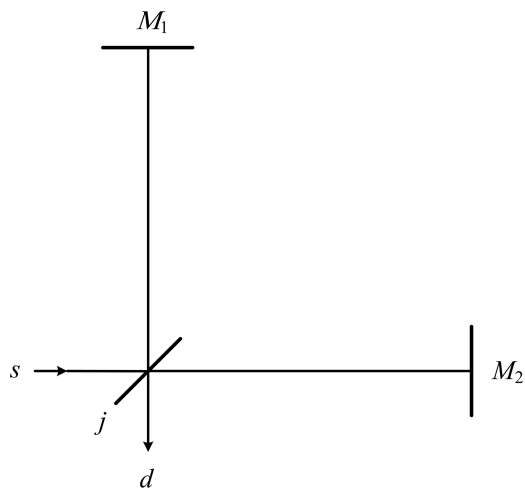

FIGURE 7.7 Michelson interferometer includes a single beam splitters and mirrors M_1 and M_2.

is sent into a path defined by the reflection on M_2 and back toward the exit beam splitter. Both beams are recombined interferometrically at the beam splitter. For the Michelson interferometer, the interference can be characterized using a probability amplitude of the form

$$\langle d|s\rangle = \langle d|j\rangle\langle j|M_2\rangle\langle M_2|j'\rangle\langle j'|s\rangle + \langle d|j'\rangle\langle j'|M_1\rangle\langle M_1|j\rangle\langle j|s\rangle \tag{7.30}$$

where j represents reflection at the beam splitter and j' stands for transmission.

Assuming perfect mirror reflectivity, Equation (7.30) can be abstracted to

$$\langle d|s\rangle = \langle d|j\rangle\langle j|j'\rangle\langle j'|s\rangle + \langle d|j'\rangle\langle j'|j\rangle\langle j|s\rangle \tag{7.31}$$

Further abstraction, using $|\phi\rangle = |j\rangle\langle j|\phi\rangle$, leads to

$$\langle d|s\rangle = \langle d|j\rangle\langle j|s\rangle + \langle d|j'\rangle\langle j'|s\rangle \tag{7.32}$$

which again leads to a probability amplitude of the form of Equation (7.29). Equation (7.32) can be expressed as

$$|s\rangle = 2^{-1/2}\left(|G\rangle \pm |H\rangle\right) \tag{7.33}$$

where

$$|G\rangle = |j\rangle\langle j|s\rangle \tag{7.34}$$

$$|H\rangle = |j'\rangle\langle j'|s\rangle \tag{7.35}$$

which is not surprising since the mirrors M_1 and M_2 are being treated as idealized perfect mirrors leaving all the physics to the beam splitter. A variant of the Michelson interferometer uses retroreflectors (Steel, 1967).

7.4.3 The Sagnac Interferometer

The Sagnac, or cyclic, interferometer is illustrated in Figure 7.8. In this interferometer, the incident light beam is divided into two subbeams by a beam splitter. The reflected beam, on the incidence beam splitter, is then sent into a path defined by the reflections on M_1, M_2, and M_3 mirrors. The transmitted beam, on the incidence beam splitter, is sent into a path defined by the reflections on M_3, M_2, and M_1 mirrors. Both counter-propagating beams are recombined at the beam splitter. The interference mechanics of the counter-propagating round trips can be described using Dirac's notation via the probability amplitude

$$\begin{aligned}\langle d|s\rangle = {} & \langle d|j\rangle\langle j|M_3\rangle\langle M_3|M_2\rangle\langle M_2|M_1\rangle\langle M_1|j\rangle\langle j|s\rangle \\ & + \langle d|j'\rangle\langle j'|M_1\rangle\langle M_1|M_2\rangle\langle M_2|M_3\rangle\langle M_3|j'\rangle\langle j'|s\rangle\end{aligned} \tag{7.36}$$

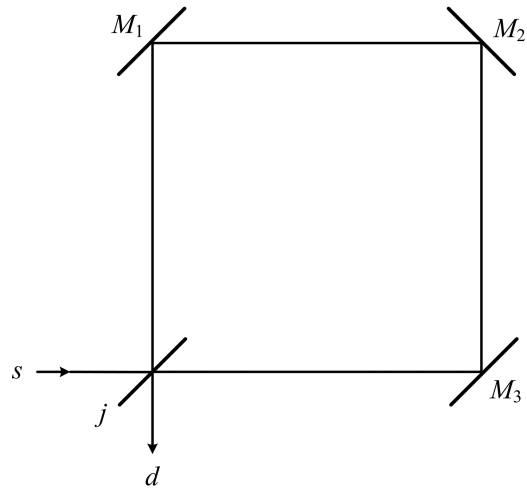

FIGURE 7.8 Sagnac interferometer. All three mirrors M_1, M_2, and M_3 are assumed to be identical. For the description given in the text, the beam splitter is assumed to be lossless and to divide the incident beam exactly into two components half the intensity of the original beam.

Assuming perfect reflectivity at the mirrors

$$\langle j|M_3\rangle\langle M_3|M_2\rangle\langle M_2|M_1\rangle\langle M_1|j\rangle = 1 \tag{7.37}$$

$$\langle j'|M_1\rangle\langle M_1|M_2\rangle\langle M_2|M_3\rangle\langle M_3|j'\rangle = 1 \tag{7.38}$$

and Equation (7.36) reduces to

$$\langle d|s\rangle = \langle d|j\rangle\langle j|s\rangle + \langle d|j'\rangle\langle j'|s\rangle \tag{7.39}$$

which can ultimately be expressed as

$$|s\rangle = 2^{-1/2}\left(|I\rangle \pm |J\rangle\right) \tag{7.40}$$

where

$$|I\rangle = |j\rangle\langle j|s\rangle \tag{7.41}$$

and

$$|J\rangle = |j'\rangle\langle j'|s\rangle \tag{7.42}$$

Again, it should be noted that the physics of Equation (7.40) can be traced back to the Dirac–Feynman probability amplitude given in Equation (7.29).

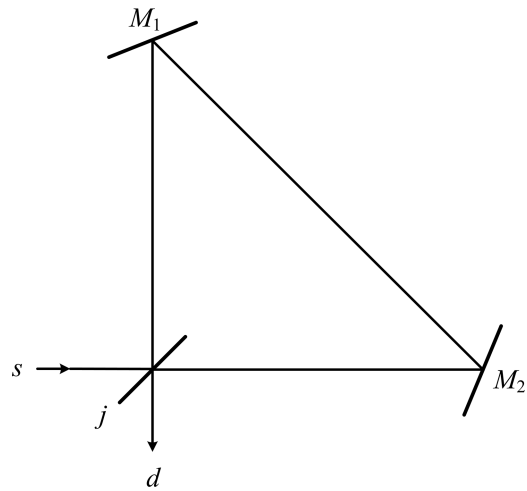

FIGURE 7.9 Sagnac interferometer in a triangular configuration.

The alternative triangular Sagnac interferometer, with only two mirrors (M_1 and M_2), illustrated in Figure 7.9, leads to

$$\begin{aligned}\langle d|s\rangle = &\langle d|j\rangle\langle j|M_2\rangle\langle M_2|M_1\rangle\langle M_1|j\rangle\langle j|s\rangle \\ &+\langle d|j'\rangle\langle j'|M_1\rangle\langle M_1|M_2\rangle\langle M_2|j'\rangle\langle j'|s\rangle\end{aligned} \tag{7.43}$$

with the same conclusions as with the Sagnac interferometer with three mirrors.

7.4.4 The HOM Interferometer

This description of the HOM interferometer (Hong et al., 1987), illustrated in Figure 7.10, follows the review given in Duarte (2022). An equivalent optical diagram, assuming identical detectors $d_1 = d_2 = d$, is given in Figure 7.11 (Duarte and Taylor, 2021). The incident quanta are assumed to be *identical* and *indistinguishable*.

Using Dirac–Feynman interferometric principle (Dirac, 1958; Feynman et al., 1965)

$$\langle d|s\rangle = \sum_{j=1}^{N}\langle d|m\rangle\langle m|s\rangle \tag{7.44}$$

$$\langle d|s\rangle = \langle d|m'\rangle\langle m'|s\rangle + \langle d|m\rangle\langle m|s\rangle \tag{7.45}$$

$$|s\rangle = |m'\rangle\langle m'|s\rangle + |m\rangle\langle m|s\rangle \tag{7.46}$$

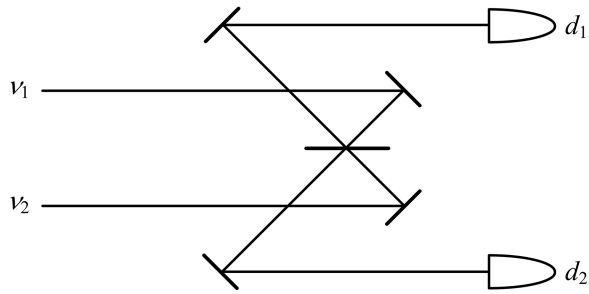

FIGURE 7.10 HOM interferometer (Duarte, F. J., *Fundamentals of Quantum Entanglement*, 2nd ed. Institute of Physics, Bristol, 2022, © IOP Publishing. Reproduced with permission. All rights reserved).

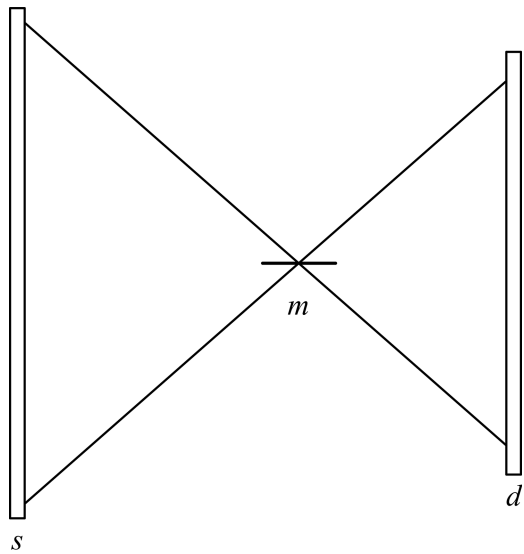

FIGURE 7.11 Optical equivalent for the HOM interferometer (Duarte, F. J., *Fundamentals of Quantum Entanglement*, 2nd ed. Institute of Physics, Bristol, 2022, © IOP Publishing. Reproduced with permission. All rights reserved).

where m is for the beam splitter in its reflection mode and m' is for the beam splitter in its transmission mode.

Using the Dirac identity $|\phi\rangle = |i\rangle\langle i|\phi\rangle$, Equation (7.46) can be abstracted into an equation of the form

$$|s\rangle = \left(|\gamma\rangle + |\delta\rangle\right) \tag{7.47}$$

Using the Dirac identity (see Chapter 6)

$$|X\rangle = |a\rangle_1 |b\rangle_2 |c\rangle_3 \ldots |g\rangle_n \tag{7.48}$$

allow us to apply the identities

$$|\gamma\rangle = |x\rangle_1 |y\rangle_2 \tag{7.49}$$

$$|\delta\rangle = |y\rangle_1 |x\rangle_2 \tag{7.50}$$

so that (see Chapter 15)

$$|\psi\rangle = \left(|x\rangle_1 |y\rangle_2 + |y\rangle_1 |x\rangle_2\right) \tag{7.51}$$

Taking into consideration its linear combination and normalizing lead again to the quantum entanglement states

$$|\psi\rangle_{\pm} = 2^{-1/2}\left(|x\rangle_1 |y\rangle_2 \pm |y\rangle_1 |x\rangle_2\right) \tag{7.52}$$

which equivalent to

$$|\psi\rangle_{+} = 2^{-1/2}\left(|\gamma\rangle + |\delta\rangle\right) \tag{7.53}$$

$$|\psi\rangle_{-} = 2^{-1/2}\left(|\gamma\rangle - |\delta\rangle\right) \tag{7.54}$$

In matrix form, Equations (7.53) and (7.54) can be expressed as

$$\begin{pmatrix} |\psi\rangle_{+} \\ |\psi\rangle_{-} \end{pmatrix} = 2^{-1/2}\begin{pmatrix} 1 & 1 \\ 1 & -1 \end{pmatrix}\begin{pmatrix} |\gamma\rangle \\ |\delta\rangle \end{pmatrix} \tag{7.55}$$

where the matrix corresponds to the matrix for the Hadamard gate (see Chapter 19)

$$H_G = 2^{-1/2}\begin{pmatrix} 1 & 1 \\ 1 & -1 \end{pmatrix} \tag{7.56}$$

which is widely associated with representing the quantum beam splitter and used in the description of the HOM interferometer.

7.5 MULTIPLE-BEAM INTERFEROMETERS

The Fabry–Perot interferometer depicted in Figure 7.12 can be described as a multiple-beam interferometer. This interferometer is also considered in Appendix B as an *intracavity etalon*. Generally, intracavity etalons are a solid slab of optical glass, or fused silica, with highly parallel surfaces coated to increase reflectivity (Figure 7.12a). These are also known as Fabry–Perot etalons. Fabry–Perot interferometers, on the other hand, are constituted by two separate slabs of optical flats with

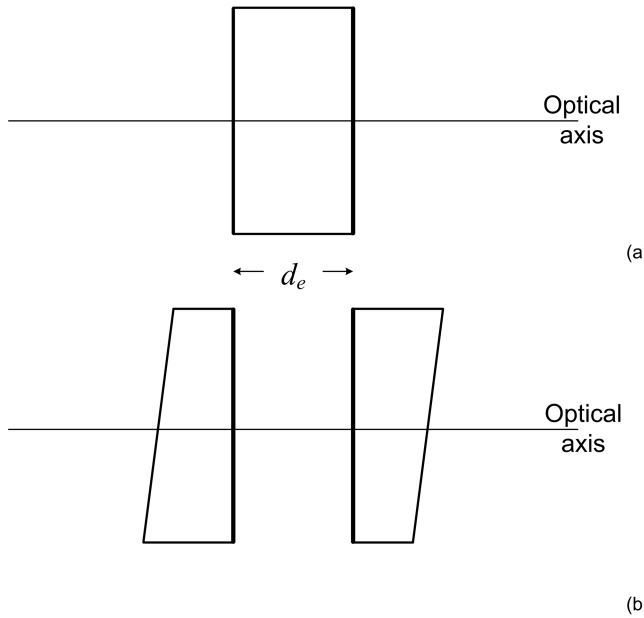

FIGURE 7.12 (a) Frabry-Perot etalon and (b) Fabry-Perot interferometer. Darker lines represent coated surfaces.

their inner surfaces coated as shown in Figure 7.12b. The space between the two coated surfaces is filled with air or other inert gas. The optical flats in a Fabry–Perot interferometer are mounted on rigid metal bars, with a low thermal expansion coefficient, such as invar. The plates can be moved, with micrometer precision or better, to vary the free spectral range (*FSR*).

These interferometers are widely used to characterize and quantify the laser linewidth.

In Chapter 3, we saw that alternative forms of the uncertainty principle

$$\Delta x\, \Delta p \approx h \tag{7.57}$$

are

$$\Delta x\, \Delta\lambda \approx \lambda^2 \tag{7.58}$$

and

$$\Delta x\, \Delta\nu \approx c \tag{7.59}$$

For *solid* Fabry–Perot etalons made of optical glass with refractive index n, $\Delta x = 2nd_e$, and $\Delta\lambda$ becomes the free spectral range (*FSR*) so that

$$FSR \approx \frac{\lambda^2}{2nd_e} \tag{7.60}$$

and in the frequency domain

$$FSR \approx \frac{c}{2nd_e} \tag{7.61}$$

For an air-spaced Fabry–Perot interferometer, $n = 1$ and $\Delta x = 2d_e$.

A Fabry–Perot interferogram generated with a narrow-linewidth laser is shown in Figure 7.13. The *FSR* corresponds to the separation of the rings, and a measure of the width of the rings determines the linewidth of the emission being observed. The minimum resolvable linewidth $\Delta\nu_{FRS}$ is given by

$$\Delta\nu_{FRS} = \frac{FRS}{\mathcal{F}} \tag{7.62}$$

where $\mathcal{F}$ is the *effective finesse*. Thus, a Fabry–Perot etalon with a $FRS = 7.0$ GHz $\mathcal{F} = 50$ provides discrimination down to $\Delta\nu_{FRS} \approx 140$ MHz. The finesse is a function of the flatness of the surfaces (often in the $\lambda/100$–$\lambda/50$ range), the dimensions of the

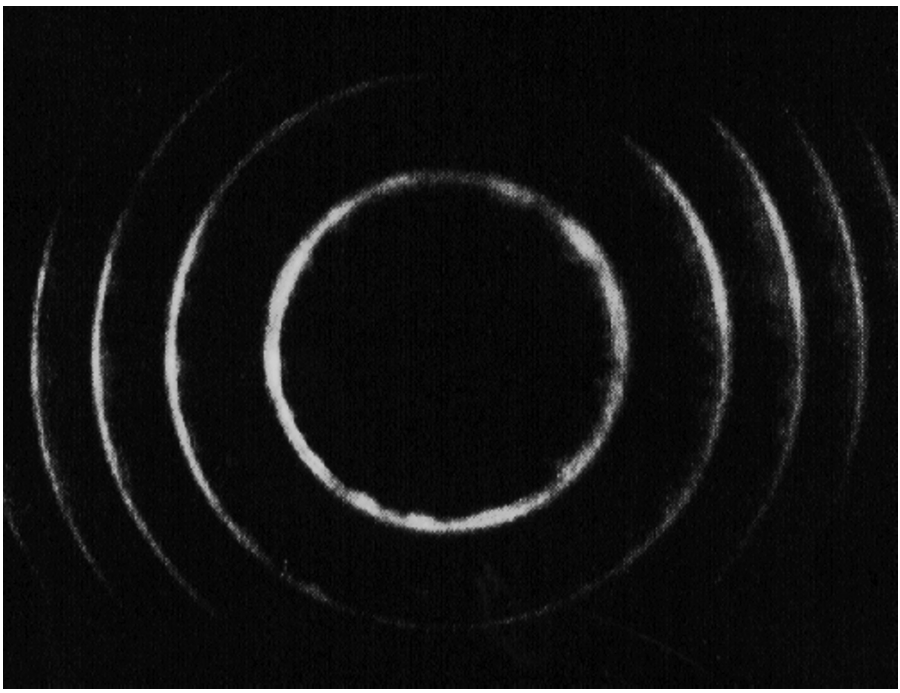

FIGURE 7.13 Fabry–Perot interferogram depicting single-longitudinal-mode oscillation, at $\Delta\nu \approx 500$ MHz, from a tunable multiple-prism grating solid-state oscillator (Reproduced from Duarte, F. J., *Opt. Commun.* **117**, 480–484, 1995, with permission from Elsevier).

aperture, and the reflectivity of the surfaces. The *FSR* concept also applies to laser cavities as discussed in Appendix B.

The effective finesse of a Fabry–Perot interferometer is given by (Meaburn, 1976)

$$\mathcal{F}^{-2} = \mathcal{F}_{\mathcal{R}}^{-2} + \mathcal{F}_{F}^{-2} + \mathcal{F}_{A}^{-2} \tag{7.63}$$

where $\mathcal{F}_{\mathcal{R}}$, $\mathcal{F}_{F}$, and $\mathcal{F}_{A}$ are the reflective, flatness, and aperture finesses, respectively. The reflective finesse is given by (Steel, 1967; Born and Wolf, 1999)

$$\mathcal{F}_{\mathcal{R}} = \frac{\pi\sqrt{\mathcal{R}}}{(1-\mathcal{R})} \tag{7.64}$$

where $\mathcal{R}$ is the reflectivity.

The mechanics of multiple-beam interferometry can be described in some detail considering the multiple reflection, and refraction, of a beam incident on two parallel surfaces separated by a region of refractive index n as illustrated in Figure 7.14. In this configuration, at each point of reflection and refraction, a fraction of the beam, or a subbeam, is transmitted toward the boundary region. Following propagation, these subbeams propagate, diverge, and subsequently interfere. In this regard, the physics is similar to that of the N-slit interferometer with the exception that each parallel beam has less intensity due to the increasing number of reflections. Here, for transmission, interference can be described using a series of probability amplitudes representing the events depicted in Figure 7.14 (Duarte, 2003).

$$\langle d|s\rangle = \sum_{m=1}^{N}\sum_{l=1}^{N}\sum_{k=1}^{N}\sum_{j=1}^{N}\langle d|m\rangle\langle m|l\rangle\langle l|k\rangle\langle k|j\rangle\langle j|s\rangle \tag{7.65}$$

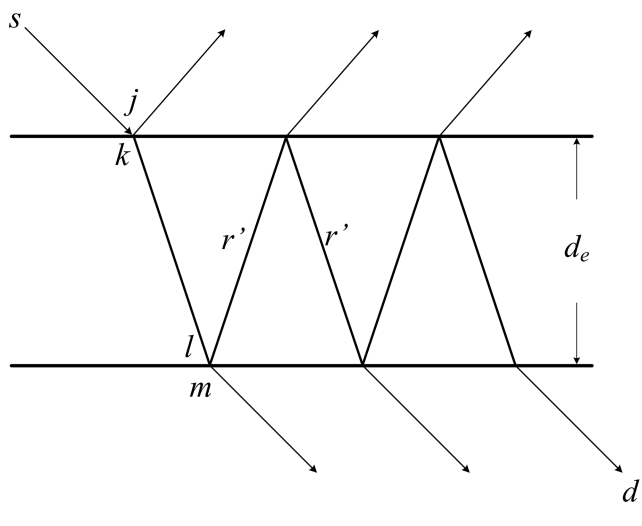

FIGURE 7.14 Multiple-beam interferometer diagram illustrating the multiple internal reflection geometry.

where j is at the reflection surface of incidence, k is immediately next to the surface of reflection, l is at the second surface of reflection, and m is immediately next to the second surface of reflection as illustrated in Figure 7.14. From s to l, the overall probability amplitude can be written as

$$\langle l|k\rangle\langle k|j\rangle\langle j|s\rangle = A_j t \tag{7.66}$$

which represents a probability amplitude attenuated by a transmission factor t. Thus, Equation (7.65) reduces to an equation of the form

$$\langle d|s\rangle = A_j t \sum_{m=1}^{N} \langle d|m\rangle\langle m|l\rangle \tag{7.67}$$

which, as seen previously, gives rise to a probability interferometric pattern. Each m point on the exit surface of the interferometric slab gives origin to a beam that will interfere with adjacent m beams while propagating to the interferometric plane d.

7.6 THE RAMSEY INTERFEROMETER

Finally, we very briefly touch on a different types of interferometer: the Ramsey interferometer, which was discovered by Norm Ramsey around 1950 (Ramsey, 1950, 1990). This is a very different type of interferometer to those described previously since it uses atoms rather than photons as the interfering entities. In the Ramsey interferometer, the laser, or photon source, is replaced by an atom source as described in Figure 7.15. In its path toward the detector, the atom beam is allowed to interact with microwave radiation at two places. The first place is near the source and the second is near the detector. At each of those spatial sections, the microwave field is allowed to modulate the state of the atoms. Defining P_g as the probability of being in the ground state and P_e the probability of being in the excited state (Haroche et al., 2013)

$$P_g = (1 - P_e) = \frac{(1 - \cos\varphi)}{2} \tag{7.68}$$

where the angle φ represents the phase difference between the ground state and the excited state. If $\varphi = 2\pi m$ (where m is an integer), the states are in phase, and thus there is constructive interference. In other words, when $\varphi = 2\pi m$ there is atomic coherence.

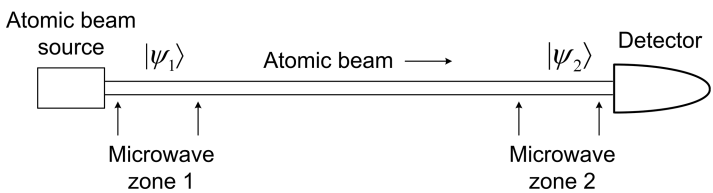

FIGURE 7.15 Simplified depiction of the Ramsey interferometer showing the source of atomic beam and microwave field regions 1 and 2. Sources of atomic beams include laser-cooled cesium and rubidium.

The origin of Equation (7.68) can be outlined using the relevant Dirac notation, introduced in Chapter 15. The probability amplitude of the initial unmodulated state can be defined as

$$|\psi\rangle_1 = 2^{-1/2}\left(|a\rangle + |b\rangle\right) \tag{7.69}$$

and the probability amplitude of the modulated state as

$$|\psi\rangle_2 = 2^{-1/2}\left(|a\rangle + e^{i\varphi}|b\rangle\right) \tag{7.70}$$

Multiplying Equation (7.70) with its complex conjugate leads to a probability of the form

$$P_e = \frac{(1+\cos\varphi)}{2} \tag{7.71}$$

and using $P_g = (1 - P_e)$ enable us to write $P_g = \dfrac{(1-\cos\varphi)}{2}$ as given in Equation (7.68).

The phase angle itself is a function of the frequency difference between the frequency of the transition (between the ground state and the excited state, i.e., ν_{eg}) and the microwave frequency ν (Haroche et al., 2013): $\varphi = 2\pi(\nu_{eg} - \nu)\Delta t$. Thus, the interference pattern produced is a function of $(\nu_{eg} - \nu)$. Locking the microwave frequency to the transition frequency, that is $\nu = \nu_{eg}$, yields a time standard anchored to the atomic transition (Haroche et al., 2013). This principle, coupled to laser-cooled atomic beams, is central to the technology of atomic clocks.

PROBLEMS

7.1 Use the generalized probability given in Equation (7.4) to arrive at an explicit

$$\langle d|s\rangle\langle d|s\rangle^* \text{ for } N = 3.$$

7.2 Interferometric measurements with a Hanbury Brown–Twiss type interferometer yield a measured angular spread of $\Delta\theta \approx 5.94$ milli arc second from the emission from the Sirius. Determine the radius of this star (Hint: 1 milli arc second is 4.8481368×10^{-9} radians and the distance to Sirius is approximately 8.6 light-years).

7.3 A laser beam fails to provide interference fringes when the length of each of the arms, in a Mach–Zehnder interferometer, is 1 m. Estimate the linewidth of the laser in Hz units. Note: the arms are defined by the beam paths $j - M_1 - k$ and $j - M_2 - k$.

7.4 Using the usual complex-wave representation for probability amplitudes use Equation (7.18) to arrive at an equation for the probability of transmission in a Mach–Zehnder interferometer.

7.5 Show that Equation (7.28) can be expressed in the form of Equation (7.25).

7.6 Show that Equation (7.43) can be expressed in the form of Equation (7.40).

7.7 Starting from Equation (7.70) arrive at Equation (7.68).

REFERENCES

Born, M., and Wolf, E. (1999). *Principles of Optics*, 7th ed. Cambridge University, Cambridge, U.K.

Demtröder, W. (2003). *Laser Spectroscopy*, 3rd ed. Springer-Verlag, Berlin.

Dirac, P. A. M. (1958). *The Principles of Quantum Mechanics*, 4th ed. Oxford University, Oxford, U.K.

Duarte, F. J. (1991). Dispersive dye lasers. In *High Power Dye Lasers* (Duarte, F. J., ed.). Springer-Verlag, Berlin, Chapter 2, pp. 7–43.

Duarte, F. J. (1993). On a generalized interference equation and interferometric measurements. *Opt. Commun.* 103, 8–14.

Duarte, F. J. (1995). Solid-sate dispersive dye laser oscillator: very compact cavity. *Opt. Commun.* 117, 480–484.

Duarte, F. J. (1998). Interference of two independent sources. *Am. J. Phys.* 66, 662–663.

Duarte, F. J. (1999). Multiple-prism grating solid-state dye laser oscillator: optimized architecture. *Appl. Opt.* 38, 6347–6349.

Duarte, F. J. (2003). *Tunable Laser Optics*, Elsevier-Academic, New York.

Duarte, F. J. (2008). Coherent electrically excited organic semiconductors: coherent or laser emission? *Appl. Phys. B*. 90, 101–108.

Duarte, F. J. (2014). *Quantum Optics for Engineers*, 1st ed. CRC, Boca Raton, FL.

Duarte, F. J. (2016). Interferometric imaging. In *Tunable Laser Applications*, 3rd ed. (Duarte, F. J., ed.). CRC, Boca Raton, FL, Chapter 10, pp. 329–369.

Duarte, F. J. (2019). *Fundamentals of Quantum Entanglement*, 1st ed. Institute of Physics, Bristol, U.K.

Duarte, F. J. (2022). *Fundamentals of Quantum Entanglement*, 2nd ed. Institute of Physics, Bristol, U.K.

Duarte, F. J., and Taylor, T. S. (2021). *Quantum Entanglement Engineering and Applications*, Institute of Physics, Bristol, U.K.

Feynman, R. P., Leighton, R. B., and Sands, M. (1965). *The Feynman Lectures on Physics*, Vol. III, Addison-Wesley, Reading, MA.

Hanbury Brown, R., and Twiss, R. Q. (1956). A test of a new type of stellar interferometer on Sirius. *Nature* 178, 1046–1048.

Haroche, S., Brune, M., and Raimond, J.-M. (2013). Atomic clocks for controlling light fields. *Phys. Today* 66 (1), 27–32.

Hong, C. K., Ou, Z. Y., and Mandel, L. (1987). Measurements of subpicosecond time intervals between two photons by interference. *Phys. Rev. Lett.* 59, 2044–2046.

Lamb, W. E. (1995). Anti-photon. *Appl. Phys. B*. 60, 77–84.

Meaburn, J. (1976). *Detection and Spectrometry of Faint Light*, Reidel, Boston, MA.

Michelson, A. A. (1927). *Studies in Optics*, University of Chicago, Chicago, IL.

Ramsey, N. F. (1950). A molecular beam resonance method with separated oscillating fields. *Phys. Rev.* 78, 695–699.

Ramsey, N. F. (1990). Experiments with separated oscillatory fields and hydrogen masers. *Rev. Mod. Phys.* 62, 541–552.

Steel, W. H. (1967). *Interferometry*, Cambridge University, Cambridge, U.K.

Wallenstein, R., and Hänsch, T. W. (1974). Linear pressure tuning of a multielement dye laser spectrometer. *Appl. Opt.* 13, 1625–1628.

8 Quantum Interferometric Communications in Free Space

8.1 INTRODUCTION

The *N*-slit laser interferometer (*N*SLI) was first introduced to secure free-space optical communications in 2002. Albeit its initial propagation distance in the laboratory was only 10 cm, it was envisioned as an interferometric tool ideally suited for propagation in the vacuum, or outer space (Duarte, 2002). Subsequently, *N*SLI experiments have also been conducted over hundreds of meters, in the field, via open atmosphere (Duarte et al., 2010, 2011).

The idea is that an *N*-slit interferometric signal, designated as an *interferometric character*, or a series of interferometric characters can be used to transmit information securely from one point in space to another point in space. The interferometric character propagates from its origin (s) to its destiny, the interference plane (d) (see Figure 8.1), while the integrity of the character itself is secured by quantum interference principles.

In other words, attempts to optically intercept the interferometric character severely distort its spatial and intensity profile, thus informing the receiver that the message has been compromised. Hence, the security of this free-space communications method rests simply on the principle that any optical attempt to intercept causes the collapse of the interferometric character. This means that, in its most basic form, no security key, or code, is necessary. However, a code could be easily added as an extra layer of security (see Figure 8.1).

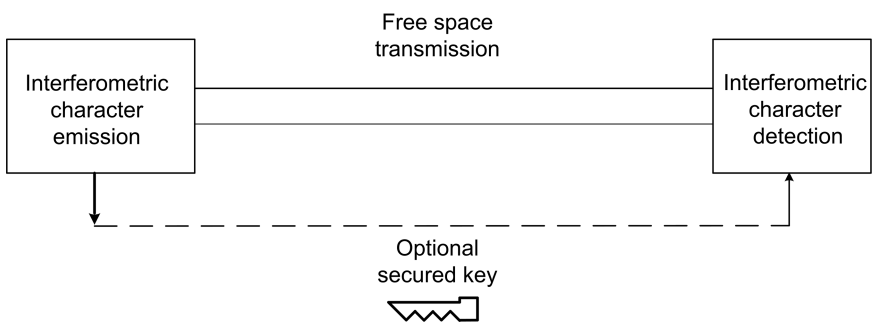

FIGURE 8.1 Cryptographic diagram applicable to *N*-slit interferometric communications in free space.

DOI: 10.1201/9781003398707-8

Interest in secure optical communications in free space appears to be driven as a matter of principle and by practical reasons such as saturation in the spectrum of traditional radio frequency communications (Hogan, 2013). A brief historical review of free-space optical communications is given by Duarte (2002).

8.2 THEORY

The probability amplitude for propagation from the source (s) to the interferometric plane (d), via the slit array (j), as illustrated in Figure 8.2, can be expressed using Dirac's notation (Duarte, 1993)

$$\langle d|s\rangle = \sum_{j=1}^{N} \langle d|j\rangle \langle j|s\rangle \tag{8.1}$$

Assigning each probability amplitude a complex wave function as taught by Dirac (1958), and following some algebra (see Chapter 4), leads to the generalized one-dimensional N-slit interferometric equation (Duarte, 1991, 1993)

$$\langle d|s\rangle\langle d|s\rangle^{*} = \sum_{j=1}^{N} \Psi(r_j)^2 + 2\sum_{j=1}^{N} \Psi(r_j) \left(\sum_{m=j+1}^{N} \Psi(r_m)\cos(\Omega_m - \Omega_j) \right) \tag{8.2}$$

where $\Psi(r_j)$ are complex wave functions (Dirac, 1958; Duarte, 2004), and the term in parenthesis is the phase that describes the exact geometry of the N-slit interferometer (Duarte, 1991, 1993). As explained by Duarte (2004), the measured intensity is proportional to the probability, that is,

$$I \propto \langle d|s\rangle\langle d|s\rangle^{*} \tag{8.3}$$

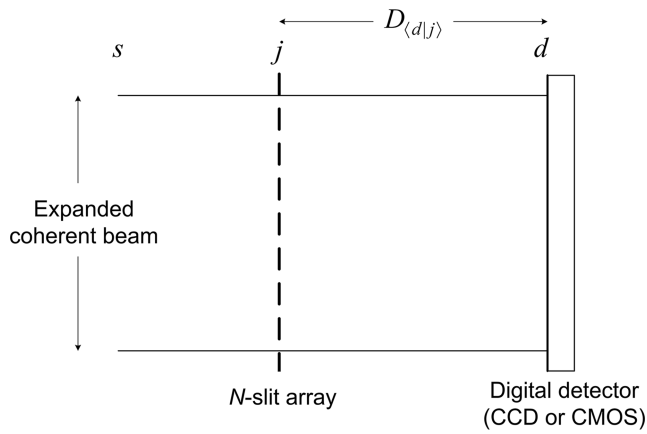

FIGURE 8.2 Top view of the N-slit laser interferometer highlighting the intra-interferometric path $D_{\langle d|j\rangle}$.

and it is this probability (Born, 1926)

$$\langle d|s\rangle\langle d|s\rangle^{*} = \left|\langle d|s\rangle\right|^{2} \tag{8.4}$$

that provides the *spatial distribution* of the observed intensity (see Chapter 4).

It is important to emphasize that this equation was originally derived for *single-photon propagation* (Duarte, 1993) albeit in practice, it also applies to the propagation of *ensembles of indistinguishable photons*, as in the case of narrow-linewidth laser emission (Duarte, 1993, 2003). In the material discussed here, the illumination is via ensembles of indistinguishable photons. The generalized *N*-slit interferometric equation accurately describes measurements performed in a macroscopic apparatus using quantum principles, and as such, it neatly follows the van Kampen (1988) criteria.

8.3 *N*-SLIT INTERFEROMETER FOR SECURE FREE-SPACE QUANTUM COMMUNICATIONS

The *N*SLI used for free-space optical communications is depicted in Figure 8.3. The essence of this method consists in the expanded beam illumination (*s*) of an *N*-slit array, or grating (*j*), where the interferometric characters are produced.

The interferometric character then propagates via the intra-interferometric distance ($D_{\langle d|j\rangle}$) until it reaches the interferometric plane at *d*. In other words, the generation, propagation, and detection of the interferometric characters take place within the *N*SLI, thus highlighting the conceptual and configurational simplicity of the interferometric approach.

The illumination section of the *N*SLI requires a single-transverse-mode narrow-linewidth laser. For the experiments described here, the coherent source is a He–Ne laser yielding 2 mW in a TEM_{00} laser beam at $\lambda = 632.82$ nm. The laser is followed by neutral density filters. Following the attenuation stage, a two-dimensional telescopic beam expander ($M \approx 10$) includes a 25 μm spatial filter. The expanded beam then undergoes one-dimensional multiple-prism beam expansion, thus yielding an

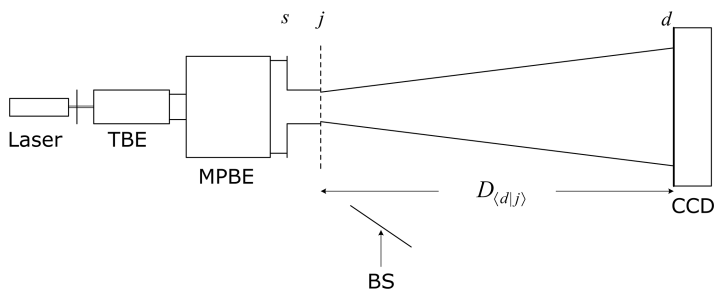

FIGURE 8.3 Top perspective of the optical architecture of the *N*-slit laser interferometer, see text for details. Also included in this diagram is a thin beam splitter (BS), inserted at the Brewster angle (relative to the optical axis), to intercept the propagating interferometer or the interferometric characters.

elongated near-Gaussian beam of ~10 mm maximum height by ~50 mm maximum width. Following the prismatic beam expander, a high-precision chromium master grating (j in Figure 8.3) is positioned.

The high-precision master gratings have rather large dimensions. For instance, one of the gratings utilized has 570 μm slits separated by 570 μm isles, and the other grating has 1000 μm slits separated by 1000 μm isles. The tolerances in the slits dimensions are quoted by the manufacturer as 0.5 μm. The 570 μm grating has a total of 44 slits and the 1000 μm grating has a total of 25 slits. The overall ruled area is 50 mm × 50 mm (Duarte et al., 2010).

The digital detector, deployed at the interferometric plane (d), is a digital detector (either CCD or CMOS) with pixels in the 20–25 μm width range. In the experiments described here, the detector was not cooled, and there was no subtraction of background noise from the measurements.

8.4 INTERFEROMETRIC CHARACTERS

The concept of *interferometric characters* was introduced when the *N*SLI was disclosed as an alternative for secure free-space optical communications (Duarte, 2002). In this approach, there is an infinite number of possible slit combinations that can lead to a set of interferometric characters. The simplest one consists to two slit interferometry resulting in the interferometric character a, that is, $N = 2 \rightarrow a$, $N = 3 \rightarrow b$, $N = 4 \rightarrow c$ … $N = 26 \rightarrow z$ (Duarte, 2002). Calculated interferograms for the interferometric characters a, b, c, and z are given in Figure 8.4.

In the N-slit interferometric approach, once the emitter, controlling the illumination of the N-slit array at j, and the receiver at d, decide on an interferometric alphabet the communications can begin immediately with the receiver reading directly the interferometric characters sent by the emitter. Since all these characters have also a theoretical counterpart, the received characters can be compared with the calculated character to verify its fidelity. As demonstrated by Duarte (2002, 2005) any attempt to optically intercept an interferometric character results in a catastrophic collapse of the interferometric signal and is immediately noticed by the receiver. The collapse sequence, and displacement, of the interferometric character a, due to the insertion of a very thin high-optical surface quality beam splitter in the intra-interferometric optical path ($D_{\langle d|j \rangle}$) is illustrated in Figure 8.5. An additional sequence of measurements, using the interferometric character c ($N = 4$), is given in Figures 8.6–8.9.

The violent distortion of the interferometric characters, following insertion of a thin beam splitter, as illustrated in Figures 8.5 and 8.7, can be explained in reference to Equation (8.2) which interferometrically entangles the probability amplitudes $\langle d|j \rangle$ originating at each slit (j). This entanglement is a function of photon wavelength, the number of slits illuminated N, slit geometry, and propagation geometry (see Chapter 4). This entanglement is violently disrupted by the insertion of an optical edge as provided by a classical, or macroscopic, beam splitter regardless of the finesse of that beam splitter.

An alternative way to think about this effect is that the mechanics of the overall superposition probability amplitude

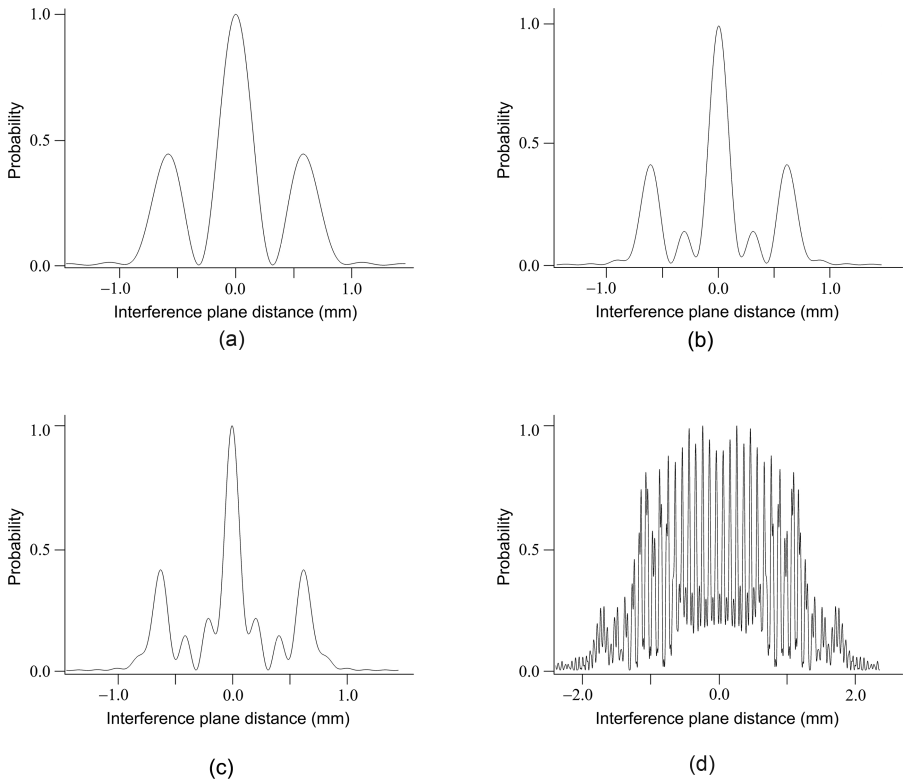

FIGURE 8.4 Interferometric characters *a* ($N = 2$), *b* ($N = 3$), *c* ($N = 4$), and *z* ($N = 26$) for $\lambda = 632.82$ nm and $D_{\langle d|j\rangle} = 10$ cm. The slit width here is 50 μm and uniformly separated by 50 μm. Note: the detailed and exact contour, as compared to measurements, of these interferograms (specially at the minima) depends on the choice of function to represent the radiation at the individual slits (Adapted from Duarte, F. J., *Opt. Commun.* **205**, 313–319, 2002, with permission from Elsevier).

$$\langle d|s\rangle = \sum_{j=1}^{N} \langle d|j\rangle \langle j|s\rangle$$

allow us to observe the input and the output but it does not allow us to obtain information while the interferometric character propagates via the intra-interferometric beam path ($D_{\langle d|j\rangle}$). In other words, the integrity of the interferometric character is protected by the very essence of interference, be it single-photon interference or interference generated by an ensemble of indistinguishable photons.

Indeed, as soon as the beam splitter is introduced, the probability Equation (8.2), that is,

$$\left|\langle d|s\rangle\right|^2 = \sum_{j=1}^{N} \Psi(r_j)^2 + 2\sum_{j=1}^{N} \Psi(r_j)\left(\sum_{m=j+1}^{N} \Psi(r_m)\cos(\Omega_m - \Omega_j)\right)$$

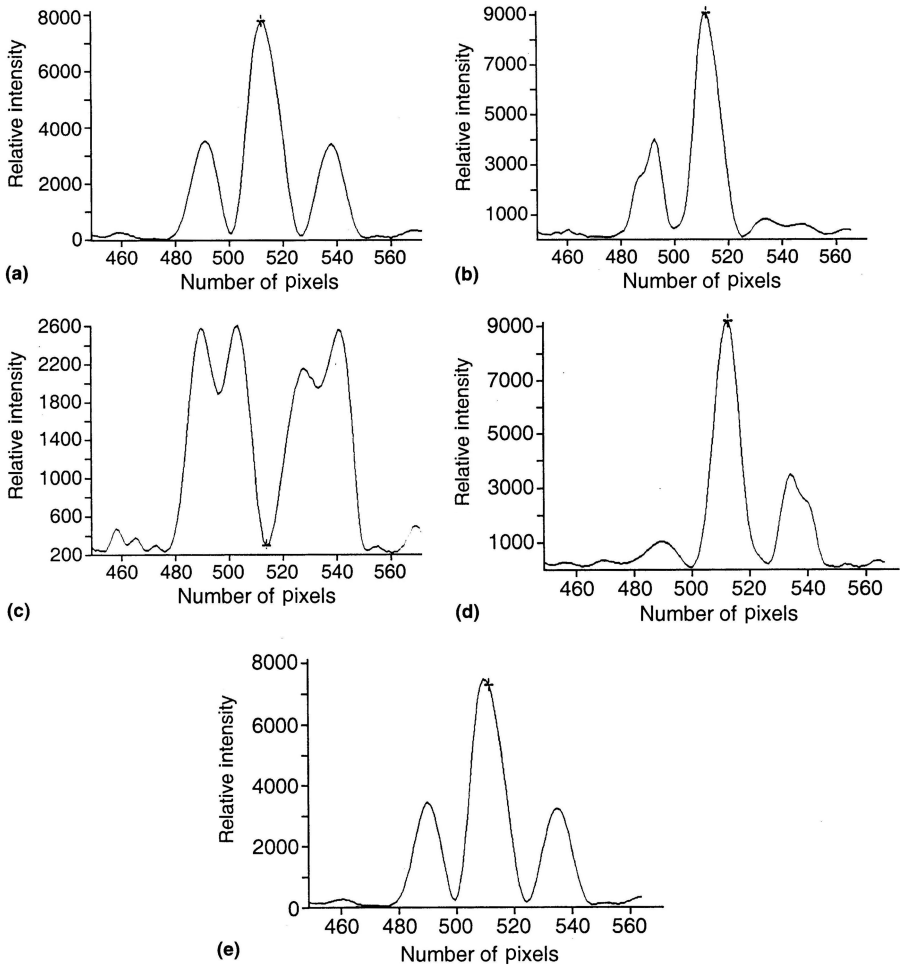

FIGURE 8.5 Collapse sequence of the interferometric characters *a*, following insertion of a thin beam splitter into the intra-interferometric path $D_{\langle d|j\rangle}$. (a) Interferometric character *a* prior to insertion of the beam splitter, (b)–(d) collapse of the interferometric character *a* during insertion, and (c) displaced interferometric character *a* once insertion is completed. Here, $N = 2$, the slit width is 50 μm, slit separation is 50 μm, and $D_{\langle d|j\rangle} = 10$ cm. Each pixel is 25 μm in width (Reproduced from Duarte, F. J., *Opt. Commun.* **205**, 313–319, 2002, with permission from Elsevier).

ceases to describe the experimental situation illustrated in Figure 8.2 which originates in the probability amplitude expressed by Equation (8.1). The new experimental situation, illustrated in Figure 8.10, is accounted for by a probability amplitude of the form

$$\langle d|s\rangle = \sum_{k=1}^{N}\sum_{j=1}^{N}\langle d|j'\rangle\langle j'|j\rangle\langle j|s\rangle \tag{8.5}$$

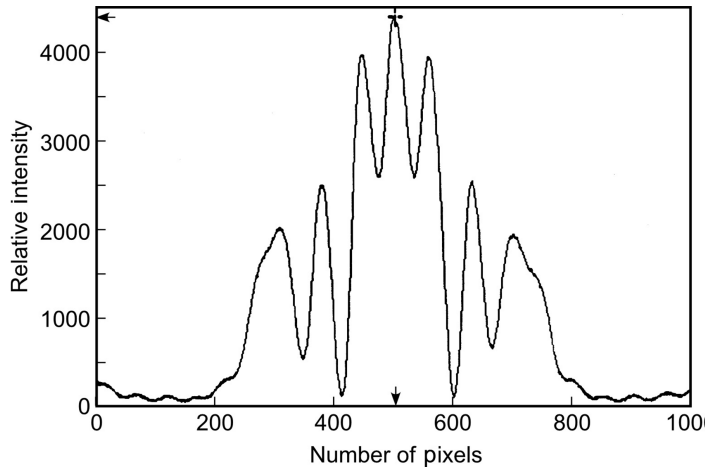

FIGURE 8.6 The interferometric character *c*, generated with $N = 4$ (570 μm slits separated by 570 μm), $\lambda = 632.8$ nm, at an intra-interferometric distance of $D_{\langle d|j\rangle} = 7.235$ m. Each pixel is 25 μm in width (Duarte, F. J., *J. Opt. A: Pure Appl. Opt.* **7**, 73–75, 2005, © IOP Publishing. Reproduced with permission. All rights reserved).

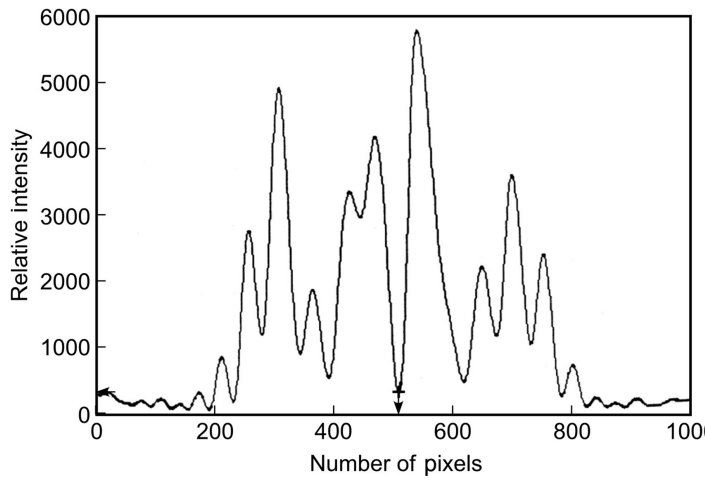

FIGURE 8.7 The interferometric character *c*, as in Figure 8.6, severely collapsed due to the insertion of a thin beam splitter, at Brewster's angle, 2 m from the grating (*j*) (Duarte, F. J., *J. Opt. A: Pure Appl. Opt.* **7**, 73–75, 2005, © IOP Publishing. Reproduced with permission. All rights reserved).

where the $\langle j'|j\rangle$ term represents the probability amplitude of transmission via the beam splitter. In reality this is an undetermined spatially unsymmetric transmission that results in the destruction of the original interferometric pattern.

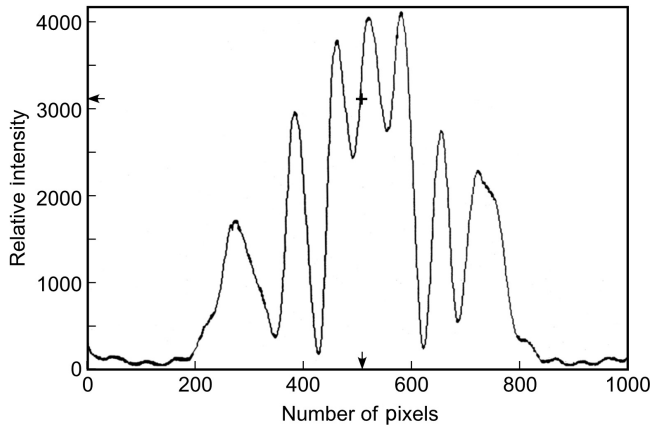

FIGURE 8.8 The interferometric character *c*, as in Figure 8.6, clearly distorted due to the static presence of a thin beam splitter, at Brewster's angle, 2 m from the grating (*j*) (Duarte, F. J., *J. Opt. A: Pure Appl. Opt.* **7**, 73–75, 2005, © IOP Publishing. Reproduced with permission. All rights reserved).

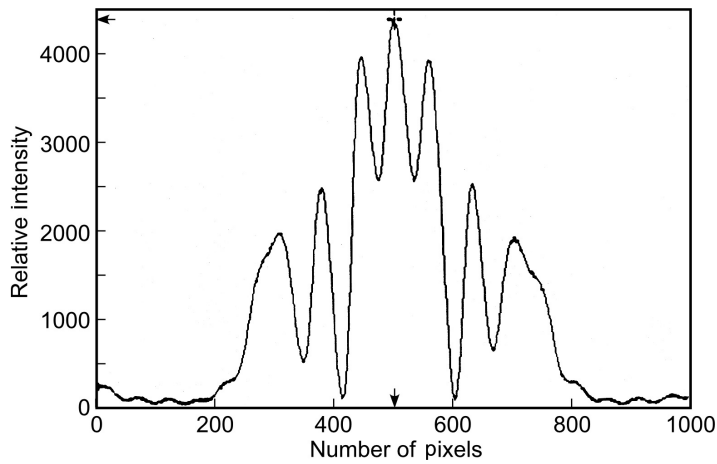

FIGURE 8.9 The interferometric character *c*, as in Figure 8.6, restored due to the removal of the thin beam splitter that caused the distortions depicted in the previous figures (Duarte, F. J., *J. Opt. A: Pure Appl. Opt.* **7**, 73–75, 2005, © IOP Publishing. Reproduced with permission. All rights reserved).

8.5 PROPAGATION IN TERRESTRIAL FREE SPACE

As mentioned at the introduction, the first experiment on the use of the *N*SLI as a tool for secured free-space optical communications took place in the laboratory over a distance of $D_{\langle d|j\rangle} = 0.10$ m (Duarte, 2002). Further series of measurements have taken place over intra-interferometric distances of $D_{\langle d|j\rangle} = 7.235$ m (Duarte, 2005), $D_{\langle d|j\rangle} = 35$ m (Duarte et al., 2010), and $D_{\langle d|j\rangle} = 527$ m (Duarte et al., 2011).

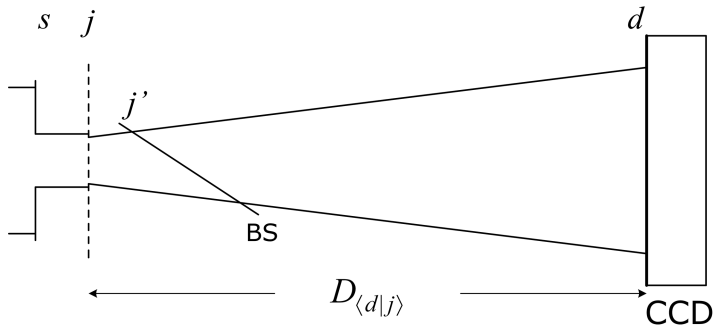

FIGURE 8.10 The N-slit laser interferometer with a thin beam splitter (BS) inserted in the intra-interferometric path $D_{\langle d|j\rangle}$. For the propagation at the top of the figure, the probability amplitude is modified from $\langle d|j\rangle\langle j|s\rangle$ to $\langle d|j'\rangle\langle j'|j\rangle\langle j|s\rangle$. The latter probability amplitude varies continuously, as a function of distance, along the beam splitter.

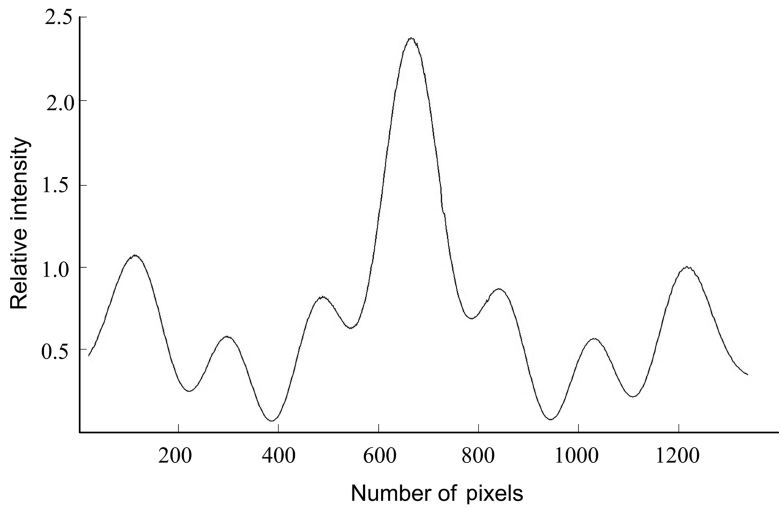

FIGURE 8.11 The interferometric character c ($N = 4$, 1000 μm slits separated by 1000 μm) for $D_{\langle d|j\rangle} = 35$ m recorded outside the laboratory. Each pixel is 20 μm wide (Duarte, F. J. et al., *J. Opt.* **12**, 015705, 2010, © IOP Publishing. Reproduced with permission. All rights reserved).

For $D_{\langle d|j\rangle} = 0.10$ m, and propagation in homogeneous laboratory air, the interferometric character a is depicted in Figure 8.5. For $D_{\langle d|j\rangle} = 7.235$ m, and propagation in homogeneous laboratory air, the interferometric character c is depicted in Figure 8.6. For $D_{\langle d|j\rangle} = 35$ m, and propagation in near-homogeneous air (at $T \approx 30°\text{C}$), the measured interferometric character c is depicted in Figure 8.11 while its calculated version is displayed in Figure 8.12. For $D_{\langle d|j\rangle} = 527$ m, and propagation in near-homogeneous air (at $T \approx 24°\text{C}$ and 66% humidity), the measured interferometric character d ($N = 5$) is shown in Figure 8.13, while its calculated version is displayed in Figure 8.14.

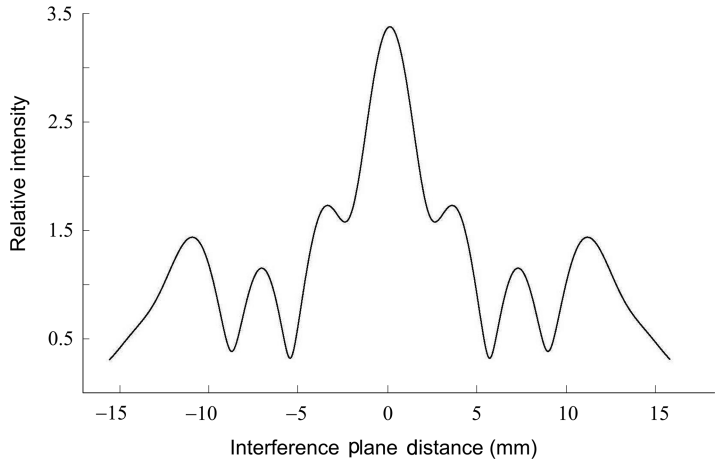

FIGURE 8.12 The calculated version of the interferometric character c ($N = 4$, 1000 μm slits separated by 1000 μm) for $D_{\langle d|j\rangle} = 35$ m (Duarte, F. J. et al., *J. Opt.* **12**, 015705, 2010, © IOP Publishing. Reproduced with permission. All rights reserved).

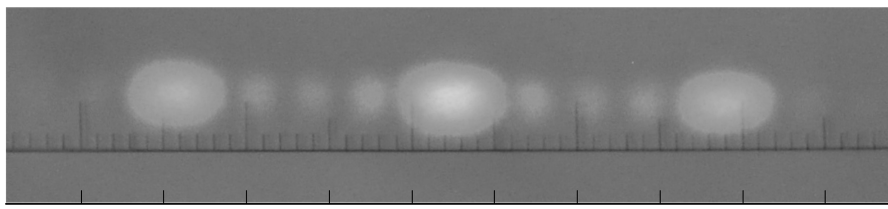

FIGURE 8.13 The interferometric character d ($N = 5$, 1000 μm slits separated by 1000 μm) for $D_{\langle d|j\rangle} = 527$m (Duarte, F. J. et al., *J. Opt.* **13**, 035710, 2011, © IOP Publishing. Reproduced with permission. All rights reserved).

8.5.1 Clear-Air Turbulence

As mentioned previously the original propagation space envisioned for communications via interferometric characters was vacuum, or outer space, where the interferometric characters can propagate free of refractive index distortions (Duarte, 2002). That is not the case for propagation in a terrestrial environment where the propagation space is subject to refractive index variations due to thermal gradients and clear-air turbulence (CAT).

The question then becomes: can we differentiate between interferometric character distortions due to CAT and distortions due to third-party intrusion into the intra-interferometric optical path $D_{\langle d|j\rangle}$?

This question can be answered empirically. To do this, attention should be paid to Figures 8.5b–d, 8.7, and 8.15, all of which illustrate the catastrophic collapse of the given interferometric character due to the insertion of a beam splitter in the $D_{\langle d|j\rangle}$ path. Now, by contrast, we consider Figure 8.16 where the distortions due to mild

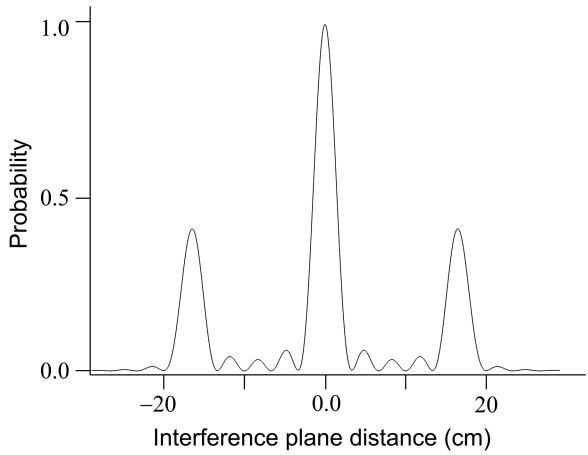

FIGURE 8.14 The calculated version of the interferometric character d (N = 5, 1000 μm slits separated by 1000 μm) for $D_{\langle d|j\rangle} = 527$ m.

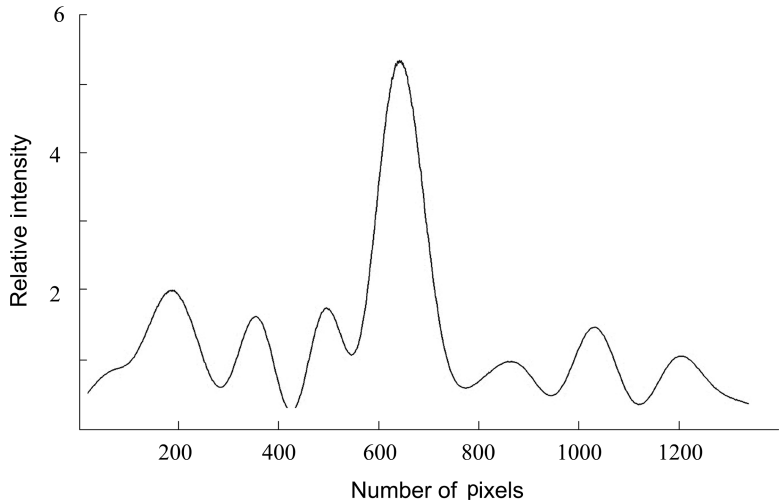

FIGURE 8.15 The interferometric character c ($N = 4$, 1000 μm slits separated by 1000 μm) for $D_{\langle d|j\rangle} = 35$ m, while a thin beam splitter is inserted at a distance 10 m from the N-slit array. Each pixel is 20 μm in width (Duarte, F. J. et al., *J. Opt.* **12**, 015705, 2010, © IOP Publishing. Reproduced with permission. All rights reserved).

clear-air turbulence detected at $D_{\langle d|j\rangle} = 7.235$ m, for the c ($N = 4$) character, are illustrated (Duarte, 2009). Severe CAT causes the interferometric character to lose all its spatial information and to tend toward a 'smooth' distribution (Duarte et. al., 2010). It appears that the effect of CAT might be statistically predictable. This is very different to the massive distortions and catastrophic collapse induced by beam splitter incursions into the $D_{\langle d|j\rangle}$ optical path.

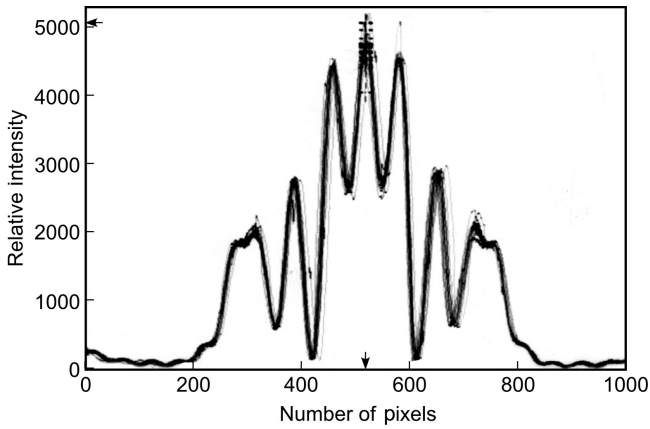

FIGURE 8.16 The effect of mild clear-air turbulence introduced in the laboratory for the interferometric character *c*, generated with $N = 4$ (570 μm slits separated by 570 μm), $\lambda = 632.82$ nm, at an intra-interferometric distance of $D_{\langle d|j\rangle} = 7.235$ m. Each pixel is 25 μm in width (From Duarte, F. J., Interferometric imaging, in *Tunable Laser Applications*, 2nd ed., (Duarte, E. J., ed.), CRC, Boca Raton, FL, Chapter 12, 2009).

Finally, it should be mentioned that CAT is a phenomenon of significant importance to aviation safety. This class of turbulence is difficult to detect with traditional radar methods. In this regard, the ability of the *N*SLI to detect CAT offers a practical and demonstrated avenue of detection, specially by installing infrared-laser based *N*-slit interferometers at airports near the runway thresholds (Duarte, 2009, 2016).

8.6 ADDITIONAL APPLICATIONS

In addition to secure free-space communications and detection of CAT, the coherent *N*-slit interferometer used in conjunction with its interferometric probability equation is useful in a series of further applications Duarte (1995, 2009, 2016). These applications include biomedicine, cytology, densitometry, film imaging, film granularity measurements, metrology, microscopy, nanoscopy, interferometry of fine textiles, wavelength measurements, surface imaging, transmission grating characterization, and x-ray film imaging.

8.7 DISCUSSION

The *N*-slit interferometer, in conjunction with the *N*-slit interferometric probability equation, has been used to generate interferometric characters that have proven extremely sensitive to interception with classical, or macroscopic, optical methods. Thus, an interferogram or interferometric character can be generated according to an established interferometric alphabet and used for free space communications knowing that attempts to intercept the optical character will lead to its catastrophic collapse. This implies that transparent communications, without the use of a classified

key, can proceed through the open space. However, a cryptographic key could be easily added and implemented, if desired.

In Chapter 21, we describe how microscopic optical methods can be used to intercept the interferometric character causing minimal distortions. Moreover, in Chapter 21, a more detailed interplay between measured and calculated interferograms is described.

As already mentioned, the *N*-slit interferometric method was originally conceived for outer space communications in vacuum (Duarte, 2002). However, here we have seen that deployment in a terrestrial environment, devoid of CAT, should be practically feasible. Moreover, given the different nature of the distortions due to CAT, as compared with macroscopic optical interception, deployment in atmospheric environments including some degree of CAT should also be possible.

The main advantages of the *N*-slit interferometric method for optical communications in free space are as follows:

1. The extraordinary simplicity of the optical architecture.
2. The use of single-transverse-mode, narrow-linewidth, lasers as illumination sources that neutralize significant signal to noise problems.
3. The ease with which additional security features could be implemented into its optical configuration: tunable infrared lasers and variable interferometric characters, among others.

In Chapter 15, it is shown how the physics of quantum entanglement is derived from the Dirac–Feynman interferometric principle utilized here. In this regard, it can be argued that the security, in space-to-space communications, provided by straightforward *N*-slit quantum interferometry is guaranteed by quantum mechanics in the same manner as the security provided by quantum entanglement is guaranteed by quantum mechanics.

PROBLEMS

8.1 Suggest an optimum laser for use in a secure interferometric character generating configuration. Explain the reasons for your selection.

8.2 Suggest an optimum laser for use in an *N*SLI for the detection of CAT. Explain the differences with the selection of Problem 8.1.

8.3 Suggest an optimum laser for use in an *N*SLI for motion picture film imaging. Explain the differences with the selection of Problem 8.1.

REFERENCES

Born, M. (1926). Zur quantenmechanik der stoßvorgänge. *Z. Phys.* 37, 863–827.

Dirac, P. A. M. (1958). *The Principles of Quantum Mechanics*, 4th ed. Oxford University, Oxford, U.K.

Duarte, F. J. (1991). Dispersive dye lasers. In *High Power Dye Lasers* (Duarte, F. J., ed.). Springer-Verlag, Berlin, Chapter 2, pp. 7–43.

Duarte, F. J. (1993). On a generalized interference equation and interferometric measurements. *Opt. Commun.* 103, 8–14.

Duarte, F. J. (1995). Interferometric imaging. In *Tunable Laser Applications*, 1st ed. (Duarte, F. J., ed.) Marcel-Dekker, New York, Chapter 5, pp. 153–178.

Duarte, F. J. (2002). Secure interferometric communications in free space. *Opt. Commun.* 205, 313–319.

Duarte, F. J. (2003). *Tunable Laser Optics*, Elsevier-Academic, New York.

Duarte, F. J. (2004). Comment on 'reflection, refraction and multislit interference'. *Eur. J. Phys.* 25, L57–L58.

Duarte, F. J. (2005). Secure interferometric communications in free space: enhanced sensitivity for propagation in the metre range. *J. Opt. A: Pure Appl. Opt.* 7, 73–75.

Duarte, F. J. (2009). Interferometric imaging. In *Tunable Laser Applications*, 2nd ed. (Duarte, F. J., ed.) CRC Press, New York, Chapter 12, pp. 341–373.

Duarte, F. J. (2016). Interferometric imaging. In *Tunable Laser Applications*, 3rd ed. (Duarte, F. J., ed.) CRC Press, Boca Raton, FL, Chapter 10, pp. 329–369.

Duarte, F. J., Taylor, T. S., Black, A. M., Davenport, W. E., and Varmette, P. G. (2011). N-slit interferometer for secure free-space optical communications: 527 m intra interferometric path length. *J. Opt.* 13, 035710.

Duarte, F. J., Taylor, T. S., Clark, A. B., and Davenport, W. E. (2010). The N-slit interferometer: an extended configuration. *J. Opt.* 12, 015705.

Hogan, F. (2013). Data demands free-space optics. *Photon. Spec.* 47 (2), 38–41.

van Kampen, N. G.(1988). Ten theorems about quantum mechanical measurements. *Phys. A.* 153, 97–113.

9 Schrödinger's Equation

9.1 INTRODUCTION

As mentioned in Chapter 1, Schrödinger's equation (Schrödinger, 1926) provides one of the three main avenues to quantum mechanics. It also has important applications in atomic and molecular physics (Herzberg, 1950; Feynman et al., 1965). Given the importance of this equation in semiconductor lasers, we examine a couple of derivational approaches. The principal aim is to gain an understanding of the physics behind this quantum wave equation. Since the application of this equation is widely and extensively treated in many textbooks (see, e.g., Saleh and Teich, 1991; Silfvast, 2008; Hooker and Webb, 2010) we only briefly describe a few applications relevant to semiconductor lasers.

It is also relevant to highlight that in the fields of quantum interference and quantum entanglement, the Schrödinger equation does not come into play since the photon is considered as a form of *nonlocal coherent energy* and *not* as a particle (see Chapter 3). Under those circumstances, the principal tools are *superposition probabilities amplitudes* effectively described by the complex wave equations mentioned by Dirac (1958).

9.2 A HEURISTIC EXPLICIT APPROACH TO SCHRÖDINGER'S EQUATION

Here, Schrödinger's equation is arrived at in an alternative heuristic path modeled after Haken (1981). This approach relies on the use of the complex wave function $\psi(x,t)$. The advantage of this approach is that the argument is much simpler and clearer.

A free particle moves with classical kinetic energy according to

$$E = \tfrac{1}{2} m v^2 \tag{9.1}$$

which, using $p = mv$, can be re-stated as

$$E = p^2/2m \tag{9.2}$$

Now, using Planck's quantum energy (Planck, 1901)

$$E = h\nu \tag{9.3}$$

in conjunction with $\lambda = c/\nu$, and $E = mc^2$, the well-known de Broglie's expression for momentum can be arrived to (de Broglie, 1923)

DOI: 10.1201/9781003398707-9

$$p = \hbar k \tag{9.4}$$

The classical 'wave functions of ordinary wave optics' (Dirac, 1958) can be written as

$$\psi(x,t) = \psi_0 e^{-i(\omega t - kx)} \tag{9.5}$$

whose derivative with respect to time becomes

$$\frac{\partial \psi(x,t)}{\partial t} = (-i\omega)\psi_0 e^{-i(\omega t - kx)} \tag{9.6}$$

Similarly, the first and second derivatives with respect to displacement are

$$\frac{\partial \psi(x,t)}{\partial x} = (+ik)\psi_0 e^{-i(\omega t - kx)} \tag{9.7}$$

$$\frac{\partial^2 \psi(x,t)}{\partial x^2} = (-k^2)\psi_0 e^{-i(\omega t - kx)} \tag{9.8}$$

Multiplying the first-time derivative by $(-i\hbar)$ yields

$$-i\hbar \frac{\partial \psi(x,t)}{\partial t} = (-\hbar\omega)\psi_0 e^{-i(\omega t - kx)} \tag{9.9}$$

and multiplying the second displacement derivative by $(-\hbar^2/2m)$ yields

$$-\frac{\hbar^2}{2m}\frac{\partial^2 \psi(x,t)}{\partial x^2} = \frac{\hbar^2 k^2}{2m}\psi_0 e^{-i(\omega t - kx)} \tag{9.10}$$

Recognizing that $E = \hbar^2 k^2/2m$, allow us to write

$$-\frac{\hbar^2}{2m}\frac{\partial^2 \psi(x,t)}{\partial x^2} = +i\hbar \frac{\partial \psi(x,t)}{\partial t} \tag{9.11}$$

which is the basic form of Schrödinger's equation. Observing Equations (9.9) to (9.11) the importance of the concept of energy in these equations becomes immediately apparent. Adding a term for a constant potential energy $V\psi$ to the LHS of Equation (9.11) yields

$$-\frac{\hbar^2}{2m}\frac{\partial^2 \psi(x,t)}{\partial x^2} + V(x)\psi(x,t) = +i\hbar \frac{\partial \psi(x,t)}{\partial t} \tag{9.12}$$

which makes Schrödinger's equation compatible with the Hamiltonian which is the sum of kinetic and potential energy.

The Schrödinger equation is a wave equation that incorporates classical particle concepts, and classical wave function concepts, in its derivation. In other words,

a heuristic approach to Schrödinger's equation utilizes Planck's quantum energy, classical kinetic energy of a free particle, and the complex wave functions. In this approach, it is clear that Schrödinger's equation refers to a *free particle* propagating in a wave motion according to wave optics. Once again, the central role of complex wave equation

$$\psi(x,t) = \psi_0 e^{-i(\omega t - kx)}$$

is highlighted.

9.3 SCHRÖDINGER'S EQUATION VIA DIRAC'S NOTATION

Here, once again the Feynman approach (Feynman et al., 1965) is adopted. In the Hamiltonian H_{ij} (see Appendix A), the time dependence of the amplitude C_i is given by (Dirac, 1958)

$$i\hbar \frac{dC_i}{dt} = \sum_j H_{ij} C_i \tag{9.13}$$

For $C_i = \langle i|\psi \rangle$, this equation can be rewritten as

$$i\hbar \frac{d\langle i|\psi\rangle}{dt} = \sum_j \langle i|H|j\rangle \langle j|\psi\rangle \tag{9.14}$$

which, for $i = x$, can be written as

$$i\hbar \frac{d\langle x|\psi\rangle}{dt} = \sum_j \langle x|H|x'\rangle \langle x'|\psi\rangle \tag{9.15}$$

Since $\langle x|\psi\rangle = \psi(x)$, this equation can be reexpressed as

$$i\hbar \frac{d\psi(x)}{dt} = \int H(x,x')\psi(x')\,dx' \tag{9.16}$$

The integral on the right-hand side is given by

$$\int H(x,x')\psi(x')\,dx' = -\frac{\hbar^2}{2m}\frac{d^2\psi(x)}{dx^2} + V(x)\psi(x) \tag{9.17}$$

About this stage, Feynman poses and asks the question: 'Where did we get that from? Nowhere… it came from the mind of Schrödinger, invented in his struggle to find an understanding of the experimental observations of the real world' (Feynman et al., 1965).

Next, combining Equations (9.16) and (9.17), we get Schrödinger's equation

$$+i\hbar \frac{d\psi(x)}{dt} = -\frac{\hbar^2}{2m}\frac{d^2\psi(x)}{dx^2} + V(x)\psi(x) \tag{9.18}$$

In three dimensions, we use $\psi(x,y,z)$ and $V(x,y,z)$ and

$$\nabla^2 = (\partial^2/\partial x^2) + (\partial^2/\partial y^2) + (\partial^2/\partial z^2) \tag{9.19}$$

so that Schrödinger's equation in three dimensions takes the succinct form

$$+i\hbar\frac{\partial\psi}{\partial t} = -\frac{\hbar^2}{2m}\nabla^2\psi + V\psi \tag{9.20}$$

It is clear that even in this approach, using the quantum tools provided by Dirac and Feynman, the derivation of Schrödinger's equation still depends on Schrödinger's classical concepts. Defining the *Hamiltonian operator* $\hat{\mathcal{H}}$ as

$$\hat{\mathcal{H}} = (-\hbar^2/2m)\nabla^2 + V \tag{9.21}$$

the Schrödinger equation can be expressed as

$$+i\hbar\frac{\partial\psi}{\partial t} = \hat{\mathcal{H}}\psi \tag{9.22}$$

Finally, for a large number of particles, Feynman restates the Schrödinger equation as

$$+i\hbar\left(\frac{\partial\psi(r_1, r_2, r_2\ldots)}{\partial t}\right) = -\frac{\hbar^2}{2}\sum_i m_i^{-1}\nabla_i^2\psi + V(r_1, r_2, r_2\ldots)\psi \tag{9.23}$$

where

$$\nabla_i^2 = (\partial^2/\partial x_i^2) + (\partial^2/\partial y_i^2) + (\partial^2/\partial z_i^2) \tag{9.24}$$

This is the type of Schrödinger's equation applied in the description of molecular physics (Herzberg, 1950).

9.4 THE TIME-INDEPENDENT SCHRÖDINGER EQUATION

As suggested by Feynman, using a solution of the form

$$\psi(x) = \Psi(x)e^{-iEt/\hbar} \tag{9.25}$$

Equation (9.20), in one dimension, takes the form of

$$\frac{\partial^2\Psi(x)}{\partial x^2} - \frac{2m}{\hbar^2}\big(V(x) - E\big)\Psi(x) = 0 \tag{9.26}$$

or

$$\frac{\partial^2\Psi(x)}{\partial x^2} = \frac{2m}{\hbar^2}\big(V(x) - E\big)\Psi(x) \tag{9.27}$$

which is known as a one-dimensional time-independent Schrödinger equation. This simple form of the Schrödinger equation is of enormous significance to semiconductor physics and semiconductor lasers. This equation has exactly the same form as Schrödinger introduced his equation originally (Schrödinger, 1926)

$$\nabla^2\psi + \frac{8\pi^2 m}{h^2}(E - V)\psi = 0 \tag{9.28}$$

9.4.1 Quantized Energy Levels

Let us consider a static potential well as described by the function $V(x)$ in Figure 9.1. Since E is a constant, it is shown on the vertical axis. From Equation (9.27), $\Psi(x)$ can be evaluated along x as E is varied, along the vertical, by small amounts. This evaluation indicates that $\Psi(x)$ shows an oscillatory behavior within the well. For certain definite vales of E, the shape of the curve is symmetrical as x increases pass the well boundary. However, for other slightly different values of E, $\Psi(x)$ diverges toward large positive or large negative values. In other words, as indicated in Figure 9.2, within a potential well, the particle is only bound for definite discrete values of $E = 0, 1, 3, 4\ldots$ (Feynman et al., 1965). The behavior of $\Psi(x)$, as a function of E, illustrates the phenomenon of quantized energy levels within a potential well.

9.4.2 Semiconductor Emission

Going back to the time-independent Schrödinger equation

$$\frac{\partial^2\psi(x)}{\partial x^2} - \frac{2m}{\hbar^2}\big(V(x) - E\big)\ \psi(x) = 0 \tag{9.29}$$

and using the spatial component of the wave function as solution

$$\psi(x) = \psi_0 e^{-ikx} \tag{9.30}$$

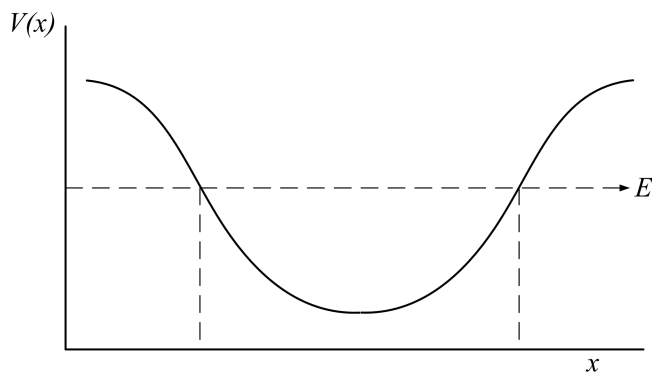

FIGURE 9.1 Static potential energy well $V(x)$.

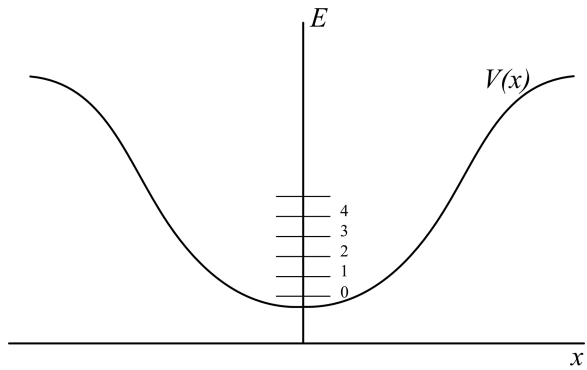

FIGURE 9.2 Potential energy well depicting a series of discrete energy levels $E = 0, 1, 3, 4\ldots$ and corresponding $\Psi(x)$ functions.

leads directly to

$$E = \frac{k^2\hbar^2}{2m} + V(x) \tag{9.31}$$

This energy expression is the sum of kinetic and potential energy so that

$$E_K + E_P = \frac{k^2\hbar^2}{2m} + V(x) \tag{9.32}$$

and

$$E_K = \frac{k^2\hbar^2}{2m} \tag{9.33}$$

The kinetic energy E_K as a function of $k = 2\pi/\lambda$ is shown graphically in Figure 9.3.

The graph is a positive parabola for positive values of m and a negative parabola for negative values of m. In a semiconductor, the positive parabola is known as the *conduction* band and the negative parabola is known as the *valence* band. The separation between the two bands is known as the *band gap*, E_G. If an electron is excited and transitions from the valence band to the conduction band, it is said to leave behind a vacancy or *hole*.

Electrons can transition from the bottom of the conduction band to the top of valence band by recombining with holes. In a material like gallium arsenide, the band gap is $E_G \approx 1.43$ eV and the recombination emission occurs around 870 nm (Silfvast, 2008).

Under certain conditions, radiation might also occur higher from the conduction band as suggested in Figure 9.4; however, that process is undermined by fast phonon relaxation.

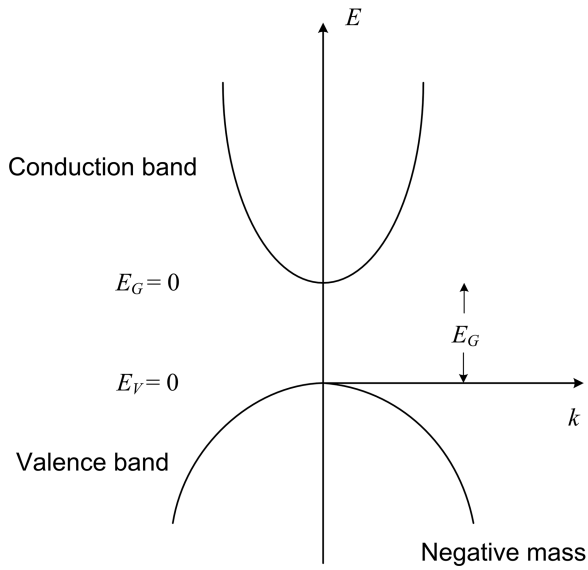

FIGURE 9.3 Conduction and valence bands according to $E_K = \pm(k^2\hbar^2/2m)$.

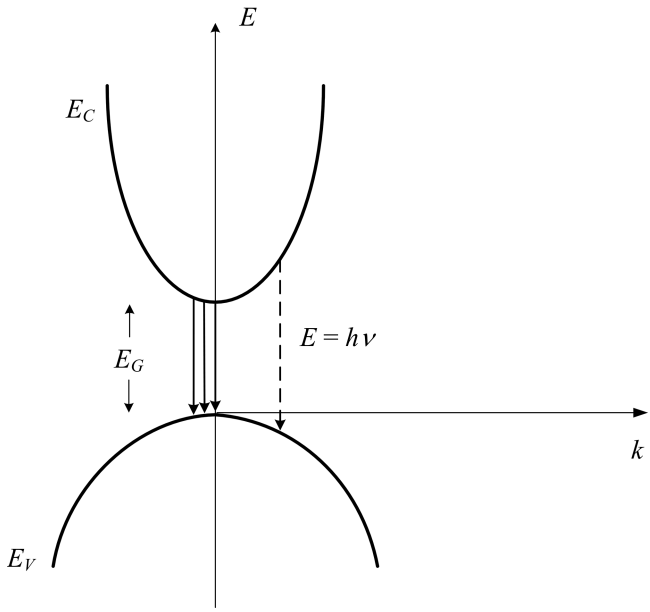

FIGURE 9.4 Emission due to recombination transitions from the bottom of the conduction band to the top of the valence band.

9.4.3 Quantum Wells

Starting with a potential well as described by Silfvast (2008): $V(x) = 0$ for $0 < x < L$; and $V(x) = \infty$ for $x = 0$ or $x = L$, illustrated in Figure 9.5, then Equation (9.27)

$$\frac{\partial^2 \psi(x)}{\partial x^2} - \frac{2m}{\hbar^2}\big(V(x) - E\big)\psi(x) = 0$$

becomes

$$\frac{\partial^2 \psi(x)}{\partial x^2} + \frac{2m}{\hbar^2} E\psi(x) = 0 \tag{9.34}$$

for $0 < x < L$. This is a wave equation of the form

$$\frac{d^2 \psi(x)}{dx^2} + k_x^2 \psi(x) = 0 \tag{9.35}$$

with

$$k_x^2 = \frac{2m_c}{\hbar^2} E \tag{9.36}$$

The solution to Equation (9.35) is

$$\psi(x) = \sin k_x x \tag{9.37}$$

Since $\psi(x) = 0$ at $x = 0$ or $x = L$, we have

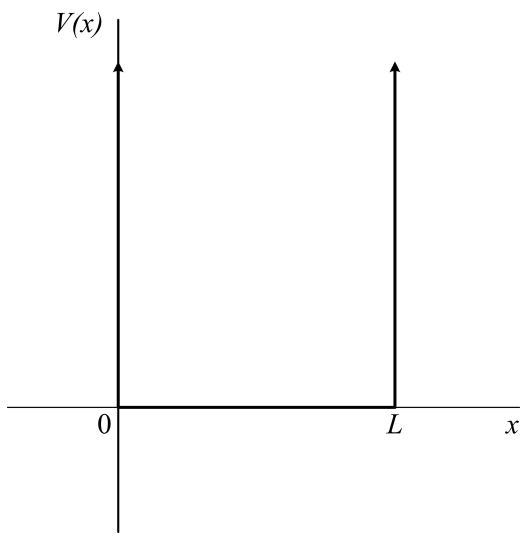

FIGURE 9.5 Potential well $V(x) = 0$ for $0 < x < L$; and $V(x) = \infty$ for $x = 0$ or $x = L$.

$$k_x = \frac{n\pi}{L} \tag{9.38}$$

for $n = 1, 2, 3\ldots$. Substituting Equation (9.38) into (9.36) leads to

$$E = \frac{n^2\pi^2\hbar^2}{2m_cL^2} \tag{9.39}$$

which should be labeled as E_n to account for the quantized nature of the energy, that is

$$E_n = \frac{n^2\pi^2\hbar^2}{2m_cL^2} \tag{9.40}$$

This quantized energy E_n indicates a series of possible discrete energy levels above the lowest point of the conduction band so that the total energy above the valence band becomes (Silfvast, 2008)

$$E = E_c + E_n \tag{9.41}$$

9.4.4 Quantum Cascade Lasers

These lasers operate via transitions between quantized levels, *within* the conduction band, of multiple quantum well structures. The carriers involved are electrons generated in an n-doped material. A single stage includes an injector and an active region. The electron is injected into the active region at $n = 3$ and the transition occurs down to $n = 2$ (see Figure 9.6). Following emission, the electron continues into the next injector region. Practical devices include a series of such stages. From Equation (9.40), the energy difference between the two levels can be expressed as (Silfvast, 2008)

$$\Delta E = (3^2 - 2^2)\frac{\pi^2\hbar^2}{2m_cL^2} \tag{9.42}$$

where L is the thickness of the well. Using $\Delta E = h\nu$, it follows that the wavelength of emission is given by

$$\lambda = (3^2 - 2^2)^{-1}\frac{8m_cL^2}{h} \tag{9.43}$$

Quantum cascade lasers (Faist et al., 1994) are tunable sources emitting in the infrared from a few micrometers to beyond 20 μm.

9.4.5 Quantum Dots

Besides the multiple quantum well configurations, other interesting semiconductor geometries include the quantum wire and the quantum dot. The quantum wire

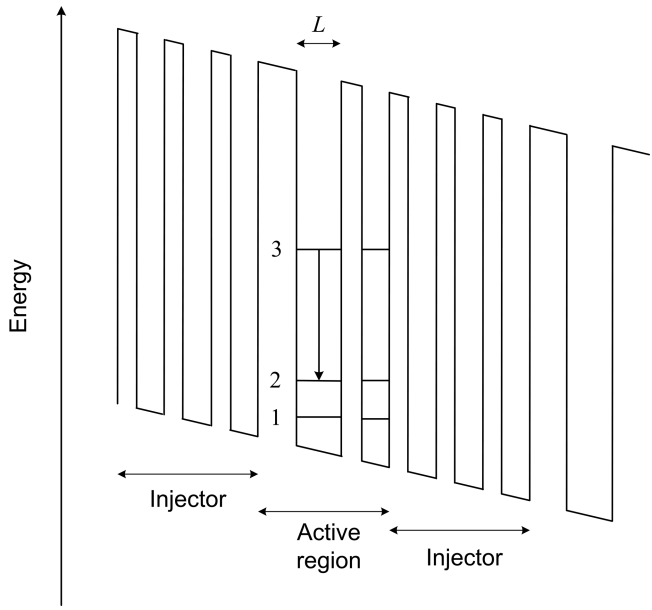

FIGURE 9.6 Simplified illustration of a multiple quantum well structure relevant to quantum cascade lasers. An electron is injected from the "injector region" into the active region at $n = 3$. Thus a photon is emitted via the $3 \rightarrow 2$ transition. The electron continues to the next region where the process is repeated. By configuring a series of such stages, one electron can generate the emission of numerous photons.

narrowly confines the electrons and holes in two directions (x, y). The quantum dot geometry severely confines the electrons in three dimensions (x, y, z). Under these circumstances, the quantized energy can be expressed as

$$E = E_c + \frac{k_x^2 \hbar^2}{2m_c} + \frac{k_y^2 \hbar^2}{2m_c} + \frac{k_x^2 \hbar^2}{2m_c} \tag{9.44}$$

where k_x, k_y, and k_z are defined according to Equation (9.38).

The concept of quantum dot is not limited to semiconductor materials; it also applies to nanoparticle gain media and nanoparticle core–shell gain media. For instance, for nanoparticle core–shells the physics can be described with a Schrödinger equation of the form

$$\nabla^2 \psi(r) - \frac{2m}{\hbar^2}\big(V(r) - E\big)\psi(r) = 0 \tag{9.45}$$

with the potential $V(r)$ defined by the core–shell geometry (Dong et al., 2013).

9.5 NONLINEAR SCHRÖDINGER EQUATION

For the sake of completeness, and without derivation, we now introduce the nonlinear Schrödinger equation (Zakharov and Manakov, 1974)

$$+i\hbar\frac{\partial\psi}{\partial t}=\left(-\frac{\hbar^2}{2m}\nabla^2+V+g|\psi|^2\right)\psi \tag{9.46}$$

that adds an extra term $\left(g|\psi|^2\psi\right)$ to the original equation. In the extra term, $|\psi|^2$ is a dimensionless probability and g is the nonlinear interaction strength. This equation is relevant to the physics of *solitons* in nonlinear optics. It should be mentioned that *multiple-prism arrays* for laser pulse compression (see Appendix C) are used to compensate for intracavity dispersion in the 'soliton shaping' of laser pulses (Spence et al., 1991).

9.6 DISCUSSION

In this chapter, we have seen that the Schrödinger equation is an emergent mathematical statement whose individual terms display units of energy (J). Derivation of the Schrödinger equation depends on more fundamental complex wave equations

$$\psi(x,t)=\psi_0 e^{-i(\omega t-kx)}$$

which are the direct physical representation of Dirac's probability amplitudes

$$\langle d|j\rangle\rightarrow e^{-i\phi_j}$$

Thus, it can be argued that the quantum mechanics based on Dirac's probability amplitudes is more basic, more fundamental, than the quantum mechanics that relies on Schrödinger's equation.

PROBLEMS

9.1 Verify that multiplication of Equation (9.8) by $(-\hbar^2/2m)$ yields a kinetic energy multiplied by the complex wave function.

9.2 Use the wave Equation (9.25) into Equation (9.20) to verify Equation (9.27).

9.3 Use the wave Equation (9.30) into Equation (9.29) to verify Equation (9.31).

9.4 For a particle in a potential well $V(x)$ assume that the wave function describing the state of the particle is given by $\psi(x,t)=\phi(x)\vartheta(t)$. Given that

$$\vartheta(t)=Ce^{-i\omega t}$$

show that $\phi(x)$ and $\vartheta(t)$ satisfy the equation

$$\frac{\partial^2\psi(x)}{\partial x^2}-\frac{2m}{\hbar^2}\left(V(x)-E\right)\ \phi(x)=0$$

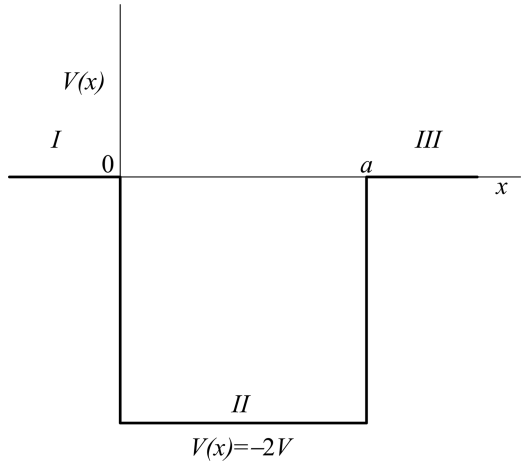

FIGURE 9.7 Potential well $V(x)$ with regions I, I, and III, applicable to Problem 9.5 $V(x) = 0$ for $x < 0$, $V(x) = -2V$ for $0 \le x \le a$, $V(x) = 0$ for $x > a$.

9.5 Find the stationary solutions to the Schrödinger equation for the three regions (I, II, and III) defined in Figure 9.7.

9.6 Verify that g, in Equation (9.46), has units of energy (J).

REFERENCES

de Broglie, L. (1923). Waves and quanta. *Nature* 112, 540.

Dirac, P. A. M. (1958). *The Principles of Quantum Mechanics*, 4th ed. Oxford University, Oxford, U.K.

Dong, L., Sugunan, A., Hu, J., Zhou, S., Li, S., Popov, S., Toprak, M. S., Friberg, A. T., and Muhammed, M. (2013). Photoluminescence from quasi-type-II spherical CdSe-CdS core-shell quantum dots. *Appl. Opt.* 52, 105–109.

Faist, J., Capasso, F., Sivco, D. L., Sirtori, C., Hutchinson, A. L., and Cho A. Y. (1994). Quantum cascade laser. *Science* 264, 553–556.

Feynman, R. P., Leighton, R. B., and Sands, M. (1965). *The Feynman Lectures on Physics*, Vol. III, Addison-Wesley, Reading, MA.

Haken, H. (1981). *Light*, North-Holland, Amsterdam.

Herzberg, G. (1950). *Spectra of Diatomic Molecules*, Van Nostrand Reinhold, New York.

Hooker, S., and Webb, E. (2010). *Laser Physics*, Oxford University, Oxford, U.K..

Planck, M (1901). Ueber das gesetz der energieverteilung im normalspectrum. *Ann. Phys.* 309 (3), 553–563.

Saleh, B. E. A., and Teich, M. C. (1991). *Fundamentals of Photonics*, Wiley, New York.

Schrödinger, E. (1926). An undulatory theory of the mechanics of atoms and molecules. *Phys. Rev.* 28, 1049–1070.

Silfvast, W. T. (2008). *Laser Fundamentals*, 2nd ed. Cambridge University, Cambridge, U.K.

Spence, D. E., Kean, P. N., and Sibbett, W. (1991). 60-fs pulse generation from self-mode-locked Ti:sapphire laser. *Opt. Lett.* 16, 42–44.

Zakharov, V. E., and Mannakov, S. V. (1974). On the complete integrability of a nonlinear Schrödinger equation. *J. Theor. Math. Phys.* 19, 551–559.

10 Introduction to Feynman Path Integrals

10.1 INTRODUCTION

Feynman's path integrals provide an alternative version of quantum mechanics (Feynman and Hibbs, 1965). This approach is outlined here since Feynman applied it to describe macroscopic beam divergence. The presentation is brief and limited since this subject was mainly selected as an example of an alternative version of quantum mechanics and is not utilized elsewhere in the book.

From a historical perspective, it should further be mentioned that *the quantum analog of the classical action* was first introduced, as a concept, by Dirac in early editions of his book *The Principles of Quantum Mechanics* where he introduced a section entitled 'The action principle' (Dirac, 1958).

10.2 THE CLASSICAL ACTION

Feynman was fascinated by the *principle of least action*, and he gave a lecture on this topic in the *Feynman Lectures of Physics* (Feynman et al., 1965). This principle can be used to describe the possible paths of a particle from an initial to a final point. There is a quantity S that can be computed for each path, and that S is a minimum. Feynman explains further that S is an extremum, that is, the value of S remains unchanged to a first order even if the path is changed slightly (Feynman and Hibbs, 1965). In his lecture, Feynman states, 'the average kinetic energy less the average potential energy is as little as possible for the path of an object.' Then he introduces the integral

$$S = \int_{t_1}^{t_2} \left(\tfrac{1}{2} m \left(\frac{dx}{dt} \right)^2 - mgx \right) dt \tag{10.1}$$

which he also writes as

$$S = \int_{t_1}^{t_2} (KE - PE)\, dt \tag{10.2}$$

$$S = \int_{t_a}^{t_b} L(\dot{x}, x, t)\, dt \tag{10.3}$$

DOI: 10.1201/9781003398707-10

where

$$L = \left(\frac{m}{2}\right)\dot{x}^2 - V(x,t) \tag{10.4}$$

is known as the *Lagrangian*.

In summary: for the true path, between an initial point x_a and a final point x_b, S is a minimum. This concept is illustrated in Figure 10.1, where S_1 and S_2 are two possible paths, S_1 is the true path, and $S_1 < S_2$.

10.3 THE QUANTUM LINK

Feynman and Hibbs (1965) introduce a notation in which a square bracket represents a path between two points in a two-dimensional space. Thus, the action S between a and b is expressed as $S[b, a]$. For the amplitudes due to successive events, Feynman writes

$$S[b,a] = S[b,c] + S[c,a] \tag{10.5}$$

and then he defines the *kernel* $K(b, a)$ as a *path integral*

$$K(b,a) = \int_a^b e^{(i/\hbar)S[b,a]} D\,x(t) \tag{10.6}$$

This is the crucial step in which he introduces the concept of quantum energy into his otherwise classical approach. This is done via de Broglie's relation

$$p = k\hbar = \frac{\partial S}{\partial x} \tag{10.7}$$

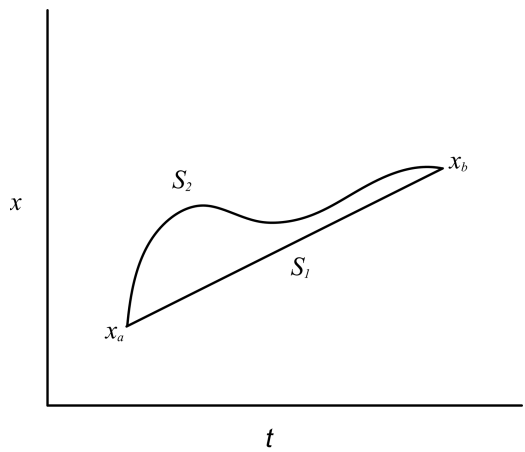

FIGURE 10.1 Least action: S_1 and S_2 are two possible paths between an initial x_0 and a final point x_n. S_1 represents the direct *true path*. S_2 represents a longer convoluted path: $S_1 < S_2$.

which dimensionally leads to an exponent of the form

$$e^{(i/\hbar)S[b,a]} \to e^{(i/2\hbar)px} \to e^{-(mx^2/2i\hbar t)} \tag{10.8}$$

Here, it should be mentioned that equations of the form

$$\left\langle q_t' \middle| q'' \right\rangle = e^{iS/\hbar} \tag{10.9}$$

were first introduced by Dirac (1958) in his discussion of the action principle.

Evaluation of the kernel, via integration, leads to (Feynman and Hibbs, 1965)

$$K(x,t;0,0) = \left(\frac{2\pi i\hbar t}{m}\right)^{-1/2} e^{(imx^2/2\hbar t)} \tag{10.10}$$

In terms that are familiar with concepts already introduced, elsewhere in this book, the probability $P(b,a)$ to go from x_a (at t_a) to x_b (at t_b) is given by

$$P(b,a) = \left|K(b,a)\right|^2 \tag{10.11}$$

and an alternative way to express the *probability amplitude* is

$$K(b,a) = \sum_{a\to b} \varphi[x(t)] = \sum_{a\to b} ce^{(i/\hbar)S[x(t)]} \tag{10.12}$$

where c is a constant and $a \to b$ means all possible paths from a to b.

Thus, Equations (10.10) and (10.12) refer to probability amplitudes and thus relate to the usual wave function.

10.4 PROPAGATION THROUGH A SLIT AND THE UNCERTAINTY PRINCIPLE

Now we consider Feynman's description of propagation through a slit, and we do this in reference to Figure 10.2. The event to be described here can be summarized in the following set of steps:

1. The particle is at $x = 0$ at $t = 0$.
2. The particle passes between $(x_0 - w)$ and $(x_0 + w)$ at $t = T$.
3. The problem is to calculate the probability of finding the particle at position x at a later time $t = T + \tau$.
4. The width of the slit, from $-w$ to $+w$, is $2w$.

The correct quantum mechanical answer must consider all possible paths, so the wave function depends on the sum of all possible paths in the range $-w$ to $+w$, or the integral in that range. Thus, Feynman and Hibbs (1965) write

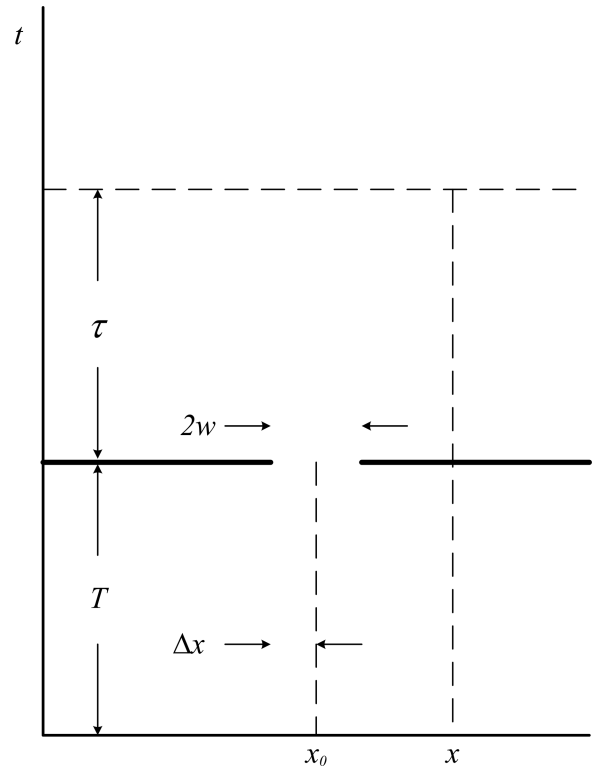

FIGURE 10.2 Propagation through a slit of width $2w$. The particle starts at $x = 0$ at $t = 0$ and passes through $2w$ at $t = T$. This passage position can also be designated as lying between $x_0 - w$ and $x_0 + w$. First, one can calculate the probability amplitude $\psi(x)$ of finding the particle at a position x at some time later denoted by $t = T + \tau$. Once $\psi(x)$ is established then the probability $|\psi(x)|^2$ can be calculated.

$$\psi(x) = \int_{-w}^{+w} K(x + x_0, T + \tau; x_0 + y, T)\, K(x_0 + y, T; 0, 0)\, dy \tag{10.13}$$

which, using Equation (10.10), can be expressed as

$$\psi(x) = \int_{-b}^{+b} \left(\frac{2\pi i\hbar t}{m}\right)^{-1/2} e^{(im(x-y)^2/2\hbar\tau)} \left(\frac{2\pi i\hbar T}{m}\right)^{-1/2} e^{(im(x_0+y)^2/2\hbar T)}\, dy \tag{10.14}$$

Feynman then argues that a Gaussian function $G(y)$ can be introduced in the integrand while extending the range of integration to $\pm\infty$. The function $G(y)$ has a value of unity in the $-w \le y \le +w$ range and zero elsewhere. The introduction of $G(y)$ with

$$G(y) = e^{-y^2/2w^2} \tag{10.15}$$

modifies Equation (10.14) to

$$\psi(x) = \int_{-\infty}^{+\infty} \left(\frac{m}{2\pi i\hbar} \right) (\tau T)^{-1/2} e^{(im(x-y)^2/2\hbar\tau)} e^{(im(x_0+y)^2/2\hbar T)} e^{-y^2/2w^2}\, dy \tag{10.16}$$

Expanding the exponentials, this equation can be written as

$$\psi(x) = \int_{-\infty}^{+\infty} \left(\frac{m}{2\pi i\hbar} \right) (\tau T)^{-1/2} e^{\alpha+\beta y+\gamma y^2}\, dy \tag{10.17}$$

where

$$\alpha = \frac{im}{2\hbar}\left(\frac{x^2}{\tau} + \frac{x_0^2}{T} \right) \tag{10.18}$$

$$\beta = \frac{im}{2\hbar}\left(-\frac{2x}{\tau} + \frac{2x_0}{T} \right) \tag{10.19}$$

$$\gamma = \frac{im}{2\hbar}\left(\frac{1}{\tau} + \frac{1}{T} + \frac{i\hbar}{mw^2} \right) \tag{10.20}$$

This integral, via the exponent described by Equation (10.20), links the quantum quantity $i\hbar$ to the width of the slit $2w$, the interesting physics is in the term $(i\hbar/mw^2)$. Feynman goes on to perform the integral and ends up with the quantity

$$\frac{im}{2\hbar}\left(\frac{1}{\tau} + \frac{1}{T} + \frac{i\hbar}{mw^2} \right) \tag{10.21}$$

as a component of the amplitude of $\psi(x)$. However, rather than performing the integral and following the steps of Feynman and Hibbs (1965), we return to our previous observation that the physics of interest is contained in the term $(i\hbar/mw^2)$ and that this term is the inverse of a temporal quantity, so that

$$\frac{1}{t} \approx \frac{i\hbar}{mw^2} \tag{10.22}$$

The absolute value of this quantity is obtained by multiplying it with its complex conjugate and taking its square root, so that

$$\left| \frac{1}{t} \right| \approx \left| \frac{\hbar}{mw^2} \right| \tag{10.23}$$

If we abstract the absolute notation and notice that the quantity w is a segment of x, that is, $w \to \Delta x$ (see Figure 10.1), then

$$\frac{\Delta x}{t} \approx \frac{\hbar}{m\Delta x} \tag{10.24}$$

$$\Delta p \approx \frac{\hbar}{\Delta x} \tag{10.25}$$

and we arrive at an expression of the form

$$\Delta p\ \Delta x \approx \hbar \tag{10.26}$$

which is a reduced expression of the uncertainty principle as compared with

$$\Delta p\ \Delta x \approx h \tag{10.27}$$

as given by Dirac (1958). In Chapter 3, we describe how to use the uncertainty principle to arrive at the diffraction-limited beam divergence

$$\Delta\theta \approx \frac{\lambda}{\pi w} \tag{10.28}$$

where $2w$ is the width of the slit.

10.4.1 Discussion

Beyond discussing the propagation through a slit and its link to Heisenberg's uncertainty principle, Feynman goes on to derive the Schrödinger equation and discuss many other applications to quantum mechanics using his path integral approach. Regarding our optics perspective, in this brief introduction, we have learned that

1. The path integral approach can be used to describe propagation of particles through macroscopic slits. Yes! Quantum mechanics also applies to macroscopic physics.
2. This approach leads to the uncertainty principle which can be used to describe diffraction-limited beam divergence (see Chapter 3).
3. The path integral approach is mathematically more involved and not as succinct and elegant as the straight-forward Dirac notation to describe basic optics phenomena such as beam divergence.

10.5 FEYNMAN DIAGRAMS IN OPTICS

Since we are discussing about the subject of Feynman, perhaps this is the best place to briefly touch on Feynman diagrams. An introduction to this subject is provided by Feynman himself in his book *QED: The Strange Theory of Light and Matter* (Feynman, 1985). Feynman is said to have invented these diagrams 'as a bookkeeping device for wading through complicated calculations' (Kaiser, 2005) in his particle physics renormalization work.

The very basics of Feynman diagrams are illustrated in Figure 10.3. Time is in the vertical axis, and space is in the horizontal axis. A photon is represented by an undulating line, while an electron is represented by a straight line. Using Feynman's language, a photon has an *amplitude* to go from point A to point B as depicted in Figure 10.3a.

Similarly, an electron has an amplitude to go from point A to point B as depicted in Figure 10.3b. Note: in Feynman's language, the concept of 'amplitude' is equivalent to 'kernel' and since $P(b,a) = \left|K(b,a)\right|^2$, it is also equivalent to probability amplitude.

An electron has an amplitude to emit or absorb a photon as depicted in Figure 10.4.

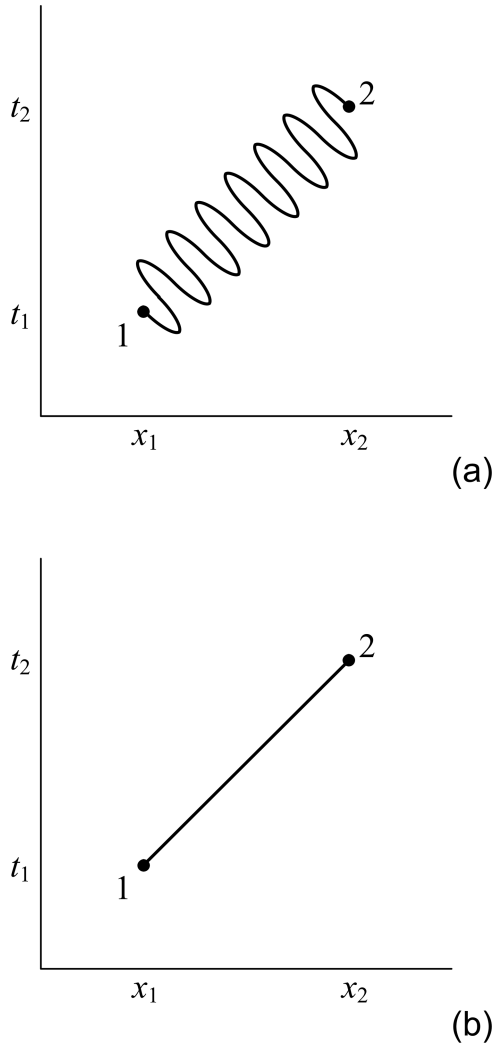

FIGURE 10.3 (a) Time–space Feynman diagram for the photon amplitude to go from point 1 to point 2. (b) Time–space Feynman diagram for the electron amplitude to go from point 1 to point 2.

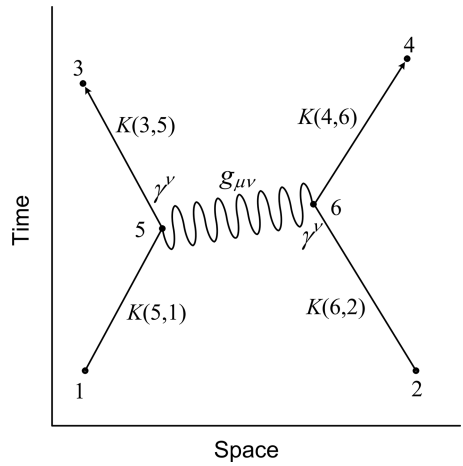

FIGURE 10.4 Feynman diagram for the most basic form of electron scattering involving emission and absorption of a photon.

Here, a photon is emitted at 5 and absorbed at 6. The emission is caused by the electron at 1 transitioning to 3, and the absorption is allowed by the electron at 2 transitioning to 4. Each of the electron lines corresponds to elements of probability amplitudes (kernels) as does the undulating line of the photon.

The overall probability amplitude of the scattering process depicted in this Feynman diagram can be written as

$$K(3,5)\, ie\gamma^{\nu} K(1,5)\left(\frac{-ig_{\mu\nu}}{p^2}\right) K(4,6)\, ie\gamma^{\nu} K(6,2) \tag{10.29}$$

The reader will observe that this is a multiplication involving the incident and output electron kernels, the amplitude representing the vertices $ie\gamma^{\nu}$, and the photon amplitude $(-ieg_{\mu\nu}/p^2)$. The quantity $g_{\mu\nu}$ is a tensor. For the complete set of rules governing Feynman diagrams, the reader should refer to Peskin and Schroeder (1995).

The scattering process depicted in Figure 10.4, involving only one photon, is the simplest alternative. Other more complicated alternatives involving two photons, or three photons, are also possible. However, the probability is significantly lower each time an extra photon is involved.

Perhaps the first use of Feynman diagrams in quantum optics was initiated via the description of 'the scattering of light by light' by Ward (1950). Yariv (1977) applied Feynman diagram concepts to the description of Raman scattering, while Butcher and Cotter (1991) applied the same diagram technique to describe the third harmonic generation. Feynman diagrams should also be useful in the description of photon absorption by electrons at single-photon detector surfaces.

PROBLEMS

10.1 Show that the exponential forms in Equation (10.8) are equivalent.
10.2 Show that Equation (10.16) can be expressed as Equation (10.17) in conjunction with Equations (10.18) to (10.20).
10.3 Draw a Feynman diagram for the scattering process illustrated in Figure 10.4 involving (a) one extra photon and (b) two extra photons.

REFERENCES

Butcher, P. N., and Cotter, D. (1991). *The Elements of Nonlinear Optics*, Cambridge University, Cambridge, U.K.
Dirac, P. A. M. (1978). *The Principles of Quantum Mechanics*, 4th ed. Oxford, London, U.K.
Feynman, R. P. (1985). *QED: The Strange Theory of Light and Matter*, Princeton University, Princeton, NJ.
Feynman, R. P., and Hibbs, A. R. (1965). *Quantum Mechanics and Path Integrals*, McGraw-Hill, New York.
Feynman, R. P., Leighton, R. B, and Sands, M. (1965). *The Feynman Lectures on Physics*, Vol. II. Addison-Wesley, Reading, MA.
Kaiser, D. (2005). *Drawing Theories Apart: The Dispersion of Feynman Diagrams in Postwar Physics*, Chicago University, Chicago, IL.
Peskin, M. E., and Schroeder, D. V. (1995). *An Introduction to Quantum Field Theory*, Perseus Books, Reading, MA.
Ward, J. C. (1950). The scattering of light by light. *Phys. Rev*. 77, 293.
Yariv, A. (1977). The application of time evolution operators and Feynman diagrams to nonlinear optics. *IEEE J. Quantum Electron*. QE-13, 943–950.

11 Matrix Aspects of Quantum Mechanics and Quantum Operators

11.1 INTRODUCTION

As mentioned in Chapter 1, Heisenberg's matrix mechanics provides one of the three main avenues of quantum mechanics. This approach to quantum mechanics was disclosed in three papers authored by Heisenberg (1925), Born and Jordan (1925), and Born et al. (1926). An iconic result from the Heisenberg–Born–Jordan contribution was the *commutation rule*

$$pq - qp = \frac{h}{2\pi i} \tag{11.1}$$

$$pq - qp = -i\hbar \tag{11.2}$$

Here, we examine the origin of the commutation rule, using Feynman's approach, and provide a brief pragmatic introduction to some salient aspects of matrix quantum mechanics with a focus on Pauli matrices. We begin with a review preamble on vector and matrix algebra.

11.2 INTRODUCTION TO VECTOR AND MATRIX ALGEBRA

Here, a few of the salient and useful features of classical vector and classical matrix algebra are introduced in a very pragmatic approach.

11.2.1 Vector Algebra

A vector in three dimensions (x, y, z) is depicted in Figure 11.1. The sum of two vectors $\mathbf{r} + \mathbf{s}$, illustrated in Figure 11.2, is defined as

$$\begin{pmatrix} r_1 \\ r_2 \\ r_3 \end{pmatrix} + \begin{pmatrix} s_1 \\ s_2 \\ s_3 \end{pmatrix} = \begin{pmatrix} r_1 + s_1 \\ r_2 + s_2 \\ r_3 + s_3 \end{pmatrix} \tag{11.3}$$

Subtraction of two vectors $\mathbf{r} - \mathbf{s}$, illustrated in Figure 11.3, is defined as

DOI: 10.1201/9781003398707-11

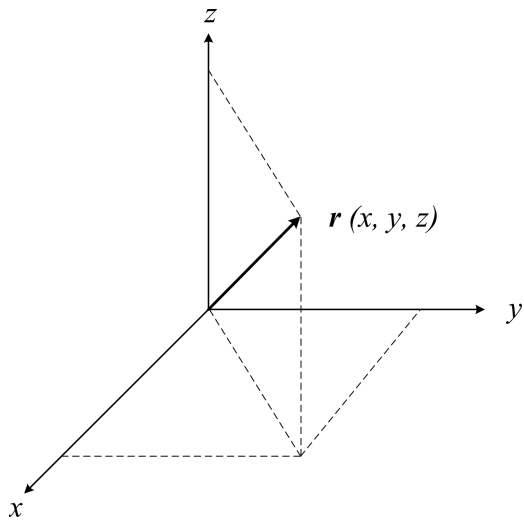

FIGURE 11.1 Vector in three dimensions.

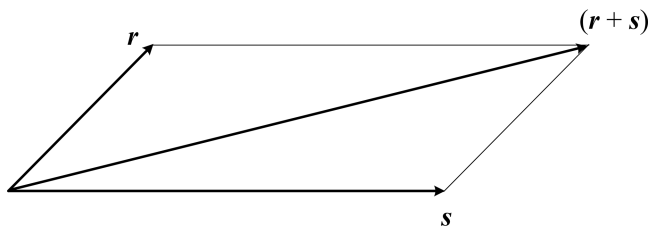

FIGURE 11.2 Vector addition $\mathbf{r}+\mathbf{s}$.

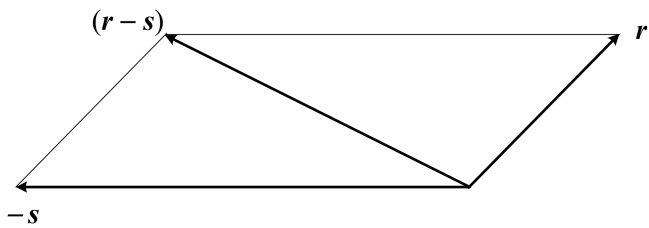

FIGURE 11.3 Vector subtraction $\mathbf{r}-\mathbf{s}$.

$$\begin{pmatrix} r_1 \\ r_2 \\ r_3 \end{pmatrix} - \begin{pmatrix} s_1 \\ s_2 \\ s_3 \end{pmatrix} = \begin{pmatrix} r_1 - s_1 \\ r_2 - s_2 \\ r_3 - s_3 \end{pmatrix} \tag{11.4}$$

Multiplication of a vector $\mathbf{r}$ with a scalar number a, thus creating a new vector $a\mathbf{r}$, is defined as

$$a\begin{pmatrix} r_1 \\ r_2 \\ r_3 \end{pmatrix} = \begin{pmatrix} ar_1 \\ ar_2 \\ ar_3 \end{pmatrix} \tag{11.5}$$

The length of a vector $\mathbf{s}$ is defined as $|\mathbf{s}|$

$$|\mathbf{s}|^2 = \begin{vmatrix} s_1 \\ s_2 \\ s_3 \end{vmatrix}^2 = (s_1^2 + s_2^2 + s_3^2)\lceil \tag{11.6}$$

and the dot product of two vectors $\mathbf{r} \cdot \mathbf{s}$, as shown in Figure 11.4, is a scalar defined as

$$\begin{pmatrix} r_1 \\ r_2 \\ r_3 \end{pmatrix} \cdot \begin{pmatrix} s_1 \\ s_2 \\ s_3 \end{pmatrix} = (r_1 s_1 + r_2 s_2 + r_3 s_3) \tag{11.7}$$

In reference to Figure 11.4, the angle between the two vectors is defined as θ and the law of cosines is applied

$$\mathbf{r} \cdot \mathbf{s} = |\mathbf{r}||\mathbf{s}|\cos\theta \tag{11.8}$$

The cross-product of two vectors $\mathbf{r} \times \mathbf{s}$ is a new vector defined as

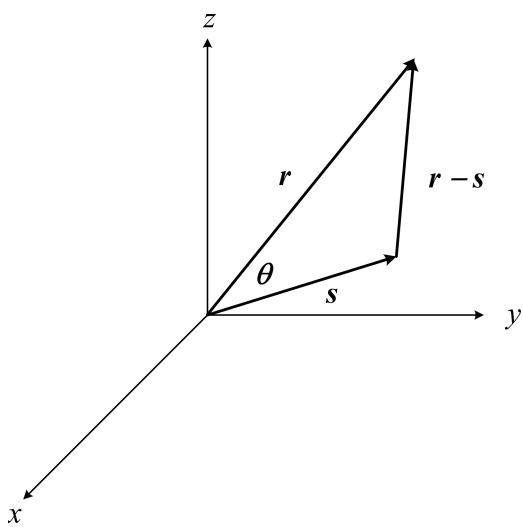

FIGURE 11.4 Dot product $\mathbf{r} \cdot \mathbf{s}$. The angle between the two vectors is θ.

$$\begin{pmatrix} r_1 \\ r_2 \\ r_3 \end{pmatrix} \times \begin{pmatrix} s_1 \\ s_2 \\ s_3 \end{pmatrix} = \begin{pmatrix} r_2 s_3 - r_3 s_2 \\ r_3 s_1 - r_1 s_3 \\ r_1 s_2 - r_2 s_1 \end{pmatrix} \tag{11.9}$$

The magnitude of $\mathbf{r} \times \mathbf{s}$ is the area of the parallelogram formed by **r** and **s**, and its direction is determined by the right-hand rule as illustrated in Figure 11.5.

Some useful vector identities involve the *derivative operators* ∇ and ∇^2

$$\nabla(\mathbf{AB}) = (\nabla \mathbf{A})\mathbf{B} + \mathbf{A}(\nabla \mathbf{B}) = \mathbf{B}\nabla \mathbf{A} + \mathbf{A}\nabla \mathbf{B} \tag{11.10}$$

$$\nabla \times (\mathbf{AB}) = \mathbf{B}(\nabla \times \mathbf{A}) - \mathbf{A} \times \nabla \mathbf{B} \tag{11.11}$$

$$\nabla \times (\nabla \times \mathbf{C}) = \nabla(\nabla \cdot \mathbf{C}) - (\nabla \cdot \nabla)\mathbf{C} \tag{11.12}$$

where

$$\nabla = \begin{pmatrix} \partial/\partial x \\ \partial/\partial y \\ \partial/\partial z \end{pmatrix} \tag{11.13}$$

and

$$\nabla^2 = (\partial^2/\partial x^2 + \partial^2/\partial y^2 + \partial/\partial z^2) \tag{11.14}$$

These identities are useful in dealing with wave equations (see Chapter 12) and a range of other applications including electromagnetism.

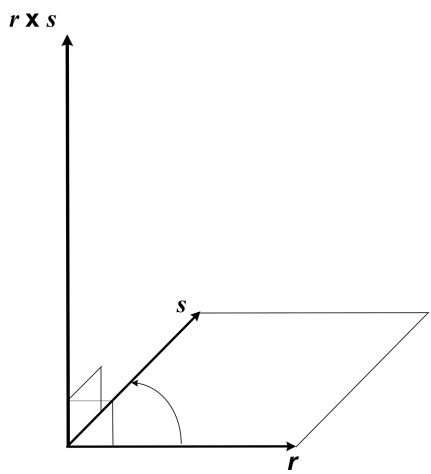

FIGURE 11.5 Cross-product $\mathbf{r} \times \mathbf{s}$ (vector diagram not to scale).

11.2.2 Matrix Algebra

For simplicity, we consider mainly 2×2 matrices albeit the algebra is also applicable to 3×3 and higher order matrices. We begin by defining the 2×2 matrix A

$$A=\begin{pmatrix} a_{11} & a_{12} \\ a_{21} & a_{22} \end{pmatrix} \tag{11.15}$$

and the 2×2 matrix B

$$B=\begin{pmatrix} b_{11} & b_{12} \\ b_{21} & b_{22} \end{pmatrix} \tag{11.16}$$

thus the matrix addition $A+B$ yields

$$A+B=\begin{pmatrix} a_{11}+b_{11} & a_{12}+b_{12} \\ a_{21}+b_{21} & a_{22}+b_{22} \end{pmatrix} \tag{11.17}$$

and the subtraction $A-B$ yields

$$A-B=\begin{pmatrix} a_{11}-b_{11} & a_{12}-b_{12} \\ a_{21}-b_{21} & a_{22}-b_{22} \end{pmatrix} \tag{11.18}$$

Multiplication of the matrix A by (-1) is equivalent to multiply each individual component of the matrix by (-1)

$$(-1)A=\begin{pmatrix} -a_{11} & -a_{12} \\ -a_{21} & -a_{22} \end{pmatrix} \tag{11.19}$$

Similarly, multiplication of the matrix A by the quantity i is equivalent to multiplying each individual component of the matrix by i

$$iA=\begin{pmatrix} ia_{11} & ia_{12} \\ ia_{21} & ia_{22} \end{pmatrix} \tag{11.20}$$

The simple product of two matrices AB is

$$AB=\begin{pmatrix} a_{11} & a_{12} \\ a_{21} & a_{22} \end{pmatrix}\begin{pmatrix} b_{11} & b_{12} \\ b_{21} & b_{22} \end{pmatrix}=\begin{pmatrix} a_{11}b_{11}+a_{12}b_{21} & a_{11}b_{12}+a_{12}b_{22} \\ a_{21}b_{11}+a_{22}b_{21} & a_{21}b_{12}+a_{22}b_{22} \end{pmatrix} \tag{11.21}$$

and the simple product of two matrices BA is

$$BA = \begin{pmatrix} b_{11} & b_{12} \\ b_{21} & b_{22} \end{pmatrix} \begin{pmatrix} a_{11} & a_{12} \\ a_{21} & a_{22} \end{pmatrix} = \begin{pmatrix} b_{11}a_{11} + b_{12}a_{21} & b_{11}a_{12} + b_{12}a_{22} \\ b_{21}a_{11} + b_{22}a_{21} & b_{21}a_{12} + b_{22}a_{22} \end{pmatrix} \tag{11.22}$$

Notice that

$$AB - BA \neq 0 \tag{11.23}$$

or

$$AB \neq BA \tag{11.24}$$

which is an iconic result in matrix algebra. However, with certain very special matrices, the condition described by Equation (11.24) might not hold as we shall see next.

Identity matrices are defined as follows: for a 2×2 matrix

$$I = \begin{pmatrix} 1 & 0 \\ 0 & 1 \end{pmatrix} \tag{11.25}$$

a 3×3 matrix

$$I = \begin{pmatrix} 1 & 0 & 0 \\ 0 & 1 & 0 \\ 0 & 0 & 1 \end{pmatrix} \tag{11.26}$$

and a 4×4 matrix

$$I = \begin{pmatrix} 1 & 0 & 0 & 0 \\ 0 & 1 & 0 & 0 \\ 0 & 0 & 1 & 0 \\ 0 & 0 & 0 & 1 \end{pmatrix} \tag{11.27}$$

$$IA = AI = A \tag{11.28}$$

Obviously, $IA - AI = 0$ which is an exception to the condition described in Equation (11.24).

The inverse, or reciprocal, matrix C^{-1} is a unique matrix that, multiplied with the original matrix C, yields the identity matrix, so that

$$C\ C^{-1} = C^{-1}C = I \tag{11.29}$$

$$(C^{-1})^{-1} = I \tag{11.30}$$

If matrices C and H have inverses, C^{-1} and H^{-1}, then

$$(C\ H)^{-1} = C^{-1}H^{-1} \tag{11.31}$$

and

$$C^{-1}H^{-1}C\ H = C\ H\ C^{-1}H^{-1} = I \tag{11.32}$$

The *determinant* of a 2×2 matrix is defined as

$$|A| = \begin{vmatrix} a_{11} & a_{12} \\ a_{21} & a_{22} \end{vmatrix} = a_{11}a_{22} - a_{21}a_{12} \tag{11.33}$$

For a 3×3 matrix the determinant is defined as

$$|A| = \begin{vmatrix} a_{11} & a_{12} & a_{13} \\ a_{21} & a_{22} & a_{23} \\ a_{31} & a_{32} & a_{33} \end{vmatrix} = a_{11}\begin{vmatrix} a_{22} & a_{23} \\ a_{32} & a_{33} \end{vmatrix} - a_{12}\begin{vmatrix} a_{21} & a_{23} \\ a_{31} & a_{33} \end{vmatrix} + a_{13}\begin{vmatrix} a_{21} & a_{22} \\ a_{31} & a_{32} \end{vmatrix} \tag{11.34}$$

and so on for $N\times N$ matrices.

Finally, in this section, we define the *trace* of a matrix: this quantity Tr is defined as the sum of the diagonal elements of a matrix

$$Tr(A) = \sum_j a_{jj} \tag{11.35}$$

so that for our 3×3 matrix

$$Tr(A) = \sum_{j=1}^{N=3} a_{jj} = a_{11} + a_{22} + a_{33} \tag{11.36}$$

For example, if

$$D = \begin{pmatrix} 1 & 1-i \\ 1+i & -1 \end{pmatrix} \tag{11.37}$$

$$D^{-1} = 3^{-1}\begin{pmatrix} 1 & 1-i \\ 1+i & -1 \end{pmatrix} \tag{11.38}$$

$$D\ D^{-1} = \begin{pmatrix} 1 & 1-i \\ 1+i & -1 \end{pmatrix} 3^{-1}\begin{pmatrix} 1 & 1-i \\ 1+i & -1 \end{pmatrix} = 3^{-1}\begin{pmatrix} 3 & 0 \\ 0 & 3 \end{pmatrix} = I \tag{11.39}$$

Moreover, the determinant of this matrix $|D|$ (see Equation (11.33)) is

$$|D| = \left| \begin{pmatrix} 1 & 1-i \\ 1+i & -1 \end{pmatrix} \right| = -1 + (1+i)(1-i) = -1+2 = 1 \tag{11.40}$$

and its trace is

$$Tr(D) = 1 + (-1) = 0 \tag{11.41}$$

11.2.3 Unitary Matrices

A complex matrix G, obeying the property

$$G\, G^* = G^* G = I \tag{11.42}$$

is considered to be a *unitary* matrix (Lipschutz, 1968). For example, if

$$G = \begin{pmatrix} i & 0 \\ 0 & i \end{pmatrix} \tag{11.43}$$

then

$$G\, G^* = \begin{pmatrix} i & 0 \\ 0 & i \end{pmatrix} \begin{pmatrix} -i & 0 \\ 0 & -i \end{pmatrix} = I \tag{11.44}$$

Here it should be noted that some authors (Tropper, 1968) define a unitary matrix as a matrix J exhibiting the more stringent property

$$(J^*)^T J = J (J^*)^T = I \tag{11.45}$$

In this regard, if

$$J = \begin{pmatrix} +i & 0 \\ 0 & -i \end{pmatrix} \tag{11.46}$$

$$(J^*)^T = \begin{pmatrix} -i & 0 \\ 0 & +i \end{pmatrix} \tag{11.47}$$

and the condition imposed in Equation (11.45) is met, namely,

$$\begin{pmatrix} -i & 0 \\ 0 & +i \end{pmatrix} \begin{pmatrix} +i & 0 \\ 0 & -i \end{pmatrix} = \begin{pmatrix} +i & 0 \\ 0 & -i \end{pmatrix} \begin{pmatrix} -i & 0 \\ 0 & +i \end{pmatrix} = \begin{pmatrix} 1 & 0 \\ 0 & 1 \end{pmatrix} \tag{11.48}$$

11.3 PAULI MATRICES

Pauli matrices are widely used in quantum polarization (see Chapter 16); thus, here we provide an introduction to the subject via the Hamiltonian following Feynman's style.

The time-dependent equation for a two-state system is (Dirac, 1958)

$$i\hbar \frac{dC_i}{dt} = \sum_j H_{ij} C_j \tag{11.49}$$

or

$$i\hbar \frac{dC_1}{dt} = H_{11} C_1 + H_{12} C_2 \tag{11.50}$$

$$i\hbar \frac{dC_2}{dt} = H_{21} C_1 + H_{22} C_2 \tag{11.51}$$

and for a spin one-half particle, such as an electron, under the influence of a magnetic field, the Hamiltonian becomes (Feynman et al., 1965)

$$\begin{pmatrix} H_{11} & H_{12} \\ H_{21} & H_{22} \end{pmatrix} = \begin{pmatrix} -\mu B_z & -\mu(B_x - iB_y) \\ -\mu(B_x + iB_y) & +\mu B_z \end{pmatrix} \tag{11.52}$$

In general, the Hamiltonian for a spin one-half particle can be defined as (Feynman et al., 1965)

$$H_{ij} = -\mu\left(\sigma_{ij}^x B_x + \sigma_{ij}^y B_y + \sigma_{ij}^z B_z\right) \tag{11.53}$$

While observing the definitions given in Equations (11.52) and (11.53), we see that for the z component, that is B_z, we have

$$H_{11} = -\mu\sigma_{11}^z B_z = -\mu B_z \tag{11.54}$$

$$H_{12} = -\mu\sigma_{12}^z B_z = 0 \tag{11.55}$$

$$H_{21} = -\mu\sigma_{21}^z B_z = 0 \tag{11.56}$$

$$H_{22} = -\mu\sigma_{22}^z B_z = +\mu B_z \tag{11.57}$$

which implies that

$$\sigma_{11}^{z} = 1 \tag{11.58}$$

$$\sigma_{12}^{z} = 0 \tag{11.59}$$

$$\sigma_{21}^{z} = 0 \tag{11.60}$$

$$\sigma_{22}^{z} = -1 \tag{11.61}$$

so that, in matrix form (Dirac, 1958)

$$\sigma_{ij}^{z} = \sigma_z = \begin{pmatrix} 1 & 0 \\ 0 & -1 \end{pmatrix} \tag{11.62}$$

Similarly, we find for the x and y components (Dirac, 1958)

$$\sigma_{ij}^{x} = \sigma_x = \begin{pmatrix} 0 & 1 \\ 1 & 0 \end{pmatrix} \tag{11.63}$$

$$\sigma_{ij}^{y} = \sigma_y = \begin{pmatrix} 0 & -i \\ i & 0 \end{pmatrix} \tag{14.64}$$

The 2×2 matrices σ_x, σ_y, and σ_z are known as Pauli matrices (Dirac, 1958) and are very important to spin and magnetic moment computations. Some properties of these matrices are (Dirac, 1958; Jordan, 1986)

$$\sigma_x^2 = \sigma_y^2 = \sigma_z^2 = 1 \tag{11.65}$$

$$\sigma_x \sigma_y = i\sigma_z \tag{11.66}$$

$$\sigma_y \sigma_x = -i\sigma_z \tag{11.67}$$

$$\sigma_y \sigma_z = i\sigma_x \tag{11.68}$$

$$\sigma_z \sigma_y = -i\sigma_x \tag{11.69}$$

$$\sigma_z \sigma_x = i\sigma_y \tag{11.70}$$

$$\sigma_x\sigma_z = -i\sigma_y \tag{11.71}$$

$$\sigma_x\sigma_y\sigma_z = i \tag{11.72}$$

The σ_y matrix is also known to be *Hermitian*, that is, this matrix is identical to its own *conjugate transpose*. In other words, the conjugate of σ_y is

$$\sigma_y^* = \begin{pmatrix} 0 & -i \\ +i & 0 \end{pmatrix}^* = \begin{pmatrix} 0 & +i \\ -i & 0 \end{pmatrix} \tag{11.73}$$

and the transpose (rows → column) of σ_y^* is $(\sigma_y^*)^T$

$$(\sigma_y^*)^T = \begin{pmatrix} 0 & +i \\ -i & 0 \end{pmatrix}^T = \begin{pmatrix} 0 & -i \\ +i & 0 \end{pmatrix} = \sigma_y \tag{11.74}$$

Comparison of Equation (11.73) and (11.74) indicate that

$$\sigma_y = (\sigma_y)^\dagger \tag{11.75}$$

where the symbol † represents the combined conjugate transpose operation, that is, the *Hermitian* property.

11.3.1 Eigenvalues of Pauli Matrices

In the matrix identity

$$AX = tX \tag{11.76}$$

the vector

$$X = \begin{pmatrix} x \\ y \end{pmatrix} \tag{11.77}$$

is an *eigenvector* and the scalar t is an eigenvalue. Setting $A = \sigma_x$:

$$\begin{pmatrix} 0 & 1 \\ 1 & 0 \end{pmatrix}\begin{pmatrix} x \\ y \end{pmatrix} = t\begin{pmatrix} x \\ y \end{pmatrix} \tag{11.78}$$

$$0x + 1y = tx \tag{11.79}$$

$$1x + 0y = ty \tag{11.80}$$

$$\begin{vmatrix} t & -1 \\ -1 & t \end{vmatrix} \tag{11.81}$$

$$t^2 - 1 = 0 \tag{11.82}$$

and the eigenvalues are

$$t = \pm 1 \tag{11.83}$$

For $t = +1$

$$\begin{pmatrix} +1 & -1 \\ -1 & +1 \end{pmatrix} \tag{11.84}$$

so that

$$x - y = 0 \tag{11.85}$$

$$-x + y = 0 \tag{11.86}$$

and an eigenvector is

$$X_1 = \begin{pmatrix} x \\ y \end{pmatrix} = \begin{pmatrix} 1 \\ 1 \end{pmatrix} \tag{11.87}$$

Similarly for $t = -1$, the second eigenvector can be

$$X_2 = \begin{pmatrix} 1 \\ -1 \end{pmatrix} \tag{11.88}$$

For$A = \sigma_y$:

$$\begin{pmatrix} 0 & -i \\ i & 0 \end{pmatrix} \begin{pmatrix} x \\ y \end{pmatrix} = t \begin{pmatrix} x \\ y \end{pmatrix} \tag{11.89}$$

$$0x - iy = tx \tag{11.90}$$

$$ix + 0y = ty \tag{11.91}$$

$$\begin{vmatrix} t & +i \\ -i & t \end{vmatrix} \tag{11.92}$$

$$t^2 - 1 = 0 \tag{11.93}$$

and the eigenvalues are

$$t = \pm 1 \tag{11.94}$$

A set of corresponding eigenvectors, for $t = \pm 1$, is

$$X_1 = \begin{pmatrix} -i \\ 1 \end{pmatrix} \tag{11.95}$$

$$X_2 = \begin{pmatrix} 1 \\ -i \end{pmatrix} \tag{11.96}$$

11.3.2 Pauli Matrices for Spin One-Half Particles

Electrons and protons are defined as Fermions and have an intrinsic angular momentum of $\hbar/2$ (Feynman et al., 1965). Thus, the electron is said to be a spin one-half, or spin $-\frac{1}{2}$, particle. Moreover, the electron can have its spin up $|+\rangle$ or it can have its spin down $|-\rangle$. Pauli introduced spin operators to describe the condition of the electron as

$$\hat{S} = \tfrac{1}{2}\hbar\hat{\sigma} \tag{11.97}$$

where

$$\hat{S}_x = \tfrac{1}{2}\hbar\begin{pmatrix} 0 & 1 \\ 1 & 0 \end{pmatrix} \tag{11.98}$$

$$\hat{S}_y = \tfrac{1}{2}\hbar\begin{pmatrix} 0 & -i \\ i & 0 \end{pmatrix} \tag{11.99}$$

$$\hat{S}_z = \tfrac{1}{2}\hbar\begin{pmatrix} 1 & 0 \\ 0 & -1 \end{pmatrix} \tag{11.100}$$

These matrices satisfy (Robson, 1974)

$$\hat{S}_x^2 + \hat{S}_y^2 + \hat{S}_z^2 = \tfrac{3}{4}\hbar^2\begin{pmatrix} 1 & 0 \\ 0 & 1 \end{pmatrix} \tag{11.101}$$

and the angular momentum commutation rules become

$$\hat{S}_x\hat{S}_y - \hat{S}_y\hat{S}_x = \frac{\hbar^2}{4}\left\{\begin{pmatrix} 0 & 1 \\ 1 & 0 \end{pmatrix}\begin{pmatrix} 0 & -i \\ i & 0 \end{pmatrix} - \begin{pmatrix} 0 & -i \\ i & 0 \end{pmatrix}\begin{pmatrix} 0 & 1 \\ 1 & 0 \end{pmatrix}\right\}$$

$$= \frac{i\hbar^2}{2}\begin{pmatrix} 1 & 0 \\ 0 & -1 \end{pmatrix} \tag{11.102}$$

so that

$$\hat{S}_x\hat{S}_y - \hat{S}_y\hat{S}_x = i\hbar\hat{S}_z \tag{11.103}$$

and similarly

$$\hat{S}_z\hat{S}_x - \hat{S}_x\hat{S}_z = i\hbar\hat{S}_y \tag{11.104}$$

$$\hat{S}_y\hat{S}_z - \hat{S}_z\hat{S}_y = i\hbar\hat{S}_x \tag{11.105}$$

as can be verified by expansion. Equations (11.98) to (11.101) are useful in the description of polarized beam of electrons (Robson, 1974).

The eigenvalues of Equation (11.101) are

$$\tfrac{3}{4}\hbar^2 = s(s+1)\hbar^2 \tag{11.106}$$

where $s = \frac{1}{2}$. By inspection, eigenvalues of $\hat{S}_z$ are

$$\pm\tfrac{1}{2}\hbar = \pm s\hbar \tag{11.107}$$

Now, without derivation, we introduce the quantum angular momentum

$$|J| = [j(j+1)]^{1/2}\hbar \tag{11.108}$$

where

$$j = l \pm s = l \pm \tfrac{1}{2} \tag{11.109}$$

Here, we already know that s is related to the spin angular momentum and can take the values $\pm\frac{1}{2}$. On the other hand, l is related to the orbital angular momentum and can take the values $l = 0, 1, 2, 3....$ Equation (11.109) in conjunction with Pauli's exclusion principle can be used to gain a glimpse of the energy level structure of hydrogen. This is an alternative way to describe the hydrogen atom to the formal Schrödinger equation path outlined in Chapter 9.

Pauli's exclusion principle: 'two electrons are never in the same state' (Dirac, 1958). This means that no two electrons can have the same quantum numbers.

11.3.3 The Tensor Product

This section is based on the brief introduction given by Duarte (2019), and it is specifically tailored to deal with tensor elements applicable to the mathematics of the probability amplitude of quantum entanglement. This is an alternative notation to the vector product notation used in Chapters 15–17.

The *tensor product* is also known as the Kronecker product $\mathbf{U} \otimes \mathbf{W}$:

$$|u\rangle \otimes |w\rangle = \begin{pmatrix} u_1 \\ u_2 \end{pmatrix} \otimes \begin{pmatrix} w_1 \\ w_2 \end{pmatrix} = \begin{pmatrix} u_1 w_1 \\ u_1 w_2 \\ u_2 w_1 \\ u_2 w_2 \end{pmatrix} \tag{11.110}$$

For the vectors

$$|1\rangle = \begin{pmatrix} 1 \\ 0 \end{pmatrix} \tag{11.111}$$

$$|0\rangle = \begin{pmatrix} 0 \\ 1 \end{pmatrix} \tag{11.112}$$

we can find the following products

$$|1\rangle \otimes |1\rangle = \begin{pmatrix} 1 \\ 0 \\ 0 \\ 0 \end{pmatrix} \tag{11.113}$$

$$|1\rangle \otimes |0\rangle = \begin{pmatrix} 0 \\ 1 \\ 0 \\ 0 \end{pmatrix} \tag{11.114}$$

$$|0\rangle \otimes |1\rangle = \begin{pmatrix} 0 \\ 0 \\ 1 \\ 0 \end{pmatrix} \tag{11.115}$$

$$|0\rangle \otimes |0\rangle = \begin{pmatrix} 0 \\ 0 \\ 0 \\ 1 \end{pmatrix} \tag{11.116}$$

For 2×2 matrices, the Kronecker product $\mathbf{U}\otimes\mathbf{W}$ is defined as

$$\begin{pmatrix} u_{11} & u_{12} \\ u_{21} & u_{22} \end{pmatrix}\otimes\begin{pmatrix} w_{11} & w_{12} \\ w_{21} & w_{22} \end{pmatrix}=\begin{pmatrix} u_{11}w_{11} & u_{11}w_{12} & u_{12}w_{11} & u_{12}w_{12} \\ u_{11}w_{21} & u_{11}w_{22} & u_{12}w_{21} & u_{12}w_{22} \\ u_{21}w_{11} & u_{21}w_{12} & u_{22}w_{11} & u_{22}w_{12} \\ u_{21}w_{21} & u_{21}w_{22} & u_{22}w_{21} & u_{22}w_{22} \end{pmatrix} \tag{11.117}$$

Kronecker multiplication of Pauli matrices yields the following 4×4 matrices

$$\sigma_x\otimes\sigma_y=\begin{pmatrix} 0 & 1 \\ 1 & 0 \end{pmatrix}\otimes\begin{pmatrix} 0 & -i \\ i & 0 \end{pmatrix}=\begin{pmatrix} 0 & 0 & 0 & -i \\ 0 & 0 & i & 0 \\ 0 & -i & 0 & 0 \\ i & 0 & 0 & 0 \end{pmatrix} \tag{11.118}$$

$$\sigma_x\otimes\sigma_z=\begin{pmatrix} 0 & 1 \\ 1 & 0 \end{pmatrix}\otimes\begin{pmatrix} 1 & 0 \\ 0 & -1 \end{pmatrix}=\begin{pmatrix} 0 & 0 & 1 & 0 \\ 0 & 0 & 0 & -1 \\ 1 & 0 & 0 & 0 \\ 0 & -1 & 0 & 0 \end{pmatrix} \tag{11.119}$$

$$\sigma_y\otimes\sigma_x=\begin{pmatrix} 0 & -i \\ i & 0 \end{pmatrix}\otimes\begin{pmatrix} 0 & 1 \\ 1 & 0 \end{pmatrix}=\begin{pmatrix} 0 & 0 & 0 & -i \\ 0 & 0 & -i & 0 \\ 0 & i & 0 & 0 \\ i & 0 & 0 & 0 \end{pmatrix} \tag{11.120}$$

$$\sigma_y\otimes\sigma_z=\begin{pmatrix} 0 & -i \\ i & 0 \end{pmatrix}\otimes\begin{pmatrix} 1 & 0 \\ 0 & -1 \end{pmatrix}=\begin{pmatrix} 0 & 0 & -i & 0 \\ 0 & 0 & 0 & i \\ i & 0 & 0 & 0 \\ 0 & -i & 0 & 0 \end{pmatrix} \tag{11.121}$$

$$\sigma_z\otimes\sigma_x=\begin{pmatrix} 1 & 0 \\ 0 & -1 \end{pmatrix}\otimes\begin{pmatrix} 0 & 1 \\ 1 & 0 \end{pmatrix}=\begin{pmatrix} 0 & 1 & 0 & 0 \\ 1 & 0 & 0 & 0 \\ 0 & 0 & 0 & -1 \\ 0 & 0 & -1 & 0 \end{pmatrix} \tag{11.122}$$

$$\sigma_z\otimes\sigma_y=\begin{pmatrix} 1 & 0 \\ 0 & -1 \end{pmatrix}\otimes\begin{pmatrix} 0 & -i \\ i & 0 \end{pmatrix}=\begin{pmatrix} 0 & -i & 0 & 0 \\ i & 0 & 0 & 0 \\ 0 & 0 & 0 & i \\ 0 & 0 & -i & 0 \end{pmatrix} \tag{11.123}$$

11.4 INTRODUCTION TO THE DENSITY MATRIX

Here we provide a brief introduction to the concept of density matrices. The description given here is aimed at illustrating the density matrix formalism applicable to the description of multiple-level transitions (see Appendix A). First, we express the Schrödinger equation as (Dirac, 1958)

$$i\hbar \frac{d|m\rangle}{dt} = H|m\rangle \tag{11.124}$$

$$i\hbar \frac{d\langle m|}{dt} = H\langle m| \tag{11.125}$$

and define the 'quantum density' as (Dirac, 1958)

$$\rho = \sum_m |m\rangle P_m \langle m| \tag{11.126}$$

where P_m is an mth state. Differentiating the quantum density with respect to time, yields

$$i\hbar \frac{d\rho}{dt} = \sum_m i\hbar \left(\frac{d|m\rangle}{dt} P_m \langle m| + |m\rangle P_m \frac{d\langle m|}{dt} \right) \tag{11.127}$$

and using Equations (11.124) and (11.125)

$$i\hbar \frac{d\rho}{dt} = \sum_m \left(H|m\rangle P_m \langle m| + |m\rangle P_m H\langle m| \right) \tag{11.128}$$

which can be written as (Dirac, 1958)

$$i\hbar \frac{d\rho}{dt} = \left(H\rho - \rho H \right) \tag{11.129}$$

$$\frac{d\rho}{dt} = -\frac{i}{\hbar}[H, \rho] \tag{11.130}$$

Dirac argues that the sum of the P_m states can be equal to unity, thus allowing Equation (11.126) to be expressed simply as

$$\rho = |m\rangle \langle m| \tag{11.131}$$

which can be expanded in an explicit form as

$$\rho = |m\rangle\langle m| = \begin{pmatrix} m_1 \\ m_2 \end{pmatrix}\begin{pmatrix} m_1^* & m_2^* \end{pmatrix} = \begin{pmatrix} m_1 m_1^* & m_1 m_2^* \\ m_2 m_1^* & m_2 m_2^* \end{pmatrix} = \begin{pmatrix} \rho_{11} & \rho_{12} \\ \rho_{21} & \rho_{22} \end{pmatrix} \tag{11.132}$$

Characteristics of the density matrix include the Hermitian property $\rho = \rho^\dagger$, $Tr(\rho) = 1$, and $\rho^2 = \rho$.

11.4.1 Examples

If a state is described by the vector

$$|m\rangle = 2^{-1/2}\begin{pmatrix} e^{-i\varphi} \\ 1 \end{pmatrix} \tag{11.133}$$

let us find out the corresponding density matrix. Using Equation (11.132)

$$|m\rangle\langle m| = \begin{pmatrix} 2^{-1/2}e^{-i\varphi} \\ 2^{-1/2} \end{pmatrix}\begin{pmatrix} 2^{-1/2}e^{i\varphi} & 2^{-1/2} \end{pmatrix} = \begin{pmatrix} 1/2 & e^{-i\varphi}/2 \\ e^{i\varphi}/2 & 1/2 \end{pmatrix} \tag{11.134}$$

Next, we can easily verify that all the conditions for a normalized density matrix, that is, $\rho = \rho^\dagger$, $Tr(\rho) = 1$, and $\rho^2 = \rho$, are met (see Problem 11.8).

If $\varphi = \pi/2$, then this equation becomes the matrix for right-handed circularly polarized light

$$|m\rangle\langle m| = \begin{pmatrix} 1/2 & -i/2 \\ i/2 & 1/2 \end{pmatrix} \tag{11.135}$$

and if $\varphi = -\pi/2$, then this equation becomes the matrix for left-handed circularly polarized light (see Chapter 13)

$$|m\rangle\langle m| = \begin{pmatrix} 1/2 & i/2 \\ -i/2 & 1/2 \end{pmatrix} \tag{11.136}$$

Dirac's definition given in Equation (11.106) suggests that density matrices can be added, thus creating mixed states. If we take linearly polarized light in the *x*-direction

$$|1\rangle\langle 1| = \begin{pmatrix} 1 \\ 0 \end{pmatrix}\begin{pmatrix} 1 & 0 \end{pmatrix} = \begin{pmatrix} 1 & 0 \\ 0 & 0 \end{pmatrix} \tag{11.137}$$

and mix it with light linearly polarized in the *y*-direction

$$|0\rangle\langle 0| = \begin{pmatrix} 0 \\ 1 \end{pmatrix}\begin{pmatrix} 0 & 1 \end{pmatrix} = \begin{pmatrix} 0 & 0 \\ 0 & 1 \end{pmatrix} \tag{11.138}$$

we get a mixed state described by the density matrix

$$\rho = \frac{1}{2}\left(|0\rangle\langle 0| + |0\rangle\langle 0|\right) = \frac{1}{2}\begin{pmatrix} 1 & 0 \\ 0 & 1 \end{pmatrix} \tag{11.139}$$

which is the density matrix for unpolarized light (Robson, 1974). The density matrix description of polarization in photons is considered in more detail in Chapter 13, including Stokes parameters and Pauli matrices.

11.4.2 Transitions Via the Density Matrix

Equation (11.131) is the starting point of the description of excitation of multi-level systems. For a two-level system, this equation can be written in vector form with wave function components

$$\rho = \begin{pmatrix} \psi_a \\ \psi_b \end{pmatrix}\begin{pmatrix} \psi_a^* & \psi_b^* \end{pmatrix} = \begin{pmatrix} \psi_a\psi_a^* & \psi_a\psi_b^* \\ \psi_b\psi_a^* & \psi_b\psi_b^* \end{pmatrix} \tag{11.140}$$

Using the waveform definitions given by Demtröder (2008), we write

$$\psi_a(r,t) = \alpha(t)u_a e^{-iE_a t/\hbar} \tag{11.141}$$

$$\psi_b(r,t) = \beta(t)u_b e^{-iE_b t/\hbar + i\phi} \tag{11.142}$$

and the density matrix becomes

$$\begin{pmatrix} \rho_{aa} & \rho_{ab} \\ \rho_{ba} & \rho_{bb} \end{pmatrix} = \begin{pmatrix} |\alpha(t)|^2 & \alpha(t)\beta(t)e^{-i[(E_a-E_b)t/\hbar+\phi]} \\ \alpha(t)\beta(t)e^{+i[(E_a-E_b)t/\hbar+\phi]} & |\beta(t)|^2 \end{pmatrix} \tag{11.143}$$

since the u factors normalize to unity Demtröder (2008). The non-diagonal terms in this matrix (ρ_{ab} and ρ_{ba}) describe the coherence of the system. If ρ_{ab} and ρ_{ba} average to zero, then the matrix

$$\rho_{in} = \begin{pmatrix} |\alpha(t)|^2 & 0 \\ 0 & |\beta(t)|^2 \end{pmatrix} \tag{11.144}$$

describes the incoherently excited system.

Equation (11.130) can be used to describe the relaxation of coherently excited systems (Demtröder, 2008). For this, the total Hamiltonian is separated into three components

$$H = H_0 + H_I(t) + H_R \tag{11.145}$$

where

$$H_0 = \begin{pmatrix} E_a & 0 \\ 0 & E_b \end{pmatrix} \tag{11.146}$$

$$H_I = \begin{pmatrix} 0 & -\mu_{ab} \cdot E_0(t) \\ -\mu_{ba} \cdot E_0(t) & 0 \end{pmatrix} \cos(\omega t + \phi) \tag{11.147}$$

$$H_R = \hbar \begin{pmatrix} \gamma_a & \gamma_a^{\varphi} \\ \gamma_b^{\varphi} & \gamma_b \end{pmatrix} \tag{11.148}$$

are the internal (H_0), interaction (H_I), and relaxation (H_R) Hamiltonians, respectively (Demtröder, 2008). The population relaxation of state $|b\rangle$ to state $|a\rangle$, with a decay rate $\gamma_b = (1/T_b)$ (see Figure 11.6), can be described, using Equation (11.130), as

$$i\hbar \frac{\rho_{bb}}{T_b} = -[H_R, \rho]_{bb} \tag{11.149}$$

$$i\hbar \frac{\rho_{bb}}{T_b} = +[H_R, \rho]_{aa} \tag{11.150}$$

Furthermore, using Equations (11.130) and (11.140), a complete set of motion equations known as 'master equations' can be derived. The density matrix formalism is particularly apt to describe quantum mechanically the transition mechanics of n-level systems. For example, this has been done in detail for lithium, a five-level system, by Olivares et al. (1998, 2002). Note that n-level transitions are considered, using rate equations, in Appendix A.

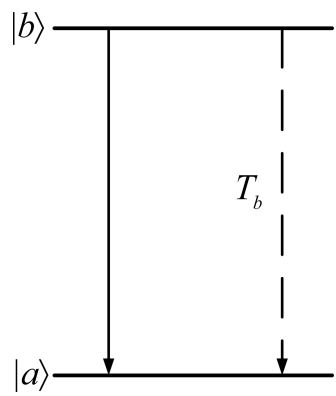

FIGURE 11.6 Spontaneous emission from level $|b\rangle$ to level $|a\rangle$.

11.5 QUANTUM OPERATORS

There are three types of operators in quantum mechanics: the position operator, the momentum operator, and the energy operator. The Hamiltonian, as an energy operator Hamiltonian, is described in Appendix A. Here, the position, momentum, and energy operators are introduced using Feynman's style and notation (Feynman et al., 1965).

Note: given the similarity of the equations involved, Feynman's approach appears to be inspired in Dirac's discussion on momentum (Dirac, 1958).

11.5.1 The Position Operator

The position operator is related to the average position of a particle. More specifically, it is related to the average value of x in a state $|\psi\rangle$. Following a probabilistic argument, Feynman defines the average of x using an integral first disclosed by Dirac (1958)†

$$\bar{x} = \int \langle \psi | x \rangle \, x \, \langle x | \psi \rangle \, dx \tag{11.151}$$

Then, Feynman identifies the average of x with the probability amplitude

$$\bar{x} = \langle \psi | \alpha \rangle \tag{11.152}$$

where

$$|\alpha\rangle = \hat{x} |\psi\rangle \tag{11.153}$$

Hence, combining Equations (11.151) and (11.152), we get

$$\bar{x} = \langle \psi | \alpha \rangle = \int \langle \psi | x \rangle \, x \, \langle x | \psi \rangle \, dx \tag{11.154}$$

and since, by definition,

$$\langle \psi | \alpha \rangle = \int \langle \psi | x \rangle \, \langle x | \alpha \rangle \, dx \tag{11.155}$$

then, a comparison of Equations (11.154) and (11.155) yields

$$\langle x | \alpha \rangle = x \langle x | \psi \rangle \tag{11.156}$$

$$|\alpha\rangle = x |\psi\rangle \tag{11.157}$$

and from the definition in Equation (11.153)

$$|\alpha\rangle = \hat{x}|\psi\rangle = x|\psi\rangle \tag{11.158}$$

Hence, the position operators $\hat{x}, \hat{y}, \hat{z}$ are related to the coordinates x, y, z according to

$$\hat{x}|\psi\rangle = x|\psi\rangle \tag{11.159}$$

$$\hat{y}|\psi\rangle = y|\psi\rangle \tag{11.160}$$

$$\hat{z}|\psi\rangle = z|\psi\rangle \tag{11.161}$$

†Equations of the form

$$\int \langle\psi|x\rangle\, x\, \langle x|\psi\rangle\, dx \tag{11.162}$$

were first introduced by Dirac in his discussion of the momentum representation (Dirac, 1958).

11.5.2 The Momentum Operator

Again, following Feynman's style, as with the position operator, the process begins by relating the average momentum $\overline{p}$ to a state $|\beta\rangle$

$$\overline{p} = \langle\psi|\beta\rangle \tag{11.163}$$

$$|\beta\rangle = p|\psi\rangle \tag{11.164}$$

$$|\beta\rangle = \hat{p}|\psi\rangle \tag{11.165}$$

Next, in analogy with the position operator approach, Feynman defines

$$\overline{p} = \langle\psi|\beta\rangle = \int \langle\psi|x\rangle\, \langle x|\beta\rangle\, dx \tag{11.166}$$

and

$$\langle p|\beta\rangle = \int \langle p|x\rangle\, \langle x|\beta\rangle\, dx \tag{11.167}$$

where, following Dirac (1958), we define

$$\langle p|x\rangle = e^{-ipx/\hbar} \tag{11.168}$$

Then, using the definitions given in Equations (11.164) and (11.168), with $\langle x|\psi\rangle = \psi(x)$

$$\langle p|\beta\rangle = p\,\langle p|\psi\rangle = p\int \langle p|x\rangle\,\langle x|\psi\rangle\,dx = \int e^{-ipx/\hbar}\,p\psi(x)\,dx \tag{11.169}$$

which can be integrated into parts (Feynman et al., 1965) to yield

$$\langle p|\beta\rangle = -i\hbar\int e^{-ipx/\hbar}\,\frac{d\psi(x)}{dx}\,dx \tag{11.170}$$

Comparison of Equations (11.167) and (11.170) renders

$$\langle x|\beta\rangle = -i\hbar\frac{d\psi(x)}{dx} \tag{11.171}$$

which is equivalent to

$$\langle x|\beta\rangle = -i\hbar\frac{d}{dx}\langle x|\psi\rangle \tag{11.172}$$

$$|\beta\rangle = -i\hbar\frac{d}{dx}|\psi\rangle \tag{11.173}$$

Now, using the definition given in Equation (11.165)

$$|\beta\rangle = \hat{p}|\psi\rangle = -i\hbar\frac{d}{dx}|\psi\rangle \tag{11.174}$$

In this manner, the three momentum operators become (Dirac, 1958; Feynman et al., 1965)

$$\hat{p}_x \to \hat{\wp}_x = -i\hbar\frac{\partial}{\partial x} \tag{11.175}$$

$$\hat{p}_y \to \hat{\wp}_y = -i\hbar\frac{\partial}{\partial y} \tag{11.176}$$

$$\hat{p}_z \to \hat{\wp}_z = -i\hbar\frac{\partial}{\partial z} \tag{11.177}$$

In three dimensions, and using vector notation, these results are nicely summarized as (Feynman et al., 1965)

$$\hat{\boldsymbol{p}} \to \hat{\boldsymbol{\wp}} = -i\hbar\nabla \tag{11.178}$$

11.5.3 Example

Letting the operator $\hat{p}_x$ operate on some function $\psi(x)$, analogously to $x\ p_x - p_x x$, yields

$$x\ \hat{p}_x\psi(x) - \hat{p}_x x\psi(x) = x(-i\hbar)\frac{\partial\psi(x)}{\partial x} - (-i\hbar)\frac{\partial(x\psi(x))}{\partial x} \tag{11.179}$$

$$x(-i\hbar)\frac{\partial\psi(x)}{\partial x} + i\hbar\psi(x) + xi\hbar\frac{\partial\psi(x)}{\partial x} = +i\hbar\psi(x) \tag{11.180}$$

$$x\ \hat{p}_x - \hat{p}_x x = i\hbar \tag{11.181}$$

as given by Dirac (1958). If both sides of this equation are multiplied by –1, we get

$$\hat{p}_x x - x\ \hat{p}_x = -i\hbar \tag{11.182}$$

which is the all-important result discovered by Heisenberg et al. in 1926, see Equation (11.1). Notice that in the classical analogy, $x\ p_x - p_x x = 0$.

In general, any two operators, $\hat{A}$ and $\hat{B}$, exhibiting the condition

$$\hat{A}\hat{B} - \hat{B}\hat{A} \neq 0 \tag{11.183}$$

are said not to commute. In other words, 'the operators do not commute' (Feynman et al., 1965). Moreover, Equation (11.181) is referred to as the *commutation rule*. Note that this result is analogous to that encountered in classical matrix algebra, see Equation (11.23).

11.5.4 The Energy Operator

The energy operator is the *Hamiltonian* and has already been introduced in Chapter 9 as (Dirac, 1958)

$$\hat{H} \to \hat{\mathcal{H}} = -\frac{\hbar^2}{2m}\nabla^2 + V(r) \tag{11.184}$$

which in vector notation becomes

$$\hat{H} \to \hat{\mathcal{H}} = \frac{1}{2m}\hat{\wp}\cdot\hat{\wp} + V(r) \tag{11.185}$$

11.5.5 The Heisenberg Equation of Motion

Feynman defines an operator $\hat{A}$ which he eventually links to the operator $\hat{H}$ via an equation of the form (Dirac, 1958)

$$\hat{\dot{A}} = \frac{i}{\hbar}[\hat{H}, \hat{A}] \tag{11.186}$$

where $[\hat{H}, \hat{A}] = (\hat{H}\hat{A} - \hat{A}\hat{H})$ is the *Poisson Bracket* introduced by Dirac (1958).

Here we'll do things a little bit differently since we are interested in Heisenberg's equation of motion. To do this, we consider Dirac's definition of $A(t)$ (Dirac, 1958)

$$A(t) = e^{iHt/\hbar} A e^{-iHt/\hbar} \tag{11.187}$$

Differentiation of this function leads to

$$\frac{dA(t)}{dt} = \frac{iH}{\hbar} A + \frac{\partial A}{\partial t} - A\frac{iH}{\hbar} \tag{11.188}$$

$$\frac{dA(t)}{dt} = \frac{i}{\hbar}(HA - AH) + \frac{\partial A}{\partial t} \tag{11.189}$$

$$\frac{dA(t)}{dt} = \frac{i}{\hbar}[H, A] + \frac{\partial A}{\partial t} \tag{11.190}$$

which is known as the *Heisenberg equation of motion*.

Finally, we should mention that operators provide the entrance stage to the subfield of 'second quantization' where a creation operator a_ξ^t creates a quantum state ξ and an annihilation operator a_η annihilates a quantum state η. Bosons satisfy several commutation rules including $[a_\xi^t, a_\eta^t] = 0$. For an introduction to this subject, see Judd (2006).

PROBLEMS

11.1 Use Equations (11.52) and (11.53) to find the Pauli matrices σ_{ij}^x and σ_{ij}^y.

11.2 Using Equations (11.62)–(11.64), prove the following Pauli matrix identities: $\sigma_x^2 = \sigma_y^2 = \sigma_z^2 = 1$

11.3 Using Equations (11.62)–(11.64), prove the following Pauli matrix identities: $\sigma_z\sigma_x = i\sigma_y$ and $\sigma_x\sigma_z = -i\sigma_y$.

11.4 Evaluate the determinant and the trace of σ_x, σ_y, and σ_z.

11.5 Find the eigenvalues for the matrix $A = (\sigma_x + \sigma_y)$ and show that $t_{\sigma_x} + t_{\sigma_y} \neq t_{\sigma_x + \sigma_y}$

11.6 Use the definitions for the spin one-half particles given in Equations (11.98)–(14.100) to verify Equation (11.101).

11.7 Use the definitions for the spin one-half particles given in Equations (11.98)–(11.100) to verify the commutation rules given in Equations (11.104) and (11.105).

11.8 Verify the conditions $\rho = \rho^\dagger$, $Tr(\rho) = 1$, and $\rho^2 = \rho$, for the normalized density matrix given in Equation (11.134).

11.9 Perform the integration by parts of the integral in Equation (11.169) and show that the result corresponds to Equation (11.170). Hint: $\psi(x) \to 0$ at $\pm\infty$.

REFERENCES

Born, M., Heisenberg, W., and Jordan, P. (1926). Zur quantenmechanik II. *Z. Phys.* 35, 557–617.

Born, M., and Jordan, P. (1925). Zur quantenmechanik. *Z. Phys.* 34, 858–888.

Demtröder, W. (2008). *Laser Spectroscopy*, 4th ed. Springer, Berlin.

Dirac, P. A. M. (1978). *The Principles of Quantum Mechanics*, 4th ed. Oxford University, Oxford, U.K.

Duarte, F. J. (2019). *Fundamentals of Quantum Entanglement*, 1st ed. Institute of Physics, Bristol, U.K.

Feynman, R. P., Leighton, R. B., and Sands, M. (1965). *The Feynman Lectures on Physics*, Vol. III, Addison-Wesley, Reading, MA.

Heisenberg, W. (1925). Uber quantenthoretische umdeutung kinematischer and mechanischer beziehungen. *Z. Phys.* 33, 879–893.

Jordan, T. F. (1986). *Quantum Mechanics in Simple Matrix Form*, Wiley, New York.

Judd, B. R. (2006). Second quantization. In *Springer Handbook of Atomic, Molecular, and Optical Physics* (Drake, G. W. F., ed.) Springer, Berlin, Part A Chapter 6, pp. 115–121.

Lipschutz, S. (1968). Linear Algebra, McGraw-Hill, New York.

Olivares, I. E., Duarte, A. E., Lokajczyk, T., Dinklage, A., and Duarte, F. J. (1998). Doppler-free spectroscopy and collisional studies with tunable diode lasers of isotopes in a heat-pipe oven. *J. Opt. Soc. Am. B*. 15, 1932–1939.

Olivares, I. E., Duarte, A. E., Saravia, E. A., and Duarte, F. J. (2002). Lithium isotope separation with tunable diode lasers. *App. Opt.* 41, 2973–2977.

Robson, B. A. (1974). *The Theory of Polarization Phenomena*, Clarendon, Oxford, U.K.

Tropper, A. M. (1968). *Linear Algebra*, Nelson, London, U.K.

12 Classical Polarization

12.1 INTRODUCTION

In this chapter, we provide a revision of concepts and techniques in classical polarization as a background to Chapter 13 that deals with quantum polarization. Moreover, various elements and techniques considered here are used as tools in optical systems in quantum optics experiments. This exposition is based on a revised version of a review given by Duarte (2003) and includes new and updated material.

12.2 MAXWELL EQUATIONS

Maxwell equations are of fundamental importance since they describe the whole of classical electromagnetic phenomena. From a classical perspective, light can be described as waves of electromagnetic radiation. As such, Maxwell equations are very useful to illustrate a number of the characteristics of light including polarization. It is customary to just state these equations without derivation. Since our goal is simply to apply them, the usual approach will be followed. However, for those interested, it is mentioned that a derivation by Dyson (1990) attributed to Feynman is available in the literature. *Maxwell equations* in the rationalized metric system are given by

$$\nabla \cdot \boldsymbol{B} = 0 \tag{12.1}$$

$$\nabla \cdot \boldsymbol{E} = \frac{\rho}{\varepsilon_0} \tag{12.2}$$

$$\nabla \times \boldsymbol{B} = c^{-2}\left(\frac{\partial \boldsymbol{E}}{\partial t} + \frac{\boldsymbol{j}}{\varepsilon_0}\right) \tag{12.3}$$

$$\nabla \times \boldsymbol{E} = -\frac{\partial \boldsymbol{B}}{\partial t} \tag{12.4}$$

Feynman et al. (1965). These equations illustrate, with succinct beauty, the unique coexistence of the electric field and the magnetic field in nature. The first two equations provide the value of the given flux through a closed surface, while the second two equations give the value of a line integral around a loop. In this notation,

$$\nabla = (\partial/\partial x, \partial/\partial y, \partial/\partial z)$$

where

$\boldsymbol{E}$ is the electric vector
$\boldsymbol{B}$ is the magnetic induction
ρ is the electric charge density

DOI: 10.1201/9781003398707-12

$\boldsymbol{j}$ is the electric current density
ε_0 is the *permittivity of free space*
c is the speed of light (see Appendix K).

In addition to Maxwell equations, the following identities are useful

$$\boldsymbol{j} = \sigma\, \boldsymbol{E} \tag{12.5}$$

$$\boldsymbol{D} = \varepsilon\, \boldsymbol{E} \tag{12.6}$$

$$\boldsymbol{B} = \mu\, \boldsymbol{H} \tag{12.7}$$

where
$\boldsymbol{D}$ is the electric displacement
$\boldsymbol{H}$ is the magnetic vector
σ is the specific conductivity
ε is the dielectric constant (or permittivity)
μ is the magnetic permeability.

In the Gaussian systems of units, the unsymmetric Maxwell equations are given in the form of

$$\nabla \cdot \boldsymbol{B} = 0 \tag{12.8}$$

$$\nabla \cdot \boldsymbol{E} = 4\pi\rho \tag{12.9}$$

$$\nabla \times \boldsymbol{H} = c^{-1}\left(\frac{\partial \boldsymbol{D}}{\partial t} + 4\pi\, \boldsymbol{j}\right) \tag{12.10}$$

$$\nabla \times \boldsymbol{E} = -c^{-1}\frac{\partial \boldsymbol{B}}{\partial t} \tag{12.11}$$

(see, e.g., Born and Wolf, 1999). It should be noted that many authors in the field of optics prefer to use Maxwell equations in the Gaussian system of units. As explained by Born and Wolf (1999), in this system $\boldsymbol{E}$, $\boldsymbol{D}$, $\boldsymbol{j}$, and ρ are measured in electrostatic units, while $\boldsymbol{H}$ and $\boldsymbol{B}$ are measured in electromagnetic units.

For the case of no charges or currents, that is $\boldsymbol{j} = 0$ and $\rho = 0$, and a homogeneous medium, Maxwell equations and the given identities can be applied in conjunction with the vector identity

$$\nabla \times \nabla \times \boldsymbol{E} = \nabla\, \nabla \cdot \boldsymbol{E} - \nabla^2 \boldsymbol{E} \tag{12.12}$$

to obtain wave equations of the form (Born and Wolf, 1999)

$$\nabla^2 \boldsymbol{E} - \frac{\varepsilon\mu}{c^2}\frac{\partial^2 \boldsymbol{E}}{\partial t^2} = 0 \tag{12.13}$$

This leads to an expression for the velocity of propagation

$$\boldsymbol{v} = c(\varepsilon\ \mu)^{-1/2} \tag{12.14}$$

Comparison of this expression with the law of positive refraction given in Chapter 5, $(\sin\Theta_m / \sin\Phi_m) = n = (c/\upsilon)$, leads to what is known as Maxwell's formula (Born and Wolf, 1999)

$$n = (\varepsilon\ \mu)^{1/2} \tag{12.15}$$

where n is the refractive index. It is useful to note that in vacuum

$$c^2 = (\varepsilon_0\ \mu_0)^{-1} \tag{12.16}$$

in the rationalized metric system, where μ_0 is the *permeability of free space* (Lorrain and Corson, 1970). The values of fundamental constants are listed in Appendix K.

12.2.1 Symmetry in Maxwell Equations

As beautiful as they are, Maxwell equations are not symmetric. Symmetry can be incorporated, however, via the introduction of the concept of the *magnetic monopole* (Dirac, 1931). If the magnetic monopole is brought into Maxwell equations, then these become symmetric and take the form of

$$\nabla \cdot \boldsymbol{B} = \frac{\rho_m}{\varepsilon_0} \tag{12.17}$$

$$\nabla \cdot \boldsymbol{E} = \frac{\rho_e}{\varepsilon_0} \tag{12.18}$$

$$\nabla \times \boldsymbol{B} = c^{-2}\left(\frac{\partial \boldsymbol{E}}{\partial t} + \frac{\boldsymbol{j}_e}{\varepsilon_0}\right) \tag{12.19}$$

$$\nabla \times \boldsymbol{E} = -\left(\frac{\partial \boldsymbol{B}}{\partial t} + \frac{j_m}{\varepsilon_0}\right) \tag{12.20}$$

There is a long history of experimental research, and the use of a variety of measurement techniques, in search of the magnetic monopole. It makes sense for it to exist, thus the reason for the inclusion of these beautiful equations.

12.3 POLARIZATION AND REFLECTION

Following the convention of Born and Wolf (1999), we consider a reflection boundary, depicted in Figure 12.1, and a plane of incidence established by the incidence ray and the normal to the reflection surface. Here, the reflected component $\mathcal{R}_{\parallel}$ is parallel to the plane of incidence, while the reflected component $\mathcal{R}_{\perp}$ is perpendicular to the plane of incidence.

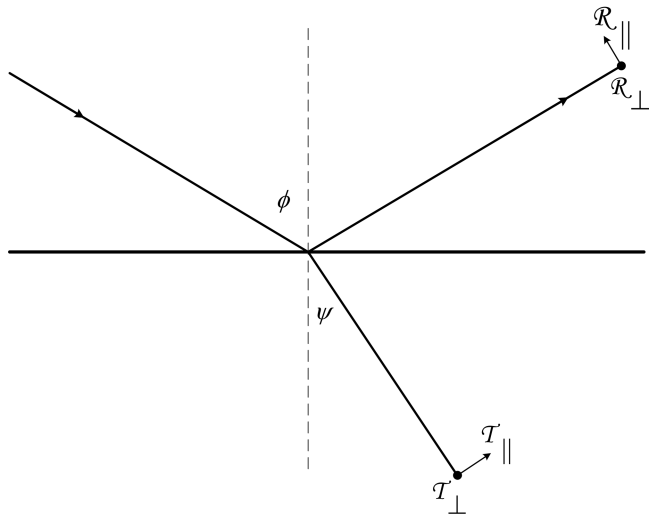

FIGURE 12.1 Reflection boundary defining the plane of incidence.

For the case of $\mu_1 = \mu_2 = 1$, Born and Wolf (1999) consider the electric, and magnetic, vectors as complex plane waves. In this approach, the incident electric vector is represented by equations of the form

$$E_x^{(i)} = -A_{\|} \cos\phi \left(e^{-i\tau_i}\right) \tag{12.21}$$

$$E_y^{(i)} = -A_{\perp} \left(e^{-i\tau_i}\right) \tag{12.22}$$

$$E_z^{(i)} = -A_{\|} \sin\phi \left(e^{-i\tau_i}\right) \tag{12.23}$$

where $\mathcal{R}_{\|}$ and $\mathcal{R}_{\perp}$ are complex amplitudes and τ_i is the usual plane wave phase factor.

Using corresponding equations for $\boldsymbol{E}$ and $\boldsymbol{H}$ for transmission and reflection in conjunction with Maxwell's relation, with $\mu = 1$, and the law or positive refraction, the Fresnel formulae can be derived (Born and Wolf, 1999). Using the Fresnel formulae, the transmissivity and reflectivity, for both polarizations, can be expressed as

$$\mathcal{T}_{\|} = \left(\frac{(\sin 2\phi \sin 2\psi)}{\sin^2(\phi+\psi)\cos^2(\phi-\psi)} \right) \tag{12.24}$$

$$\mathcal{T}_{\perp} = \left(\frac{(\sin 2\phi \sin 2\psi)}{\sin^2(\phi+\psi)} \right) \tag{12.25}$$

$$\mathcal{R}_{\|} = \left(\frac{\tan^2(\phi-\psi)}{\tan^2(\phi+\psi)} \right) \tag{12.26}$$

$$\mathcal{R}_{\perp} = \left(\frac{\sin^2(\phi - \psi)}{\sin^2(\phi + \psi)} \right) \tag{12.27}$$

and

$$\mathcal{R}_{\parallel} + \mathcal{T}_{\parallel} = 1 \tag{12.28}$$

$$\mathcal{R}_{\perp} + \mathcal{T}_{\perp} = 1 \tag{12.29}$$

Using these expressions for transmissivity and reflectivity, the degree of polarization $\mathcal{P}$ is defined as (Born and Wolf, 1999)

$$\mathcal{P} = \frac{(\mathcal{R}_{\parallel} - \mathcal{R}_{\perp})}{(\mathcal{R}_{\parallel} + \mathcal{R}_{\perp})} \tag{12.30}$$

The usefulness of these equations is self-evident once $\mathcal{R}_{\parallel}$ is calculated, as a function of the angle of incidence (Figure 12.2), for fused silica at $\lambda \approx 590$ nm ($n = 1.4583$). Here we see that $\mathcal{R}_{\parallel} = 0$ at 55.5604°. At this angle, $(\phi + \psi)$ becomes 90° so that $\tan(\phi + \psi)$

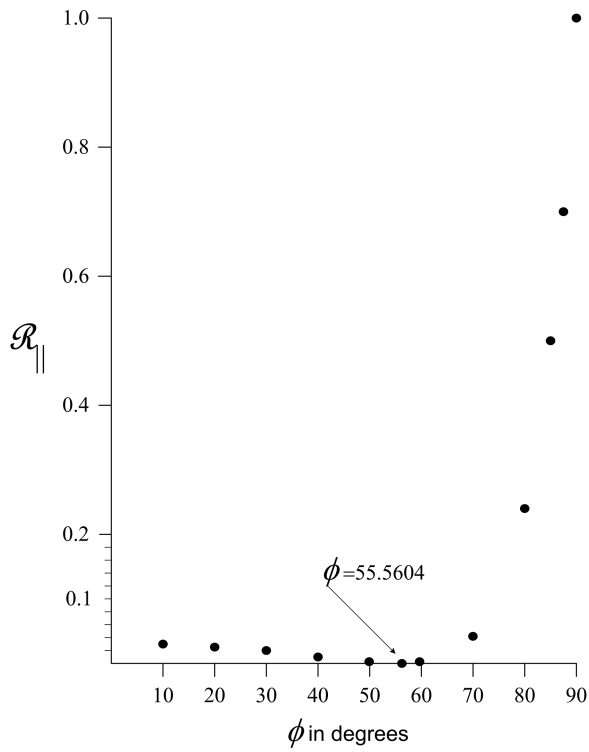

FIGURE 12.2 Reflection intensity as a function of angle of incidence. The angle at which the reflection vanishes is known as the Brewster angle.

approaches infinity, thus causing $\mathcal{R}_{\parallel} = 0$. This particular ϕ is known as the *Brewster angle* (ϕ_B) and has a very important role in laser optics. Since at $\phi = \phi_B$, the angle of refraction becomes $\psi = (90 - \phi)°$ and the law of refraction takes the form of

$$\tan \phi_B = n \tag{12.31}$$

For orthogonal, or normal, incidence, the difference between the two polarizations vanishes. Using the law of positive refraction and the appropriate trigonometric identities, in Equations (12.24)–(12.27), it can be shown that (Born and Wolf, 1999)

$$\mathcal{R} = \left(\frac{(n-1)}{(n+1)} \right)^2 \tag{12.32}$$

and

$$\mathcal{T} = \left(\frac{4n}{(n+1)} \right)^2 \tag{12.33}$$

12.3.1 The Plane of Incidence

The discussion in the preceding section uses parameters such as $\mathcal{R}_{\parallel}$ and $\mathcal{R}_{\perp}$. In this convention, $\parallel$ means parallel to the plane of incidence and $\perp$ means perpendicular, orthogonal, or normal to the plane of incidence. The plane of incidence is defined, following Born and Wolf (1999), in Figure 12.1. However, in more explicit terms, let us consider a laser beam propagating on a plane parallel to the surface of an optical table.

If that beam is made to illuminate the hypotenuse of a right-angle prism, whose triangular base is parallel to the surface of the table, then the plane of incidence is established by the incident laser beam and the perpendicular to the hypotenuse of the prism. In other words, in this case, the plane of incidence is parallel to the surface of the optical table.

Moreover, if that prism is allowed to expand the transmitted beam, as discussed later in this chapter, then the beam expansion is parallel to the plane of incidence.

The linear polarization of a laser can often be orthogonal to an external plane of incidence. When that is the case, and maximum transmission of the laser through external optics is desired, the laser is rotated by $\pi/2$ about its axis of propagation as will be discussed later in this chapter.

12.4 JONES CALCULUS

Jones calculus is a matrix approach to describe, in a unified form, both linear and circular polarization. It was introduced by Jones (1947) and a good review of the subject is given by Robson (1974). Here, salient features of the Jones calculus are described without derivation.

A more general approach to express the electric field in complex terms in x and y coordinates is in vector form

$$\begin{pmatrix} E_{0x} \\ E_{0y} \end{pmatrix} = \begin{pmatrix} E_0 e^{i\phi_x} \\ E_0 e^{i\phi_y} \end{pmatrix} \tag{12.34}$$

In this notation, linear polarization in the x direction is represented by

$$\begin{pmatrix} E_{0x} \\ E_{0y} \end{pmatrix} = \begin{pmatrix} 1 \\ 0 \end{pmatrix} \tag{12.35}$$

while linear polarization in the y direction is described by

$$\begin{pmatrix} E_{0x} \\ E_{0y} \end{pmatrix} = \begin{pmatrix} 0 \\ 1 \end{pmatrix} \tag{12.36}$$

Subsequently,

$$\begin{pmatrix} E_{0x} \\ E_{0y} \end{pmatrix} = 2^{-1/2} \begin{pmatrix} 1 \\ \pm 1 \end{pmatrix} \tag{12.37}$$

describes diagonal (or oblique) polarization at a $\pi/4$ angle, relative to the x axis (+), or relative to the y axis (−).

Circular polarization is described by the vector

$$\begin{pmatrix} E_{0x} \\ E_{0y} \end{pmatrix} = 2^{-1/2} \begin{pmatrix} 1 \\ \pm i \end{pmatrix} \tag{12.38}$$

where $+i$ applies to right-circularly polarized light and $-i$ to left-circularly polarized light (Appendix G for a description of i). Figure 12.3 illustrates the various polarization alternatives.

Jones calculus introduces 2×2 matrices to describe optical elements transforming the polarization of the incidence radiation in the following format:

$$\begin{pmatrix} a_{11} & a_{12} \\ a_{21} & a_{22} \end{pmatrix} \begin{pmatrix} A_x \\ A_y \end{pmatrix} = \begin{pmatrix} a_{11}A_x + a_{12}A_y \\ a_{21}A_x + a_{22}A_y \end{pmatrix} \tag{12.39}$$

where the 2×2 matrix represents the optical element, the polarization vector multiplying this matrix corresponds to the incident radiation, and the resulting vector describes the polarization of the resulting radiation.

Useful Jones matrices include the matrix for transmission of linearly polarized light in the x direction

$$\begin{pmatrix} a_{11} & a_{12} \\ a_{21} & a_{22} \end{pmatrix} = \begin{pmatrix} 1 & 0 \\ 0 & 0 \end{pmatrix} \tag{12.40}$$

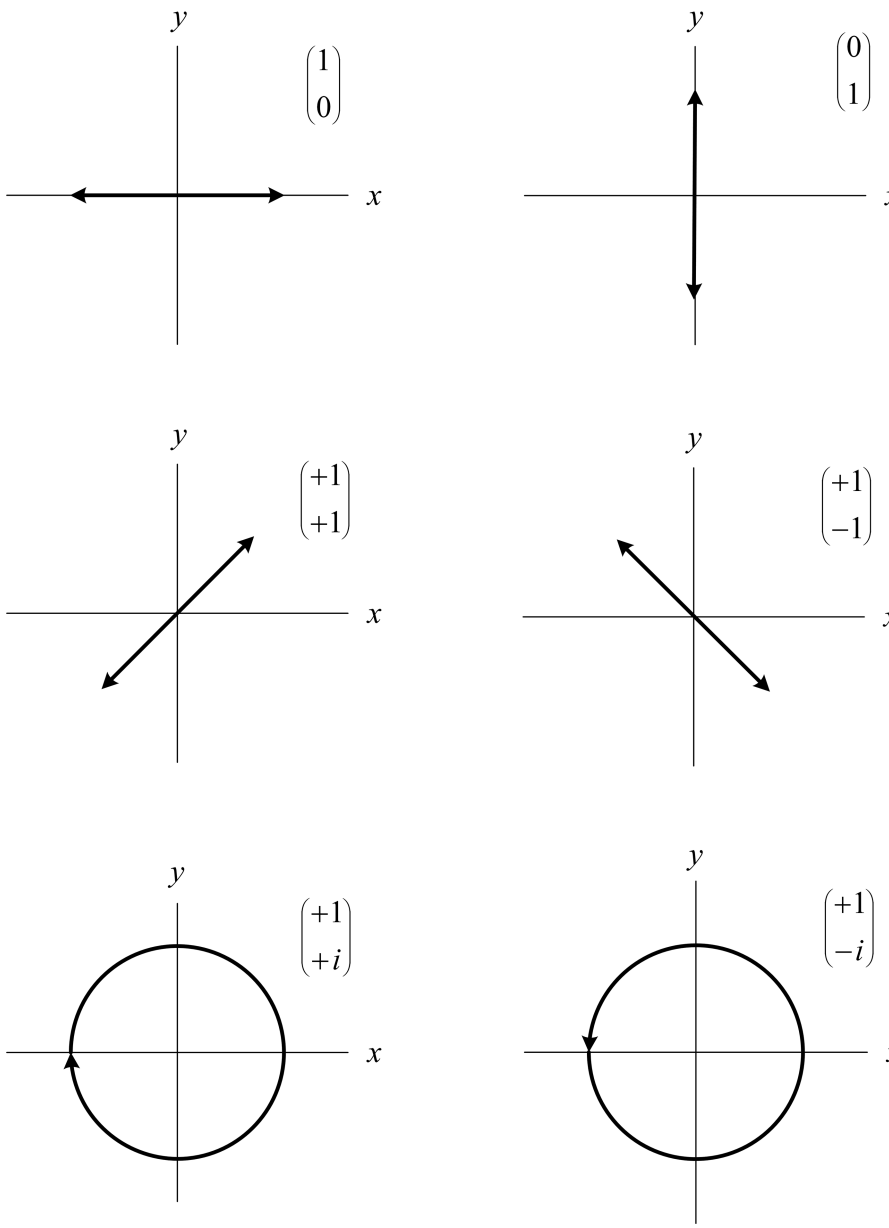

FIGURE 12.3 The various forms of polarization.

and the y direction

$$\begin{pmatrix} a_{11} & a_{12} \\ a_{21} & a_{22} \end{pmatrix} = \begin{pmatrix} 0 & 0 \\ 0 & 1 \end{pmatrix} \tag{12.41}$$

For light linearly polarized at a $\pi/4$ angle, the matrix becomes

$$\begin{pmatrix} a_{11} & a_{12} \\ a_{21} & a_{22} \end{pmatrix} = 2^{-1}\begin{pmatrix} 1 & 1 \\ 1 & 1 \end{pmatrix} \tag{12.42}$$

The generalized polarization Jones matrix for linearly polarized light, at an angle θ to the x axis, is given by

$$\begin{pmatrix} a_{11} & a_{12} \\ a_{21} & a_{22} \end{pmatrix} = \begin{pmatrix} \cos^2\theta & \sin\theta\cos\theta \\ \sin\theta\cos\theta & \sin^2\theta \end{pmatrix} \tag{12.43}$$

The right-circular polarizer is described as

$$\begin{pmatrix} a_{11} & a_{12} \\ a_{21} & a_{22} \end{pmatrix} = 2^{-1}\begin{pmatrix} 1 & -i \\ i & 1 \end{pmatrix} \tag{12.44}$$

while the left-circular polarizer is described as

$$\begin{pmatrix} a_{11} & a_{12} \\ a_{21} & a_{22} \end{pmatrix} = 2^{-1}\begin{pmatrix} 1 & i \\ -i & 1 \end{pmatrix} \tag{12.45}$$

In Chapter 13, we see how these matrices can be obtained from the density matrix formalism.

The generalized rotation matrix for birefringent rotators is given by (Robson, 1974)

$$\begin{pmatrix} a_{11} & a_{12} \\ a_{21} & a_{22} \end{pmatrix} = \begin{pmatrix} \cos\theta & \sin\theta \\ -e^{i\delta}\sin\theta & e^{i\delta}\cos\theta \end{pmatrix} \tag{12.46}$$

where δ is the phase angle and α is the rotation angle about the z axis. For a quarter-wave plate, $\delta = \pi/2$, the rotation matrix becomes

$$\begin{pmatrix} a_{11} & a_{12} \\ a_{21} & a_{22} \end{pmatrix} = \begin{pmatrix} \cos\theta & \sin\theta \\ -i\sin\theta & i\cos\theta \end{pmatrix} \tag{12.47}$$

12.4.1 Example

A laser beam polarized in the x direction is sent through an optical element that allows the transmission of y polarization only, thus using Equations (12.31) and (12.37)

$$\begin{pmatrix} 0 & 0 \\ 0 & 1 \end{pmatrix}\begin{pmatrix} 1 \\ 0 \end{pmatrix} = \begin{pmatrix} 0 \\ 0 \end{pmatrix} \tag{12.48}$$

we find that no light is transmitted as can be demonstrated by a simple experiment.

12.5 POLARIZING PRISMS

There are two avenues to induce polarization using prisms. The first involves simple reflection as characterized by the equations of reflectivity and straightforward refraction.

This approach is valid for windows, prisms, or multiple-prism arrays, made from homogeneous optical materials such as optical glass or fused silica. The second approach involves double refraction in crystalline transmission media exhibiting birefringence.

12.5.1 Transmission Efficiency in Multiple-Prism Arrays

For a generalized multiple-prism array, as shown in Figure 12.4, the cumulative reflection losses at the incidence surface of the mth prism are given by (Duarte et al., 1990)

$$L_{1,m} = L_{2,(m-1)} + (1 - L_{2,(m-1)})\mathcal{R}_{1,m} \tag{12.49}$$

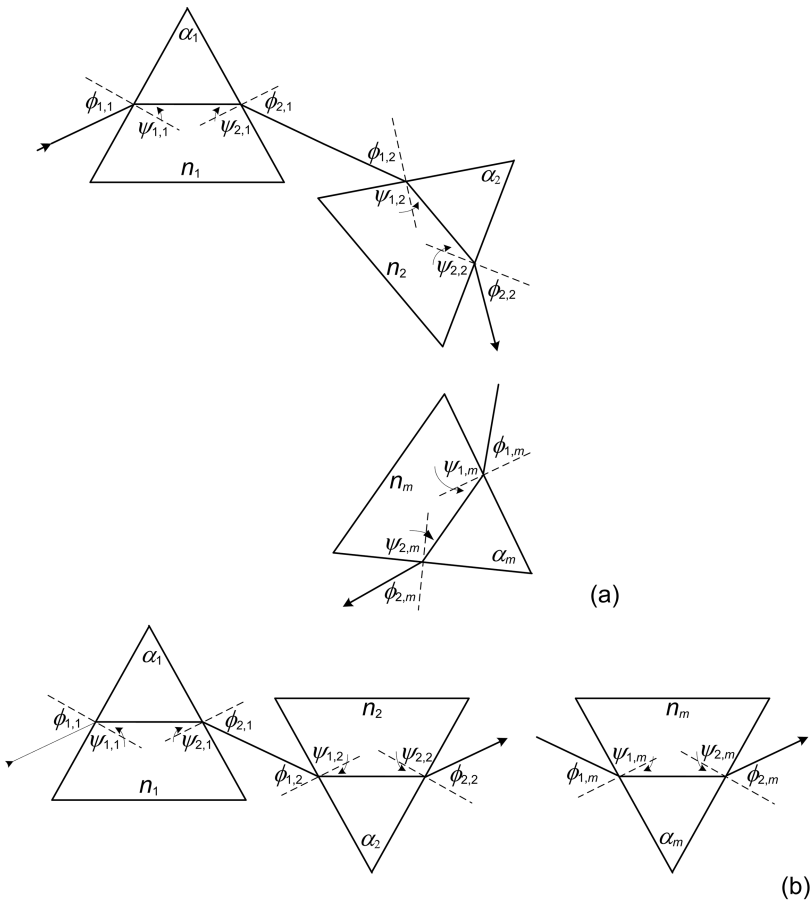

FIGURE 12.4 Generalized multiple-prism array (Reproduced from Duarte, F. J., and Piper, J. A., *Am. J. Phys.* **51**, 1132–1134, 1983, with permission of the American Association of Physics Teachers).

while the losses at the mth exit surface are given by

$$L_{2,m} = L_{1,m} + (1 - L_{1,m})\mathcal{R}_{2,m} \tag{12.50}$$

where $\mathcal{R}_{1,m}$ and $\mathcal{R}_{2,m}$ are given by either $\mathcal{R}_{\parallel}$ or $\mathcal{R}_{\perp}$. In practice, the optics is deployed so that the polarization of the propagation beam is parallel to the plane of incidence meaning that the reflection coefficient is given by $\mathcal{R}_{\parallel}$. It should be noted that these equations apply not only to prisms but also to optical wedges and any homogeneous optical element, with an input and exit surface, used in the transmission domain.

12.5.2 Induced Polarization in a Double-Prism Beam Expander

Polarization induction in multiple-prism beam expanders should be apparent once the reflectivity equations are combined with the transmission Equations (12.49) and (12.50). In this section, this effect is made clear by considering the transmission efficiency, for both components of polarization, of a simple double-prism beam expander as illustrated in Figure 12.5. This beam expander is a modified version of one described by Duarte (2003) and consists of two identical prisms made of fused silica, with $n = 1.4583$ at $\lambda \approx 590$ nm, and an apex angles of 42.7098°. Both prism are deployed to yield identical magnifications and for orthogonal beam exit. This implies that $\phi_{1,1} = \phi_{1,2} = 81.55°$, $\psi_{1,1} = \psi_{1,2} = 42.7098°$, $\phi_{2,1} = \phi_{2,2} = 0°$, $\psi_{2,1} = \psi_{2,2} = 0°$.

Thus, for radiation polarized parallel to the plane of incidence

$$L_{1,1} = \mathcal{R}_{1,1} = 0.3008$$

$$L_{2,1} = L_{1,1}$$

$$L_{1,2} = L_{2,1} + (1 - L_{2,1})\mathcal{R}_{1,2} = 0.5111$$

$$L_{2,2} = L_{1,2}$$

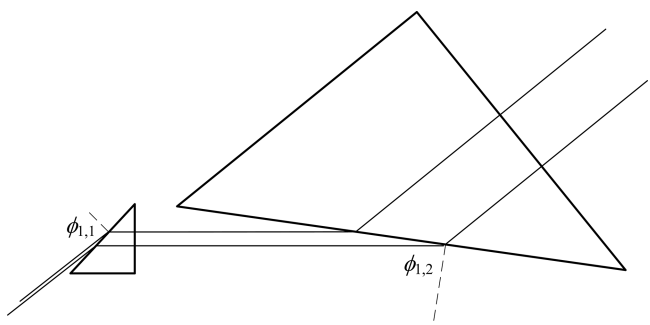

FIGURE 12.5 Double-prism expander as described in the text.

while for radiation polarized perpendicular to the plane of incidence

$$L_{1,1} = \mathcal{R}_{1,1} = 0.5758$$

$$L_{2,1} = L_{1,1}$$

$$L_{1,2} = L_{2,1} + (1 - L_{2,1})\mathcal{R}_{1,2} = 0.8200$$

$$L_{2,2} = L_{1,2}$$

also

$$k_{1,1} = k_{1,2} = 5.0005$$

$$M = k_{1,1}k_{1,2} = 25.0045$$

Thus, for this particular beam expander, the cumulative reflection losses are 51.11% for light polarized parallel to the plane of incidence, while they increase to 82.00% for radiation polarized perpendicular to the plane of incidence. This example helps to illustrate the fact that multiple-prism beam expanders exhibit a clear polarization preference. It is easy to see that the addition of further stages of beam magnification leads to increased discrimination. When incorporated in frequency selective dispersive laser cavities, these beam expanders contribute significantly toward the emission of laser emission polarized parallel to the plane of propagation.

The reader should refer to Appendix C for a generalized description of multiple-prism dispersion. Appendix B describes the use of multiple-prism arrays in laser oscillators.

12.5.3 Double-Refraction Polarizers

These are crystalline prism pairs that exploit the birefringence effect in crystals. In birefringent materials, the dielectric constant, ε, is different in each of the x, y, and z directions so that the propagation velocity is different in each direction

$$\boldsymbol{v}_a = c(\varepsilon_x)^{-1/2} \tag{12.51}$$

$$\boldsymbol{v}_b = c(\varepsilon_y)^{-1/2} \tag{12.52}$$

$$\boldsymbol{v}_c = c(\varepsilon_z)^{-1/2} \tag{12.53}$$

Since polarization of a transmission medium is determined by the $\boldsymbol{D}$ vector, it is possible to describe the polarization characteristics in each direction. Further, it can be shown that there are two different velocities, for the refracted radiation, in any given direction (Born and Wolf, 1999). As a consequence of the law of refraction, these two velocities lead to two different propagation paths in the crystal and give origin to the *ordinary* and *extraordinary* ray. In other words, the two velocities lead to *double refraction*.

Of particular interest in this class of polarizers are those known as the Nicol prism, the Rochon prism, the Glan–Foucault prism, the Glan–Thompson prism, and the Wollaston prism. According to Bennett and Bennett (1978), a Glan–Foucault prism pair is an air-spaced Glan–Thompson prism pair. In Glan-type polarizers, the extraordinary ray is transmitted from the first to the second prism in the propagation direction of the incident beam. On the other hand, the diagonal surface of the two prisms is predetermined to induce total internal reflection for the ordinary ray (see Figure 12.6).

Glan-type polarizers are very useful since they can be oriented to discriminate in favor of either polarization component with negligible beam deviation. Normally, these polarizers are made of either quartz or calcite. Commercially available calcite Glan–Thompson polarizer with a useful aperture of 10 mm provides extinction ratios of ~5× showing that there are two different velocities, for the refracted radiation, in any given direction (Born and Wolf, 1999). As a consequence of the law of refraction, these two velocities lead to two different propagation paths in the crystal and give origin to the *ordinary* and *extraordinary* rays. In other words, the two velocities lead to *double refraction.*

Of particular interest in this class of polarizers are those known as the Nicol prism, the Rochon prism, the Glan–Foucault prism, the Glan–Thompson prism, and the Wollaston prism. According to Bennett and Bennett (1978), a Glan–Foucault prism pair is an air-spaced Glan–Thompson prism pair. In Glan-type polarizers, the extraordinary ray is transmitted from the first to the second prism in the propagation direction of the incident beam. On the other hand, the diagonal surface of the two prisms is predetermined to induce total internal reflection for the ordinary ray (see Figure 12.6).

Glan-type polarizers are very useful since they can be oriented to discriminate in favor of either polarization component with negligible beam deviation. Normally, these polarizers are made of either quartz or calcite. Commercially available calcite Glan–Thompson polarizer with a useful aperture of 10 mm provides extinction ratios of $\sim 5 \times 10^{-5}$. It should be noted that Glan-type polarizers are used in straightforward propagation applications as well as intracavity elements. For instance, the tunable single-longitudinal-mode laser oscillator depicted in Figure 12.7 incorporates a

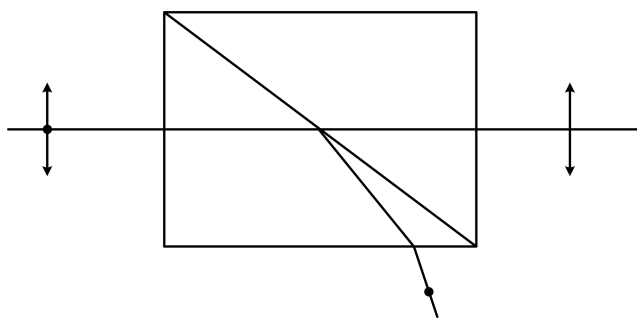

FIGURE 12.6 Generic Glan–Thompson polarizer. The beam polarized parallel to the plane of incidence is transmitted while the complementary component is deviated (drawing not to scale). For further details refer to Jenkins and White (1957).

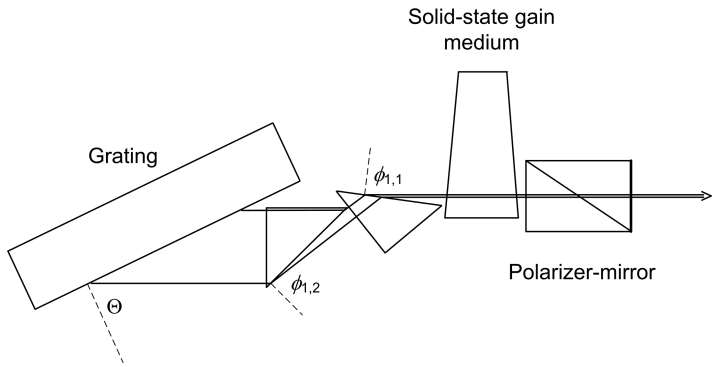

FIGURE 12.7 Solid-state MPL grating dye laser oscillator, yielding single-longitudinal-mode emission, incorporating a Glan–Thompson polarizer output coupler. The reflective coating is applied to the outer surface of the polarizer (Reproduced from Duarte, F. J., *Opt. Commun*. **117**, 480–484, 1995, with permission from Elsevier).

Glan–Thompson polarizer as an output coupler. In this particular polarizer, the inner window is antireflection coated, while the outer window is coated for partial reflectivity to act as an output coupler mirror. The laser emission from multiple-prism grating oscillators is highly polarized parallel to the plane of incidence by the interaction of the intracavity flux with the multiple-prism expander and the grating. The function of the polarizer output coupler here is to provide further discrimination against unpolarized single-pass amplified spontaneous emission. These dispersive tunable laser oscillators yield extremely low levels of broadband amplified spontaneous emission measured to be in the 10^{-7}–10^{-6} range (Duarte, 1995, 1999).

The Wollaston prism, illustrated in Figure 12.8, is usually fabricated with either crystalline quartz or calcite. These prisms are assembled from two matched and complimentary right-angled prisms whose crystalline optical axes are oriented orthogonal to each other. The Wollaston prisms are widely used as beam splitters of beams with orthogonal polarizations. The beam separation provided by calcite is significantly greater than the beam separation achievable with crystalline quartz. Moreover, for both materials, the beam separation is wavelength-dependent.

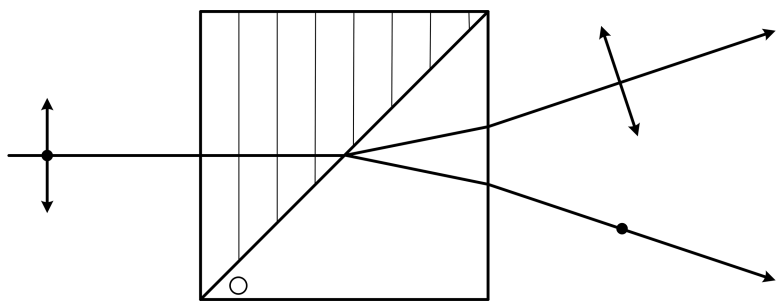

FIGURE 12.8 Generic Wollaston prism. The lines and circle represent the direction of the crystalline optical axis of the prism components (drawing not to scale).

The use of these prisms in quantum cryptography optical configurations is outlined in Chapter 20. In those optical configurations, a Wollaston prism is used after an electro-optical polarization rotator (such as a Pockels cell) to spatially separate photons corresponding to orthogonal polarizations. For a description of electro-optical polarization rotators, see Saleh and Teich (1991).

12.5.4 Attenuation of the Intensity of Laser Beams Using Polarization

A very simple yet powerful technique to attenuate the intensity of linearly polarized laser beams involves the transmission of the laser beam through a prism pair such as a Glan–Thompson polarizer followed by rotation of the polarizer. This technique has been illustrated in Figure 12.9. In this technique for a ~100% laser beam polarized parallel to the plane of incidence, there is almost total transmission when the Glan–Thompson prism pair is oriented as in Figure 12.9a. As the prism pair is rotated about the axis of propagation, the intensity of the transmission

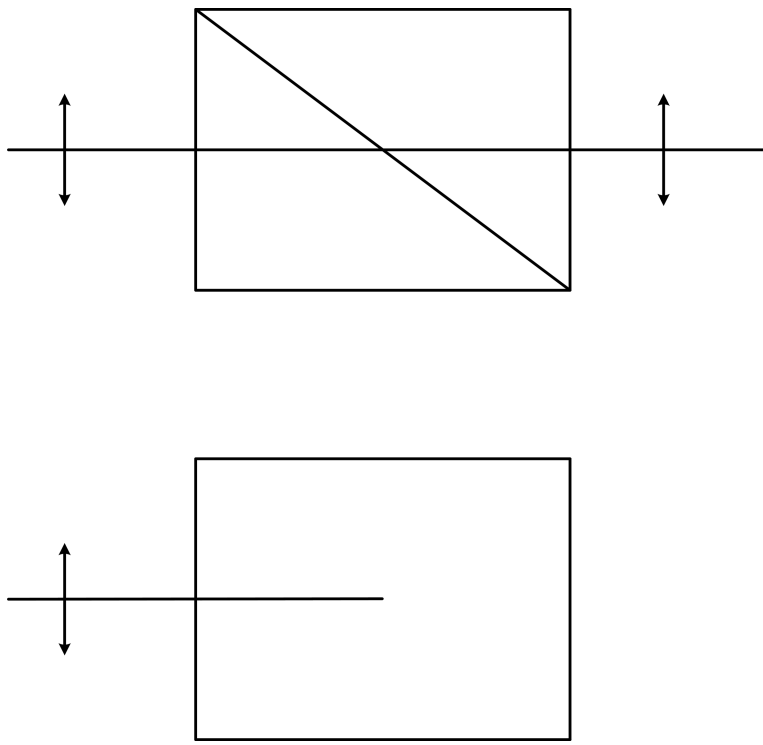

FIGURE 12.9 Attenuation of polarized laser beams using a Glan–Thompson polarizer. (a) Polarizer set for ~100% transmission. (b) Rotation of the polarizer, about the axis of propagation by $\pi/2$, yields ~0% transmission. The amount of transmitted light can be varied continuously by rotating the polarizer in the $0 \le \theta \le \pi/2$ range (From Duarte, F. J., Laser sensitometer using a multiple-prism beam expander and a polarizer. *US Patent* 6236461 B1, 2001).

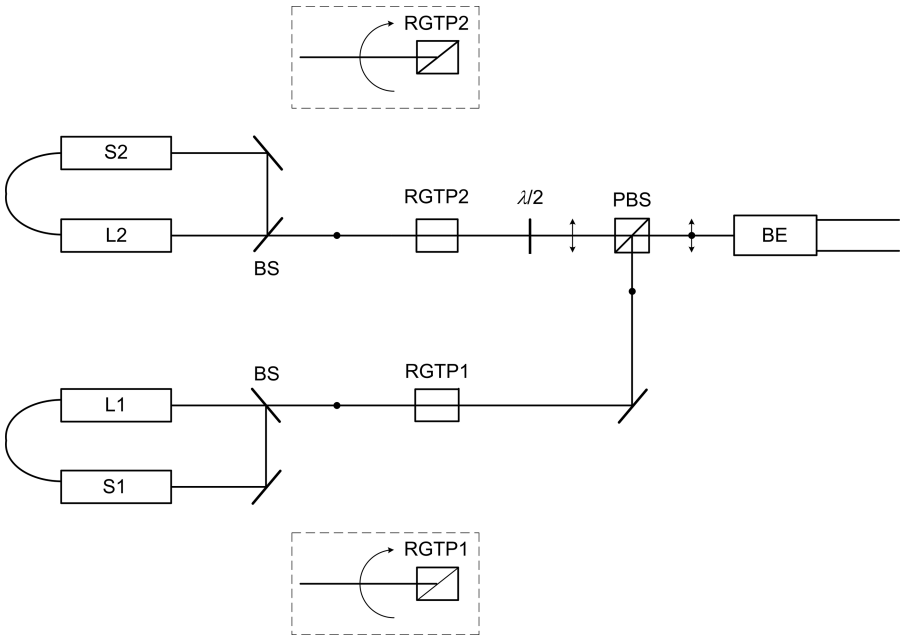

FIGURE 12.10 Top view of schematics of a laser cooling experiment including Glan–Thompson polarizers to independently control the laser intensity of the cooling lasers (L1) and the repumping laser (L2). S1 and S2 are stabilizer systems, RGTP1 and RGTP2 are the rotating Glan–Thompson polarizers, $\lambda/2$ is a half-wave plate, PBS is a polarizer beam splitter, and BE a beam expander. Polarizations perpendicular to the plane of propagation are indicated by the solid dot. Rotation by $\pi/2$ of an RGTP extinguishes the transmission of the laser beam which is polarized perpendicular to the plane of propagation (Adapted from Olivares, I. E. et al., *J. Mod. Opt.* **56**, 1780–1784, 2009, with permission).

decreases until it becomes zero once the angular displacement has reached $\pi/2$. With a precision rotation of the prism pair, a scale of well-determined intensities can be easily obtained (Duarte, 2001). This has a number of applications including the generation of precise laser intensity scales for exposing instrumentation, and laser printers, used in imaging (Duarte, 2001). Moreover, this technique has been successfully applied to *laser cooling* experiments to independently vary the intensity of the cooling and repumping lasers as illustrated in Figure 12.10 (Olivares et al., 2009).

12.6 POLARIZATION ROTATORS

Maximum transmission efficiency is always a goal in optical systems. If the polarization of a laser is mismatched to the polarization preference of the optics, then transmission efficiency will be poor. Furthermore, efficiency can be significantly improved if the polarization of a pump laser is matched to the polarization preference of the laser being excited (Duarte, 1990). Although sometimes the efficiency can be improved, or even optimized, by the simple rotation of a laser, it is highly desirable

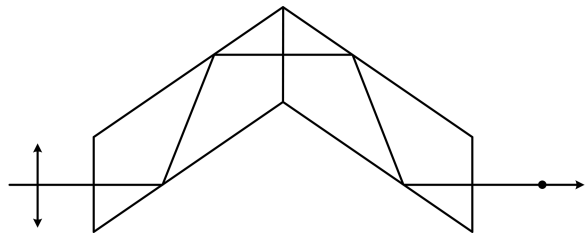

FIGURE 12.11 Side view of double Fresnel rhomb. Linearly polarized light is rotated by $\pi/2$ and exits with polarized orthogonally to the original polarization.

and practical to have optical elements to perform this function. In this section, we shall consider three alternatives to perform such rotation: birefringent polarization rotators and prismatic rotators. An additional alternative to rotate polarization is the use of rhomboids (Figure 12.11), which is described in Duarte (2003).

12.6.1 Birefringent Polarization Rotators

In birefringent uniaxial crystalline materials, the ordinary and extraordinary rays propagate at different velocities. The generalized matrix for birefringent rotators is given by Equation (12.46)

$$\begin{pmatrix} a_{11} & a_{12} \\ a_{21} & a_{22} \end{pmatrix} = \begin{pmatrix} \cos\theta & \sin\theta \\ -e^{i\delta}\sin\theta & e^{i\delta}\cos\theta \end{pmatrix}$$

For a quarter-wave plate $\delta = \pi/2$, the phase term is $e^{i\pi/2} = +i$, and the rotation matrix becomes

$$\begin{pmatrix} a_{11} & a_{12} \\ a_{21} & a_{22} \end{pmatrix} = \begin{pmatrix} \cos\theta & \sin\theta \\ -i\sin\theta & i\cos\theta \end{pmatrix} \tag{12.54}$$

For a half-wave plate $\delta = \pi$ and the phase term is $e^{i\pi} = -1$. Thus, the rotation matrix becomes

$$\begin{pmatrix} a_{11} & a_{12} \\ a_{21} & a_{22} \end{pmatrix} = \begin{pmatrix} \cos\theta & \sin\theta \\ \sin\theta & -\cos\theta \end{pmatrix} \tag{12.55}$$

From experiment, we know that a half-wave plate causes a rotation of a linearly polarized beam by $\theta = \pi/2$ so that Equation (12.55) reduces to

$$\begin{pmatrix} a_{11} & a_{12} \\ a_{21} & a_{22} \end{pmatrix} = \begin{pmatrix} 0 & 1 \\ 1 & 0 \end{pmatrix} \tag{15.56}$$

12.6.2 Example

Thus, if we send a beam polarized in the x direction through a half-wave plate, the emerging beam polarization will be

$$\begin{pmatrix} 0 & 1 \\ 1 & 0 \end{pmatrix}\begin{pmatrix} 1 \\ 0 \end{pmatrix}=\begin{pmatrix} 0 \\ 1 \end{pmatrix} \tag{12.57}$$

which corresponds to a beam polarized in the y direction as observed experimentally and as illustrated in Figure 12.10 (Duarte, 2003; Olivares et al., 2009).

12.6.3 Broadband Prismatic Polarization Rotators

An alternative to frequency selective polarization rotators is prismatic rotators (Duarte, 1989). These devices work at normal incidence and apply the principle of total internal reflection. The basic operation of polarization rotation, by $\pi/2$, due to total internal reflection is shown in Figure 12.12. This operation, however, reflects the beam into a direction that is orthogonal to the original propagation. Furthermore, the beam is not in the same plane. To achieve collinear polarization rotation, by $\pi/2$, the beam must be displaced upwards and then be brought into alignment with the incident beam while conserving the polarization rotation achieved by the initial double reflection operation. A collinear prismatic polarization rotator, which performs this task using seven total internal reflections, is depicted in Figure 12.13. For high-power laser applications, this rotator is best assembled using a high-precision mechanical mount that allows air interfaces between the individual prisms. The useful aperture in this rotator is about 10 mm and its physical length is 30 mm.

It should be noted that despite the apparent complexity of this collinear polarization rotator, the transmission efficiency is relatively high using antireflection coatings. In fact, using broadband (425–675 nm) antireflection coatings with a nominal loss of 0.5% per surface, the measured transmission efficiency becomes 94.7% at $\lambda = 632.82$ nm.

The predicted transmission losses using

$$L_r = 1-(1-L)^r \tag{12.58}$$

are 4.9%, with $L = 0.5$ %, as compared with a measured value of 5.3%. Equation (12.58) is derived by combining Equations (12.49) and (12.50) for the special case of identical reflection losses. Here, r is the total number of reflection surfaces. For this particular collinear rotator, $r = 10$. A further parameter of interest is the transmission fidelity of the rotator since it is also important to keep spatial distortions of the rotated beam to a minimum. The integrity of the beam due to transmission and rotation is quantified in Figure 12.14 where a very slight beam expansion, of ~3.2% at full-width-half-maximum (FWHM), is evident (Duarte, 1992).

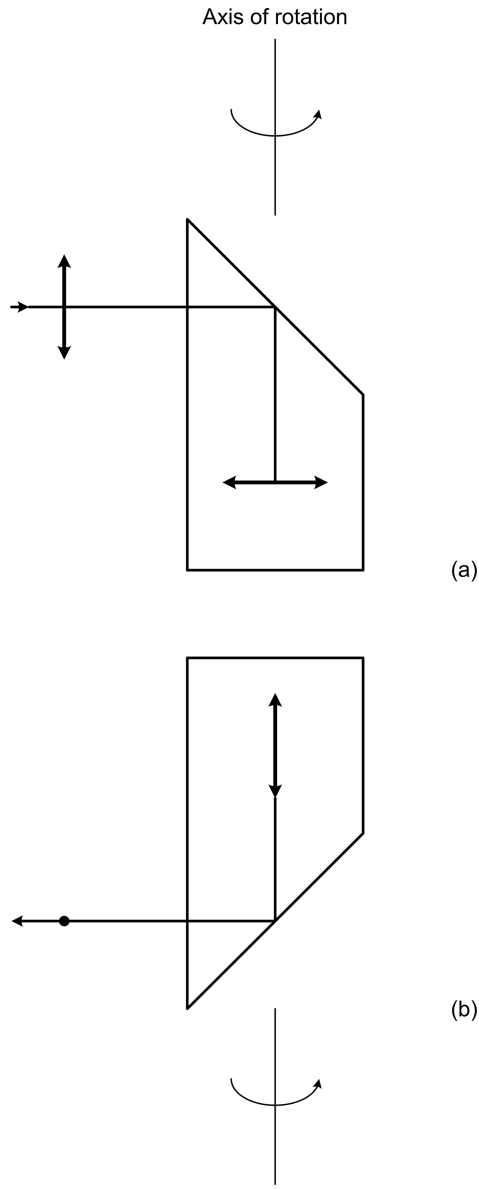

FIGURE 12.12 Basic prism operator for polarization rotation using two reflections. This can be composed of two 45° prisms adjoined $\pi/2$ to each other (note that it is also manufactured as one piece). (a) Side view of the rotator illustrating the basic rotation operation due to one reflection. The beam with the rotated polarization exists the prism into the plane of the figure. (b) The prism rotator is itself rotated anti clockwise by $\pi/2$ about the rotation axis (as indicated), thus providing an alternative perspective of the operation: the beam is now incident into the plane of the figure and it is reflected downwards with is polarization rotated by $\pi/2$ relative to the original orientation (From Duarte, F. J., Optical device for rotating the polarization of a light beam. *US Patent* 4822150, 1989).

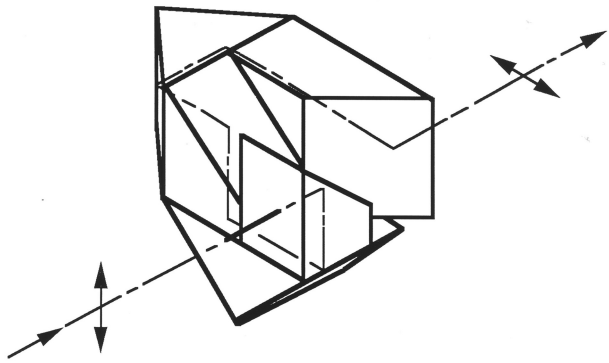

FIGURE 12.13 Broadband collinear prism polarization rotator (From Duarte, F. J., Optical device for rotating the polarization of a light beam. *US Patent* 4822150, 1989).

12.6.4 Example

The $\pi/2$ prismatic polarization rotator just described rotates linearly x polarized radiation into linearly y polarized radiation and vice versa. Here we will find the Jones matrix that describes its rotational capability. Considering first the case of $x \rightarrow y$ and using the Jones matrix formalism, we can write

$$\begin{pmatrix} a_{11} & a_{12} \\ a_{21} & a_{22} \end{pmatrix}\begin{pmatrix} 1 \\ 0 \end{pmatrix}=\begin{pmatrix} 1a_{11}+0a_{12} \\ 1a_{21}+0a_{22} \end{pmatrix}=\begin{pmatrix} 0 \\ 1 \end{pmatrix} \tag{12.59}$$

which means that $a_{11}=0$ and $a_{21}=1$. To find the other two components, we use the complementary rotation $y \rightarrow x$ which can be described as

$$\begin{pmatrix} a_{11} & a_{12} \\ a_{21} & a_{22} \end{pmatrix}\begin{pmatrix} 0 \\ 1 \end{pmatrix}=\begin{pmatrix} 0a_{11}+1a_{12} \\ 0a_{21}+1a_{22} \end{pmatrix}=\begin{pmatrix} 1 \\ 0 \end{pmatrix} \tag{12.60}$$

which implies that $a_{12}=1$ and $a_{22}=0$. Thus, the Jones matrix for $\pi/2$ rotation, which applies directly to the prismatic rotator described in Figure 12.13, becomes

$$R=\begin{pmatrix} a_{11} & a_{12} \\ a_{21} & a_{22} \end{pmatrix}=\begin{pmatrix} 0 & 1 \\ 1 & 0 \end{pmatrix} \tag{12.61}$$

Thus, we have again arrived at the $\pi/2$ rotation matrix Equation (12.56), by observation, using simple linear algebra.

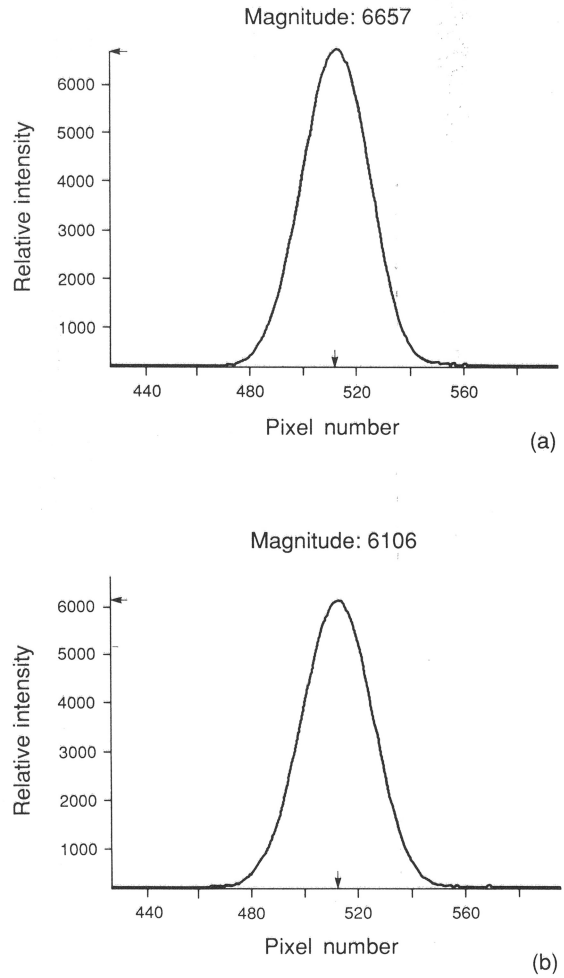

FIGURE 12.14 Transmission fidelity of the broadband collinear polarization rotator: (a) intensity profile of incident beam, prior to rotation, and (b) intensity profile of transmitted beam with rotated polarization (Reproduced from Duarte, F. J., *Appl. Opt.* **31**, 3377–3378, 1992, with permission from Optica).

PROBLEMS

12.1 Design a single right-angle prism, made of fused silica, to expand a laser beam by a factor of two with an orthogonal beam exit. Calculate $\mathcal{R}_{\parallel}$ and $\mathcal{R}_{\perp}$. (Use $n = 1.4583$ at $\lambda \approx 590$ nm.)

12.2 For a four-prism beam expander, with orthogonal beam exit, using fused silica prisms with an apex angle of 41°, calculate the overall beam magnification factor M. Moreover, calculate the overall transmission efficiency for a laser beam polarized parallel to the plane of incidence. (Use $n = 1.4583$ at $\lambda \approx 590$ nm.)

12.3 Use Maxwell equations in the Gaussian system, for the $\boldsymbol{j} = 0$ and $\rho = 0$ case, to derive the wave equations

$$\nabla^2 \boldsymbol{E} - (\varepsilon\mu)c^{-2}\frac{\partial^2 \boldsymbol{E}}{\partial t^2} = 0$$

$$\nabla^2 \boldsymbol{H} - (\varepsilon\mu)c^{-2}\frac{\partial^2 \boldsymbol{H}}{\partial t^2} = 0$$

12.4 Using the values for ε_0 and μ_0 given in Appendix K, verify that $c^2 = (\varepsilon_0\mu_0)^{-1}$.

12.5 Compare the set of symmetric Maxwell equation to Equations (12.1)–(12.4). In light of the final observation stipulated in Section 12.2.1 comment on the likely synergy between mathematical beauty and nature.

12.6 If a linearly polarized beam in the x direction is sent through a rotator plate represented by the matrix

$$\begin{pmatrix} a_{11} & a_{12} \\ a_{21} & a_{22} \end{pmatrix} = \begin{pmatrix} 0 & 1 \\ -i & 0 \end{pmatrix}$$

What will be the polarization of the transmitted beam? What kind of plate would that be?

REFERENCES

Bennett, J. M., and Bennett, H. E. (1978). Polarization. In *Handbook of Optics* (Driscoll, W. G., and Vaughan, W., eds.). McGraw-Hill, New York, Chapter 10, pp. 10-1–10-164.

Born, M., and Wolf, E. (1999). *Principles of Optics*, 7th ed. Cambridge, New York.

Dirac, P. A. M. (1931). Quantized singularities in the magnetic field. Proc. *Royal Soc. A*. **133**, 60–72.

Duarte, F. J. (1989). Optical device for rotating the polarization of a light beam. *US Patent* 4822150.

Duarte, F. J. (1990). Technology of pulsed dye lasers. In *Dye Laser Principles* (Duarte, F. J., and Hillman, L. W., eds.). Academic, New York, Chapter 6, pp. 239–285.

Duarte, F. J. (1992). Beam transmission characteristics of a collinear polarization rotator. *Appl. Opt*. **31**, 3377–3378.

Duarte, F. J. (1995). Solid-state dispersive dye laser oscillator: very compact cavity. *Opt. Commun*. **117**, 480–484.

Duarte, F. J. (1999). Multiple-prism grating solid-state dye laser oscillator: optimized architecture. *Appl. Opt*. **38**, 6347–6349.

Duarte, F. J. (2001). Laser sensitometer using a multiple-prism beam expander and a polarizer. *US Patent* 6236461 B1.

Duarte, F. J. (2003). *Tunable Laser Optics*, Elsevier-Academic, New York.

Duarte, F. J., Ehrlich, J. J., Davenport, W. E., and Taylor, T. S. (1990). Flashlamp pumped narrow-linewidth dispersive dye laser oscillators: very low amplified spontaneous emission levels and reduction of linewidth instabilities. *Appl. Opt*. **29**, 3176–3179.

Duarte, F. J., and Piper, J. A. (1983). Generalized prism dispersion theory, *Am. J. Phys.* **51,** 1132–1134.

Dyson, F. J. (1990). Feynman's proof of Maxwell equations, *Am. J. Phys*. **58**, 209–211.

Feynman, R. P., Leighton, R. B, and Sands, M. (1965). *The Feynman Lectures on Physics*, Vol. II. Addison-Wesley, Reading, MA.

Jenkins, F. A., and White, H. E. (1957). *Fundamentals of Optics*, MacGraw-Hill, New York.
Jones, R. C. (1947). A new calculus for the treatment of optical systems, *J. Opt. Soc. Am*. **37**, 107–110.
Lorrain, P., and Corson, D. (1970). *Electromagnetic Fields and Waves*, Freeman, San Francisco, CA.
Olivares, I. E., Cuadra, J. A., Aguilar, F. A., Aguirre Gomez, J. G., and Duarte, F. J. (2009). Optical method using rotating Glan-Thompson polarizers to independently vary the power of the excitation and repumping lasers in laser cooling experiments. *J. Mod. Opt*. **56**, 1780–1784.
Robson, B. A. (1974). *The Theory of Polarization Phenomena*, Clarendon, Oxford, U.K.
Saleh, B. E. A., and Teich, M. C. (1991). *Fundamentals of Photonics*, Wiley, New York.

13 Quantum Polarization

13.1 INTRODUCTION

In this chapter, we examine the quantum aspects of polarization primarily via Dirac's notation (Dirac, 1958) and also using density matrices. The approach follows the style of Feynman (Feynman et al., 1965). Classical polarization is examined in Chapter 12.

13.2 LINEAR POLARIZATION

This section contains all of the elements included in the first edition of this book (Duarte, 2014) while extended by further details introduced in Duarte (2022).

Linear polarization in the x direction represented in Jones calculus by (Jones, 1947)

$$\begin{pmatrix} E_{0x} \\ E_{0y} \end{pmatrix} = \begin{pmatrix} 1 \\ 0 \end{pmatrix} \tag{13.1}$$

is expressed simply as $|x\rangle$ in the *bra ket* representation. Linear polarization in the y direction described in Jones calculus by

$$\begin{pmatrix} E_{0x} \\ E_{0y} \end{pmatrix} = \begin{pmatrix} 0 \\ 1 \end{pmatrix} \tag{13.2}$$

is expressed as simply as $|y\rangle$ in the *bra ket* representation.

The rotation of axes, $x \rightarrow x'$ and $y \rightarrow y'$, as illustrated in Figure 13.1, leads directly to the following rotation identities

$$\frac{x}{x'} = \cos\varphi \tag{13.3}$$

$$\frac{x}{y'} = -\sin\varphi \tag{13.4}$$

$$\frac{y}{x'} = \sin\varphi \tag{13.5}$$

$$\frac{y}{y'} = \cos\varphi \tag{13.6}$$

DOI: 10.1201/9781003398707-13

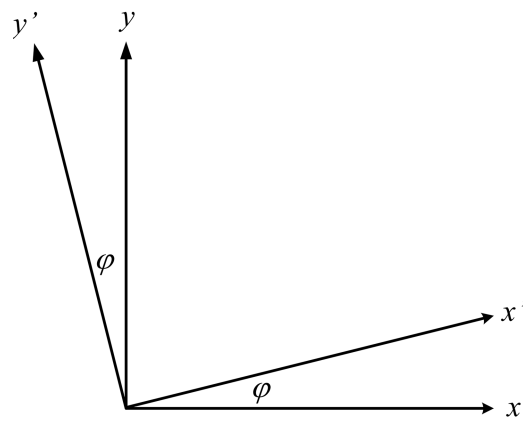

FIGURE 13.1 x and y axes and rotating x' and y' axes.

Using the simple geometrical rotations given above

$$\langle x|x'\rangle = \langle x'|x\rangle = \cos\varphi \tag{13.7}$$

$$\langle y|x'\rangle = \langle x'|y\rangle = \sin\varphi \tag{13.8}$$

$$\langle x|y'\rangle = \langle y'|x\rangle = -\sin\varphi \tag{13.9}$$

$$\langle y|y'\rangle = \langle y'|y\rangle = \cos\varphi \tag{13.10}$$

Probability amplitudes of interest are

$$\langle x|x'\rangle = \langle x|x\rangle\langle x|x'\rangle + \langle x|y\rangle\langle y|x'\rangle \tag{13.11}$$

$$\langle y'|x\rangle = \langle y'|x'\rangle\langle x'|x\rangle + \langle y'|y'\rangle\langle y'|x\rangle \tag{13.12}$$

$$\langle x'|y\rangle = \langle x'|y'\rangle\langle y'|y\rangle + \langle x'|x'\rangle\langle x'|y\rangle \tag{13.13}$$

$$\langle y|y'\rangle = \langle y|y\rangle\langle y|y'\rangle + \langle y|x\rangle\langle x|y'\rangle \tag{13.14}$$

Using Equations (13.11)–(13.14) leads to the following probability amplitudes:

$$\langle x|x'\rangle = \langle x|x\rangle\cos\varphi + \langle x|y\rangle\sin\varphi \tag{13.15}$$

$$\langle y'|x\rangle = \langle y'|x'\rangle\cos\varphi + \langle y'|y'\rangle(-\sin\varphi) \tag{13.16}$$

$$\langle x'|y\rangle = \langle x'|y'\rangle\cos\varphi + \langle x'|x'\rangle\sin\varphi \tag{13.17}$$

$$\langle y|y'\rangle = \langle y|y\rangle\cos\varphi + \langle y|x\rangle(-\sin\varphi) \tag{13.18}$$

In abstract form, these equations become (Duarte, 2014)

$$|x'\rangle = |x\rangle\cos\varphi + |y\rangle\sin\varphi \tag{13.19}$$

$$|x\rangle = |x'\rangle\cos\varphi - |y'\rangle\sin\varphi \tag{13.20}$$

$$|y\rangle = |y'\rangle\cos\varphi + |x'\rangle\sin\varphi \tag{13.21}$$

$$|y'\rangle = |y\rangle\cos\varphi - |x\rangle\sin\varphi \tag{13.22}$$

It should be noticed that Equation (13.19) is the one equation given by Feynman et al. (1965) in their description of quantum polarization.

Since $\langle x|x\rangle = 1$, $\langle y|y\rangle = 1$, and $\langle x|y\rangle = 0$, $\langle y|x\rangle = 0$, then

$$\langle x|x'\rangle = \cos\varphi \tag{13.23}$$

$$\langle y'|y\rangle = -\sin\varphi \tag{13.24}$$

$$\langle x'|y\rangle = \sin\varphi \tag{13.25}$$

$$\langle y|y'\rangle = \cos\varphi \tag{13.26}$$

which is consistent with the geometrical identities (13.7) to (13.10). Hence, using Born's rule, the polarization probabilities are

$$|\langle x|x'\rangle|^2 = \cos^2\varphi \tag{13.27}$$

$$|\langle y'|x\rangle|^2 = \sin^2\varphi \tag{13.28}$$

$$|\langle x'|y\rangle^2 = \sin^2\varphi \tag{13.29}$$

$$|\langle y|y'\rangle|^2 = \cos^2\varphi \tag{13.30}$$

13.2.1 Example

Consider the polarization configuration described in Figure 13.2: a source *s* is followed by a polarizer deployed to allow *y* polarization only which is followed by a polarizer deployed to allow *x* polarization only. The light is then detected at detector *d*. The probability amplitude of this transmission configuration can be described as

$$\langle d|s\rangle = \langle d|x\rangle\,\langle x|y\rangle\,\langle y|s\rangle \tag{13.31}$$

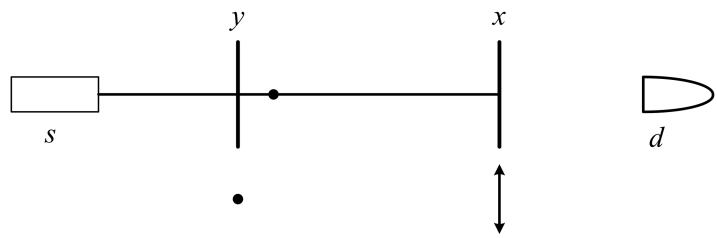

FIGURE 13.2 Top view of polarization configuration including a polarizer set for *y* transmission followed by a polarized set for transmission in the *x* direction. No light reaches the detector *d*. The *y* direction is perpendicular to the plane of incidence and is indicated by a dot.

and assuming $\langle y|s\rangle = \langle d|x\rangle = 1$, the probability amplitude reduces to $\langle x|y\rangle$

$$\langle d|s\rangle = \langle x|y\rangle \tag{13.32}$$

which, by definition, is $\langle x|y\rangle = 0$, so that

$$\langle d|s\rangle = 0 \tag{13.33}$$

If, instead, we now add a $\pi/4$ polarizer in between *x* and *y* polarizers, as illustrated in Figure 13.3, the probability amplitude becomes

$$\langle d|s\rangle = \langle d|x\rangle \langle x|x'\rangle \langle x'|y\rangle \langle y|s\rangle \tag{13.34}$$

Assuming, as before, that $\langle y|s\rangle = \langle d|x\rangle = 1$

$$\langle d|s\rangle = \langle x|x'\rangle \langle x'|y\rangle \tag{13.35}$$

and using Equation (13.7)

$$\langle d|s\rangle = \cos\varphi \langle x'|y\rangle \tag{13.36}$$

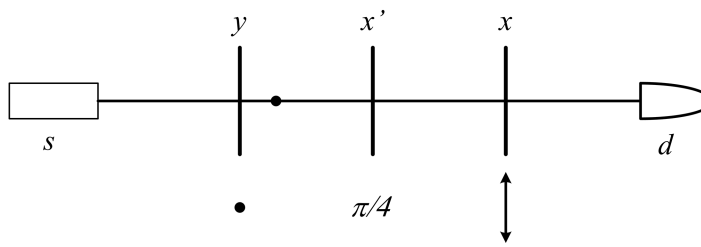

FIGURE 13.3 Top view of polarization configuration including a polarizer set for *y* transmission followed by a polarizer set for transmission in the *x* direction. A polarizer set for $\pi/4$ is inserted between the two polarizers. As explained in the text, some light is now allowed to reach the detector *d*.

Now, substituting Equation (13.9) for $\langle x'|y\rangle$ yields

$$\langle d|s\rangle = \sin\varphi\cos\varphi \tag{13.37}$$

so that the probability of transmission at $\varphi = \pi/4$ becomes

$$\left|\langle d|s\rangle\right|^2 = (\sin\varphi\cos\varphi)^2 = 1/4 \tag{13.38}$$

13.3 POLARIZATION AS A TWO-STATE SYSTEM

From the solution to the two-state system described by (Feynman et al., 1965)

$$i\hbar\frac{dC_i}{dt} = \sum H_{ij}C_j \tag{13.39}$$

where H_{ij} is the Hamiltonian, we obtain (see Appendix A)

$$C_{II} = 2^{-1/2}(C_1 + C_2) \tag{13.40}$$

and

$$C_I = 2^{-1/2}(C_1 - C_2) \tag{13.41}$$

which eventually leads to probability amplitudes of the form

$$|s\rangle = 2^{-1/2}\left(|B\rangle + |A\rangle\right) \tag{13.42}$$

$$|s\rangle = 2^{-1/2}\left(|B\rangle - |A\rangle\right) \tag{13.43}$$

13.3.1 Diagonal Polarization

In Chapter 12, the classical vector representation for diagonally polarized light was introduced as

$$\begin{pmatrix} E_{0x} \\ E_{0y} \end{pmatrix} = 2^{-1/2}\begin{pmatrix} 1 \\ \pm 1 \end{pmatrix} \tag{13.44}$$

Linearly polarized light sustaining a $\pi/4$ angle relative to the x-axis is referred to as diagonally polarized light and is described by the probability amplitude

$$|D\rangle = 2^{-1/2}\left(|x\rangle + |y\rangle\right) \tag{13.45}$$

If the angle is $-(\pi/4)$, this obliquely polarized light is represented by the probability amplitude

$$|A\rangle = 2^{-1/2}\left(|x\rangle - |y\rangle\right) \tag{13.46}$$

Diagonally polarized light is described in Figure 13.4.

13.3.2 Circular Polarization

In Chapter 12, the classical vector representation for circularly polarized light was introduced as

$$\begin{pmatrix} E_{0x} \\ E_{0y} \end{pmatrix} = 2^{-1/2}\begin{pmatrix} 1 \\ \pm i \end{pmatrix} \tag{13.47}$$

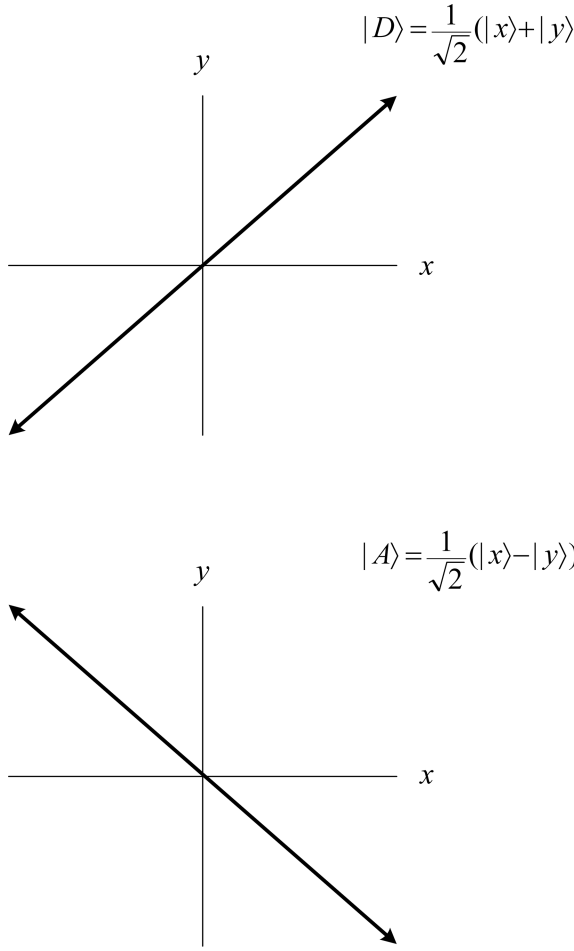

FIGURE 13.4 Diagonally polarized light depicting quantum notation.

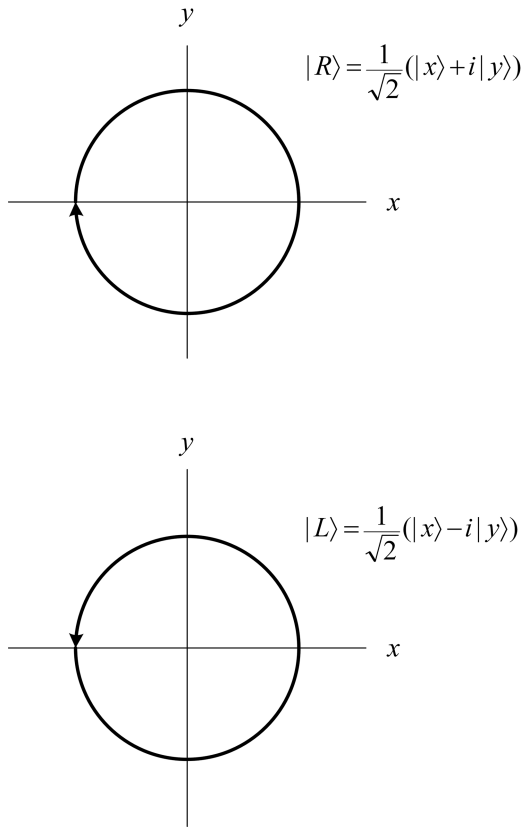

FIGURE 13.5 Circularly polarized light depicting quantum notation.

where the $+i$ factor applies to right-handed polarization and the $-i$ factor applies to left-handed polarization. Circularly polarized light is described in Figure 13.5.

Using Equations (13.30) and (13.31), the probability amplitude representation for right-handed polarization $(|R\rangle)$ and left-handed polarization $(|L\rangle)$ becomes

$$|R\rangle = 2^{-1/2}\left(|x\rangle - i|y\rangle\right) \tag{13.48}$$

$$|R\rangle = 2^{-1/2}\left(|x\rangle - i|y\rangle\right) \tag{13.49}$$

Adding and subtracting Equations (13.48) and (13.49) yield

$$|x\rangle = 2^{-1/2}\left(|R\rangle + |R\rangle\right) \tag{13.50}$$

$$|y\rangle = -2^{-1/2}i(|R\rangle - |L\rangle) \tag{13.51}$$

Further, we can write

$$|R'\rangle = 2^{-1/2}(|x'\rangle + i|y'\rangle) \tag{13.52}$$

and from Equations (13.19) and (13.22), we get (Feynman et al., 1965)

$$|R'\rangle = 2^{-1/2}\left(\cos\theta|x\rangle + \sin\theta|y\rangle + i\cos\theta|y\rangle - i\sin\theta|x\rangle\right) \tag{13.53}$$

$$|R'\rangle = 2^{-1/2}\left((\cos\theta - i\sin\theta)\left(|x\rangle + i|y\rangle\right)\right) \tag{13.54}$$

$$|R'\rangle = \left(e^{-i\theta}|R\rangle\right) \tag{13.55}$$

so that

$$|L'\rangle = \left(e^{+i\theta}|R\rangle\right) \tag{13.56}$$

13.4 DENSITY MATRIX NOTATION

Here we return to the Jones calculus initially to consider the classical density matrix for polarization followed by the quantum description. The notation used is consistent with that of Robson (1974) in the matrix case and that of Feynman in the *bra ket* approach.

Jones calculus does not offer a direct representation for unpolarized or partially polarized light. However, Robson (1974) points out that Jones vectors of the form

$$\begin{pmatrix} a \\ be^{i\delta} \end{pmatrix} \tag{13.57}$$

generally describe polarized beams. If we define the above vector as a state $|J\rangle$

$$|J\rangle = \begin{pmatrix} a_1 \\ a_2 e^{i\delta} \end{pmatrix} \tag{13.58}$$

then, using the definition for the density matrix given in Chapter 11, we can write

$$|J\rangle\langle J| = \begin{pmatrix} a_1 \\ a_2 e^{i\delta} \end{pmatrix}\begin{pmatrix} a_1 & a_2 e^{-i\delta} \end{pmatrix} = \begin{pmatrix} a_1 a_1 & a_1 a_2 e^{-i\delta} \\ a_2 a_1 e^{i\delta} & a_2 a_2 \end{pmatrix} \tag{13.59}$$

and the resulting matrix is a 2×2 density matrix

$$\rho = \begin{pmatrix} \rho_{11} & \rho_{12} \\ \rho_{21} & \rho_{22} \end{pmatrix} = \begin{pmatrix} a_1 a_1 & a_1 a_2 e^{-i\delta} \\ a_2 a_1 e^{i\delta} & a_2 a_2 \end{pmatrix} \tag{13.60}$$

The trace of this matrix

$$Tr(\rho) = a_1 a_1 + a_2 a_2 \tag{13.61}$$

corresponds to the intensity of the beam and the off-diagonal terms provide information about the phase of the two components (Robson, 1974).

The *Stokes parameters* (see Appendix J) are defined in terms of combinations of the density matrix elements (Robson, 1974)

$$I = \rho_{11} + \rho_{22} \tag{13.62}$$

$$P_1 = \rho_{11} - \rho_{22} \tag{13.63}$$

$$P_2 = \rho_{12} + \rho_{21} \tag{13.64}$$

$$P_3 = i(\rho_{12} - \rho_{21}) \tag{13.65}$$

Thus, for polarized light, the density matrix can be re-expressed as

$$\rho = \begin{pmatrix} \rho_{11} & \rho_{12} \\ \rho_{21} & \rho_{22} \end{pmatrix} = 2^{-1} \begin{pmatrix} I + P_1 & P_2 - iP_3 \\ P_2 + iP_3 & I - P_1 \end{pmatrix} \tag{13.66}$$

For unpolarized light $P_1 = P_2 = P_3 = 0$ so that the matrix reduces to

$$\rho_u = 2^{-1} \begin{pmatrix} I & 0 \\ 0 & I \end{pmatrix} \tag{13.67}$$

As seen in Chapter 11, we can write the $|J\rangle$ state in a general form, so that

$$|J\rangle = \begin{pmatrix} j_1 \\ j_2 \end{pmatrix} \begin{pmatrix} j_1^* & j_2^* \end{pmatrix} = \begin{pmatrix} j_1 j_1^* & j_1 j_2^* \\ j_2 j_1^* & j_2 j_2^* \end{pmatrix} = \begin{pmatrix} \rho_{11} & \rho_{12} \\ \rho_{21} & \rho_{22} \end{pmatrix} = \rho_q \tag{13.68}$$

The trace of this matrix

$$Tr(\rho_q) = |j_1|^2 + |j_2|^2 \tag{13.69}$$

gives information on the relative intensities of the two linearly polarized, and orthogonal components. If we define $j_1 = |x\rangle$ and $j_2 = |y\rangle$, then the trace of the matrix provides information on the relative probabilities of finding a photon in the $|x\rangle$ and $|y\rangle$ polarization states (Robson, 1974).

13.4.1 Stokes Parameters and Pauli Matrices

Previously in Chapter 11, we found that the identity matrix and the x, y, and z Pauli matrices are given by

$$I = \begin{pmatrix} 1 & 0 \\ 0 & 1 \end{pmatrix} \tag{13.70}$$

$$\sigma_x = \begin{pmatrix} 0 & 1 \\ 1 & 0 \end{pmatrix} \tag{13.71}$$

$$\sigma_y = \begin{pmatrix} 0 & -i \\ i & 0 \end{pmatrix} \tag{13.72}$$

$$\sigma_z = \begin{pmatrix} 1 & 0 \\ 0 & -1 \end{pmatrix} \tag{13.73}$$

Multiplication of the density matrix with these matrices yield

$$\rho I = \begin{pmatrix} \rho_{11} & \rho_{12} \\ \rho_{21} & \rho_{22} \end{pmatrix}\begin{pmatrix} 1 & 0 \\ 0 & 1 \end{pmatrix} = \begin{pmatrix} \rho_{11} & \rho_{12} \\ \rho_{21} & \rho_{22} \end{pmatrix} \tag{13.74}$$

$$\rho\sigma_x = \begin{pmatrix} \rho_{11} & \rho_{12} \\ \rho_{21} & \rho_{22} \end{pmatrix}\begin{pmatrix} 0 & 1 \\ 1 & 0 \end{pmatrix} = \begin{pmatrix} \rho_{12} & \rho_{11} \\ \rho_{22} & \rho_{21} \end{pmatrix} \tag{13.75}$$

$$\rho\sigma_y = \begin{pmatrix} \rho_{11} & \rho_{12} \\ \rho_{21} & \rho_{22} \end{pmatrix}\begin{pmatrix} 0 & -i \\ i & 0 \end{pmatrix} = \begin{pmatrix} i\rho_{12} & -i\rho_{11} \\ i\rho_{22} & -i\rho_{21} \end{pmatrix} \tag{13.76}$$

$$\rho\sigma_z = \begin{pmatrix} \rho_{11} & \rho_{12} \\ \rho_{21} & \rho_{22} \end{pmatrix}\begin{pmatrix} 1 & 0 \\ 0 & -1 \end{pmatrix} = \begin{pmatrix} \rho_{11} & -\rho_{12} \\ \rho_{21} & -\rho_{22} \end{pmatrix} \tag{13.77}$$

Computing the trace of these matrices leads directly to

$$Tr(\rho I) = \rho_{11} + \rho_{22} = I \tag{13.78}$$

$$Tr(\rho\sigma_z) = \rho_{11} - \rho_{22} = P_1 \tag{13.79}$$

$$Tr(\rho\sigma_x) = \rho_{12} + \rho_{21} = P_2 \tag{13.80}$$

$$Tr(\rho\sigma_y) = i(\rho_{12} - \rho_{21}) = P_3 \tag{13.81}$$

Due to Stoke's nomenclature, Robson (1974) uses a different notation (see Appendix J):

$$\sigma_x \rightarrow \hat{\sigma}_2 = \begin{pmatrix} 0 & 1 \\ 1 & 0 \end{pmatrix} \tag{13.82}$$

$$\sigma_y \rightarrow \hat{\sigma}_3 = \begin{pmatrix} 0 & -i \\ i & 0 \end{pmatrix} \tag{13.83}$$

$$\sigma_z \rightarrow \hat{\sigma}_1 = \begin{pmatrix} 1 & 0 \\ 0 & -1 \end{pmatrix} \tag{13.84}$$

Here, Robson (1974) points out that while the σ_x, σ_y, and σ_z matrices refer to ordinary space, the matrices $\hat{\sigma}_1$, $\hat{\sigma}_2$, and $\hat{\sigma}_3$ correspond to the Poincaré space that defines P_1, P_2, and P_3. Moreover, notice the use of the operator hat to designate these matrices. By introducing the operator $\hat{\gamma}$ to designate the identity matrix, the set of relations just described becomes (Robson, 1974)

$$Tr(\rho\hat{\gamma}) = \rho_{11} + \rho_{22} = I \tag{13.85}$$

$$Tr(\rho\hat{\sigma}_1) = \rho_{11} - \rho_{22} = P_1 \tag{13.86}$$

$$Tr(\rho\hat{\sigma}_2) = \rho_{12} + \rho_{21} = P_2 \tag{13.87}$$

$$Tr(\rho\hat{\sigma}_3) = i(\rho_{12} - \rho_{21}) = P_3 \tag{13.88}$$

Albeit most of the applications of Pauli matrices are found in the context of spin one-half particles (Fermions), such as electrons, some applications are found for spin one particles (Bosons) such as the photon. For instance, in Chapter 11, we discovered that the matrix describing a $\pi/2$ rotator of linear polarization, for either a half-wave plate or a prismatic rotator, is given by

$$R = \begin{pmatrix} 0 & 1 \\ 1 & 0 \end{pmatrix} \tag{13.89}$$

This matrix is identical to either σ_x or $\hat{\sigma}_2$. This means that $\hat{\sigma}_2$ is a rotation operator of linear polarization by $\theta = \pi/2$. In general, $\hat{\sigma}_1$ and $\hat{\sigma}_2$ are used in the description of linearly polarized photons, while $\hat{\sigma}_3$ is used in the description of circularly polarized photons.

13.4.2 The Density Matrix and Circular Polarization

Using the probability amplitude representation for right-handed polarization ($|R\rangle$) and left-handed polarization ($|L\rangle$) given previously, we can write

$$|R\rangle = 2^{-1/2}\left(|x\rangle + i|y\rangle\right)$$

$$|L\rangle = 2^{-1/2}\left(|x\rangle - i|y\rangle\right)$$

which can be expressed in vector form as

$$|R\rangle = 2^{-1/2}\begin{pmatrix} 1 \\ +i \end{pmatrix} \tag{13.90}$$

$$|L\rangle = 2^{-1/2}\begin{pmatrix} 1 \\ -i \end{pmatrix} \tag{13.91}$$

Using these vectors, the density matrix for right-handed polarization becomes (see Chapter 11)

$$|R\rangle\langle R| = 2^{-1}\begin{pmatrix} 1 \\ +i \end{pmatrix}\begin{pmatrix} 1 & -i \end{pmatrix} = 2^{-1}\begin{pmatrix} 1 & -i \\ +i & 1 \end{pmatrix} \tag{13.92}$$

and the density matrix for left-handed polarization becomes

$$|L\rangle\langle L| = 2^{-1}\begin{pmatrix} 1 \\ -i \end{pmatrix}\begin{pmatrix} 1 & +i \end{pmatrix} = 2^{-1}\begin{pmatrix} 1 & +i \\ -i & 1 \end{pmatrix} \tag{13.93}$$

13.4.3 Example

Setting $a_1 = a_2 = 2^{-1/2}$ and $\delta = \pi/2$, in Equation (13.60), gives us again

$$\begin{pmatrix} \rho_{11} & \rho_{12} \\ \rho_{21} & \rho_{22} \end{pmatrix} = 2^{-1}\begin{pmatrix} 1 & -i \\ +i & 1 \end{pmatrix} \tag{13.94}$$

which is the density matrix for right-handed polarized light.

PROBLEMS

13.1 Starting from Equations (13.11) to (13.14) arrive at Equations (13.19)–(13.22).

13.2 Circular polarization: using the same approach outlined in Equations (13.52)–(13.55) derive the expression for $|L'\rangle$ given in Equation (13.56).

13.3 Set $a_1 = a_2 = 2^{-1/2}$ and $\delta = -\pi/2$, in Equation (13.60), to obtain the density matrix for left-handed polarized light.

13.4 Use the definition of the Stokes parameters given in Equations (13.62)–(13.65) to express the polarization density matrix given in Equation (13.66).

13.5 For the density matrix applicable to unpolarized light, Equation (13.67), find the values of ρ_{11} and ρ_{22} so that $Tr(\rho) = 1$.

REFERENCES

Dirac, P. A. M. (1958). *The Principles of Quantum Mechanics*, 4th ed. Oxford University, Oxford, U.K.

Duarte, F. J. (2014). *Quantum Optics for Engineers*, 1st ed. CRC, Boca Raton, FL.

Duarte, F. J. (2022). *Fundamentals of Quantum Entanglement*, 2nd ed. Institute of Physics, Bristol, U.K.

Feynman, R. P., Leighton, R. B, and Sands, M. (1965). *The Feynman Lectures on Physics*, Vol. III. Addison-Wesley, Reading, MA.

Jones, R. C. (1947). A new calculus for the treatment of optical systems, *J. Opt. Soc. Am*. 37, 107–110.

Robson, B. A. (1974). *The Theory of Polarization Phenomena*, Clarendon, Oxford, U.K.

14 Bell's Theorem

14.1 INTRODUCTION

Bell wrote a breakthrough paper in the interpretational realm of quantum mechanics. His paper was entitled *On the Einstein-Podolsky-Rosen paradox* (Bell, 1964). Bell's paper provided a transparent mathematical avenue to show that *hidden variable theories* were incompatible with the predictions of quantum mechanics. Bell's starting point was the famous contribution of Einstein et al. (1935) and their claim that quantum mechanics was incomplete and should be 'supplemented by additional variables.' He then continues 'that idea will be formulated mathematically and shown to be incompatible with the statistical predictions of quantum mechanics' (Bell, 1964). This mathematical statement became known as either *Bell's theorem* or *Bell's inequality.*

As a preamble to a discussion on Bell's work, it should be mentioned that as early as 1932, John von Neumann wrote about quantum mechanics and hidden variables theories. In this regard, von Neumann states that 'hidden parameters' are *incompatible* with the fundamental postulates of quantum mechanics (von Neumann, 1932). However, Bell reconsidered von Neumann's work and arrived at the conclusion that von Neumann's proof was 'wanting' (Bell, 1964). He then proceeded to offer his own proof on the incompatibility of hidden variables with quantum mechanics.

In the interest of fairness, it should be mentioned that Bell's dismissal of von Neumann's proof has been questioned by Bub (2010) who concludes that von Neumann's work still excludes two classes of hidden variable theories.

The following exposition of Bell's theorem is based on Bell's own work and on the reviews of this theorem by Duarte (2014, 2019, 2022).

14.2 BELL'S THEOREM

Bell's work begins defining a *hidden variable* λ, or *hidden variables*, as having a probability density $\rho(\lambda)$. In turn, this probability density $\rho(\lambda)$ obeys the normalization property (Bell, 1964)

$$\int \rho(\lambda)\, d\lambda = 1 \tag{14.1}$$

The *correlation* between observables, which are a function of this hidden variable λ, $A(x,\lambda)$ and $B(y,\lambda)$ is stated by Bell as

$$P(x,y) = \int A(x,\lambda)\, B(y,\lambda)\, \rho(\lambda)\, d\lambda \tag{14.2}$$

where x and y are 'setting directions,' and the condition of *locality* requires that A depends only on x and B depends only on y. The variables x' and y' are assumed to

 DOI: 10.1201/9781003398707-14

be 'alternative settings' in the two measuring instruments. The experimenter *freely determines* these settings. Further assumptions made (Bell, 1964) are

$$A(x,\lambda) = \pm 1 \tag{14.3}$$

$$B(y,\lambda) = \pm 1 \tag{14.4}$$

$$\left|A(x,\lambda)\right| \leq 1 \tag{14.5}$$

$$\left|B(y,\lambda)\right| \leq 1 \tag{14.6}$$

Bell provides at least two approaches to derive his theorem (Bell, 1964, 1971). Our approach begins by following Bell, but it is also influenced by the discussion of Mandel and Wolf (1995).

Using the nomenclature of Equation (14.2)

$$\left|P(x,y) - P(x,y')\right| \leq \int \left|\left[A(x,\lambda)\, B(y,\lambda) - A(x,\lambda)\, B(y',\lambda)\right]\right| \rho(\lambda)\, d\lambda \tag{14.7}$$

and

$$\left|P(x',y') + P(x',y)\right| \leq \int \left|\left[A(x',\lambda)\, B(y',\lambda) + A(x',\lambda)\, B(y,\lambda)\right]\right| \rho(\lambda)\, d\lambda \tag{14.8}$$

Adding Equations (14.7) and (14.8)

$$\begin{aligned}\left|P(x,y) - P(x,y')\right| + \left|P(x',y') + P(x',y)\right| \leq \int \left|A(x,\lambda)[B(y,\lambda) - B(y',\lambda)]\right| + \\ \left|A(x',\lambda)[B(y',\lambda) + B(y,\lambda)]\right| \rho(\lambda)\, d\lambda\end{aligned} \tag{14.9}$$

The right-hand-side (RHS) of this inequality includes *four distinct probabilities* as does the left-hand-side (LHS) (Duarte and Taylor 2021). Thus, the mathematical expression is balanced. Since the probabilities obey the definitions $A(x,\lambda) = \pm 1$, $A(x',\lambda) = \pm 1$, $B(y,\lambda) = \pm 1$, $B(y',\lambda) = \pm 1$, then

$$\int \left|A(x,\lambda)[B(y,\lambda) - B(y',\lambda)]\right| + \left|A(x',\lambda)[B(y',\lambda) + B(y,\lambda)\right|] \rho(\lambda)\, d\lambda = 2 \tag{14.10}$$

Substituting the result of Equation (14.10) for the RHS of inequality (14.9) yields

$$\left|P(x,y) - P(x,y')\right| + \left|P(x',y') + P(x',y)\right| \leq 2 \tag{14.11}$$

as required by the central result of *Bell's theorem* (Bell, 1964, 1971).

Up to this stage, Bell's theorem is a statement in classical statistics. The quantum aspect is introduced *ad hoc* via the substitution of quantum mechanical superposition

probabilities, from polarization quantum entanglement measurements, for $P(x,y)$, $P(x',y')$, $P(x',y)$, and $P(x,y')$. More explicitly

$$P(x,y) \rightarrow P(\varphi_1,\varphi_2) \tag{14.12}$$

$$P(x,y') \rightarrow P(\varphi_1,\varphi_2') \tag{14.13}$$

$$P(x',y') \rightarrow P(\varphi_1',\varphi_2') \tag{14.14}$$

$$P(x',y) \rightarrow P(\varphi_1',\varphi_2) \tag{14.15}$$

So that inequality (14.11) becomes

$$\left|P(\varphi_1,\varphi_2)-P(\varphi_1,\varphi_2')\right|+\left|P(\varphi_1',\varphi_2')+P(\varphi_1',\varphi_2)\right| \le 2 \tag{14.16}$$

In reality, however, substituting experimentally measured quantum superposition probabilities for $P(\varphi_1,\varphi_2)$, $P(\varphi_1,\varphi_2')$, $P(\varphi_1',\varphi_2')$, and $P(\varphi_1',\varphi_2)$ leads to

$$\left|P(\varphi_1,\varphi_2)-P(\varphi_1,\varphi_2{}')\right|+\left|P(\varphi_1{}',\varphi_2{}')+P(\varphi_1{}',\varphi_2)\right| \ge 2 \tag{14.17}$$

thus violating Bell's inequality (14.11).

14.3 QUANTUM ENTANGLEMENT PROBABILITIES

In Chapter 17, it is shown that the Pryce–Ward probability amplitude for quantum entanglement is

$$|\psi\rangle = 2^{-1/2}\left(|x\rangle_1|y\rangle_2 - |y\rangle_1|x_2\rangle\right) \tag{14.18}$$

Completing the *bra ket* expression on the RHS leads to

$$|\psi\rangle = 2^{-1/2}\left(\langle x'|x\rangle_1\,\langle x'|y\rangle_2 - \langle x'|y\rangle_1\,\langle x'|x\rangle_2\right) \tag{14.19}$$

and, via Born's rule $|\psi\rangle|\psi\rangle^*$, the probability becomes (Duarte, 2014)

$$\left\||\psi\rangle\right\|^2 = 2^{-1}\left(\langle x'|x\rangle_1\,\langle x'|y\rangle_2 - \langle x'|y\rangle_1\,\langle x'|x_2\rangle\right)^2 \tag{14.20}$$

Substitution of the corresponding individual probability amplitudes (see Chapter 13) into Equation (14.20) yields

$$\left\||\psi\rangle\right\|^2 = 2^{-1}(\cos\varphi_1\sin\varphi_2 - \sin\varphi_1\cos\varphi_2)^2 \tag{14.21}$$

Using the appropriate geometrical identity (see Appendix H), this probability reduces to

$$\left\||\psi\rangle\right\|^2 = 2^{-1}\sin^2(\varphi_2-\varphi_1) \tag{14.22}$$

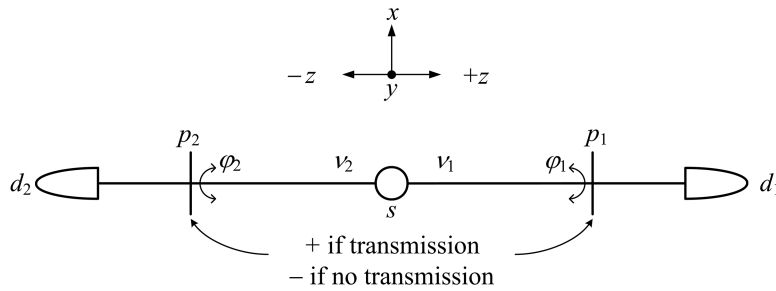

FIGURE 14.1 Quantum entanglement experimental configuration.

Revisiting Equation (14.19) and assuming that quantum 1 is incident on p_1, as illustrated in Figure 14.1, and quantum 2 is incident p_2, then

$$|\psi\rangle = 2^{-1/2}\left(\cos\varphi_1 \sin\varphi_2 - \sin\varphi_1 \cos\varphi_2\right) \tag{14.23}$$

$$|\psi\rangle = 2^{-1/2}\sin(\varphi_2 - \varphi_1) \tag{14.24}$$

Rotating the polarization analyzers by $\pi/2$

$$|\psi\rangle = 2^{-1/2}\cos(\varphi_2 - \varphi_1) \tag{14.25}$$

Using the convention of Mandel and Wolf (1995): transmission through a polarization analyzer is denoted by + and absorption through a polarization analyzer by – then the corresponding probabilities become

$$p(+\varphi_1,+\varphi_2) = p(-\varphi_1,-\varphi_2) = 2^{-1}\sin^2(\varphi_2 - \varphi_1) \tag{14.26}$$

$$p(+\varphi_1,-\varphi_2) = p(-\varphi_1,+\varphi_2) = 2^{-1}\cos^2(\varphi_2 - \varphi_1) \tag{14.27}$$

Noting that the overall probability $P(\varphi_1,\varphi_2)$ is the sum of the individual probability alternatives (Mandel and Wolf, 1995)

$$P(\varphi_1,\varphi_2) = p(+\varphi_1,+\varphi_2) + p(-\varphi_1,-\varphi_2) - p(+\varphi_1,-\varphi_2) - p(-\varphi_1,+\varphi_2) \tag{14.28}$$

$$P(\varphi_1,\varphi_2) = \sin^2(\varphi_2 - \varphi_1) - \cos^2(\varphi_2 - \varphi_1) \tag{14.29}$$

and using the geometrical identities given in Appendix H, the overall probability becomes

$$P(\varphi_1,\varphi_2) = -\cos 2(\varphi_2 - \varphi_1) \tag{14.30}$$

Moreover,

$$-\cos 2(\varphi_2 - \varphi_1) = -\cos 2(\varphi_1 - \varphi_2) \tag{14.31}$$

so that

$$P(\varphi_1,\varphi_2) = -\cos 2(\varphi_1 - \varphi_2) \tag{14.32}$$

Hence, the probability depends on the angular difference of the polarization settings φ_1 and φ_2 as shown by Pryce and Ward (1947).

From Equation (14.32), the complete set of quantum probabilities is given by

$$P(\varphi_1,\varphi_2) = -\cos 2(\varphi_1 - \varphi_2) \tag{14.33}$$

$$P(\varphi_1,\varphi_2') = -\cos 2(\varphi_1 - \varphi_2') \tag{14.34}$$

$$P(\varphi_1',\varphi_2') = -\cos 2(\varphi_1' - \varphi_2') \tag{14.35}$$

$$P(\varphi_1',\varphi_2) = -\cos 2(\varphi_1' - \varphi_2) \tag{14.36}$$

14.4 EXAMPLE

For $\varphi_1 = 0$, $\varphi_2 = 4\pi/11$, $\varphi_1' = \pi/7$, $\varphi_2' = 0$

$$\Sigma_P = \left|P(\varphi_1,\varphi_2) - P(\varphi_1,\varphi_2')\right| + \left|P(\varphi_1',\varphi_2') + P(\varphi_1',\varphi_2)\right|$$

leads to the numerical expression

$$\Sigma_P \approx |+0.65+1.0|+|-0.62-0.18| \approx 2.45 \tag{14.37}$$

so that $\Sigma_P \geq 2$. In other words, Bell's inequality is violated when using probabilities derived from the Pryce–Ward probability amplitude for quantum entanglement.

14.5 DISCUSSION

Bell's theorem is a statement in classical probability theory. The quantum probabilities are introduced *ad hoc* replacing the original classical probabilities in the final inequality expression.

Moreover, Bell's theorem is disconnected from the physics leading to the derivation of $|\psi\rangle_+$, $|\psi\rangle_-$, $|\psi\rangle^+$, and $|\psi\rangle^-$, and unrelated to the quantum probabilities calculated from these probability amplitudes (see Chapters 15–17).

In Duarte (2022), a simple all-quantum approach (see Chapter 20) leads to

$$\Sigma_{|\psi\rangle_-|\psi\rangle_-^*} = \left|P(\varphi_1,\varphi_2)\right| + \left|P(\varphi_1,\varphi_2')\right| + \left|P(\varphi_1',\varphi_2')\right| + \left|P(\varphi_1,\varphi_2')\right| \tag{14.38}$$

which can also be used to determine the security of quantum communications, via quantum entanglement.

The main significance of Bell's theorem was to reinforce that hidden variable theories were incompatible with quantum mechanics, thus neutralizing much of the criticism and discomfort, within some academic circles, toward quantum mechanics for being 'incomplete.'

PROBLEMS

14.1 Work out what happens if $|P(x,y)-P(x,y')|$ becomes $|P(x,y)+P(x,y')|$.

14.3 Verify that for non-quantum probabilities Equation (14.10) holds.

14.3 Use $P(\varphi_1,\varphi_2)=-\cos 2(\varphi_1-\varphi_2)$ to calculate

$$\Sigma_P=|P(\varphi_1,\varphi_2)-P(\varphi_1,\varphi_2')|+|P(\varphi_1',\varphi_2')+P(\varphi_1',\varphi_2)|$$

for $\varphi_1=4\pi/11,\ \varphi_2=0,\ \varphi_1'=0,\ \varphi_2'=2\pi/11$.

14.4 Use $P(\varphi_1,\varphi_2)=-\cos 2(\varphi_1-\varphi_2)$ to calculate

$$\Sigma_{|\psi\rangle|\psi\rangle^*}=|P(\varphi_1,\varphi_2)|+|P(\varphi_1,\varphi_2')|+|P(\varphi_1',\varphi_2')|+|P(\varphi_1',\varphi_2)|$$

for $\varphi_1=4\pi/11,\ \varphi_2=0,\ \varphi_1'=0,\ \varphi_2'=2\pi/11$.

REFERENCES

Bell, J. S. (1964). On the Einstein-Podolsky-Rosen paradox. *Physics* 1, 195–200.

Bell, J. S. (1971). Introduction to the hidden variable question. In *Proceedings of the International School of Physics Enrico Fermi: Foundations of Quantum Mechanics.* Academic, New York, pp. 171–181.

Bub, J. (2010). von Neumann's 'no hidden variables proof': a re-appraisal. *Found. Phys.* 40, 1333–1340.

Duarte, F. J. (2014). *Quantum Optics for Engineering*, 1st ed. CRC, Boca Raton, FL.

Duarte, F. J. (2019). *Fundamentals of Quantum Entanglement*, 1st ed. Institute of Physics, Bristol, U.K.

Duarte, F. J. (2022). *Fundamentals of Quantum Entanglement*, 2nd ed. Institute of Physics, Bristol, U.K.

Duarte, F. J., and Taylor, T. S. (2021). *Quantum Entanglement Engineering and Applications*, Institute of Physics, Bristol, U.K.

Einstein, A., Podolsky, B., and Rosen, N. (1935). Can quantum mechanical description of physical reality be considered complete? *Phys. Rev*. 47, 777–780.

Mandel, L., and Wolf, E. (1995). *Optical Coherence and Quantum Optics*, Cambridge University, Cambridge, U.K.

Pryce, M. L. H., and Ward, J. C. (1947). Angular correlation effects with annihilation radiation, Nature 160, 435.

von Neumann, J. (1932). *Mathematische Grundlagen der Quanten-Mechanik*, Springer, Berlin.

15 Quantum Entanglement Probability Amplitude for $n = N = 2$

15.1 INTRODUCTION

In this chapter, the probability amplitude for quantum entanglement is derived from the Dirac–Feynman principle (Dirac 1939, 1958; Feynman et al., 1965) as shown by Duarte (2013, 2014). This derivation applies to the most basic quantum entanglement cases, that of two quanta ($n = 2$) and two propagation channels ($N = 2$), and it is thus referred to as $n = N = 2$.

15.2 THE DIRAC–FEYNMAN PROBABILITY AMPLITUDE

The Dirac–Feynman probability amplitude (Dirac 1939, 1958; Feynman et al., 1965)

$$\langle d|s\rangle = \sum_{j=1}^{N} \langle d|j\rangle\langle j|s\rangle \tag{15.1}$$

applies to single photon propagation or to the propagation of an *ensemble of indistinguishable* photons (Duarte, 1993). This principle is crucial to quantum mechanics. It is quite a succinct mathematical statement and yet profound:

1. It states that 'all the indistinguishable photons illuminate the array of N slits, or grating, simultaneously. If only one photon propagates… then that individual photon illuminates the whole array of N slits simultaneously' (Duarte, 2003).
2. To obtain the correct result, the interaction of the probability amplitude via every slit, under illumination, with the probability amplitude via every other slit in the array must be included in the calculation.
3. It inherently includes information about *space*, that is $\langle d|j\rangle\langle j|s\rangle$, and *time* since photons propagate with velocity c.

If an array of two thousand slits is illuminated, either by a single photon or by an ensemble of indistinguishable photons, it means that the interaction of the probability amplitude of slit number 1 with all the other 1999 slits must be accounted for, and so on (Duarte, 1993). In other words, *all the probability amplitudes are interconnected* in accordance with Dirac's superposition principle (Dirac, 1958).

 DOI: 10.1201/9781003398707-15

The material in this section is based on original descriptions of Duarte (2013a, 2013b, 2014) and on the review of Duarte (2022).

15.3 THE QUANTUM ENTANGLEMENT PROBABILITY AMPLITUDE

The experimental situation applicable to the basic $n = N = 2$ configuration of quantum entanglement is depicted in Figure 15.1. Here, s is a photon source of ν_1 and ν_2 emitted in the $+z$ and $-z$ directions, respectively. The quanta propagate along the optical axis, in the $+z$ and $-z$ directions, through the polarization analyzers p_1 and p_2 toward the detectors d_1 and d_2, respectively.

The first essential, and experimentally sound, assumption is that the quanta emitted by the source are *indistinguishable*, that is, $\nu_1 = \nu_2 = \nu$. Then, expanding the Dirac interferometric principle stated in Equation (15.1), for $N = 2$

$$\langle d|s\rangle = \langle d|p_2\rangle\langle p_2|s\rangle + \langle d|p_1\rangle\langle p_1|s\rangle \tag{15.2}$$

Implicitly, this equation assumes that $d_1 = d_2 = d$, which is quite reasonable for a pair of matched detectors. Abstracting d from Equation (15.2)

$$|s\rangle = |p_2\rangle\langle p_2|s\rangle + |p_1\rangle\langle p_1|s\rangle \tag{15.3}$$

Next, using the Dirac identity

$$|\psi\rangle = |j\rangle\langle j|\psi\rangle \tag{15.4}$$

allows the expression of

$$|D\rangle_2 = |p_2\rangle\langle p_2|s\rangle \tag{15.5}$$

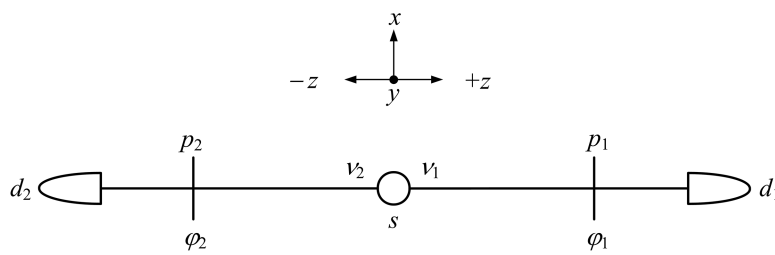

FIGURE 15.1 The Pryce–Ward quantum entanglement experiment simplified for the visible spectrum. The photon pair source s emits photon ν_1 and photon ν_2 in the $+Z$ and minus sign Z directions. The two linear polarization states $|x\rangle$ and $|y\rangle$ are orthogonal to each other. The angles ϕ_2 and are ϕ_2 the polarization angles measured on a plane perpendicular to the propagation axis, while d_1 and d_2 are the corresponding detectors (Duarte, F. *J., Fundamentals of Quantum Entanglement*, 2nd ed. Institute of Physics, Bristol, U.K., 2022, © IOP Publishing. Reproduced with permission. All rights reserved).

and

$$|D\rangle_1 = |p_1\rangle\langle p_1|s\rangle\frac{1}{2} \tag{15.6}$$

Substituting identities (15.5) and (15.6) into Equation (15.3) yields

$$|s\rangle = \left(|D\rangle_2 + |D\rangle_1\right) \tag{15.7}$$

Equation (15.7) is a probability amplitude $|s\rangle$ that represents the linear combination of two probability amplitudes, $|D\rangle_1$ and $|D\rangle_2$, and applies equally to an interferometric situation involving a single photon, or a population of indistinguishable photons, and to the $n = N = 2$ quantum entanglement situation. The crucial difference between interference and entanglement occurs at this very stage. For the entanglement situation, $|D\rangle_1$ and $|D\rangle_2$ are expanded via the Dirac identity for 'similar particles'

$$|X\rangle = |a\rangle_1|b\rangle_2|c\rangle_3 \ldots |g\rangle_n \tag{15.8}$$

This very step diverges from a purely interferometric situation given that the possibility of identifiable quanta, quanta 1 and quanta 2, is allowed with each quanta in different alternative states, that is, state $|x\rangle$ and state $|y\rangle$. Rewriting $|D\rangle_1$ and $|D\rangle_2$ in terms of polarization states as per identity (15.8), and using $|C\rangle_1$ and $|C\rangle_2$ to distinguish from a pure interferometric event, leads to

$$|s\rangle = \left(|C\rangle_2 + |C\rangle_1\right) \tag{15.9}$$

where

$$|C\rangle_2 = |x\rangle_1|y\rangle_2 \tag{15.10}$$

and

$$|C\rangle_1 = |y\rangle_1|x\rangle_2 \tag{15.11}$$

Inserting identities (15.10) and (15.11) in the expression for the probability amplitude in Equation (15.9) leads to

$$|s\rangle = \left(|x\rangle_1|y\rangle_2 + |y\rangle_1|x\rangle_2\right) \tag{15.12}$$

Following normalization, and designating $|s\rangle$ as $|\psi\rangle$, Equation (15.12) can be expressed as

$$|\psi\rangle_+ = 2^{-1/2}(|x\rangle_1|y\rangle_2 + |y\rangle_1|x\rangle_2) \tag{15.13}$$

and its linear combination is (Duarte 2013a, 2013b, 2014)

$$|\psi\rangle_- = 2^{-1/2}\left(|x\rangle_1|y\rangle_2 - |y\rangle_1|x\rangle_2\right) \tag{15.14}$$

which is the iconic probability amplitude for quantum entanglement.

Equations (15.13) and (15.14) also be expressed in a 2×2 arrangement as Duarte (2022)

$$\begin{matrix} +|C\rangle_1 & +|C\rangle_2 \\ +|C\rangle_1 & -|C\rangle_2 \end{matrix} \tag{15.15}$$

15.4 IDENTICAL STATES OF POLARIZATION

If the two quanta pairs have identical states of polarization, then Equations (15.10) and (15.11) become (Duarte, 2022)

$$|C\rangle_2 = |x\rangle_1 |x\rangle_2 \tag{15.16}$$

$$|C\rangle_1 = |y\rangle_1 |y\rangle_2 \tag{15.17}$$

so that

$$|\psi\rangle^+ = 2^{-1/2}\left(|x\rangle_1 |x\rangle_2 + |y\rangle_1 |y\rangle_2\right) \tag{15.18}$$

and

$$|\psi\rangle^- = 2^{-1/2}\left(|x\rangle_1 |x\rangle_2 - |y\rangle_1 |y\rangle_2\right) \tag{15.19}$$

The probability amplitudes $|\psi\rangle^+$ and $|\psi\rangle^-$ are also of interest in quantum computing. In summary, the whole family of probability amplitudes relevant to the quantum entanglement situation of $n = N = 2$ is represented by $|\psi\rangle_+$, $|\psi\rangle_-$, $|\psi\rangle^+$, and $|\psi\rangle^-$.

15.5 ENTANGLEMENT OF INDISTINGUISHABLE ENSEMBLES

The original Pryce–Ward probability amplitude for quantum entanglement can be re-expressed as (Duarte, 2022)

$$|\psi\rangle_- = 2^{-1/2}\left(|x\rangle_I |y\rangle_{II} - |y\rangle_I |x\rangle_{II}\right) \tag{15.20}$$

Dirac's rules for bosons do not prevent states such as $|x\rangle_I$ and $|y\rangle_{II}$ from becoming combined states of indistinguishable polarized quanta ensembles like

$$|x\rangle_I = |x\rangle_1 |x\rangle_2 |x\rangle_3 \ldots |x\rangle_g \ldots \tag{15.21}$$

$$|y\rangle_{II} = |y\rangle_1 |y\rangle_2 |y\rangle_3 \ldots |y\rangle_g \ldots \tag{15.22}$$

so that, via Equation (15.20), ensembles $|x\rangle_I$ and $|y\rangle_{II}$ are themselves entangled. This allows the design of sources of *entangled laser emission* thus vastly improving the signal-to-noise ratio for quantum communications and other applications.

It should be noted that identities (15.21) and (15.22) explain beautifully the coherent emission from electrically-pumped organic semiconductors at a very fundamental level (Duarte and Taylor, 2022). Indeed, narrow-linewidth laser sources randomly emitting $|x\rangle_I$ and $|y\rangle_{II}$ states in opposite directions, via the use of intracavity elements driven by quantum random number generators (QRNG), have been proposed and designed by Duarte (2018).

15.6 DISCUSSION

The probability amplitude for quantum entanglement was first applied in 1947 by Pryce and Ward, and a semi-heuristic derivation was disclosed in 1949 by Ward (Pryce and Ward 1947; Ward 1949). Since 1949, and until 2013, there is no record in the open literature of additional derivations. In 1965, Feynman wrote down the physics, via a two-level Hamiltonian, which leads to equations of the form of $|s\rangle = \left(|D\rangle_2 + |D\rangle_1\right)$ but did not consider the relevant Dirac identity nor the additional steps that would have led to the probability amplitude for quantum entanglement $|\psi\rangle_-$. When Feynman considers the issue of quantum entanglement, he brings in an equation of the relevant form in an ad hoc manner and he writes 'theoretical physicist have shown' (Feynman et al., 1965).

The derivation detailed here shows that the Dirac–Feynman interferometric principle

$$\langle d|s\rangle = \sum_{j=1}^{N} \langle d|j\rangle\langle j|s\rangle$$

that is central to the development of generalized interferometric probability equations is also at the foundations of quantum entanglement. The derivation of the quantum entanglement probability amplitude, *à la Dirac*, flows naturally, it is transparent, straightforward, and free of 'paradoxes' (Duarte 2022, 2023).

PROBLEMS

15.1 Expand Equation (15.1) to arrive at an equation of the form of (15.2) for $N = 2$.

15.2 Show that Equations (15.13) and (15.14) can be written in a matrix-like form as expressed in (15.15).

15.3 Express Equations (15.18) and (15.19) in matrix-like form.

REFERENCES

Dirac, P. A. M. (1939). A new notation for quantum mechanics. *Math. Proc. Cam. Phil. Soc*. 35, 416–418.

Dirac, P. A. M. (1958). *The Principles of Quantum Mechanics*, 4th edn. Oxford University, Oxford, U.K.

Duarte, F. J. (1993). On a generalized interference equation and interferometric measurements. Opt. Comm. 103, 8–14.

Duarte, F. J. (2003). *Tunable Laser Optics*, Elsevier-Academic, New York.
Duarte, F. J. (2013a). The probability amplitude for entangled polarizations: an interferometric approach. *J. Mod. Opt*. 60, 1585–1587.
Duarte, F. J. (2013b). Tunable laser optics: applications to optics and quantum optics. *Prog. Quantum Electron*. 37, 326–347.
Duarte, F. J. (2014). *Quantum Optics for Engineers*, 1st edn. CRC, Boca Raton, FL.
Duarte, F. J. (2018). Organic lasers for N-channel quantum entanglement. In *Organic Lasers and Organic Photonics* (Duarte, F. J., ed.). Institute of Physics, Bristol, U.K., Chapter 15, pp. 15-1–15-21.
Duarte, F. J. (2022). *Fundamentals of Quantum Entanglement*, 2nd edn. Institute of Physics, Bristol, U.K.
Duarte, F. J. (2023). Quantum entanglement free of paradoxes. *Laser Focus World* 59 (1), 55–56.
Duarte, F. J. and Taylor, T. S. (2022). Quantum coherence in electrically-pumped organic interferometric emitters. *Appl. Phys*. B. 128, 11.
Feynman, R. P., Leighton, R. B., and Sands, M. (1965). *The Feynman Lectures on Physics*, vol. III, Addison-Wesley, Reading, MA.
Pryce, M. L. H. and Ward, J. C. (1947). Angular correlation effects with annihilation radiation, *Nature* 160, 435.
Ward, J. C. (1949). *Some Properties of the Elementary Particles*, Oxford University, Oxford, U.K.

16 Quantum Entanglement Probability Amplitude for $n = N = 2^1, 2^2, 2^3, \ldots, 2^r$

16.1 INTRODUCTION

The interferometric derivation, *à la Dirac*, of the iconic superposition quantum entanglement probability amplitude

$$|\psi\rangle_{-} = 2^{-1/2}\left(|x\rangle_1|y\rangle_2 - |y\rangle_1|x\rangle_2\right) \tag{16.1}$$

for $n = N = 2$ is described in Chapter 15. In this chapter, the interferometric derivational approach is extended to the cases of $n = N = 4$, $n = N = 8$, and $n = N = 16$. Moreover, generalized equations applicable to $n = N = 2^1, 2^2, 2^3, 2^4, \ldots 2^r$ or simply $n = N = 2^r$, where $r = 1,\ 2,\ 3,\ 4,\ 5...$, are also given.

The physics in this chapter is a revision, in a handbook style, of various treatments previously considered by Duarte (2013a, 2013b, 2014, 2015, 2016, 2022) and Duarte and Taylor (2017).

16.2 QUANTUM ENTANGLEMENT PROBABILITY AMPLITUDE FOR $n = N = 4$

The quantum entanglement experimental configuration for $n = N = 4$ is given in Figure 16.1. The photon source s emits two pairs of quanta in opposite directions relative to each other: (ν_1, ν_2) and (ν_3, ν_4). Quanta ν_1 and ν_2 are emitted in the $+z$ and $-z$ directions, while quanta ν_3 and ν_4 are emitted in the $+x$ and $-x$ directions, respectively. Traditional axes labels are obviated and only polarization alternatives are assigned in pairs, in this case (x, y) along the $+z$ and $-z$ directions, and (φ, φ') along the corresponding orthogonal direction.

For the case $n = N = 2^2$, the Dirac–Feynman interferometric principle (Dirac, 1958; Feynman et al., 1965)

$$\langle d|s\rangle = \sum_{j=1}^{N} \langle d|j\rangle\langle j|s\rangle \tag{16.1}$$

can be expanded for $N = 4$, while assuming that the quanta emitted by the source are *indistinguishable*, $d_1 = d_2 = d_3 = d_4 = d$, and that $j \rightarrow p_j$, so that

$$\langle d|s\rangle = \langle d|p_4\rangle\langle p_4|s\rangle + \langle d|p_3\rangle\langle p_3|s\rangle + \langle d|p_2\rangle\langle p_2|s\rangle + \langle d|p_1\rangle\langle p_1|s\rangle \tag{16.2}$$

DOI: 10.1201/9781003398707-16

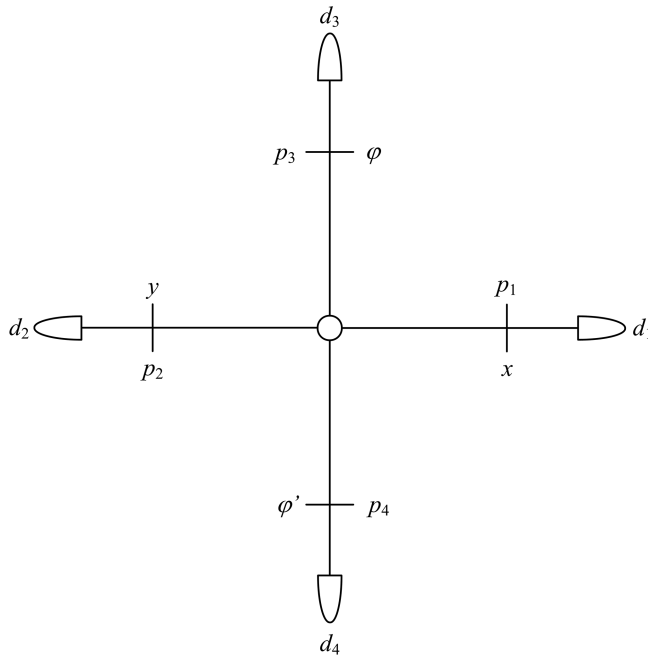

FIGURE 16.1 Schematics for a quantum entanglement situation of $n = N = 2^2$ (Duarte, F. J., *Fundamentals of Quantum Entanglement*, 2nd ed. Institute of Physics, Bristol, U.K., 2022, © IOP Publishing. Reproduced with permission. All rights reserved).

and following the procedure introduced in Chapter 15

$$|D\rangle_4 = |p_4\rangle\langle p_4|s\rangle \tag{16.3}$$

$$|D\rangle_3 = |p_3\rangle\langle p_3|s\rangle \tag{16.4}$$

$$|D\rangle_2 = |p_2\rangle\langle p_2|s\rangle \tag{16.5}$$

$$|D\rangle_1 = |p_1\rangle\langle p_1|s\rangle \tag{16.6}$$

so that Equation (16.2) becomes

$$|s\rangle = \left(|D\rangle_4 + |D\rangle_3 + |D\rangle_2 + |D\rangle_1\right) \tag{16.7}$$

Using the Dirac identity (Dirac, 1958)

$$|X\rangle = |a\rangle_1 |b\rangle_2 |c\rangle_3 \ldots |g\rangle_n \tag{16.8}$$

and using $|D\rangle_m \rightarrow |C\rangle_m$ to differentiate from the interferometric situation

$$|C\rangle_1 = |x\rangle_1 |y\rangle_2 |\varphi\rangle_3 |\varphi'\rangle_4 \tag{16.9}$$

$$|C\rangle_2 = |y\rangle_1 |x\rangle_2 |\varphi'\rangle_3 |\varphi\rangle_4 \tag{16.10}$$

$$|C\rangle_3 = |\varphi\rangle_1 |\varphi'\rangle_2 |x\rangle_3 |y\rangle_4 \tag{16.11}$$

$$|C\rangle_4 = |\varphi'\rangle_1 |\varphi\rangle_2 |y\rangle_3 |x\rangle_4 \tag{16.12}$$

The normalized probability amplitude $|\psi\rangle_R$, where R is a *Roman numeral*, is given by (Duarte, 2015)

$$|\psi\rangle_R = N^{-1/2} |s\rangle \tag{16.13}$$

and the normalization condition for $N = 4$ is

$$1 = \left| |\psi\rangle_I \right|^2 + \left| |\psi\rangle_{II} \right|^2 + \left| |\psi\rangle_{III} \right|^2 + \left| |\psi\rangle_{IV} \right|^2 \tag{16.14}$$

Hence, the normalization condition leads to

$$|\psi\rangle_I = 4^{-1/2} \left(|C\rangle_1 + |C\rangle_2 + |C\rangle_3 + |C\rangle_4 \right) \tag{16.15}$$

$$|\psi\rangle_{II} = 4^{-1/2} \left(|C\rangle_1 + |C\rangle_2 - |C\rangle_3 - |C\rangle_4 \right) \tag{16.16}$$

$$|\psi\rangle_{III} = 4^{-1/2} \left(|C\rangle_1 - |C\rangle_2 + |C\rangle_3 - |C\rangle_4 \right) \tag{16.17}$$

$$|\psi\rangle_{IV} = 4^{-1/2} \left(|C\rangle_1 - |C\rangle_2 - |C\rangle_3 + |C\rangle_4 \right) \tag{16.18}$$

Substituting identities (16.9)–(16.12) into Equations (16.15)–(16.18) reveals the explicit expressions for the relevant superposition probability amplitudes

$$\begin{aligned} |\psi\rangle_I = 4^{-1/2} \big(& |x\rangle_1 |y\rangle_2 |\varphi\rangle_3 |\varphi'\rangle_4 + |y\rangle_1 |x\rangle_2 |\varphi'\rangle_3 |\varphi\rangle_4 \\ & + |\varphi\rangle_1 |\varphi'\rangle_2 |x\rangle_3 |y\rangle_4 + |\varphi'\rangle_1 |\varphi\rangle_2 |y\rangle_3 |x\rangle_4 \big) \end{aligned} \tag{16.19}$$

$$\begin{aligned} |\psi\rangle_{II} = 4^{-1/2} \big(& |x\rangle_1 |y\rangle_2 |\varphi\rangle_3 |\varphi'\rangle_4 + |y\rangle_1 |x\rangle_2 |\varphi'\rangle_3 |\varphi\rangle_4 \\ & - |\varphi\rangle_1 |\varphi'\rangle_2 |x\rangle_3 |y\rangle_4 + |\varphi'\rangle_1 |\varphi\rangle_2 |y\rangle_3 |x\rangle_4 \big) \end{aligned} \tag{16.20}$$

$$\begin{aligned} |\psi\rangle_{III} = 4^{-1/2} \big(& |x\rangle_1 |y\rangle_2 |\varphi\rangle_3 |\varphi'\rangle_4 - |y\rangle_1 |x\rangle_2 |\varphi'\rangle_3 |\varphi\rangle_4 \\ & + |\varphi\rangle_1 |\varphi'\rangle_2 |x\rangle_3 |y\rangle_4 - |\varphi'\rangle_1 |\varphi\rangle_2 |y\rangle_3 |x\rangle_4 \big) \end{aligned} \tag{16.21}$$

$$\begin{aligned} |\psi\rangle_{IV} = 4^{-1/2} \big(& |x\rangle_1 |y\rangle_2 |\varphi\rangle_3 |\varphi'\rangle_4 - |y\rangle_1 |x\rangle_2 |\varphi'\rangle_3 |\varphi\rangle_4 \\ & - |\varphi\rangle_1 |\varphi'\rangle_2 |x\rangle_3 |y\rangle_4 + |\varphi'\rangle_1 |\varphi\rangle_2 |y\rangle_3 |x\rangle_4 \big) \end{aligned} \tag{16.22}$$

The symmetry pattern in the sign convention of the $|C\rangle_m$ states can be best observed via a 4×4 mathematical arrangement (Duarte, 2018)

$$\begin{array}{cccc} +|C\rangle_1 & +|C\rangle_2 & +|C\rangle_3 & +|C\rangle_4 \\ +|C\rangle_1 & +|C\rangle_2 & -|C\rangle_3 & -|C\rangle_4 \\ +|C\rangle_1 & -|C\rangle_2 & +|C\rangle_3 & -|C\rangle_4 \\ +|C\rangle_1 & -|C\rangle_2 & -|C\rangle_3 & +|C\rangle_4 \end{array} \tag{16.23}$$

16.3 QUANTUM ENTANGLEMENT PROBABILITY AMPLITUDE FOR $n = N = 8$

The quantum entanglement experimental configuration for $n = N = 8$ is given in Figure 16.2. Four axes are involved, each adjacent axis at $\theta = \pi/4$ rad relative to each other. If each axis has a + and a − direction, then there are $N = 8$ channels of propagation. Here, s is the photon source of *four pairs* of quanta emitted in opposite directions relative to each other. Axes labeling in reference to Figure 16.2: (x, y) along the $+z$ and $-z$ directions, and (φ, φ') along the corresponding orthogonal direction.

The first axis at $\theta = \pi/4$, relative to the z axis, involves the (ϕ, ϕ') polarizations, and the axis orthogonal to it involves the (ϑ, ϑ') polarizations.

Following the same methodology as in the previous section

$$|s\rangle = |D\rangle_8 + |D\rangle_7 + |D\rangle_6 + |D\rangle_5 + |D\rangle_4 + |D\rangle_3 + |D\rangle_2 + |D\rangle_1 \tag{16.24}$$

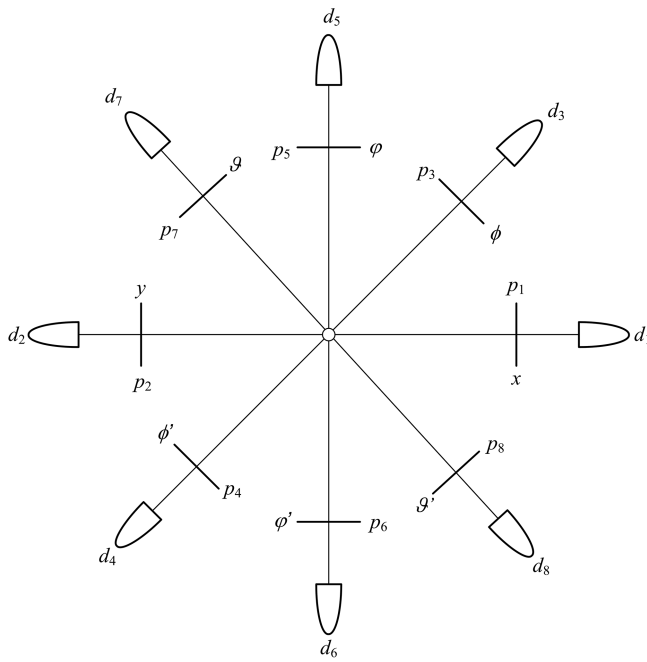

FIGURE 16.2 Schematics for a quantum entanglement situation of $n = N = 2^3$ (Duarte, F. J., *Fundamentals of Quantum Entanglement*, 2nd ed. Institute of Physics, Bristol, U.K., 2022, © IOP Publishing. Reproduced with permission. All rights reserved).

Applying the Dirac identity (Dirac, 1958)

$$|X\rangle = |a\rangle_1 |b\rangle_2 |c\rangle_3 \ldots |g\rangle_n \tag{16.25}$$

and using $|D\rangle_m \to |C\rangle_m$ to differentiate from the interferometric situation

$$|C\rangle_1 = |x\rangle_1 |y\rangle_2 |\varphi\rangle_3 |\varphi'\rangle_4 |\phi\rangle_5 |\phi'\rangle_6 |\vartheta\rangle_7 |\vartheta'\rangle_8 \tag{16.26}$$

$$|C\rangle_2 = |y\rangle_1 |x\rangle_2 |\varphi'\rangle_3 |\varphi\rangle_4 |\phi'\rangle_5 |\phi\rangle_6 |\vartheta'\rangle_7 |\vartheta\rangle_8 \tag{16.27}$$

$$|C\rangle_3 = |\varphi\rangle_1 |\varphi'\rangle_2 |\phi\rangle_3 |\phi'\rangle_4 |\vartheta\rangle_5 |\vartheta'\rangle_6 |x\rangle_7 |y\rangle_8 \tag{16.28}$$

$$|C\rangle_4 = |\varphi'\rangle_1 |\varphi\rangle_2 |\phi'\rangle_3 |\phi\rangle_4 |\vartheta'\rangle_5 |\vartheta\rangle_6 |y\rangle_7 |x\rangle_8 \tag{16.29}$$

$$|C\rangle_5 = |\phi\rangle_1 |\phi'\rangle_2 |\vartheta\rangle_3 |\vartheta'\rangle_4 |x\rangle_5 |y\rangle_6 |\varphi\rangle_7 |\varphi'\rangle_8 \tag{16.30}$$

$$|C\rangle_6 = |\phi'\rangle_1 |\phi\rangle_2 |\vartheta'\rangle_3 |\vartheta\rangle_4 |y\rangle_5 |x\rangle_6 |\varphi'\rangle_7 |\varphi\rangle_8 \tag{16.31}$$

$$|C\rangle_7 = |\vartheta\rangle_1 |\vartheta'\rangle_2 |x\rangle_3 |y\rangle_4 |\varphi\rangle_5 |\varphi'\rangle_6 |\phi\rangle_7 |\phi'\rangle_8 \tag{16.32}$$

$$|C\rangle_8 = |\vartheta'\rangle_1 |\vartheta\rangle_2 |y\rangle_3 |x\rangle_4 |\varphi'\rangle_5 |\varphi\rangle_6 |\phi'\rangle_7 |\phi\rangle_8 \tag{16.33}$$

For $n = N = 2^3$, the normalized probability amplitudes become

$$|\psi\rangle_I = 8^{-1/2}\left(|C\rangle_1 + |C\rangle_2 + |C\rangle_3 + |C\rangle_4 + |C\rangle_5 + |C\rangle_6 + |C\rangle_7 + |C\rangle_8\right) \tag{16.34}$$

$$|\psi\rangle_{II} = 8^{-1/2}\left(|C\rangle_1 + |C\rangle_2 + |C\rangle_3 + |C\rangle_4 - |C\rangle_5 - |C\rangle_6 - |C\rangle_7 - |C\rangle_8\right) \tag{16.35}$$

$$|\psi\rangle_{III} = 8^{-1/2}\left(|C\rangle_1 + |C\rangle_2 - |C\rangle_3 - |C\rangle_4 + |C\rangle_5 + |C\rangle_6 - |C\rangle_7 - |C\rangle_8\right) \tag{16.36}$$

$$|\psi\rangle_{IV} = 8^{-1/2}\left(|C\rangle_1 + |C\rangle_2 - |C\rangle_3 - |C\rangle_4 - |C\rangle_5 - |C\rangle_6 + |C\rangle_7 + |C\rangle_8\right) \tag{16.37}$$

$$|\psi\rangle_V = 8^{-1/2}\left(|C\rangle_1 - |C\rangle_2 + |C\rangle_3 - |C\rangle_4 + |C\rangle_5 - |C\rangle_6 + |C\rangle_7 - |C\rangle_8\right) \tag{16.38}$$

$$|\psi\rangle_{VI} = 8^{-1/2}\left(|C\rangle_1 - |C\rangle_2 + |C\rangle_3 - |C\rangle_4 - |C\rangle_5 + |C\rangle_6 - |C\rangle_7 + |C\rangle_8\right) \quad (16.39)$$

$$|\psi\rangle_{VII} = 8^{-1/2}\left(|C\rangle_1 - |C\rangle_2 - |C\rangle_3 + |C\rangle_4 + |C\rangle_5 - |C\rangle_6 - |C\rangle_7 + |C\rangle_8\right) \quad (16.40)$$

$$|\psi\rangle_{VIII} = 8^{-1/2}\left(|C\rangle_1 - |C\rangle_2 - |C\rangle_3 + |C\rangle_4 - |C\rangle_5 + |C\rangle_6 + |C\rangle_7 - |C\rangle_8\right) \quad (16.41)$$

A better appreciation of the sign alternatives is offered if the $|C\rangle_m$ amplitudes are expressed in an 8×8 format with the *bra ket* $(|\ \rangle)$ symbols abstracted, so that (Duarte, 2018)

$$\begin{array}{cccccccc}
+C_1 & +C_2 & +C_3 & +C_4 & +C_5 & +C_6 & +C_7 & +C_8 \\
+C_1 & +C_2 & +C_3 & +C_4 & -C_5 & -C_6 & -C_7 & -C_8 \\
+C_1 & +C_2 & -C_3 & -C_4 & +C_5 & +C_6 & -C_7 & -C_8 \\
+C_1 & +C_2 & -C_3 & -C_4 & -C_5 & -C_6 & +C_7 & +C_8 \\
+C_1 & -C_2 & +C_3 & -C_4 & +C_5 & -C_6 & +C_7 & -C_8 \\
+C_1 & -C_2 & +C_3 & -C_4 & -C_5 & +C_6 & -C_7 & +C_8 \\
+C_1 & -C_2 & -C_3 & +C_4 & +C_5 & -C_6 & -C_7 & +C_8 \\
+C_1 & -C_2 & -C_3 & +C_4 & -C_5 & +C_6 & +C_7 & -C_8
\end{array} \quad (16.42)$$

For the row and column originating at $+C_1$, the sign sequences (right and down) are +, +, +, +, +, +, +, + and +, +, +, +, +, +, +, +. On the other hand, for the terms on the diagonal, the sign sequence is +, +, −, −, +, +, −, −. The sign sequence for the second column and the second row is +, +, +, +, −, −, −, −, while the sequence for the third column and the third row is +, +, −, −, +, +, −, −, and so on.

16.4 QUANTUM ENTANGLEMENT PROBABILITY AMPLITUDE FOR $n = N = 16$

For $n = N = 2^4$, the first normalized probability $|\psi\rangle_I$ amplitudes becomes

$$\begin{aligned}|\psi\rangle_I = 16^{-1/2}\big(&|C\rangle_1 + |C\rangle_2 + |C\rangle_3 + |C\rangle_4 + |C\rangle_5 + |C\rangle_6 + |C\rangle_7 + |C\rangle_8 \\ &+ |C\rangle_9 + |C\rangle_{10} + |C\rangle_{11} + |C\rangle_{12} + |C\rangle_{13} + |C\rangle_{14} + |C\rangle_{15} + |C\rangle_{16}\big)\end{aligned} \quad (16.43)$$

and so on for $|\psi\rangle_{II}, |\psi\rangle_{III}, |\psi\rangle_{IV} \ldots |\psi\rangle_{XVI}$. Going straight to the sign alternatives for the $|C\rangle_m$ probability amplitudes expressed in an 16×16 format, with the *bracket* $(|\ \rangle)$ symbols abstracted (Duarte, 2018)

$$
\begin{array}{cccccccccccccccc}
+C_1 & +C_2 & +C_3 & +C_4 & +C_5 & +C_6 & +C_7 & +C_8 & +C_9 & +C_{10} & +C_{11} & +C_{12} & +C_{13} & +C_{14} & +C_{15} & +C_{16} \\
+C_1 & +C_2 & +C_3 & +C_4 & +C_5 & +C_6 & +C_7 & +C_8 & -C_9 & -C_{10} & -C_{11} & -C_{12} & -C_{13} & -C_{14} & -C_{15} & -C_{16} \\
+C_1 & +C_2 & +C_3 & +C_4 & -C_5 & -C_6 & -C_7 & -C_8 & +C_9 & +C_{10} & +C_{11} & +C_{12} & -C_{13} & -C_{14} & -C_{15} & -C_{16} \\
+C_1 & +C_2 & +C_3 & +C_4 & -C_5 & -C_6 & -C_7 & -C_8 & -C_9 & -C_{10} & -C_{11} & -C_{12} & +C_{13} & +C_{14} & +C_{15} & +C_{16} \\
+C_1 & +C_2 & -C_3 & -C_4 & +C_5 & +C_6 & -C_7 & -C_8 & +C_9 & +C_{10} & -C_{11} & -C_{12} & +C_{13} & +C_{14} & -C_{15} & -C_{16} \\
+C_1 & +C_2 & -C_3 & -C_4 & +C_5 & +C_6 & -C_7 & -C_8 & -C_9 & -C_{10} & +C_{11} & +C_{12} & -C_{13} & -C_{14} & +C_{15} & +C_{16} \\
+C_1 & +C_2 & -C_3 & -C_4 & -C_5 & -C_6 & +C_7 & +C_8 & +C_9 & +C_{10} & -C_{11} & -C_{12} & -C_{13} & -C_{14} & +C_{15} & +C_{16} \\
+C_1 & +C_2 & -C_3 & -C_4 & -C_5 & -C_6 & +C_7 & +C_8 & -C_9 & -C_{10} & +C_{11} & +C_{12} & +C_{13} & +C_{14} & -C_{15} & -C_{16} \\
+C_1 & -C_2 & +C_3 & +C_4 & +C_5 & -C_6 & +C_7 & -C_8 & +C_9 & -C_{10} & +C_{11} & -C_{12} & +C_{13} & -C_{14} & +C_{15} & -C_{16} \\
+C_1 & -C_2 & +C_3 & +C_4 & +C_5 & -C_6 & +C_7 & -C_8 & -C_9 & +C_{10} & -C_{11} & +C_{12} & -C_{13} & +C_{14} & -C_{15} & +C_{16} \\
+C_1 & -C_2 & +C_3 & -C_4 & -C_5 & +C_6 & -C_7 & +C_8 & +C_9 & -C_{10} & +C_{11} & -C_{12} & -C_{13} & +C_{14} & -C_{15} & +C_{16} \\
+C_1 & -C_2 & +C_3 & -C_4 & -C_5 & +C_6 & -C_7 & +C_8 & -C_9 & +C_{10} & -C_{11} & +C_{12} & +C_{13} & -C_{14} & +C_{15} & -C_{16} \\
+C_1 & -C_2 & -C_3 & +C_4 & +C_5 & -C_6 & -C_7 & +C_8 & +C_9 & +C_{10} & -C_{11} & -C_{12} & +C_{13} & -C_{14} & -C_{15} & +C_{16} \\
+C_1 & -C_2 & -C_3 & +C_4 & +C_5 & -C_6 & -C_7 & +C_8 & -C_9 & -C_{10} & +C_{11} & +C_{12} & -C_{13} & +C_{14} & +C_{15} & -C_{16} \\
+C_1 & -C_2 & -C_3 & +C_4 & -C_5 & +C_6 & +C_7 & -C_8 & +C_9 & -C_{10} & -C_{11} & +C_{12} & -C_{13} & +C_{14} & +C_{15} & -C_{16} \\
+C_1 & -C_2 & -C_3 & +C_4 & -C_5 & +C_6 & +C_7 & -C_8 & -C_9 & +C_{10} & +C_{11} & -C_{12} & +C_{13} & -C_{14} & -C_{15} & +C_{16}
\end{array}
\tag{16.44}
$$

16.5 QUANTUM ENTANGLEMENT PROBABILITY AMPLITUDE FOR $n = N = 2^1, 2^2, 2^3, \ldots 2^r$

First, the probability amplitude $|s\rangle$ can generally be expressed as (Duarte, 2016, 2018)

$$|s\rangle = \sum_{j=1}^{N} (\pm)|C\rangle_{N+1-j} \tag{16.45}$$

and for notational consistency, the normalized probability amplitude is expressed as

$$|\psi\rangle_R = N^{-1/2}|s\rangle \tag{16.46}$$

which means

$$|\psi\rangle_R = N^{-1/2}\sum_{j=1}^{N} (\pm)|C\rangle_{N+1-j} \tag{16.47}$$

where the subscript R is a *Roman numeral*, the $N^{-1/2}$ factor is derived from the normalization operation

$$1 = \left|\|\psi\rangle_I\right|^2 + \left|\|\psi\rangle_{II}\right|^2 + \left|\|\psi\rangle_{III}\right|^2 + \left|\|\psi\rangle_{IV}\right|^2 + \ldots \tag{16.48}$$

and the sign alternative $(\pm)$ means that every possible sign alternative in the series is allowed. Equation (16.47) is the generalized superposition probability amplitude for quantum entanglement for situations applicable to $n = N = 2^1, 2^2, 2^3 \ldots 2^r$.

The individual path probability amplitudes $|C\rangle_{N+1-j}$ are expressed in a generalized form as (Duarte, 2016, 2018)

$$|C\rangle_{N+1-j} = \prod_{m=1,\,3,\,5\ldots}^{n} |a\rangle_m |b\rangle_{m+1} \tag{16.49}$$

Equation (16.49) is a mathematical expression for a series of probability amplitudes beginning at $|C\rangle_{N+1-j}$ with $j = 1$, and ending at $|C\rangle_1$ which is reached when $j = N$.

In this notation, n is the total number of quanta, which is an even number since quanta participate in pairs. For each pair, $(1, 2), (3, 4) \ldots (m, m+1)$, $|a\rangle_m, |b\rangle_{m+1}$ represent a set of orthogonal polarization alternatives such as (x, y), (φ, φ'), and so on (Duarte, 2018).

16.5.1 Example

Consider the case of $n = N = 2^3$: expanding $|C\rangle_{N+1-j}$, that is Equation (16.49) for $j = 8,\ 7,\ 6,\ 5,\ 4,\ 3,\ 2,\ 1$, explicit values for $|C\rangle_1, |C\rangle_2, |C\rangle_3 \ldots |C\rangle_8$ are obtained.

Substitution of the corresponding $|C\rangle_{N+1-j}$ amplitudes, that is $|C\rangle_1, |C\rangle_2, |C\rangle_3 \ldots |C\rangle_8$ into Equation (16.47), lead to the explicit series of probability amplitudes $|\psi\rangle_I, |\psi\rangle_{II}, |\psi\rangle_{III} \ldots |\psi\rangle_{VIII}$ in terms of the polarization coordinates $(x, y), (\varphi, \varphi'), (\phi, \phi')$, and (ϑ, ϑ') (Duarte and Taylor, 2017)

$$
\begin{aligned}
|\psi\rangle_I = 8^{-1/2}\big(&|x\rangle_1|y\rangle_2|\varphi\rangle_3|\varphi'\rangle_4|\phi\rangle_5|\phi'\rangle_6|\vartheta\rangle_7|\vartheta'\rangle_8\\
&+|y\rangle_1|x\rangle_2|\varphi'\rangle_3|\varphi\rangle_4|\phi'\rangle_5|\phi\rangle_6|\vartheta'\rangle_7|\vartheta\rangle_8\\
&+|\varphi\rangle_1|\varphi'\rangle_2|\phi\rangle_3|\phi'\rangle_4|\vartheta\rangle_5|\vartheta'\rangle_6|x\rangle_7|y\rangle_8\\
&+|\varphi'\rangle_1|\varphi\rangle_2|\phi'\rangle_3|\phi\rangle_4|\vartheta'\rangle_5|\vartheta\rangle_6|y\rangle_7|x\rangle_8\\
&+|\phi\rangle_1|\phi'\rangle_2|\vartheta\rangle_3|\vartheta'\rangle_4|x\rangle_5|y\rangle_6|\varphi\rangle_7|\varphi'\rangle_8\\
&+|\phi'\rangle_1|\phi\rangle_2|\vartheta'\rangle_3|\vartheta\rangle_4|y\rangle_5|x\rangle_6|\varphi'\rangle_7|\varphi\rangle_8\\
&+|\vartheta\rangle_1|\vartheta'\rangle_2|x\rangle_3|y\rangle_4|\varphi\rangle_5|\varphi'\rangle_6|\phi\rangle_7|\phi'\rangle_8\\
&+|\vartheta'\rangle_1|\vartheta\rangle_2|y\rangle_3|x\rangle_4|\varphi'\rangle_5|\varphi\rangle_6|\phi'\rangle_7|\phi\rangle_8\big)
\end{aligned}
\tag{16.50}
$$

$$
\begin{aligned}
|\psi\rangle_{II} = 8^{-1/2}\big(&|x\rangle_1|y\rangle_2|\varphi\rangle_3|\varphi'\rangle_4|\phi\rangle_5|\phi'\rangle_6|\vartheta\rangle_7|\vartheta'\rangle_8\\
&+|y\rangle_1|x\rangle_2|\varphi'\rangle_3|\varphi\rangle_4|\phi'\rangle_5|\phi\rangle_6|\vartheta'\rangle_7|\vartheta\rangle_8\\
&+|\varphi\rangle_1|\varphi'\rangle_2|\phi\rangle_3|\phi'\rangle_4|\vartheta\rangle_5|\vartheta'\rangle_6|x\rangle_7|y\rangle_8\\
&+|\varphi'\rangle_1|\varphi\rangle_2|\phi'\rangle_3|\phi\rangle_4|\vartheta'\rangle_5|\vartheta\rangle_6|y\rangle_7|x\rangle_8\\
&-|\phi\rangle_1|\phi'\rangle_2|\vartheta\rangle_3|\vartheta'\rangle_4|x\rangle_5|y\rangle_6|\varphi\rangle_7|\varphi'\rangle_8\\
&-|\phi'\rangle_1|\phi\rangle_2|\vartheta'\rangle_3|\vartheta\rangle_4|y\rangle_5|x\rangle_6|\varphi'\rangle_7|\varphi\rangle_8\\
&-|\vartheta\rangle_1|\vartheta'\rangle_2|x\rangle_3|y\rangle_4|\varphi\rangle_5|\varphi'\rangle_6|\phi\rangle_7|\phi'\rangle_8\\
&-|\vartheta'\rangle_1|\vartheta\rangle_2|y\rangle_3|x\rangle_4|\varphi'\rangle_5|\varphi\rangle_6|\phi'\rangle_7|\phi\rangle_8\big)
\end{aligned}
\tag{16.51}
$$

$$
\begin{aligned}
|\psi\rangle_{III} = 8^{-1/2}\big(&|x\rangle_1|y\rangle_2|\varphi\rangle_3|\varphi'\rangle_4|\phi\rangle_5|\phi'\rangle_6|\vartheta\rangle_7|\vartheta'\rangle_8\\
&+|y\rangle_1|x\rangle_2|\varphi'\rangle_3|\varphi\rangle_4|\phi'\rangle_5|\phi\rangle_6|\vartheta'\rangle_7|\vartheta\rangle_8\\
&-|\varphi\rangle_1|\varphi'\rangle_2|\phi\rangle_3|\phi'\rangle_4|\vartheta\rangle_5|\vartheta'\rangle_6|x\rangle_7|y\rangle_8\\
&-|\varphi'\rangle_1|\varphi\rangle_2|\phi'\rangle_3|\phi\rangle_4|\vartheta'\rangle_5|\vartheta\rangle_6|y\rangle_7|x\rangle_8\\
&+|\phi\rangle_1|\phi'\rangle_2|\vartheta\rangle_3|\vartheta'\rangle_4|x\rangle_5|y\rangle_6|\varphi\rangle_7|\varphi'\rangle_8\\
&+|\phi'\rangle_1|\phi\rangle_2|\vartheta'\rangle_3|\vartheta\rangle_4|y\rangle_5|x\rangle_6|\varphi'\rangle_7|\varphi\rangle_8\\
&-|\vartheta\rangle_1|\vartheta'\rangle_2|x\rangle_3|y\rangle_4|\varphi\rangle_5|\varphi'\rangle_6|\phi\rangle_7|\phi'\rangle_8\\
&-|\vartheta'\rangle_1|\vartheta\rangle_2|y\rangle_3|x\rangle_4|\varphi'\rangle_5|\varphi\rangle_6|\phi'\rangle_7|\phi\rangle_8\big)
\end{aligned}
\tag{16.52}
$$

$$
\begin{aligned}
|\psi\rangle_{IV} = 8^{-1/2}\big(&|x\rangle_1|y\rangle_2|\varphi\rangle_3|\varphi'\rangle_4|\phi\rangle_5|\phi'\rangle_6|\vartheta\rangle_7|\vartheta'\rangle_8\\
&+|y\rangle_1|x\rangle_2|\varphi'\rangle_3|\varphi\rangle_4|\phi'\rangle_5|\phi\rangle_6|\vartheta'\rangle_7|\vartheta\rangle_8\\
&-|\varphi\rangle_1|\varphi'\rangle_2|\phi\rangle_3|\phi'\rangle_4|\vartheta\rangle_5|\vartheta'\rangle_6|x\rangle_7|y\rangle_8\\
&-|\varphi'\rangle_1|\varphi\rangle_2|\phi'\rangle_3|\phi\rangle_4|\vartheta'\rangle_5|\vartheta\rangle_6|y\rangle_7|x\rangle_8\\
&-|\phi\rangle_1|\phi'\rangle_2|\vartheta\rangle_3|\vartheta'\rangle_4|x\rangle_5|y\rangle_6|\varphi\rangle_7|\varphi'\rangle_8\\
&-|\phi'\rangle_1|\phi\rangle_2|\vartheta'\rangle_3|\vartheta\rangle_4|y\rangle_5|x\rangle_6|\varphi'\rangle_7|\varphi\rangle_8\\
&+|\vartheta\rangle_1|\vartheta'\rangle_2|x\rangle_3|y\rangle_4|\varphi\rangle_5|\varphi'\rangle_6|\phi\rangle_7|\phi'\rangle_8\\
&+|\vartheta'\rangle_1|\vartheta\rangle_2|y\rangle_3|x\rangle_4|\varphi'\rangle_5|\varphi\rangle_6|\phi'\rangle_7|\phi\rangle_8\big)
\end{aligned}
\tag{16.53}
$$

$$
\begin{aligned}
|\psi\rangle_{V} = 8^{-1/2}\big(&|x\rangle_1|y\rangle_2|\varphi\rangle_3|\varphi'\rangle_4|\phi\rangle_5|\phi'\rangle_6|\vartheta\rangle_7|\vartheta'\rangle_8\\
&-|y\rangle_1|x\rangle_2|\varphi'\rangle_3|\varphi\rangle_4|\phi'\rangle_5|\phi\rangle_6|\vartheta'\rangle_7|\vartheta\rangle_8\\
&+|\varphi\rangle_1|\varphi'\rangle_2|\phi\rangle_3|\phi'\rangle_4|\vartheta\rangle_5|\vartheta'\rangle_6|x\rangle_7|y\rangle_8\\
&-|\varphi'\rangle_1|\varphi\rangle_2|\phi'\rangle_3|\phi\rangle_4|\vartheta'\rangle_5|\vartheta\rangle_6|y\rangle_7|x\rangle_8\\
&+|\phi\rangle_1|\phi'\rangle_2|\vartheta\rangle_3|\vartheta'\rangle_4|x\rangle_5|y\rangle_6|\varphi\rangle_7|\varphi'\rangle_8\\
&-|\phi'\rangle_1|\phi\rangle_2|\vartheta'\rangle_3|\vartheta\rangle_4|y\rangle_5|x\rangle_6|\varphi'\rangle_7|\varphi\rangle_8\\
&+|\vartheta\rangle_1|\vartheta'\rangle_2|x\rangle_3|y\rangle_4|\varphi\rangle_5|\varphi'\rangle_6|\phi\rangle_7|\phi'\rangle_8\\
&-|\vartheta'\rangle_1|\vartheta\rangle_2|y\rangle_3|x\rangle_4|\varphi'\rangle_5|\varphi\rangle_6|\phi'\rangle_7|\phi\rangle_8\big)
\end{aligned}
\tag{16.54}
$$

$$
\begin{aligned}
|\psi\rangle_{VI} = 8^{-1/2}\big(&|x\rangle_1|y\rangle_2|\varphi\rangle_3|\varphi'\rangle_4|\phi\rangle_5|\phi'\rangle_6|\vartheta\rangle_7|\vartheta'\rangle_8\\
&-|y\rangle_1|x\rangle_2|\varphi'\rangle_3|\varphi\rangle_4|\phi'\rangle_5|\phi\rangle_6|\vartheta'\rangle_7|\vartheta\rangle_8\\
&+|\varphi\rangle_1|\varphi'\rangle_2|\phi\rangle_3|\phi'\rangle_4|\vartheta\rangle_5|\vartheta'\rangle_6|x\rangle_7|y\rangle_8\\
&-|\varphi'\rangle_1|\varphi\rangle_2|\phi'\rangle_3|\phi\rangle_4|\vartheta'\rangle_5|\vartheta\rangle_6|y\rangle_7|x\rangle_8\\
&-|\phi\rangle_1|\phi'\rangle_2|\vartheta\rangle_3|\vartheta'\rangle_4|x\rangle_5|y\rangle_6|\varphi\rangle_7|\varphi'\rangle_8\\
&+|\phi'\rangle_1|\phi\rangle_2|\vartheta'\rangle_3|\vartheta\rangle_4|y\rangle_5|x\rangle_6|\varphi'\rangle_7|\varphi\rangle_8\\
&-|\vartheta\rangle_1|\vartheta'\rangle_2|x\rangle_3|y\rangle_4|\varphi\rangle_5|\varphi'\rangle_6|\phi\rangle_7|\phi'\rangle_8\\
&+|\vartheta'\rangle_1|\vartheta\rangle_2|y\rangle_3|x\rangle_4|\varphi'\rangle_5|\varphi\rangle_6|\phi'\rangle_7|\phi\rangle_8\big)
\end{aligned}
\tag{16.55}
$$

$$
\begin{aligned}
|\psi\rangle_{VII} = 8^{-1/2}\big(&|x\rangle_1|y\rangle_2|\varphi\rangle_3|\varphi'\rangle_4|\phi\rangle_5|\phi'\rangle_6|\vartheta\rangle_7|\vartheta'\rangle_8\\
&-|y\rangle_1|x\rangle_2|\varphi'\rangle_3|\varphi\rangle_4|\phi'\rangle_5|\phi\rangle_6|\vartheta'\rangle_7|\vartheta\rangle_8\\
&-|\varphi\rangle_1|\varphi'\rangle_2|\phi\rangle_3|\phi'\rangle_4|\vartheta\rangle_5|\vartheta'\rangle_6|x\rangle_7|y\rangle_8\\
&+|\varphi'\rangle_1|\varphi\rangle_2|\phi'\rangle_3|\phi\rangle_4|\vartheta'\rangle_5|\vartheta\rangle_6|y\rangle_7|x\rangle_8\\
&+|\phi\rangle_1|\phi'\rangle_2|\vartheta\rangle_3|\vartheta'\rangle_4|x\rangle_5|y\rangle_6|\varphi\rangle_7|\varphi'\rangle_8\\
&-|\phi'\rangle_1|\phi\rangle_2|\vartheta'\rangle_3|\vartheta\rangle_4|y\rangle_5|x\rangle_6|\varphi'\rangle_7|\varphi\rangle_8\\
&-|\vartheta\rangle_1|\vartheta'\rangle_2|x\rangle_3|y\rangle_4|\varphi\rangle_5|\varphi'\rangle_6|\phi\rangle_7|\phi'\rangle_8\\
&+|\vartheta'\rangle_1|\vartheta\rangle_2|y\rangle_3|x\rangle_4|\varphi'\rangle_5|\varphi\rangle_6|\phi'\rangle_7|\phi\rangle_8\big)
\end{aligned}
\tag{16.56}
$$

$$
\begin{aligned}
|\psi\rangle_{VIII} = 8^{-1/2}\big(&|x\rangle_1|y\rangle_2|\varphi\rangle_3|\varphi'\rangle_4|\phi\rangle_5|\phi'\rangle_6|\vartheta\rangle_7|\vartheta'\rangle_8\\
&-|y\rangle_1|x\rangle_2|\varphi'\rangle_3|\varphi\rangle_4|\phi'\rangle_5|\phi\rangle_6|\vartheta'\rangle_7|\vartheta\rangle_8\\
&-|\varphi\rangle_1|\varphi'\rangle_2|\phi\rangle_3|\phi'\rangle_4|\vartheta\rangle_5|\vartheta'\rangle_6|x\rangle_7|y\rangle_8\\
&+|\varphi'\rangle_1|\varphi\rangle_2|\phi'\rangle_3|\phi\rangle_4|\vartheta'\rangle_5|\vartheta\rangle_6|y\rangle_7|x\rangle_8\\
&-|\phi\rangle_1|\phi'\rangle_2|\vartheta\rangle_3|\vartheta'\rangle_4|x\rangle_5|y\rangle_6|\varphi\rangle_7|\varphi'\rangle_8\\
&+|\phi'\rangle_1|\phi\rangle_2|\vartheta'\rangle_3|\vartheta\rangle_4|y\rangle_5|x\rangle_6|\varphi'\rangle_7|\varphi\rangle_8\\
&+|\vartheta\rangle_1|\vartheta'\rangle_2|x\rangle_3|y\rangle_4|\varphi\rangle_5|\varphi'\rangle_6|\phi\rangle_7|\phi'\rangle_8\\
&-|\vartheta'\rangle_1|\vartheta\rangle_2|y\rangle_3|x\rangle_4|\varphi'\rangle_5|\varphi\rangle_6|\phi'\rangle_7|\phi\rangle_8\big)
\end{aligned}
\tag{16.57}
$$

16.6 SUMMARY

1. The generalized quantum entanglement equations for the $n = N = 2^1, 2^2, 2^3 \ldots 2^r$ configurations are (Duarte, 2016, 2022)

$$|\psi\rangle_R = N^{-1/2}\sum_{j=1}^{N}(\pm)|C\rangle_{N+1-j}$$

$$1 = \left|\langle\psi|_I\right|^2 + \left|\langle\psi|_{II}\right|^2 + \left|\langle\psi|_{III}\right|^2 + \left|\langle\psi|_{IV}\right|^2 + \ldots$$

$$|C\rangle_{N+1-j} = \prod_{m=1,3,5\ldots}^{n}|a\rangle_m|b\rangle_{m+1}$$

2. Each individual probability amplitude includes $n = N$ terms.
3. The normalization factor for a quantum entanglement configuration including N propagation channels is $N^{-1/2}$.
4. For a given $n = N$ entanglement configuration, there are $n = N$ probability amplitudes obeying sign permutations leading to symmetric sign distributions starting with all + signs for the first row and the first column of the arrangement.

It can be observed that the interferometric derivation *à la Dirac* of the generalized equations for quantum entanglement, that is Equations (16.47)–(16.49), is beautifully transparent, completely free of paradoxes (Duarte, 2023), and entirely decoupled from Bell's theorem.

PROBLEMS

16.1 Expand Equation (16.49) for $j = 8, 7, 6, 5, 4, 3, 2, 1$, to arrive at explicit expressions for $|C\rangle_1, |C\rangle_2, |C\rangle_3 \ldots |C\rangle_8$.

16.2 Use the explicit results for $|C\rangle_1, |C\rangle_2, |C\rangle_3 \ldots |C\rangle_8$ to arrive at the corresponding explicit probability amplitudes given in Equations (16.50)–(16.57) for $n = N = 2^3$.

16.3 Use Equations (16.47) to (16.49), to derive explicit probability amplitudes, $|\psi\rangle_I, |\psi\rangle_{II}, |\psi\rangle_{III}, |\psi\rangle_{IV} \ldots |\psi\rangle_{XVI}$ for $n = N = 2^4$.

REFERENCES

Dirac, P. A. M. (1958). *The Principles of Quantum Mechanics*, 4th ed. Oxford University, Oxford, U.K.

Duarte, F. J. (2013a). The probability amplitude for entangled polarizations: an interferometric approach. *J. Mod. Opt*. 60, 1585–1587.

Duarte, F. J. (2013b). Tunable laser optics: applications to optics and quantum optics. *Prog. Quantum Electron*. 37, 326–347.

Duarte, F. J. (2014). *Quantum Optics for Engineers*, 1st ed. CRC, Boca Raton, FL.

Duarte, F. J. (2015). *Tunable Laser Optics*, 2nd ed. CRC, Boca Raton, FL.

Duarte, F. J. (2016). Secure space-to-space interferometric communications and its nexus to the physics of quantum entanglement. *Appl. Phys*. Rev 3, 041301.

Duarte, F. J. (2018). Organic lasers for *N*-channel quantum entanglement. In *Organic Lasers and Organic Photonics* (Duarte, F. J., ed.). Institute of Physics, Bristol, U.K., Chapter 15, pp. 15-1–15-21.

Duarte, F. J. (2022). *Fundamentals of Quantum Entanglement*, 2nd ed. Institute of Physics, Bristol, U.K.

Duarte, F. J. (2023). Quantum entanglement free of paradoxes. *Laser Focus World* 59 (1), 55–56.

Duarte, F. J. and Taylor, T. S. (2017). Quantum entanglement probability amplitudes in multiple channels: an interferometric approach. *Optik* 139, 222–230.

Feynman, R. P., Leighton, R. B., and Sands, M. (1965). *The Feynman Lectures on Physics*, Vol. III, Addison-Wesley, MA.

17 Quantum Entanglement Probability Amplitudes for $n = N = 3, 6$

17.1 INTRODUCTION

In the chapter, interferometric derivation, *à la Dirac*, of the probability amplitude for quantum entanglement applicable to three quanta ($n = 3$) and three propagation channels ($N = 3$), that is $n = N = 3$, is described. The same approach is then extended to $n = N = 6$.

The presentation in this chapter is a summary and revision of previous publications by Duarte (2015, 2016, 2022).

17.2 QUANTUM ENTANGLEMENT PROBABILITY AMPLITUDE FOR $n = N = 3$

The quantum entanglement experimental configuration applicable to $n = N = 3$ is depicted in Figure 17.1. Here, s is the photon source of three quanta emitted in three directions at a relative angle of $2\pi/3$.

For the case $n = N = 3$, the Dirac–Feynman interferometric principle (Dirac, 1958; Feynman et al., 1965)

$$\langle d|s\rangle = \sum_{j=1}^{N} \langle d|j\rangle\langle j|s\rangle \tag{17.1}$$

can be expanded for $N = 3$ while assuming that the quanta emitted by the source are *indistinguishable*, $d_1 = d_2 = d_3 = d$, and that $j \to p_j$, so that

$$\langle d|s\rangle = \langle d|p_3\rangle\langle p_3|s\rangle + \langle d|p_2\rangle\langle p_2|s\rangle + \langle d|p_1\rangle\langle p_1|s\rangle \tag{17.2}$$

is obtained, and observing the methodology introduced in Chapter 15

$$|D\rangle_3 = |p_3\rangle\langle p_3|s\rangle \tag{17.3}$$

$$|D\rangle_2 = |p_2\rangle\langle p_2|s\rangle \tag{17.4}$$

$$|D\rangle_1 = |p_1\rangle\langle p_1|s\rangle \tag{17.5}$$

DOI: 10.1201/9781003398707-17

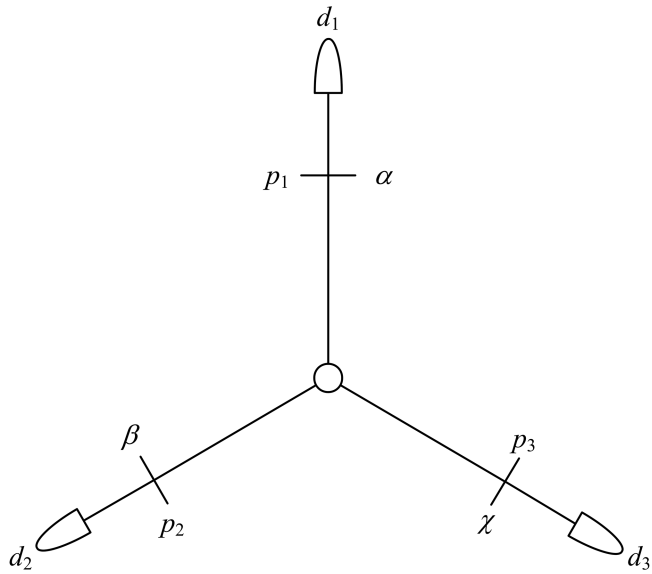

FIGURE 17.1 Experimental diagram applicable to quantum entanglement for the $n = N = 3$ configuration (Duarte, F. J., *Fundamentals of Quantum Entanglement*, 2nd ed. Institute of Physics, Bristol, U.K., 2022, © IOP Publishing. Reproduced with permission. All rights reserved).

so that Equation (17.2) can be written as

$$|s\rangle = \left(|D\rangle_3 + |D\rangle_2 + |D\rangle_1\right) \tag{17.6}$$

Again, applying the Dirac identity (Dirac, 1958)

$$|X\rangle = |a\rangle_1 |b\rangle_2 |c\rangle_3 ... |g\rangle_n \tag{17.7}$$

for $n = 3$ and using $|C\rangle_m$ s to differentiate from a pure interferometric situation

$$|C\rangle_1 = |\alpha\rangle_1 |\beta\rangle_2 |\chi\rangle_3 \tag{17.8}$$

$$|C\rangle_2 = |\chi\rangle_1 |\alpha\rangle_2 |\beta\rangle_3 \tag{17.9}$$

$$|C\rangle_3 = |\beta\rangle_1 |\chi\rangle_2 |\alpha\rangle_3 \tag{17.10}$$

The generalized superposition probability amplitude for quantum entanglement (Duarte 2016), introduced in Chapter 16, with a slight modification in notation is expressed as

$$|\psi\rangle_R = N^{-1/2}\sum_{j=1}^{N}(\pm)q|C\rangle_{N+1-j} \tag{17.11}$$

where

$$|C\rangle_{N+1-j} = \prod_{m=1,\ 3,\ 5\ldots}^{n}|a\rangle_m|b\rangle_{m+1} \tag{17.12}$$

and the condition for normalization is

$$1 = \left|\|\psi\rangle_I\right|^2 + \left|\|\psi\rangle_{II}\right|^2 + \left|\|\psi\rangle_{III}\right|^2 + \ldots \tag{17.13}$$

Since $n = 3$, there is a need to introduce *Hamilton's quaternions* (Hamilton, 1866) (see Appendix G) to satisfy the odd normalization conditions such as

$$1 = \left|\|\psi\rangle_I\right|^2 + \left|\|\psi\rangle_{II}\right|^2 + \left|\|\psi\rangle_{III}\right|^2 \tag{17.14}$$

Hence, the superposition probability amplitudes become

$$|\psi\rangle_I = 3^{-1/2}\left(|C\rangle_1 + |C\rangle_2 + i|C\rangle_3\right) \tag{17.15}$$

$$|\psi\rangle_{II} = 3^{-1/2}\left(|C\rangle_1 - |C\rangle_2 + i|C\rangle_3\right) \tag{17.16}$$

$$|\psi\rangle_{III} = 3^{-1/2}\left(i|C\rangle_1 + j|C\rangle_2 + k|C\rangle_3\right) \tag{17.17}$$

Substituting Equations (17.8)–(17.10) into Equations (17.15)–(17.17), the explicit probability amplitudes become (Duarte, 2016, 2022)

$$|\psi\rangle_I = 3^{-1/2}\left(|\alpha\rangle_1|\beta\rangle_2|\chi\rangle_3 + |\chi\rangle_1|\alpha\rangle_2|\beta\rangle_3 + i|\beta\rangle_1|\chi\rangle_2|\alpha\rangle_3\right) \tag{17.18}$$

$$|\psi\rangle_{II} = 3^{-1/2}\left(|\alpha\rangle_1|\beta\rangle_2|\chi\rangle_3 + |\chi\rangle_1|\alpha\rangle_2|\beta\rangle_3 - i|\beta\rangle_1|\chi\rangle_2|\alpha\rangle_3\right) \tag{17.19}$$

$$|\psi\rangle_{III} = 3^{-1/2}\left(i|\alpha\rangle_1|\beta\rangle_2|\chi\rangle_3 + j|\chi\rangle_1|\alpha\rangle_2|\beta\rangle_3 + k|\beta\rangle_1|\chi\rangle_2|\alpha\rangle_3\right) \tag{17.20}$$

17.3 QUANTUM ENTANGLEMENT PROBABILITY AMPLITUDE FOR $n = N = 6$

The quantum entanglement experimental configuration applicable to $n = N = 3$ is depicted in Figure 17.2. Here, s is the photon source of three quanta emitted in three directions at a relative angle of $\pi/3$.

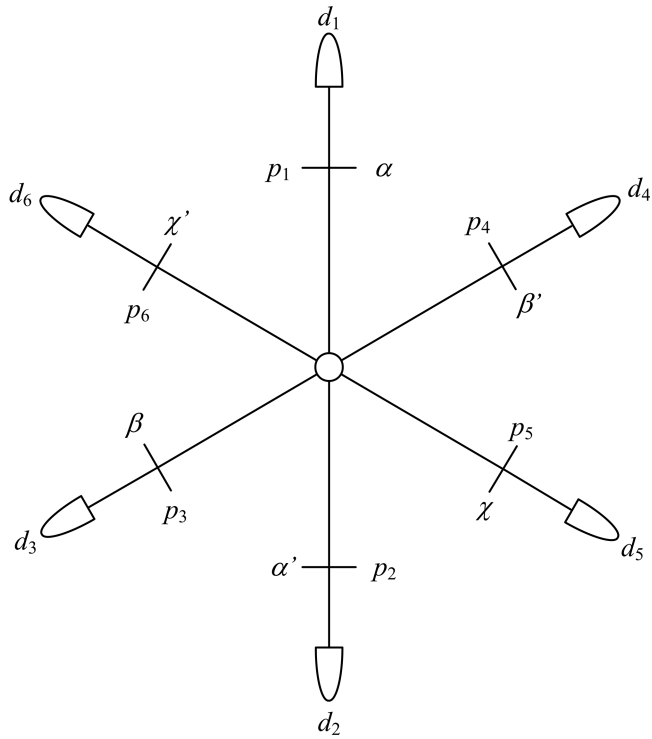

FIGURE 17.2 Experimental diagram applicable to quantum entanglement for the $n = N = 6$ configuration (Duarte, F. J., *Fundamentals of Quantum Entanglement*, 2nd ed. Institute of Physics, Bristol, U.K., 2022, © IOP Publishing. Reproduced with permission. All rights reserved).

For $n = 6$ *indistinguishable* quanta, $d_1 = d_2 = d_3 = d_4 = d_5 = d_6 = d$, and $j \to p_j$, the Dirac–Feynman interferometric principle (Equation (17.1) leads to

$$\langle d|s\rangle = \langle d|p_6\rangle\langle p_6|s\rangle + \ldots + \langle d|p_3\rangle\langle p_3|s\rangle + \langle d|p_2\rangle\langle p_2|s\rangle + \langle d|p_1\rangle\langle p_1|s\rangle \quad (17.21)$$

so that

$$|s\rangle = \left(|D\rangle_6 + |D\rangle_5 + |D\rangle_4 + |D\rangle_3 + |D\rangle_2 + |D\rangle_1\right) \quad (17.22)$$

Using the Dirac identity $|X\rangle = |a\rangle_1|b\rangle_2|c\rangle_3 \ldots |g\rangle_n$ for $n = 6$ while observing the mechanics applied in the previous section leads to

$$|C\rangle_1 = |\alpha\rangle_1|\alpha'\rangle_2|\beta\rangle_3|\beta'\rangle_4|\chi\rangle_5|\chi'\rangle_6 \quad (17.23)$$

$$|C\rangle_2 = |\alpha'\rangle_1|\alpha\rangle_2|\beta'\rangle_3|\beta\rangle_4|\chi'\rangle_5|\chi\rangle_6 \quad (17.24)$$

$$|C\rangle_3 = |\chi\rangle_1 |\chi'\rangle_2 |\alpha\rangle_3 |\alpha'\rangle_4 |\beta\rangle_5 |\beta'\rangle_6 \tag{17.25}$$

$$|C\rangle_4 = |\chi'\rangle_1 |\chi\rangle_2 |\alpha'\rangle_3 |\alpha\rangle_4 |\beta'\rangle_5 |\beta\rangle_6 \tag{17.26}$$

$$|C\rangle_5 = |\beta\rangle_1 |\beta'\rangle_2 |\chi\rangle_3 |\chi'\rangle_4 |\alpha\rangle_5 |\alpha'\rangle_6 \tag{17.27}$$

$$|C\rangle_6 = |\beta'\rangle_1 |\beta\rangle_2 |\chi'\rangle_3 |\chi\rangle_4 |\alpha'\rangle_5 |\alpha\rangle_6 \tag{17.28}$$

where the polarization alternatives (α, α'), (β, β'), and (χ, χ') are indicated in Figure 17.2.

The generalized superposition probability amplitude is

$$|\psi\rangle_R = N^{-1/2} \sum_{j=1}^{N} (\pm) q |C\rangle_{N+1-}$$

where q represents either 1 or a quaternion i, j, k needed to satisfy the normalization condition

$$1 = \left|\|\psi\rangle_I\right|^2 + \left|\|\psi\rangle_{II}\right|^2 + \left|\|\psi\rangle_{III}\right|^2 + \left|\|\psi\rangle_{IV}\right|^2 + \left|\|\psi\rangle_V\right|^2 + \left|\|\psi\rangle_{VI}\right|^2 \tag{17.29}$$

Thus, the individual superposition probability amplitudes become

$$|\psi\rangle_I = 6^{-1/2} \left(|C\rangle_1 + |C\rangle_2 + |C\rangle_3 + |C\rangle_4 + i|C\rangle_5 + i|C\rangle_6\right) \tag{17.30}$$

$$|\psi\rangle_{II} = 6^{-1/2} \left(|C\rangle_1 + |C\rangle_2 + |C\rangle_3 + |C\rangle_4 - i|C\rangle_5 - i|C\rangle_6\right) \tag{17.31}$$

$$|\psi\rangle_{III} = 6^{-1/2} \left(|C\rangle_1 + |C\rangle_2 - |C\rangle_3 - |C\rangle_4 + i|C\rangle_5 + i|C\rangle_6\right) \tag{17.32}$$

$$|\psi\rangle_{IV} = 6^{-1/2} \left(|C\rangle_1 + |C\rangle_2 - |C\rangle_3 - |C\rangle_4 - i|C\rangle_5 - i|C\rangle_6\right) \tag{17.33}$$

$$|\psi\rangle_V = 6^{-1/2} \left(i|C\rangle_1 + i|C\rangle_2 + j|C\rangle_3 + j|C\rangle_4 + k|C\rangle_5 + k|C\rangle_6\right) \tag{17.34}$$

$$|\psi\rangle_{VI} = 6^{-1/2} \left(-i|C\rangle_1 - i|C\rangle_2 - j|C\rangle_3 - j|C\rangle_4 - k|C\rangle_5 - k|C\rangle_6\right) \tag{17.35}$$

Substitution of the states (19.23)–(19.28) into Equations (19.30)–(19.35) yields the explicit probability amplitudes as a function for (α, α'), (β, β'), and (χ, χ').

17.4 DISCUSSION

The teaching of this chapter on the quantum entanglement physics applying to $n = N = 3,\ 6$ situations can be summarized as follows:

1. The generalized quantum entanglement equations for the $n = N = 3,\ 6$ configurations are (Duarte 2016, 2022)

$$|\psi\rangle_R = N^{-1/2}\sum_{j=1}^{N}(\pm)q|C\rangle_{N+1-j}$$

$$|C\rangle_{N+1-j} = \prod_{m=1,\ 3,\ 5...}^{n}|a\rangle_m|b\rangle_{m+1}$$

$$1 = \left|\psi\right\rangle_I\Big|^2 + \left|\psi\right\rangle_{II}\Big|^2 + \left|\psi\right\rangle_{III}\Big|^2 + \ldots$$

2. Each individual probability amplitude includes $n = N$ terms.
3. The normalization factor for a quantum entanglement configuration including N propagation channels is $N^{-1/2}$.
4. To satisfy the normalization condition the use of Hamilton's quaternions is necessary.
5. For a given $n = N$ entanglement configuration, there are $n = N$ probability amplitudes.

By applying the mechanics utilized to derive Equations (17.15)–(17.17) and (17.30)–(17.35), the equations applicable to $n = N = 9$ can also be obtained. Again, it can be observed that the interferometric derivation *à la Dirac* for quantum entanglement situations, in this case $n = N = 3,\ 6$, is beautifully transparent, completely free of paradoxes (Duarte, 2023), and entirely decoupled from Bell's theorem.

PROBLEMS

17.1 Show that the generalized equations for the quantum entanglement probability amplitudes, Equations (17.11)–(17.13), lead to Equations (17.18)–(17.20) for $n = N = 3$.

17.2 Verify that the normalization condition given in Equation (17. 29) is satisfied via the use of quaternions for the $n = N = 6$ quantum entanglement situation.

17.3 Use the generalized quantum entanglement Equations (19.11)–(19.13) to derive explicit superposition probability amplitudes for the case $n = N = 9$.

REFERENCES

Dirac, P. A. M. (1958). *The Principles of Quantum Mechanics*, 4th ed. Oxford University, Oxford, U.K.

Duarte, F. J. (2015). *Tunable Laser Optics*, 2nd ed. CRC, Boca Raton, FL.

Duarte, F. J. (2016). Secure space-to-space interferometric communications and its nexus to the physics of quantum entanglement. *Appl. Phys. Rev.* 3, 041301.

Duarte, F. J. (2022). *Fundamentals of Quantum Entanglement*, 2nd ed. Institute of Physics, Bristol, U.K.

Duarte, F. J. (2023). Quantum entanglement free of paradoxes. *Laser Focus World* 59 (1), 55–56.

Hamilton, W. R. (1866). *Elements of Quaternions*, Longman Green & Co., London, U.K.

18 Quantum Entanglement in Matrix Form

18.1 INTRODUCTION

Here, the complete set of probability amplitudes for $n = N = 2$ quantum entanglement is expressed in matrix form. These are 2×2 matrices that describe the polarization of the quanta in the states $|x\rangle$ and $|y\rangle$. This is very useful from an optical-engineering perspective given that a number of crucial optical components are also represented in 2×2 matrix form.

The mathematical link between the probability amplitudes for quantum entanglement, also known as Bell states, and Pauli matrices is explored in detail. The same is done regarding the nexus between these probability amplitudes and the Hadamard matrix. This chapter is a handbook-type review version of the work disclosed by Duarte et al. (2020), Duarte and Taylor (2021), and Duarte (2022).

18.2 QUANTUM ENTANGLEMENT PROBABILITY AMPLITUDES

The superposition probability amplitudes for the $n = N = 2$ quantum entanglement situation, involving entangled orthogonal polarizations $|x\rangle$ and $|y\rangle$, is given by (Pryce and Ward, 1947; Duarte, 2013, 2014, 2019)

$$|\psi\rangle_{+} = 2^{-1/2}\left(|x\rangle|y\rangle + |y\rangle|x\rangle\right) \tag{18.1}$$

$$|\psi\rangle_{-} = 2^{-1/2}\left(|x\rangle|y\rangle - |y\rangle|x\rangle\right) \tag{18.2}$$

$$|\psi\rangle^{+} = 2^{-1/2}\left(|x\rangle|x\rangle + |y\rangle|y\rangle\right) \tag{18.3}$$

$$|\psi\rangle^{-} = 2^{-1/2}\left(|x\rangle|x\rangle - |y\rangle|y\rangle\right) \tag{18.4}$$

Using the definitions $|x\rangle = |1\rangle$ and $|y\rangle = |0\rangle$, the complete set of probability amplitudes for quantum entanglement can be expressed as (Duarte, 2019)

$$|\psi\rangle_{+} = 2^{-1/2}\left(|1\rangle|0\rangle + |0\rangle|1\rangle\right) \tag{18.5}$$

$$|\psi\rangle_{-} = 2^{-1/2}\left(|1\rangle|0\rangle - |0\rangle|1\rangle\right) \tag{18.6}$$

DOI: 10.1201/9781003398707-18

$$|\psi\rangle^{+} = 2^{-1/2}\left(|1\rangle|1\rangle + |0\rangle|0\rangle\right) \tag{18.7}$$

$$|\psi\rangle^{-} = 2^{-1/2}\left(|1\rangle|1\rangle - |0\rangle|0\rangle\right) \tag{18.8}$$

Equations (18.5)–(18.8) are to be expressed in matrix 2×2 form in this chapter.

18.3 QUANTUM ENTANGLEMENT VIA PAULI MATRICES

As taught by Duarte (2019, 2022) and Duarte et al. (2020), a useful mathematical transformation, applicable to quantum notation, is the *vector direct product* defined as (Ayres, 1965)

$$|x\rangle|y\rangle = |x\rangle \cdot |y\rangle^{T} \tag{18.9}$$

$$|x\rangle \cdot |y\rangle^{T} = \begin{pmatrix} x_1 \\ x_2 \end{pmatrix}\begin{pmatrix} y_1 \\ y_2 \end{pmatrix}^{T} = \begin{pmatrix} x_1y_1 & x_1y_2 \\ x_2y_1 & x_2y_2 \end{pmatrix} \tag{18.10}$$

by which Dirac's *ket vectors* can be multiplied to yield 2×2 matrices.

Defining the ket vectors $|x\rangle$ and $|y\rangle$ as

$$|x\rangle = |1\rangle = \begin{pmatrix} 1 \\ 0 \end{pmatrix} \tag{18.11}$$

$$|y\rangle = |0\rangle = \begin{pmatrix} 0 \\ 1 \end{pmatrix} \tag{18.12}$$

the quantum entanglement equations for ψ_{+}, ψ_{-}, ψ^{+}, and ψ^{-} can be expressed in matrix form via

$$|\psi\rangle_{+} = 2^{-1/2}\left(\begin{pmatrix} 1 \\ 0 \end{pmatrix}\cdot\begin{pmatrix} 0 \\ 1 \end{pmatrix} + \begin{pmatrix} 0 \\ 1 \end{pmatrix}\cdot\begin{pmatrix} 1 \\ 0 \end{pmatrix}\right) = 2^{-1/2}\left(\begin{pmatrix} 0 & 1 \\ 0 & 0 \end{pmatrix} + \begin{pmatrix} 0 & 0 \\ 1 & 0 \end{pmatrix}\right) \tag{18.13}$$

$$|\psi\rangle_{-} = 2^{-1/2}\left(\begin{pmatrix} 1 \\ 0 \end{pmatrix}\cdot\begin{pmatrix} 0 \\ 1 \end{pmatrix} - \begin{pmatrix} 0 \\ 1 \end{pmatrix}\cdot\begin{pmatrix} 1 \\ 0 \end{pmatrix}\right) = 2^{-1/2}\left(\begin{pmatrix} 0 & 1 \\ 0 & 0 \end{pmatrix} - \begin{pmatrix} 0 & 0 \\ 1 & 0 \end{pmatrix}\right) \tag{18.14}$$

$$|\psi\rangle^{+} = 2^{-1/2}\left(\begin{pmatrix} 1 \\ 0 \end{pmatrix}\cdot\begin{pmatrix} 1 \\ 0 \end{pmatrix}+\begin{pmatrix} 0 \\ 1 \end{pmatrix}\cdot\begin{pmatrix} 0 \\ 1 \end{pmatrix}\right) = 2^{-1/2}\left(\begin{pmatrix} 1 & 0 \\ 0 & 0 \end{pmatrix}+\begin{pmatrix} 0 & 0 \\ 0 & 1 \end{pmatrix}\right) \tag{18.15}$$

$$|\psi\rangle^{-} = 2^{-1/2}\left(\begin{pmatrix} 1 \\ 0 \end{pmatrix}\cdot\begin{pmatrix} 1 \\ 0 \end{pmatrix}-\begin{pmatrix} 0 \\ 1 \end{pmatrix}\cdot\begin{pmatrix} 0 \\ 1 \end{pmatrix}\right) = 2^{-1/2}\left(\begin{pmatrix} 1 & 0 \\ 0 & 0 \end{pmatrix}-\begin{pmatrix} 0 & 0 \\ 0 & 1 \end{pmatrix}\right) \tag{18.16}$$

Matrix Equations (18.13)–(18.16) are expressed as (Duarte, 2022)

$$|\psi\rangle_{+} = 2^{-1/2}\begin{pmatrix} 0 & 1 \\ 1 & 0 \end{pmatrix} \tag{18.17}$$

$$|\psi\rangle_{-} = 2^{-1/2}i\begin{pmatrix} 0 & -i \\ i & 0 \end{pmatrix} \tag{18.18}$$

$$|\psi\rangle^{+} = 2^{-1/2}\begin{pmatrix} 1 & 0 \\ 0 & 1 \end{pmatrix} \tag{18.19}$$

$$|\psi\rangle^{-} = 2^{-1/2}\begin{pmatrix} 1 & 0 \\ 0 & -1 \end{pmatrix} \tag{18.20}$$

and Equations (18.17)–(18.20) are directly equivalent to (Duarte et al., 2020)

$$|\psi\rangle_{+} = 2^{-1/2}\sigma_x \tag{18.21}$$

$$|\psi\rangle_{-} = 2^{-1/2}i\sigma_y \tag{18.22}$$

$$|\psi\rangle^{+} = 2^{-1/2}I \tag{18.23}$$

$$|\psi\rangle^{-} = 2^{-1/2}\sigma_z \tag{18.24}$$

where

$$\sigma_x = \begin{pmatrix} 0 & 1 \\ 1 & 0 \end{pmatrix} \tag{18.25}$$

$$\sigma_y = \begin{pmatrix} 0 & -i \\ i & 0 \end{pmatrix} \tag{18.26}$$

$$\sigma_z = \begin{pmatrix} 1 & 0 \\ 0 & -1 \end{pmatrix} \tag{18.27}$$

$$I = \begin{pmatrix} 1 & 0 \\ 0 & 1 \end{pmatrix} \tag{18.28}$$

are the σ_x, σ_y, σ_z Pauli matrices and I is the identity matrix (Dirac, 1958).

18.3.1 Example

The *conjugate* of σ_y is given by

$$\sigma_y^* = \begin{pmatrix} 0 & -i \\ +i & 0 \end{pmatrix}^* = \begin{pmatrix} 0 & +i \\ -i & 0 \end{pmatrix} \tag{18.29}$$

and the *transpose* (rows → column) of σ_y^* is denoted by $(\sigma_y^*)^T$

$$(\sigma_y^*)^T = \begin{pmatrix} 0 & +i \\ -i & 0 \end{pmatrix}^T = \begin{pmatrix} 0 & -i \\ +i & 0 \end{pmatrix} = \sigma_y \tag{18.30}$$

so that

$$(\sigma_y^*)^T = \sigma_y \tag{18.31}$$

The identity exhibited in Equation (18.31) is also expressed as

$$\sigma_y = \sigma_y^{\mathscr{H}} \tag{18.32}$$

where the symbol $\mathscr{H}$ represents the combined *conjugate transpose* operation also known as the *Hermitian property.* All three Pauli matrices are Hermitian.

18.3.2 Pauli Matrices Identities

Additional properties of Pauli matrices are (Dirac, 1958; Jordan, 1986)

$$\sigma_x^2 = \sigma_y^2 = \sigma_z^2 = I \tag{18.31}$$

$$\sigma_x \sigma_y = i\sigma_z \tag{18.32}$$

$$\sigma_y \sigma_x = -i\sigma_z \tag{18.33}$$

$$\sigma_y \sigma_z = i\sigma_x \tag{18.34}$$

$$\sigma_z\sigma_y = -i\sigma_x \tag{18.35}$$

$$\sigma_z\sigma_x = i\sigma_y \tag{18.36}$$

$$\sigma_x\sigma_z = -i\sigma_y \tag{18.37}$$

$$\sigma_x\sigma_y\sigma_z = iI \tag{18.38}$$

18.4 QUANTUM ENTANGLEMENT VIA THE HADAMARD GATE

The widely used Hadamard matrix

$$H = \begin{pmatrix} 1 & 1 \\ 1 & -1 \end{pmatrix} \tag{18.39}$$

can be written as the sum of two matrices

$$H = \begin{pmatrix} 0 & 1 \\ 1 & 0 \end{pmatrix} + \begin{pmatrix} 1 & 0 \\ 0 & -1 \end{pmatrix} \tag{18.40}$$

which, by inspection, can also be expressed as (Duarte, 2019)

$$H = \sigma_x + \sigma_z \tag{18.41}$$

Considering the quantum entanglement states $|\psi\rangle_+$ and $|\psi\rangle_-$, that is

$$|\psi\rangle_+ = 2^{-1/2}\left(|x\rangle_1|y\rangle_2 + |y\rangle_1|x\rangle_2\right)$$

$$|\psi\rangle_- = 2^{-1/2}(|x\rangle_1|y\rangle_2 - |y\rangle_1|x\rangle_2)$$

one can write (Dirac, 1958; Duarte, 2013)

$$|\alpha\rangle = |x\rangle_1|y\rangle_2 \tag{18.42}$$

$$|\beta\rangle = |y\rangle_1|x\rangle_2 \tag{18.43}$$

which leads directly to the equations describing beam splitter-based interferometers such as the Mach–Zehnder interferometer (Duarte, 2003, 2014, 2019)

$$|\Psi\rangle_{+} = 2^{-1/2}\left(|\alpha\rangle + |\beta\rangle\right) \tag{18.44}$$

$$|\Psi\rangle_{-} = 2^{-1/2}\left(|\alpha\rangle - |\beta\rangle\right) \tag{18.45}$$

Equations (18.44) and (18.45) can be expressed in matrix form as

$$\begin{pmatrix} |\Psi\rangle_{+} \\ |\Psi\rangle_{-} \end{pmatrix} = 2^{-1/2}\begin{pmatrix} 1 & 1 \\ 1 & -1 \end{pmatrix}\begin{pmatrix} |\alpha\rangle \\ |\beta\rangle \end{pmatrix} \tag{18.46}$$

where

$$2^{-1/2}\begin{pmatrix} 1 & 1 \\ 1 & -1 \end{pmatrix} = H_G \tag{18.47}$$

is known as the *Hadamard gate* H_G widely used in the literature in the absence of a transparent derivation. Furthermore, this is precisely the physics behind the HOM interferometer (see Chapter 7).

The Hadamard gate H_G can also be defined via the multiplication of the Hadamard matrix by the normalization factor $2^{-1/2}$, so that

$$H_G = 2^{-1/2}\begin{pmatrix} 1 & 1 \\ 1 & -1 \end{pmatrix} = 2^{-1/2}H \tag{18.48}$$

which can be expressed in terms of the probability amplitudes for quantum entanglement as done by Duarte et al. (2020)

$$H_G = \left(|\psi\rangle_{+} + |\psi\rangle^{-}\right) \tag{18.49}$$

$$H_G = 2^{-1/2}(\sigma_x + \sigma_z) \tag{18.50}$$

18.5 QUANTUM ENTANGLEMENT PROBABILITY AMPLITUDE MATRICES

Certainly, new matrices become immediately apparent via the combination, in various permutations, of $|\psi\rangle_{+}, |\psi\rangle_{-}, |\psi\rangle^{+}$, and $|\psi\rangle^{-}$ (Duarte and Taylor, 2021; Duarte 2022)

$$J = \left(|\psi\rangle_{+} - |\psi\rangle^{-}\right) \tag{18.51}$$

$$K = \left(|\psi\rangle^{+} + |\psi\rangle_{-} \right) \tag{18.52}$$

$$L = \left(|\psi\rangle^{+} - |\psi\rangle_{-} \right) \tag{18.53}$$

$$M = \left(|\psi\rangle^{+} + |\psi\rangle_{+} \right) \tag{18.54}$$

$$N = \left(|\psi\rangle^{+} - |\psi\rangle_{+} \right) \tag{18.55}$$

$$O = \left(|\psi\rangle^{-} + |\psi\rangle_{-} \right) \tag{18.56}$$

$$P = \left(|\psi\rangle^{-} - |\psi\rangle_{-} \right) \tag{18.57}$$

where

$$J = 2^{-1/2} \begin{pmatrix} -1 & 1 \\ 1 & 1 \end{pmatrix} \tag{18.58}$$

$$K = 2^{-1/2} \begin{pmatrix} 1 & 1 \\ -1 & 1 \end{pmatrix} \tag{18.59}$$

$$L = 2^{-1/2} \begin{pmatrix} 1 & -1 \\ 1 & 1 \end{pmatrix} \tag{18.60}$$

$$M = 2^{-1/2} \begin{pmatrix} 1 & 1 \\ 1 & 1 \end{pmatrix} \tag{18.61}$$

$$N = 2^{-1/2} \begin{pmatrix} 1 & -1 \\ -1 & 1 \end{pmatrix} \tag{18.62}$$

$$O = 2^{-1/2} \begin{pmatrix} 1 & 1 \\ -1 & -1 \end{pmatrix} \tag{18.63}$$

$$P = 2^{-1/2} \begin{pmatrix} 1 & -1 \\ 1 & -1 \end{pmatrix} \tag{18.64}$$

It should be noted that $M = \left(|\psi\rangle^{+} + |\psi\rangle_{+}\right)$ can be configured with a combination of an ordinary beam splitter and a polarization rotator (Duarte and Taylor, 2021).

18.6 QUANTUM ENTANGLEMENT POLARIZATION ROTATOR MATHEMATICS

Polarization rotators can be used to perform quantum operations for quantum computing applications. If the entangled photons are made to be incident on a generalized $\theta = \pi/2$ polarization rotator (Duarte, 2003) represented by the matrix

$$R = \begin{pmatrix} 0 & 1 \\ 1 & 0 \end{pmatrix} \tag{18.65}$$

then it can be shown that (Duarte et al., 2020)

$$R|\psi\rangle^{+} = |\psi\rangle_{+} = 2^{-1/2}\sigma_x \tag{18.66}$$

$$R|\psi\rangle^{-} = -|\psi\rangle_{-} = -2^{-1/2} i\sigma_y \tag{18.67}$$

$$R|\psi\rangle_{+} = |\psi\rangle^{+} = 2^{-1/2} I \tag{18.68}$$

$$R|\psi\rangle_{-} = -|\psi\rangle^{-} = -2^{-1/2}\sigma_z \tag{18.69}$$

This demonstrates the inherent capability for mathematical operations utilizing polarization rotators and entangled states. This simple concept means that beams of entangled photons interacting with optical apparata configured with optical elements capable of transforming the entangled polarization states can be used to perform optical quantum computations.

18.7 QUANTUM MATHEMATICS VIA HADAMARD'S GATE

The Hadamard matrix operation on the probability amplitudes for quantum entanglement yields the following mathematical identities (Duarte et al., 2020)

$$H_G|\psi\rangle_{+} = 2^{-1/2}\left(|\psi\rangle^{+} + |\psi\rangle_{-}\right) \tag{18.70}$$

$$H_G|\psi\rangle_{-} = 2^{-1/2}\left(|\psi\rangle_{+} - |\psi\rangle^{-}\right) \tag{18.71}$$

$$H_G|\psi\rangle^{+} = 2^{-1/2}\left(|\psi\rangle_{+} + |\psi\rangle^{-}\right) \tag{18.72}$$

$$H_G|\psi\rangle^{-} = 2^{-1/2}\left(|\psi\rangle^{+} - |\psi\rangle_{-}\right) \tag{18.73}$$

which are equivalent to (Duarte et al., 2020)

$$H_G|\psi\rangle_+ = 2^{-1}(I + i\sigma_y) \tag{18.74}$$

$$H_G|\psi\rangle_- = 2^{-1}(\sigma_x - \sigma_z) \tag{18.75}$$

$$H_G|\psi\rangle^+ = 2^{-1}(\sigma_x + \sigma_z) \tag{18.76}$$

$$H_G|\psi\rangle^- = 2^{-1}(I - i\sigma_y) \tag{18.77}$$

18.8 REVERSIBILITY IN QUANTUM MECHANICS

Duarte (2013, 2014, 2016, 2022) has shown that the Dirac–Feynman interferometric principle leads to the superposition probability amplitudes for quantum entanglement

$$\langle d|s\rangle = \sum_{j=1}^{N} \langle d|j\rangle \langle j|s\rangle \rightarrow |\psi\rangle = 2^{-1/2}\left(|x\rangle_1|y\rangle_2 \pm |y\rangle_1|x\rangle_2\right) \tag{18.78}$$

Consequently, the Pauli matrices also have a Diracian interferometric origin (Duarte et al., 2020; Duarte, 2022)

$$\langle d|s\rangle = \sum_{j=1}^{N} \langle d|j\rangle \langle j|s\rangle \rightarrow |\psi\rangle_+, |\psi\rangle_-, |\psi\rangle^+, |\psi\rangle^- \rightarrow \sigma_x, \sigma_y, \sigma_z, I \tag{18.79}$$

Further understanding of this physics also allows for the reverse mathematical flow (Duarte, 2019, 2022; Duarte and Taylor, 2021)

$$\sum_{j=1}^{N} \langle d|j\rangle \langle j|s\rangle \leftarrow |\psi\rangle_+, |\psi\rangle_-, |\psi\rangle^+, |\psi\rangle^- \leftarrow \sigma_x, \sigma_y, \sigma_z, I \tag{18.80}$$

or

$$\sigma_x, \sigma_y, \sigma_z, I \rightarrow |\psi\rangle_+, |\psi\rangle_-, |\psi\rangle^+, |\psi\rangle^- \rightarrow \sum_{j=1}^{N} \langle d|j\rangle \langle j|s\rangle \tag{18.81}$$

and it ultimately points toward an interferometric origin of Pauli matrices (Duarte, 2022)

$$\sum_{j=1}^{N} \langle d|j\rangle \langle j|s\rangle \rightarrow \ldots \rightarrow \sigma_x, \sigma_y, \sigma_z, I \tag{18.82}$$

The mathematical flow depicted in (18.79) indicates that the Dirac–Feynman principle neatly and transparently leads to the superposition probability amplitudes of quantum entanglement $|\psi\rangle_+, |\psi\rangle_-, |\psi\rangle^+$, and $|\psi\rangle^-$.

However, from a first-principle perspective, the complete mathematical flow culminating in the Dirac–Feynman interferometric principle is (Duarte and Taylor, 2021)

$$\sum_j H_{ij}C_j \to \sigma_x, \sigma_y, \sigma_z, I \to |\psi\rangle_+, |\psi\rangle_-, |\psi\rangle^+, |\psi\rangle^- \to \sum_{j=1}^{N} \langle d|j\rangle \langle j|s\rangle \tag{18.83}$$

which indicates that to go in reverse, from foundational principles, it is necessary first to derive the Pauli matrices, which needs to differentiate C_i with respect to time (Feynman et al., 1965)

$$i\hbar \frac{dC_i}{dt} = \sum_j^2 H_{ij}C_j \tag{18.84}$$

where the C_i amplitude originates directly from the Dirac–Feynman interferometric principle. This appears to indicate that quantum interference is a more fundamental principle than quantum entanglement with both, quantum interference and quantum entanglement, linked at a most fundamental level at the foundations of quantum mechanics.

PROBLEMS

18.1 Starting from Equation (18.14), verify that $|\psi\rangle_= = 2^{-1/2} i\sigma_y$.
18.2 Starting from Equation (18.16), verify that $|\psi\rangle^= = 2^{-1/2}\sigma_z$.
18.3 Show that $H_G = (\psi_+ + \psi^-)$.
18.4 Show that $J = \left(|\psi\rangle_+ - |\psi\rangle^-\right)$.
18.5 Show that $O = \left(|\psi\rangle^- + |\psi\rangle_-\right)$.
18.6 Show that $R|\psi\rangle^+ = |\psi\rangle_- = 2^{-1/2}\sigma_x$.
18.7 Show that $R|\psi\rangle_+ = |\psi\rangle^+ = 2^{-1/2} I$.
18.8 Show that $H_G|\psi\rangle_+ = 2^{-1/2}\left(|\psi\rangle^+ + |\psi\rangle_-\right)$.
18.9 Show that $H_G|\psi\rangle^- = 2^{-1/2}\left(|\psi\rangle^+ - |\psi\rangle_-\right)$.

REFERENCES

Ayres, F. (1965). *Modern Algebra*, McGraw-Hill, New York.
Dirac, P. A. M. (1958). *The Principles of Quantum Mechanics*, 4th ed. Oxford University, Oxford, U.K.
Duarte, F. J. (2003). *Tunable Laser Optics*, 1st ed. Elsevier-Academic, New York.
Duarte, F. J. (2013). The probability amplitude for entangled polarizations: an interferometric approach. *J. Mod. Opt.* **60**, 1585–1587.
Duarte, F. J. (2014). *Quantum Optics for Engineers*, 1st ed. CRC, Boca Raton, FL.

Duarte, F. J. (2016). Secure space-to-space interferometric communications and its nexus to the physics of quantum entanglement. *Appl. Phys. Rev.* **3**, 041301.

Duarte, F. J. (2019). *Fundamentals of Quantum Entanglement*, 1st ed. Institute of Physics, Bristol, U.K.

Duarte, F. J. (2022). *Fundamentals of Quantum Entanglement*, 2nd edn. Institute of Physics, Bristol, U.K.

Duarte, F. J., and Taylor, T. S. (2021). *Quantum Entanglement Engineering and Applications*, Institute of Physics, Bristol, U.K.

Duarte, F. J., Taylor, T. S., and Slaten, J. C. (2020). On the probability amplitude of quantum entanglement and the Pauli matrices. *Opt. Quantum Electron.* **52**, 106.

Feynman, R. P., Leighton, R. B., and Sands, M. (1965). *The Feynman Lectures on Physics*, Vol. III, Addison-Wesley, Reading, MA.

Jordan, T. E. (1986). *Quantum Mechanics in Simple Matrix Form*, Wiley, New York.

Pryce, M. L. H., and Ward, J. C. (1947). Angular correlation effects with annihilation radiation. *Nature* **160**, 435.

19 Quantum Computing in Matrix Notation

19.1 INTRODUCTION

The first discussion of *quantum logic* was due to von Neumann in 1932. In this regard, von Neumann associates a quantum quantity with the values of 1 and 0. If verified, the value of this quantity is 1. If not, the value of this quantity is 0 (von Neumann, 1932).

Quantum computing is an extremely active field producing an enormous number of publications. Following the initial introduction à la Feynman, and revision of basic concepts, attention is focused on the matrices already developed in previous chapters and their application to quantum computing.

In the discussion that follows, the term *universal computer* is applied to traditional transistor-based computers using Boolean algebra executed by logical gates such as AND, OR, NOT, NAND, and NOR. The beauty of universal computers is that by using mathematical equations, expressed in the logical language of the computer, it can accurately simulate scientific processes of interest. Their scope of applications is extremely wide. A disadvantage of the universal computer is that, for certain classes of calculations, they can consume large amounts of energy, and they can be slower than desired. From a practical perspective, the issue of computational speed is very important.

There is a cost and efficiency motivation to replace universal computers that take too much time to perform computationally intensive calculations. This stimulates the interest in quantum computing.

Physical computers, such as optical computers, can be *extremely fast* to perform certain computational tasks that demand very long computational times in universal computers; however, the range of applications that physical computers offer is limited. An example of this class of computer, an interferometric computer, is described in the next section.

A quantum computer, as the name suggests, is a computer that can operate at the quantum level, thus offering enormous improvements in energy consumption and size reductions (Bennett, 1982; Feynman, 1985, 1986). Significant size reductions and the use of photons should also lead to vast improvements in computational speed. The concept of a quantum computer goes beyond physical computers and seeks to offer an alternative universal computer. It does so by utilizing analogs to bits known as *qbits*.

These qbits can take a physical representation at the quantum level and allow the performance of Boolean logic operations. Here an introduction to this fascinating subject is provided while using the mathematical tools and quantum concepts already introduced in this book.

 DOI: 10.1201/9781003398707-19

This chapter is based on a revision of the original chapter (Duarte, 2014) and introduces new material as disclosed in subsequent publications (Duarte, 2019, 2022).

19.2 INTERFEROMETRIC COMPUTER

The *N*-slit laser interferometer (*N*SLI), as an example of a physical, or optical, computer is discussed by Duarte (2003). This interferometric computer utilizes either single photon illumination or illumination via *ensembles of indistinguishable photons* as available from narrow-linewidth lasers. A simplified diagram of the *N*SLI is shown in Figure 19.1.

Interferograms recorded with the *N*SLI have been compared for numerous geometrical and wavelength parameters with interferograms calculated via the quantum interferometric equation, which is a quantum probability equation (Duarte, 1993)

$$\langle d|s\rangle\langle d|s\rangle^{*} = \sum_{j=1}^{N}\Psi(r_j)\sum_{m=1}^{N}\Psi(r_m)e^{i(\Omega_m-\Omega_j)} \tag{19.1}$$

$$\langle d|s\rangle\langle d|s\rangle^{*} = \sum_{j=1}^{N}\Psi(r_j)^2 + 2\sum_{j=1}^{N}\Psi(r_j)\left(\sum_{m=j+1}^{N}\Psi(r_m)\cos(\Omega_m-\Omega_j)\right) \tag{19.2}$$

One such case is considered in Figure 19.2. The measured interferogram is displayed at the top of Figure 19.2, and the corresponding theoretical interferogram is included in the lower trace of Figure 19.2. In this regard, it should be mentioned that good agreement, between theory and experiment, exists from the near to the far field. Observed differences, especially at the baseline, are due to thermal noise in the digital detector that is used at room temperature. The original program was written in Fortran 77.

Subsequent software versions have utilized Visual Fortran and MATLAB (Duarte, 1993, 2014). For calculations involving a large number of slits, especially for $N = 2000$ or more, Fortran is preferred, given its superior computational speed. Further comparative aspects have been discussed in Chapter 4.

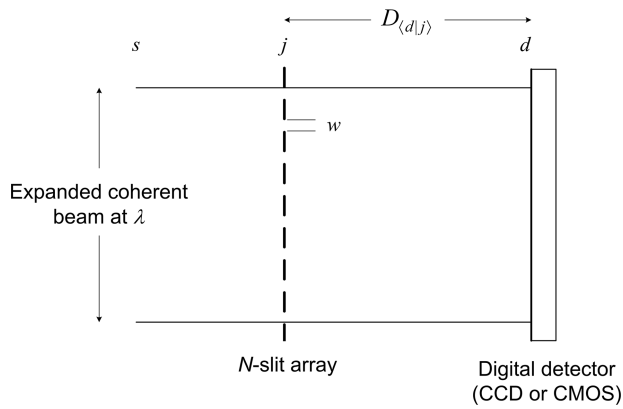

FIGURE 19.1 *N*-slit laser interferometer (*N*SLI) configuration. Critical parameters are the laser wavelength λ, the number of slits *N*, the dimension of the slits *w*, and the intra-interferometric distance $D_{\langle d|j\rangle}$.

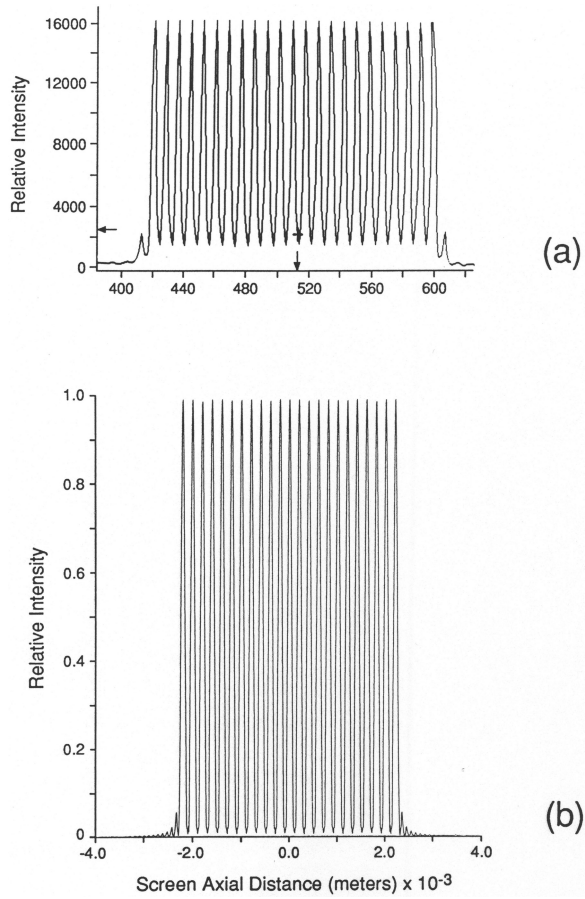

FIGURE 19.2 (a) Measured near field interferogram using the *N*SLI for $N = 23$, $\lambda = 632.8$ nm, $D_{\langle d|j\rangle} = 1.5$ cm. Slits are 100 μm wide separated by 100 μm. (b) Calculated near field interferogram using the *N*SLI for $N = 23$, $\lambda = 632.8$ nm, $D_{\langle d|j\rangle} = 1.5$ cm. Slits are 100 μm wide separated by 100 μm (Reproduced from Duarte, F. J., *Opt. Commun.* **103**, 8–14, 1993, with permission from Elsevier).

The interferometric calculations, using the interferometric probability equation to program a universal computer, require the following input information:

1. Slit dimensions: w
2. Standard of deviation of the slit dimensions: Δw
3. Interslit dimensions
4. Standard of deviation of interslit dimensions
5. Wavelength: λ
6. N-slit array-, or grating-, screen distance: $D_{\langle d|j\rangle}$
7. Number of slits: N

The Boolean algebra program, based on the quantum probability interferometric equation, also provides options for the illumination profile and allows for multiple-stage calculations. That is, it allows for the propagation through several sequential *N*-slit arrays prior to arrival at *d* as considered in Chapter 4.

An interesting aspect of comparisons, between theory and experiment, is that for a given wavelength, set of slit dimensions, and distance from *j* to *d*, the time taken to calculate in a conventional universal computer increases with an increase in the number of slits *N*. In fact, the computational time $t(N)$ behaves in a nonlinear fashion as *N* increases. This is clearly illustrated in Figure 19.3, where $t = 0.96$ s for $N = 2$ and $t = 3111.2$ for $N = 1500$ s (Duarte, 1996). By contrast, all of these calculations can be performed in the *N*SLI at a constant time of ~30 ms which is a time mainly imposed by the electronic integration time of the digital detector. Certainly, the generation and propagation of the interferogram are performed at a speed that is approximate to that of the speed of light *c*.

In this regard, following the criteria outlined by Deutsch (1992), the *N*SLI can be classified as a physical, or quantum interferometric, computer that can perform certain specific computations at times orders of magnitude below the computational time required by a universal computer. Among the computations that the *quantum interferometric computer* can perform are

1. *N*-slit array interference calculations
2. Near- or far-field diffraction calculations

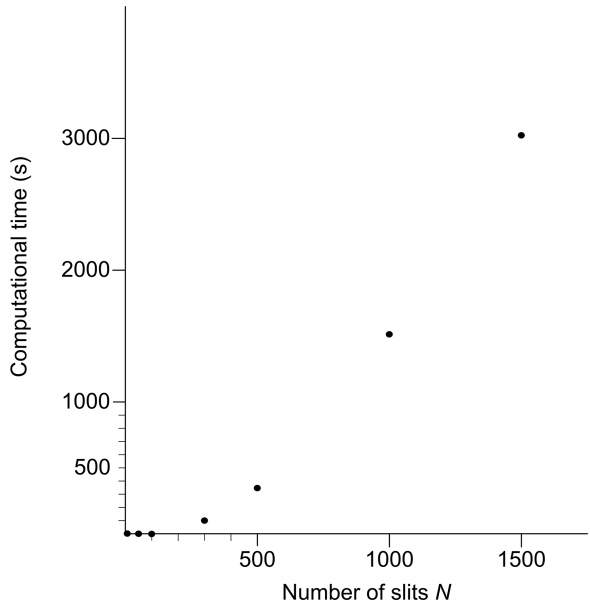

FIGURE 19.3 Computational time in a mainframe universal computer as a function of number of slits. The first four points are 0.96 s for $N = 2$, 1.14 s for $N = 10$, 7.03 s for $N = 50$, and 14.33 s for $N = 100$. For these calculations $\lambda = 632.8$ nm, $D_{\langle d|j\rangle} = 75$ cm. Slits are 30 μm wide separated by 30 μm.

3. Beam divergence calculations
4. Wavelength calculations

For this limited set of tasks, the interferometric computer based on the *N*SLI outperforms, by some *5 orders of magnitude*, universal computers. Hence, it can be classified as a very fast, albeit limited in scope, quantum optical computer. The advantage of the universal computer remains its versatility. Moreover, in the universal computer, there is access to intermediate results at all stages of the computation. This is not allowed in the *N*SLI where access is strictly limited to the input stage and the final stage of the computation. Attempts to acquire information about intermediate stages of the computation can destroy the final answer (see Chapter 21).

The interferometric computer is a macroscopic apparatus that allows the control of photon propagation via the probabilistic laws of quantum mechanics. Since it can function either via single photon illumination or illumination via ensembles of indistinguishable photons, while following the laws of quantum mechanics, it can be classified as a quantum optics computer.

19.3 CLASSICAL LOGIC GATES

Classical universal computers function based on logical operations performed by a series of gates such as the OR, AND gates, and the negation gates NOT, NOR, and NAND.

Feynman, in his article, focuses, in particular, on the *primitive elements* NOT, AND, FAN OUT, and EXCHANGE. To this list, he also adds the *reversible primitives* NOT, CONTROLLED NOT, and CONTROLED CONTROLLED NOT.

Figure 19.4 illustrates the NOT gate, Figure 19.5 the NAND, and Figure 19.6 the NOR gates with their corresponding transistor circuitry.

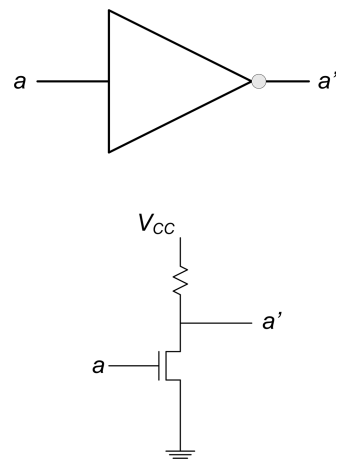

FIGURE 19.4 Symbol for NOT gate and transistor circuit of NOT gate using NMOS technology. NMOS technology refers to field effect transistors fabricated with n-type metal-oxide-semiconductors (MOS).

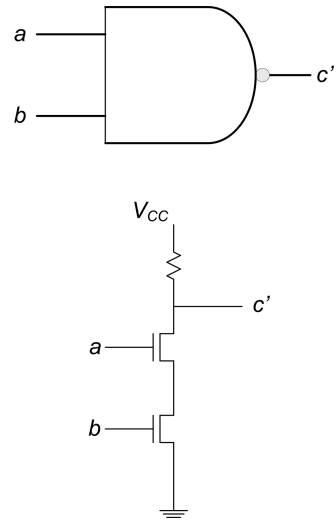

FIGURE 19.5 Symbol for NAND gate and transistor circuit of NAND gate using NMOS technology.

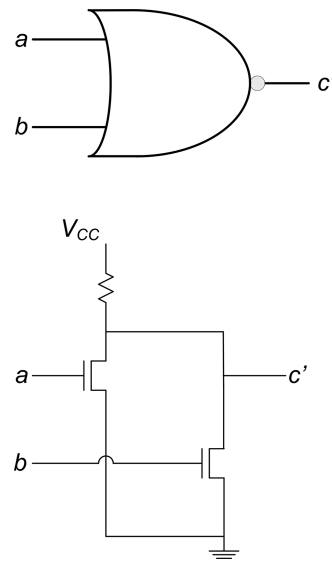

FIGURE 19.6 Symbol for NOR gate and transistor circuit of NOR gate using NMOS technology.

For an input a and an output a', the truth table for the NOT gate is

a	a'
0	1
1	0

For inputs a and b and output c', the truth table for the AND gate is

a	b	c'
0	0	0
0	1	0
1	0	0
1	1	1

For inputs a and b and output c', the truth table for the NAND gate is

a	b	c'
0	0	1
0	1	1
1	0	1
1	1	0

For inputs a and b and output c', the truth table for the OR gate is

a	b	c'
0	0	0
0	1	1
1	0	1
1	1	1

For inputs a and b and output c', the truth table for the NOR gate is

a	b	c'
0	0	1
0	1	0
1	0	0
1	1	0

19.4 von NEUMANN ENTROPY

Entropy can be defined as the change, as a function of time, from an orderly state to a disorderly state. Duarte (2022) discusses entropy from an interferometric perspective where the initial state consists of a well-defined interferometric pattern in space, at t_i. At a subsequent state, at $t = t_i + \Delta t$, the interferometric pattern loses its initial well-defined structure and becomes a uniform near-Gaussian distribution. The well-defined interferometric pattern in space, at t_i, is indicative of low entropy, while the near-Gaussian distribution, at $t = t_i + \Delta t$, is indicative of high, or higher, entropy.

Relevant to quantum computing is the von Neumann entropy

$$S(\rho) = -Tr[\rho \ln \rho] \tag{19.3}$$

where ρ is the density matrix describing an ensemble of states of a relevant quantum system and *Tr* is the trace of the matrix $[\rho \ln \rho]$ (von Neumann, 1932). This means that the larger the number of states involved, the larger the entropy. This is an important caveat given that for effective practical quantum computing, a large number of states are needed.

19.5 QBITS

Richard Feynman (1985, 1986) introduced the nexus between the concept of the *bit* and the quantum states $|1\rangle$ and $|0\rangle$. He then went on to propose that one bit can be represented by a single atom being either in the $|1\rangle$ state or the $|0\rangle$ state.

From the Dirac–Feynman principle (Dirac, 1958; Feynman et al., 1965)

$$\langle \phi|\psi\rangle = \sum_{j=1}^{N} \langle \phi|j\rangle \langle j|\psi\rangle \tag{19.4}$$

for $j = 1,\ 2$

$$\langle \phi|\psi\rangle = \langle \phi|2\rangle \langle 2|\psi\rangle + \langle \phi|1\rangle \langle 1|\psi\rangle \tag{19.5}$$

and abstracting $\langle \phi|$

$$|\psi\rangle = |2\rangle \langle 2|\psi\rangle + |1\rangle \langle 1|\psi\rangle \tag{19.6}$$

leads to

$$|\psi\rangle = C_2|2\rangle + C_1|1\rangle \tag{19.7}$$

where

$$C_1 = \langle 1|\psi\rangle \tag{19.8}$$

$$C_2 = \langle 2|\psi\rangle \tag{19.9}$$

Equation (19.7) is a general principle that means that a single state, or probability amplitude, can be expressed as a linear combination of two other states (Feynman et al., 1965).

In the case of the $|1\rangle$ and $|0\rangle$ states, the combined probability amplitude is

$$|\psi\rangle = C_1|1\rangle + C_2|0\rangle \tag{19.10}$$

where C_1 and C_2 are themselves probability amplitudes and therefore *complex numbers*.

This is an example of a *superposition*. Once normalized, this probability amplitude becomes

$$|\psi\rangle = 2^{-1/2}\left(C_1|1\rangle - C_2|0\rangle\right) \tag{19.11}$$

The $|1\rangle$ and $|0\rangle$ states are known in the literature as *qbits* for 'quantum bits' (Schumacher, 1995).

The $|1\rangle$ and $|0\rangle$ states can also be entangled. The four possible probability amplitudes related to qbits $|1\rangle$ and $|0\rangle$ are

$$|\psi\rangle = 2^{-1/2}\left(|1\rangle|0\rangle \pm |0\rangle|1\rangle\right) \tag{19.12}$$

$$|\psi\rangle = 2^{-1/2}\left(|1\rangle|1\rangle \pm |0\rangle|0\rangle\right) \tag{19.13}$$

For spin −½ particles, the individual states are also abbreviated as $|\uparrow\rangle$ and $|\downarrow\rangle$ so that the four probability amplitudes are written as

$$|\psi\rangle = 2^{-1/2}\left(|\uparrow\rangle|\downarrow\rangle \pm |\downarrow\rangle|\uparrow\rangle\right) \tag{19.14}$$

$$|\psi\rangle = 2^{-1/2}\left(|\uparrow\rangle|\uparrow\rangle \pm |\downarrow\rangle|\downarrow\rangle\right) \tag{19.15}$$

States written in this fashion are known in the literature as 'Bell states' or 'EPR pairs,' even though neither Bell nor EPR had a hand in their development.

19.6 QUANTUM ENTANGLEMENT VIA PAULI MATRICES

The probability amplitudes of quantum entanglement can be re-expressed individually as (Duarte, 2019, 2022)

$$|\psi\rangle_+ = 2^{-1/2}\left(|1\rangle|0\rangle + |0\rangle|1\rangle\right) \tag{19.16}$$

$$|\psi\rangle_- = 2^{-1/2}\left(|1\rangle|0\rangle - |0\rangle|1\rangle\right) \tag{19.17}$$

$$|\psi\rangle^+ = 2^{-1/2}\left(|1\rangle|1\rangle + |0\rangle|0\rangle\right) \tag{19.18}$$

$$|\psi\rangle^- = 2^{-1/2}\left(|1\rangle|1\rangle - |0\rangle|0\rangle\right) \tag{19.19}$$

where

$$|1\rangle = \begin{pmatrix} 1 \\ 0 \end{pmatrix} \tag{19.20}$$

and

$$|0\rangle = \begin{pmatrix} 0 \\ 1 \end{pmatrix} \tag{19.21}$$

As seen previously, the quantum entanglement probability amplitudes can also be expressed in matrix form using the *direct vector product* defined as (Ayres, 1965)

$$|x\rangle|y\rangle = |x\rangle \cdot |y\rangle^T \tag{19.22}$$

or

$$|x\rangle \cdot |y\rangle^T = \begin{pmatrix} x_1 \\ x_2 \end{pmatrix} \begin{pmatrix} y_1 \\ y_2 \end{pmatrix}^T = \begin{pmatrix} x_1 y_1 & x_1 y_2 \\ x_2 y_1 & x_2 y_2 \end{pmatrix} \tag{19.23}$$

In general, this means that any optical component associated with a 2×2 matrix operator operating on one of the entangled vector states can yield a new transformed state. For instance, if an optical component is represented by the matrix operator B, then

$$B|\psi\rangle_+ \rightarrow |\xi\rangle \tag{19.24}$$

where $|\xi\rangle$ is a new or transformed state. More specifically, Equations (19.16)–(19.19) can be expressed in matrix form as (Duarte et al., 2020; Duarte and Taylor, 2021)

$$|\psi\rangle_+ = 2^{-1/2}\sigma_x \tag{19.25}$$

$$|\psi\rangle_- = 2^{-1/2} i\sigma_y \tag{19.26}$$

$$|\psi\rangle^+ = 2^{-1/2} I \tag{19.27}$$

$$|\psi\rangle^- = 2^{-1/2}\sigma_z \tag{19.28}$$

which are equivalent to

$$\sigma_x = 2^{1/2}|\psi\rangle_+ \tag{19.29}$$

$$i\sigma_y = 2^{1/2}|\psi\rangle_- \tag{19.30}$$

$$I = 2^{1/2}|\psi\rangle^+ \tag{19.31}$$

$$\sigma_z = 2^{1/2}|\psi\rangle^- \tag{19.32}$$

where

$$\sigma_x = \begin{pmatrix} 0 & 1 \\ 1 & 0 \end{pmatrix} \tag{19.33}$$

$$\sigma_y = \begin{pmatrix} 0 & -i \\ i & 0 \end{pmatrix} \tag{19.34}$$

$$\sigma_z = \begin{pmatrix} 1 & 0 \\ 0 & -1 \end{pmatrix} \tag{19.35}$$

$$I = \begin{pmatrix} 1 & 0 \\ 0 & 1 \end{pmatrix} \tag{19.36}$$

are the σ_x, σ_y, and σ_z Pauli matrices and I is the identity matrix.

These identities show yet an additional avenue to derive the quantum entanglement probability amplitudes provided that the Pauli matrices are arrived at independently and from first principles (Duarte et al., 2020; Duarte, 2022).

19.7 ROTATION OF QUANTUM ENTANGLEMENT STATES

A $\pi/2$ polarization rotator can be realized experimentally using a half-wave plate, a wavelength-specific double Fresnel rhomb, or a broadband collinear prismatic rotator (Duarte, 1989, 2014). These $\pi/2$ polarization rotators, illustrated in Figures 19.7–19.9, are mathematically represented by the matrix

$$R = \begin{pmatrix} 0 & 1 \\ 1 & 0 \end{pmatrix} \tag{19.37}$$

Using this matrix, it can be shown that (Duarte et al., 2020; Duarte, 2022)

$$R|\psi\rangle_+ = |\psi\rangle^+ \tag{19.38}$$

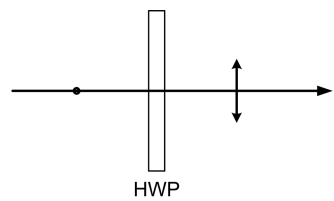

FIGURE 19.7 Schematics for a wavelength-specific half-wave plate $\pi/2$ polarization rotator.

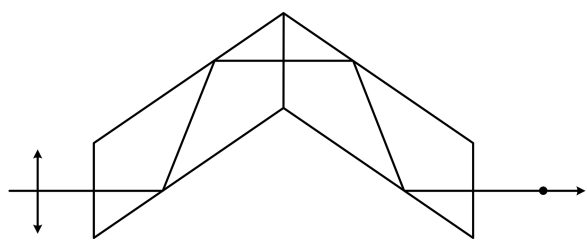

FIGURE 19.8 Schematics for a wavelength-specific double Fresnel rhomb $\pi/2$ polarization rotator.

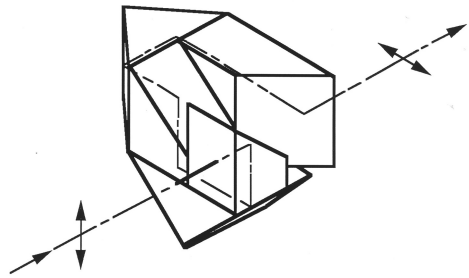

FIGURE 19.9 Multiple-prism broadband $\pi/2$ polarization rotator (Duarte, 1989).

$$R|\psi\rangle_{-} = -|\psi\rangle^{-} \tag{19.39}$$

$$R|\psi\rangle^{+} = |\psi\rangle_{+} \tag{19.40}$$

$$R|\psi\rangle^{-} = -|\psi\rangle_{-} \tag{19.41}$$

which are equivalent to

$$R|\psi\rangle_{+} = 2^{-1/2} I \tag{19.42}$$

$$R|\psi\rangle_{-} = -2^{-1/2}\sigma_z \tag{19.43}$$

$$R|\psi\rangle^{+} = 2^{-1/2}\sigma_x \tag{19.44}$$

$$R|\psi\rangle^{-} = -2^{-1/2} i\sigma_y \tag{19.45}$$

thus demonstrating an inherent capability for mathematical operations. This simple concept has significant practical implications. It means that beams of entangled photons interacting with optical apparata configured with optical elements that are capable of transforming the entangled states can be used to perform optical quantum computations.

In addition to the polarization rotator, other optical components of interest in optical computers are the beam splitter and the Mach–Zehnder interferometer.

19.8 QUANTUM GATES

In this section, the characteristics of some basic quantum gates linked to the probability amplitude of quantum entanglement are introduced.

In the previous section, the reader should have noticed that the matrix R for the $\pi/2$ polarization rotator

$$R = \sigma_x = \begin{pmatrix} 0 & 1 \\ 1 & 0 \end{pmatrix} \tag{19.46}$$

In other words, a polarization rotator behaves mathematically exactly as the σ_x Pauli matrix. Indeed, the Pauli σ_x matrix is the mathematical realization of a quantum NOT gate whose truth table is given below:

a	a'
0	1
1	0

Using the Feynman approach, the quantum NOT gate is illustrated pictorially in Figure 19.10. Furthermore, the observation summarized in Equation (19.54) implies that any optical element that can be related to one of Pauli's matrices is capable of implementing a gate for a quantum computer. A quantum NOT gate was demonstrated by Pelliccia et al. (2003) via polarization methods.

In classical universal computers, logical gates such as AND, NAND, OR, NOR, and NOT form the bases for logical operations. In quantum computing, a gate that was of particular interest to Feynman (1985) was the controlled NOT gate or CNOT gate. The truth table for the CNOT gate is given by (Feynman, 1985)

a	b	a'	b'
0	0	0	0
0	1	0	1
1	0	1	1
1	1	1	0

In the truth table of the CNOT gate, the value of b' is changed, with respect to b, *if and only if* the value of $a = 1$. The pictorial representation of the CNOT gate is illustrated in Figure 19.11.

The interest in the CNOT gate emerges from the fact that this is a fundamental gate for the generation of quantum entanglement states. The first realization of a quantum CNOT gate was reported by Wineland et al. (Monroe et al., 1995).

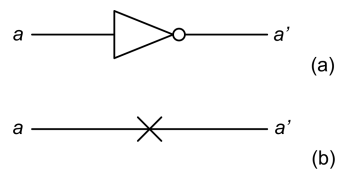

FIGURE 19.10 Generic schematics of the quantum NOT gate.

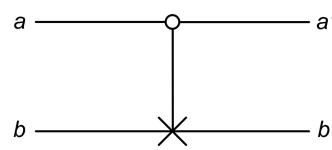

FIGURE 19.11 Generic schematics of the quantum CNOT gate.

A quantum computer with 127 qbits has been demonstrated by Kim et al. (2023) based on CNOT gates and Pauli gates.

19.8.1 Pauli Gates

Each Pauli matrix (σ_x, σ_y, σ_z) is related to a corresponding gate, and they are depicted as illustrated in Figure 19.12. Each of the Pauli gates act on a single qbit. The Pauli-X gate is equivalent to the NOT gate and physically, as already indicated in Equation (19.54), it induces a polarization rotation of $\pi/2$ radians. In other words, it converts $|x\rangle$ to $|y\rangle$, or $|y\rangle$ to $|x\rangle$. Specifically,

$$\begin{pmatrix} 0 & 1 \\ 1 & 0 \end{pmatrix}\begin{pmatrix} 1 \\ 0 \end{pmatrix}=\begin{pmatrix} 0 \\ 1 \end{pmatrix} \tag{19.47}$$

$$\begin{pmatrix} 0 & 1 \\ 1 & 0 \end{pmatrix}\begin{pmatrix} 0 \\ 1 \end{pmatrix}=\begin{pmatrix} 1 \\ 0 \end{pmatrix} \tag{19.48}$$

which can be summarized as

$$\sigma_x|1\rangle \rightarrow |0\rangle \tag{19.49}$$

$$\sigma_x|0\rangle \rightarrow |1\rangle \tag{19.50}$$

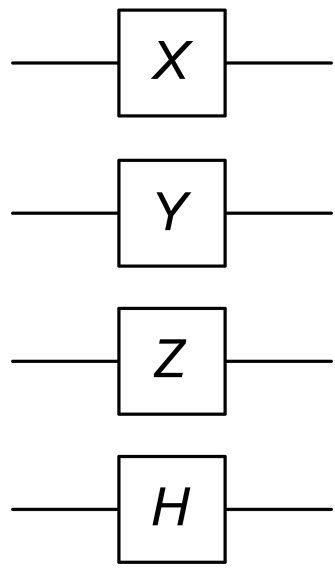

FIGURE 19.12 Generic representation of the Pauli σ_x, σ_y, and σ_z gates. The Hadamard gate is represented by *H*.

The Pauli-Y gate performs the following transformations:

$$\begin{pmatrix} 0 & -i \\ i & 0 \end{pmatrix}\begin{pmatrix} 1 \\ 0 \end{pmatrix}=\begin{pmatrix} 0 \\ i \end{pmatrix} \tag{19.51}$$

$$\begin{pmatrix} 0 & -i \\ i & 0 \end{pmatrix}\begin{pmatrix} 0 \\ 1 \end{pmatrix}=\begin{pmatrix} -i \\ 0 \end{pmatrix} \tag{19.52}$$

that can be summarized as

$$\sigma_y|1\rangle \rightarrow i|0\rangle \tag{19.53}$$

$$\sigma_y|0\rangle \rightarrow -i|1\rangle \tag{19.54}$$

The Pauli-Z gate conducts the transformations

$$\begin{pmatrix} 1 & 0 \\ 0 & -1 \end{pmatrix}\begin{pmatrix} 1 \\ 0 \end{pmatrix}=\begin{pmatrix} 1 \\ 0 \end{pmatrix} \tag{19.55}$$

$$\begin{pmatrix} 1 & 0 \\ 0 & -1 \end{pmatrix}\begin{pmatrix} 0 \\ 1 \end{pmatrix}=\begin{pmatrix} 0 \\ -1 \end{pmatrix} \tag{19.56}$$

which can be summarized as

$$\sigma_z|1\rangle \rightarrow |1\rangle \tag{19.57}$$

$$\sigma_z|0\rangle \rightarrow -|0\rangle \tag{19.58}$$

19.8.2 The Hadamard Gate

The Hadamard gate H_G is related to the matrices of the same name which are designated after the mathematician J. Hadamard. The matrix of interest is

$$H_G = 2^{-1/2}\begin{pmatrix} 1 & 1 \\ 1 & -1 \end{pmatrix} \tag{19.59}$$

which can be derived from the following operation involving Pauli matrices:

$$H_G = 2^{-1/2}(\sigma_x + \sigma_z) \tag{19.60}$$

This gate performs the following transformations:

$$2^{-1/2}\begin{pmatrix} 1 & 1 \\ 1 & -1 \end{pmatrix}\begin{pmatrix} 1 \\ 0 \end{pmatrix} = 2^{-1/2}\begin{pmatrix} 1 \\ 1 \end{pmatrix} = 2^{-1/2}\left(\begin{pmatrix} 1 \\ 0 \end{pmatrix}+\begin{pmatrix} 0 \\ 1 \end{pmatrix}\right) \tag{19.61}$$

$$2^{-1/2}\begin{pmatrix} 1 & 1 \\ 1 & -1 \end{pmatrix}\begin{pmatrix} 0 \\ 1 \end{pmatrix} = 2^{-1/2}\begin{pmatrix} 1 \\ -1 \end{pmatrix} = 2^{-1/2}\left(\begin{pmatrix} 1 \\ 0 \end{pmatrix} - \begin{pmatrix} 0 \\ 1 \end{pmatrix}\right) \quad (19.62)$$

which can be summarized as

$$H_G|1\rangle \rightarrow 2^{-1/2}\left(|1\rangle + |0\rangle\right) \quad (19.63)$$

$$H_G|0\rangle \rightarrow 2^{-1/2}\left(|1\rangle - |0\rangle\right) \quad (19.64)$$

The Hadamard gate can be configured experimentally via a HOM interferometer (Duarte, 2022). The HOM interferometer has been described in Chapter 7.

19.8.3 The CNOT Gate

The truth table for the CNOT gate can be written as a sum of states

$$C_{NOT} = \sum_j |ab\rangle_j \langle a'b'|_j \quad (19.65)$$

$$C_{NOT} = |00\rangle\langle 00| + |01\rangle\langle 01| + |10\rangle\langle 11| + |11\rangle\langle 10| \quad (19.66)$$

which, using the tensor products $|00\rangle = |0\rangle \otimes |0\rangle$, $|01\rangle = |0\rangle \otimes |1\rangle$, $|10\rangle = |1\rangle \otimes |0\rangle$, $|11\rangle = |1\rangle \otimes |1\rangle$ (see Chapter 11), can be expressed as

$$\begin{aligned} C_{NOT} = &\begin{pmatrix} 0 \\ 0 \\ 0 \\ 1 \end{pmatrix}\begin{pmatrix} 0 & 0 & 0 & 1 \end{pmatrix} + \begin{pmatrix} 0 \\ 0 \\ 1 \\ 0 \end{pmatrix}\begin{pmatrix} 0 & 0 & 1 & 0 \end{pmatrix} \\ &+ \begin{pmatrix} 0 \\ 1 \\ 0 \\ 0 \end{pmatrix}\begin{pmatrix} 1 & 0 & 0 & 0 \end{pmatrix} + \begin{pmatrix} 1 \\ 0 \\ 0 \\ 0 \end{pmatrix}\begin{pmatrix} 0 & 1 & 0 & 0 \end{pmatrix} \end{aligned} \quad (19.67)$$

Utilizing the direct vector product, this becomes the sum of four matrices

$$C_{NOT} = \begin{pmatrix} 0 & 0 & 0 & 0 \\ 0 & 0 & 0 & 0 \\ 0 & 0 & 0 & 0 \\ 0 & 0 & 0 & 0 \\ 0 & 0 & 0 & 1 \end{pmatrix} + \begin{pmatrix} 0 & 0 & 0 & 0 \\ 0 & 0 & 0 & 0 \\ 0 & 0 & 0 & 0 \\ 0 & 0 & 1 & 0 \\ 0 & 0 & 0 & 0 \end{pmatrix} + \begin{pmatrix} 0 & 0 & 0 & 0 \\ 1 & 0 & 0 & 0 \\ 0 & 0 & 0 & 0 \\ 0 & 0 & 0 & 0 \\ 0 & 0 & 0 & 0 \end{pmatrix} + \begin{pmatrix} 0 & 1 & 0 & 0 \\ 0 & 0 & 0 & 0 \\ 0 & 0 & 0 & 0 \\ 0 & 0 & 0 & 0 \\ 0 & 0 & 0 & 0 \end{pmatrix} \quad (19.68)$$

$$C_{NOT} = \begin{pmatrix} 0 & 1 & 0 & 0 \\ 1 & 0 & 0 & 0 \\ 0 & 0 & 0 & 0 \\ 0 & 0 & 1 & 0 \\ 0 & 0 & 0 & 1 \end{pmatrix} \tag{19.69}$$

as given by Aradhyamath et al. (2017).

19.9 QUANTUM ENTANGLEMENT MATHEMATICS VIA THE HADAMARD GATE

It can also be shown that the Hadamard matrix operation on the probability amplitudes for quantum entanglement yields the following mathematical identities (Duarte, 2019, 2022; Duarte et al., 2020; Duarte and Taylor, 2021):

$$H_G|\psi\rangle_+ = 2^{-1/2}\left(|\psi\rangle^+ + |\psi\rangle^-\right) \tag{19.70}$$

$$H_G|\psi\rangle_- = 2^{-1/2}\left(|\psi\rangle_+ - |\psi\rangle^-\right) \tag{19.71}$$

$$H_G|\psi\rangle^+ = 2^{-1/2}\left(|\psi\rangle_+ + |\psi\rangle^-\right) \tag{19.72}$$

$$H_G|\psi\rangle^- = 2^{-1/2}\left(|\psi\rangle^+ - |\psi\rangle_-\right) \tag{19.73}$$

19.9.1 Example

It can be shown that Equations (19.70)–(19.83) are equivalent to (Duarte, 2019; Duarte and Taylor, 2021)

$$H_G|\psi\rangle_+ = 2^{-1}(I + i\sigma_y) \tag{19.74}$$

$$H_G|\psi\rangle_- = 2^{-1}(\sigma_x - \sigma_z) \tag{19.75}$$

$$H_G|\psi\rangle^+ = 2^{-1}(\sigma_x + \sigma_z) \tag{19.76}$$

$$H_G|\psi\rangle^- = 2^{-1}(I - i\sigma_y) \tag{19.77}$$

Moreover, it can be shown that (Duarte et al., 2020)

$$H_G = \left(|\psi\rangle_+ + |\psi\rangle^-\right) \tag{19.78}$$

19.10 MULTIPLE ENTANGLED STATES

Binary quantum computing should be based on $n = N = 2^1,\ 2^2,\ 2^3 ... 2^r$. For the case $n = N = 2^2$, the states $|0\rangle$ and $|1\rangle$ can form a series of combined states such as (Duarte, 2019)

$|1\rangle|1\rangle|1\rangle|1\rangle,\ |1\rangle|1\rangle|0\rangle|1\rangle,\ |1\rangle|1\rangle|1\rangle|0\rangle,\ |1\rangle|1\rangle|0\rangle|0\rangle,\ |1\rangle|0\rangle|1\rangle|1\rangle,\ |1\rangle|0\rangle|0\rangle|1\rangle,$
$|1\rangle|0\rangle|1\rangle|0\rangle,\ |1\rangle|0\rangle|0\rangle|0\rangle,\ |0\rangle|1\rangle|1\rangle|1\rangle,\ |0\rangle|1\rangle|1\rangle|0\rangle,\ |0\rangle|1\rangle|0\rangle|1\rangle,\ |0\rangle|1\rangle|0\rangle|0\rangle,$
$|0\rangle|0\rangle|1\rangle|1\rangle,\ |0\rangle|0\rangle|1\rangle|0\rangle,\ |0\rangle|0\rangle|0\rangle|1\rangle,\ |0\rangle|0\rangle|0\rangle|0\rangle$

Four of these combined states observe inter-pair orthogonality:

$$|C\rangle_1 = |1\rangle|0\rangle|0\rangle|0\rangle \tag{19.79}$$

$$|C\rangle_2 = |1\rangle|0\rangle|1\rangle|0\rangle \tag{19.80}$$

$$|C\rangle_3 = |0\rangle|1\rangle|0\rangle|1\rangle \tag{19.81}$$

$$|C\rangle_4 = |0\rangle|1\rangle|1\rangle|0\rangle \tag{19.82}$$

and the corresponding combined and normalized probability amplitudes become (Duarte, 2015, 2016)

$$|\psi\rangle_I = 4^{-1/2}\left(|C\rangle_1 + |C\rangle_2 + |C\rangle_3 + |C\rangle_4\right) \tag{19.83}$$

$$|\psi\rangle_{II} = 4^{-1/2}\left(|C\rangle_1 + |C\rangle_2 - |C\rangle_3 - |C\rangle_4\right) \tag{19.84}$$

$$|\psi\rangle_{III} = 4^{-1/2}\left(|C\rangle_1 - |C\rangle_2 + |C\rangle_3 - |C\rangle_4\right) \tag{19.85}$$

$$|\psi\rangle_{IV} = 4^{-1/2}\left(|C\rangle_1 - |C\rangle_2 - |C\rangle_3 + |C\rangle_4\right) \tag{19.86}$$

The principles of $n = N = 2^3,\ 2^4$ quantum entanglement, which are applicable to binary quantum computing, are described in Chapter 16 and also discussed by Duarte and Taylor (2017). The principles applicable to $n = N = 3$ and $n = N = 6$ are outlined in Chapter 17.

This is the path forward toward quantum computing with a large number of qbits at room temperature.

19.11 DISCUSSION

Quantum optics computing, based on interferometric configurations, can perform interferometric calculations at least $\times 10^5$ times faster than the same calculations carried out in optimally-programmed conventional universal computers (Duarte 1993, 2003). From the temporal vantage point alone, the promise of quantum computing is very bright.

Principal areas of development concern the generation and handling of a large number of qbits, in the $10^3 \le N_{qbit} \le 10^6$ let's say, with high fidelity (Duarte, 2019).

This is a fast-moving field and, at present, it is difficult to gauge which technological approach to quantum computing has the upper hand. Pauli gates and CNOT gates appear to become the workhorses of circuit design.

The beauty of the optical approach to quantum computing is that it can be performed without cooling and, at least in principle, it is apt to generate and handle large number of qbits. In other words, quantum computing with $n = N = 2^2, 2^3 \ldots 2^r$ and $n = N = 3, 6, 9\ldots$, at *room temperature*, is wide open using photon qbits.

The material presented in this chapter adheres exclusively to quantum boson principles. It demonstrates the kind of quantum mathematics that can be performed by utilizing known optical elements such as the $\pi/2$ polarization rotators. The Hadamard gate can be configured via a HOM interferometer.

PROBLEMS

19.1 Use the direct vector product mechanics to show that $|\psi\rangle_{\pm}^{\pm} = 2^{-1/2}\sigma_x$.
19.2 Use the direct vector product mechanics to show that $|\psi\rangle^{\pm} = 2^{-1/2}\sigma_z$.
19.3 Use the direct vector product mechanics to show that $R|\psi\rangle_{-} = -|\psi\rangle^{-}$.
19.4 Use the direct vector product mechanics to show that $R|\psi\rangle^{\mp} = 2^{-1/2}\sigma_x$.
19.5 Verify that Equation (19.66) can be expressed as Equation (19.67)
19.6 Verify the identity $H_G|\psi\rangle_{-} = 2^{-1/2}\left(|\psi\rangle_{+} - |\psi\rangle^{-}\right)$.
19.7 Verify the identity $H_G|\psi\rangle^{-} = 2^{-1}(I - i\sigma_y)$.
19.8 Verify the identity $H_G = \left(|\psi\rangle_{+} + |\psi\rangle^{-}\right)$.

REFERENCES

Aradhyamath, P., Naghabhushana, N. M., and Rohitha, U. (2017). Matrix representation of quantum gates, *Int. J. Comp. Appl.* **159**, 1–6.

Ayres, F. (1965). *Modern Algebra*, McGraw-Hill, New York.

Bennett, C. H. (1982). Thermodynamics of computation – a review. *Int. J. Theor. Phys*. **21**, 905–940.

Deutsch, D. (1992). Quantum computation. *Phys. World* **5** (6), 57–61.

Dirac, P. A. M. (1958). *The Principles of Quantum Mechanics*, 4th ed. Oxford University, Oxford, U.K.

Duarte, F. J. (1993). On a generalized interference equation and interferometric measurements. *Opt. Comm.* **103**, 8–14.

Duarte, F. J. (1996). Generalized interference equation and optical processing. In *Proceedings of the International Conference on Lasers '95* (Corcoran, V. J., and Goldman, T. A., eds.). STS Press, McLean, VA, pp. 615–617.

Duarte, F. J. (2003). *Tunable Laser Optics*, 1st ed. Elsevier-Academic, New York.

Duarte, F. J. (2014). *Quantum Optics for Engineers*, 1st ed. CRC, Boca Raton, FL.

Duarte, F. J. (2015). *Tunable Laser Optics*, 2nd ed. CRC, Boca Raton, FL.

Duarte, F. J. (2016). Secure space-to-space interferometric communications and its nexus to the physics of quantum entanglement. *Appl. Phys. Rev.* **3**, 041301.

Duarte, F. J. (2019). *Fundamentals of Quantum Entanglement*, 1st ed. Institute of Physics, Bristol, U.K.

Duarte, F. J. (2022). *Fundamentals of Quantum Entanglement*, 2nd ed. Institute of Physics, Bristol, U.K.

Duarte, F. J., and Taylor, T. S. (2021). *Quantum Entanglement Engineering and Applications*, Institute of Physics, Bristol, U.K.

Duarte, F. J., Taylor, T. S., and Slaten, J. C. (2020). On the probability amplitude of quantum entanglement and the Pauli matrices. *Opt. Quantum Electron.* **52**, 106.

Feynman, R. P. (1985). Quantum mechanical computers. *Opt. News* **11** (2), 11–20.

Feynman, R. P. (1986). Quantum mechanical computers. *Found. Phys.* **16**, 507–531.

Feynman, R. P., Leighton, R. B., and Sands, M. (1965). *The Feynman Lectures on Physics*, vol. **III**, Addison-Wesley, Reading, MA.

Kim, Y., Eddins, A., Anand, S., Wei, K. X., van der Berg, E., Rosenblatt, S., Nayfeh, H., Zaletet, M., Temme, K., and Kandala, A. (2023). Evidence for the utility of quantum computing before fault tolerance. *Nature* **618**, 500–505.

Monroe, C., Meekhof, D. M., King, B. E., Itano, W. M., and Wineland, D. J. (1995). Demonstration of a fundamental quantum logic gate. *Phys. Rev. Lett.* **75**, 4714–4717.

Pelliccia, D., Schettini, V., Sciarrino, F., Sias, C., and De Martini, F. (2003). Contextual realization of the universal quantum cloning machine and of the universal-NOT gate by quantum-injected optical parametric amplification. *Phys. Rev. A.* **68**, 042306.

Schumacher, B. (1995). Quantum coding. *Phys. Rev. Lett.* **51**, 2738–2747.

von Newmann, J. (1932). *Mathematische Grundlagen der Quanten-Mechanik*, Springer, Berlin.

20 Quantum Cryptography and Quantum Teleportation

20.1 INTRODUCTION

Cryptography is a word derived from the Greek that is approximately translated as *hidden writing*. There are various forms and styles of cryptography; however, since ancient times, the aim of cryptography has been the same: secure the transmission of information from an emitter to a receiver. A classical form of cryptography involves the sharing of a code between the emitter and the receiver. The emitter writes a message, using the shared code, and sends it to the intended receiver who uses the code to decipher the message. The integrity of the message is secured if and only if the code remains in the knowledge of the emitter and the intended receiver. If the code is acquired, or broken, by a third party, then the message is no longer secured. An example of a simple classical numerical code is illustrated in Figure 20.1 and used to write the number π to ten decimal places.

Albeit still in use, paper-based code systems have been largely replaced by various computerized mathematical methods that enable the electronic transmission of encrypted messages. The message is encrypted before transmission, transmitted via an unsecured channel in encrypted form, and decoded, once received. A widely used system of encryption, of this class, is known as *symmetric key algorithm*. This approach utilizes the same cryptographic key, or classical algorithm, for encryption and decryption, see Figure 20.2.

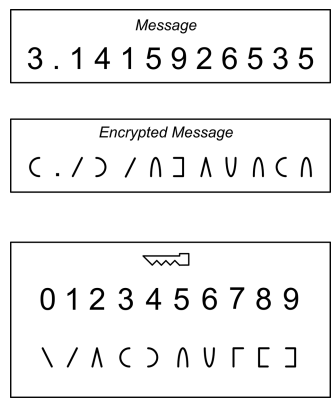

FIGURE 20.1 Classical code representation for the truncated value of π, to ten decimal places. The key is included as a third item.

DOI: 10.1201/9781003398707-20

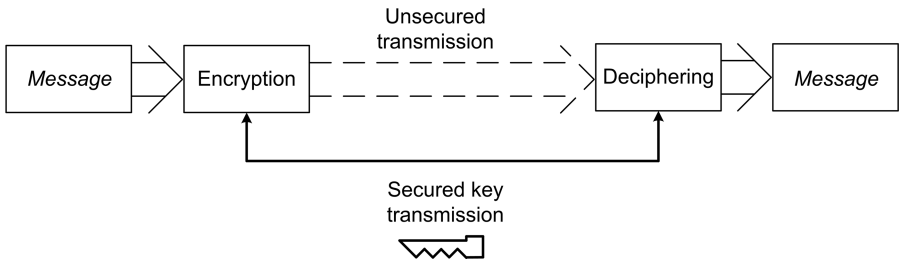

FIGURE 20.2 Classical symmetric key distribution. The same cryptographic key, or classical algorithm, is used for encryption and decryption,

A different algorithmic approach allows the use of a public key and is known as *public key cryptography.* This approach uses a public key and a secured key, both of which are mathematically connected. One key encrypts the plaintext, and the other unlocks the ciphertext (see Figure 20.3). The algorithmic methods just described enjoy compatibility with the vast array of existing computer networks and are thus widely used.

There are many extensions and variations of these classical algorithmic methods. Against this background, optical methods of communication offer alternatives that include some inherent advantages. In Chapter 8, we described a method of secure optical communications known as interferometric communications that involve the transmission of *interferometric characters* at luminal speeds. This method does not require a key, although one might be introduced for added security, and is based on the fact that the interferometric character is catastrophically distorted or destroyed by attempts of interception. Thus, any external intrusion is immediately detected by the receiver (Duarte, 2002).

An alternative method, which has received widespread attention in the open literature, is *quantum cryptography.* That method is described here in addition to a closely related discipline called *quantum teleportation*.

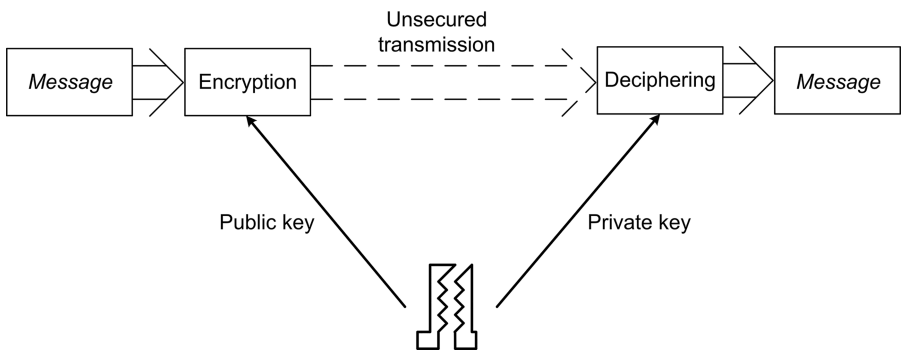

FIGURE 20.3 Classical public key cryptography. This approach uses a public key and a secured key, both of which are mathematically related.

20.2 QUANTUM CRYPTOGRAPHY

Quantum cryptography was first introduced by Weisner in 1983 and then by Bennett and Brassard (BB) (1984). A refined protocol was introduced by Bennett et al. (1992a). The BB approach relies on the straightforward polarization property of single photons. An alternative method, based on the quantum entanglement of pairs of photons, was introduced by Ekert (1991). Here, these two approaches to quantum cryptography are described.

20.2.1 Bennett and Brassard Cryptography

In the BB approach, we have a single photon emitter and a receiver. There is also an adversary intruder, or eavesdropper, whose function is to optically intercept the transmission.

The BB approach relies on the quantum polarization properties of single photons: the polarization states of the photon are referred to as *base* states and two bases are said to be conjugated in the sense that an attempt to measure one base randomizes the other.

Bennett et al. (1992a) refer to these conjugate bases as *canonical bases*. The canonical bases for polarized photons are

$$|H\rangle = |x\rangle \tag{20.1}$$

$$|V\rangle = |y\rangle \tag{20.2}$$

$$|L\rangle = 2^{-1/2}\left(|x\rangle - i|y\rangle\right) \tag{20.3}$$

$$|R\rangle = 2^{-1/2}\left(|x\rangle + i|y\rangle\right) \tag{20.4}$$

which correspond to horizontally ($|H\rangle$ or $\leftrightarrow$), vertically ($|V\rangle$ or $\updownarrow$), left-circularly ($|L\rangle$), and right-circularly ($|R\rangle$), polarized photons.

Bennett et al. (1992a) describe a quantum key distribution protocol that involves the emitter sending a random series of photons polarized in the canonical bases, the receiver choosing independently how to measure the polarizations (either rectilinearly (+) or circularly (O)), the receiver publicly announcing his measuring sequence (but not the results), the emitter publishing which of the receiver's bases were correct, then both parties agree to discard the data from incorrect measurements and null measurements, and finally, the measurements are in bit form according to their polarization.

20.2.2 Quantum Entanglement Cryptography Using Bell's Theorem

As mentioned in the previous section, an alternative approach, in quantum cryptography, involves the use of pairs of photons with entangled polarizations. Interest in this methodology was triggered by a paper by Ekert (1991) that described a cryptographic approach using spin one-half particles and Bell's theorem to ensure security.

The complete set of probability amplitudes for $n = N = 2$ quantum entanglement is (see Chapter 15)

$$|\psi\rangle_{+} = 2^{-1/2}\left(|x\rangle_1|y\rangle_2 + |y\rangle_1|x\rangle_2\right) \tag{20.5}$$

$$|\psi\rangle_{-} = 2^{-1/2}\left(|x\rangle_1|y\rangle_2 - |y\rangle_1|x\rangle_2\right) \tag{20.6}$$

$$|\psi\rangle^{+} = 2^{-1/2}\left(|x\rangle_1|x\rangle_2 + |y\rangle_1|y\rangle_2\right) \tag{20.7}$$

$$|\psi\rangle^{-} = 2^{-1/2}\left(|x\rangle_1|x\rangle_2 - |y\rangle_1|y\rangle_2\right) \tag{20.8}$$

From this set of probability amplitudes, Equations (20.5) and (20.6) were *implicitly* used by Ekert (1991). The transmission security of this technique is tested via Bell's theorem (Bell, 1964).

The quantum entanglement probability applicable to two quanta propagating in opposite directions, while exhibiting orthogonal polarizations, is calculated from the superposition probability amplitude (20.6) and is given by Pryce and Ward (1947).

$$|\psi\rangle|\psi\rangle^{*} = P(\varphi_1, \varphi_2) = -\cos 2(\varphi_1 - \varphi_2) \tag{20.9}$$

In Bell's inequality, the ordinary probabilities originally related to hidden variables ultimately are, in an ad-hoc manner, replaced by quantum probabilities (Bell 1964).

More specifically, for $\varphi_1 = 0, \varphi_2 = \pi/3, \varphi_1' = \pi/6, \varphi_2' = 0$, the probabilities in Bell's expression become quantum superposition probabilities $P(\varphi_1, \varphi_2)$, $P(\varphi_1', \varphi_2)$, $P(\varphi_1', \varphi_2')$, and $P(\varphi_1, \varphi_2')$ (see Chapter 14) and

$$\Sigma_P = |P(\varphi_1, \varphi_2) - P(\varphi_1, \varphi_2')| + |P(\varphi_1', \varphi_2') + P(\varphi_1', \varphi_2)| \tag{20.10}$$

with a numerical value of

$$\Sigma_P = |+0.5 + 1.0| + |-0.5 - 0.5| \tag{20.11}$$

so that $\Sigma_P = 2.5$. A result of $\Sigma_P \geq 2$ indicates that Bell's inequality *is violated* when using probabilities calculated from the probability amplitudes for quantum entanglement.

A generic depiction of a quantum entanglement cryptography experiment is given in Figure 20.4. Some notable free-space quantum cryptography experiments include the following: Ursin et al. (2007) communicated at a distance of over 144 km while reporting a clear violation of Bell's inequality with $\Sigma_P = 2.508 \pm 0.037$; Yin et al. (2017) communicated in an Earth–satellite–Earth scheme over distances up to 1700 km while reporting $\Sigma_P = 2.37 \pm 0.09$; Villar et al. (2020) have demonstrated polarization quantum entanglement experiments on board a 'nanosatellite' launched from the International Space Station at an altitude of 408 km, while reporting $\Sigma_P = 2.63 \pm 0.067$.

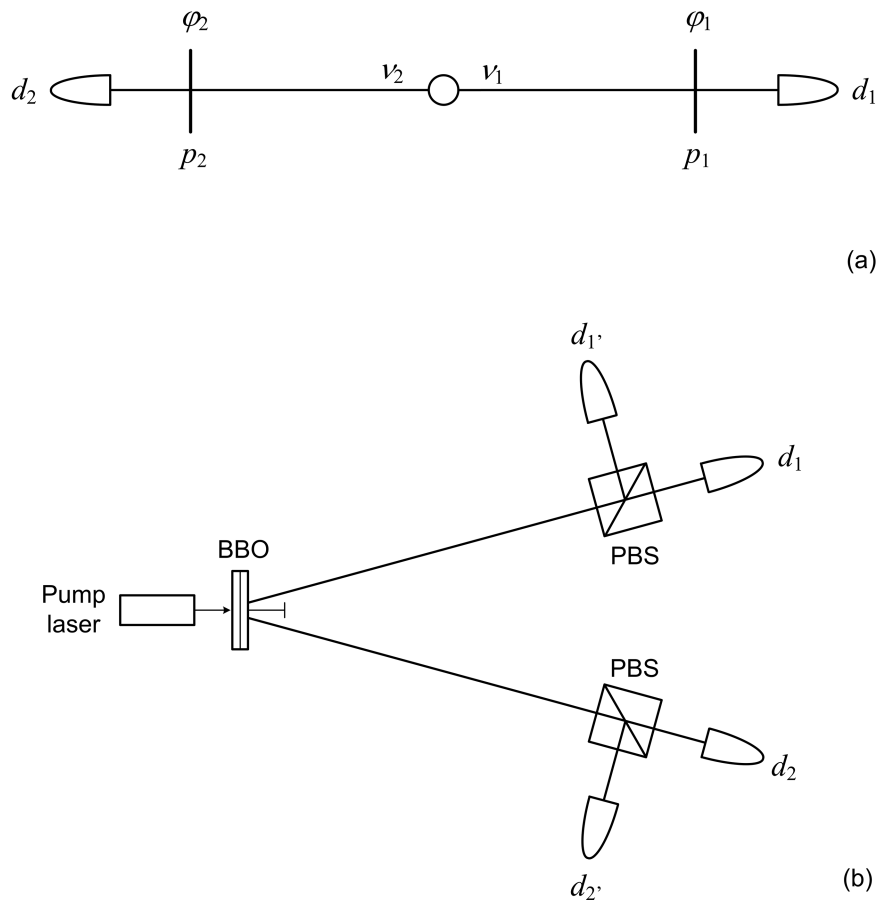

FIGURE 20.4 (a) Generic experimental configuration for cryptography via quantum entanglement based on the original Pryce–Ward γ-ray configuration (Pryce and Ward, 1947). (b) Generic quantum entanglement configuration for cryptographic applications based on a photon pair source. These experimental alternatives use polarizers (p) and polarizing beam splitters (PBS).

20.2.3 All-Quantum Quantum Entanglement Cryptography

The Pryce-Ward superposition probability, in its four alternative forms for φ_1, φ_2, φ_1', and φ_2', is given by

$$P(\varphi_1,\varphi_2) = -\cos 2(\varphi_1 - \varphi_2) \tag{20.12}$$

$$P(\varphi_1,\varphi_2') = -\cos 2(\varphi_1 - \varphi_2') \tag{20.13}$$

$$P(\varphi_1',\varphi_2') = -\cos 2(\varphi_1' - \varphi_2') \tag{20.14}$$

$$P(\varphi_1',\varphi_2) = -\cos 2(\varphi_1' - \varphi_2) \tag{20.15}$$

Duarte and Taylor (2021) introduced a simple *all-quantum* approach to quantum cryptography independent of Bell's theorem. In this approach, the overall quantum probability of the experiment is given by the straight-forward addition of the absolute value of *each of the four* quantum superposition probabilities (Duarte and Taylor 2021; Duarte, 2022)

$$\Sigma_{|\psi\rangle\_|\psi\rangle^*_-} = |P(\varphi_1,\varphi_2)| + |P(\varphi_1,\varphi_2')| + |P(\varphi_1',\varphi_2')| + |P(\varphi_1,\varphi_2')| \tag{20.16}$$

which is clearly distinct from the probability equation given by Bell (1964) and included previously as Equation (20.10). The use of Equations (20.12)–(20.15) and the overall superposition probability, Equation (20.16), is *completely free of the assumptions* used to arrive at Bell's theorem.

As an example, consider the following angular settings: $\varphi_1 = \pi/20$, $\varphi_2 = 9\pi/20$, $\varphi_1' = \pi/3$, $\varphi_2' = \pi/6$. This leads directly to

$$\Sigma_{|\psi\rangle\ |\psi\rangle^*} = |0.8090| + |-0.7431| + |-0.5000| + |-0.7431| = 2.7952 \tag{20.17}$$

The *all-quantum measurement protocol* for secure quantum entanglement communications as developed by Duarte and Taylor (2021) consists of three steps:

1. Via a series of measurements, in free space, while ensuring that no third-party intruders are present, arrive at a measurement determined *intrinsic quantum superposition probability* (IQSP)

$$\Sigma_{|\psi\rangle\_|\psi\rangle^*_-} \pm \Delta\Sigma_{|\psi\rangle\_|\psi\rangle^*_-} \tag{20.18}$$

2. Once the IQSP has been determined, only polarization data giving rise to measured probabilities within the $\Sigma_{|\psi\rangle\_|\psi\rangle^*_-} \pm \Delta\Sigma_{|\psi\rangle\_|\psi\rangle^*_-}$ range are to be considered as secure. Polarization data, leading to probabilities outside the intrinsic measured range (20.18), is to be discarded.
3. Determining $\Sigma_{|\psi\rangle\_|\psi\rangle^*_-} \pm \Delta\Sigma_{|\psi\rangle\_|\psi\rangle^*_-}$ also yields a set of completely correlated measurements that can be used as the key. However, this key is not necessary.

It should be reemphasized that the crucial IQSP, or $\Sigma_{|\psi\rangle\_|\psi\rangle^*_-} \pm \Delta\Sigma_{|\psi\rangle\_|\psi\rangle^*_-}$, is an *experimental quantity* to be determined by measurements exclusively. This approach is in total agreement with Born's quantum experimental doctrine (Born, 1949).

20.3 QUANTUM TELEPORTATION

Quantum teleportation, as described by Bennett et al. (1993), consists in the disintegration of one quantum state, at the emitter's site, and in the subsequent reintegration of that quantum state at the receiver's site.

In this section, *the mechanics of quantum teleportation* is described. This description is based on the descriptions previously given by Duarte and Taylor (2021) and

Duarte (2022). The style and notation of previous reviews on the subject by Duarte (2014, 2019) are preserved.

As a first step, Pauli's matrices and the identity matrix I and are restated

$$\sigma_x = \begin{pmatrix} 0 & 1 \\ 1 & 0 \end{pmatrix} \tag{20.19}$$

$$\sigma_y = \begin{pmatrix} 0 & -i \\ i & 0 \end{pmatrix} \tag{20.20}$$

$$\sigma_z = \begin{pmatrix} 1 & 0 \\ 0 & -1 \end{pmatrix} \tag{20.21}$$

$$I = \begin{pmatrix} 1 & 0 \\ 0 & 1 \end{pmatrix} \tag{20.22}$$

The complete set of Pryce-Ward probability amplitudes are expressed in vector notation (Duarte, 2019)

$$|s\rangle_+ = 2^{-1/2}\left(|1\rangle_1|0\rangle_2 + |0\rangle_1|1\rangle_2\right) \tag{20.23}$$

$$|s\rangle_- = 2^{-1/2}\left(|1\rangle_1|0\rangle_2 - |0\rangle_1|1\rangle_2\right) \tag{20.24}$$

$$|r\rangle_+ = 2^{-1/2}\left(|1\rangle_1|1\rangle_2 + |0\rangle_1|0\rangle_2\right) \tag{20.25}$$

$$|r\rangle_- = 2^{-1/2}\left(|1\rangle_1|1\rangle_2 - |0\rangle_1|0\rangle_2\right) \tag{20.26}$$

Addition and subtraction of these superposition probability amplitudes yield the following combined states:

$$2^{-1/2}(|s\rangle_+ + |s\rangle_-) = |1\rangle_1|0\rangle_2 \tag{20.27}$$

$$2^{-1/2}(|s\rangle_+ - |s\rangle_-) = |0\rangle_1|1\rangle_2 \tag{20.28}$$

$$2^{-1/2}(|r\rangle_+ + |r\rangle_-) = |1\rangle_1|1\rangle_2 \tag{20.29}$$

$$2^{-1/2}(|r\rangle_+ - |r\rangle_-) = |0\rangle_1|0\rangle_2 \tag{20.30}$$

Now, assume that the following quantum state is to be teleported

$$|\phi\rangle_1 = (\alpha|1\rangle_1 + \beta|0\rangle_1) \tag{20.31}$$

In explicit vector notation, this state is equivalent to

$$|\phi\rangle_1 = \left(\begin{pmatrix} \alpha \\ 0 \end{pmatrix}_1 + \begin{pmatrix} 0 \\ \beta \end{pmatrix}_1 \right) = \begin{pmatrix} \alpha \\ \beta \end{pmatrix}_1 \tag{20.32}$$

Here, the α and β factors are related by $|\alpha|^2 + |\beta|^2 = 1$. This probability amplitude, $|\phi\rangle_1 = (\alpha|1\rangle_1 + \beta|0\rangle_1)$, is the state to be *disassembled* at the emitter's site and *reassembled* at the receiver's site. This is what is known as *quantum teleportation*.

Next, select one of the quantum entanglement states given in Equations (20.23)–(20.26). Assuming that Equation (20.23) is selected, then replacing $|s\rangle_+$ by $|s\rangle_{23+}$ leads to

$$|s\rangle_{23+} = 2^{-1/2}\left(|1\rangle_2|0\rangle_3 + |0\rangle_2|1\rangle_3\right) \tag{20.33}$$

Now, a three quanta state $|\phi\rangle_{123}$ is created by the emitter via the multiplication of $|\phi\rangle_1$ and $|s\rangle_{23+}$

$$|\phi\rangle_{123} = 2^{-1/2}\left(\alpha|1\rangle_1|1\rangle_2|0\rangle_3 + \alpha|1\rangle_1|0\rangle_2|1\rangle_3 + \beta|0\rangle_1|1\rangle_2|0\rangle_3 + \beta|0\rangle_1|0\rangle_2|1\rangle_3\right) \tag{20.34}$$

this step disassembles the original state $|\phi\rangle_1$.

Using Equations (20.27)–(20.30) while noting that $|s\rangle_+ = |s\rangle_{12+}$, $|s\rangle_- = |s\rangle_{12-}$, $|r\rangle_+ = |r\rangle_{12+}$, $|r\rangle_- = |r\rangle_{12-}$, Equation (20.34) can be rewritten as

$$|\phi\rangle_{123} = 2^{-1}\left(|s\rangle_{12+}|\phi\rangle_{3+} + |s\rangle_{12-}|\varphi\rangle_{3-} + |r\rangle_{12+}|\vartheta\rangle_{3+} + |r\rangle_{12-}|\vartheta\rangle_{3-}\right) \tag{20.35}$$

meaning that each of the internal states of this probability amplitude has an equal chance of existing. Thus, attention is now given to $|\phi\rangle_{3+}$, $|\phi\rangle_{3-}$, $|\vartheta\rangle_{3+}$, and $|\vartheta\rangle_{3-}$.

Via Equation (20.31), photon 3 is projected into the following states:

$$|\phi\rangle_{3+} = \left(\alpha|1\rangle_3 + \beta|0\rangle_3\right) \tag{20.36}$$

$$|\phi\rangle_{3+} = \left(\alpha|1\rangle_3 + \beta|0\rangle_3\right) \tag{20.37}$$

$$|\vartheta\rangle_{3+} = \left(\alpha|0\rangle_3 + \beta|1\rangle_3\right) \tag{20.38}$$

$$|\vartheta\rangle_{3-} = \left(\alpha|0\rangle_3 - \beta|1\rangle_3\right) \tag{20.39}$$

which in direct vector notation become

$$|\phi\rangle_{3+} = \begin{pmatrix} \alpha \\ \beta \end{pmatrix}_3 \tag{20.40}$$

$$|\phi\rangle_{3-} = \begin{pmatrix} \alpha \\ -\beta \end{pmatrix}_3 \tag{20.41}$$

$$|\vartheta\rangle_{3+} = \begin{pmatrix} \beta \\ \alpha \end{pmatrix}_3 \tag{20.42}$$

$$|\vartheta\rangle_{3-} = \begin{pmatrix} -\beta \\ \alpha \end{pmatrix}_3 \tag{20.43}$$

In summary: the emitter measures the probability corresponding to $|s\rangle_{12+}$ and the qbit communicated to the receiver is $|\phi\rangle_{3+}$. For this case, the unitary transformation needed is the identity matrix I which is communicated classically to the receiver (Kim et al., 2001).

In the nomenclature $|s\rangle_{12+} \rightarrow |\phi\rangle_{3+}$, $\rightarrow$ stands for 'quantum communicate to receiver'. The mechanics for the four cases $|s\rangle_{12+} \rightarrow |\phi\rangle_{3+}$, $|s\rangle_{12-} \rightarrow |\phi\rangle_{3-}$, $|r\rangle_{12+} \rightarrow |\vartheta\rangle_{3+}$, and $|r\rangle_{12-} \rightarrow |\vartheta\rangle_{3-}$ is explicitly described in the following equations.

For $|s\rangle_{12+} \rightarrow |\phi\rangle_{3+}$:

$$I|\phi\rangle_{3+} = \left(\alpha|1\rangle_3 + \beta|0\rangle_3\right) \tag{20.44}$$

$$I|\phi\rangle_{3+} = \begin{pmatrix} 1 & 0 \\ 0 & 1 \end{pmatrix}\begin{pmatrix} \alpha \\ \beta \end{pmatrix}_3 = \begin{pmatrix} \alpha \\ \beta \end{pmatrix}_3 \tag{20.45}$$

$$I|\phi\rangle_{3+} = |\phi\rangle_{3+} \tag{20.46}$$

For $|s\rangle_{12-} \rightarrow |\phi\rangle_{3-}$:

$$\sigma_z|\phi\rangle_{3-} = \sigma_z(\alpha|1\rangle_3 - \beta|0\rangle_3) \tag{20.47}$$

$$\begin{pmatrix} 1 & 0 \\ 0 & -1 \end{pmatrix}\begin{pmatrix} \alpha \\ -\beta \end{pmatrix}_3 = \begin{pmatrix} \alpha \\ \beta \end{pmatrix}_3 \tag{20.48}$$

$$\sigma_z|\phi\rangle_{3-} = |\phi\rangle_{3+} \tag{20.49}$$

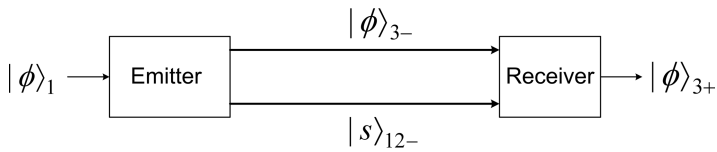

FIGURE 20.5 Simplified generic overview of quantum teleportation. At the emitter's site, a single photon source creates $|\phi_1\rangle$, the state to be teleported. In addition, entangled photon pairs are produced. This emission is used in the creation, for example, of the $|r_{12}\rangle_-$ and $|\vartheta_3\rangle_-$ states by mixing the $|\phi_1\rangle$ state with the entangled photon pair, thus $|\phi_1\rangle$ is disassembled. Synchronized emission via free-space enables the $|\vartheta_3\rangle_-$ state to reach the receiver where $|\vartheta_3\rangle_-$ undergoes the $i\sigma_y$ transformation to reassemble $|\phi_1\rangle$.

For $|r\rangle_{12+} \rightarrow |\vartheta\rangle_{3+}$:

$$\sigma_x|\vartheta\rangle_{3+} = \sigma_x\left(\alpha|0\rangle_3 + \beta|1\rangle_3\right) \tag{20.50}$$

$$\begin{pmatrix} 0 & 1 \\ 1 & 0 \end{pmatrix}\begin{pmatrix} \beta \\ \alpha \end{pmatrix}_3 = \begin{pmatrix} \alpha \\ \beta \end{pmatrix}_3 \tag{20.51}$$

$$\sigma_x|\vartheta\rangle_{3+} = |\phi\rangle_{3+} \tag{20.52}$$

For $|r\rangle_{12-} \rightarrow |\vartheta\rangle_{3-}$:

$$i\sigma_y|\vartheta\rangle_{3-} = i\sigma_y\left(\alpha|0\rangle_3 - \beta|1\rangle_3\right) \tag{20.53}$$

$$i\begin{pmatrix} 0 & -i \\ i & 0 \end{pmatrix}\begin{pmatrix} -\beta \\ \alpha \end{pmatrix}_3 = \begin{pmatrix} \alpha \\ \beta \end{pmatrix}_3 \tag{20.54}$$

$$i\sigma_y|\vartheta\rangle_{3-} = |\phi\rangle_{3+} \tag{20.55}$$

A simplified schematic of the quantum state teleportation scheme is outlined in Figure 20.5.

PROBLEMS

20.1 Show that $\sigma_x|0\rangle = |1\rangle$ and $\sigma_x|1\rangle = |0\rangle$.

20.2 Evaluate $i\sigma_y|0\rangle$ and $i\sigma_y|1\rangle$.

20.3 Using the Pryce-Ward probabilities given in Equations (20.12) to (20.15) and Bell's Equation (20.10) calculate Σ_P for $\varphi_1 = \pi/20$, $\varphi_2 = 9\pi/20$, $\varphi_1' = \pi/3$, $\varphi_2' = \pi/6$.

20.4 Using the Pryce-Ward probabilities given in Equations (20.12)–(20.15) and Equation (20.16) calculate $\Sigma_{|\psi\rangle_-|\psi\rangle_-^*}$ for $\varphi_1 = \pi/20$, $\varphi_2 = 9\pi/20$, $\varphi_1' = \pi/3$, $\varphi_2' = \pi/6$.

20.5 If the state to be quantum teleported is $|\phi\rangle_1 = \left(\alpha|0\rangle_1 + \beta|1\rangle_1\right)$ derive equations, in vector notation, for $|\phi\rangle_{3+}$, $|\phi\rangle_{3-}$, $|\vartheta\rangle_{3+}$, and $|\vartheta\rangle_{3-}$.

20.6 Using the vector states for $|\phi\rangle_{3+}$, $|\varphi\rangle_{3-}$, $|\vartheta\rangle_{3+}$, and $|\vartheta\rangle_{3-}$, found in the previous problem, derive the matrix equations for $I|\phi\rangle_{3+}$, $\sigma_z|\phi\rangle_{3-}$, $\sigma_x|\vartheta\rangle_{3+}$, and $i\sigma_y|\vartheta\rangle_{3-}$.

REFERENCES

Bell, J. S. (1964). On the Einstein-Podolsky-Rosen paradox. *Physics* **1**, 195–200.

Bennett, C. H. (1992). Quantum cryptography using any two nonorthogonal states. *Phys. Rev. Lett*. **68**, 3121–3124.

Bennett, C. H., Bessette, F., Brassard, G., Salvail, L., and Smolin, J. (1992a). Experimental quantum cryptography. *J. Cryptol*. **5**, 3–28.

Bennett, C. H., Brassard, G., and Mermin, N. D. (1992b). Quantum cryptography without Bells theorem. *Phys. Rev. Lett*. **68**, 557–559.

Bennett, C. H., and Brassard, G. (1984). Quantum cryptography: public key distribution and coin tossing. *Proceedings of IEEE International Conference on Computers Systems and Signal Processing*, Bangalore, India.

Bennett, C. H., Brassard, G., Crépeau, C., Jozsa, R., Peres, A., and Wootters, W. K. (1993). Teleporting an unknown quantum state via dual classical and Einstein-Podolsky-Rosen channels. *Phys. Rev. Lett*. **70**, 1895–1899.

Born, M. (1949). *Natural Philosophy of Cause and Chance*, Clarendon Press, Oxford, U.K.

Duarte, F. J. (2002). Secure interferometric communications in free space. *Opt.Commun*. **205**, 313–319.

Duarte, F. J. (2014). *Quantum Optics for Engineers*, 1st ed., CRC, Boca Raton, FL.

Duarte, F. J. (2019). *Fundamentals of Quantum Entanglement*, 1st ed., Institute of Physics, Bristol, U.K.

Duarte, F. J. (2022). *Fundamentals of Quantum Entanglement*, 2nd ed., Institute of Physics, Bristol, U.K.

Duarte, F. J. and Taylor, T. S. (2021). *Quantum Entanglement Engineering and Applications*, Institute of Physics, Bristol, U.K.

Ekert, A. K. (1991). Quantum cryptography based on Bell's theorem. *Phys. Rev.Lett*. **67**, 661–663.

Gobby, C., Yuan, Z. L., and Shields, A. J. (2004). Quantum key distribution over 122 km of standard telecom fiber. Appl. Phys. Lett. **84**, 3762–3764.

Kim, Y.-H., Kulik, S. P., and Yanhua Shih, Y (2001). Quantum teleportation of a polarization state with a complete Bell state measurement. *Phys. Rev. Lett*. **86**, 1370–1373.

Pryce, M. H. L., and Ward, J. C. (1947). Angular correlation effects with annihilation radiation. *Nature* **160**, 435.

Ursin, R., Tiefenbacher, F., Schmitt-Manderbach, T., Weier, H., Scheidl, T., Lindenthal, M., Blauensteiner, B., Jennewein, T., Perdigues, J., Trojek, P., Ömer, B., Fürst, M., Meyenburg, M., Rarity, J., Sodnik, Z., Barbieri, C., Weinfurter, H., and Zeilinger, A. (2007). Free-space distribution of entanglement and single photons over 144 km. *Nature Phys*. **3**, 481–486.

Villar, A., Lohrmann, A., Bai, X., Vergoossen, T., Bedington, R., Perumangatt, C., Lim, H. Y., Islam, T., Reezwana, A., Tang, Z., Chandrasekara, R., Sachidananda, S., Durak, K., Wildfeuer, C. F., Griffin, D., Oi, D. K. L., and Lin, A. (2020). Entanglement demonstration on board a nano-satellite. *Optica* **7**, 734–737.

Yin, J., Cao, Y., Li, Y. H., Liao, S. K., Zhang, L., Ren, J. G., Cai, W. Q., Liu, W. Y., Li, B., Dai, H., and Li, G. B. (2017). Satellite based entanglement distribution over 1200 kilometers. *Science* **356**, 1140–1144.

21 Quantum Measurements

21.1 INTRODUCTION

Classically, the process of a measurement is relatively straight forward. The objects measured are macroscopic, and they can be measured repeatedly without being disturbed in a non-destructive process. For example, using a meter rule or a metric caliper, one can measure repeatedly the length of an object, thus obtaining a series of measurements that can lead to an average dimension and a corresponding standard of deviation. In other words, the experimental physicist obtains the measurement and the error associated with that measurement $(x \pm \Delta x)$. Thus, classically speaking, the measurement issue is settled.

All experimental measurements include an error. Measurements without an error, or without uncertainty, are not physically possible.

Quantum mechanically speaking, the measurement problem is not as straightforward, as in the classical domain, since we are using relatively massive macroscopic classical instruments to obtain measurements on minute quantum objects such as photons and electrons. Therefore, the issue of uncertainties becomes even more important.

Going back to basics, we find that Dirac (1958) refers to the measurement process in a fairly abstract manner indicating that a succession of measurements should give identical results, thus implying that the measurement should be non-destructive. von Neumann (1932) introduced the reduction of the wave function hypothesis. Lamb (1989) is of the opinion that the Dirac and the von Neumann approaches are 'essentially equivalent.' Lamb (1989) further states that 'neither Dirac nor von Neumann discussed his measurements in physical terms.'

Furthermore, according to Lamb (1989), Pauli introduced a concept to use Stern–Gerlach type measurements to determine probability distributions which were fine in principle but in practice 'always destroyed the system of interest' (Lamb, 1989). Here, we should also add that one of van Kampen's theorems states explicitly that the measuring apparatus in quantum mechanics is *macroscopic* (van Kampen, 1988).

Thus, it is not surprising to read articles by noted physicists entitled *Against measurement* (Bell, 1990) where the concepts of Dirac, von Neumann, and van Kampen are criticized. In this chapter, we attempt to describe practical approaches to the measurement of physical parameters associated with quantum entities such as the photons and ensembles of indistinguishable photons.

21.1.1 The Two Realms of Quantum Mechanics

In quantum mechanics, as articulated by Dyson (2007), there are two realms – the first realm is the beautiful mathematical realm of probability amplitudes, wave functions,

DOI: 10.1201/9781003398707-21

and complex numbers. The second realm is the measurement realm of probabilities, intensity measurements, and polarization measurements. The transition from the first realm to the second realm is performed via Born's rule (Born, 1926)

$$\langle d|s\rangle\langle d|s\rangle^{*} = \left|\langle d|s\rangle\right|^{2} \tag{21.1}$$

That is how we transition from purely mathematical probability amplitudes to measurable probabilities. That's it. Nothing else is needed. There is no need to conceptualize a 'collapse of the wave function' or a 'collapse of the probability amplitude' (Duarte, 2022). In this regard, the 'measurement problem' becomes an unnecessary conceptual problem to be discarded (Duarte, 2022).

Also important, from our perspective, is that we are dealing almost exclusively with photons and indistinguishable quanta. Photons and/or indistinguishable quanta *are not* particles (Lamb, 1995).

21.2 THE INTERFEROMETRIC IRREVERSIBLE MEASUREMENTS

The interferometric measurements described in Chapter 8 are macroscopic physical permanent records of interferometric photon distributions. As such, these recordings represent an inherently irreversible transformation of the event to be recorded. In other words, these measurements are destructive and they illustrate what happens when a massive macroscopic classical system interacts with a quantum entity such as a photon or an indistinguishable quanta interferometric distribution.

Photon intensities are proportional to quantum mechanical probabilities (see Appendix A). Thus, when we measure an intensity distribution or an interferometric intensity distribution, we are recording the spatial information originally contained in the interferometric distribution which is a *quantum probability distribution* such as the generalized one-dimensional *N*-slit interferometric distribution (Duarte, 1991, 1993)

$$\langle d|s\rangle\,\langle d|s\rangle^{*} = \sum_{j=1}^{N}\Psi(r_j)\sum_{m=1}^{N}\Psi(r_m)e^{i(\Omega_m-\Omega_j)} \tag{21.2}$$

$$\left|\langle d|s\rangle\right|^{2} = \sum_{j=1}^{N}\Psi(r_j)^{2} + 2\sum_{j=1}^{N}\Psi(r_j)\left(\sum_{m=j+1}^{N}\Psi(r_m)\cos(\Omega_m-\Omega_j)\right) \tag{21.3}$$

where $\Psi(r_j)$ are wave functions (Dirac, 1958; Duarte, 2004), and the term in parentheses represents the phase that describes the exact geometry of the *N*-slit interferometer (Duarte, 1991, 1993). Again, the measured intensity is proportional to the probability $\left|\langle d|s\rangle\right|^{2}$, and it is this probability that gives origin to the spatial distribution of the observed intensity. These equations were originally derived for *single-photon propagation* (Duarte, 1993, 2004) albeit in practice, they also apply to the propagation of an *ensemble of indistinguishable photons*, as in the case of narrow-linewidth laser emission.

Note: the quantum probability is expressed in Equations (21.2) and (21.3) are entirely equivalent. This is restated here to dissipate any doubts on the quantumness of Equation (21.3) which does not explicitly include imaginary exponents due to the use of the identity

$$2\cos(\Omega_m - \Omega_j) = e^{-i(\Omega_m - \Omega_j)} + e^{i(\Omega_m - \Omega_j)} \tag{21.4}$$

21.2.1 The Quantum Measurement Mechanics

In the interferometric measuring process, a photon distributed in the interferometric distribution described by Equations (21.2) or (21.3) arrives at the interference plane or detection surface *d*. Here, the photon is considered as a nonlocal form of coherent energy.

The arrival of each individual photon, with an energy $E = h\nu$, means that the quantum intensity distribution

$$I(\lambda, N, \Omega) = K\ h\nu\ \langle d|s\rangle\ \langle d|s\rangle^* \tag{21.5}$$

interacts with the pixels at the detector's surface. This single-photon interaction with the detector might or might not lead to the creation of a charge within the spatial boundaries of the $\langle d|s\rangle\ \langle d|s\rangle^*$ distribution. Repeated interactions of $I(\lambda, N, \Omega)$ with the detector surface eventually lead to the creation of a charge at any of the individual pixel sites within the $\langle d|s\rangle\langle d|s\rangle^*$ distribution.

For light associated with the emission of large numbers of *r* indistinguishable photons, as in the case of narrow-linewidth laser emission, the intensity distribution becomes

$$I_r(\lambda, N, \Omega) = rK\ h\nu\ \ \langle d|s\rangle\langle d|s\rangle^* \tag{21.6}$$

and the energy associated with this distribution becomes $E = rh\nu$. In this case, a cumulative spatial charge distribution closely resembling $\langle d|s\rangle\ \langle d|s\rangle^*$ is registered at the detector (Duarte, 2004). Once the single photon, or the ensemble of indistinguishable photons, interacts with the detection surface, the process becomes *irreversible*, thus representing a destructive measurement.

If the interferometric plane is comprised of a photographic plate, then the incident photon energy develops a charge in one of the grains within the $\langle d|s\rangle\ \langle d|s\rangle^*$ distribution. If the interferometric plane is comprised of a photo-electric surface, the incident photon generates a charge, within the $\langle d|s\rangle\ \langle d|s\rangle^*$ distribution, that is amplified in a cascade process until it produces a classical manifestation.

In the case of illumination via ensembles of indistinguishable photons, this process is highly reproducible and repeatable with nearly identical ensembles of indistinguishable photons, giving rise to nearly identical $\langle d|s\rangle\ \langle d|s\rangle^*$ probability distributions.

The intensity distributions represented by Equations (21.5) and (21.6) follow from the observation that $I(\nu) \propto \langle d|s\rangle\ \langle d|s\rangle^*$ (see Appendix A). We also know, from

comparisons from measurements and theory (Duarte, 1993) that this intensity distribution, $I_r(\lambda,N,\Omega)$, closely reproduces the calculated quantum probability distribution $\langle d|s\rangle\langle d|s\rangle^*$. In turn, $\langle d|s\rangle\langle d|s\rangle^*$ originates from the multiplication of the superposition probability amplitude series.

Note: in this section, the original material, was expanded and revised in light of the review by Duarte (2022).

21.2.2 Additional Irreversible Quantum Measurements

In addition to the interferometric measurements just described, other irreversible quantum measurements in optics include the following:

1. The original quantum polarization entanglement measurements made by Wu and Shaknov (1950).
2. Quantum polarization measurements to test Bell's inequalities (see, for example, Aspect et al., 1982).
3. Quantum cryptography measurements (see, for example, Gobby et al., 2004).
4. Measurements of quantum teleported states (see, for example, Ma et al., 2012).

In all these cases, quantum entities, namely the photon, interact with massive macroscopic detectors in an irreversible manner.

21.3 QUANTUM NON-DEMOLITION MEASUREMENTS

Lamb wrote several papers on measurements in quantum mechanics. The first paper (Lamb, 1986) considers a sequence of quantum mechanical measurements on an isolated large macroscopic system, such as a gravity wave detector. In the second paper, Lamb (1989) is still interested in a large macroscopic system where 'only the detector is treated quantum mechanically.' He then discloses his idea of 'making purely classical measurements on a quantum system' (Lamb, 1989). This approach appears to be consistent with van Kampen's fifth theorem which states that a measuring instrument in quantum mechanics 'consists of a macroscopic system' (van Kampen, 1988). Lamb's work is mainly mentioned here to highlight the interplay between quantum mechanics and macroscopic measurement apparata.

21.3.1 Soft Probing of Quantum States

Soft, non-destructive, optical probing of propagating quanta in superposition polarization states of the form

$$|\psi\rangle = 2^{-1/2}\left(|x\rangle + |y\rangle\right) \tag{21.7}$$

can be performed via the insertion of *microscopic* means that alter the polarization state as described by the density matrix

$$|\psi'\rangle\langle\psi'| = 2^{-1}\begin{pmatrix} 1 & e^{-i\varphi} \\ e^{i\varphi} & 1 \end{pmatrix} \tag{21.8}$$

If quanta are involved in an interferometric situation, then insertion of microscopic means causes the interferometric pattern to be slightly altered. The fact that the interference pattern *is altered*, indicates that the soft probing conducted does indeed modify the interference pattern, as would be expected from Feynman's teachings (Feynman et al., 1965). The insertion of macroscopic means, such as beam splitters, to probe propagating quanta in a given superposition state, causes catastrophic alterations to the propagating state (Duarte, 2002).

21.4 SOFT INTERSECTION OF INTERFEROMETRIC CHARACTERS

In Chapter 8, we saw that beam path proving via conventional high-surface quality beam splitters can be immediately detected due to the catastrophic collapse induced by the spatial disruption caused by the beam splitter. This is the case even if the classical beam splitter is highly transparent and only a fraction of a millimeter in thickness, since the observed phenomenon is a diffractive edge effect brought about by an abrupt change in the spatial distribution of the refractive index.

The question then becomes: can we probe in the intra-interferometric path $D_{\langle d|j\rangle}$ ever so gently as to avoid a violent disruption of the homogeneous refractive index serving as propagation medium between the N-slit array and the interference plane? The answer to this question *is in the affirmative*: soft intersection of propagating N-slit interferometric characters, microscopic spider web silk fibers, was demonstrated by Duarte et al. (2011) using an experimental configuration described in Figure 21.1. The fibers used in these experiments are ultra-thin semi-transparent and ultra-thin transparent natural fibers.

Two such fibers are fine human blond hair and spider web fibers. The fibers have a diameter of $d \approx 50$ μm in the case of blond human hair and $25 \leq d \leq 30$ μm in the case of transparent spider web fibers which were collected in Western New York, near Lake Ontario (Duarte et al., 2011).

The interferometric character $a(N = 2)$, for an intra-interferometric distance of $D_{\langle d|j\rangle} = 7.235$ m, is illustrated in Figure 21.2. For the same interferometric character $(N = 2)$ with the spider web fiber, positioned 15 cm from the interferometric plane at d (D_3), and displaced laterally, a diffraction pattern is superimposed over one of the outer wings of the interferogram (see Figure 21.3). The important and interesting effect here is that the propagating interferogram is physically intercepted but *it is not destroyed*. It is modified, or altered, in a suave orderly and controllable manner.

21.4.1 Comparison between Theoretical and Measured N-Slit Interferograms

Next, we describe in detail a series of additional soft probing experiments, conducted by Duarte et al. (2013), that involve the gentle and controlled insertion of the spider silk web fiber into the optical path $D_{\langle d|j\rangle}$ of the propagating interferometric character.

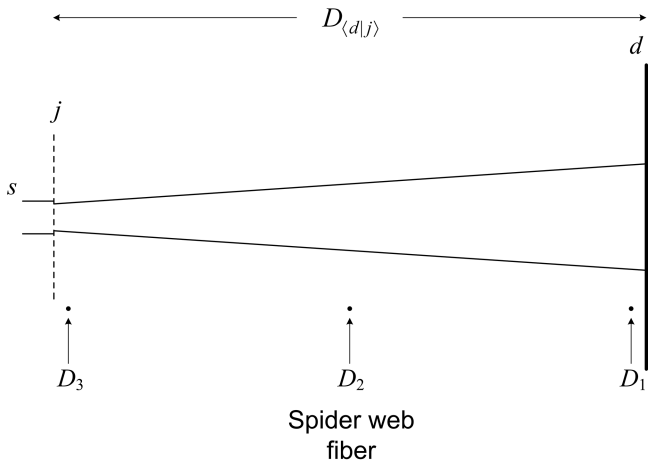

FIGURE 21.1 Top view schematics of the intra-interferometric path of the *N*-slit interferometer indicating (approximately) the three positions D_1, D_2, and D_3, in the $D_{\langle d|j\rangle}$ propagation path, where the spider web fiber is inserted perpendicular to the plane of incidence (i.e., orthogonal to the plane of the figure).

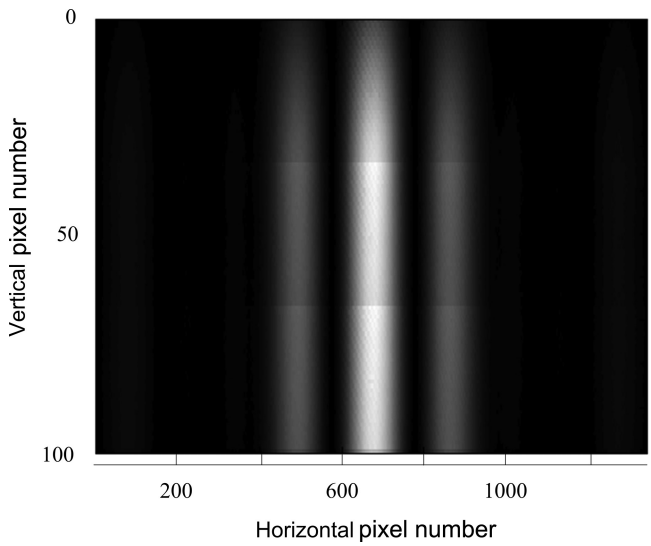

FIGURE 21.2 Interferometric distribution registered at x, for $D_{\langle d|j\rangle} = 7.235$ m, $\lambda = 632.82$ nm, and $N = 2$ (570 μm slits separated by 570 μm). This interferogram corresponds to the interferometric character a. This measurement was performed at a temperature of $T \approx 22$°C. Each pixel on the CCD screen is 20 μm wide (Duarte, F. J. et al., *J. Opt.* **13**, 035710, 2011, © IOP Publishing. Reproduced with permission. All rights reserved).

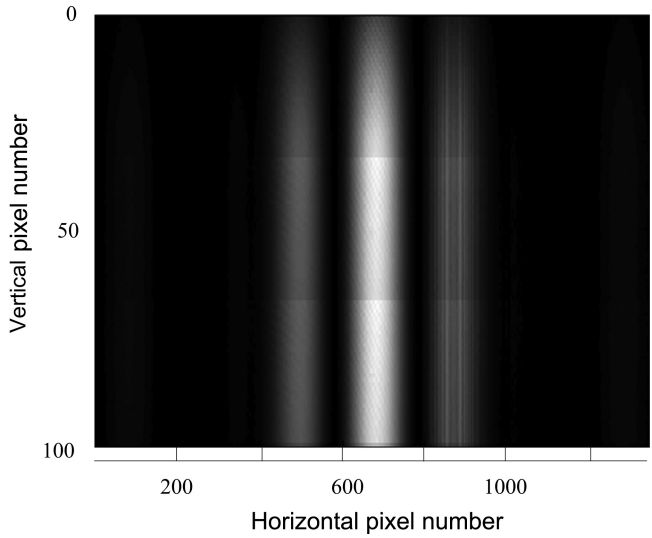

FIGURE 21.3 Photograph of the interferometric distribution registered at x, for $D_{\langle d|j\rangle} = 7.235$ m, $\lambda = 632.82$ nm, and $N = 2$ (570 μm slits separated by 570 μm) showing a superimposed diffractive pattern over the *outer right wing* of the interferogram. The superimposed diffractive distribution is caused by a spider web fiber deployed orthogonally to the propagation plane (that is, perpendicular to the plane of Figure 21.1) at the distance of $D_1 = D_{\langle d|j\rangle} - 0.150$ m, or 15 cm from d (Duarte, F. J. et al., *J. Opt.* **13**, 035710, 2011, © IOP Publishing. Reproduced with permission. All rights reserved).

The silk fiber is inserted into the intra-interferometric propagation path, under tension, perpendicular to the plane of incidence at D_1, D_2, and D_3 (see Figure 21.1). That is, the spider web fiber is inserted orthogonal to the beam expansion defined by the multiple-prism expander. As illustrated in Figure 21.1, the N-slit array, or grating, is also deployed with the direction of the slits perpendicular to the plane of incidence.

The intra-interferometric distances of silk fiber insertion are (Duarte et al., 2013):

1. $D_1 = D_{\langle d|j\rangle} - 0.150$ m (15 cm from the detector).
2. $D_2 = D_{\langle d|j\rangle} / 2$ (midway).
3. $D_3 = D_{\langle d|j\rangle} - 7.085$ m (15 cm from the grating).

while the overall intra-interferometric distance is maintained at $D_{\langle d|j\rangle} = 7.235$ m.

First, a control interferogram is generated from the illumination of $N = 3$ slits of the grating comprised with 570 μm slits separated by 570 μm, at $\lambda = 632.82$ nm, for an intra-interferometric distance of $D_{\langle d|j\rangle} = 7.235$ m, as illustrated in Figure 21.4. This interferometric character b, is recorded at room temperature ($T \approx 22°C$) which becomes the standard measurement temperature.

An interferogram under identical propagation conditions, for $N = 3$, with the spider web silk fiber deployed orthogonally to the propagation plane, at D_1, is shown in

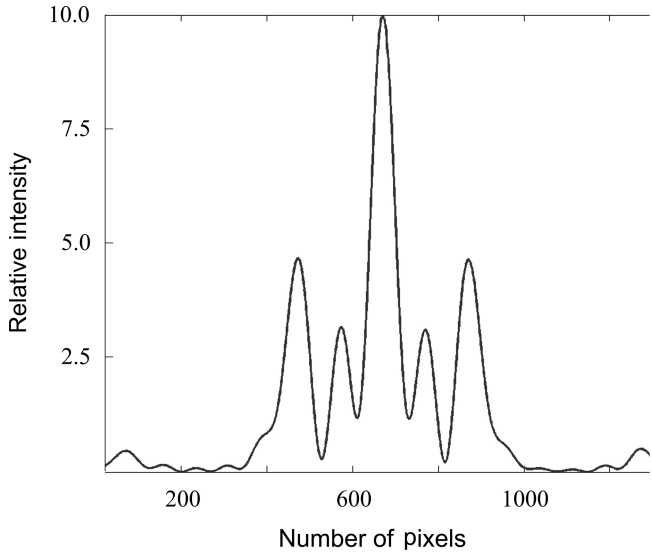

FIGURE 21.4 Control intensity profile of interferogram registered at d, for $D_{\langle d|j\rangle} = 7.235$ m, $\lambda = 632.8$ nm, and $N = 3$ (570 μm slits separated by 570 μm). The interferogram generated with $N = 3$ corresponds to the interferometric character *b*. This measurement was performed at a temperature of $T \approx 22^{\circ}$C. Each pixel on the CCD screen is 20 μm wide. These parameters apply to all the measurements considered in the next set of figures (Reproduced from Duarte, F. J. et al., *J. Mod. Opt.* **56**, 1780–1784, 2013, with permission).

Figure 21.5. The interferometric distribution thus obtained demonstrates a diffraction pattern superimposed over the outer right wing of the interferogram in Figure 21.5.

An interferogram under identical propagation conditions, for $N = 3$, but now with the spider web silk fiber deployed orthogonally to the propagation plane, at $D_2 = D_{\langle d|j\rangle}/2$, is shown in Figure 21.6.

An interferogram under identical propagation conditions, for $N = 3$, but now with the spider web silk fiber deployed orthogonally to the propagation plane, at D_3, is shown in Figure 21.7. For this experiment, the fiber is positioned 15 cm from the slits near the first (right) slit relative to the configuration of Figure 21.1.

A theoretical control interferogram, equivalent to the measured interferogram of Figure 21.4, is generated using the interferometric equation

$$\left|\langle d|s\rangle\right|^2 = \sum_{j=1}^{N} \Psi(r_j)^2 + 2\sum_{j=1}^{N} \Psi(r_j)\left(\sum_{m=j+1}^{N} \Psi(r_m)\cos(\Omega_m - \Omega_j)\right)$$

and displayed in Figure 21.8. Reproduction, or prediction, of the interferograms with superimposed diffraction patterns is performed by adopting the interferometric *cascade approach* (Duarte, 1993; Duarte et al., 2011). This cascade approach consists in using the interferometric equation, that is Equation (21.1), to create an interferometric distribution that becomes the illumination field of the next N-slit array (Duarte, 1993)

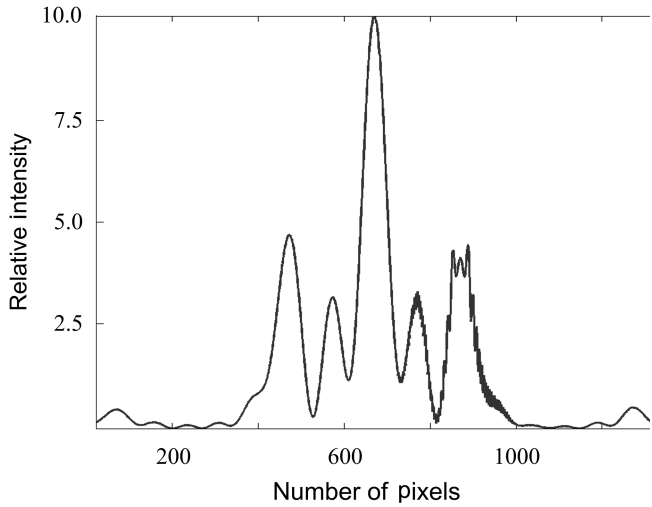

FIGURE 21.5 Measured intensity profile of interferogram registered at d, for $D_{\langle d|j\rangle} = 7.235$ m, $\lambda = 632.82$ nm, and $N = 3$ showing a superimposed diffractive intensity distribution over the *outer right wing* of the interferogram. The superimposed diffractive pattern is caused by a spider web fiber deployed orthogonally to the propagation plane (i.e., perpendicular to the plane of Figure 21.1) at the distance of $D_1 = D_{\langle d|j\rangle} - 0.150$ m, or 15 cm from d (Reproduced from Duarte, F. J. et al., *J. Mod. Opt.* **56**, 1780–1784, 2013, with permission).

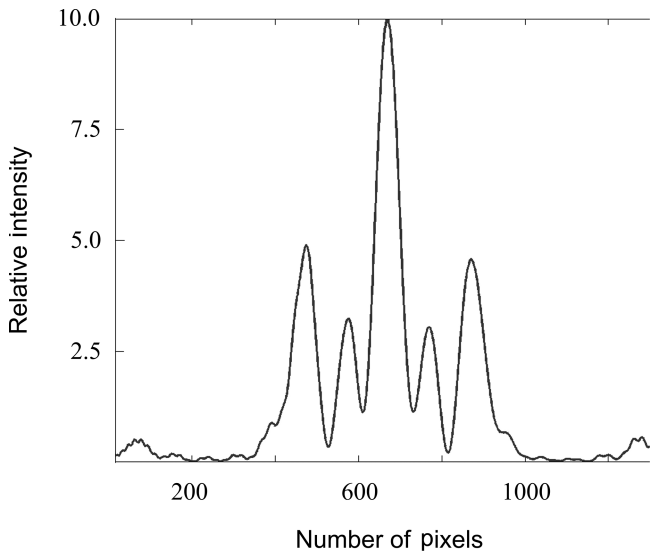

FIGURE 21.6 Measured intensity profile of interferogram registered at x, for $D_{\langle d|j\rangle} = 7.235$ m, $\lambda = 632.8$ nm, and $N = 3$ with a spider web fiber deployed orthogonally to the propagation plane at an intra-interferometric distance of $D_2 = D_{\langle d|j\rangle}/2$ (Reproduced from Duarte, F. J. et al., *J. Mod. Opt.* **56**, 1780–1784, 2013, with permission).

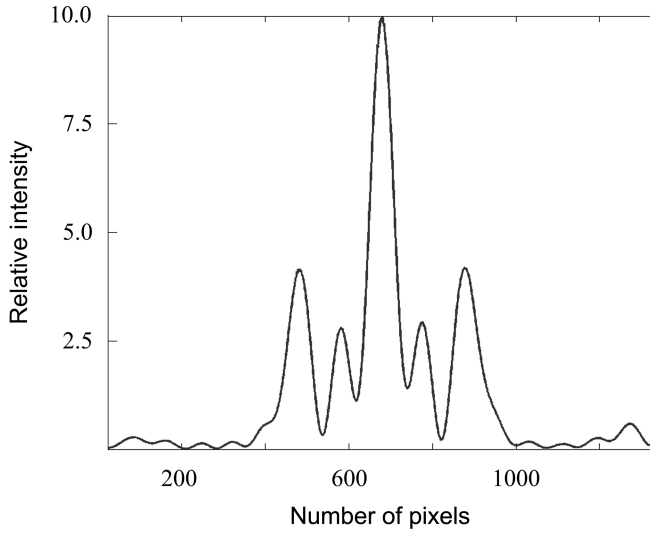

FIGURE 21.7 Measured intensity profile of interferogram registered at d, for $D_{\langle d|j\rangle} = 7.235$ m, $\lambda = 632.82$ nm, and $N = 3$ with a spider web fiber deployed orthogonally to the propagation plane at an intra-interferometric distance of $D_3 = D_{\langle d|j\rangle} - 7.085$ m (15 cm from the slits) (Reproduced from Duarte, F. J. et al., *J. Mod. Opt.* **56**, 1780–1784, 2013, with permission).

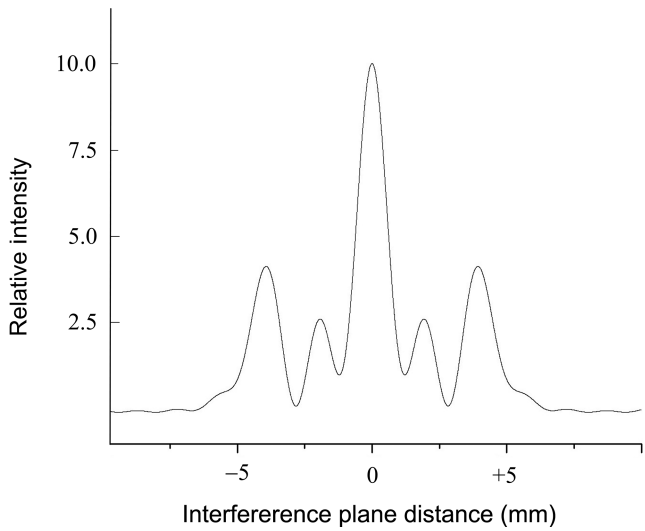

FIGURE 21.8 Calculated control interferogram at d, using Equation (21.1), for $D_{\langle d|j\rangle} = 7.235$ m, $\lambda = 632.82$ nm, and $N = 3$. This calculated interferogram corresponds to the measured interferogram displayed in Figure 21.4 (Reproduced from Duarte, F. J. et al., *J. Mod. Opt.* **56**, 1780–1784, 2013, with permission).

(see Chapter 22 for further details). Using this approach, the spider web silk fiber is represented by two wide slits separated by the diameter of the fiber. Thus, we can predict or replicate the diffraction effect induced by the spider web fiber at various intra-interferometric distances.

The calculations representing insertion of a 25 μm fiber in the intra-interferometric path $D_{\langle d|j\rangle}$ at D_1, D_2, and D_3 are displayed in Figures 21.9, 21.10, and 21.11, respectively. At D_1, the superposition of the diffraction signal over the interferometric distribution is beautifully predicted as illustrated in Figure 21.9. At D_2, the silk fiber induces only a minor effect as shown in Figure 21.10. Furthermore, at D_3, the silk fiber produces almost no disturbance when placed between slits and tends to only very slightly modify the whole interferometric distribution when positioned at the center of one of the slits (Figure 21.11). Either in the case of the beautiful superimposed diffraction distribution (Figure 21.9) or in the other two more subtle interactions, the theoretical interferograms nicely reproduce the corresponding measured interferograms.

Previously, it was demonstrated that insertion of a conventional thin and highly transparent beam splitter into the intra-interferometric path led, as expected (see Chapter 8), immediately to a *catastrophic collapse* of the interferometric character or signal (Duarte, 2002, 2005; Duarte et al., 2010). However, the experiments described by Duarte et al. (2013) demonstrate a remarkable suave and controlled way to alter the propagating interferograms in a soft and non-demolition manner. Thus, we have transitioned from a regime of *total signal collapse*, using classical beam

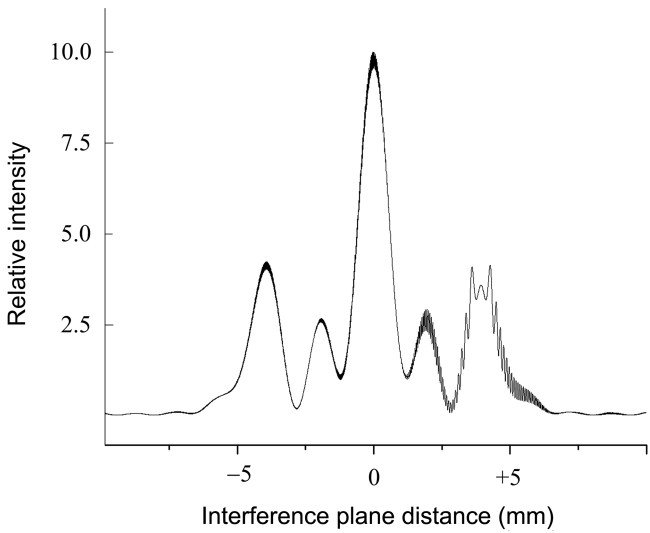

FIGURE 21.9 Calculated interferogram at d, for $D_{\langle d|j\rangle} = 7.235$ m, $\lambda = 632.82$ nm, and $N = 3$ with a 30 μm diameter fiber deployed orthogonally to the propagation plane at a distance of 15 cm from d, or $D_1 = D_{\langle d|j\rangle} - 0.150$ m. The fiber is positioned 4 mm from the center. This calculated interferogram corresponds to the measured interferogram displayed in Figure (21.5) (Reproduced from Duarte, F. J. et al., *J. Mod. Opt.* **56**, 1780–1784, 2013, with permission).

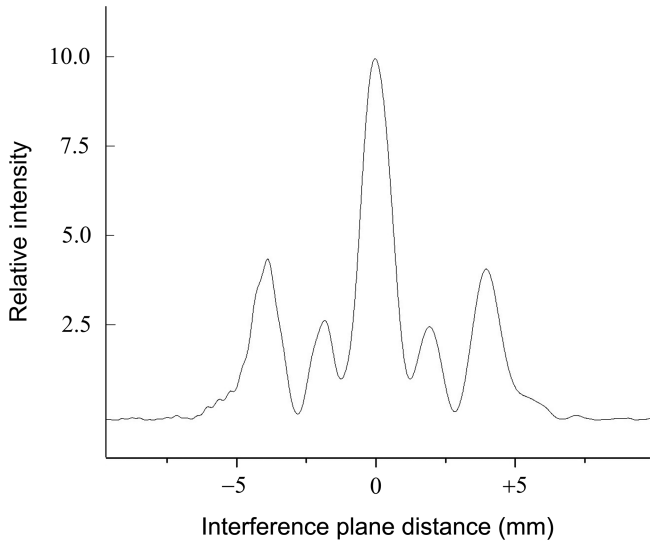

FIGURE 21.10 Calculated interferogram at d, for $D_{\langle d|j\rangle} = 7.235$ m, $\lambda = 632.82$ nm, and $N = 3$ with a 30 μm web fiber deployed orthogonally to the propagation plane at an intra-interferometric distance of $D_2 = D_{\langle d|j\rangle}/2$ (that is, 3.6175 m). The fiber is positioned 2.227 mm from the center. This calculated interferogram corresponds to the measured interferogram displayed in Figure 21.6 (Reproduced from Duarte, F. J. et al., *J. Mod. Opt.* **56**, 1780–1784, 2013, with permission).

splitters, to a soft regime of *non-destructive* gentle detection with the use of spider silk threads. This appears to be allowed by the unusual geometry of the N-slit interferometer where the dimensions and separation of the slits (570 μm) are relatively enormous to the dimensions of the fiber diameter (25–30 μm).

21.4.2 Soft Interferometric Probing

As indicated earlier, Equation (21.2) is a quantum probability expression that was originally derived for single-photon propagation that also describes accurately the interferometric propagation generated by ensembles of indistinguishable photons as available from narrow-linewidth lasers. Thus, as previously observed (Duarte, 2002, 2005), and according to Feynman's teachings, we have expected and observed the *catastrophic collapse* of interferometric characters at any macroscopic attempt to extract information. These attempts involved the insertion of very thin highly transparent beam splitters. In this regard, the orderly non-destructive diffractive effects reported by Duarte et al. (2011, 2013), following soft interrogation via the insertion of a microscopic spider web fiber, are extremely relevant given that the information contained in the interferometric character is largely preserved albeit the presence of the fiber is nicely detected. Even more interesting are the results obtained at $D_2 = D_{\langle d|j\rangle}/2$ and D_3.

Probing with the fiber at those positions causes a *nearly indistinguishable* effect. These results demonstrate the capability of interacting with the propagating interferograms non-destructively causing only slight alterations to the information relative to the pristine interferograms.

21.4.3 The Mechanics of Soft Interferometric Probing

According to Willis Lamb, quantum mechanics can be extended to measurements on a 'rather large and otherwise macroscopic system' (Lamb, 1989). He goes on to explain that the detector is treated quantum mechanically; in other words, the process of the measurement that in our case refers directly to the interferometric probability distribution, that is Equations (21.2) or (21.3), arising either from the propagation of single photons or an ensemble of indistinguishable photons (Duarte, 2004).

Albeit the measured interferograms are neatly reproduced using the cascade interferometric approach, where the interferometric distribution at one plane becomes the input for the next plane, as described by Duarte (1993), next we use an alternative approach to describe the physics of the fiber intersection with the propagating interferogram (Duarte et al., 2013).

In a straight forward interferometric propagation, as outlined in Figure 21.1, and in the absence of the probing fibers, the interferograms generated are the corresponding control interferogram as shown in Figure 21.4 (measured) and Figure 21.8 (calculated), the probability amplitudes from the grating to the interferometric plane are

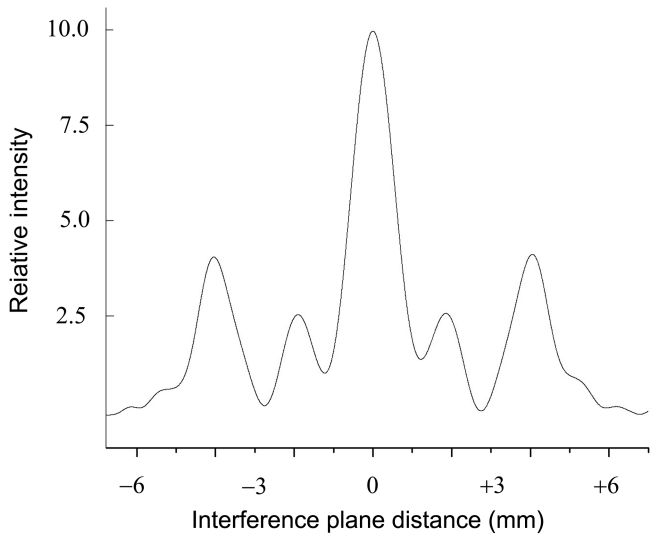

FIGURE 21.11 Calculated interferogram at d, for $D_{\langle d|j\rangle} = 7.235$ m, $\lambda = 632.82$ nm, and $N = 3$ with a 30 μm web fiber deployed orthogonally to the propagation plane at an intra-interferometric distance of $D_3 = D_{\langle d|j\rangle} - 7.085$ m. The fiber is positioned at the center-right slit. This calculated interferogram corresponds to the measured interferogram displayed in Figure 21.7 (Reproduced from Duarte, F. J. et al., *J. Mod. Opt.* **56**, 1780–1784, 2013, with permission).

simply given by $\langle d|\, j\rangle$; however, with the insertion of the spider web fiber, the probability amplitudes are altered, so that

$$\langle d|\, j\rangle \rightarrow \langle d|\, j'\rangle\, \langle j'|\, j\rangle \tag{21.9}$$

Indeed, as soon as the spider web fiber is introduced, the original probability amplitude

$$\langle d|\, s\rangle = \sum_{j=1}^{N} \langle d|\, j\rangle\, \langle j|s\rangle \tag{21.10}$$

is replaced by a probability amplitude relevant to the experimental configuration of Figure 21.1, that is,

$$\langle d|\, s\rangle' = \sum_{j'=1}^{N} \sum_{j=1}^{N} \langle d|\, j'\rangle\, \langle j'|\, j\rangle\, \langle j|s\rangle \tag{21.11}$$

where the $\langle j'|\, j\rangle$ term represents the probability amplitude of transmission via the fiber's plane. In reality, this is an undetermined spatially un-symmetric transmission that results in the alteration of the original interferometric pattern. Under those circumstances, and using the wave function notation of Chapter 4, the probability amplitude has the form of

$$\langle d|\, s\rangle' = \sum_{j'=1}^{N} \Psi(r_{j'}) e^{-i\Lambda_{j'}} \sum_{j=1}^{N} \Psi(r_j) e^{-i\Omega_j} \tag{21.12}$$

An alternative and complementary description is to think of $\langle j'|\, j\rangle$ as representing the propagation from the grating to the new plane established by two narrowly separated large slits. The width of the separation corresponds to the diameter of the spider web fiber. Toward the sides, away from the fiber,

$$\langle j'|\, j\rangle \approx 1 \tag{21.13}$$

and Equation (21.10) reduces to

$$\langle d|\, s\rangle' \approx \sum_{j=1}^{N} \langle x|\, j\rangle\, \langle j|\, s\rangle \tag{21.14}$$

so that the interferometric probability distribution is very close to Equation (21.2) or

$$\left|\langle d|\, s\rangle'\right|^2 = \sum_{j=1}^{N} \Psi(r_j) \sum_{m=1}^{N} \Psi(r_m) e^{i(\Omega_m - \Omega_j)} \tag{21.15}$$

as shown in Figures 21.10 and 21.11.

However, in the strong interferometric regime and immediately around the spider web fiber $\langle j' | j \rangle$ alters the overall probability amplitude in a subtle but measurable manner leading to the beautiful effect illustrated in Figure 21.5 (measured) and Figure 21.9 (calculated). In that case, the probability amplitude given in Equation (21.11) applies.

From a dimensional perspective, the experiments described here document the unusual opportunity to softly prove, non-destructively, the intra-interferometric propagation using natural fibers with diameters 11–22 times smaller than the width of the grating slits.

21.5 ON THE QUANTUM MEASURER

Physics experiments are performed by experimental physicists or experimentalists. These experimentalists play a critical role in the quality of the measurements and the overall outcome of the experiment. The reasons for this dependence on the experimentalist, or the measurer, have been roughly enumerated as follows (Duarte, 2022):

1. The measurer decides what experiment to perform.
2. The measurer decides on what optics to select and on the quality of the optics. The measurer also decides on coherent sources, the measurement electronics, and its quality.
3. The experiment then depends on the skill of the measurer to optimally configure the experiment and to align the optics. As the experimental configuration is improved, the measurer performs fine and minute adjustments to optimize and thus reduce experimental errors. In a somewhat ineffable manner, it is as if a good experimenter gets *in tune* with the experiment almost intuitively knowing what optical element to adjust to compensate for a given temperature change, for instance.
4. Once the experiment is in progress, the measurer must ensure that the experiment is *free of external intrusions* that might alter the measurements. This is particularly so in the quantum situation since *external intrusions catastrophically demolish the superposition states*. This is entirely compatible with van Kampen's second theorem that emphasizes that quantum measurements must 'not be perturbed by observation' (van Kampen, 1998).
5. It is the implicit 'freedom of thought'†, or 'free will' of the experimentalist that leads to innovations, inventions, and discoveries.

In this brief exposition the words experimentalist, measurer, and observer, are equivalent. † Explicitly Feynman refers in his writing to 'freedom to doubt' (Feynman, 1998).

21.5.1 External Intrusions

The effect of external intrusions or 'observations' on a quantum experiment in progress can be illustrated via the superposition probability amplitude for the double-slit experiment. Expanding Equation (21.10) for $N = 2$

$$\langle d|\, s\rangle = \langle d|\, 2\rangle\, \langle 2|\, s\rangle + \langle d|\, 1\rangle\, \langle 1|\, s\rangle \tag{21.16}$$

will lead to an interferometric probability distribution as shown in Figure 21.2. This superposition depends on a single unified detection plane d. Introducing a second 'observation' detector d_2, in the intra-interferometric space $D_{\langle d|j\rangle}$, nearby slit 2, as illustrated in Figure 21.12, and labeling the original unified detector d as d_1 leads to the following superposition probability amplitude

$$\langle d_1|\, s\rangle = \langle d_1|\, d_2\rangle\, \langle d_2|\, 2\rangle\, \langle 2|\, s\rangle + \langle d_1|\, d_2\rangle\, \langle d_2|\, 1\rangle\, \langle 1|\, s\rangle + \langle d_1|\, 2\rangle\, \langle 2|\, s\rangle + \langle d_1|\, 1\rangle\, \langle 1|\, s\rangle \tag{21.17}$$

The probability amplitude for a photon arriving at d_2 to reach d_1 is close to zero since any photon reaching d_2 is absorbed by this detector. Thus $\langle d_1|\, d_2\rangle \approx 0$ and

$$\langle d_1|\, s\rangle \approx \langle d_1|\, 2\rangle\, \langle 2|\, s\rangle + \langle d_1|\, 1\rangle\, \langle 1|\, s\rangle \tag{21.18}$$

It can also be argued that the weight of $\langle d_1|\, 2\rangle\, \langle 2|\, s\rangle$ will be diminished, given the proximity of d_2 to slit 2, leading to a distorted interferogram, thus informing the measurer of the presence d_2. In the *extreme case* of $\langle d_1|\, 1\rangle\, \langle 1|\, s\rangle >> \langle d_1|\, 2\rangle\, \langle 2|\, s\rangle$

$$\langle d_1|\, s\rangle \approx \langle d_1|\, 1\rangle\, \langle 1|\, s\rangle \tag{21.19}$$

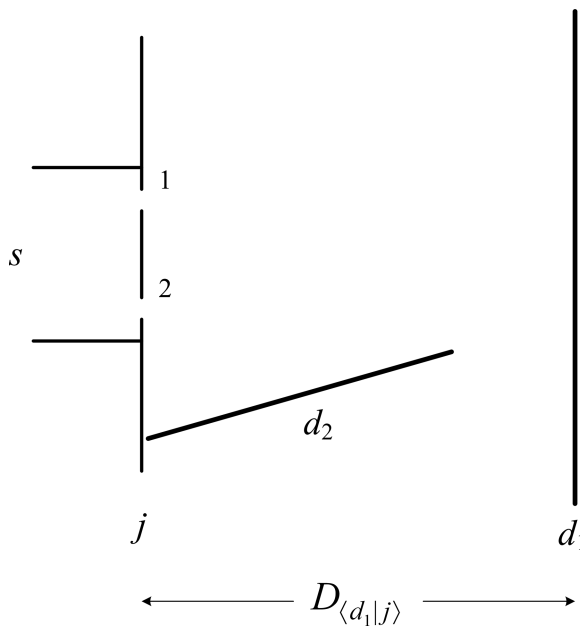

FIGURE 21.12 Double-slit experiment incorporating additional d_2 detector in the $D_{\langle d_1|j\rangle}$ intra-interferometric space.

$$\left|\langle d_1|s\rangle\right|^2 \approx \left|\langle d_1|1\rangle\langle 1|s\rangle\right|^2 \tag{21.20}$$

which is a non-interferometric probability. In other words, the interference distribution of Equation (21.18) tends to disappear.

Positioning d_2 symmetrically above or below the slits leads to interferometric distributions at both d_1 and d_2.

21.6 QUANTUM ENTROPY

The generalized interferometric quantum probability Equations (21.2) and (21.3) intrinsically incorporate information about time (Duarte and Taylor 2021). For an infinitesimally short intra interferometric propagation distance $D_{\langle d|j\rangle}$ the propagation time $t_{\langle d|j\rangle}$can be very short. For instance for $D_{\langle d|j\rangle} = 1\,\mu\text{m}$ the propagation time is $t_{\langle d|j\rangle} \approx 3.33\times10^{-15}$ s. For $D_{\langle d|j\rangle} = 1\,\text{mm}$ the propagation time is $t_{\langle d|j\rangle} \approx 3.33\times10^{-12}$ s and for $D_{\langle d|j\rangle} = 10$ m the propagation time is $t_{\langle d|j\rangle} \approx 3.33\times10^{-8}$ s, and so on. Then it can be easily envisioned that the interferometric quantum probability equation can be used to characterize the *arrow of time* in the interferometric regime. Consequently, a highly structured interferogram measured at $D_{\langle d|j\rangle} = 1\,\text{mm}$, let us say, represents a lower entropy regime than a smoother interferogram measured at $D_{\langle d|j\rangle} = 10\,\text{m}$.

Furthermore, it is possible to use the information provided by a measured interferogram at $D_{\langle d|j\rangle} = 10\,\text{m}$, let us say, plus the preexisting parameters of the interferometer N, λ, slit width, and slit separation, to *go back in time* and reconstruct an interferogram at $D_{\langle d|j\rangle} = 1\,\text{mm}$, let us say. Thus the transition in time is from $t_{\langle d|j\rangle} \approx 3.33\times10^{-8}$ s to $t_{\langle d|j\rangle} \approx 3.33\times10^{-12}$ s. This reconstruction of interferograms at earlier times was first suggested for interferometric measurements applied to imaging (Duarte, 1995).

21.7 DISCUSSION

The soft proving technique described here illustrates that an interferogram can be delicately contacted in a non-destructive manner by a microscopic semi-transparent fiber.

Illumination of the N-slit array by a single photon means that a single photon illuminates the N-slit array and that probability amplitudes $\langle d|j\rangle$ are generated at each slit. In this case, insertion of a detecting micro-fiber, or a detecting nanofiber, results in the alteration of the superposition probability amplitude and the transformation of the interferogram.

Illumination of the N-slit array by an ensemble of indistinguishable photons means that the ensemble generates indistinguishable probability amplitudes at each slit.

Insertion of a detecting micro-fiber, or a detecting nanofiber, results in the generation of new superposition probability amplitudes, such as $\langle d|s\rangle'$.

Once the idea that a single photon illuminates the whole N-slit array is accepted, the questions of 'which hole' or 'which slit' the photon went through does not apply – it does not arise. Similarly, once the idea that an ensemble of indistinguishable photons illuminates the whole N-slit array simultaneously, the question of 'which hole' or 'which slit' the photon went through is irrelevant. What is relevant are the $\langle d|j\rangle$ probability

amplitudes that contribute to the final $\langle d|s\rangle$ superposition probability amplitude that provide the measurable $\langle d|s\rangle\langle d|s\rangle^*$.

The laws of quantum mechanics, *á la Dirac*, perfectly predict and/or reproduce the measurements at hand be it in straightforward interferometric propagation, via an *N*-slit array, or via propagation through an *N*-slit array followed by a soft probing optics as characterized by a transparent microscopic fiber.

Key to the correct interpretation of the interplay between superposition quantum probability amplitudes, *á la Dirac*, and measurements is the description of the photon as a nonlocal coherent energy entity.

PROBLEMS

21.1 Show that Equation (21.2) can be expressed as Equation (21.3).

21.2 In addition to the list provided in Section 21.2, provide three further examples, from the open literature, of photon-based, irreversible quantum measurements.

21.3 Rewrite the probability amplitude given in Equation (21.7) in density matrix notation. That is, as $|\psi\rangle\langle\psi|$.

21.4 Rewrite the density matrix given in Equation (21.8) in the usual probability amplitude notation. That is, simply as $|\psi'\rangle$.

21.5 For $N = 2$, expand Equation (21.11) and multiply it by its complex conjugate to obtain the corresponding probability.

21.6 Extend the equations of Section 21.5.1 to the generalized case of *N* slits.

REFERENCES

Aspect, A., Grangier, P., and Roger, G. (1982). Experimental test of Bell's inequalities using time-varying analyzers. *Phys. Rev. Lett.* **49**, 1804–1807.

Bell, J. S. (1990). Against measurement. *Phys. World* **3** (8), 33–39.

Born, M. (1926). Zur quantenmechanik der stoßvorgänge. *Z. Phys.* **37**, 863–827.

Dirac, P. A. M. (1958). *The Principles of Quantum Mechanics*, 4th ed. Oxford University, Oxford, U.K.

Duarte, F. J. (1991). Dispersive dye lasers. In *High Power Dye Lasers* (Duarte, F. J., ed.). Springer, Berlin, Chapter 2, pp. 7–43.

Duarte, F. J. (1993). On a generalized interference equation and interferometric measurements. *Opt. Commun.* **103**, 8–14.

Duarte, F. J. (1995). Interferometric imaging. In *Tunable Laser Applications*, (Duarte, F. J., ed.). Marcel Dekker, New York, pp. 153–178.

Duarte, F. J. (2002). Secure interferometric communications in free space. *Opt. Commun.* **205**, 313–319.

Duarte, F. J. and Taylor T. S. (2021). *Quantum Entanglement Engineering and Applications*, Institute of Physics, Bristol, U. K.

Duarte, F. J. (2004). Comment on 'reflection, refraction and multislit interference'. *Eur. J. Phys.* **25**, L57–L58.

Duarte, F. J. (2005). Secure interferometric communications in free space: enhanced sensitivity for propagation in the metre range. *J. Opt. A: Pure Appl. Opt.* **7**, 73–75.

Duarte, F. J. (2022). *Fundamentals of Quantum Entanglement*, 2nd ed. Institute of Physics, Bristol, U.K.

Duarte, F. J., Taylor, T. S., Black, A. M., Davenport, W. E., and Varmette, P. G. (2011). *N*-slit interferometer for secure free-space optical communications: 527 m intra interferometric path length. *J. Opt.* **13**, 035710.

Duarte, F. J., Taylor, T. S., Black, A. M., and Olivares, I. E.. (2013). Diffractive patterns superimposed over propagating N-slit interferograms. *J. Mod. Opt.* **60**, 136–140.

Duarte, F. J., Taylor, T. S., Clark, A. B., and Davenport, W. E. (2010). The *N*-slit interferometer: an extended configuration. *J. Opt.* **12**, 015705.

Dyson, F. J. (2007). Why is Maxwell's theory so hard to understand? In *Proceedings of 2nd European Conferfence on Antennas and Propagation*, EuCAP, Edinburgh, U.K.

Feynman, R. P. (1998). *The Meaning of It All*, Addison-Wesley, Reading, MA.

Gobby, C., Yuan, Z. L., and Shields, A. J. (2004). Quantum key distribution over 122 km of standard telecom fiber. *Appl. Phys. Lett*. **84**, 3762–3764.

Feynman, R. P., Leighton, R. B., and Sands, M. (1965). *The Feynman Lectures on Physics*, Vol. **I**, Addison-Wesley, Reading, MA.

Lamb, W. E. (1986). Theory of quantum mechanical measurements. In *Proceeding of the 2nd International Symposium Foundations of Quantum Mechanics*, Physical Society of Japan, Tokyo, pp. 185–192.

Lamb, W. E. (1989). Classical measurements on a quantum mechanical system. *Nucl. Phys. B*. **6**, 197–201.

Lamb, W. E. (1995). Anti-photon. *Appl. Phys. B*. **60**, 77–84.

Ma, X., Herbst, T., Scheidl, T., Wang, D., Kropatschek, S., Naylor, W., Mech, A., Wittmann, B., Koer, J., Anisimova, E., Makarov, V., Jennewein, T., Ursin, R., and Zeilinger, A. (2012). Quantum teleportation over 143 kilometres using active feed-forward. *Nature* **489**, 269–273.

van Kampen, N. G. (1988). Ten theorems about quantum mechanical measurements. *Phys. A*. **153**, 97–113.

von Neumann, J. (1932). *Mathematical Foundations of Quantum Mechanics*, Springer, Berlin.

Wu, C. S., and Shaknov, I. (1950). The angular correlation of scattered annihilation radiation. *Phys. Rev.* **77**, 13.

22 Quantum Principles and the Probability Amplitude

22.1 INTRODUCTION

In this chapter, we summarize the fundamental principles of quantum mechanics from an interferometric perspective. The approach followed here provides a compendium of principles most of which are mathematical. The material in this chapter is based on discussions on this subject matter published previously by Duarte (2014, 2019, 2022).

22.2 FUNDAMENTAL PRINCIPLES OF QUANTUM MECHANICS

From a quantum interference and quantum entanglement perspective, where the *nonlocality* of the photon takes center stage, the fundamental principles of quantum mechanics can be listed as follows:

1. The *probability amplitude* for a single quantum, or an ensemble of r indistinguishable quanta, is given by the Dirac–Feynman interferometric superposition probability amplitude (Feynman et al., 1965)

$$\langle d|s\rangle = \sum_{j=1}^{N} \langle d|j\rangle \langle j|s\rangle \tag{22.1}$$

   The sum from $j = 1$ to $j = N$ in this superposition series means that *every* propagation path must be incorporated in the calculation.
2. The *principle of superposition*: 'Any state may be considered as the result of a superposition of two or more other states… conversely any two or more states may be superposed to give a new state' (Dirac, 1958). Feynman refers to the j states as base states… 'any state in the world can be expressed as a superposition… of base states' (Feynman et al., 1965). The Dirac–Feynman interferometric principle, expressed in Equation (22.1), is the essence of superposition.
3. Theorem: *The interferometric probability amplitude for a single quantum is* mathematically identical to the interferometric probability amplitude for an ensemble of *indistinguishable quanta*.
4. The probability amplitudes are represented by complex wave functions of the form (Dirac, 1958)

$$\Psi(x,t) = \Psi_0 e^{-i(\omega t - kx)} \tag{22.2}$$

DOI: 10.1201/9781003398707-22

or

$$\langle j|\, s\rangle = \Psi(r_{j\leftarrow s})e^{-i\theta} \tag{22.3}$$

$$\langle d|\, j\rangle = \Psi(r_{d\leftarrow j})e^{-i\varphi} \tag{22.4}$$

These complex wave functions assume a fundamental role in the theory. Note that since we are dealing here only with non-local quanta the use of the Schrödinger equation does not arise.

5. Additional Dirac principles as outlined by Feynman et al. (1965)

$$\langle d|\, s\rangle = \langle s|\, d\rangle^{*} \tag{22.5}$$

$$\langle j|\, i\rangle = \delta_{ji} \tag{22.6}$$

6. *Reversibility*: The physics of quantum mechanics is *reversible*. The probability amplitude for quantum entanglement can be derived from the Dirac–Feynman principle (Duarte, 2013a, 2019)

$$\langle d|\, s\rangle = \sum_{j=1}^{N} \langle d|\, j\rangle\, \langle j|\, s\rangle \rightarrow |\psi\rangle = 2^{-1/2}\left(|x\rangle_1 |y\rangle_2 \pm |y\rangle_1 |x\rangle_2\right) \tag{22.7}$$

or *vice versa* (Duarte 2019)

$$|\psi\rangle = 2^{-1/2}\left(|x\rangle_1 |y\rangle_2 \pm |y\rangle_1 |x\rangle_2\right) \rightarrow \langle d|\, s\rangle = \sum_{j=1}^{N} \langle d|\, j\rangle\, \langle j|\, s\rangle \tag{22.8}$$

7. Dirac's identity for indistinguishable quanta in different states (Dirac, 1958)

$$|X\rangle = |a\rangle_1 |b\rangle_2 |c\rangle_3 \ldots |g\rangle_n \tag{22.9}$$

8. *Nonlocality of the photon*: 'Photons cannot be localized… and they do not behave at all like particles' (Lamb, 1995). This is totally compatible with Heisenberg's uncertainty principle.
9. *Heisenberg's uncertainty principle* (Heisenberg, 1927)

$$\Delta p\, \Delta x \approx h \tag{22.10}$$

10. *Born's rule*: The probability is given by multiplying the probability amplitude with its complex conjugate (Born, 1926)

$$\left|\langle d|\, s\rangle\right|^2 = \langle d|\, s\rangle\, \langle d|\, s\rangle^{*} \tag{22.11}$$

Quantum probabilities are measurable quantities. It is Born's rule that allows the probability amplitudes to become measurable probabilities.

11. *Measurables*: the measured intensity I, at a given frequency ν, is proportional to the quantum probability

$$I \propto \langle d|s\rangle \langle d|s\rangle^* \tag{22.12}$$

Intensity is given in units of energy per square meter per second ($J/m^2/s^1$). Besides intensities and quantum probabilities, polarizations are also measurable quantities.

12. The energy of a single photon is given by Planck's quantum energy equation (Planck, 1901)

$$E = h\nu \tag{22.13}$$

For an ensemble or population of r indistinguishable photons, the energy is given by

$$E = rh\nu \tag{22.14}$$

These straightforward principles of quantum mechanics provide the foundations of the knowledge needed to quantify generalized quantum interference and generalized quantum entanglement.

In summary, from our perspective, the absolute essentials of quantum mechanics are the Dirac–Feynman principle, probability amplitudes represented by complex wave functions, Dirac's identity for indistinguishable quanta, Born's rule, Heisenberg's uncertainty principle, Planck's energy, and the nonlocality of the photon.

22.3 PROBABILITY AMPLITUDES

Probability amplitudes, *à la Dirac*, exist in a mathematical realm described by *imaginary numbers* and *complex numbers*, and yet they intrinsically contain information about *space* and *time*. For instance, the probability amplitude $\langle d|j\rangle$ describes the propagation, of a photon, in space from plane j to plane d. Since the photon propagates at a speed c then, information about time is also encoded in $\langle d|j\rangle$.

Expansion of the Dirac–Feynman interferometric principle equation, Equation (22.1), leads to

$$\langle d|s\rangle = \langle d|1\rangle \langle 1|s\rangle + \langle d|2\rangle \langle 2|s\rangle + \langle d|3\rangle \langle 3|s\rangle \ldots + \langle d|N\rangle \langle N|s\rangle \tag{22.15}$$

For instance, for a transmission grating including two thousand slits, that is $N = 2000$, the interaction of every slit, with every other slit, must be included in the calculation of $\langle d|s\rangle \langle d|s\rangle^*$ to obtain the correct intensity distribution as judged by the measurement. In other words, the probability amplitude description must accurately and faithfully represent the physical configuration at hand (Duarte, 1993).

If the physics is modified even in the most minute manner, let's say via the insertion of a single strand of a transparent microscopic fiber, then the probability amplitude is immediately transformed and becomes (Duarte et al., 2013, Duarte 2019)

$$\langle d|s\rangle = \sum_{j=1}^{N} \langle d|k\rangle \langle k|j\rangle \langle j|s\rangle \tag{22.16}$$

This probability amplitude introduces three intra-interferometric propagation distances $D_{\langle j|s\rangle}$, $D_{\langle k|j\rangle}$, and $D_{\langle d|k\rangle}$ rather than the two original intra-interferometric distances $D_{\langle j|s\rangle}$ and $D_{\langle d|j\rangle}$. The microscopic transparent fiber allows *information to be extracted* from the propagating interferogram. Thus, the original propagating interferogram described by Equation (22.1) ceases to exist and immediately a new interferogram, described by Equation (22.16), is observed (Duarte et al., 2013; Duarte 2019, 2022).

Here, there is a profound observation to be made: albeit probability amplitudes exist in the mathematical realm dominated by imaginary numbers and complex numbers, experimental measurements demand an accurate and detailed description of the physics configuration via probability amplitudes. For a relevant description of imaginary and complex numbers, see Appendix G.

22.3.1 Probability Amplitude Refinement

In 1975, Dirac, while on a visit to Australia, did refer to a possible improvement to quantum mechanics without further elaboration. In 1949, Born hinted that the 'indeterministic foundations will be permanent' (Born, 1949).

From our perspective, an 'improvement' to quantum mechanics means further revelation of physical details… *a refined spatial accuracy.* As suggested by Duarte (2022), this can already be achieved indeterministically via the Dirac–Feynman interferometric principle since

$$\langle d|\, s\rangle = \sum_{j=1}^{N} \langle d|\, j\rangle\, \langle j|\, s\rangle$$

can be applied to further diminishing spatial dimensions or to provide greater and greater spatial detail. In the case of the *N*-slit coherent interferometer, for instance, *a single slit* in the *j* array can be further finessed as being comprised of 200 subslits, 400 subslits, or 800 subslits (Duarte, 1993, 2022). It is found, however, that depending on the wavelength λ, there is an optimum correspondence between theory and experiment beyond which no further improvements in the spatial information of the interferometric distribution are gained. The experiment reigns, Nature reigns.

The Dirac–Feynman interferometric principle has been successfully applied to *N*-slit interferometers with intra-interferometric distances in the $0.1 \leq D_{\langle d|j\rangle} \leq 527$ m range with slit widths in the $50 \leq \Delta w \leq 1000$ μm range for wavelengths in the visible.

This range of applicability has been extended via the design of nanometer *N*-slit interferometers, for the assessment of fibers with diameters in the femtometer (fm) regime. In these nano interferometers, $D_{\langle d|j\rangle} = 7.5$ nm and $\Delta w = 0.01$ nm, for γ-ray illumination at $\lambda \approx 100$ fm (Duarte and Olivares, 2023). Indeed, the only 'limitation' to the applicability of the Dirac–Feynman superposition probability amplitude appears to be provided by Nature itself via the availability of photon wavelengths. Any observation of wavelengths shorter than γ-rays will open up further refinements and further application regimes. In principle, the only wavelength limit appears to be provided by Planck's length. This brings into attention Feynman's sentence 'there is plenty of room at the bottom' (Feynman, 1960).

22.4 FROM PROBABILITY AMPLITUDES TO PROBABILITIES

Born's rule is crucial to quantum mechanics: $\left|\langle d|s\rangle\right|^2 = \langle d|s\rangle\langle d|s\rangle^*$ is the key that takes us from the mathematical realm of superposition probability amplitudes to the measurable physical realm of probabilities, intensities, and polarizations.

The superposition probability amplitude

$$\langle d|s\rangle = \langle d|1\rangle\langle 1|s\rangle + \langle d|2\rangle\langle 2|s\rangle + \langle d|3\rangle\langle 3|s\rangle \ldots + \langle d|N\rangle\langle N|s\rangle$$

evolves unperturbed until the measurement is performed. At that precise instant, $\langle d|s\rangle$ is multiplied with its complex conjugate, thus giving rise to the probability $\langle d|s\rangle\langle d|s\rangle^*$ which in turn allows the intensity measurement via

$$I(\nu) = \mathrm{K}\, h\nu\, \langle d|s\rangle\langle d|s\rangle^* \tag{22.17}$$

$$I(\nu) = \mathrm{K}\, h\nu \sum_{j=1}^{N} \Psi(r_j) \sum_{m=1}^{N} \Psi(r_m) e^{i(\Omega_m - \Omega_j)} \tag{22.18}$$

For a population of indistinguishable photons, or an ensemble of r indistinguishable photons, the intensity is simply modified to

$$I(\nu)_r = r\,\mathrm{K}\, h\nu\ \langle d|s\rangle\langle d|s\rangle^* \tag{22.19}$$

$$I(\nu)_r = r\,\mathrm{K}\, h\nu \sum_{j=1}^{N} \Psi(r_j) \sum_{m=1}^{N} \Psi(r_m) e^{i(\Omega_m - \Omega_j)} \tag{22.20}$$

For $n = N = 2$ quantum entanglement, as described in Figure 22.1, the superposition probability amplitude is

$$|\psi\rangle_- = 2^{-1/2}\left(|x\rangle_1|y\rangle_2 - |y\rangle_1|x\rangle_2\right) \tag{22.21}$$

The superposition probability $P(\varphi_1, \varphi_2)$ is calculated by multiplying the superposition $|\psi\rangle$ with its complex conjugate $|\psi\rangle^*$, according to Born's rule, so that (Pryce and Ward, 1947)

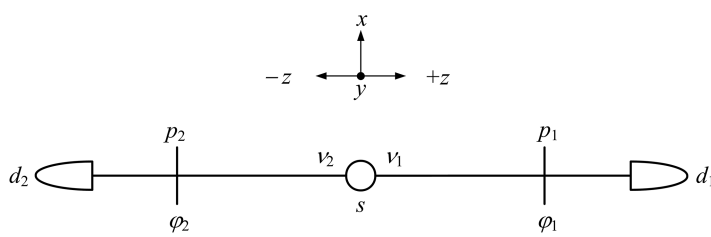

FIGURE 22.1 Generic two-photon entanglement experimental configuration. φ_1 and φ_2 refer to the orientation of the polarizers.

$$P(\varphi_1, \varphi_2) = |\psi\rangle|\psi\rangle^* \tag{22.22}$$

$$P(\varphi_1, \varphi_2) = -\cos 2(\varphi_1 - \varphi_2) \tag{22.23}$$

It should be emphasized that at no time, it is necessary to invoke a 'collapse of the wave function' or a 'collapse of the probability amplitude' to obtain the correct physics in agreement with the measurement. Furthermore, neither Dirac nor Feynman devotes space to 'the collapse of the wave function' in their iconic books (Dirac, 1958; Feynman et al., 1965).

22.4.1 Interferometric Cascade

It is useful to consider an interferometric cascade approach when propagating from one interferometric plane to another interferometric plane and so on (Duarte, 1993). Thus, the quantum interferometric probability distribution generated at the initial plane becomes the input at the subsequent plane. Assuming that the input interferometric probability is

$$P(\lambda, N, \Omega) = \sum_{j=1}^{N} \vartheta(r_j) \sum_{m=1}^{N} \vartheta(r_m) e^{i(\Omega_m - \Omega_j)} \tag{22.24}$$

the corresponding intensity is given by

$$I(P, \nu) = \mathrm{K}\, h\nu\, P(\lambda, N, \Omega) \tag{22.25}$$

If the undisturbed propagating interferogram, described by Equation (22.25), is allowed to illuminate a new interferometric plane (j), composed of N slits, a whole new array of probability amplitudes is generated (see Figure 22.2). Once this interaction occurs, the original $I(P, \nu)$ distribution gives origin to a whole new *array* of probability amplitudes represented by $\langle d|\, j\rangle\langle j|\, s\rangle$, where s is the source and d the new interferometric plane.

The new series of probability amplitudes is described by the Dirac–Feynman principle

$$\langle d|\, s\rangle = \sum_{j=1}^{N} \langle d|\, j\rangle\, \langle j|\, s\rangle$$

and the corresponding probability becomes

$$\left|\langle d|\, s\rangle\right|^2 = \sum_{j=1}^{N} \Psi(r_j) \sum_{m=1}^{N} \Psi(r_m) e^{i(\Omega_m - \Omega_j)} \tag{22.26}$$

Thus, the new probability distribution at d is given

$$\mathcal{P}(\lambda, N, \Omega) = \left|\langle d|\, s\rangle\right|^2 \tag{22.27}$$

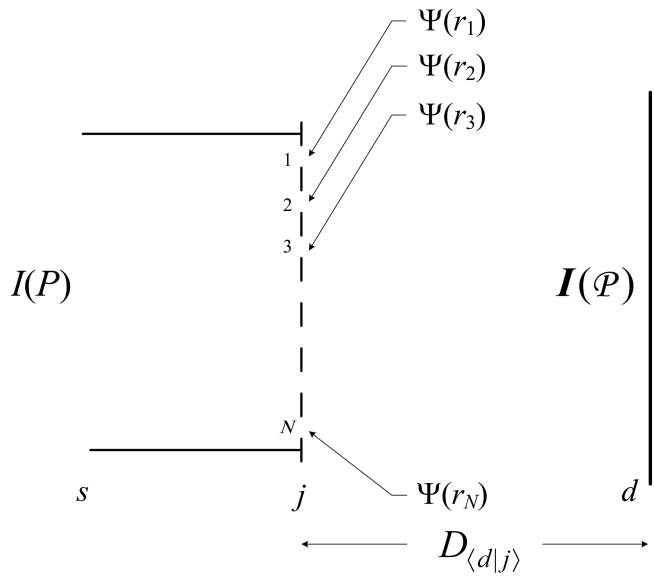

FIGURE 22.2 Interferometric intensity distribution $I(P)$interacts with an N-slit array thus producing a new interferometric intensity distribution $I(\mathscr{P})$. Wave function $\Psi(r_1)$ is associated with slit $j=1$, $\Psi(r_2)$with $j=2$, $\Psi(r_3)$ is with $j=3$, and so on.

and the new intensity distribution is given by

$$\boldsymbol{I}(\mathscr{P}) = \mathrm{K}\,\mathscr{P}(\lambda, N, \Omega) \tag{22.28}$$

In summary, a measurable interferometric distribution $I(P)$ interacts with a new interferometric array ($j=1,2,3,\ldots N$), thus creating a whole new series of probability amplitudes. This new series of probability amplitudes are represented by a corresponding series of complex wave functions

$$\Psi(r_{\mathrm{l}1}), \Psi(r_2), \Psi(r_3), \ldots \Psi(r_N)$$

Immediately following passage of the N-slit array, and due to diffraction, these wave functions become entangled and give rise to a new measurable interferometric intensity distribution as described by Equations (22.26)–(22.28).

22.5 NONLOCALITY OF THE PHOTON

The nonlocality of the photon is crucial to the correct understanding of quantum interferometry and quantum entanglement. Heisenberg's uncertainty principle

$$\Delta p\, \Delta x \approx h \tag{22.29}$$

leads directly to the space–frequency identity

$$\Delta\nu\,\Delta x \approx c \tag{22.30}$$

This is quite real to any observant experimental physicist who has made linewidth measurements using a Mach–Zehnder interferometer, for instance. If this interferometer is configured to measure the $\Delta\nu$ from a narrow-linewidth laser, then the overall linear space of intra-interferometric distance for which interference will be observed is $\Delta x \approx c/\Delta\nu$. If the length of the arms of the interferometer is less than $\Delta x \approx c/\Delta\nu$, then interference will not be observed.

Single photons exhibit extremely narrow linewidths and correspondingly can exhibit *enormous* coherence lengths. In a $n = N = 2$ quantum entanglement configuration, two indistinguishable, extremely narrow-linewidth photons, are emitted in opposite directions. This extremely narrow linewidth allows an extremely large coherence length determined by $\Delta x \approx c/\Delta\nu$. Hence, the emitted quanta will continue to interact after emission from their common source. Photon nonlocality has yet to be fully explored experimentally.

Following Lamb's lead on the nonlocality of the photon (Lamb, 1995), the statement 'All the indistinguishable photons illuminate the array of *N* slits, or grating, simultaneously. If only one photon propagates, at any given time, then that individual photon illuminates the whole array of *N* slits simultaneously' (Duarte, 2003) comes into focus. Nonlocality of the photon is a unique quantum feature completely at odds with traditional 'classical expectations' (Duarte, 2022).

It should be added that in quantum interferometric surroundings, not even the electron behaves like a particle.

22.6 INDISTINGUISHABILITY AND DIRAC'S IDENTITIES

As described in Chapter 15, crucial to the interferometric derivation of the quantum entanglement probability amplitude (Duarte, 2013a, 2013b, 2014) is the Dirac identity (Dirac, 1958)

$$|X\rangle = |a\rangle_1 |b\rangle_2 |c\rangle_3 \ldots |g\rangle_n \tag{22.31}$$

which refers to quanta of the 'absolutely indistinguishable from one another' (Dirac, 1958). At the same time, he is also contemplating arrays of *identical* quanta in different states such as $|a\rangle_1, |b\rangle_1, |c\rangle_1 \ldots$ and $|a\rangle_2, |b\rangle_2, |c\rangle_2 \ldots$. Extension of these ideas leads to the expression of identities of the form (Duarte, 2022)

$$|Y\rangle = |a\rangle_1 |b\rangle_1 |c\rangle_1 \ldots |g\rangle_1 \tag{22.32}$$

and

$$|Z\rangle = |a\rangle_2 |b\rangle_2 |c\rangle_2 \ldots |g\rangle_2 \tag{22.33}$$

that describe indistinguishable, quanta in different states. In turn, this allows the description of a series of indistinguishable quanta in identical states such as

$$|\alpha\rangle = |x\rangle_1 |x\rangle_2 |x\rangle_3 \ldots |x\rangle_n \tag{22.34}$$

and

$$|\beta\rangle = |y\rangle_1 |y\rangle_2 |y\rangle_3 \ldots |y\rangle_n \tag{22.35}$$

These Diracian identities are directly applicable to the description of single-transverse-mode single-longitudinal-mode laser beams comprised by ensembles of indistinguishable quanta. The state $|\alpha\rangle$ describes an ensemble of indistinguishable quanta in the $|x\rangle$ state of polarization while the state $|\beta\rangle$ describes an ensemble of indistinguishable quanta in the $|y\rangle$ state of polarization. These concepts have been applied to describe highly coherent directional emission from electrically-pumped organic semiconductors within an interferometric configuration (Duarte and Taylor, 2022).

22.7 QUANTUM ENTANGLEMENT AND THE FOUNDATIONS OF QUANTUM MECHANICS

The generalized equations for quantum entanglement can be expressed as (Duarte, 2016, 2019; Duarte and Taylor, 2017)

$$|\psi\rangle_R = N^{-1/2} \sum_{j=1}^{N} (\pm) |C\rangle_{N+1-j} \tag{22.36}$$

$$1 = \left| |\psi\rangle_I \right|^2 + \left| |\psi\rangle_{II} \right|^2 + \left| |\psi\rangle_{III} \right|^2 + \left| |\psi\rangle_{IV} \right|^2 + \ldots \tag{22.37}$$

$$|C\rangle_{N+1-j} = \prod_{m=1,\,3,\,5\ldots}^{n} |a\rangle_m |b\rangle_{m+1} \tag{22.38}$$

For $n = N = 2$, these equations reduce to

$$|\psi\rangle = 2^{-1/2} \left(|x\rangle_1 |y\rangle_2 \pm |y\rangle_1 |x\rangle_2 \right) \tag{22.39}$$

In Chapter 15, it was shown that

$$\sum_{j=1}^{N} \langle d|\, j\rangle\, \langle j|\, s\rangle \rightarrow 2^{-1/2} \left(|x\rangle_1 |y\rangle_2 \pm |y\rangle_1 |x_2\rangle \right) \tag{22.40}$$

flows naturally while utilizing the Dirac identities $|C\rangle_2 = |y\rangle_1 |x\rangle_2$ and $|C\rangle_1 = |x\rangle_1 |y\rangle_2$ (Duarte, 2013a, 2013b, 2014, 2016).

Given the reversibility of quantum mechanical equations,

$$2^{-1/2}\left(|x\rangle_1|y\rangle_2 \pm |y\rangle_1|x\rangle_2\right) \rightarrow \sum_{j=1}^{N}\langle d|\, j\rangle\,\langle j|\, s\rangle \tag{22.41}$$

is also clear and transparent. However, the derivation of the superposition probability amplitude for quantum entanglement, via non-interferometric physics, involves extra mathematical steps so that (Duarte, 2019, 2022)

$$\sum_j H_{ij}C_j \rightarrow \sigma_x, \sigma_y \rightarrow 2^{-1/2}(|x\rangle_1|y\rangle_2 \pm |y\rangle_1|x\rangle_2) \rightarrow \sum_{j=1}^{N}\langle d|\, j\rangle\,\langle j|\, s\rangle \tag{22.42}$$

This observation implies that quantum interference is a slightly more fundamental principle.

Assuming that

$$\langle d|\, s\rangle = \sum_{j=1}^{N}\langle d|\, j\rangle\,\langle j|\, s\rangle$$

and

$$|\psi\rangle = 2^{-1/2}\left(|x\rangle_1|y\rangle_2 \pm |y\rangle_1|x\rangle_2\right)$$

are both *intrinsic foundational principles* of quantum mechanics, then these two principles are inextricably and profoundly interconnected

$$\langle d|\, s\rangle = \sum_{j=1}^{N}\langle d|\, j\rangle\ \langle j|\, s\rangle\ \leftrightarrow\ |\psi\rangle_+, |\psi\rangle_-, |\psi\rangle^+, |\psi\rangle^- \leftrightarrow \sigma_x, \sigma_y, \sigma_z, I \tag{22.43}$$

at the most fundamental level.

22.8 THE DIRAC–FEYNMAN INTERFEROMETRIC PRINCIPLE

Feynman did not provide any mathematical derivation of the Dirac–Feynman principle

$$\langle d|\, s\rangle = \sum_{j=1}^{N}\langle d|\, j\rangle\,\langle j|\, s\rangle$$

The Dirac–Feynman principle describes *how Nature works* at its most fundamental level; thus, it is worth discussing its origin albeit briefly.

Duarte (2013a, 2014) shows that

$$\sum_{j=1}^{N}\langle d|\, j\rangle\,\langle j|\, s\rangle \rightarrow 2^{-1/2}\left(|y\rangle_1|y\rangle_2 \pm |y\rangle_1|x_2\rangle\right)$$

Furthermore (Duarte 2019; Duarte et al., 2020)

$$\sigma_x, \sigma_y, \sigma_z, I \rightarrow |\psi\rangle_+, |\psi\rangle_-, |\psi\rangle^+, |\psi\rangle^- \tag{22.44}$$

and (Duarte, 2022)

$$|\psi\rangle_+, |\psi\rangle_-, |\psi\rangle^+, |\psi\rangle^- \rightarrow \sum_{j=1}^{N} \langle d|j\rangle \langle j|s\rangle \tag{22.45}$$

Hence, there is a transparent mathematical path to arrive at the Dirac–Feynman principle, assuming that the quantum entanglement probability amplitude is the most fundamental mathematical–physical statement in quantum mechanics (Duarte, 2022).

PROBLEMS

22.1 Verify that $\langle d|s\rangle = \langle s|d\rangle^*$.

22.2 Show that $\Delta p\, \Delta x \approx h$ is equivalent to $\Delta \nu\, \Delta t \approx 1$.

22.3 Expand Equation (22.1) for $N = 2$ and provide an explicit expression for $\langle d|s\rangle \langle d|s\rangle^*$.

22.4 Nonlocality of the photon: what other interferometer, besides the Mach–Zehnder, can be used to determine the coherence length Δx of a narrow-linewidth laser?

22.5 Show that the generalized quantum entanglement Equation (22.36) reduces, for $n = N = 2$, to the probability amplitude for quantum entanglement given in Equation (22.39).

REFERENCES

Born, M. (1926). Zur quantenmechanik der stoßvorgänge. *Z. Phys*. **37**, 863–827.

Born, M. (1949). *Natural Philosophy of Cause and Chance*, Clarendon, Oxford, U.K.

Dirac, P. A. M. (1958). *The Principles of Quantum Mechanics*, 4th ed. Oxford University, Oxford, U.K.

Duarte, F. J. (1993). On a generalized interference equation and interferometric measurements. *Opt. Comm*. **103**, 8–14.

Duarte, F. J. (2003). *Tunable Laser Optics*, 1st ed. Elsevier-Academic, New York.

Duarte, F. J. (2013a). The probability amplitude for entangled polarizations: an interferometric approach. *J. Mod. Opt*. **60**, 1585–1587.

Duarte, F. J. (2013b). Tunable laser optics: applications to optics and quantum optics. *Prog. Quantum Electron*. **37**, 326–347.

Duarte, F. J. (2014). *Quantum Optics for Engineers*, 1st ed. CRC, Boca Raton, FL.

Duarte, F. J. (2016). Secure space-to-space interferometric communications and its nexus to the physics of quantum entanglement. *Appl. Phys. Rev*. **3**, 041301.

Duarte, F. J. (2019). *Fundamentals of Quantum Entanglement*, 1st ed. Institute of Physics, Bristol, U.K.

Duarte, F. J. (2022). *Fundamentals of Quantum Entanglement*, 2nd ed. Institute of Physics, Bristol, U.K.

Duarte, F. J. and Olivares, I. O. (2023). N-slit quantum interferometers in the nanometer domain. *Appl. Phys*. B. **129**, 88.

Duarte, F. J., and Taylor, T. S. (2017). Quantum entanglement probability amplitudes in multiple channels: an interferometric approach. *Optik* **139**, 222–230.

Duarte, F. J., and Taylor, T. S. (2022). Quantum coherence in electrically pumped organic interferometric emitters, *Appl. Phys. B*. **128**, 11.

Duarte, F. J., Taylor, T. S., Black, A. M., and Olivares, I. E. (2013) Diffractive patters superimposed over propagating N-slit interferograms. *J. Mod. Opt*. **60**, 136–140.

Duarte, F. J., Taylor, T. S., and Slaten, J. C. (2020). On the probability amplitude of quantum entanglement and the Pauli matrices. *Opt. Quantum Electron*. **52**, 106.

Feynman, R. P. (1960). There is plenty of room at the bottom. *Eng. Sci*. **23** (5), 22–36.

Feynman, R. P., Leighton, R. B., and Sands, M. (1965). *The Feynman Lectures on Physics*, Vol. III, Addison-Wesley, Reading, MA.

Heisenberg, W. (1927). Über den anschaulichen inhalt der quantentheoretishen kinematik und mechanic. *Z. Phys*. **43**, 172–198.

Lamb, W. E. (1995). Anti-photon. *Appl. Phys. B*. **60**, 77–84.

Planck, M. (1901). Ueber das gesetz der energieverteilung im normalspectrum. *Ann. Phys.* **309**, 553–563.

Pryce, M. L. H., and Ward, J. C. (1947). Angular correlation effects with annihilation radiation. *Nature* **160**, 435.

23 On the Interpretation of Quantum Mechanics

23.1 INTRODUCTION

The first edition of this book closed with the sentence: 'the most efficient and practical interpretation of quantum mechanics, is… *no interpretation at all*' (Duarte, 2014). Here, the issue of interpretation in quantum mechanics is revisited.

There is a large plethora of interpretations of quantum mechanics (Freire, 2022), and albeit this is a fascinating area of discussion, it is not our intention to enter this vast arena.

In this chapter, we adopt a pragmatic perspective of physics. Our approach to quantum mechanics is to use the Dirac principles, as presented by Dirac (1958) and further elucidated by Feynman et al. (1965), while being perfectly aware that it is *the experiment* that has the final say.

23.2 EINSTEIN PODOLSKY AND ROSEN (EPR)

In 1935, Einstein, Podolsky, and Rosen (1935) wrote a famous paper entitled *Can quantum mechanical description of physical reality considered complete?* This is a cleverly crafted document that argues, in essence, that in quantum mechanics '*when the momentum of a particle is known, its coordinate has no physical reality*' (Einstein et al., 1935). Subsequently, the authors go on to conclude that '*the quantum mechanical description of reality given by the wave function is not complete*' (Einstein et al., 1935).

In a reply, under the same title, Bohr (1935) uses Heisenberg's uncertainty principle and the principle of *complementarity* in an attempt to refute the argument of Einstein Podolsky and Rosen (EPR).

Although the matter was considered by many quantum physicists to have been resolved, Bohr's reply, in six-plus pages, was somewhat non-transparent and convoluted. Thus, it was not surprising that clever critics, such as Bell (1990), persisted in their criticism.

The central argument from Einstein et al., from now on referred to as EPR, is that '*when the momentum of a particle is known, its coordinate has no physical reality*' (Einstein et al., 1935). This is the essence of the EPR argument. It should also be added that EPR concluded their paper stating that 'we believe' that a 'complete description of physical reality' is possible (Einstein et al., 1935). It is that expressed belief that subsequently provided impetus to the development of *hidden variable theories* (HVTs).

DOI: 10.1201/9781003398707-23

As a historical note, it should be mentioned that it was Schrödinger (1935) who first related the EPR criticism toward quantum mechanics with the concept of *entanglement*.

Later on, it was Bohm and Aharanov (1957) who made the connection between the EPR argument and the polarization-based annihilation experiments of Wu and Shaknov (1950): 'we have essentially the same puzzling kind of correlations in the properties of distant particles, in which the property of anyone photon that is definite is determined by a measurement of a far away photon. Thus, the paradox of EPR can equally well be tested by polarization properties of pairs of photons' (Bohm and Aharanov, 1957).

However, Bohm and Aharanov did not cite Pryce and Ward (1947), who introduced the experimental schematics and calculated the correct quantum probability for polarization entanglement (Duarte, 2012).

23.3 HEISENBERG'S UNCERTAINTY PRINCIPLE AND EPR

'*When the momentum of a particle is known, its coordinate has no physical reality*' (Einstein et al., 1935) is the crucial component of the EPR argument. As mentioned previously, Bohr (1935) used both the principle of complementarity and Heisenberg's uncertainty principle in response to the EPR argument. However, Bohr did not develop a transparent direct response based on the uncertainty principle.

Here, a simple and direct approach to this issue is taken making explicit use of the uncertainty principle itself (Duarte, 2014). Heisenberg's uncertainty principle is given by (Dirac, 1958)

$$\Delta x \, \Delta p \approx h \tag{23.1}$$

and one of its alternative forms is (Feynman et al., 1965)

$$\Delta x \approx \frac{h}{\Delta p} \tag{23.2}$$

Now, if we measure the momentum p of a particle, we can only measure

$$p \pm \Delta p \tag{23.3}$$

An *absolutely exact measurement of momentum* p with $\Delta p = 0$ is *physically impossible* (Duarte, 2014). The presence of uncertainties and errors in measurements has been known to physicists since the dawn of physics and optics (Newton, 1687, 1704). The EPR sentence '*when the momentum of a particle is known, its coordinate has no physical reality*' (Einstein et al., 1935) implies an idealized *exact measurement* of momentum p with $\Delta p = 0$. Once a real physical measurement of momentum is made with a non-zero estimate of the error in the measurement, that is $p \pm \Delta p$, then the coordinate can be determined according to Heisenberg's uncertainty principle

$$\Delta x \approx \frac{h}{\Delta p} \tag{23.4}$$

and the '*all values*' spread in the coordinate, as feared by Einstein et al. (1935), is not allowed. Once the '*all values*' spread in the coordinate is found physically untenable, the claim of '*no physical reality*' is neutralized. Hence, the EPR conclusion that '*the quantum mechanical description of physical reality … is not complete*' can be negated.

In summary, the EPR claim of an '*all values*' spread in the coordinate depends on an idealized absolute and exact measurement of p with $\Delta p = 0$. Since this is physically impossible, the claim of '*no physical reality*' can be nullified.

While writing the first edition of this book (Duarte, 2014), we came across a paragraph in Dirac's book which very succinctly reinforces the argument made here: 'it is evident physically that a state for which all values of q are equally probable, or one for which all values of p are equally probable, cannot be attained in practice' (Dirac, 1958). Notice that the book we are using is a revised printing of the 1947 edition. This means that observant physicists such as Feynman, Lamb, and Ward might have been very much aware of the existence of this little-known Dirac dictum.

23.4 QUANTUM PHYSICISTS ON THE INTERPRETATION OF QUANTUM MECHANICS

Here we present the orthodox–pragmatic perspective on quantum mechanics followed by criticisms of orthodox quantum mechanics as articulated by EPR, Schrödinger, and Bell.

23.4.1 The Pragmatic Practitioners

Quantum mechanics is a wondrous branch of physics. As such, this section should begin by stating the thoughts John Clive Ward on quantum mechanics (Ward, 2004): '*The inner mysteries of quantum mechanics require a willingness to extend one's mental processes into a strange world of phantom possibilities, endlessly branching into more and more abstruse chains of coupled logical networks, endlessly extending themselves forward and even backwards in time.*' John Ward was one of those prominent quantum physicists who never expressed doubts about the correctness or effectiveness of quantum mechanics. Nor did he *bother* with issues of interpretation (Ward, 2004).

The interpretation of quantum mechanics has been the subject of many publications and books (Bell, 1988; Selleri, 1988; Wallace, 1996; Freire, 2022). In this section, a pragmatic perspective on this topic is presented that is mainly derived from Feynman's school of thought: '*unless a thing can be defined by measurement, it has no place in the theory*' and '*already in classical mechanics there was indeterminability*' (Feynman et al., 1965). In this regard, Feynman was keenly aware of the crucial role of Heisenberg's uncertainty principle in the formulation of quantum mechanics: '*the uncertainty principle protects quantum mechanics*' (Feynman et al., 1965).

Dirac was famously not impressed by discussions on the interpretation of quantum mechanics, and in one of his last papers he wrote, '*The interpretation of quantum*

mechanics has been dealt with by many authors, and I do not want to discuss it here. I want to deal with more fundamental things' (Dirac, 1987). Nevertheless, in a visit to Sydney, in August 1975, Dirac briefly did refer to the interpretation of quantum mechanics and did refer to the Bohr–Einstein controversy. In this regard, he went on to say that according to standard atomic physics, 'Bohr was right.' In this regard, he left open the possibility of some kind of improved quantum mechanics of the future (Duarte, 2012b). Born was of the opinion that for quantum mechanics 'its indeterministic foundations will be permanent' and added 'there remains now only to show how the ordinary, apparently deterministic laws of physics can be obtained from these foundations' (Born, 1949).

Willis Lamb, yet another noted quantum physicist, assigned the interpretational problems of quantum mechanics to '*historical misunderstandings*' (Lamb, 2001). In his broad critique, Lamb included the EPR argument in a list associated to these misunderstandings and went as far as describing Bell's inequalities as 'unnecessary' (Lamb, 2001). Certainly, Bell's theorem is not a factor in the derivation of the probability amplitude of quantum entanglement as described in Chapters 15–17 and previous publications (Duarte, 2013a, 2014).

For a while, many people criticized Dirac's description of interference due to the sentence: '*Each photon then interferes only with itself*' (Dirac, 1958). This sentence is the conclusion of an argument that begins by considering a beam of monochromatic light 'with a large number of photons' (Dirac, 1958). The beam is made to split into two components of equal intensity and then made to interfere (as in a Mach-Zehnder interferometer). Dirac then explains that each photon goes partially into each component and '*each photon then interferes with itself*' (Dirac, 1958). That is, each photon has a probability amplitude to propagate via each of the paths, and it is the addition of these probability amplitudes, multiplied with its corresponding complex conjugate, that accurately and correctly describes the observed interference patterns (Duarte, 1998, 2003). That is, Dirac writes about a beam of monochromatic light, with a large number of photons, which is equivalent to a single *narrow-linewidth* high-power laser beam.

This is equivalent to a laser beam comprised of a population of indistinguishable photons. The key principle here is that photon interference is a phenomenon that involves either single photons or *ensembles of indistinguishable photons*. In this regard, Dirac outlined the principles of laser interference back in 1947, and thus he should be considered the father of *laser optics* and *quantum optics* (Duarte, 2003).

Dirac's statement does not exclude interference between two different lasers as long as the emission from these two sources is indistinguishable. In other words, interference from two separate narrow-linewidth lasers at the same central wavelength will register with sharp high-contrast interferograms with high visibility approaching unity ($\mathcal{V} \approx 1$).

Going back to Dirac's observation about a possible future improved quantum mechanics: that might well be possible. However, that should not be necessary since, as discussed in Chapter 22, the Dirac–Feynman principle can be readily applied to yield unprecedented improvements in spatial finesse as demonstrated in the design of N-slit interferometers with dimensions in the nanometer regime using γ-ray quanta for metrology in the femtometer domain. It all depends on the availability of shorter

and shorter wavelengths (Duarte, 2022; Duarte and Olivares, 2023). van Kampen (1988) published a paper entitled *Ten theorems about quantum mechanical measurements*. Theorem I of van Kampen simply states, '*Quantum mechanics works*.' From the teaching of Born, Dirac, Feynman, Lamb, and Ward, two salient conclusions are provided: first, these luminaries were not concerned with the 'incompleteness' of quantum mechanics, and when they did refer to interpretational matters, they did so to reaffirm indeterminism, as in the case of Born, and to criticize alternative interpretations, as in the case of Lamb.

Note: the main pitfall incurred by critics of quantum mechanics while describing *N*-slit interference, which they mainly describe as 'two-slit interference,' is to erroneously think of the photon as a 'particle.' Via this basic error, they depart from Dirac's lucid description (Duarte, 2013b) and enter a path fraught with conceptual difficulties.

23.4.2 Bell's Criticisms

Criticisms toward orthodox quantum mechanics are nothing new. The original critique by EPR concluded that quantum mechanics 'is not complete' and was immediately seconded by Schrödinger in the context of quantum entanglement using the word 'disconcerting' to describe the fact that there is no independence between separated systems that were originally entangled (Schrödinger, 1935). These criticisms were expanded in a second paper where he reaffirms his displeasure with 'the present theory' (Schrödinger, 1936).

In a subsequent scenario, it was J. S. Bell himself – a key figure in cementing the concept that HVTs were incompatible with the predictions of quantum mechanics (Bell, 1964), who paradoxically became a clever and eloquent critic of orthodox quantum mechanics (Bell and Nauenberg, 1966; Bell, 1990).

This subject is considered in detail by Duarte (2022), and here, only the more salient aspects are brought into context. Bell's first critical work was entitled *The moral aspects of quantum mechanics* in which he concluded that the theory is 'at best, incomplete' and that 'it carries in itself the seeds of its own destruction' (Bell and Nauenberg, 1966). In that paper, Bell discusses the double-slit, or Young's, interference experiment while invoking the 'de Broglie-Bohm pilot wave' or 'hidden parameter' interpretation of quantum mechanics (Bell and Nauenberg, 1966). From our perspective, Bell's interpretation of the two-slit experiment is not only unnecessary but it is also at odds with the lucid-transparent description given by Dirac (1958), and with the non-local nature of the photon. Furthermore, in an extension to the *N*-slit interferometer, Duarte (2003) explains that 'all the indistinguishable photons illuminate the array of *N* slits, or grating, simultaneously. If only one photon propagates at any given time, then that individual photon illuminates the whole array of *N* slits simultaneously.' Also relevant is the existence of experimental evidence that points directly against the 'pilot wave' interpretation (Andersen et al., 2015).

Bell and Nauenberg (1966) arrive at the conclusion that quantum mechanics is 'at best incomplete.' This argument has already been neutralized here, via $\Delta x\, \Delta p \approx h$. In conclusion, from a pragmatic perspective, quantum mechanics *does not* carry 'the seeds of its own destruction.'

Bell's second paper on this subject was entitled *Against* '*measurement*' (Bell 1990).

Very sharp and cleverly written, it was Bell's last paper. In it, Bell criticizes all books on quantum mechanics and Dirac for having a '*why bother*' attitude toward the possibility of an 'exact' formulation of the theory. In this paper, Bell suggests to replace the word *measurement* by the word *experiment*: 'A serious formulation will not exclude the big world outside the laboratory' (Bell, 1990). In this regard, experiments with very large *N*-slit interferometers, utilizing ensembles of indistinguishable photons and measurement predictions based on Diracian probability amplitudes have taken place within the laboratory at an intra-interferometric distance of $D_{\langle d|j\rangle} = 35$ m and *outside* the laboratory at $D_{\langle d|j\rangle} = 527$ m (Duarte et al., 2010, 2011). Furthermore, space-to-Earth quantum entanglement experiments, utilizing the quantum entanglement probability amplitudes, have been reported over a propagation distance of 1200 km (Yin et al., 2017).

Bell also criticizes Landau and Lifshitz (1977) mainly due to their *ambiguity* in regard to 'what is microscopic, what is macroscopic, what [is] quantum, what [is] classical' (Bell, 1990). In principle, quantum mechanics applies both to the microscopic and the macroscopic: the first description of quantum interference was provided by Dirac, while discussing macroscopic two-beam interference (Dirac, 1958).

Indeed, from the perspectives of Lamb and van Kampen, quantum mechanics does apply to large-scale phenomena. Moreover, Feynman and Hibbs (1965) applied quantum path integrals to the description of macroscopic diffraction and Duarte (1997, 2003) derived the physics of diffraction, refraction, and reflection from quantum interferometric principles.

Finally, it should be indicated that Bell's criticisms were mainly of a philosophical nature and he abstained from introducing his own description, or interpretation, of quantum mechanics and relied mainly on 'pilot wave' concepts.

23.5 ON HIDDEN VARIABLE THEORIES

HVTs apparently were first mentioned, as the '*hidden parameter*', by von Neumann (1932) who was aware of their existence and dismissed them. At least two HVTs have been proposed: those of Bohm (1952a, 1952b) and Bohm and Bub (1966). The HVT introduced by Bohm (1952a) concludes that 'the probability density of particles will cease to be equal to $|\Psi(x)|^2$' (Bohm 1952a).

It also introduces the concept of precise measurements of position and momentum, thus violating $\Delta p\, \Delta x \approx h$ (Bohm, 1952b). The second HTV introduces an *irreversible* set of equations (Bohm and Bub 1966). The concept of HTVs was highly influential in a section of the physics community. Optical experiments designed to test for HVTs were proposed and performed by Clauser et al. (1969), Freedman and Clauser (1972), and Clauser and Horne (1974). The first Aspect experiments were also inspired by HVTs (Aspect et al., 1981), while the emphasis shifted toward Bell's theorem in the subsequent experiments (Aspect et al., 1982a, 1982b). These experiments reaffirmed the correctness of quantum mechanics.

Since Born's rule (Born, 1926), stated as $|\Psi(x,t)|^2 = \Psi(x,t)\Psi(x,t)^*$ or $|\langle d|s\rangle|^2 = \langle d|s\rangle\langle d|s\rangle^*$, is a crucial principle of quantum mechanics, it can be concluded that *a theory that does not observe Born's rule is not a quantum mechanical theory* (Duarte, 2022). Similarly with a theory that violates $\Delta p\, \Delta x \approx h$. Hence, it follows that the HVT introduced by Bohn (1952a, 1952b) is not a quantum mechanical theory. A similar conclusion can be reached in regard to the HVT of Bohm and Bub (1966) (Duarte and Taylor, 2021) given that *reversibility* is a key feature in the flow of quantum mechanical equations (von Neumann, 1932; Duarte, 2019).

HVTs have not led to any practical physics and their only application appears to have been their use as a platform to project doubts toward early quantum entanglement experiments, inspired on *Dirac's pair theory* (Dirac, 1930), utilizing positron–electron annihilation sources $e^+e^- \rightarrow \gamma_1\gamma_2$ (Bleuler and Bradt, 1948; Hanna, 1948; Wu and Shaknov, 1950). Here, it is relevant to mention that Feynman also dismissed the concept of HTVs (Feynman et al., 1965) and Willis Lamb (2001) cataloged HVTs as 'unnecessary.'

From a historical perspective and beyond the original dismissal from von Neumann (1932), it was Bell's theorem (Bell, 1964) (see Chapter 14) that precipitated the widespread acceptance of the concept that HVTs were indeed incompatible with quantum mechanics. Nevertheless, 'The two photons are entangled and according to local realism, their polarizations planes should become independent… a typical EPR situation. Already in 1948, observations agreed with quantum mechanics… not with local realism' (Dalitz and Duarte, 2000; Duarte, 2012).

23.6 ON THE ABSENCE OF 'THE MEASUREMENT PROBLEM'

'Quantum mechanics works' as stated by van Kampen's first theorem (van Kampen, 1988). Quantum mechanics gave us the transistor, the laser, and laser cooling.

Furthermore, quantum mechanics predicts quite accurately *N*-slit interferometric measurements using ensembles of indistinguishable quanta (see Chapter 4). In quantum electrodynamics, the electron magnetic moment is measured to be $(g/2) = 1.00115965218073$ in Bohr magnetons (Hanneke et al., 2008) while predicted to be $(g/2) = 1.0011596$ (Petermann, 1956). An agreement to the seventh decimal place between theory and experiment is not indicative of a 'measurement problem' especially for a theory based on 'indeterminacy' (Duarte, 2022). Of course, we know that the agreement is even better since Petermann, in 1956, used only two Feynman diagrams, while today large numbers of Feynman diagrams are employed in computerized calculations.

The measurement problem in quantum mechanics is not a practical existing problem. It is a conceptual problem. Contemporaneous critics of quantum mechanics often link the measurement problem to 'the collapse of the wave function' (Albert and Vaidman, 1989; Namiki and Pascazio, 1992; Penrose, 1996). However, as indicated by Duarte and Taylor (2021), the collapse of the wave function is absent from the discussion on quantum superposition in Dirac's book (Dirac 1958) and it is absent in Feynman's lectures on quantum mechanics (Feynman et al., 1965). In the next sections, it becomes quite transparent that the concept of the collapse of the wave

function is absent and unnecessary in the measurement methodology of quantum interference and quantum entanglement.

23.7 THE PHYSICAL BASES OF QUANTUM ENTANGLEMENT

Derivational methods for the probability amplitude of quantum entanglement include Ward's heuristic conservational approach (Ward, 1949), the use of Feynman's Hamiltonian method (Duarte, 2014), the quantum interferometric method (Duarte, 2013a, 2014), and the use of Pauli matrices (Duarte, 2019, Duarte et al., 2020). The quantum interferometric approach is summarized by

$$\sum_{j=1}^{N} \langle d|\, j\rangle\, \langle j|s\rangle \rightarrow |\psi\rangle_{+}, |\psi\rangle_{-}, |\psi\rangle^{+}, |\psi\rangle^{-} \tag{23.5}$$

while the Pauli matrix approach can be described by

$$\sum_{j} H_{ij} C_j \rightarrow \sigma_x, \sigma_y, \sigma_z, I \rightarrow |\psi\rangle_{+}, |\psi\rangle_{-}, |\psi\rangle^{+}, |\psi\rangle^{-} \tag{23.6}$$

These methodologies are direct and mathematically transparent. They are free of mysteries and free of paradoxes (Duarte, 2023).

23.8 THE MECHANISMS OF QUANTUM MECHANICS

Here we describe, succinctly and directly, the workings of quantum mechanics from interferometric and quantum entanglement perspectives.

23.8.1 The Quantum Interference Mechanics

The Dirac–Feynman interferometric probability amplitude (Dirac, 1958; Feynman et al., 1965)

$$\langle d|s\rangle = \sum_{j=1}^{N} \langle d|\, j\rangle\, \langle j|s\rangle \tag{23.7}$$

is a superposition probability amplitude involving all the base states related to the physics of the experimental configuration

$$\langle d|s\rangle = \langle d|1\rangle\, \langle 1|s\rangle + \langle d|2\rangle \langle 2|s\rangle + \langle d|3\rangle\, \langle 3|s\rangle \ldots + \langle d|\, N\rangle\, \langle N|\, s\rangle \tag{23.8}$$

This superposition probability amplitude, or state, becomes a probability via Born's rule

$$\left|\langle d|s\rangle\right|^2 = \langle d|s\rangle\, \langle d|s\rangle^{*} \tag{23.9}$$

as the measurement is performed. This interferometric probability distribution

$$P(\lambda, N, \Omega) = \left|\langle d|\, s\rangle\right|^2 \tag{23.10}$$

immediately gives rise to a measurable intensity

$$I(P, \nu) = \mathrm{K}\, h\nu\, P(\lambda, N, \Omega) \tag{23.11}$$

This is an intensity spatial distribution which, at a frequency ν, is entirely dependent on the spatial distribution of the dimensionless quantum probability distribution.

If only a single photon is involved in the measurement process, this means that, at the detector surface, this single quantum can generate an electron charge anywhere within the boundaries of the $\langle d|\, s\rangle\, \langle d|\, s\rangle^*$ distribution.

If an *ensemble of r indistinguishable photons* is involved in the measurement process, the physics is again correctly described by the superposition probability amplitude $\langle d|\, s\rangle = \langle d|\, 1\rangle\, \langle 1|\, s\rangle + \langle d|\, 2\rangle\, \langle 2|\, s\rangle + \langle d|\, 3\rangle\, \langle 3|\, s\rangle \ldots + \langle d|\, N\rangle\, \langle N|\, s\rangle$, but the intensity becomes

$$I(\nu) = r\mathrm{K}\, h\nu\, \langle d|\, s\rangle\, \langle d|\, s\rangle^* \tag{23.12}$$

This 'ensemble intensity' is now sufficient to generate electron charges throughout the entire the $\langle d|\, s\rangle\, \langle d|\, s\rangle^*$ spatial distribution.

It is the correct superposition probability amplitude $\langle d|\, s\rangle$, describing the physics of the experimental configuration that provides us the measurable via $\langle d|\, s\rangle\, \langle d|\, s\rangle^*$.

Nowhere in this description, it is necessary to invoke a 'collapse of the wave function.'

23.8.2 The Quantum Entanglement Mechanics

From the Dirac–Feynman interferometric probability amplitude

$$\langle d|\, s\rangle = \sum_{j=1}^{N} \langle d|\, j\rangle\, \langle j|\, s\rangle$$

emerges the superposition probability amplitude for quantum entanglement

$$|\psi\rangle_- = 2^{-1/2}\left(|x\rangle_1 |y\rangle_2 - |y\rangle_1 |x\rangle_2\right) \tag{23.13}$$

Once two polarized entangled, and indistinguishable, quanta are emitted in opposite directions, the polarizations are orthogonal to each other. For example, if the polarization of the photon toward the detector in the $+z$ direction is in the $|x\rangle$ state, then the polarization of the photon emitted in the $-z$ direction is in the $|y\rangle$ state. Once the photons are emitted, their superposition probability amplitude evolves according to $|\psi\rangle_-$.

Immediately as the polarization measurement is performed, the superposition probability is given by

$$P(\varphi_1, \varphi_2) = |\psi\rangle_{\_} \, |\psi\rangle_{\_}^{*} \tag{23.14}$$

$$P(\varphi_1, \varphi_2) = -\cos 2(\varphi_1 - \varphi_2) \tag{23.15}$$

and it is this superposition probability that determines whether the experimentalist will measure a photon in the $|x\rangle$ state or a photon in the $|y\rangle$ state.

It is the correct superposition probability amplitude $|\psi\rangle_{\_}$ that provides the measurable via $|\psi\rangle_{\_} \, |\psi\rangle_{\_}^{*}$. Nowhere in this description it is necessary to invoke a 'collapse of the wave function' and, furthermore, the description is entirely independent of Bell's theorem.

23.9 PHILOSOPHY

Quantum mechanics, via quantum entanglement, has generated intense interest in the philosophical world (see, for instance, Godoy, 2018; Trotter, 2021; Silva, 2022) and even garnered serious attention in literature (Dark, 2023). In this regard, the uncertainty of Heisenberg, the indeterminacy of Born, the doubts of Feynman, and the nonlocality of the photon should serve as the foundations for a philosophical approach based on an indeterminism free from preestablished notions and prejudices. Inspired by Born (1949) and Feynman (1998), this indeterministic, and pragmatic, school of thought accepts with humility our ignorance and leaves the experiment, the measurement, and their uncertainties, as the main conduits toward Nature. Indeed, Nature is the supreme judge.

In this regard, no theory is final and all good theories should be able to adapt to integrate new experimental evidence.

23.10 DISCUSSION

Here, we very humbly assume that Nature is far subtler than our philosophical abilities and accept, as Born, Dirac, Feynman, Lamb, Ward and others have done, the physics of quantum entanglement and the intricacy of the machinery of quantum interference, as *Nature's way.*

In this pragmatic approach to quantum mechanics, the physics, or experimental configuration, is faithfully and transparently described by the superposition probability amplitude. It is this superposition probability amplitude, $\langle d|s\rangle$ or $|\psi\rangle_{\_}$, that must correctly relate to the experimental configuration. The transition from the mathematical realm of probability amplitudes to the measurable realm of probabilities, intensities, and polarizations is naturally and effortlessly provided via Born's rule. This transition occurs continuously and spontaneously throughout the course of the experiment, and it is up to the experimenter to decide *when* to observe. At the instant, the experimenter decides to perform the measurement $\langle d|s\rangle \rightarrow \langle d|s\rangle \, \langle d|s\rangle^{*}$

or $|\psi\rangle_- \rightarrow |\psi\rangle_- |\psi\rangle_-^*$ occur. Once in the measurements realm, we can express $\langle d|s\rangle \langle d|s\rangle^* \rightarrow I(\nu)$ or $|\psi\rangle_- |\psi\rangle_-^* \rightarrow P(\varphi_1, \varphi_2)$.

As far as a possible, 'improved' quantum mechanics is concerned: we agree with Born's suggestion that the bases of quantum mechanics will remain indeterministic. In this regard, as already suggested in Chapter 22, the Dirac–Feynman interferometric principle

$$\langle d|s\rangle = \sum_{j=1}^{N} \langle s|j\rangle \langle j|s\rangle$$

already contains the mechanics for further and further spatial and temporal refinements (Duarte, 2022; Duarte and Olivares, 2023).

Indeterminism plays a crucial role in quantum mechanics and a real, yet unrecognized, role in classical physics given that no measurement – no matter how classical – is free from experimental error (Duarte, 2014, 2022). Indeed, the stochastic nature of classical physics has been observed for a while now (Newton, 1687; Feynman et al., 1965). In this regard, it is clear that indeterminism and uncertainty are intrinsic features of Nature itself.

It should be reemphasized that crucial to this pragmatic approach to quantum mechanics is the awesome *nonlocality* of the photon, a unique quantum feature. It is this wonderful nonlocality of the photon, *itself a physical reality* confirmed by experiments, that reaffirms quantum mechanics… and not 'local realism' (Dalitz and Duarte, 2000)

PROBLEMS

23.1 How would the argument in Section 23.3 change if the general form of the uncertainty principle, as given in Chapter 3, were used rather than $\Delta x\, \Delta p \approx h$? Would the conclusion remain unchanged?

23.2 Besides the transistor, the laser, and laser cooling, name one or more unique technologies made possible by quantum mechanics.

23.3 Besides the approaches to derive the probability amplitudes of quantum entanglement identified in Section 23.7, identify or describe any other transparent approach to arrive at $|\psi\rangle_+, |\psi\rangle_-, |\psi\rangle^+, |\psi\rangle^-$, from first principles.

23.4 In reference to Equation (23.11): Comment on the possible components that might comprise the constant **K**.

23.5 Provide a physical argument to justify that Equation (23.11) follows from Equation (23.10).

REFERENCES

Albert, D. Z., and Vaidman, L. (1989). On a theory of the collapse of the wave function. In *Bell's Theorem, Quantum Theory and Conception of the Universe* (Kafatos, M. ed.). Springer, Berlin, pp. 1–6.

Andersen, A., Madsen, J., Reichelt, C., Ahl, S. R., Lautrup, B., Ellegaard, C., Levinsen, M. T. and Bohr, T. (2015). Double-slit experiment with single wave-driven particles and its relation to quantum mechanics. *Phys. Rev. E.* **92**, 013006.

Aspect, A., Grangier, P., and Roger, G. (1981). Experimental tests of realistic local theories via Bell's theorem. *Phys. Rev. Lett.* **47**, 460–463.

Aspect, A., Grangier, P., and Roger, G. (1982a). Experimental realization of Einstein-Podolsky-Rosen-Bohm gedanken experiment: a new violation of Bell's inequalities. *Phys. Rev. Lett.* **49**, 91–94.

Aspect, A., Grangier, P., and Roger, G. (1982b). Experimental test of Bell's inequality using time-varying analyzers. *Phys. Rev. Lett.* **49**, 1804–1807.

Bell, J. S. (1964). On the Einstein-Podolsky-Rosen paradox. *Physics* **1**, 195–200.

Bell, J. S. (1990). Against measurement. *Phys. World* **3** (8) 33–39.

Bell, J. S. (1988). *Speakable and Unspeakable in Quantum Mechanics*, Cambridge University, Cambridge, U.K.

Bell, J. S., and Nauenberg, M. (1966). The moral aspects of quantum mechanics. In *Preludes in Theoretical Physics* (De Shalit, A., Feshbach, H., and Van Hove, L., eds.). North Holland, Amsterdam, pp. 279–286.

Bleuler, E. and Bradt, H. L. (1948). Correlation between the states of polarization of the two quanta of annihilation radiation. *Phys. Rev.* **73**, 1398.

Bohm, D., and Aharonov, Y. (1957). Discussion of experimental proof for the paradox of Einstein, Rosen, and Podolsky. *Phys. Rev.* **108**, 1070–1076.

Bohm, D. (1952a). A suggested interpretation of quantum theory using 'hidden' variables I. *Phys. Rev.* **85**, 166–179.

Bohm, D. (1952b). A suggested interpretation of quantum theory using 'hidden' variables II. *Phys. Rev.* **85**, 180–193.

Bohm, D., and Bub, J. (1966). A proposed solution of the measurement problem in quantum mechanics by hidden variable theory. *Rev. Mod. Phys.* **38**, 453–469.

Bohr, N. (1935). Can quantum-mechanical description of physical reality be considered complete? *Phys. Rev.* **48**, 696–701.

Born, M. (1926). Zur quantenmechanik der stoßvorgänge. *Z. Phys.* **37**, 863–827.

Born, M. (1949). *Natural Philosophy of Cause and Chance*, Clarendon Press, Oxford, U.K.

Clauser, J. F. and Horner, M. A. (1974). Experimental consequences of objective local theories. *Phys. Rev. D.* **10**, 526–535.

Clauser, J. F., Horner, M. A., Shimony, A., and Holt, R. A. (1969). Proposed experiment to test local hidden variable theories. *Phys. Rev. Lett.* **23**, 880–883.

Dalitz, R. H., and Duarte, F. J. (2000). John Clive Ward. *Phys. Today* **53**, 99–100.

Dark, S. (2023). *The Shadows of Woolf's Universe*. University of Sydney, Sydney.

Dirac, P. A. M. (1930). On the annihilation of electrons and protons. *Math. Proc. Camb. Phil. Soc.* **2**, 361–375

Dirac, P. A. M. (1958). *The Principles of Quantum Mechanics*, 4th ed. Oxford University, Oxford, U.K.

Dirac, P. A. M. (1987). The inadequacies of quantum field theories. In *Paul Adrien Maurice Dirac* (Kursunoglu, B. N., and Wigner, E. P., eds.). Cambridge University, Cambridge, U.K., Chapter 15, pp. 194–198.

Duarte, F. J. (1997). Interference, diffraction, and refraction, via Dirac's notation. *Am. J. Phys.* **65**, 637–640.

Duarte, F. J. (1998). Interference of two independent sources. *Am. J. Phys.* **66**, 662–663.

Duarte, F. J. (2003). Tunable Laser Optics, Elsevier-Academic, New York.

Duarte, F. J. (2012). The origin of quantum entanglement experiments based on polarization measurements. *Eur. Phys. J. H* **37**, 311–318.

Duarte, F. J. (2013a). The probability amplitude for entangled polarizations: an interferometric approach. *J. Mod. Opt.* **60**, 1585–1587.

Duarte, F. J. (2013b). Electron interference, part deux. *Opt. Photon. News* **24**, 7.
Duarte, F. J. (2014). Quantum Optics for Engineers, 1st ed. CRC, Boca Raton, FL.
Duarte, F. J. (2019). *Fundamentals of Quantum Entanglement*, 1st ed. Institute of Physics, Bristol, U.K.
Duarte, F. J. (2022). *Fundamentals of Quantum Entanglement*, 2nd ed. Institute of Physics, Bristol, U.K.
Duarte, F. J. (2023). Quantum entanglement free of paradoxes. *Laser Focus World* 59 (1), 55–56.
Duarte, F. J., and Olivares, I. O. (2023). *N*-slit quantum interferometers in the nanometer domain. *Appl. Phys. B*. **129**, 88.
Duarte, F. J., and Taylor, T. S. (2021). *Quantum Entanglement Engineering and Applications*, Institute of Physics, Bristol, U.K.
Duarte, F. J., Taylor, T. S., Black, A. M., Davenport, W. E., and Varmette, P. G. (2011). *N*-slit interferometer for secure free-space optical communications: 527 m intra interferometric path length. *J. Opt.* **13**, 035710.
Duarte, F. J., Taylor, T. S., Clark, A. B., and Davenport, W. E. (2010). The *N*-slit interferometer: an extended configuration. *J. Opt.* **12**, 015705.
Duarte, F. J., Taylor, T. S., and Slaten, J. C. (2020). On the probability amplitude of quantum entanglement and the Pauli matrices. *Opt. Quantum Electron.* **52**, 106.
Einstein, A., Podolsky, B., and Rosen, N. (1935). Can quantum mechanical description of physical reality be considered complete? *Phys. Rev.* **47**, 777–780.
Feynman, R. P., Leighton, R. B., and Sands, M. (1965). *The Feynman Lectures on Physics*, Vol. III, Addison-Wesley, Reading, MA.
Feynman, R. P., and Hibbs, A. R. (1965). *Quantum Mechanics and Path Integrals*, McGraw-Hill, New York.
Feynman, R. P. (1989). *The Meaning of It All*. Addison-Wesley, Reading, MA.
Freedman, S. J. and Clauser, J. F. (1972). Experimental test of local hidden-variable theories. *Phys. Rev. Lett.* **28**, 938–941.
Freire, O. (2022). *The History of Quantum Interpretations*, Oxford University, Oxford, U.K.
Godoy, W. (2018). *Explorações Filosóficas da Não-Localidade em Física Quântica*. Universidade de São Paulo, São Paulo.
Hanna, R. C. (1948). Polarization of annihilation radiation. *Nature* **162**, 332.
Hanneke, D., Fogwell, S., and Gabrielse, G. (2008). New measurement of the electro magnetic moment and the fine structure constant. *Phys. Rev. Lett.* **100**, 120801.
Lamb, W. E. (2001). Super classical quantum mechanics: the best interpretation of non- relativistic quantum mechanics. *Am. J. Phys.* **69**, 413–421.
Landau, L. D., and Lifshitz, E. M. (1977). *Quantum Mechanics*, Pergamon, New York.
Namiki, M., and Pascazio, S. (1992). Many-Hilbert-spaces approach to the wave-function Collapse. *Found. Phys.* **22**, 451–466.
Newton, I. (1687). *Principia Mathematica*, Royal Society, London, U.K.
Newton, I. (1704). *Opticks*, Royal Society, London, U.K.
Penrose, R. (1996). On gravity's role in quantum state reduction. *Gen. Rel. Grav.* **28** 581-600.
Petermann, A. (1956). Fourth order magnetic moment of the electron. *Helv. Phys. Acta* **30**, 407–408.
Pryce, M. H. L., and Ward, J. C. (1947). Angular correlation effects with annihilation radiation. *Nature* **160**, 435.
Schrödinger, E. (1935). Discussion of probability relations between separated systems *Math. Proc. Camb. Phil. Soc.* **31**, 555–563.
Schrödinger, E. (1936). Probability relations between separated systems *Math. Proc. Camb. Phil. Soc.* **32**, 446–452.
Selleri, F. (1988). *Quantum Mechanics Versus Local Realism*, Plenum, New York.

Silva, I. (2022). Chien-Shiung Wu's contributions to experimental philosophy. In *The History of Quantum Interpretations* (Freire, O., ed.). Oxford University, Oxford, U.K., Chapter 29, 735–754.

Trotter, F. (2021). *A Philosophical Observation in Quantum Mechanics*, Université de Lausanne, Lausane.

van Kampen, N. G. (1988). Ten theorems about quantum mechanical measurements. *Phys. A.* **153**, 97–113.

Wallace, R. P. (1996). *Paradox Lost*, Springer, Berlin.

Ward, J. C. (1949). *Some Properties of the Elementary Particles*. D. Phil Thesis, Oxford University, Oxford, U.K.

Ward, J. C. (2004). *Memoirs of a Theoretical Physicists*, Optics Journal, Rochester, N.Y.

Wu, C. S., and Shaknov, I. (1950). The angular correlation of scattered annihilation radiation. *Phys. Rev.* **77**, 136.

Yin, J., Cao, Y., Li, Y. H., Liao, S. K., Zhang, L., Ren, J. G., Cai, W. Q., Liu, W. Y., Li, B., Dai, H., and Li, G. B. (2017). Satellite based entanglement distribution over 1200 kilometers. *Science* **356**, 1140–1144.

Appendix A
Laser Excitation

A.1 INTRODUCTION

Lasers are quantum devices. The process of stimulated emission is a quantum phenomenon. Stimulated emission is essential to the generation of spatially and spectrally coherent radiation, which are also quantum phenomena. Thus, albeit initially a macroscopic device, the laser emits radiation that is intrinsically quantum in character. In this chapter, we consider the first and essential step in the creation of a laser: laser excitation.

Here, we consider the process of laser excitation and emission, in a gain medium, from a semi-classical and quantum perspective. In Appendices B and C, we examine the optics phenomena applicable to generate spatially and spectrally coherent radiation.

A.2 BRIEF LASER OVERVIEW

The word *laser* has its origin in an acronym of the words *light amplification* by *stimulated emission* of *radiation*. However, the laser is readily associated with the spatial and spectral coherence characteristics of its emission.

A laser is a device that transforms electrical energy, chemical energy, or incoherent optical energy, into coherent optical emission. This coherence is both spatial and spectral. Spatial coherence means a highly directional light beam, with little divergence, and, spectral coherence means an extremely pure color of emission. These concepts of spatial and spectral coherence are intimately related to Heisenberg's uncertainty principle $\Delta p\, \Delta x \approx h$ (see Chapter 3).

An alternative way to cast this idea is to think of the laser as a device that transforms ordinary incoherent energy into an extremely well-defined form of energy, both in the spatial and the spectral domains.

Physically, the laser consists of an atomic or molecular gain medium optically aligned within an optical resonator, or optical cavity, as depicted in Figure A.1. When excited by electrical energy, or optical energy, the atoms or molecules in the gain medium oscillate at optical frequencies. This oscillation is maintained and sustained by the optical resonator or optical cavity. In this regard, the laser is analogous to a mechanical or radio oscillator but oscillating at extremely high frequencies. For the green color of $\lambda \approx 500$ nm, the equivalent frequency is $\nu \approx 5.99 \times 10^{14}$ Hz. A direct comparison between a *laser oscillator* and an old radio oscillator makes the atomic, or molecular gain medium, equivalent to the vacuum tube, and the elements of the optical cavity, equivalent to the resistances, capacitances, and inductances.

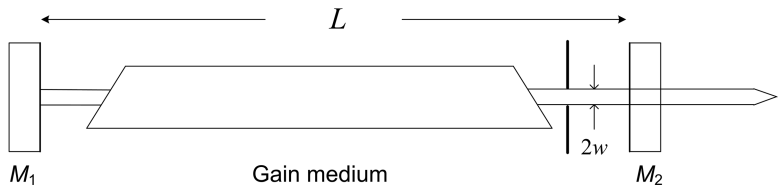

FIGURE A.1 Basic laser resonator. It is comprised of an atomic, or molecular, gain medium, and two mirrors aligned along the optical axis. The length of the cavity is L and the diameter of the beam is $2w$. The gain medium can be excited either optically or electrically.

The spectral purity of the emission of a laser is related to how narrow its linewidth ($\Delta\nu$) is. High-power broadband tunable lasers can exhibit a linewidth in the $4.5 \leq \Delta\lambda \leq 10$ nm range (see, for example, Schäfer et al., 1966). High-power pulsed narrow-linewidth lasers can have single-longitudinal-mode linewidths of $\Delta\nu \approx 350$ MHz (i.e., $\Delta\lambda \approx 0.0004$ nm, at 590 nm) near the limit allowed by Heisenberg's uncertainty principle (Duarte, 1999). Single longitudinal mode means that all the emission radiation is contained in a single electromagnetic mode.

Low power CW narrow-linewidth lasers can offer much narrower linewidths approaching the kHz regime. Cooled-stabilized CW lasers can yield $\Delta\nu \approx 1$ Hz or even less (Kessler et al., 2012).

In the language of the laser literature, a laser emitting narrow-linewidth radiation is referred to as a *laser oscillator* or *master oscillator* (MO). High-power narrow-linewidth emission is attained when an MO is used to inject a *laser amplifier*, or *power amplifiers* (PA). Large high-power systems include several MOPA chains with each chain including several amplifiers. The difference between an oscillator and an amplifier is that the amplifier simply stores energy to be released up on the arrival of the narrow-linewidth oscillator signal. In some cases, the amplifiers are configured within unstable resonator cavities in what is referred to as a *forced oscillator* (FO). When that is the case the amplifier is called a FO and the integrated configuration is referred to as a MOFO system.

A.2.1 Laser Optics

Laser optics, as defined in Duarte (2003), refers to the individual optics elements that comprise laser cavities, to the optics ensembles that comprise laser cavities, and to the physics that results from the propagation of laser radiation. In addition, the subject of laser optics includes instrumentation employed to characterize laser radiation and instrumentation that incorporates lasers. A broad survey of laser cavities is given in Appendix B, while the physics and architecture of tunable narrow-linewidth laser oscillators are presented in Appendix C.

A.3 LASER EXCITATION

As already mentioned, lasers can be excited via several forms of energy, including electrical, optical, chemical, and even nuclear. Electrical excitation for lasers can be

either in the gaseous or the solid state. Electrical excitation in the gaseous state give origin to gas lasers while in the solid state gives origin mainly to semiconductor lasers. Optical excitation can be used in gaseous, liquid, or solid state gain media. Here we provide a brief survey of examples of laser gain media in the gaseous, liquid, and solid states.

A.3.1 Electrically Excited Gas Lasers

Electrically excited gas lasers are a very broad class of lasers that includes high-power excimer lasers, metal-vapor lasers, and CO_2 lasers. It also includes an array of continuous wave (CW) metal ion lasers.

To illustrate how some of these lasers are excited, we'll refer to metal ion lasers such as the He–Zn laser, and in particular to a subclass of lasers known as the He–Zn halogen lasers, that is, He–$ZnBr_2$, He–$ZnCl_2$, and He–ZnI_2.

These lasers need a buffer gas which is rare. In this case, that rare gas is helium. Very briefly, the rare-gas metal hollow-cathode discharge is excited electrically as the impedance of an electrical circuit as depicted in Figure A.2. The metal, in this case zinc, is evaporated into the discharge, thus creating an He–Zn discharge. The metal species are excited via Duffendack reactions, that is,

$$\mathrm{He}^{+} + \mathrm{M} \rightarrow \mathrm{He} + (\mathrm{M}^{+})^{*} + \Delta\mathrm{E} \tag{A.1}$$

This means that electrons ionize helium atoms, thus creating He^{+} which in turn collide with metal atoms, thus yielding excited metal ions $(\mathrm{M}^{+})^{*}$. The energy defect of the reaction is $\Delta\mathrm{E}$. These lasers need very energetic electrons to ionize helium and thus utilize hollow-cathode discharges (Piper and Gill, 1975).

An additional excitation mechanism is known as Penning ionization in which electrons excite helium atoms to a metastable state $\mathrm{He}^{*}(2^3\mathrm{S}_1)$, so that

$$\mathrm{He}^{*}(2^3\mathrm{S}_1) + \mathrm{M} \rightarrow \mathrm{He} + (\mathrm{M}^{+})^{*} + \Delta\mathrm{E} \tag{A.2}$$

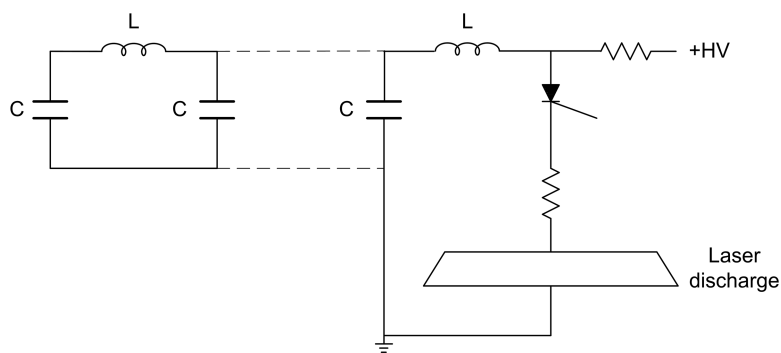

FIGURE A.2 Transmission line excitation circuit of rare-gas metal-vapor laser discharge. An LC circuit of up to ten sections serves as a pulsed forming network and the pulse is switched via a high-voltage thyristor (From Duarte, F. J., *Excitation Processes in Continuous Wave Rare Gas-Metal Halide Vapour Lasers*, Macquarie University, Sydney, 1977.)

An energy level diagram illustrating the zinc transitions due to both Duffendack reactions and Penning ionization is illustrated in Figure A.3. Notice that since the laser transitions occur between specific atomic levels, these transitions are specific in wavelength and intrinsically narrow-linewidth.

In lasers such as He–CdI_2, in addition to the metal transitions, iodine transitions are added to the emission, thus giving rise to white-light lasing (Piper, 1976). An advantage of the metal-halide vapor lasers over the pure metal-vapor lasers is that they need lower operational temperatures. However, this complicates the excitation cycle since the metal-halide molecule needs to be dissociated prior to excitation and needs to recombine following laser emission. Chemical recombination is critical to the successful continuation of the excitation cycle. A time-resolved study in the

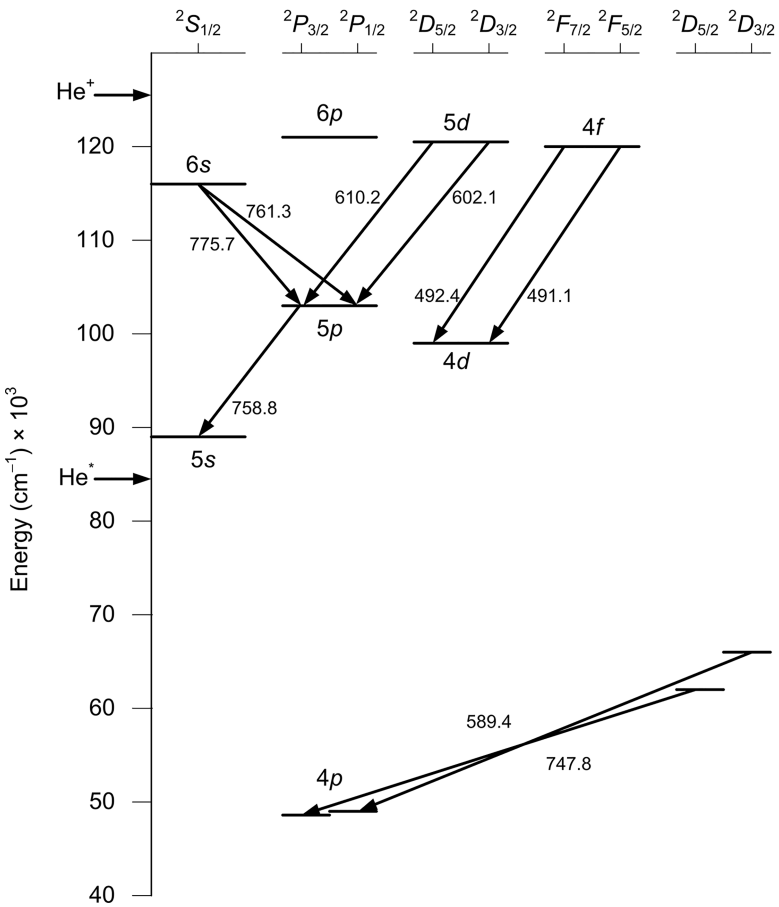

FIGURE A.3 Partial energy level diagram of the He–Zn laser. Upper transitions are excited via Duffendack reactions in hollow-cathode discharge lasers while the lower transitions originate from Penning ionization. The energies corresponding to helium ionization and the relevant helium metastable are indicated. Transition wavelengths are given in nm.

He–ZnX_2 systems, where X_2 refers to the halogen, led to the conclusion that second-order reactions of the form

$$M + X_m \xrightarrow{k_1} MX_2 \tag{A.3}$$

is the likely process of recombination. The solution is (Duarte, 1977)

$$M(t) = \left([X_m]_0 - [M]_0\right)\left(\frac{[X_m]_0}{[M]_0} e^{\tau_1 t} - 1\right)^{-1} \tag{A.4}$$

where the initial concentrations are $[X_m]_0 > [M]_0$. Here, the decay rate (in s^{-1}) is given by

$$\tau_1 = \left([X_m]_0 - [M]_0\right) k_1 \tag{A.5}$$

For hollow-cathode rare-gas metal-vapor lasers, the measured neutral metal decay rates are $(1.6 \le \tau_1 \le 2.0) \times 10^4$ s^{-1} for $ZnBr_2$ and$(0.8 \le \tau_1 \le 1.0) \times 10^4$ s^{-1} for ZnI_2 (Duarte, 1977; Duarte and Piper, 1985).

In summary, for rare-gas metal-halide vapor lasers, the excitation cycle begins with the dissociation of the MX_2 molecules, followed by either Duffendack or Penning excitation of the metal atom. Following excitation and emission, the metal atom decays to its neutral state and undergoes chemical recombination with the halogen, and the cycle continues.

The population dynamics of this type of laser can be analyzed using rate equations while the transition cross sections can either be measured or estimated using quantum methods (Willett, 1974).

A.3.2 Optically Pumped Gas and Liquid Lasers

Optical excitation of lasers can be accomplished either by using incoherent means, such as flashlamps, or by using direct laser excitation (see, e.g., Duarte, 2003). Here, we consider two examples of laser excitation of two types of distinct molecular lasers.

First, we briefly consider the laser-pumped molecular iodine dimer laser, I_2. This molecule has sufficient vapor pressure at room temperature and can be excited longitudinally using a laser compatible with its absorption characteristics. Excitation lasers include pulsed copper vapor lasers (Kaslin et al., 1980), frequency-doubled Nd:YAG lasers (Byer et al., 1972), and narrow-linewidth tunable dye lasers (Duarte and Piper, 1986). Laser excitation of molecular dimer lasers has also been accomplished in the CW regime (see, e.g., Wellegehausen, 1979).

The transitions for molecular iodine belong to the $B^3\Pi_{ou}^+ - X^1\Sigma_g^+$ electronic system. Specific narrow-linewidth excitation of lower lying vibrational–rotational levels in the lower electronic state $X^1\Sigma_g^+$ results in the population of higher lying vibrational–rotational levels in the $B^3\Pi_{ou}^+$ state. Subsequently, transitions from those higher lying vibrational–rotational levels, in the $B^3\Pi_{ou}^+$ state, are observed toward higher lying vibrational–rotational levels, in the $X^1\Sigma_g^+$ state. This type of

selective narrow-linewidth excitation leads to a series of specific, and discrete, narrow-linewidth vibrational–rotational transitions. For instance, narrow-linewidth excitation at $\lambda_p \approx 510.55$ yields a series of *discrete* lines in the red to near infrared (Duarte and Piper, 1986).

A different class of optically pumped molecular laser is the liquid organic dye laser. Organic laser dyes are enormous molecules with very large molecular weights (in the 175–1000 m_u range, see Duarte, 2003). A consequence of this extraordinary characteristic is that each electronic state of a laser dye molecule includes multitudes of closely lying, and overlapping, vibrational–rotational levels. This is the feature that provides the continuous tunability of the dye laser. Figure A.4 shows the molecular structure of the coumarin 545 tetramethyl laser dye that exhibits an approximate tuning range of $500 \leq \lambda \leq 570$ nm (Duarte et al., 2006). The tuning curve of a simple grating resonator using this green laser dye is shown in Figure A.5. The emission available from laser dyes spans the spectrum continuously from ~330 to ~900 nm (Duarte, 2003). The excitation dynamics of dye lasers is described later in this chapter.

Liquid organic dye lasers are enormously versatile and lase either in the CW regime (see, e.g., Hollberg, 1990) or in the pulsed regime (Duarte, 2003). Their liquid gain media is particularly apt for the removal of excess heat. Hence, dye lasers are very suitable for the generation of high average powers and very large pulsed energy.

Transverse laser excitation of a narrow-linewidth tunable dye laser oscillator is illustrated in Figure A.6 (Duarte et al., 1998). As will be discussed later, the population dynamics of dye lasers can be analyzed using rate equations, and the transition cross section is mainly obtained from measurements (Duarte, 2003).

A.3.3 Optically Pumped Solid-State Lasers

The first visible laser was a flashlamp-pumped crystalline laser: the ruby laser (Maiman, 1960). Cr^{3+}:Al_3O_2 lases at $\lambda = 694.3$ nm via the $^2E(\bar{E}) - {}^4A_2$ transition in a three-level energy excitation scheme as illustrated in Figure A.7. On the other hand, the widely tunable Ti:sapphire laser emits in the $660 \leq \lambda \leq 986$ nm range in a two-level energy system that operates like a four-level laser, thus allowing its wide tuning range (Barnes, 1995a).

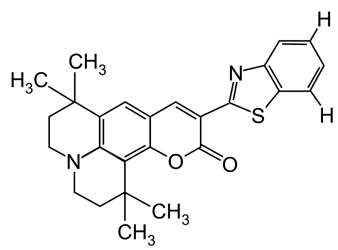

FIGURE A.4 Molecular structure of Coumarin 545 T laser dye. A laser dye molecule, such as this, in an ethanol solution becomes the gain medium for a dye laser (Duarte, F. J. et al., *J. Opt. A: Pure Appl. Opt.* **8**, 172–174, 2006, © IOP Publishing. Reproduced with permission. All rights reserved).

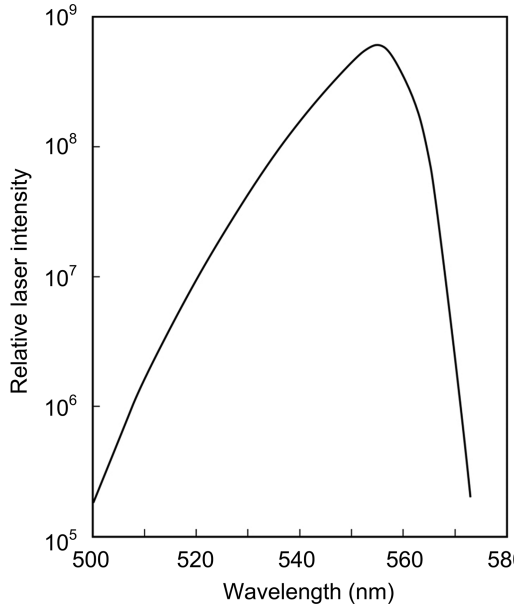

FIGURE A.5 Tuning curve of the emission from the Coumarin 545 T dye laser (Duarte, F. J. et al., *J. Opt. A: Pure Appl. Opt.* **8**, 172–174, 2006, © IOP Publishing. Reproduced with permission. All rights reserved).

There is a large variety of optically pumped solid-state lasers that include transition metal solid-state lasers (Barnes, 1995a) and optical parametric oscillators (Barnes, 1995b; Orr et al., 2016). More recently, fiber lasers have become highly developed and widely used in many applications (Popov, 2016).

Diode-laser excitation has become widely applied in the excitation of solid-state lasers. Figure A.8 shows the simplified energy level diagram for diode-laser excitation of an Nd:YAG laser and a schematics of a longitudinal excitation scheme.

The population dynamics of optically-excited solid-state lasers can be analyzed using rate equations, while the transition cross sections can be derived from spectral measurements (Barnes, 1995a). Emission characteristics of the lasers mentioned here are given in Duarte (2014, 2015).

A.3.4 Electrically Excited Semiconductor Lasers

The excitation and emission process in semiconductor lasers can be described via Schrödinger's equation as discussed in Chapter 9. The beauty of semiconductor lasers is that they can be directly excited using basic electric circuitry as illustrated in Figure A.9.

In semiconductor laser materials, emission occurs between a conduction band and a lower valence band as illustrated in Figure A.10. This is intrinsically a quantum effect. The emission wavelength in these lasers depends on the energy difference between the conduction and the valence band, the *band gap* ($E_G = h\nu$), and is inherently tunable.

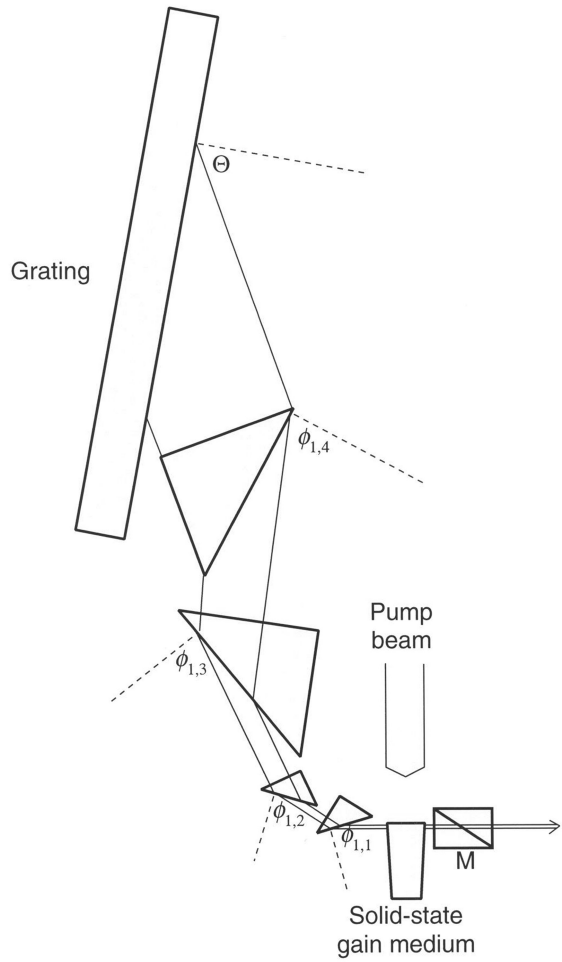

FIGURE A.6 Transverse excitation of narrow-linewidth dye laser oscillator. The gain medium here is a laser dye-doped polymer (Reproduced from Duarte, F. J. et al., *Appl. Opt.* **37**, 3987–3989, 1998, with permission from Optica).

Most semiconductor lasers emit in the visible and near infrared. An interesting semiconductor laser is the quantum cascade laser (QCL) that covers an impressive segment of the infrared spectrum $3 \leq \lambda \leq 24$ μm (Silfvast, 2008). These lasers operate on transitions between quantized conduction-band states of multiple quantum well structures. The only carries are electrons. A single stage consists of an injector and an active region. An electron is injected at $n = 3$ of the quantum well, and as a photon is emitted, the electron transitions to $n = 2$. This is a multiple process so that one electron can emit a large number of photons. The emission wavelength is given by (see Chapter 9)

$$\lambda = (3^2 - 2^2)^{-1} \frac{8mcL_x^2}{h} \tag{A.6}$$

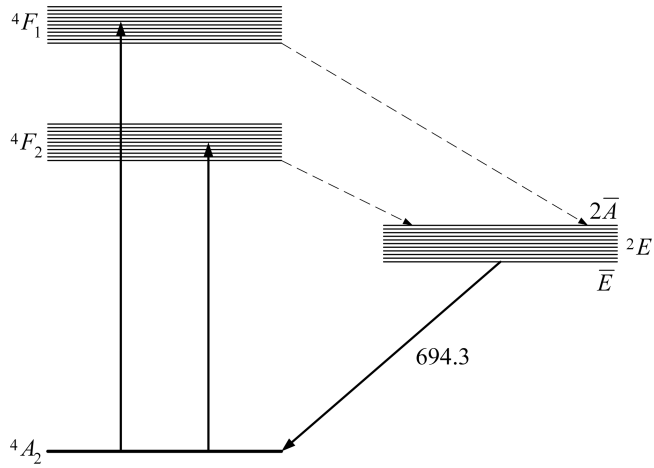

FIGURE A.7 Three-level energy diagram for the ruby laser. Optical pumping to either $^4F_1$ or $^4F_2$ results in rapid nonradiative decay to ^2E from where laser action takes place to the ground level $^4A_2$. The wavelength corresponding to the transition $^2E(\bar{E}) - {}^4A_2$ is $\lambda = 694.3$ nm.

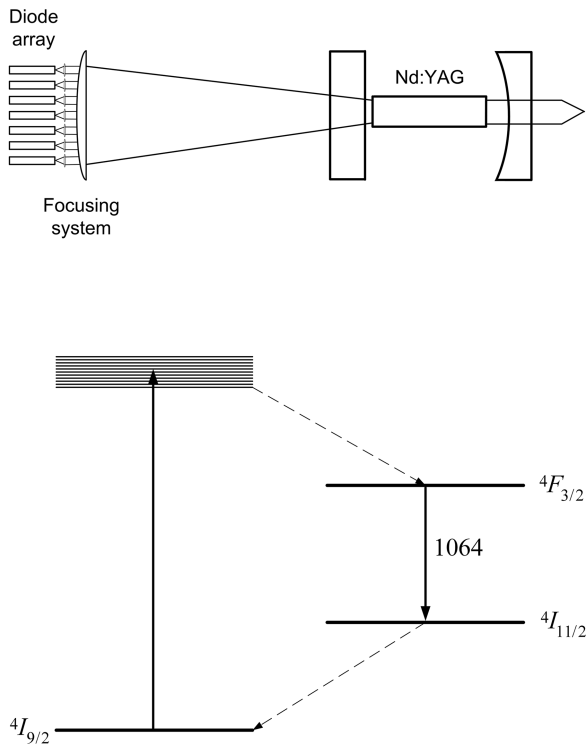

FIGURE A.8 Diode-pumped Nd:YAG laser, using longitudinal pumping with a near IR diode-laser array, and corresponding four-level energy diagram. Optical pumping leads to rapid nonradiative decay to $^4F_{3/2}$ from where laser action takes place to the $^4I_{11/2}$ level. The wavelength corresponding to the transition $^4F_{3/2} - {}^4I_{11/2}$ is $\lambda = 1064$ nm.

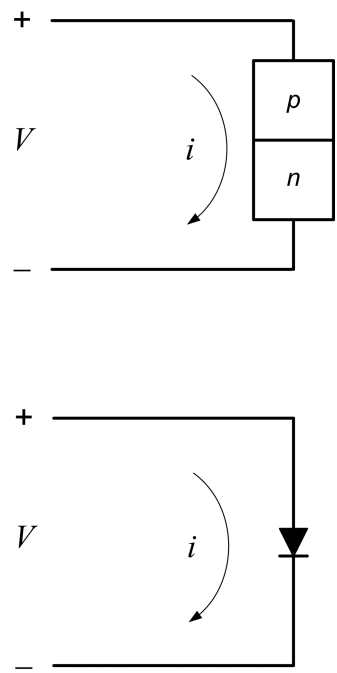

FIGURE A.9 Simple excitation circuit of generic semiconductor laser.

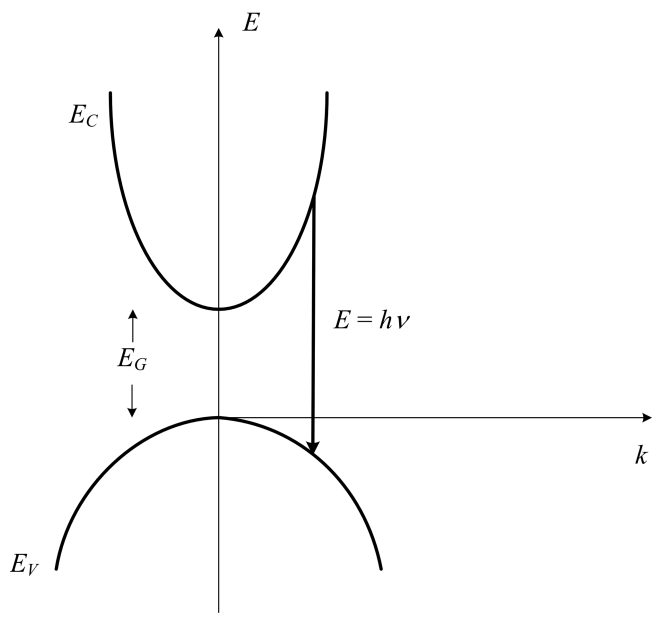

FIGURE A.10 Conduction and valence bands in a semiconductor emitter.

where L_x is the thickness of the quantum well. For emission characteristics of QCLs, the reader may refer to Duarte (2014).

A.4 EXCITATION AND EMISSION DYNAMICS

There are various methods and approaches to describe the dynamics of excitation in the gain media of lasers. Approaches range from complete quantum mechanical treatments to rate equation descriptions (Haken, 1970). A complete survey of energy level diagrams corresponding to gain media in the gaseous, liquid, and solid-state is given by Silfvast (2008). Here, a basic description of laser excitation mechanisms is given using energy levels and classical rate equations applicable to tunable organic molecular gain media. This description is based on the standard approach to the subject (see, e.g., Peterson, 1979) and follows a review given by Duarte (2003).

A.4.1 Rate Equations for a Two-Level System

A simplified two-level molecular system is depicted in Figure A.11. The pump laser intensity $I_p(t)$ populates the upper energy level N_1 from the ground state N_0. The emission from the upper state is designated as $I_l(x, t, \lambda)$. Thus, the time evolution of the upper-, or excited-state-, population is written as

$$\frac{\partial N_1}{\partial t} = N_0 \sigma_{0,1} I_p(t) - N_1 \sigma_e I_l(x, t, \lambda) \tag{A.7}$$

Here, σ_{01} is the absorption cross section and σ_e is the emission cross section. Cross sections have units of cm^2, time has units of seconds (s), the populations have units of molecules cm^{-3}, and the intensities have units of photons cm^{-2}/s^1. The transition cross sections are quantum mechanical in origin and are described later in this chapter.

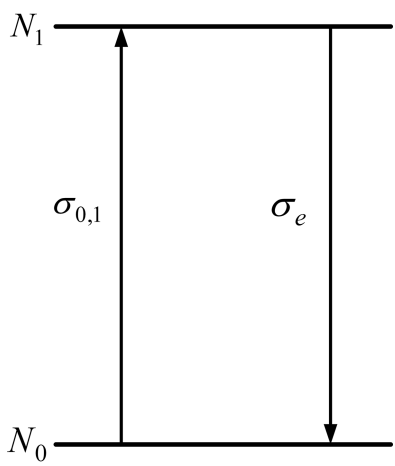

FIGURE A.11 Simplified two-level energy diagram used to describe a basic rate equation system.

The dynamics of the pump intensity $I_p(t)$ is described by

$$c^{-1}\frac{\partial I_p(t)}{\partial t} = -N_0\sigma_{0,1}I_p(t) \tag{A.8}$$

where c is the speed of light. In reference to Figure A.11, the dynamics of the emission intensity $I_l(x, t, \lambda)$ depends on the difference between the upper level population and lower level population so that

$$c^{-1}\frac{\partial I_l(x,t,\lambda)}{\partial t} + \frac{\partial I_l(x,t,\lambda)}{\partial x} = \left(N_1\sigma_e - N_0\sigma_{0,1}^l\right)I_l(x,t,\lambda) \tag{A.9}$$

In the steady state, this equation reduces to

$$\frac{\partial I_l(x,\lambda)}{\partial x} \approx \left(N_1\sigma_e - N_0\sigma_{0,1}^l\right)I_l(x,\lambda) \tag{A.10}$$

and integration yields

$$I_l(x,\lambda) = I_l(0,\lambda)e^{(N_1\sigma_e - N_0\sigma_{0,1}^l)L} \tag{A.11}$$

The exponential terms in Equation (A.11) are referred to as the *gain*. It can be easily seen that the laser threshold is reached for $N_1\sigma_e \geq N_0\sigma_{0,1}^l$ and that for strong laser action, we need $N_1\sigma_e >> N_0\sigma_{0,1}^l$.

A.4.2 Dynamics of Multiple-Level System

The literature on rate equations includes the works of Ganiel et al. (1975), Teschke et al. (1976), Penzkofer and Falkenstein (1978), Dujardin and Flamant (1978), Peterson (1979), Munz and Haag (1980), Haag et al. (1983), Nair and Dasgupta (1985), and Jensen (1991). The rate equation approach given here incorporates several of the elements common in the published literature and emphasizes the frequency-selective aspects of the dynamics as outlined by Duarte (2003). This approach applies to laser dye gain media either in the *liquid* or the *solid state*.

An energy level diagram for a laser dye molecule is included in Figure A.12. S_0, S_1, and S_1 are the *electronic states* of the molecule while T_1 and T_2 represent the *triplet states*, which are detrimental to laser emission. Laser emission occurs via $S_1 \rightarrow S_0$ transitions.

An important feature of laser dyes is that each electronic state contains a large number of overlapping vibrational–rotational levels. This multitude of closely lying vibrational–rotational levels is the origin of the broadband gain and tunability in dye lasers.

In reference to the energy level diagram of Figure A.12, and considering only vibrational manifolds at each electronic state, a set of rate equations for transverse excitations can be written as (Duarte, 2003)

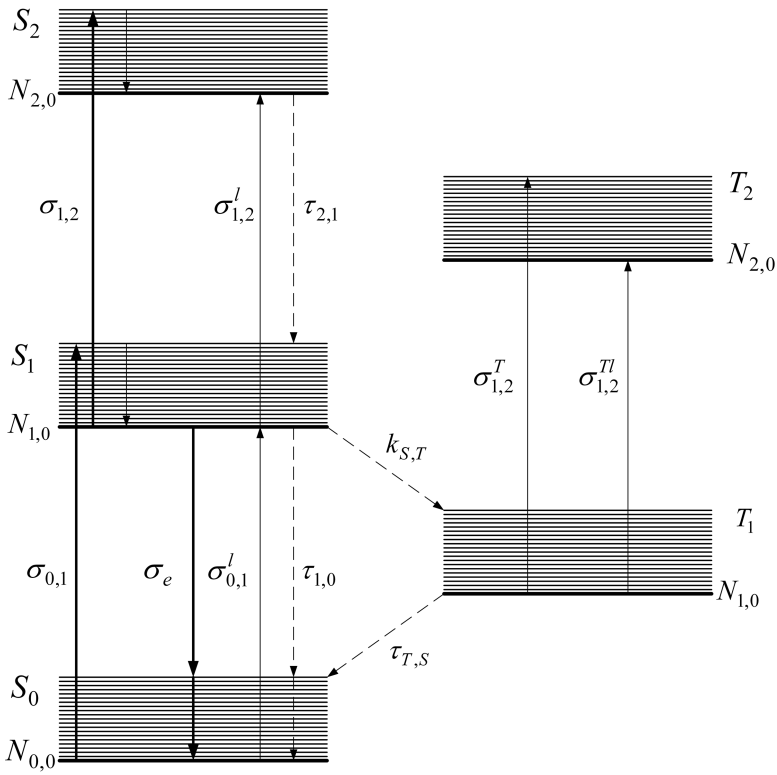

FIGURE A.12 Energy level diagram corresponding to a laser dye molecule. The electronic singlet states are It includes the electronic states S_0, S_1, and S_2 plus the triplet levels T_1 and T_2. Notice that each electronic level includes a multitude of closely lying vibrational–rotational levels. Laser emission takes place from the lowest vibro-rotational level in S_1 to S_0. The presence of a manifold of closely lying vibro-rotational levels at S_0, allowing a range of energies, is what gives rise to wavelength tunability. Using cavity design techniques described in Appendix B, and Appendix C, tunable narrow-linewidth oscillation can be achieved.

$$N = \sum_{S=0}^{m} \sum_{v=0}^{m} N_{S,v} + \sum_{T=1}^{m} \sum_{v=0}^{m} N_{T,v} \tag{A.12}$$

$$\begin{aligned} \frac{\partial N_{1,0}}{\partial t} \approx & \sum_{v=0}^{m} N_{0,v}\sigma_{0,1_{0,v}} I_p(t) + \sum_{v=0}^{m} N_{0,v}\sigma^l_{0,1_{0,v}} I_l(x,t,\lambda_v) + \frac{N_{2,0}}{\tau_{2,1}} \\ & - N_{1,0}\left(\sum_{v=0}^{m} \sigma_{1,2_{0,v}} I_p(t) + \sum_{v=0}^{m} \sigma_{e_{0,v}} I_l(x,t,\lambda_v) \right. \\ & \left. + \sum_{v=0}^{m} \sigma^l_{1,2_{0,v}} I_l(x,t,\lambda_v) + \left(k_{S,T} + \tau^{-1}_{1,0}\right) \right) \end{aligned} \tag{A.13}$$

$$\frac{\partial N_{T_{1,0}}}{\partial t} \approx N_{1,0} k_{S,T} - \frac{N_{T_{1,0}}}{\tau_{T,S}} - N_{T_{1,0}} \left(\sum_{v=0}^{m} \sigma^{T}_{1,2_{0,v}} I_P(t) + \sum_{v=0}^{m} \sigma^{Tl}_{1,2_{0,v}} I_l(x,t,\lambda_v) \right) \quad \text{(A.14)}$$

$$c^{-1} \frac{\partial I_P(t)}{\partial t} \approx -\left(N_{0,0} \sum_{v=0}^{m} \sigma_{0,1_{0,v}} + N_{1,0} \sum_{v=0}^{m} \sigma_{1,2_{0,v}} + N_{T_{1,0}} \sum_{v=0}^{m} \sigma^{T}_{1,2_{0,v}} \right) I_P(t) \quad \text{(A.15)}$$

$$c^{-1} \frac{\partial I_l(x,t,\lambda}{\partial t} + \frac{\partial I_l(x,t,\lambda)}{\partial x} \approx N_{1,0} \sum_{v=0}^{m} \sigma_{e_{0,v}} I_l(x,t,\lambda_v) - \sum_{v=0}^{m} N_{0,v} \sigma^{l}_{0,1_{0,v}} I_l(x,t,\lambda_v)$$
$$- N_{1,0} \sum_{v=0}^{m} \sigma^{l}_{1,2_{0,v}} I_l(x,t,\lambda_v) - N_{T_{1,0}} \sum_{v=0}^{m} \sigma^{Tl}_{1,2_{0,v}} I_l(x,t,\lambda_v) \quad \text{(A.16)}$$

$$I_l(x,t,\lambda) = \sum_{v=0}^{m} I_l(x,t,\lambda_v) \quad \text{(A.17)}$$

$$I_l(x,t,\lambda) = I_l^{+}(x,t,\lambda) + I_l^{-}(x,t,\lambda) \quad \text{(A.18)}$$

In this set of equations, frequency dependence is incorporated via the summation terms, and variables, depending on the vibrational assignment v. The equations parameters are as follows (see Figure A.12):

1. $I_p(t)$ is the intensity of the pump laser beam. Units are photons cm^{-2} s^{-1}.
2. $I_l(x,t,\lambda)$ is the laser emission from the gain medium. Units are photons cm^{-2} s^{-1}.
3. $N_{S,v}$ refers to the population of the S electronic state at the v vibrational level. It is given as a number per unit volume (cm^{-3}).
4. $N_{T,v}$ refers to the population of the T triplet state at the v vibrational level. It is given as a number per unit volume (cm^{-3}).
5. The absorption cross sections, such as $\sigma_{0,1_{0,v}}$, are identified by a subscript $S'', S''_{v'',v'}$ that refers the electronic $S'' \rightarrow S'$ transition and the vibrational transition $v'' \rightarrow v'$.

   The same convention applies to the triplet levels. Units are cm^2.
6. The *emission* cross sections, $\sigma_{e_{0,v}}$, are identified by the subscript $e_{v',v''}$. Units are cm^2.
7. Radiationless decay times, such as $\tau_{1,0}$, are identified by subscripts that denote the corresponding $S' \rightarrow S''$ transition. Units are s.
8. $k_{S,T}$ is a radiationless decay rate from the singlet to the triplet. Units are s^{-1}.

   Ignoring the vibrational manifolds and other finer details, Equations (A.12)–(A.16) can be expressed in reduced form as

$$N = N_0 + N_1 + N_T \quad \text{(A.19)}$$

$$\frac{\partial N_1}{\partial t} \approx N_0\sigma_{0,1}I_p(t) + \left(N_0\sigma_{0,1}^{l} - N_1\sigma_e - N_1\sigma_{1,2}^{l}\right)I_l(x,t,\lambda) - N_1\left(k_{S,T} + \tau_{1,0}^{-1}\right) \quad \text{(A.20)}$$

$$\frac{\partial N_T}{\partial t} = N_1 k_{S,T} - N_T\,\tau_{T,S}^{-1} - N_T\sigma_{1,2}^{Tl}I_l(x,t,\lambda) \quad \text{(A.21)}$$

$$c^{-1}\frac{\partial I_p(t)}{\partial t} = -\left(N_0\sigma_{0,1} + N_1\sigma_{1,2}\right)I_p(t) \quad \text{(A.22)}$$

$$c^{-1}\frac{\partial I_l(x,t,\lambda)}{\partial t} + \frac{\partial I_l(x,t,\lambda)}{\partial x} = \left(N_1\sigma_e - N_0\sigma_{0,1}^{l} - N_1\sigma_{1,2}^{l} - N_T\sigma_{1,2}^{Tl}\right)I_l(x,t,\lambda) \quad \text{(A.23)}$$

This simplified set of equations is similar to the equations disclosed by Teschke et al. (1976). This type of rate equations can be effectively applied to simulate numerically the dynamics of dye laser intensity as a function of the laser-pump intensity and dye molecular concentration. Relevant cross sections and excitation rates are given in Table A.1.

It should be noted that since organic dye gain media exhibits homogeneous broadening, the introduction of intracavity frequency-selective optics (see Appendix B) enables all the molecules to contribute efficiently to tunable narrow-linewidth emission.

A.4.3 Long-Pulse Approximation

For long pulse, or CW emission, a simplified set of equations is possible, thus opening the alternative to closed-form solutions. Assuming that the time derivatives vanish, Equations (A.20)–(A.23) reduce to

TABLE A.1
Laser Excitation Parameters for the Rhodamine 6G Molecule

Symbol	Measured Value	λ (nm)	References
$\sigma_{0,1}$	1.66×10^{-16} cm^2	510	Hargrove and Kan (1980)
$\sigma_{0,1}$	4.50×10^{-16} cm^2	530	Everett (1991)
$\sigma_{1,2}$	0.40×10^{-16} cm^2	510	Hammond (1979)
σ_e	1.86×10^{-16} cm^2	572	Hargrove and Kan (1980)
σ_e	1.30×10^{-16} cm^2	600	Everett (1991)
$\sigma_{0,1}^{l}$	1.0×10^{-19} cm^2	600	Everett (1991)
$\sigma_{1,2}^{l}$	1.0×10^{-17} cm^2	600	Everett (1991)
$\sigma_{1,2}^{T}$	1.0×10^{-17} cm^2	530	Everett (1991)
$\sigma_{1,2}^{Tl}$	4.0×10^{-17} cm^2	600	Everett (1991)
$\tau_{1,0}$	4.8×10^{-9} s		Tuccio and Strome (1972)
$\tau_{2,1}$	1.0×10^{-12} s		Hargrove and Kan (1980)
$\tau_{T,S}$	1.1×10^{-7} s		Tuccio and Strome (1972)
$k_{S,T}$	8.2×10^{6} s^{-1}		Tuccio and Strome (1972)

$$N_0\sigma_{0,1}I_p + \left(N_0\sigma_{0,1}^l - N_1\sigma_e - N_1\sigma_{1,2}^l\right)I_l(x,\lambda) = N_1\left(k_{S,T} + \tau_{1,0}^{-1}\right) \tag{A.24}$$

$$N_1 k_{S,T} = N_T\ \tau_{T,S}^{-1} + N_T\sigma_{1,2}^{Tl}I_l(x,\lambda) \tag{A.25}$$

$$N_0\sigma_{0,1} = -N_1\sigma_{1,2} \tag{A.26}$$

$$\frac{\partial I_l(x,\lambda)}{\partial x} = \left(N_1\sigma_e - N_0\sigma_{0,1}^l - N_1\sigma_{1,2}^l - N_T\sigma_{1,2}^{Tl}\right)I_l(x,\lambda) \tag{A.27}$$

Using a *triplet level quenchers* such as O_2 or C_8H_8 (see, e.g., Duarte (1990)), it is possible to neutralize the effect of triplets so that the intensity given in Equation (A.27) simplifies to

$$\frac{\partial I_l(x,\lambda)}{\partial x} = \left(N_1\sigma_e - N_0\sigma_{0,1}^l - N_1\sigma_{1,2}^l\right)I_l(x,\lambda) \tag{A.28}$$

from which it follows that

$$I_l(x,\lambda) = I(0,\lambda)e^{\left(N_1(\sigma_e-\sigma_{1,2}^l)-N_0\sigma_{0,1}^l\right)L} \tag{A.29}$$

Thus, the gain can be expressed as

$$g = \left(N_1(\sigma_e - \sigma_{1,2}^l) - N_0\sigma_{0,1}^l\right)L \tag{A.30}$$

A.4.4 Example

From Equation (A.30), it can be deduced that, in the absence of triplet losses, gain can be achieved when

$$N_1\left(\sigma_e - \sigma_{1,2}^l\right) > N_0\sigma_{0,1}^l \tag{A.31}$$

or

$$\frac{N_1}{N_0} > \frac{\sigma_{0,1}^l}{\sigma_e - \sigma_{1,2}^l} \tag{A.32}$$

For rhodamine 6G, this ratio can be estimated using the cross sections given in Table A.1.

A.5 QUANTUM TRANSMISSION PROBABILITIES AND CROSS SECTIONS

Albeit the dynamics of laser excitation can be described using classical rate equations, an examination of transition probabilities, and transition cross sections, require a quantum treatment. Here, this is done via Dirac's notation (Dirac, 1958) while adopting Feynman's approach (Feynman et al., 1965). An introduction to Dirac's

notation is given in Chapter 4 and a summary of useful identities is available in Chapter 6. The following description is based on a review given by Duarte (2003).

Here, we begin with the basic Dirac principles

$$\langle \phi | \psi \rangle = \sum_j \langle \phi | j \rangle \langle j | \psi \rangle \tag{A.33}$$

$$\langle \phi | \psi \rangle = \langle \psi | \phi \rangle^* \tag{A.34}$$

$$\langle i | j \rangle = \delta_{ij} \tag{A.35}$$

For $j = 1, 2$, Equation (A.33) can be expanded into

$$\langle \phi | \psi \rangle = \langle \phi | 2 \rangle \langle 2 | \psi \rangle + \langle \phi | 1 \rangle \langle 1 | \psi \rangle \tag{A.36}$$

or

$$\langle \phi | \psi \rangle = \langle \phi | 2 \rangle C_2 + \langle \phi | 1 \rangle C_1 \tag{A.37}$$

where

$$C_1 = \langle 1 | \psi \rangle \tag{A.38}$$

and

$$C_2 = \langle 2 | \psi \rangle \tag{A.39}$$

Following Feynman, we express the derivative of the C_j amplitudes, with respect to time, as (Dirac, 1958; Feynman et al., 1965)

$$i\hbar \frac{dC_j}{dt} = \sum_k^2 H_{jk} C_k \tag{A.40}$$

where H_{jk} is the *Hamiltonian*.

Next, using Feynman's notation, new amplitudes C_I and C_{II} are defined as linear combinations of C_1 and C_2. Furthermore, since

$$\langle II | II \rangle = \langle II | 1 \rangle \langle 1 | II \rangle + \langle II | 2 \rangle \langle 2 | II \rangle = 1 \tag{A.41}$$

the normalization factor $2^{-1/2}$ is introduced, so that

$$C_{II} = 2^{-1/2}(C_1 + C_2) \tag{A.42}$$

$$C_I = 2^{-1/2}(C_1 - C_2) \tag{A.43}$$

Next, the Hamiltonian of the molecule under the effect of an electrical field is allowed to be perturbed so that the matrix elements of the Hamiltonian become

$$H_{11} = E_0 + \mu\mathcal{E} \tag{A.44}$$

$$H_{12} = -A \tag{A.45}$$

$$H_{21} = -A \tag{A.46}$$

$$H_{22} = E_0 - \mu\mathcal{E} \tag{A.47}$$

where

$$\mathcal{E} = \mathcal{E}_0(e^{i\omega t} + e^{-i\omega t}) \tag{A.48}$$

and μ corresponds to the electric dipole moment. The term $\mu\mathcal{E}$ is known as the *perturbation term*. Expanding Equation (A.40), followed by subtraction and addition, leads to

$$i\hbar\frac{dC_I}{dt} = (E_0 + A)C_I + \mu\mathcal{E}\, C_{II} \tag{A.49}$$

$$i\hbar\frac{dC_{II}}{dt} = (E_0 - A)C_{II} + \mu\mathcal{E}\, C_I \tag{A.50}$$

Assuming a small electric field, solutions are of the form

$$C_I = D_I e^{-i(E_I/\hbar)t} \tag{A.51}$$

$$C_{II} = D_{II} e^{-i(E_{II}/\hbar)t} \tag{A.52}$$

where

$$E_I = E_0 + A \tag{A.53}$$

and

$$E_{II} = E_0 - A \tag{A.54}$$

Assuming that $(\omega + \omega_0)$ oscillates too rapidly to contribute to the rate of change of D_I and D_{II}, we can write

$$i\hbar\frac{dD_I}{dt} = \mu\mathcal{E}_0 D_{II} e^{-i(\omega-\omega_0)t} \tag{A.55}$$

$$i\hbar\frac{dD_{II}}{dt} = \mu\mathcal{E}_0 D_I e^{i(\omega-\omega_0)t} \tag{A.56}$$

If at $t = 0$, $D_I \approx 1$, then integration of Equation (A.56) leads to

$$D_{II} = \frac{\mu \mathcal{E}_0}{\hbar}\left(\frac{1 - e^{i(\omega-\omega_0)T}}{(\omega - \omega_0)}\right) \tag{A.57}$$

and following multiplication with its complex conjugate

$$|D_{II}|^2 = \left(\frac{\mu \mathcal{E}_0}{\hbar}\right)^2 \left(\frac{2 - 2\cos(\omega - \omega_0)T}{(\omega - \omega_0)^2}\right) \tag{A.58}$$

which can be written as (Feynman et al., 1965)

$$|D_{II}|^2 = \left(\frac{\mu \mathcal{E}_0 T}{\hbar}\right)^2 \frac{\sin^2\left(\frac{1}{2}(\omega - \omega_0)T\right)}{\left(\frac{1}{2}(\omega - \omega_0)T\right)^2} \tag{A.59}$$

This is the probability for the transition $I \rightarrow II$ during the time segment T. This result is central to the theory of absorption and radiation of light by atoms and molecules. It can be further shown that

$$|D_I|^2 = |D_{II}|^2 \tag{A.60}$$

which means that the physics for the stimulated emission probability is the same as the physics for the absorption probability.

Using $I = 2\varepsilon_0 c \mathcal{E}_0^2$, the transition probability can be written as

$$|D_{II}|^2 = 2\pi\left(\frac{\mu^2 T^2}{4\pi\varepsilon_0 c\hbar^2}\right) I(\omega) \frac{\sin^2\left(\frac{1}{2}(\omega - \omega_0)T\right)}{\left(\frac{1}{2}(\omega - \omega_0)T\right)^2} \tag{A.61}$$

where, μ is the dipole moment in units of Cm, $(1/4\pi\varepsilon_0)$ is in units of $\mathrm{Nm^2\ C^{-2}}$, and $I(\omega)$ is the intensity in units of $\mathrm{Js^{-1}\ m^{-2}}$. There are two approaches to further evaluate this probability. The first alternative consists in evaluating $|D_{II}|^2$ at $\frac{1}{2}(\omega - \omega_0)T = \pi/2$ which yields

$$|D_{II}|^2 = \frac{8}{\pi}\left(\frac{\mu^2}{4\pi\varepsilon_0 c\hbar^2}\right) T^2 I(\omega_0) \tag{A.62}$$

$$|D_{II}|^2 = \frac{8}{\pi}\left(\frac{\sigma}{\hbar}\right) T^2 I(\omega_0) \tag{A.63}$$

$$|D_{II}|^2 = \frac{8}{\pi}\kappa^{-1} T^2 I(\omega_0) \tag{A.64}$$

where

$$\sigma = \left(\frac{\mu^2}{4\pi\varepsilon_0 c\hbar} \right) \tag{A.65}$$

is the cross section in units of m^2 and the constant

$$\kappa = \frac{\hbar}{\sigma} \tag{A.66}$$

is in units of Js/m^2. The intensity can then be written as

$$I(\omega_0) = \frac{\pi}{8} \kappa\, T^{-2} |D_{II}|^2 \tag{A.67}$$

An additional alternative is outlined by Feynman et al. (1965) and consists in evaluating the integral of the sine function in Equation (A.61) in which case

$$|D_{II}|^2 = 2\pi^2 \left(\frac{\sigma}{\hbar} \right) T^2 I(\omega_0) \tag{A.68}$$

From both approaches, it can be learned that the intensity, in units of $Js^{-1}\ m^{-2}$ or $W\ m^{-2}$, becomes

$$I(\omega_0) = \eta\, \kappa\, T^{-2} |D_{II}|^2 \tag{A.69}$$

where η is a numerical weight that depends on the approach selected to evaluate the sinusoidal function in (A.61). It should be noted that the probability equation given by Feynman et al. (1965) is dimensionally incorrect. Sargent et al. (1974) provide a slightly different approach to this transition probability.

A direct application of the quantum cross section σ evaluated here is in calculating the gain of molecular vibrational–rotational transitions, which can be expressed in the form (Chutjian and James, 1969; Byer et al., 1972)

$$g = \sigma NL \tag{A.70}$$

A.5.1 Long-Pulse Approximation

For a very long pulse, or a CW situation, $\frac{1}{2}(\omega - \omega_0)T$ dominates and Equation (A.61) can be approximated as

$$|D_{II}|^2 \approx 8\pi \left(\frac{\sigma}{\hbar} \right) (\omega - \omega_0)^{-2} I(\omega_0) \tag{A.71}$$

so that the intensity becomes

$$I(\omega_0) \approx \frac{\kappa}{8\pi} (\Delta\omega)^2 |D_{II}|^2 \tag{A.72}$$

This approximation indicates that the intensity is proportional to the square of the frequency linewidth multiplied by the probability of the transition, or $(\Delta\omega)^2|D_{II}|^2$.

PROBLEMS

A.1 Show that in the steady state Equation (A.20) becomes Equation (A.24).
A.2 Show that in the steady state Equation (A.23) becomes Equation (A.27).
A.3 In the absence of triplets, that is $k_{S,T} \approx 0$, set $I_I(x, \lambda) \approx 0$ in Equation (A.24) to arrive at an equation for I_p to estimate the necessary pump intensity to overcome the threshold.
A.4 Show that by neglecting the triplet state Equation (A.27) can be expressed as Equation (A.29).
A.5 Starting from Equations (A.49) and (A.50) derive an expression for $|D_I|^2$ and show that it is equal to $|D_{II}|^2$.
A.6 Show that Equation (A.58) can be written as Equation (A.59).
A.7 Verify that for a very long pulse, or a CW situation, Equation (A.61) becomes Equation (A.72).
A.8 Show that the dimensions of the intensity given in Equation (A.72) are in W m^{-2}.

REFERENCES

Barnes, N. P. (1995a). Transition metal solid-state lasers. In *Tunable Lasers Handbook* (Duarte, F. J., ed.). Academic, New York, Chapter 6, pp. 219–291.

Barnes, N. P. (1995b). Optical parametric oscillators. In *Tunable Lasers Handbook* (Duarte, F. J., ed.). Academic, New York, Chapter 7, pp. 293–348.

Byer, R. L., Herbst, R. L., Kildal, H., and Levenson, M. D. (1972). Optically pumped molecular iodine vapor-phase laser. *Appl. Phys. Lett.* **20**, 463–466.

Chutjian, A., and James, T. C. (1969). Intensity measurements in the system of I2. *J. Chem. Phys.* **51**, 1242–1249.

Dirac, P. A. M. (1958). *The Principles of Quantum Mechanics*, 4th ed. Oxford University, Oxford, U.K.

Duarte, F. J. (1977). *Excitation Processes in Continuous Wave Rare Gas-Metal Halide Vapour Lasers*, Macquarie University, Sydney.

Duarte, F. J. (1990). Technology of pulsed dye lasers. In *Dye Laser Principles* (Duarte, F. J., and Hillman, L. W., eds.). Academic, New York, Chapter 6, pp. 239–285.

Duarte, F. J. (1999). Solid-state multiple-prism grating dye laser oscillator: optimized architecture. *Appl. Opt.* **38**, 6347–6349.

Duarte, F. J. (2003). *Tunable Laser Optics*, Elsevier-Academic, New York.

Duarte, F. J. (2014). *Quantum Optics for Engineers*, 1st ed. CRC, Boca Raton, FL.

Duarte, F. J. (2015). *Tunable Laser Optics*, 2nd ed. CRC, Boca Raton, FL.

Duarte, F. J., Liao, L. S., Vaeth, K. M., and Miller, A. M. (2006). Widely tunable green laser emission using the coumarin 545 tetramethyl dye as the gain medium, *J. Opt. A*: *Pure Appl. Opt*. **8**, 172–174.

Duarte, F. J., and Piper, J. A. (1985). Measurements of neutral metal decay rates in CW rare-gas metal-halide vapor lasers. In *Proceedings of the International Conference on Lasers '84* (Corcoran, K. M. ed.). STS, McLean, VA, pp. 261–267.

Duarte, F. J., and Piper, J. A. (1986). Pulsed dye laser study of the B-X system in the I2 laser medium. In *Proceedings of the International Conference on Lasers '85* (Wang, C. P. ed.). STS, McLean, VA, pp. 789–796.

Duarte, F. J., Taylor, T. S., Costela, A., Garcia-Moreno, I., and Sastre, R. (1998). Long pulse narrow-linewidth dispersive solid-state dye-laser oscillator. *Appl. Opt.* **37**, 3987–3989.

Dujardin, G., and Flamant, P. (1978). Amplified spontaneous emission and spatial dependence of gain in dye amplifiers. *Opt. Commun.* **24**, 243–247.

Everett, P.N. (1991). Flashlamp-excited dye lasers. In *High Power Dye Lasers* (Duarte, F. J., ed.). Springer-Verlag, Berlin, Chapter 6, pp. 183–245.

Feynman, R. P., Leighton, R. B., and Sands, M. (1965). *The Feynman Lectures on Physics*, Vol. III, Addison-Wesley, Reading, MA.

Ganiel, U., Hardy, A., Neumann, G., and Treves, D. (1975). Amplified spontaneous emission and signal amplification in dye-laser systems. *IEEE J. Quantum Electron.* **QE-11**, 881–892.

Haag, G., Munz, M., and Marowski, G. (1983). Amplified spontaneous emission (ASE) in laser oscillators and amplifiers. *IEEE J. Quantum Electron.* **QE-19**, 1149.

Haken, H. (1970). *Light and Matter*. Springer-Verlag, Berlin.

Hammond, P. (1979). Spectra of the lowest excited singlet states of rhodamine 6G and rhodamine B. *IEEE J. Quantum Electron.* **QE-15**, 624–632.

Hargrove, R. S., and Kan, T. K. (1980). High power efficient dye amplifier pumped by copper vapor lasers. *IEEE J. Quantum Electron.* **QE-16**, 1108–1113.

Hollberg, L. (1990). CW dye lasers. In *Dye Laser Principles* (Duarte, F. J., and Hillman, L. W., eds.). Academic, New York, Chapter 5, pp. 185–238.

Jensen, C., (1991). Pulsed dye laser gain analysis and amplifier design. In *High Power Dye Lasers* (Duarte, F. J., ed.). Springer-Verlag, Berlin, Chapter 3, pp. 45–91.

Kaslin, V. M., Petrash, G. G., and Yakushev, O. F. (1980). Laser action at the B-X transition of the I2 molecule using a copper-vapor laser for optical pumping. *Sov. Phys. JETP.* **51**, 679–686.

Kessler, T., Hagemann, C., Grebing, C., Legero, T., Sterr, U., Riehle, F., Martin, M. J., Chen, L., and Ye, J. (2012). A sub-40-mHz-linewidth laser based on a silicon single-crystal optical cavity. *Nature Photon.* **6**, 687–692.

Maiman, T. H. (1960). Stimulated optical radiation in ruby. *Nature* **187**, 493–494.

Munz, M., and Haag, G. (1980). Optimization of dye-laser output coupling by consideration of the spatial gain distribution. *Appl. Phys.* **22**, 175–184.

Nair, L. G., and Dasgupta, K. (1985). Amplified spontaneous emission in narrow-band pulsed dye laser oscillators -theory and experiment. *IEEE J. Quantum Electron.* **21**, 1782–1794.

Orr, B. J., He, Y., and White, R. T. (2016). Spectroscopic applications of pulsed tunable optical parametric oscillators. In *Tunable Laser Applications*, 3rd ed. (Duarte, F. J., ed.). CRC, Boca Raton, FL, Chapter 2, 17–142.

Penzkofer, A., and Falkenstein, W. (1978). Theoretical investigation of amplified spontaneous emission with picosecond light pulses in dye solutions. *Opt. Quantum Electron.* **10**, 399–423.

Peterson, O. G. (1979). Dye lasers. In *Methods of Experimental Physics*, Vol. 15 (Tang, C. L. ed.). Academic, New York, Chapter 5, pp. 251–359.

Piper, J. A. (1976). Simultaneous CW laser oscillation on transitions of Cd+ and I+ in a hollow-cathode He-CdI2 discharge. *Opt. Commun.* **19**, 189–192.

Piper, J. A., and Gill, P. (1975). Output characteristics of the He-Zn laser. *J. Phys. D: Appl. Phys.* **8**, 127–134.

Popov, S. (2016). Fiber laser overview and medical applications. In *Tunable Laser Applications*, 3rd ed. (Duarte, F. J., ed.). CRC, Boca Raton, FL, Chapter 7, pp. 263–292.

Sargent, M., Scully, M. O, and Lamb, W. E. (1974). *Laser Physics*, Addison Wesley, Reading, MA.

Schäfer, F. P., Schmidt, W., and Volze, J. (1966). Organic dye solution laser. *Appl. Phys. Lett.* **9**, 306–309.

Silfvast, W. T. (2008). *Laser Fundamentals*, 2nd ed. Cambridge University, Cambridge, U.K.

Teschke, O., Dienes, A., and Whinnery, J. R. (1976). Theory and operation of high- power CW and long-pulse dye lasers. *IEEE J. Quantum Electron.* **QE-12**, 383–395.

Tuccio, S. A., and Strome, F. C. (1972). Design and operation of a tunable continuous dye laser. *Appl. Opt.* **11**, 64–73.

Wellegehausen, B. (1979). Optically pumped CW dimer lasers. *IEEE J. Quantum Electron.* **QE-15**, 1108–1130.

Willett, C. S. (1974). *An introduction to Gas Lasers: Population Inversion Mechanisms*, Pergamon, New York.

Appendix B
Laser Oscillators and Laser Cavities via Dirac's Notation

B.1 INTRODUCTION

Here we derive the classical linewidth cavity equation

$$\Delta\lambda \approx \Delta\theta\left(\frac{\partial\theta}{\partial\lambda}\right)^{-1} \tag{B.1}$$

using the Dirac's notation approach. First, we notice that in this equation, $\Delta\theta$ is the beam divergence previously related to the uncertainty principle (see Chapter 3)

$$\Delta p\,\Delta x \approx h \tag{B.2}$$

and $\left(\partial\theta/\partial\lambda\right)^{-1}$ is the overall cavity angular dispersion (Duarte, 2003).

We should also mention that Equation (B.1) is the single-pass version of the *multiple-pass* linewidth cavity equation (Duarte and Piper, 1984; Duarte 1990, 2001)

$$\Delta\lambda = \Delta\theta_R\left(MR\nabla_\lambda\Theta_G + R\nabla_\lambda\Phi_P\right)^{-1} \tag{B.3}$$

where the multiple return-pass beam divergence is given by (Duarte, 1989, 1990)

$$\Delta\theta_R = \frac{\lambda}{\pi w}\left(1+\left(\frac{L_{\mathscr{R}}}{B_R}\right)^2+\left(\frac{A_R L_{\mathscr{R}}}{B_R}\right)^2\right)^{1/2} \tag{B.4}$$

In Equations (B.3) and (B.4), R is the number of return-cavity passes necessary to reach laser threshold, $L_{\mathscr{R}} = (\pi w^2/\lambda)$ is the Rayleigh length (Duarte, 1990), and w is the beam waist. $A_{\mathscr{R}}$ and B_R are the corresponding multi-return-pass matrix elements (Duarte, 2003) as indicated in Appendix F. For high-power, high-gain, tunable narrow-linewidth oscillators (as depicted in Figures B.1 and B.2), this factor has been measured to be $R \approx 3$ (Duarte, 2001). Equation (B.3) has been found to be fairly successful to predict, and account for, measured laser linewidths in high-gain, pulsed tunable lasers (Duarte, 2001).

In this chapter, we shall see that equations and concepts previously developed in a classical context can also be outlined and derived from a quantum perspective. Here, it should be mentioned that these laser-linewidth concepts have been successfully

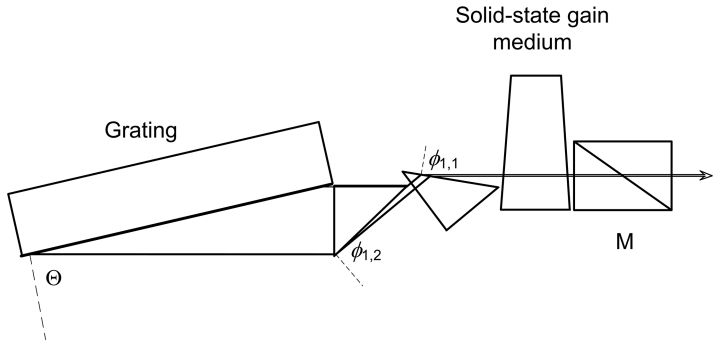

FIGURE B.1 Optimized multiple-prism grating solid-state dye laser oscillator using a 3000 lines/mm diffraction grating deployed in Littrow configuration. The measured laser linewidth is $\Delta\nu \approx 350$ MHz (Duarte, 1999). This is a *closed cavity* configuration, where the laser output is coupled via a partially reflective mirror rather than from the reflection loss of a diffractive element (Reproduced from Duarte, F. J., *Appl. Opt.* **38**, 6347–6349, 1999, with permission from Optica).

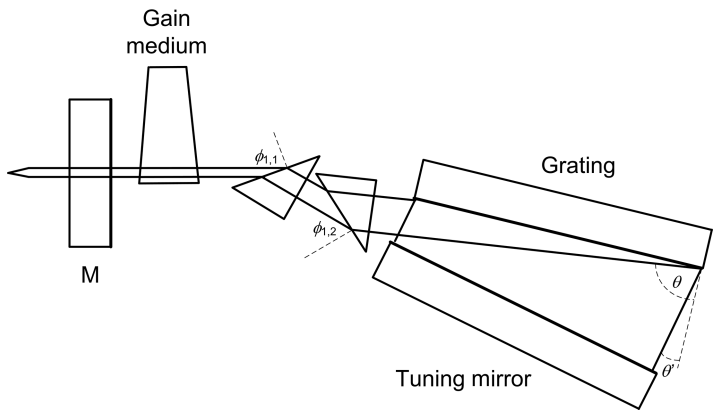

FIGURE B.2 Hybrid multiple-prism near grazing incidence (HMPGI) grating oscillator (Duarte and Piper, 1981; Duarte, 1990). For the organic solid-state HMPGIG oscillator, the measured laser linewidth is $\Delta\nu \approx 375$ MHz (Duarte, 1997a). This is a *closed cavity* configuration.

applied to lasers with gain media the gaseous (Duarte, 1985), the liquid (Duarte and Piper, 1984), and the solid state (Duarte, 1994).

B.2 TRANSVERSE AND LONGITUDINAL MODES

The unrestricted initial emission from laser gain media is both spatially and spectrally broad, in other words, it lacks spectral purity. This is the essence of broadband emission. Spatially, this broad emission contains many spatial modes, and each of those spatial modes includes a multitude of longitudinal modes. Albeit exhibiting a

directional beam, this type of broadband emission is essentially chaotic and exhibits a high degree of entropy.

To achieve highly selective, controllable, narrow-linewidth, spectrally pure emission, it is imperative to:

1. Restrict the spatial emission to a single transverse electromagnetic mode, that is TEM_{00}.
2. Restrict the longitudinal modes, *within* that single transverse mode (TEM_{00}), to a single-longitudinal mode (SLM).

In other words, highly coherent, spectrally pure, low entropy laser emission requires the selection of a single transverse electromagnetic mode, followed by the selection of a single longitudinal mode within that single transverse mode. The discussion that follows next includes concepts and elements from a review given by Duarte (2003).

B.2.1 Transverse-Mode Structure

A fundamental laser cavity is comprised of a gain medium and two mirrors, as illustrated in Figure B.3. The physical dimension of the intracavity aperture ($2w$)relative to the separation of mirrors, or cavity length (L), determines the number of transverse electromagnetic modes. A typical broadband laser cavity, under optical excitation, has an aperture in the few mm range and a cavity length of about 10 cm. For the same cavity length, the aperture size in a narrow-linewidth cavity is reduced to the $100 \leq 2w \leq 200$ μm range.

The narrower the width of the intracavity aperture and the longer the cavity length, the lower the number of transverse modes (Duarte, 2003). The single-pass

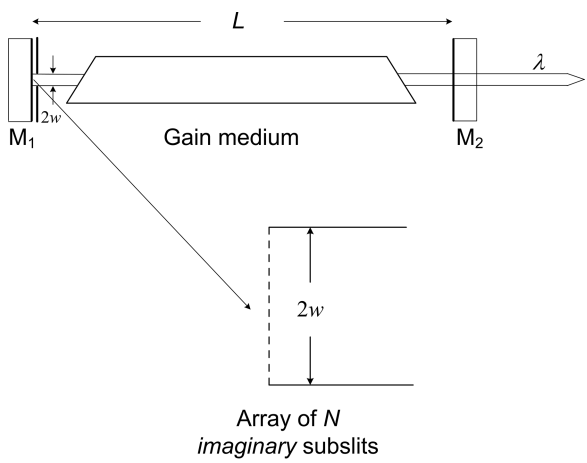

FIGURE B.3 Mirror-mirror laser cavity. The physical dimensions of the intracavity aperture relative to the cavity length determine the number of transverse modes. Parameters that enter the calculation are laser wavelength (λ), cavity length (L), and number of subslits (N).

transverse mode structure in one dimension can be characterized using the generalized interferometric equation introduced in Chapter 4 (Duarte, 1991, 1993a)

$$\left|\langle d|s\rangle\right|^2 = \sum_{j=1}^{N} \Psi(r_j)^2 + 2\sum_{j=1}^{N} \Psi(r_j)\left(\sum_{m=j+1}^{N} \Psi(r_m)\cos(\Omega_m - \Omega_j)\right) \tag{B.5}$$

and in two dimensions by (Duarte, 1995a)

$$\left|\langle d|s\rangle\right|^2 = \sum_{z=1}^{N}\sum_{y=1}^{N} \Psi(r_{zy}) \sum_{q=1}^{N}\sum_{p=1}^{N} \Psi(r_{pq}) e^{i(\Omega_{qp} - \Omega_{zy})} \tag{B.6}$$

The single-pass approximation to estimate the transverse mode structure assumes that in a laser with a given cavity length, most of the emission generated next to the output-coupler mirror is in the form of spontaneous emission and thus highly divergent. Thus, only the emission generated at the opposite end of the cavity and that propagates via an intracavity length L contributes to the initial transverse mode structure.

To illustrate the use of these equations, let us consider a hypothetical laser with a 10 cm cavity emitting at $\lambda = 590$ nm incorporating a one-dimensional aperture $(2w) = 2$ mm wide. Using Equation (B.5), the intensity distribution of the emission is calculated as shown in Figure B.4. Each ripple represents a transverse mode. An estimate of this number can be obtained by counting the ripples in Figure B.4 which yields an approximate number of 17. The Fresnel number (Siegman, 1986) for the given dimensions is

$$N_F = \left(\frac{w^2}{L\lambda}\right) = 16.95 \tag{B.7}$$

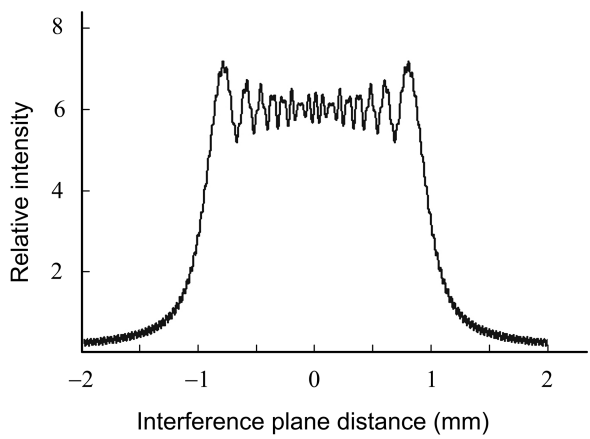

FIGURE B.4 Cross-section of diffraction distribution corresponding to a large number of transverse modes. Here, $\lambda = 590$ nm, $2w = 2$ mm, $L = 10$ cm, and $N_F \approx 17$. The wide aperture is assumed to be composed of $N = 1000$ 'imaginary' subslits.

For the same wavelength at $\lambda = 590$ nm and cavity length ($L = 10$ cm), if the aperture is reduced to $2w = 250$ μm, the calculated intensity distribution, using Equation (B.5), is given in Figure B.5. In this case, the Fresnel number becomes $N_F \approx 0.26$.

The distribution in Figure B.5 indicates that most of the emission intensity is contained in a central near-Gaussian distribution. A measured single-transverse-mode beam, with an ovaloid profile, from a narrow-linewidth tunable solid-state dye laser (Duarte, 1995b), is displayed in Figure B.6.

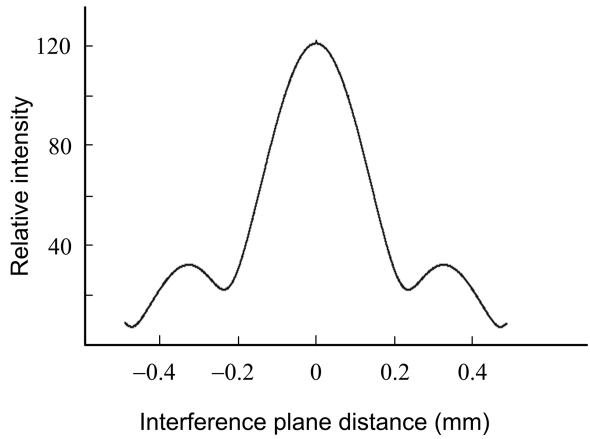

FIGURE B.5 Cross-section of diffraction distribution corresponding to a near single-Transverse-mode corresponding to $\lambda = 590$ nm, $2w = 250$ μm, $L = 10$ cm, and $N_F \approx 0.26$. In practice, the lower intensity higher-order maxima are not observed due to cavity losses and often only the central mode remains.

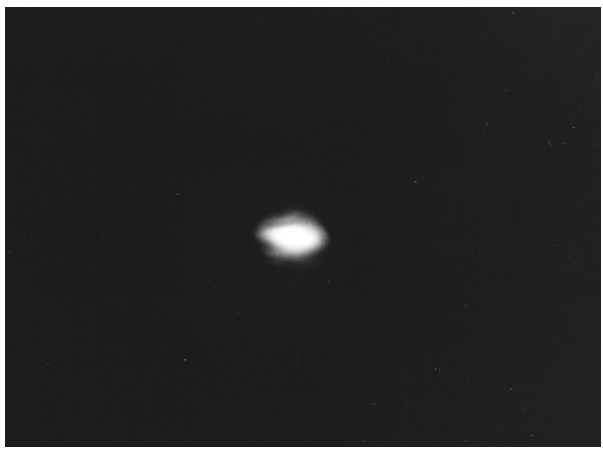

FIGURE B.6 Single-transverse mode beam originating from a single-longitudinal-mode ($\Delta\nu \approx 420$ MHz) multiple-prism grating solid-state dye laser (Reproduced from Duarte, F. J., *Opt. Commun.* **117**, 480–484, 1995b, with permission from Elsevier).

In summary: reducing the transverse mode distribution to TEM_{00} emission is the first step in the design of narrow-linewidth tunable lasers. The task of the designer consists in achieving TEM_{00} emission within desirable geometrical parameters that include the shortest possible cavity length.

B.2.2 Double- and Single-Longitudinal-Mode Emission

Successful discrimination toward a single-transverse-mode is the first step toward the attainment of tunable narrow-linewidth emission. The next task consists in controlling the number of longitudinal modes in the cavity. In a laser resonator with cavity length L, the longitudinal-mode spacing ($\delta\nu$), in the frequency domain, is given by an alternative form of the uncertainty principle (see Chapter 3)

$$\delta\nu = \frac{c}{2L} \tag{B.8}$$

and the number of longitudinal modes N_{LM} is given

$$N_{LM} = \frac{\Delta\nu}{\delta\nu} \tag{B.9}$$

where $\Delta\nu$ is the measured laser linewidth (Duarte, 2003). From Equations (B.8) and (B.9), it is clear that the number of allowed longitudinal modes (N_{LM}) decreases as the cavity length decreases. Thus, the importance of cavity compactness is highlighted.

An additional, and complementary, approach to achieve SLM emission is to optimize the beam divergence and increase the intracavity dispersion to yield a narrower cavity linewidth that would restrict oscillation to the SLM regime. In this context, the linewidth

$$\Delta\lambda \approx \Delta\theta\left(\frac{\partial\theta}{\partial\lambda}\right)^{-1} \tag{B.10}$$

is converted to $\Delta\nu$ units (Hz) using the identity

$$\Delta\nu = \Delta\lambda\left(\frac{c}{\lambda^2}\right) \tag{B.11}$$

and applying the criterion

$$\Delta\nu \leq \delta\nu \tag{B.12}$$

to guide the design of the dispersive oscillator.

Multiple-longitudinal-mode emission is complex and chaotic, both in the frequency and temporal domains. Double-longitudinal-mode (DLM) and SLM emission can be characterized in the frequency domain using Fabry–Perot interferometry or in the temporal domain by observing the shape of the temporal pulsed. In the case of DLM-emission, the interferometric rings appear to be double. In the temporal

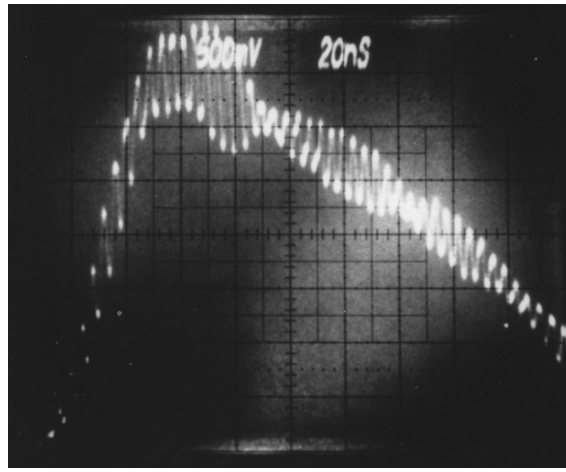

FIGURE B.7 Measured mode beating resulting from double-longitudinal-mode oscillation. Temporal scale is 20 ns/div (Reproduced from Duarte, F. J. et al., *Appl. Opt.* **27**, 843–846, 1988, with permission from Optica).

domain, *mode beating* is still observed when the intensity ratio of the primary to the secondary mode is 100:1 or even higher. Mode-beating of two longitudinal modes, as illustrated in Figure B.7, can be characterized using a wave function representation where the modes of frequencies ω_1 and ω_2, combine to produce a resulting field of the form

$$\left|\langle d|s\rangle\right|^2 = \Psi(r_1)^2 + \Psi(r_2)^2 + 2\Psi(r_1)\Psi(r_2)\cos(\Omega_2 - \Omega_1) \tag{B.13}$$

Setting $\Omega_2 = \omega_2 t$ and $\Omega_1 = \omega_1 t$, this probability becomes

$$\left|\langle d|s\rangle\right|^2 = \Psi(r_1)^2 + \Psi(r_2)^2 + 2\Psi(r_1)\Psi(r_2)\cos(\omega_2 - \omega_1)t \tag{B.14}$$

The reader should have observed that Equation (B.13) is the generalized interferometric probability for $N = 2$. Also relevant is that the quantum intensity is $I \propto \langle d|s\rangle\langle d|s\rangle^*$ as described in Appendix A. It should also be mentioned that the original description of this phenomenon was done classically using the concept of electric fields (Pacala et al., 1984).

Using this approximation and a non-Gaussian temporal representation, derived from experimental data, for the amplitudes of the form

$$E_1(t) = (a_2 t^2 + a_1 t + a_0)(b_1 t + b_0)^{-1} \tag{B.15}$$

a calculated version of the experimental waveform exhibiting mode beating can be obtained as shown in Figure B.8 (Duarte et al., 1988). For the oscillator under consideration, which was lasing in the double-longitudinal mode regime, the ratio of frequency jitter $\delta\omega$ to cavity mode spacing $\Delta\omega \approx (\omega_2 - \omega_1)$ was represented by a

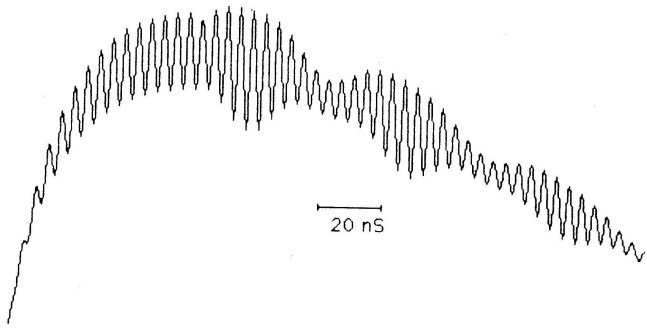

FIGURE B.8 Calculated temporal pulse assuming interference between the two longitudinal modes (Reproduced from Duarte, F. J. et al., *Appl. Opt.* **27**, 843–846, 1988, with permission from Optica).

sinusoidal function at 20 MHz. The initial mode intensity ratio is 200:1 (Duarte et al., 1988; Duarte, 1990).

In the case of SLM emission, the Fabry–Perot interferometric rings appear singular and well defined (see Figure B.9). Mode beating in the temporal domain is absent and the pulses assume a near Gaussian distribution (see Figure B.10). These results were obtained in an optimized solid-state multiple-prism grating dye laser oscillator

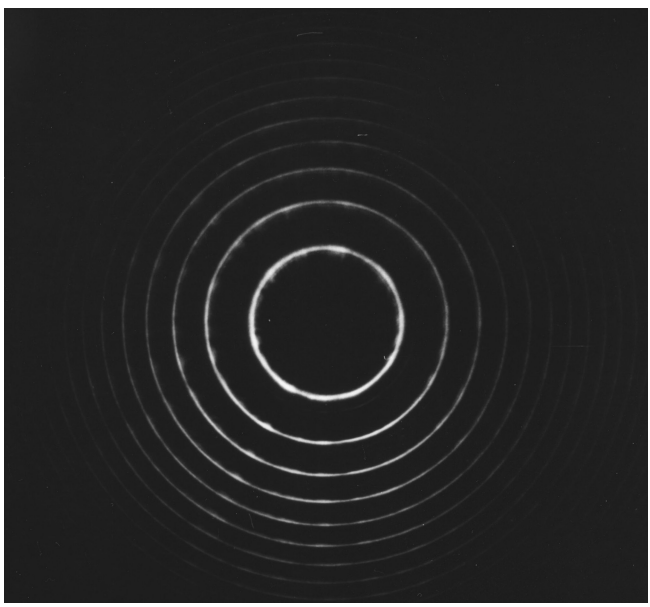

FIGURE B.9 Fabry–Perot interferogram corresponding to single-longitudinal-mode emission at $\Delta\nu \approx 350$ MHz (Reproduced from Duarte, F. J., *Appl. Opt.* **38**, 6347–6349, 1999, with permission from Optica).

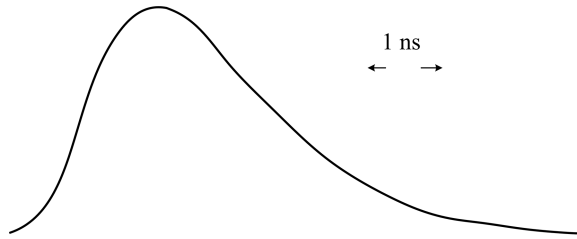

FIGURE B.10 Near-Gaussian temporal pulse corresponding to single-longitudinal-mode emission. The temporal scale is 1 ns/div (Reproduced from Duarte, F. J., *Appl. Opt.* **38**, 6347–6349, 1999, with permission from Optica).

for which $\Delta\nu\,\Delta t \approx 1$, which is near the limit allowed by Heisenberg's uncertainty principle (Duarte, 1999).

B.2.3 Example

For a laser with a 15 cm cavity length ($\delta\nu \approx 1$ GHz, using Equation (B.8), and a measured linewidth of $\Delta\nu = 3$ GHz, the number of longitudinal modes becomes $N_{LM} \approx 3$ (using Equation (B.9). If the cavity length is reduced to 10 cm ($\delta\nu \approx 1.5$ GHz), then the number of longitudinal modes is reduced to $N_{LM} \approx 2$ and the emission would be called DLM emission. Furthermore, if the cavity length is reduced to 5 cm, then $N_{LM} \approx 1$, and the laser is said to be undergoing SLM oscillation. This example highlight the advantages of compact cavity designs.

B.3 THE LASER CAVITY EQUATION: AN INTUITIVE APPROACH

We now describe an intuitive approach to the laser cavity equation using Dirac's notation as applied to a multiple-prism grating cavity as illustrated in Figures B.1 and B.2 (Duarte, 1992). A close-up view of the frequency selective assembly, in an unfolded configuration, is shown in Figure B.11.

In reference to this figure, the probability amplitude describing the propagation from the active region emitter s to the entrance of the multiple-prism array at an incidence angle $\phi_{1,m}$ can be expressed as

$$\langle \phi_{1,m} | s \rangle \tag{B.16}$$

while the probability amplitude to propagate, through the dispersive multiple-prism grating assembly D, from an incidence angle $\phi_{1,m}$ to a return angle $\phi'_{1,m}$ can be written as

$$\langle \phi'_{1,m} | D | \phi_{1,m} \rangle \tag{B.17}$$

Similarly, the probability amplitude to exit the multiple-prism array at an angle $\phi'_{1,m}$ back to the gain medium is

$$\langle s' | \phi'_{1,m} \rangle \tag{B.18}$$

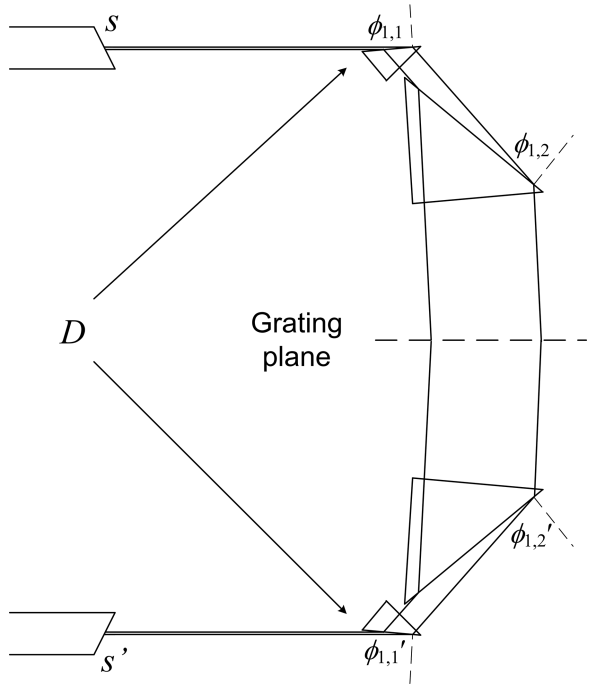

FIGURE B.11 Unfolded optical path of a dispersive multiple-prism grating configuration showing the emission source *S* followed by the entrance of the multiple-prism grating assembly ($\phi_{1,m}$ with $m = 1$), the dispersive assembly *D*, and the corresponding quantities to the return path back to the gain region (Adapted from Duarte, F. J., *Appl. Opt.* **31**, 6979–6982, 1992, with permission from Optica).

Thus, the overall probability amplitude for a photon to propagate from the active medium *s*, through the dispersive multiple-prism grating assembly, and back to the gain medium, is

$$\langle s'|D|s\rangle = \sum_{\phi'_{1,m}} \sum_{\phi_{1,m}} \langle s'|\phi'_{1,m}\rangle \langle \phi'_{1,m}|D|\phi_{1,m}\rangle \langle \phi_{1,m}|s\rangle \tag{B.19}$$

Since $\phi_{1,m}$ is a *unique angle* of incidence on the gain axis, at the multiple-prism expander, that is necessary to induce diffraction at the grating followed by an exact return passage to the gain medium, the probability amplitude can be reduced to (Duarte, 1992)

$$|\langle s'|D|s\rangle| = \langle s'|\phi'_{1,m}\rangle \langle \phi'_{1,m}|D|\phi_{1,m}\rangle \langle \phi_{1,m}|s\rangle \tag{B.20}$$

so that the probability for the intracavity photon propagation just described becomes

$$|\langle s'|D|s\rangle|^2 = |\langle s'|\phi'_{1,m}\rangle|^2 \, |\phi'_{1,m}|D|\phi_{1,m}|^2 \, |\langle \phi_{1,m}|s\rangle|^2 \tag{B.21}$$

The different components of this probability can be identified by describing the propagation at each segment. Immediately, at the exit of the gain region, in the first segment, the probability of narrow linewidth emission propagation is inversely proportional to the beam divergence $\Delta\theta$ of the emission, so that

$$\left|\langle\phi_{1,m}|s\rangle\right|^2 = \kappa_1\left(\frac{1}{\Delta\theta}\right) \tag{B.22}$$

Once the photon flux arrives at the dispersive multiple-prism grating assembly, the return of resonant narrow linewidth emission is proportional to the dispersion of the configuration. The higher the dispersion, the narrower the linewidth

$$\left|\langle\phi'_{1,m}|D|\phi_{1,m}\rangle\right|^2 = \kappa_2\left(\frac{\partial\theta}{\partial\lambda}\right) \tag{B.23}$$

For highly selective resonant emission that returns precisely at $\phi'_{1,m}$, the probability to return to the gain region for further amplification is high so that

$$\left|\langle s'|\phi'_{1,m}\rangle\right|^2 \approx 1 \tag{B.24}$$

Now, since the overall probability for resonant narrow-linewidth amplification is inversely proportional to the wavelength spread of the emission

$$\left|\langle s'|D|s\rangle\right|^2 = \kappa_3\left(\frac{1}{\Delta\lambda}\right) \tag{B.25}$$

Combining Equations (B.22)–(B.25) into (B.21), we get

$$\Delta\lambda \approx \Delta\theta\left(\frac{\kappa_1\kappa_2}{\kappa_3}\right)\left(\frac{\partial\theta}{\partial\lambda}\right)^{-1} \tag{B.26}$$

which, for $\kappa_3 \approx (\kappa_1\kappa_2)$, takes the form

$$\Delta\lambda \approx \Delta\theta\left(\frac{\partial\theta}{\partial\lambda}\right)^{-1} \tag{B.27}$$

Albeit fairly intuitive, this approach lends itself to illustrate the refinement process that occurs with multiple intra-cavity passes.

B.4 THE LASER CAVITY EQUATION VIA THE INTERFEROMETRIC EQUATION

By now, the reader should be getting the message that interference is at the heart of many phenomena in laser optics. We just saw how the interferometric equation applied to a single aperture can be used to describe the transverse mode structure of a laser cavity. In other words, we saw how the geometrical ratio of aperture width to

cavity length affects the transverse-mode distribution of the emission. Now, we apply the generalized, one-dimensional, interferometric equation

$$\left|\langle d|s\rangle\right|^2 = \sum_{j=1}^{N}\Psi(r_j)^2 + 2\sum_{j=1}^{N}\Psi(r_j)\left(\sum_{m=j+1}^{N}\Psi(r_m)\cos(\Omega_m - \Omega_j)\right)$$

to describe the origin of the cavity linewidth equation. We do this by focusing attention on the phase term of the *N*-slit interferometric equation (Duarte, 1997b)

$$\cos\left((\theta_m - \theta_j) \pm (\phi_m - \phi_j)\right) = \cos\left(|l_m - l_{m-1}|k_1 \pm |L_m - L_{m-1}|k_2\right) \tag{B.28}$$

from which the well-known *grating equation* can be derived (see Chapter 5)

$$d_m(\sin\Theta_m \pm \sin\Phi_m) = m\lambda \tag{B.29}$$

where $m = 0, \pm 1, \pm 2, \pm 3, \ldots$ For a grating deployed in the reflection domain, and at *Littrow* configuration, $\Theta_m = \Phi_m = \Theta$ (that is, the diffracted light goes back at the same angle of the incident beam) so that the grating equation reduces to

$$m\lambda = 2d_m \sin\Theta \tag{B.30}$$

where $m = 0, 1, 2, 3, \ldots$ are the various *diffraction orders*.

Considering two slightly different wavelengths, an expression for the wavelength difference can be written as

$$\Delta\lambda = \frac{2d_m}{m}(\sin\Theta_1 - \sin\Theta_2) \tag{B.31}$$

for $\Theta_1 \approx \Theta_2 (= \Theta)$ this equation can be restated as

$$\Delta\lambda \approx \frac{2d_m}{m}\Delta\theta\left(1 - \frac{3\Theta^2}{3!} + \frac{5\Theta^4}{5!} - \ldots\right) \tag{B.32}$$

Differentiation of the grating equation leads to

$$\left(\frac{\partial\theta}{\partial\lambda}\right)\cos\Theta = \frac{m}{2d_m} \tag{B.33}$$

and substitution into Equation (B.33) yields

$$\Delta\lambda \approx \Delta\theta\left(\frac{\partial\theta}{\partial\lambda}\right)^{-1}\left(1 - \frac{\Theta^2}{2!} + \frac{\Theta^4}{4!} - \ldots\right)(\cos\Theta)^{-1} \tag{9.34}$$

which reduces to the well-known cavity linewidth equation (Duarte, 1992)

$$\Delta\lambda \approx \Delta\theta \left(\frac{\partial\theta}{\partial\lambda} \right)^{-1} \tag{B.35}$$

or

$$\Delta\lambda \approx \Delta\theta \, (\nabla_{\lambda}\theta)^{-1} \tag{B.36}$$

where $\nabla_{\lambda}\theta = (\partial\theta/\partial\lambda)$. This equation has been used extensively to determine the emission linewidth in pulsed narrow-linewidth dispersive laser oscillators (Duarte, 1990). It originates in the generalized *N*-slit interference equation and incorporates $\Delta\theta$ whose value can be determined either from Heisenberg's uncertainty principle or from the interferometric equation itself. This equation is also well known in the field of classical spectrometers where it has been introduced using geometrical arguments (Robertson, 1955). In addition to its technical and computational usefulness, Equations (B.35) and/or (B.36) illustrate the inherent interdependence between spectral and spatial coherence.

PROBLEMS

B.1 Show that for $R = 1$, and in the absence of a grating, Equation (B.3) reduces to an equation of the form of Equation (B.1) where the dispersion is provided by the multiple-prism assembly.

B.2 For an optimized multiple-prism grating oscillator, as shown in Figure B.1, the measured laser linewidth is $\Delta\nu \approx 350$ MHz. Given that the free spectral range of the cavity is $FSR \approx 1.6$ GHz, determine (a) the approximate length of the cavity and (b) the value of the overall intracavity dispersion given that the measured beam divergence is $\Delta\theta \approx 2.2$ m rad.

B.3 For the case of laser radiation in the visible spectrum, show that Equation (B.14) reduces to Equation (B.15) for detectors with a time response in the nanosecond regime.

B.4 Show in detail how Equation (B.32) reduces to the cavity linewidth equation: Equation (B.35).

REFERENCES

Duarte, F. J. (1985). Multiple-prism Littrow and grazing-incidence pulsed CO_2 lasers. *Appl. Opt.* **24**, 1244–1245.

Duarte, F. J. (1989). Ray transfer matrix analysis of multiple-prism dye laser oscillators. *Opt. Quantum Electron*. **21**, 47–54.

Duarte, F. J. (1990). Narrow linewidth pulsed dye laser oscillators. In *Dye Laser Principles* (Duarte, F. J., and Hillman, L. W., eds.). Academic, New York, Chapter 4, pp. 133–183.

Duarte, F. J. (1991). Dispersive dye lasers. In *High Power Dye Lasers* (Duarte, F. J., ed.). Springer-Verlag, Berlin, Chapter 2, pp. 7–43.

Duarte, F. J. (1992). Cavity dispersion equation : a note on its origin. *Appl. Opt.* **31**, 6979–6982.
Duarte, F. J. (1993). On a generalized interference equation and interferometric measurements. *Opt. Commun.* **103**, 8–14.
Duarte, F. J. (1994). Solid-state multiple-prism grating dye-laser oscillators. *Appl. Opt.* **33**, 3857–3860.
Duarte, F. J. (1995a). Interferometric imaging. In *Tunable Laser Applications* (Duarte, F. J., ed.). Marcel Dekker, New York, Chapter 5, pp. 153–178.
Duarte, F. J. (1995b). Solid-state dispersive dye laser oscillator: very compact cavity, *Opt. Commun.* **117**, 480–484.
Duarte, F. J. (1997a). Multiple-prism near-grazing-incidence grating solid-state dye laser oscillator, *Opt. Laser Technol.* **29**, 513–516.
Duarte, F. J. (1997a). Interference, diffraction, and refraction, via Dirac's notation. *Am. J. Phys.* **65**, 637–640.
Duarte, F. J. (1999). Multiple-prism grating solid-state dye laser oscillator: optimized architecture, *Appl. Opt.* **38**, 6347–6349.
Duarte, F. J. (2001). Multiple-return-pass beam divergence and the linewidth equation. *Appl. Opt.* **40**, 3038–3041.
Duarte, F. J. (2003). *Tunable Laser Optics*, Elsevier-Academic, New York.
Duarte, F. J., and Piper, J. A. (1981). A prism preexpanded grazing incidence pulsed dye laser, *Appl. Opt.* **20**, 2113–2116.
Duarte, F. J., and Piper, J. A. (1984). Multi-pass dispersion theory of prismatic pulsed dye lasers. *Optica Acta* **31**, 331–335.
Duarte, F. J., Ehrlich, J. J., Patterson, S. P., Russell, S. D., and Adams, J. E. (1988). Linewidth instabilities in narrow-linewidth flashlamp-pumped dye laser oscillators. *Appl. Opt.* **27**, 843–846.
Pacala, T. J., McDermid, I. S., and Laudenslager, J. B. (1984). Single-longitudinal-mode operation of an XeCl laser. *Appl. Phys. Lett.* **45**, 507–509.
Robertson, J. K. (1955). *Introduction to Optics: Geometrical and Physical*, Van Nostrand, New York.
Siegman, A. E. (1986). *Lasers*, University Science Books, Mill Valley, CA.

Appendix C
Generalized Multiple-Prism Dispersion

C.1 INTRODUCTION

Now that we have dealt with the fundamentals, we'll focus on the derived phenomenon of angular dispersion. Angular dispersion is an important quantity in optics which describes the ability of an optical element, such as a diffraction grating or prism, to geometrically spread a beam of light as a function of wavelength. Mathematically, it is expressed by the differential ($\partial\Theta/\partial\lambda$). For spectrophotometers and wavelength meters based on dispersive elements, such as diffraction gratings and prism arrays, the dispersion should be as large as possible since that enables a higher wavelength spatial resolution. Further, in the case of dispersive laser oscillators, a high dispersion leads to the achievement of narrow linewidth emission since the dispersive cavity linewidth is given by

$$\Delta\lambda \approx \Delta\theta\left(\frac{\partial\theta}{\partial\lambda}\right)^{-1} \tag{C.1}$$

where $(\partial\theta / \partial\lambda)$ is the overall intracavity dispersion (Duarte, 1992). In Appendix B, the cavity linewidth equation is derived from Dirac's quantum principles (Dirac, 1958) via the interferometric equation (Duarte, 1991, 1993)

$$\left|\langle d|s\rangle\right|^2 = \sum_{j=1}^{N}\Psi(r_j)^2 + 2\sum_{j=1}^{N}\Psi(r_j)\left(\sum_{m=j+1}^{N}\Psi(r_m)\cos(\Omega_m - \Omega_j)\right) \tag{C.2}$$

In this chapter, however, we concentrate on the dispersive term $(\partial\theta / \partial\lambda)$ of generalized multiple-prism arrays since these arrays are widely used in optics in a variety of optics and quantum optics applications such as

1. Laser intracavity beam expanders, in narrow-linewidth tunable laser oscillators.
2. Extracavity beam expanders.
3. Laser pulse compressors, in femtosecond and ultrafast pulse lasers.
4. Dispersive elements in a variety of optical instruments such as spectrometers.

Albeit multiple-prism arrays were first introduced by Newton (1704), a mathematical description of their dispersion had to wait, a long time, until their application as intracavity beam expanders in narrow-linewidth tunable lasers (Duarte and Piper, 1982).

C.2 GENERALIZED MULTIPLE-PRISM DISPERSION

Generalized multiple-prism arrays are illustrated in Figure C.1. The aim here is to obtain generalized angular dispersion equations based on the basic prismatic geometry and the generalized refraction equations obtained in Chapter 5 (Duarte and Piper, 1982; Duarte, 2006). Considering the *m*th prism, of the arrangements, the angular relations are given by

$$\phi_{1,m} + \phi_{2,m} = \varepsilon_m \pm \alpha_m \tag{C.3}$$

$$\psi_{1,m} + \psi_{2,m} = \alpha_m \tag{C.4}$$

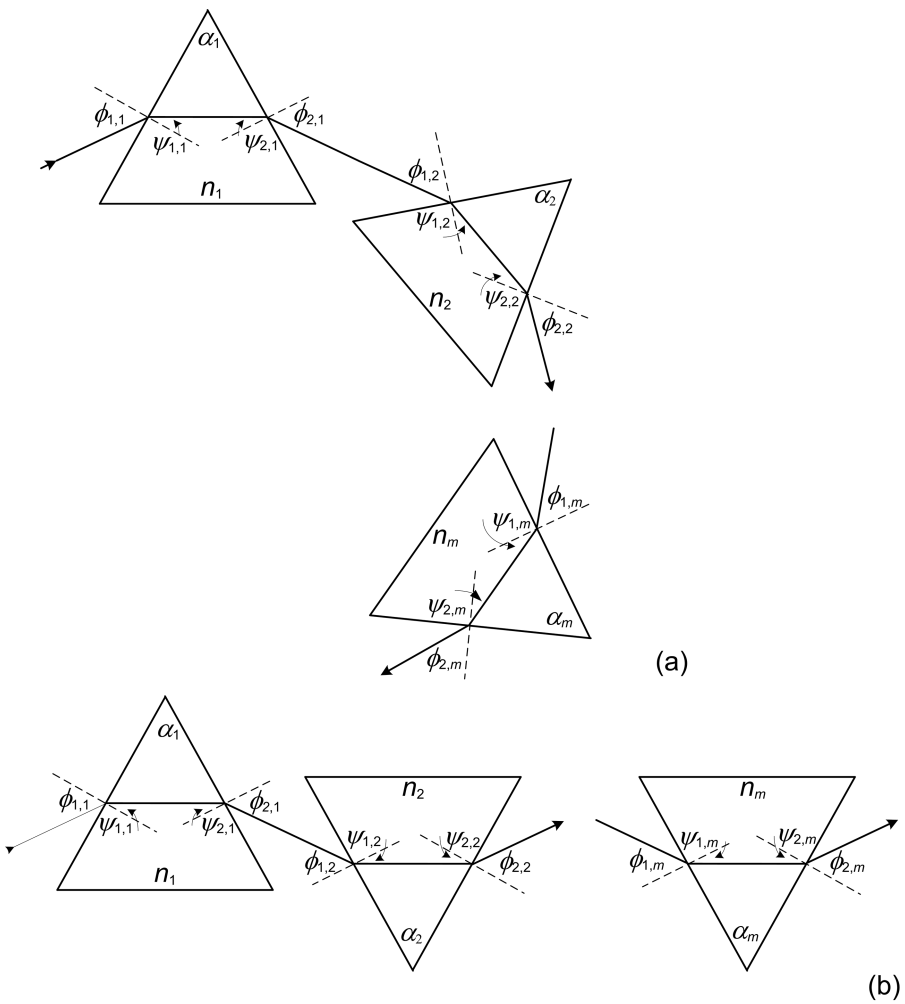

FIGURE C.1 Generalized multiple-prism sequences: (a) positive configuration and (b) compensating configuration (Reproduced from Duarte, F. J., and Piper, J. A., *Am. J. Phys.* **51**, 1132–1134, 1983, with permission of the American Association of Physics Teachers).

$$\sin\phi_{1,m} = \pm n_m \sin\psi_{1,m} \tag{C.5}$$

$$\sin\phi_{2,m} = \pm n_m \sin\psi_{2,m} \tag{C.6}$$

As illustrated in Figure C.1, $\phi_{1,m}$ and $\phi_{2,m}$ are the angles of incidence and emergence and $\psi_{1,m}$ and $\psi_{2,m}$ are the corresponding angles of refraction, at the mth prism. The sign alternative ± allows for either positive refraction or negative refraction.

Differentiating Equations (C.5) and (C.6), and using

$$\frac{d\psi_{1,m}}{dn} = -\frac{d\psi_{2,m}}{dn} \tag{C.7}$$

the single-pass dispersion following the mth prism is given by (Duarte and Piper, 1982; Duarte, 2006)

$$\nabla_\lambda \phi_{2,m} = \pm \mathcal{H}_{2,m} \nabla_\lambda n_m \pm (k_{1,m} k_{2,m})^{-1} \left(\mathcal{H}_{1,m} \nabla_\lambda n_m (\pm) \nabla_\lambda \phi_{2,(m-1)} \right) \tag{C.8}$$

where $\nabla_\lambda = \partial / \partial\lambda$ and the following geometrical identities apply

$$k_{1,m} = \frac{\cos\psi_{1,m}}{\cos\phi_{1,m}} \tag{C.9}$$

$$k_{2,m} = \frac{\cos\phi_{2,m}}{\cos\psi_{2,m}} \tag{C.10}$$

$$\mathcal{H}_{1,m} = \frac{\tan\phi_{1,m}}{n_m} \tag{C.11}$$

$$\mathcal{H}_{2,m} = \frac{\tan\phi_{2,m}}{n_m} \tag{C.12}$$

The $k_{1,m}$ and $k_{2,m}$ factors represent the physical beam expansion experienced, at the mth prism, by the incidence and the emergence beams, respectively. In Equation (C.8), the sign ± alternative refers to either positive(+) or negative (−) refraction, while the same sign alternative in parenthesis (±) indicates whether the prismatic configuration is positive (+) or compensating (−). For positive refraction alone, Equation (C.8) becomes

$$\nabla_\lambda \phi_{2,m} = \mathcal{H}_{2,m} \nabla_\lambda n_m + (k_{1,m} k_{2,m})^{-1} \left(\mathcal{H}_{1,m} \nabla_\lambda n_m \pm \nabla_\lambda \phi_{2,(m-1)} \right) \tag{C.13}$$

The generalized *single-pass dispersion equation* indicates that the cumulative dispersion at the mth prism, namely $\nabla_\lambda \phi_{2,m}$, is a function of the geometry of the mth prism, the position of the light beam relative to this prism, the material of this prism, and the cumulative dispersion up to the previous prism, $\nabla_\lambda \phi_{2,(m-1)}$ (Duarte and Piper, 1982, 1983).

For the special case of orthogonal beam exit, that is $\phi_{2,m} = 0$ and $\psi_{2,m} = 0$, we have $\mathcal{H}_{2,m} = 0$, $k_{2,m} = 1$, and Equation (C.13) reduces to

$$\nabla_\lambda \phi_{2,m} = (k_{1,m})^{-1}\left(\mathcal{H}_{1,m}\nabla_\lambda n_m \pm \nabla_\lambda \phi_{2,(m-1)}\right) \tag{C.14}$$

For an array of r identical isosceles, or equilateral, prisms deployed symmetrically, in an additive configuration, for positive refraction, so that $\phi_{1,m} = \phi_{2,m}$, the cumulative dispersion reduces to (Duarte, 1990a)

$$\nabla_\lambda \phi_{2,r} = r\nabla_\lambda \phi_{2,1} \tag{C.15}$$

This is a simple dispersion equation that applies to the design of multiple-prism spectrometers incorporating identical, isosceles, or equilateral prisms arranged in symmetrical additive configurations.

The generalized single-pass dispersion equation for positive refraction (Equation 6.13) can be restated in a more practical and explicit notation (Duarte, 1989, 1990a)

$$\begin{aligned}\nabla_\lambda \phi_{2,r} = &\sum_{m=1}^{r} (\pm 1)\mathcal{H}_{1,m}\left(\prod_{j=m}^{r} k_{1,j}\prod_{j=m}^{r} k_{2,j}\right)^{-1}\nabla_\lambda n_m \\ &+ (M_1 M_2)^{-1}\sum_{m=1}^{r} (\pm 1)\mathcal{H}_{2,m}\left(\prod_{j=1}^{m} k_{1,j}\prod_{j=1}^{m} k_{2,j}\right)\nabla_\lambda n_m\end{aligned} \tag{C.16}$$

where

$$M_1 = \prod_{j=1}^{r} k_{1,j} \tag{C.17}$$

$$M_2 = \prod_{j=1}^{r} k_{2,j} \tag{C.18}$$

are the respective beam expansion factors. For the important practical case of r right angle prism, designed for orthogonal beam exit (i.e., $\phi_{2,m} = \psi_{2,m} = 0$), Equation (C.16) reduces to

$$\nabla_\lambda \phi_{2,r} = \sum_{m=1}^{r} (\pm 1)\mathcal{H}_{1,m}\left(\prod_{j=m}^{r} k_{1,j}\right)^{-1}\nabla_\lambda n_m \tag{C.19}$$

If in addition, the prism have identical apex angle ($\alpha_1 = \alpha_2 = \alpha_3 = \ldots = \alpha_m$) and are configured to have the same angle of incidence ($\phi_{1,1} = \phi_{1,2} = \phi_{1,3} = \ldots = \phi_{1,m}$), then Equation (C.19) can be written as (Duarte, 1985a)

$$\nabla_\lambda \phi_{2,r} = \tan\psi_{1,1}\sum_{m=1}^{r} (\pm 1)\left(1/k_{1,m}\right)^{m-1}\nabla_\lambda n_m \tag{C.20}$$

Further, if the angle of incidence for all prisms is Brewster's angle, then the single-pass dispersion reduces to the elegant expression

$$\nabla_\lambda \phi_{2,r} = \sum_{m=1}^{r} (\pm 1)\left(1/n_m\right)^m \nabla_\lambda n_m \tag{C.21}$$

Alternative forms of expressing the generalized multiple-prism dispersion equation in series are given in Appendix D.

C.2.1 Example: Generalized Single-Prism Dispersion

For a single generalized prism, it is easy to show that the elegant generalized multiple-prism dispersion, Equation (C.13), reduces to

$$\nabla_\lambda \phi_{2,1} = \left(\frac{\sin\psi_{2,1}}{\cos\phi_{2,1}}\right)\nabla_\lambda n_1 + \left(\frac{\cos\psi_{2,1}}{\cos\phi_{2,1}}\right)\tan\psi_{1,1}\nabla_\lambda n_1 \tag{C.22}$$

as given in well-known textbooks (Duarte, 1990a; Born and Wolf, 1999). Further, for the case of orthogonal beam exit ($\phi_{2,m} \approx \psi_{2,m} \approx 0$), Equation (C.22) reduces to (Wyatt, 1978)

$$\nabla_\lambda \phi_{2,1} \approx \tan\psi_{1,1}\nabla_\lambda n_1 \tag{C.23}$$

The above-given examples are included to show that albeit general and elegant in its complete form, Equation (C.13) quickly leads to concrete results of practical interest to designers, laser practitioners, and optical engineers.

C.3 DOUBLE-PASS GENERALIZED MULTIPLE-PRISM DISPERSION

The evaluation of intracavity dispersion in tunable laser oscillators incorporating multiple-prism beam expanders requires the assessment of the double-pass, or return-pass, dispersion (Duarte and Piper, 1984; Duarte, 1990a). The double-pass dispersion of multiple-prism beam expanders was derived by thinking of the return pass as a mirror image of the first light passage as illustrated in Figure C.2. The return-pass dispersion corresponds to the dispersion experienced by the return light beam at the first prism.

Thus, it is given by $\partial\phi'_{1,m}/\partial\lambda = \nabla_\lambda \phi'_{1,m}$ where the prime character indicates a return pass (Duarte and Piper, 1982, 1984)

$$\nabla_\lambda \phi'_{1,m} = \mathcal{H}'_{1,m}\nabla_\lambda n_m + (k'_{1,m}k'_{2,m})\left(\mathcal{H}'_{2,m}\nabla_\lambda n_m \pm \nabla_\lambda \phi'_{1,(m+1)}\right) \tag{C.24}$$

where

$$k'_{1,m} = \frac{\cos\psi'_{1,m}}{\cos\phi'_{1,m}} \tag{C.25}$$

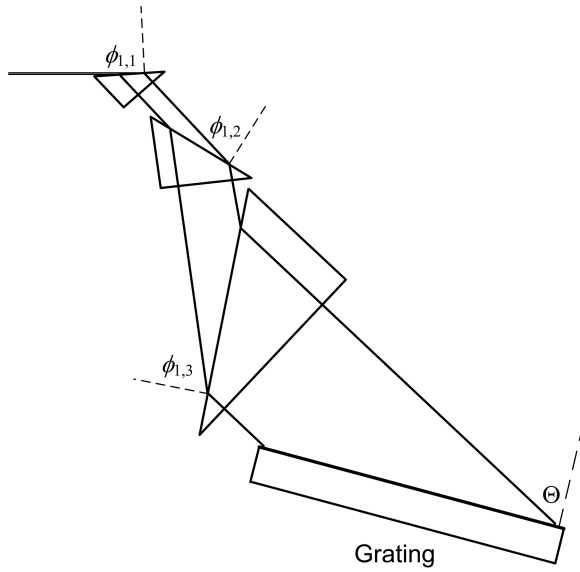

FIGURE C.2 Multiple-prism grating assembly incorporating a three-prism beam expander designed for orthogonal beam exit.

$$k'_{2,m} = \frac{\cos\phi'_{2,m}}{\cos\psi'_{2,m}} \tag{C.26}$$

$$\mathcal{H}'_{1,m} = \frac{\tan\phi'_{1,m}}{n_m} \tag{C.27}$$

$$\mathcal{H}'_{2,m} = \frac{\tan\phi'_{2,m}}{n_m} \tag{C.28}$$

Here, $\nabla_\lambda \phi'_{1,(m+1)}$ provides the cumulative single-pass multiple-prism dispersion plus the dispersion of the diffraction grating, that is,

$$\nabla_\lambda \phi'_{1,(m+1)} = \left(\nabla_\lambda \Theta_G \pm \nabla_\lambda \phi_{2,r}\right) \tag{C.29}$$

where $\nabla_\lambda \Theta_G$ is the grating dispersion. If the grating is replaced by a mirror, then we simply have the prismatic contribution and

$$\nabla_\lambda \phi'_{1,(m+1)} = \nabla_\lambda \phi_{2,r} \tag{C.30}$$

Defining $\nabla_\lambda \phi'_{1,m} = \nabla\Phi_P$, where the capital ϕ stands for return pass and P for multiple prism, the explicit version of the generalized double-pass dispersion for a multiple-prism mirror system is given by (Duarte, 1985a, 1989)

$$\nabla_\lambda \Phi_P = 2M_1M_2 \sum_{m=1}^{r} (\pm 1)\mathcal{H}_{1,m} \left(\prod_{j=m}^{r} k_{1,j} \prod_{j=m}^{r} k_{2,j} \right)^{-1} \nabla_\lambda n_m + 2\sum_{m=1}^{r} (\pm 1)\mathcal{H}_{2,m} \left(\prod_{j=1}^{m} k_{1,j} \prod_{j=1}^{m} k_{2,j} \right) \nabla_\lambda n_m \tag{C.31}$$

For the case of r right angle prism, designed for orthogonal beam exit (i.e., $\phi_{2,m} = \psi_{2,m} = 0$), Equation (C.31) reduces to

$$\nabla_\lambda \Phi_P = 2M_1 \sum_{m=1}^{r} (\pm 1)\mathcal{H}_{1,m} \left(\prod_{j=m}^{r} k_{1,j} \right)^{-1} \nabla_\lambda n_m \tag{C.32}$$

which can also be expressed as (Duarte, 1985a)

$$\nabla_\lambda \Phi_P = 2\sum_{m=1}^{r} (\pm 1) \left(\prod_{j=1}^{m} k_{1,j} \right) \tan \psi_{1,m} \nabla_\lambda n_m \tag{C.33}$$

If the angle of incidence for all prisms in the array is made equal to the Brewster angle, this equation simplifies further to (Duarte, 1990a)

$$\nabla_\lambda \Phi_P = 2\sum_{m=1}^{r} (\pm 1)\left(n_m\right)^{m-1} \nabla_\lambda n_m \tag{C.34}$$

The equations given here are quite highly applicable to the design of multiple-prism beam expanders for narrow-linewidth tunable lasers (see Figure C.3).

C.3.1 Design of Zero-Dispersion Multiple-Prism Beam Expanders

In practice, the dispersion of the grating, multiplied by the beam expansion, that is $M(\nabla_\lambda \Theta_G)$, amply dominates the overall intracavity dispersion. Thus, it is sometimes advantageous to remove the dispersion component originating from the multiple-prism beam expander so that

$$\Delta\lambda \approx \Delta\theta_R \left(MR\nabla_\lambda \Theta_G \right)^{-1} \tag{C.35}$$

In such designs, the tuning characteristics of the laser are those of the grating alone, around a specific wavelength.

The design of zero dispersion, or quasi-achromatic, multiple-prism beam expanders exhibiting orthogonal beam exit ($\phi_{2,m} \approx \psi_{2,m} \approx 0$), and made of identical material, involves the direct application of Equation (C.33) while setting $\nabla_\lambda \Phi_P = 0$. Thus, for a double-prism expander yielding zero dispersion, we obtain

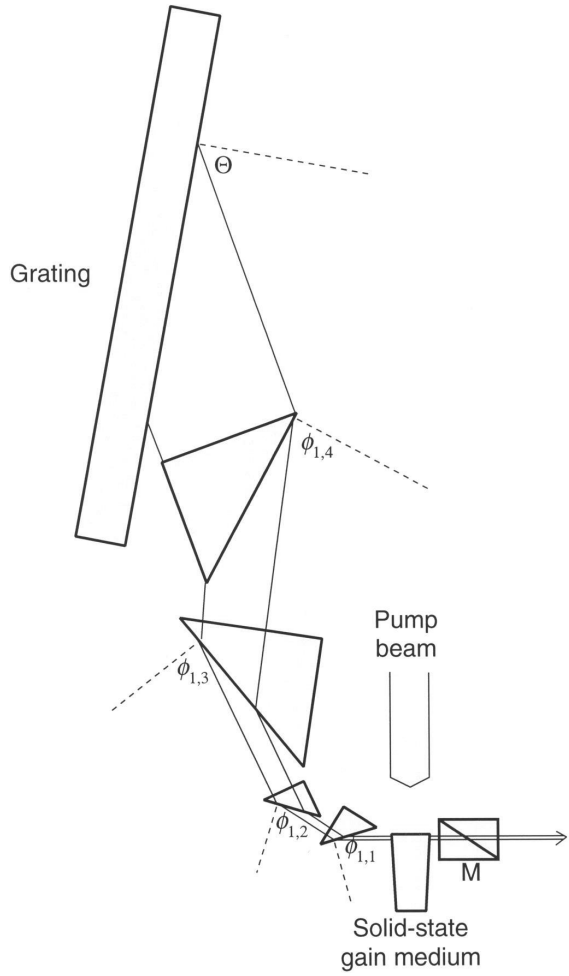

FIGURE C.3 Dispersive long-pulse solid-state tunable laser oscillator incorporating a multiple-prism grating assembly (Reproduced from Duarte, F. J. et al., *Appl. Opt.* **37**, 3987–3989, 1998, with permission from Optica).

$$(k_{1,1})\tan\psi_{1,1} = (k_{1,1})k_{1,2}\tan\psi_{1,2} \tag{C.36}$$

For a three-prism expander yielding zero dispersion, we obtain

$$(k_{1,1} + k_{1,1}k_{1,2})\tan\psi_{1,1} = (k_{1,1}k_{1,2})k_{1,3}\tan\psi_{1,3} \tag{C.37}$$

For a four-prism expander yielding zero dispersion, we obtain

$$(k_{1,1} + k_{1,1}k_{1,2} + k_{1,1}k_{1,2}k_{1,3})\tan\psi_{1,1} = (k_{1,1}k_{1,2}k_{1,3})k_{1,4}\tan\psi_{1,4} \tag{C.38}$$

For a five-prism expander yielding zero dispersion, we obtain

$$(k_{1,1} + k_{1,1}k_{1,2} + k_{1,1}k_{1,2}k_{1,3} + k_{1,1}k_{1,2}k_{1,3}k_{1,4}) \tan\psi_{1,1} = (k_{1,1}k_{1,2}k_{1,3}k_{1,4})k_{1,5} \tan\psi_{1,5} \quad \text{(C.39)}$$

and so on. Here we should just re-emphasize that all these configurations yield zero dispersion at the design wavelength, thus the use of the term quasi-achromatic.

Optimized compact high-power solid-state multiple-prism laser oscillators have been demonstrated to yield single-longitudinal-mode oscillation at $\Delta\nu \approx 350$ MHz, at pulses $\Delta t \approx 3$ ns, near the limit allowed by Heisenberg's uncertainty principle (Duarte, 1999). The oscillator, illustrated in Figure C.4, requires the use of a small fused silica double-prism beam expander with $M \approx 42$, and $\phi_{2,m} \approx \psi_{2,m} \approx 0$, at $\lambda = 590$ nm. Thus, we use Equation (C.33) to obtain Equation (C.36), which reduces to

$$\tan\psi_{1,1} = k_{1,2} \tan\psi_{1,2} \quad \text{(C.40)}$$

For $n = 1.4583$ and $\phi_{1,1} = 88.60°$, we get $\psi_{1,1} \approx 43.28°$, and $k_{1,1} \approx 29.80$. With these initial parameters, Equation (C.40) yields for the second prism $\phi_{1,2} \approx 53.93°$, $\psi_{1,2} \approx 33.66°$, and $k_{1,2} \approx 1.41$. Therefore, the overall intracavity beam expansion becomes

$$M = k_{1,1}k_{1,2} \approx 42.13$$

For a beam waist of $w = 100$ μm this implies $2wM \approx 8.43$ mm. These dimensions require the first prism to have a hypotenuse of ~ 8 mm and the second prism a hypotenuse of ~10 mm. In this particular oscillator, this intracavity beam expansion is used to illuminate a 3300 lines/mm grating deployed at an angle of incidence ~ 77° in Littrow configuration (Duarte, 1999).

Duarte (2003) describes in detail the design of a zero dispersion four-prism beam expander for $M = 103.48$, at $\lambda = 590$ nm. Shay and Duarte (2009) describe the design of a zero dispersion five-prism beam expander for fused silica, at $\lambda = 1550$ nm ($n = 1.44402$), yielding an overall beam expansion of $M \approx 987$.

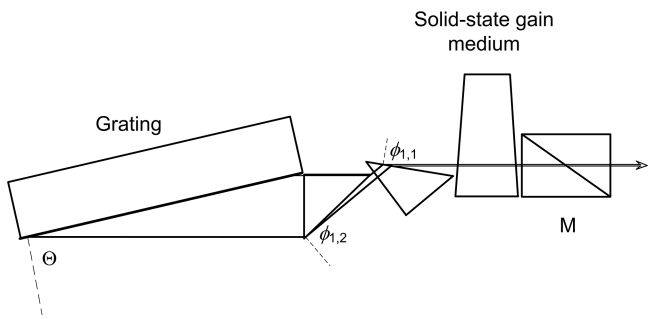

FIGURE C.4 Optimized multiple-prism ($m = 2$) grating solid-state tunable laser oscillator delivering a linewidth ($\Delta\nu \approx 350$ MHz) near the limit allowed by Heisenberg's uncertainty principle (Reproduced from Duarte, F. J., *Appl. Opt.* **38**, 6347–6349, 1999, with permission from Optica).

C.4 MULTIPLE RETURN-PASS GENERALIZED MULTIPLE-PRISM DISPERSION

Here we consider a multiple-prism grating or multiple-prism mirror assembly, for positive refraction, as illustrated in Figure C.5. The light beam enters the first prism of the array, it is then expanded, and it is either diffracted back or reflected back into the multiple-prism array. In a dispersive laser oscillator, this process goes forth and back multiple times, thus giving rise to the concept of intracavity double pass or intracavity multiple return pass. For the first return pass, toward the first prism in the array, the dispersion is given by

$$\nabla_\lambda \phi_{2,m} = \mathcal{H}_{2,m} \nabla_\lambda n_m + (k_{1,m} k_{2,m})^{-1} \left(\mathcal{H}_{1,m} \nabla_\lambda n_m \pm \nabla_\lambda \phi_{2,(m-1)} \right)$$

If N denotes the number of passes toward the grating, or reflecting element, and $2N$, the number of return passes, toward the first prism in the sequence, we have (Duarte and Piper, 1984)

$$(\nabla_\lambda \phi_{2,m})_N = \mathcal{H}_{2,m} \nabla_\lambda n_m + (k_{1,m} k_{2,m}) \left(\mathcal{H}_{1,m} \nabla_\lambda n_m \pm (\nabla_\lambda \phi_{2,(m-1)})_N \right) \tag{C.41}$$

and

$$(\nabla_\lambda \phi'_{1,m})_{2N} = \mathcal{H}'_{1,m} \nabla_\lambda n_m + (k'_{1,m} k'_{2,m}) \left(\mathcal{H}'_{2,m} \nabla_\lambda n_m \pm (\nabla_\lambda \phi'_{1,(m+1)})_{2N} \right) \tag{C.42}$$

For the first prism of the array (next to the gain medium), $(\nabla_\lambda \phi_{2,(m-1)})_N$ (with $N = 3, 5, 7\ldots$) in Equation (C.41) is replaced by $(\nabla_\lambda \phi'_{1,1})_{2N}$ (with $N = 1, 2, 3\ldots$). Likewise, for the last prism of the assembly (next to the grating), $(\nabla_\lambda \phi'_{1,(m+1)})_{2N}$ (with $N = 1, 2, 3\ldots$) in Equation (C.42) is replaced by $\left(\nabla_\lambda \Theta_G + (\nabla_\lambda \phi_{2,r})_N \right)$ (with $N = 1, 3, 5\ldots$).

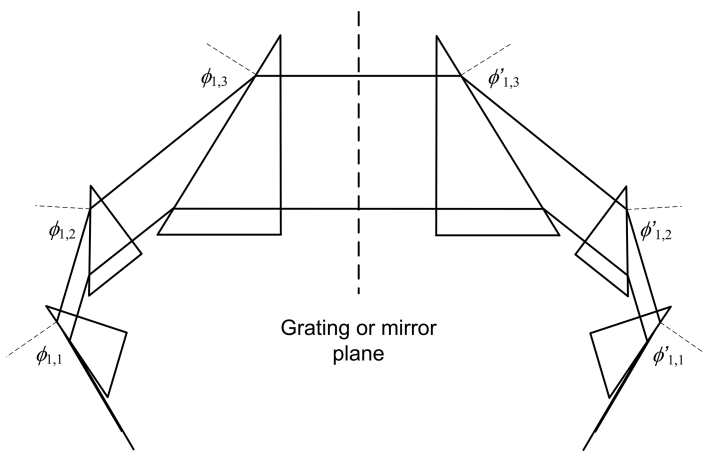

FIGURE C.5 Multiple-prism grating assembly in its unfolded depiction (Adapted from Duarte, F. J., and Piper, J. A., *Opt. Commun.* **43**, 303–307, 1982, with permission from Elsevier).

Thus, the multiple return-pass dispersion for a multiple-prism grating assembly is given by (Duarte and Piper, 1984)

$$(\nabla_\lambda \theta)_R = \left(RM\nabla_\lambda \Theta_G + R\nabla_\lambda \Phi_P \right) \tag{C.43}$$

where $R = 2N$ is the number of return passes. This equation illustrates the very important fact that in the return-pass dispersion of a multiple-prism grating assembly, the dispersion of a grating is multiplied by the factor RM, where M is the overall beam magnification of the multiple-prism beam expander. Subsequently, the multiple return-pass linewidth equation becomes (Duarte, 2001)

$$\Delta\lambda = \Delta\theta_R \left(RM\nabla_\lambda \Theta_G + R\nabla_\lambda \Phi_P \right)^{-1} \tag{C.44}$$

where $\Delta\theta_R$ is the multiple return-pass beam divergence (Duarte, 2001, 2003) described in Appendix B. Once again, if the grating is replaced by a mirror, that is $\nabla_\lambda \Theta_G = 0$, the dispersion reduces to

$$(\nabla_\lambda \theta)_R = R\nabla_\lambda \Phi_P \tag{C.45}$$

which implies that the multiple-prism intracavity dispersion increases linearly as a function of R. The finite number R can be determined experimentally from the time delay observed between the leading edge of the excitation pulse and the leading edge of the narrow-linewidth emission pulse (Duarte and Piper, 1984). For narrow-linewidth high-power dispersive dye-laser oscillators, this number is typically $R \approx 3$ (Duarte, 2001).

One further insight from Equation (C.44) is that the laser linewidth is a function of the intracavity beam expansion M. Hence, varying M allows control of $\Delta\lambda$. This led to the introduction of high-power variable-linewidth lasers (Duarte, 1985b).

C.4.1 Multiple-Prism Beam Compressors

Observing Figure C.5, it becomes immediately apparent that, in a multiple-prism array, propagation from left to right leads to beam expansion while propagation from right lo left leads to *beam compression* as described by Duarte (2006). This is a geometrical beam compression effect different from temporal pulse compression as described in the next section.

Beam expansion and beam compression, in a given multiple-prism configuration, are symmetric phenomena. If beam expansion occurs in one direction, then beam compression occurs in the opposite direction as illustrated in Figure C.5. Certainly, the equations of multiple-prism dispersion given here equally apply to both beam compressors and beam expanders. An explicit beam compressor is depicted in Figure C.6 showing propagation from right to left. Numerous further examples of geometrical beam compressors are given by Duarte (2006). The beauty of multiple-prism beam compressors is that, ideally, they reduce the cross section of the propagating beam without inducing traditional focusing that leads to divergence of the beam beyond the focal point.

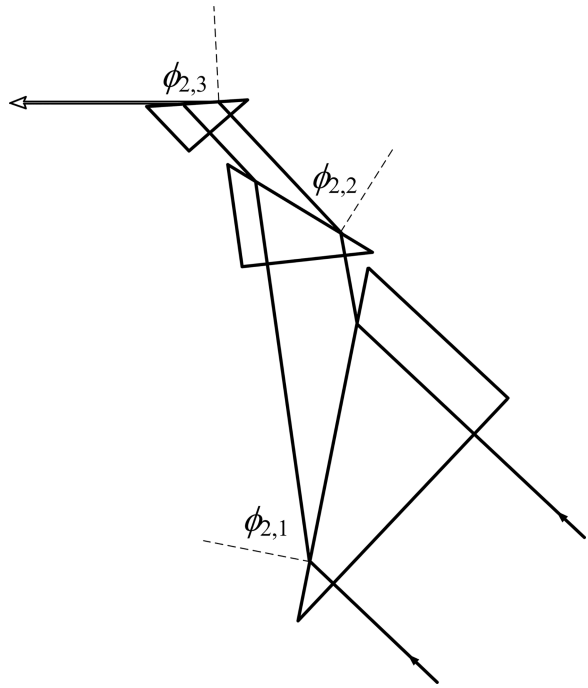

FIGURE C.6 Multiple-prism geometrical beam compressor. In this configuration, the incident beam enters orthogonally to the first larger prism. The arrows indicate the direction of the propagation. If the direction of the beam is reversed then the compressor becomes an expander.

C.5 MULTIPLE-PRISM DISPERSION AND LASER PULSE COMPRESSION

The generation of femtosecond, attosecond, or ultrashort laser pulses is of fundamental interest to optics, quantum optics, and laser science in general (Diels and Rudolph, 2006).

From the uncertainty relation

$$\Delta\nu\,\Delta t \approx 1 \tag{C.46}$$

it is immediately apparent that the generation of ultrashort time pulses (Δt) require the simultaneous generation of a very wide spectral distribution ($\Delta\nu$). From the cavity linewidth equation

$$\Delta\lambda \approx \Delta\theta \left(\frac{\partial\theta}{\partial\lambda}\right)^{-1}$$

it also clear that the generation of very wide spectral emission requires the least amount of intracavity dispersion. Thus, it is necessary to understand and control all aspects of intracavity dispersion.

Pulse compression in ultrashort pulse, or femtosecond, lasers requires control of the first, second, and third derivatives of the intracavity dispersion. Using the identity

$$\nabla_n \phi_{2,m} = \nabla_\lambda \phi_{2,m} (\nabla_\lambda n_m)^{-1} \tag{C.47}$$

Equation (C.13) can be restated as (Duarte, 2009)

$$\nabla_n \phi_{2,m} = \mathcal{H}_{2,m} + (\mathcal{M})^{-1} \left(\mathcal{H}_{1,m} \pm \nabla_n \phi_{2,(m-1)} \right) \tag{C.48}$$

where the identity

$$k_{1,m}^{-1} k_{2,m}^{-1} = (\mathcal{M})^{-1} \tag{C.49}$$

applies. Hence, the complete second derivative of the refraction angle, or first derivative of the dispersion $\nabla_\lambda \phi_{2,m}$, is given by (Duarte, 1987)

$$\begin{aligned} \nabla_n^2 \phi_{2,m} &= \nabla_n \mathcal{H}_{2,m} \\ &+ (\nabla_n \mathcal{M}^{-1})(\mathcal{H}_{1,m} \pm \nabla_n \phi_{2,(m-1)}) \\ &+ (\mathcal{M}^{-1})(\nabla_n \mathcal{H}_{1,m} \pm \nabla_n^2 \phi_{2,(m-1)}) \end{aligned} \tag{C.50}$$

The second derivative of the dispersion $\nabla_\lambda \phi_{2,m}$ is given by (Duarte, 2009)

$$\begin{aligned} \nabla_n^3 \phi_{2,m} &= \nabla_n^2 \mathcal{H}_{2,m} \\ &+ (\nabla_n^2 \mathcal{M}^{-1})(\mathcal{H}_{1,m} \pm \nabla_n \phi_{2,(m-1)}) \\ &+ 2(\nabla_n \mathcal{M}^{-1})(\nabla_n \mathcal{H}_{1,m} \pm \nabla_n^2 \phi_{2,(m-1)}) \\ &+ (\mathcal{M}^{-1})(\nabla_n^2 \mathcal{H}_{1,m} \pm \nabla_n^3 \phi_{2,(m-1)}) \end{aligned} \tag{C.51}$$

the third derivative of the dispersion $\nabla_\lambda \phi_{2,m}$ is given by (Duarte, 2009)

$$\begin{aligned} \nabla_n^4 \phi_{2,m} &= \nabla_n^3 \mathcal{H}_{2,m} \\ &+ (\nabla_n^3 \mathcal{M}^{-1})(\mathcal{H}_{1,m} \pm \nabla_n \phi_{2,(m-1)}) \\ &+ 3(\nabla_n^2 \mathcal{M}^{-1})(\nabla_n \mathcal{H}_{1,m} \pm \nabla_n^2 \phi_{2,(m-1)}) \\ &+ 3(\nabla_n \mathcal{M}^{-1})(\nabla_n^2 \mathcal{H}_{1,m} \pm \nabla_n^3 \phi_{2,(m-1)}) \\ &+ (\mathcal{M}^{-1})(\nabla_n^3 \mathcal{H}_{1,m} \pm \nabla_n^4 \phi_{2,(m-1)}) \end{aligned} \tag{C.52}$$

and the fourth derivative of the dispersion $\nabla_{\lambda}\phi_{2,m}$ is given by (Duarte, 2009)

$$\begin{aligned}\nabla_n^5\phi_{2,m} &= \nabla_n^4\mathcal{H}_{2,m} \\ &+ (\nabla_n^4\mathcal{M}^{-1})(\mathcal{H}_{1,m} \pm \nabla_n\phi_{2,(m-1)}) \\ &+ 4(\nabla_n^3\mathcal{M}^{-1})(\nabla_n\mathcal{H}_{1,m} \pm \nabla_n^2\phi_{2,(m-1)}) \\ &+ 6(\nabla_n^2\mathcal{M}^{-1})(\nabla_n^2\mathcal{H}_{1,m} \pm \nabla_n^3\phi_{2,(m-1)}) \\ &+ 4(\nabla_n\mathcal{M}^{-1})(\nabla_n^3\mathcal{H}_{1,m} \pm \nabla_n^4\phi_{2,(m-1)}) \\ &+ (\mathcal{M}^{-1})(\nabla_n^4\mathcal{H}_{1,m} \pm \nabla_n^5\phi_{2,(m-1)})\end{aligned} \tag{C.53}$$

and so on, for higher derivatives. By inspection, as stated by Duarte (2009), it can be seen that from the second term on the numerical factors can be predetermined from Pascal's triangle relative to N where $(N+1)$ is the order of the derivative.

Albeit the preceding exposition might appear a little bit abstract these equations lead to specific numerical results (Duarte, 1987, 1990b). Osvay et al. (2004, 2005) have used the lower order derivatives, given here, in practical femtosecond lasers to determine dispersions and laser pulse durations, for double-prism compressors, with excellent agreement between theory and experiments. The equations described here represent the complete description of the generalized multiple-prism dispersion theory applicable to pulse compression prismatic arrays in femtosecond, or ultrashort, pulse lasers and nonlinear optics.

Exact numerical calculations to determine $\nabla_n\phi_{2,m}$ and $\nabla_n^2\phi_{2,m}$, for $m = 1, 2, 3, 4$ were performed by Duarte (1990). In these calculations the angle of incidence was deviated by minute amounts from the Brewster angle of incidence. Duarte (2009) provides exact values, as a function of the refractive index n, for $\nabla_n\phi_{2,m}$, $\nabla_n^2\phi_{2,m}$, and $\nabla_n^3\phi_{2,m}$. Simplifying assumptions include incidence at the Brewster angle of incidence, prisms of identical isosceles geometry, and made of the same material with refractive index $n_m = n$.

C.5.1 Example: Single-Prism Pulse Compressor

For the single-prism laser pulse compressor (Dietel et al., 1983) $(m = 1)$ of isosceles geometry, made of material with refractive index $n_m = n$, and deployed at the Brewster angle of incidence (see Figure C.7) we find

$$\nabla_n\phi_{2,1} = 2 \tag{C.54}$$

$$\nabla_n^2\phi_{2,1} = \left(4n - 2n^{-3}\right) \tag{C.55}$$

$$\nabla_n^3\phi_{2,1} = \left(24n^2 + 8n^0 - 12n^{-2} + 6n^{-4} + 6n^{-6}\right) \tag{C.56}$$

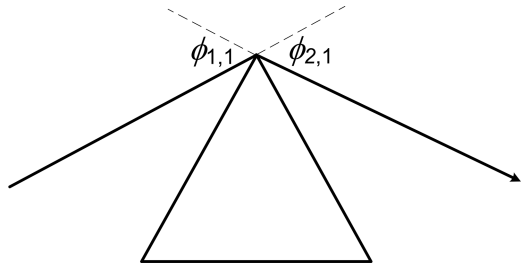

FIGURE C.7 Single-prism pulse compressor.

C.5.2 Example: Double-Prism Pulse Compressor

A prism pulse compressor integrated by $m = 2$ prisms of identical isosceles geometry, made of the same material with refractive index $n_m = n$, and deployed at the Brewster angle of incidence in *compensating configuration* is depicted in Figure C.8 (Diels et al., 1985). The compensating configuration requires the subtraction of the previous dispersive derivatives and the use of $\nabla_n \phi_{1,2} = \nabla_n \phi_{2,1}$ as a geometrical nexus between stages. Careful evaluation of all relevant identities and their correct substitution yield

$$\nabla_n \phi_{2,2} = 0 \tag{C.57}$$

$$\nabla_n^2 \phi_{2,2} = 0 \tag{C.58}$$

$$\nabla_n^3 \phi_{2,2} = 0 \tag{C.59}$$

as would be expected from geometrical and symmetrical arguments. However, the correct mathematical evaluation of $(\nabla_n^3 \phi_{2,2})$ requires considerable attention to detail given the numerous identities involved.

C.5.3 Example: Four-Prism Pulse Compressor

A four-prism compressor (Fork et al., 1984) is formed by unfolding the double-prism configuration about a symmetry axis perpendicular to the exit beam depicted in

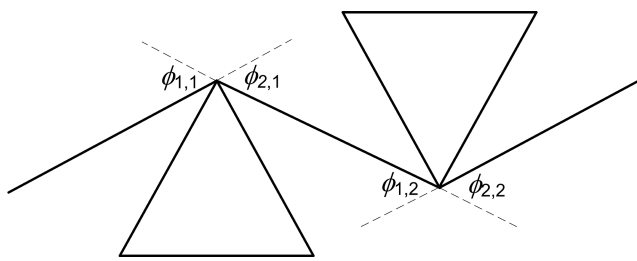

FIGURE C.8 Double-prism pulse compressor.

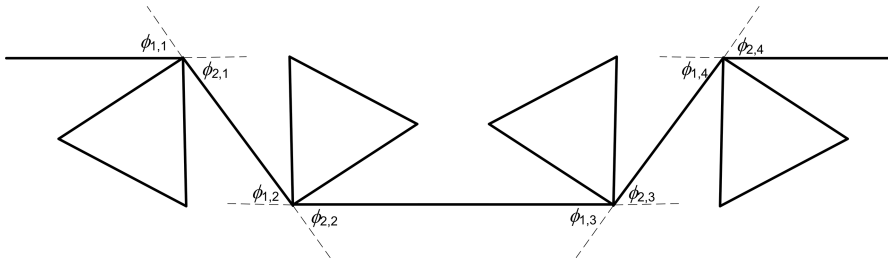

FIGURE C.9 Four-prism pulse compressor.

Figure C.7, as illustrated in Figure C.9. For exactly-balanced compensating prism arrays composed of two pairs of compensating prisms, it can be shown that

$$\nabla_n \phi_{2,1} = \nabla_n \phi_{2,3} = 2 \tag{C.60}$$

$$\nabla_n^2 \phi_{2,1} = \nabla_n^2 \phi_{2,3} = \left(4n - 2n^{-3}\right) \tag{C.61}$$

$$\nabla_n^3 \phi_{2,1} = \nabla_n^3 \phi_{2,3} = \left(24n^2 + 8n^0 - 12n^{-2} + 6n^{-4} + 6n^{-6}\right) \tag{C.62}$$

$$\nabla_n \phi_{2,2} = \nabla_n \phi_{2,4} = 0 \tag{C.63}$$

$$\nabla_n^2 \phi_{2,2} = \nabla_n^2 \phi_{2,4} = 0 \tag{C.64}$$

$$\nabla_n^3 \phi_{2,2} = \nabla_n^3 \phi_{2,4} = 0 \tag{C.65}$$

A six-prism pulse compressor has been used in semiconductor laser pulse compression by Pang et al. (1992).

PROBLEMS

C.1 Use Equation (C.4) to obtain the identity given in Equation (C.7).
C.2 Derive Equation (C.14) from Equation (C.13) using for $\phi_{2,m} \approx \psi_{2,m} \approx 0$.
C.3 Derive Equation (C.15).
C.4 Derive Equation (C.20) from Equation (C.19).
C.5 Use Equation (C.13) to obtain the single-prism Equation (C.22).
C.6 Use Equation (C.33), set $\nabla_\lambda \Phi_P = 0$, to derive Equation (C.39), for a five-prism zero-dispersion beam expander.
C.7 For a single-prism laser pulse compressor, derive Equations (C.54)–(C.56) [Hint: see Duarte (2009)].
C.8 Using the methodology described in the three prism pulse-compressor examples given, develop a set of equations applicable to a symmetrical six-prism pulse compressor [Hint: the dispersions of the first three prisms, deployed in additive configuration, is compensated by the second set of three prisms].

REFERENCES

Born, M., and Wolf, E. (1999). *Principles of Optics*, 7th ed. Cambridge University, Cambridge, U.K.

Diels, J.-C., Dietel, W., Fontaine, J. J., Rudolph, W., and Wilhelmi, B. (1985). Analysis of a mode-locked ring laser: chirped-solitary-pulse solutions. *J. Opt. Soc. Am. B*. **2**, 680–686.

Diels, J.-C., and Rudolph, W. (2006). *Ultrafast Laser Pulse Phenomena*, 2nd ed. Academic, New York.

Dietel, W., Fontaine, J. J., and Diels, J.-C. (1983). Intracavity pulse compression with glass: a new method of generating pulses shorter than 60 fs. *Opt. Lett.* **8**, 4–6.

Dirac, P. A. M. (1958). *The Principles of Quantum Mechanics*, 4th ed. Oxford University, Oxford, U.K.

Duarte, F. J. (1985a). Note on achromatic multiple-prism beam expanders. *Opt. Commun.* **53**, 259–262.

Duarte, F. J. (1985b). Variable linewidth high-power TEA CO_2 laser. *Appl. Opt.* **24**, 34–37.

Duarte, F. J. (1987). Generalized multiple-prism dispersion theory for pulse compression in ultrafast dye lasers. *Opt. Quantum Electron.* **19**, 223–229.

Duarte, F. J. (1989). Transmission efficiency in achromatic nonorthogonal multiple-prism laser beam expanders. *Opt. Commun.* **71**, 1–5.

Duarte, F. J. (1990a). Narrow-linewidth pulsed dye laser oscillators. In *Dye Laser Principles* (Duarte, F. J., and Hillman, L. W., eds.). Academic, New York, Chapter 4, pp. 133–183.

Duarte, F. J. (1990b). Prismatic pulse compression: beam deviations and geometrical perturbations. *Opt. Quantum Electron.* **22**, 467–471.

Duarte, F. J. (1991). Dispersive dye lasers. In *High Power Dye Lasers* (Duarte, F. J., ed.). Springer-Verlag, Berlin, Chapter 2, pp. 7–43.

Duarte, F. J. (1992). Cavity dispersion equation: a note on its origin. *Appl. Opt.* **31**, 6979–6982.

Duarte, F. J. (1993). On a generalized interference equation and interferometric measurements. *Opt. Commun.* **103**, 8–14.

Duarte, F. J. (1999). Multiple-prism grating solid-state dye laser oscillator: optimized architecture. *Appl. Opt.* **38**, 6347–6349.

Duarte, F. J. (2001). Multiple-return-pass beam divergence and the linewidth equation. *Appl. Opt.* **40**, 3038–3041.

Duarte, F. J. (2003). *Tunable Laser Optics*, Elsevier-Academic, New York.

Duarte, F. J. (2006). Multiple-prism dispersion equations for positive and negative refraction. *Appl. Phys. B*. **82**, 35–38.

Duarte, F. J. (2009). Generalized multiple-prism dispersion theory for laser pulse compression: higher order phase derivatives. *Appl. Phys. B*. **96**, 809–814.

Duarte, F. J., and Piper, J. A. (1982). Dispersion theory of multiple-prism beam expander for pulsed dye lasers. *Opt. Commun.* **43**, 303–307.

Duarte, F. J., and Piper, J. A. (1983). Generalized prism dispersion theory. *Am. J. Phys.* **51**, 1132–1134.

Duarte, F. J., and Piper, J. A. (1984). Multi-pass dispersion theory of prismatic pulsed dye lasers. *Optica Acta* **31**, 331–335.

Fork, R. L., Martinez, O. M., and Gordon, J. P. (1984). Negative dispersion using pairs of prisms. *Opt. Lett.* **9**, 150–152.

Newton, I. (1704). *Opticks*, Royal Society, London, U.K.

Osvay, K., Kovács, A. P., Heiner, Z., Kurdi, G., Klebniczki, J., Csatári, M. (2004). Angular dispersion and temporal change of femtosecond pulses from misaligned pulse compressors. *IEEE J. Selec. Top. Quantum Electron*. **10**, 213–220.

Osvay, K., Kovács, A. P., Kurdi, G., Heiner, Z., Divall, M., Klebniczki, J., Ferincz, I. E. (2005). Measurement of non-compensated angular dispersion and the subsequent temporal lengthening of femtosecond pulses in a CPA laser. *Opt. Commun.* **248**, 201–209.

Pang, L. Y., Fujimoto, J. G., and Kintzer, E. S. (1992). Ultrashort-pulse generation from high-power diode arrays by using intracavity optical nonlinearities. *Opt. Lett.* **17**, 1599–1601.

Shay, T. M., and Duarte, F. J. (2009). Tunable fiber lasers. In *Tunable Laser Applications*, 2nd ed. (Duarte, F. J., ed.). CRC, Boca Raton, FL, Chapter 6, pp. 179–196.

Wyatt, R. (1978). Comment on "on the dispersion of a prism used as a beam expander in a nitrogen laser." *Opt. Commun.* **26**, 9–11.

Appendix D
Multiple-Prism Dispersion Power Series

D.1 MULTIPLE-PRISM DISPERSION SERIES

In Appendix C, the generalized multiple-prism dispersion equation, applicable to multiple-prism arrays of any geometry, configuration, or materials, is given as (Duarte, 2009)

$$\nabla_\lambda \phi_{2,m} = \pm \mathcal{H}_{2,m} \nabla_\lambda n_m \pm (k_{1,m} k_{2,m})^{-1} \left(\mathcal{H}_{1,m} \nabla_\lambda n_m (\pm) \nabla_\lambda \phi_{2,(m-1)} \right) \tag{D.1}$$

For positive refraction only, this equation becomes (Duarte and Piper, 1982, 1983)

$$\nabla_\lambda \phi_{2,m} = \mathcal{H}_{2,m} \nabla_\lambda n_m + (k_{1,m} k_{2,m})^{-1} \left(\mathcal{H}_{1,m} \nabla_\lambda n_m \pm \nabla_\lambda \phi_{2,(m-1)} \right) \tag{D.2}$$

where the ± sign refers to either a positive (+) or compensating configuration (−).

In Appendix C, Equation (D.2) is expressed in a series format directly applicable to the geometry at hand. Duarte and Piper (1982) also provide further examples of simple special cases leading to explicit engineering type equations. For instance, for increasing values of m, for the *very special case* of r identical prisms deployed at the same angle of incidence (i.e., $\phi_{1,1} = \phi_{1,2} = \ldots = \phi_{1,m}$, and $\psi_{1,1} = \psi_{1,2} = \ldots = \psi_{1,m}$) and orthogonal beam exit (i.e., $\phi_{2,1} = \phi_{2,2} = \ldots = \phi_{2,m} = 0$ and $\psi_{2,1} = \psi_{2,2} = \ldots = \psi_{2,m} = 0$), Equation (D.2) reduces to a simple power series (Duarte and Piper, 1982; Duarte, 1990)

$$\nabla_\lambda \phi_{2,r} = \tan \psi_{1,1} \nabla n_1 \left(1 \pm k_{1,1}^{-1} \pm k_{1,1}^{-2} \pm k_{1,1}^{-3} \pm \ldots \pm k_{1,1}^{-(r-1)} \right) \tag{D.3}$$

Moreover, as shown in Appendix C, for orthogonal beam exit, Equation (D.2) reduces to the explicit series

$$\nabla_\lambda \phi_{2,r} = \sum_{m=1}^{r} (\pm 1) \mathcal{H}_{1,m} \left(\prod_{j=m}^{r} k_{1,j} \right)^{-1} \nabla_\lambda n_m \tag{D.4}$$

which was disclosed in print, in its double-pass version by Duarte (1985). This simple explicit equation obviously can be expressed in its long-hand version (Duarte, 2012)

$$\nabla_\lambda \phi_{2,r} = \pm \mathcal{H}_{1,1} (k_{1,1} k_{1,2} \ldots k_{1,r})^{-1} \nabla_\lambda n_1 \pm \mathcal{H}_{1,2} (k_{1,2} \ldots k_{1,r})^{-1} \nabla_\lambda n_2 \pm \ldots \pm \mathcal{H}_{1,r} (k_{1,r})^{-1} \nabla_\lambda n_r \tag{D.5}$$

These examples are included here to illustrate that the generalized dispersion Equation (D.1) leads directly to practical and explicit series.

PROBLEMS

D.1 Show that the generalized multiple-prism dispersion given in Equation (D.2) can be expressed as the series in (D.3).

D.1 Show that the multiple-prism dispersion given in Equation (D.4) can be expressed as the series in (D.5).

REFERENCES

Duarte, F. J. (1985). Note on achromatic multiple-prism beam expanders. *Opt. Commun.* **53**, 259–262.

Duarte, F. J. (1990). Narrow linewidth pulsed dye laser oscillators. In *Dye Laser Principles* (Duarte, F. J., and Hillman, L. W., eds.). Academic, New York, Chapter 4, pp. 133–183.

Duarte, F. J. (2009). Generalized multiple-prism dispersion theory for laser pulse compression: higher order phase derivatives, *Appl. Phys. B* **96**, 809–814.

Duarte, F. J. (2012). Tunable organic dye lasers: physics and technology of high- performance liquid and solid-state narrow-linewidth oscillators. *Prog. Quantum Electron.* **36**, 29–50.

Duarte, F. J., and Piper, J. A. (1982). Dispersion theory of multiple-prism beam expander for pulsed dye lasers. *Opt. Commun.* **43**, 303–307.

Duarte, F. J., and Piper, J. A. (1983). Generalized prism dispersion theory. *Am. J. Phys.* **51**, 1132–1134.

Appendix E
N-Slit Interferometric Calculations

E.1 INTRODUCTION

In this appendix, we further explain, in plain language, how to proceed with numerical calculations based on the generalized one-dimensional interferometric equation (Duarte, 1991, 1993). This explanation, provided in addition to the description given in Chapter 4, is intended to help in the construction of logical pathways and flowcharts for computer-based numerical calculations.

E.2 THE INTERFEROMETRIC EQUATION

The physics is described by the probability amplitude equation

$$\langle d|s\rangle = \sum_{j=1}^{N} \langle d|j\rangle \langle j|s\rangle \tag{E.1}$$

where

$$\langle j|s\rangle = \Psi(r_{j,s}) e^{-i\theta_j} \tag{E.2}$$

$$\langle d|j\rangle = \Psi(r_{x,j}) e^{-i\phi_j} \tag{E.3}$$

Multiplying by the complex conjugate and rearranging yields the interferometric quantum probability equation (Duarte, 1993)

$$\left|\langle d|s\rangle\right|^2 = \sum_{j=1}^{N} \Psi(r_j)^2 + 2\sum_{j=1}^{N} \Psi(r_j) \left(\sum_{m=j+1}^{N} \Psi(r_m) \cos(\Omega_m - \Omega_j) \right) \tag{E.4}$$

Key in these calculations is the phase angle

$$\Omega_j = (\theta_j + \phi_j) \tag{E.5}$$

which is related to the wavelength and the exact geometry of the interferometer.

A good simplifying assumption is to set

$$\langle j|s\rangle = \Psi(r_{j,s}) e^{-i\theta_j} = 1 \tag{E.6}$$

which represents uniform illumination of the grating. In a more advanced version of the program, this assumption is not used and the illumination can be varied at will. Hence the only wave function needed is

$$\langle d|j\rangle = \Psi(r_{x,j})e^{-i\phi_j} \tag{E.7}$$

where the amplitude can take the form of a Gaussian or a similar mathematical representation.

E.3 GEOMETRY

In these calculations, it is very important to get the geometry represented in measurable spatial quantities. The usual geometrical and angular approximations are not allowed.

The geometrical configuration, illustrated in Figure E.1, includes

1. w is the slit width.
2. ϕ_j is the jth phase angle.
3. d_1 is the center to center slit distance.
4. $D_{\langle d|j\rangle}$ is the distance from the N-slit array (j) to the interference plane (d).
5. $\Delta\delta_m$ is the distance from the center of the mth slit to the reference position at the interference plane.

As seen in Chapter 4, the phase difference term in the interferometric quantum probability equation can be expressed as (Duarte, 1997)

$$\cos\left((\theta_m - \theta_j) \pm (\phi_m - \phi_j)\right) = \cos\left(|l_m - l_{m-1}|k_1 \pm |L_m - L_{m-1}|k_2\right) \tag{E.8}$$

where $k_1 = (2\pi n_1/\lambda)$ and $k_2 = (2\pi n_2/\lambda)$ so that

$$(\phi_m - \phi_j) = \frac{2\pi n_2}{\lambda}|L_m - L_{m-1}| \tag{E.9}$$

$$(\phi_m - \phi_j) = \frac{2\pi d_1}{\lambda}\Delta\delta_m\left(D^2_{\langle d|j\rangle} + \Delta\delta^2_m\right)^{-1/2} \tag{E.10}$$

Using these equations and the geometry depicted in Figure E.1, the phase angles are given by

$$(\phi_1 - \phi_2) = \left(\frac{2\pi d_1}{\lambda}\right)\left(\frac{\Delta\delta_1}{(D^2_{\langle d|j\rangle} + \Delta\delta^2_1)^{1/2}}\right) \tag{E.11}$$

$$(\phi_1 - \phi_3) = \left(\frac{4\pi d_1}{\lambda}\right)\left(\frac{\Delta\delta_2}{(D^2_{\langle d|j\rangle} + \Delta\delta^2_2)^{1/2}}\right) \tag{E.12}$$

$$(\phi_1 - \phi_4) = \left(\frac{6\pi\delta}{\lambda}\right)\left(\frac{\Delta d_3}{(D^2_{\langle d|j\rangle} + \Delta d^2_3)^{1/2}}\right) \tag{E.13}$$

$$(\phi_2 - \phi_3) = \left(\frac{2\pi d_1}{\lambda}\right)\left(\frac{\Delta\delta_2}{(D^2_{\langle d|j\rangle} + \Delta\delta^2_2)^{1/2}}\right) \tag{E.14}$$

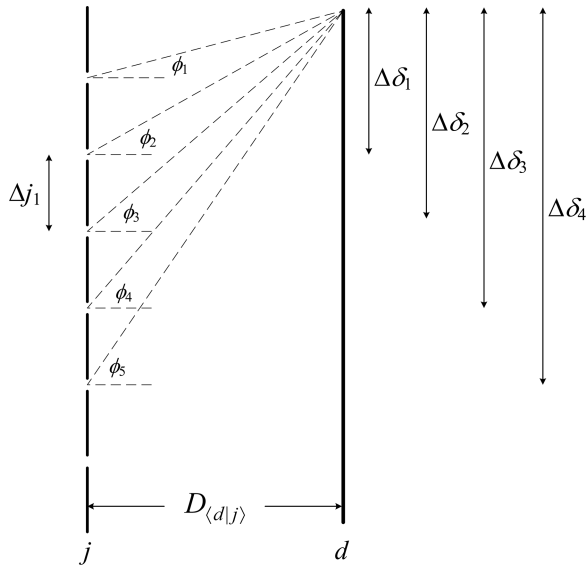

FIGURE E.1 Detailed view of the N-slit array (j) and the interferometric plane (d). See the text for a description of the quantities involved.

$$(\phi_2 - \phi_4) = \left(\frac{4\pi d_1}{\lambda}\right)\left(\frac{\Delta\delta_3}{(D^2_{\langle d|j\rangle} + \Delta\delta_3^2)^{1/2}}\right) \tag{E.15}$$

$$(\phi_3 - \phi_4) = \left(\frac{2\pi d_1}{\lambda}\right)\left(\frac{\Delta\delta_3}{(D^2_{\langle d|j\rangle} + \Delta\delta_3^2)^{1/2}}\right) \tag{E.16}$$

and so on, where λ is the wavelength of the narrow-linewidth laser.

Note that in this example, both the slit width (w) and the separation of the slits (d_1) are assumed to be constant. As shown in Duarte (1993), this is a special case as these parameters can be numerically varied (allowing for dimensional errors), thus introducing an element of variability in the calculations. Also note that in Chapter 2 of *Tunable Laser Optics* (Duarte, 2003), an alternative and equivalent description (also included in Chapter 4) of the geometry is given.

REFERENCES

Duarte, F. J. (1991). Dispersive dye lasers. In *High Power Dye Lasers* (Duarte, F. J., ed.). Springer-Verlag, Berlin, Chapter 2, pp. 7–43.

Duarte, F. J. (1993). On a generalized interference equation and interferometric measurements. *Opt. Commun.* **103**, 8–14.

Duarte, F. J. (1997). Interference, diffraction, and refraction, via Dirac's notation. *Am. J. Phys.* **65**, 637–640.

Duarte, F. J. (2003). *Tunable Laser Optics*, Elsevier-Academic, New York.

Appendix F
Ray Transfer Matrices

F.1 INTRODUCTION

A practical method to characterize and design laser optics systems is the use of beam propagation matrices also known as *ray transfer matrices*. This method applies to the propagation of laser beams with a Gaussian profile. In other words, it applies to the propagation of single-transverse-mode beams or *spatially coherent* beams which is a crucial characteristic of the concept of laser emission.

From our perspective, the main interest in ray transfer matrices arises from their usability in the determination of beam divergence from narrow-linewidth multiple-prism grating laser oscillators.

In this appendix, the basic principles of propagation matrices are outlined and a survey of matrices for various widely applicable optical elements is given. This appendix follows the style of a review on the subject by Duarte (2003, 2015). For early references on the subject, the reader is referred to Brouwer (1964), Kogelnik (1979), Siegman (1986), and Wollnik (1987).

F.2 *ABCD* PROPAGATION MATRICES

The basic idea with propagation matrices is that one vector, at a given plane, is related to a second vector, at a different plane, via a linear transformation. This transformation is represented by a propagation matrix. This concept is applicable to the characterization of the deviation of a ray, or beam, of light through either free space or any linear optical media. The rays of light are assumed to be paraxial rays that propagate in proximity and almost parallel to the optical axis (Kogelnik, 1979).

Consider the propagation of a paraxial ray of light from an original plane to a secondary plane, in free space, as depicted in Figure F.1. Here it is noted that, in moving from the original plane to the secondary plane, the ray of light experiences a linear displacement in the x direction and a small angular deviation, that is,

$$x_2 = x_1 + l\theta_1 \tag{F.1}$$

$$\theta_2 = \theta_1 \tag{F.2}$$

which in matrix form becomes

$$\begin{pmatrix} x_2 \\ \theta_2 \end{pmatrix} = \begin{pmatrix} 1 & l \\ 0 & 1 \end{pmatrix} \begin{pmatrix} x_1 \\ \theta_1 \end{pmatrix} \tag{F.3}$$

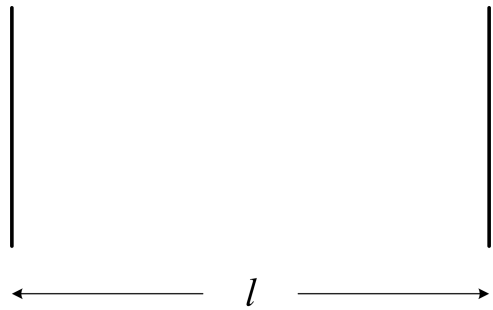

FIGURE F.1 Geometry for propagation through distance l in vacuum-free space.

the resulting 2×2 matrix is known as a *ray transfer matrix*. Here, it should be noted that some authors use derivatives instead of the angular quantities, that is, $dx_1/dz = \theta_1$ and $dx_2/dz = \theta_2$.

For a thin lens, the geometry of propagation is illustrated in Figure F.2. In this case, there is no displacement in the x direction and the ray is concentrated, or focused, toward the optical axis so that

$$x_2 = x_1 \tag{F.4}$$

$$\theta_2 = -(1/f)\, x_1 + \theta_1 \tag{F.5}$$

which can be expressed as

$$\begin{pmatrix} x_2 \\ \theta_2 \end{pmatrix} = \begin{pmatrix} 1 & l \\ f^{-1} & 1 \end{pmatrix} \begin{pmatrix} x_1 \\ \theta_1 \end{pmatrix} \tag{F.6}$$

In more general terms, the $\boldsymbol{X}_2$ vector is related to the $\boldsymbol{X}_1$ vector by a transfer matrix $\boldsymbol{T}$ known as the *ABCD* matrix so that

$$\boldsymbol{X}_2 = \boldsymbol{T}\, \boldsymbol{X}_1 \tag{F.7}$$

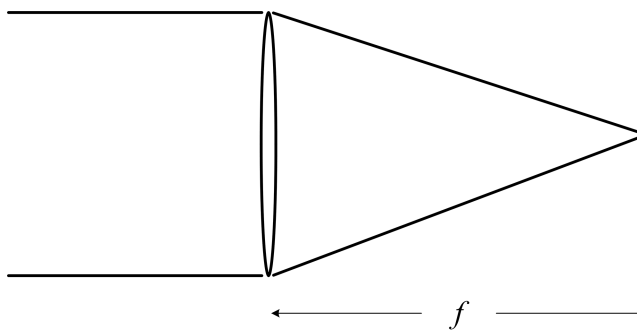

FIGURE F.2 Geometry depicting a thin convex lens with a focal length f.

where

$$\boldsymbol{T} = \begin{pmatrix} A & B \\ C & D \end{pmatrix} \tag{F.8}$$

Dimensions: by inspection, it is found that

$$\begin{pmatrix} x_2 \\ \theta_2 \end{pmatrix} = \begin{pmatrix} \partial x_2/\partial x_1 & \partial x_2/\partial \theta_1 \\ \partial \theta_2/\partial x_1 & \partial \theta_2/\partial \theta_1 \end{pmatrix} \begin{pmatrix} x_1 \\ \theta_1 \end{pmatrix} \tag{F.9}$$

This implies that A is a ratio of spatial dimensions and B is an optical length, while C is the reciprocal of an optical length. Consideration of various imaging systems leads to the conclusion that the spatial ratio represented by A is a beam magnification factor (M), while D is the reciprocal of such magnification (M^{-1}). These observations are very useful to verify the physical validity of newly derived matrices.

F.2.1 Properties of *ABCD* Matrices

ABCD matrices can be cascaded, via matrix multiplication, to produce a single overall matrix describing the propagation properties of an optical system. For example, if a linear optical system is composed of N optical elements deployed from left to right, as depicted in Figure F.3, then the overall transfer matrix is given by the multiplication of the individual matrices *in the reverse order*, that is (Duarte, 2003)

$$\prod_{m=1}^{N} \boldsymbol{T}_m = \boldsymbol{T}_N \ldots \boldsymbol{T}_3 \boldsymbol{T}_2 \boldsymbol{T}_1 \tag{F.10}$$

It is easy to see that the complexity in the form of these product matrices can increase rather rapidly. Thus, it is always useful to remember that any resulting matrix must have the dimensions of Equation (F.9) and a determinant equal to unity, that is

$$AD - BC = 1 \tag{F.11}$$

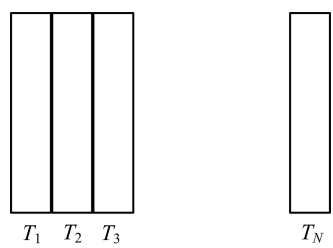

FIGURE F.3 N optical elements in series (Reproduced from Duarte, F. J., *Tunable Laser Optics*, 2nd ed. CRC, Boca Raton, FL, 2015).

F.2.2 Survey of *ABCD* Matrices

Here, a number of representative and widely used optical components are represented in ray transfer matrix form. This is done without derivation and using the published literature as reference:

Distance l in free space (Kogelnik, 1979):

$$\begin{pmatrix} A & B \\ C & D \end{pmatrix} = \begin{pmatrix} 1 & l \\ 0 & 1 \end{pmatrix} \tag{F.12}$$

Distance l in a medium with refractive index n (Kogelnik, 1979):

$$\begin{pmatrix} A & B \\ C & D \end{pmatrix} = \begin{pmatrix} 1 & l/n \\ 0 & 1 \end{pmatrix} \tag{F.13}$$

Slab of material with refractive index n where ϕ is the angle of incidence and ψ is the angle of refraction (Duarte, 1991):

$$\begin{pmatrix} A & B \\ C & D \end{pmatrix} = \begin{pmatrix} 1 & (l/n)(\cos\phi/\cos\psi)^2 \\ 0 & 1 \end{pmatrix} \tag{F.14}$$

Thin convex (positive) lens of focal length f (Kogelnik, 1979):

$$\begin{pmatrix} A & B \\ C & D \end{pmatrix} = \begin{pmatrix} 1 & 0 \\ -1/f & 1 \end{pmatrix} \tag{F.15}$$

Thin concave (negative) lens (Siegman, 1986):

$$\begin{pmatrix} A & B \\ C & D \end{pmatrix} = \begin{pmatrix} 1 & 0 \\ 1/|f| & 1 \end{pmatrix} \tag{F.16}$$

Galilean telescope (Siegman, 1986):

$$\begin{pmatrix} A & B \\ C & D \end{pmatrix} = \begin{pmatrix} f_2/|f_1| & f_2 - |f_1| \\ 0 & |f_1|/f_2 \end{pmatrix} \tag{F.17}$$

Astronomical telescope (Siegman, 1986):

$$\begin{pmatrix} A & B \\ C & D \end{pmatrix} = \begin{pmatrix} -f_2/f_1 & f_2 + f_1 \\ 0 & -f_1/f_2 \end{pmatrix} \tag{F.18}$$

Curved mirror with curvature radius R (Siegman, 1986):

$$\begin{pmatrix} A & B \\ C & D \end{pmatrix} = \begin{pmatrix} 1 & 0 \\ -2/R & 1 \end{pmatrix} \tag{F.19}$$

Double-pass in Cassegrain telescope with beam magnification M (Siegman, 1986):

$$\begin{pmatrix} A & B \\ C & D \end{pmatrix} = \begin{pmatrix} M & (M+1)L/M \\ 0 & M^{-1} \end{pmatrix} \tag{F.20}$$

Flat grating where Θ is the angle of incidence and Φ is the angle of diffraction (Siegman, 1986):

$$\begin{pmatrix} A & B \\ C & D \end{pmatrix} = \begin{pmatrix} \cos\Theta/\cos\Phi & 0 \\ 0 & \cos\Phi/\cos\Theta \end{pmatrix} \tag{F.21}$$

Flat grating in Littrow configuration[1] ($\Theta = \Phi$) (Duarte, 1991):

$$\begin{pmatrix} A & B \\ C & D \end{pmatrix} = \begin{pmatrix} 1 & 0 \\ 0 & 1 \end{pmatrix} \tag{F.22}$$

Single right-angle prism where ϕ is the angle of incidence and ψ is the angle of refraction (Duarte, 1989):

$$\begin{pmatrix} A & B \\ C & D \end{pmatrix} = \begin{pmatrix} \cos\psi/\cos\phi & (l/n)\cos\phi/\cos\psi \\ 0 & \cos\phi/\cos\psi \end{pmatrix} \tag{F.23}$$

F.2.3 The Astronomical Refractive Telescope

The astronomical refractive telescope (Figure F.4) is composed of an input lens with focal length f_1, an intra-lens distance L, and an output lens with focal lens f_2. Following Equation (F.10), the matrix multiplication proceeds as

$$\begin{pmatrix} A & B \\ C & D \end{pmatrix} = \begin{pmatrix} 1 & 0 \\ f_2^{-1} & 1 \end{pmatrix} \begin{pmatrix} 1 & L \\ 0 & 1 \end{pmatrix} \begin{pmatrix} 1 & 0 \\ f_1^{-1} & 1 \end{pmatrix} \tag{F.24}$$

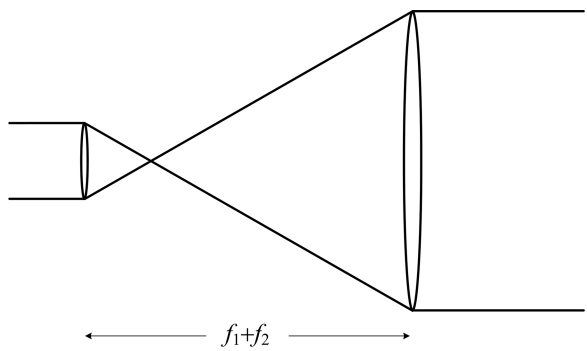

FIGURE F.4 Schematics of an astronomical refractive telescope comprised of two convex lenses.

[1] Also applies to a flat mirror.

For a well-adjusted telescope, where

$$L = f_2 + f_1 \tag{F.25}$$

the transfer matrix becomes

$$\begin{pmatrix} A & B \\ C & D \end{pmatrix} = \begin{pmatrix} -f_2 f_1^{-1} & L \\ 0 & -f_1 f_2^{-1} \end{pmatrix} \tag{F.26}$$

which is the corresponding matrix given by Siegman (1986). Defining

$$-M = -f_2 f_1^{-1} \tag{F.27}$$

this matrix can be restated as

$$\begin{pmatrix} A & B \\ C & D \end{pmatrix} = \begin{pmatrix} -M & L \\ 0 & -M^{-1} \end{pmatrix} \tag{F.28}$$

For this matrix it can be easily verified that the condition $|AD - BC| = 1$ holds.

F.2.4 Multiple-Prism Beam Expanders

For a generalized multiple-prism array, as illustrated in Figure F.5, the ray transfer matrix is given by (Duarte, 1989, 1991)

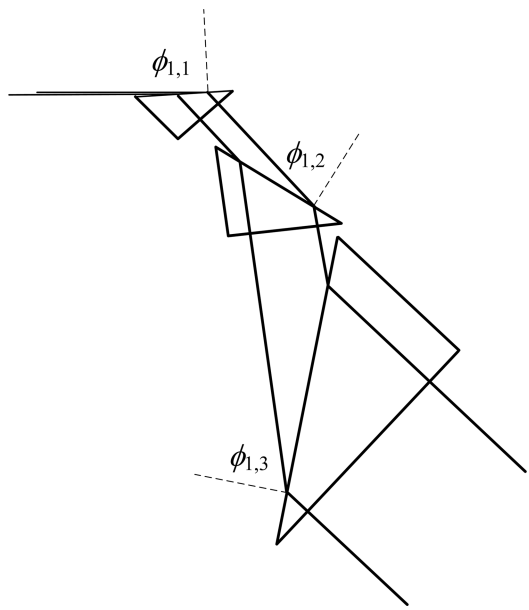

FIGURE F.5 Multiple-prism beam expander.

$$\begin{pmatrix} A & B \\ C & D \end{pmatrix} = \begin{pmatrix} M_1 M_2 & B \\ 0 & (M_1 M_2)^{-1} \end{pmatrix} \tag{F.29}$$

where

$$M_1 = \prod_{m=1}^{r} k_{1,m} \tag{F.30}$$

$$M_2 = \prod_{m=1}^{r} k_{2,m} \tag{F.31}$$

and

$$B = M_1 M_2 \sum_{m=1}^{r-1} L_m \left(\prod_{j=1}^{m} k_{1,j} \prod_{j=1}^{m} k_{2,j} \right)^{-2} + (M_1 / M_2) \sum_{m=1}^{r} (l_m / n_m) \left(\prod_{j=1}^{m} k_{1,j} \right)^{-2} \left(\prod_{j=m}^{r} k_{2,j} \right)^{2} \tag{F.32}$$

For a straightforward multiple-prism beam expander with orthogonal beam exit, $\cos\psi_{2,j} = 0$ and $k_{2,j} = 1$, so that the equations reduce to

$$\begin{pmatrix} A & B \\ C & D \end{pmatrix} = \begin{pmatrix} M_1 & B \\ 0 & M_1^{-1} \end{pmatrix} \tag{F.33}$$

where

$$B = M_1 \sum_{m=1}^{r-1} L_m \left(\prod_{j=1}^{m} k_{1,j} \right)^{-2} + M_1 \sum_{m=1}^{r} (l_m / n_m) \left(\prod_{j=1}^{m} k_{1,j} \right)^{-2} \tag{F.34}$$

For a single prism, these equations reduce further to

$$M_1 = k_{1,1} \tag{F.35}$$

$$B = l(nk_{1,1})^{-1} \tag{F.36}$$

Thus the matrix for a single prism can be expressed as

$$\begin{pmatrix} A & B \\ C & D \end{pmatrix} = \begin{pmatrix} k_{1,1} & l(nk_{1,1})^{-1} \\ 0 & k_{1,1}^{-1} \end{pmatrix} \tag{F.37}$$

which is an alternative version of the single-prism matrix given in Equation (F.23) where

$$k_{1,1} = \cos\phi_{1,1} / \cos\psi_{1,1} \tag{F.38}$$

F.2.5 Telescopes in Series

For some applications, it is necessary to propagate TEM_{00} laser beams through optical systems, including telescopes in series. For a series comprised of a telescope followed by a free-space distance, followed by a second telescope, and so on, the single-pass cumulative matrix is given by (Duarte, 2003)

$$A = M^r \tag{F.39}$$

$$B = \sum_{m=1}^{r} M^{r-2m+2} L_m + M^{r-2m+1} B_{T_m} \tag{F.40}$$

$$C = 0 \tag{F.41}$$

$$D = M^{-r} \tag{F.42}$$

where r is the total number of telescopes and B_{T_m} is the B term of the mth telescope.

This result applies to a series of well-adjusted Galilean or astronomical telescopes or a series of prismatic telescopes.

F.3 MULTIPLE-RETURN PASS LASER LINEWIDTH AND BEAM DIVERGENCE

The *ABCD* matrices considered so far are entirely classical. Previously, however, we have seen that both the cavity laser linewidth equation $\Delta\lambda = \Delta\theta\ (\nabla_\lambda \theta)^{-1}$ and the laser beam divergence $\Delta\theta \approx \lambda/\Delta x$ are quantum in origin (see Chapter 3 and Appendix B).

Here, we describe the interaction of these essential laser emission parameters with ray transfer matrices.

The multiple-return pass laser linewidth in a multiple-prism grating tunable laser oscillator is given by (Duarte, 2001)

$$\Delta\lambda = \Delta\theta_R \left(RM\ \nabla_\lambda \Theta_G + R\ \nabla_\lambda \Phi_P \right)^{-1} \tag{F.43}$$

where M is the overall intracavity beam magnification, R is the number of return passes, $\nabla_\lambda \Theta_G$ is the grating dispersion, $\nabla_\lambda \Phi_P$ is the return-pass multiple-prism dispersion, and the multiple return-pass beam divergence is given by (Duarte, 2001)

$$\Delta\theta_R = \frac{\lambda}{\pi w} \left(1 + \left(\frac{L_{\mathcal{R}}}{B_R} \right)^2 + \left(\frac{A_R L_{\mathcal{R}}}{B_R} \right)^2 \right)^{1/2} \tag{F.44}$$

where $L_{\mathcal{R}} = (\pi w^2/\lambda)$ while A_R and B_R are the cumulative multiple-return pass-ray transfer matrix coefficients given by (Duarte, 2001)

$$\begin{aligned} A_R = {} & (\alpha A_{R-1} + \chi \mathcal{L}_{R-1}) \left(\alpha + \chi (\Xi - L_2) \right) + \chi \mathcal{L}_{R-1} (\chi L_2 + \delta) \\ & + \chi A_{R-1} (\alpha L_2 + \beta) \end{aligned} \tag{F.45}$$

$$B_R = A_R\Lambda + (\alpha A_{R-1} + \chi \mathcal{L}_{R-1})\left(\beta + \delta(\Xi - L_2)\right) + \delta \mathcal{L}_{R-1}(\chi L_2 + \delta) + \delta A_{R-1}(\alpha L_2 + \beta) \tag{F.46}$$

where

$$\Lambda = \frac{L_P}{n_P} + L_1 \tag{F.47}$$

$$\mathcal{L}_{R-1} = \Lambda A_{R-1} + B_{R-1} \tag{F.48}$$

$$\Xi = 2L_2 + \frac{2B_{MP}}{M} + \frac{2L_3}{M^2} \tag{F.49}$$

and α, β, χ, and δ are the corresponding matrix elements for the gain medium. Moreover, L_P is the thickness of the output-couple polarizer and n_P its refractive index.

By definition $A_0 = 1$ and $B_0 = 0$, thus for an ideal gain medium, with little or no thermal lensing, with $\alpha \approx \delta \approx 1$, $\chi \approx 0$, and $\beta \approx \beta$, Equations (F.45) and (F.46) reduce to

$$A_R \approx 1 \tag{F.50}$$

$$B_R \approx 2\Lambda + 2\beta + \Xi \tag{F.51}$$

A discussion on the application of these equations to the design and evaluation of single-transverse-mode low-divergence narrow-linewidth tunable lasers has been given by Duarte (2001).

In addition to providing the parameters of interest to perform beam divergence calculations, the *ABCD* matrix also gives information about the stability of a cavity or resonator. The condition for lasing in the unstable regime is determined by the inequality (Siegman, 1986)

$$\left|2^{-1}(A + D)\right| > 1 \tag{F.52}$$

It should be noted that narrow-linewidth multiple-prism grating tunable laser oscillators can also meet the conditions for unstable resonators when incorporating a gain medium that exhibits some thermal lensing (Figure F.6) (Duarte et al., 1997).

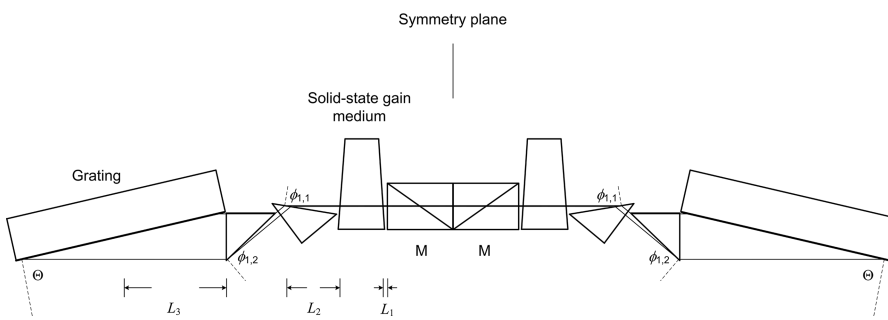

FIGURE F.6 Unfolded multiple-prism grating laser oscillator.

The description of optical systems using 3×3, 4×4, and 6×6 matrices has been considered by several authors (Brouwer, 1964; Siegman, 1986; Wollnik, 1987). Multiple-prism expanders have been described in 4×4 matrices by Duarte (1992, 2003). These matrices are also applicable to multiple-prism laser pulse compression.

PROBLEMS

F.1 For the matrix in Equation (F.24), verify that $|AD-BC|=1$ holds.
F.2 For the matrix in Equation (F.30), verify that $|AD-BC|=1$ holds.
F.3 Verify that performing the matrix multiplication in (F.24) leads to Equation (F.26).
F.4 Verify that for a series comprised of a telescope followed by a free-space distance, followed by a second telescope, and so on the single-pass cumulative ABCD matrix is given by the components in Equations (F.39)–(F.42).
F.5 Verify that for $\alpha\approx\delta\approx1$, $\chi\approx0$, and $\beta\approx\beta$ Equation (F.46) reduces to Equation (F.51).

REFERENCES

Brouwer, W. (1964). *Matrix Methods in Optical Design*, Benjamin, New York.
Duarte, F. J. (1989). Ray transfer matrix analysis of multiple-prism dye laser oscillators, *Opt. Quantum Electron*. **21**, 47–54.
Duarte, F. J. (1991). Dispersive dye lasers. In *High Power Dye Lasers* (Duarte, F. J., ed.). Springer-Verlag, Berlin, Chapter 2, pp. 7–43.
Duarte, F. J. (1992). Multiple-prism dispersion and 4×4 ray transfer matrices, *Opt. Quantum Electron*. **24**, 49–53.
Duarte, F. J. (2001). Multiple-return-pass-beam divergence and the linewidth equation. *Appl. Opt.* **40**, 3038–3041.
Duarte, F. J. (2003). *Tunable Laser Optics*, 1st ed. Elsevier-Academic, New York.
Duarte, F. J. (2015). *Tunable Laser Optics*, 2nd ed. CRC, Boca Raton, FL.
Duarte, F. J., Costela, A., Garcia-Moreno, I., Sastre, R., Ehrlich, J. J., and Taylor, T. S. (1997). Dispersive solid-state dye laser oscillators, *Opt. Quantum Electron.* **29**, 461–472.
Kogelnik, H. (1979). Propagation of laser beams. In *Applied Optics and Optics Engineering* (Shannon, R. R., and Wyant., J. C., eds.). Academic, New York, pp. 155–190.
Siegman, A. (1986). *Lasers*, University Science Books, Mill Valley, CA.
Wollnik, H. (1987). *Optics of Charged Particles*, Academic, New York.

Appendix G
Complex Numbers and Quaternions

G.1 COMPLEX NUMBERS

Imaginary and complex numbers are crucial to a complete and functional description of *Nature*. Imaginary and complex numbers are essential to the mathematics of quantum mechanics. Without complex numbers, there would be no lasers, no transistors, and no computers.

Here we offer a brief and pragmatic introduction to complex numbers and some well-known trigonometric identities based on complex numbers.

The imaginary part of a complex number is represented by i. The number i has the basic property

$$i^2 = -1 \tag{G.1}$$

so that

$$i \cdot i = -1 \tag{G.2}$$

and

$$i \cdot (-i) = +1 \tag{G.3}$$

A complex number has a real and an imaginary part denoted by i. A complex number c is defined as

$$c = a + ib \tag{G.4}$$

where a and b are real. This complex number is depicted in Figure G.1. The complex conjugate of this number c is denoted by c^*

$$c^* = a - ib \tag{G.5}$$

These two numbers can be multiplied as

$$cc^* = (a + ib)(a - ib) = a^2 + b^2 \tag{G.6}$$

and the magnitude of $c = a + ib$ is denoted by $|c|$

$$|c| = \left(a^2 + b^2\right)^{1/2} \tag{G.7}$$

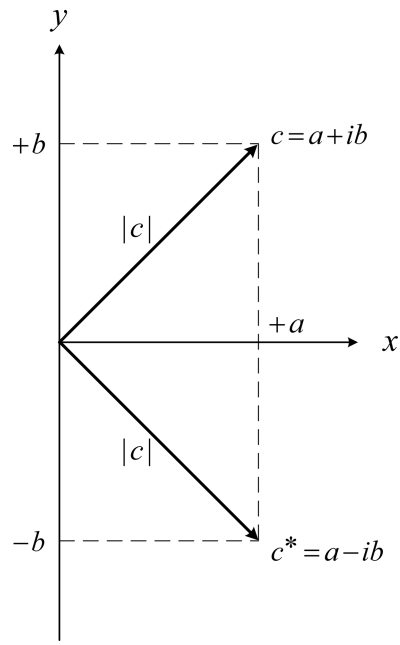

FIGURE G.1 Geometrical representation of a complex number.

and it represents the length of the vector $(a+ib)$ (see Figure G.1). Moreover,

$$|c|^2 = cc^* \tag{G.8}$$

Useful complex trigonometric identities include the Euler formulae

$$e^{i\theta} = \cos\theta + i\sin\theta \tag{G.9}$$

$$e^{-i\theta} = \cos\theta - i\sin\theta \tag{G.10}$$

which means that

$$e^{i\pi} = -1 \tag{G.11}$$

$$e^{-i\pi} = +1 \tag{G.12}$$

$$e^{i\pi/2} = +i \tag{G.13}$$

$$e^{-i\pi/2} = -i \tag{G.14}$$

Also

$$2\cos\theta = \left(e^{i\theta} + e^{-i\theta}\right) \tag{G.15}$$

$$2i\sin\theta = \left(e^{i\theta} - e^{-i\theta}\right) \tag{G.16}$$

$$2\cosh\theta = \left(e^{\theta} + e^{-\theta}\right) \tag{G.17}$$

$$2\sinh\theta = \left(e^{\theta} - e^{-\theta}\right) \tag{G.18}$$

The beautiful expression $e^{i\pi} = -1$ was discovered by Euler (1748) and has been classified as 'the most remarkable formula in mathematics… our jewel' (Feynman et al., 1963). Indeed, complex numbers should be celebrated!

G.2 QUATERNION IDENTITIES

Hamilton's quaternions (Hamilton, 1866) apply to quantum entanglement for the configurations of $n = N = 3, 6, 9\ldots$ (Duarte, 2015, 2016). Quaternions extend beyond the realm of complex numbers and obey the main relation

$$i^2 = j^2 = k^2 = ijk = -1 \tag{G.19}$$

and the elements i, j, and k obey the commutative law when multiplied by 1

$$i \times 1 = 1 \times i = i \tag{G.20}$$

$$j \times 1 = 1 \times j = j \tag{G.21}$$

$$k \times 1 = 1 \times k = k \tag{G.22}$$

The self-consistency of the main relation given in Equation (G.19) also implies that

$$ij = k \tag{G.23}$$

$$ji = -k \tag{G.24}$$

$$jk = i \tag{G.25}$$

$$kj = -i \tag{G.26}$$

$$ki = j \tag{G.27}$$

$$ik = -j \tag{G.28}$$

PROBLEMS

G.1 Use Equations (G.4) and (G.5) to verify Equation (G.6).
G.2 Verify that $2\cos\theta = (e^{i\theta} + e^{-i\theta})$.

G.3 Verify that $2i\sin\theta = (e^{i\theta} - e^{-i\theta})$.
G.4 Use Equation (G.19) to show that $jk = i$.
G.5 Use Equation (G.19) to show that $ki = j$.

REFERENCES

Duarte, F. J. (2015). *Tunable Laser Optics*, 2nd ed. CRC, Boca Raton, FL.
Duarte, F. J. (2016). Secure space-to-space interferometric communications and its nexus to the physics of quantum entanglement. *Appl. Phys. Rev.* **3**, 041301.
Euler, L. (1748). *Introductio in Analysin Infinitorun*, Marcum-Michaelem Bousquet & Socios, Lausanne.
Hamilton, W. R. (1866). *Elements of Quaternions*, Longman Green & Co, London, U.K.
Feynman, R. P., Leighton, R. B., and Sands, M. (1963). *The Feynman Lectures on Physics*, Vol. I, Addison-Wesley, Reading, MA.

Appendix H
Trigonometric Identities

H.1 TRIGONOMETRIC IDENTITIES

Here we list a number of trigonometric identities applied in various places throughout this book:

$$\sin^2\varphi + \cos^2\varphi = 1 \tag{H.1}$$

$$\sin(-\varphi) = -\sin\varphi \tag{H.2}$$

$$\cos(-\varphi) = \cos\varphi \tag{H.3}$$

$$\sin(\varphi + \theta) = \sin\varphi\cos\theta + \cos\varphi\sin\theta \tag{H.4}$$

$$\sin(\varphi - \theta) = \sin\varphi\cos\theta - \cos\phi\sin\theta \tag{H.5}$$

$$\cos(\varphi + \theta) = \cos\varphi\cos\theta - \sin\varphi\sin\theta \tag{H.6}$$

$$\cos(\varphi - \theta) = \cos\varphi\cos\theta + \sin\varphi\sin\theta \tag{H.7}$$

$$\sin 2\varphi = 2\sin\varphi\cos\varphi \tag{H.8}$$

$$\cos 2\varphi = \cos^2\varphi - \sin^2\varphi \tag{H.9}$$

$$\cos 2\varphi = 1 - 2\sin^2\varphi \tag{H.10}$$

$$\cos 2\varphi = 2\cos^2\varphi - 1 \tag{H.11}$$

$$2\sin^2\varphi = 1 - \cos 2\varphi \tag{H.12}$$

$$2\cos^2\varphi = 1 + \cos 2\varphi \tag{H.13}$$

$$\cos\varphi + \cos\varphi = 2\cos\tfrac{1}{2}(\varphi - \theta)\cos\tfrac{1}{2}(\varphi + \theta) \tag{H.14}$$

$$\cos\varphi - \cos\theta = -2\sin\tfrac{1}{2}(\varphi - \theta)\sin\tfrac{1}{2}(\varphi + \theta) \tag{H.15}$$

$$-\cos\varphi - \cos\theta = -2\cos\tfrac{1}{2}(\varphi-\theta)\cos\tfrac{1}{2}(\varphi+\theta) \tag{H.16}$$

$$\sin\varphi + \sin\theta = 2\cos\tfrac{1}{2}(\varphi-\theta)\sin\tfrac{1}{2}(\varphi+\theta) \tag{H.17}$$

$$\sin\varphi - \sin\theta = 2\sin\tfrac{1}{2}(\varphi-\theta)\cos\tfrac{1}{2}(\varphi+\theta) \tag{H.18}$$

$$-\sin\varphi - \sin\theta = -2\cos\tfrac{1}{2}(\varphi-\theta)\sin\tfrac{1}{2}(\varphi+\theta) \tag{H.19}$$

$$\sin\varphi\sin\theta = \tfrac{1}{2}\big(\cos(\varphi-\theta) - \cos(\varphi+\theta)\big) \tag{H.20}$$

$$\cos\varphi\cos\theta = \tfrac{1}{2}\big(\cos(\varphi-\theta) + \cos(\varphi+\theta)\big) \tag{H.21}$$

$$\sin\varphi\cos\theta = \tfrac{1}{2}\big(\sin(\varphi+\theta) + \sin(\varphi-\theta)\big) \tag{H.22}$$

$$\cos\varphi\sin\theta = \tfrac{1}{2}\big(\sin(\varphi+\theta) - \sin(\varphi-\theta)\big) \tag{H.23}$$

References used in this compilation of trigonometric identities include Crawford (1968) and Flanders et al. (1970).

PROBLEMS

H.1 Show that $\sin(\varphi+\theta) = \sin\varphi\cos\theta + \cos\varphi\sin\theta$.

H.2 show that $\cos 2\varphi = 1 - 2\sin^2\varphi$.

H.3 Show that $2\sin^2\varphi = 1 - \cos 2\varphi$.

H.4 Show that $\cos\varphi - \cos\theta = -2\sin\tfrac{1}{2}(\varphi-\theta)\sin\tfrac{1}{2}(\varphi+\theta)$

H.5 Show that $\sin\varphi\sin\theta = \tfrac{1}{2}\big(\cos(\varphi-\theta) - \cos(\varphi+\theta)\big)$

REFERENCES

Crawford, F. S. (1968). *Waves*, McGraw-Hill, New York.
Flanders, H., Korfhage, R. R., and Price, J. J. (1970). *Calculus*, Academic, New York.

Appendix I
Calculus Basics

I.1 CALCULUS BASICS

In this appendix, we provide a brief and pragmatic survey of some useful well-known calculus mechanics and rules. A good reference on calculus is Flanders et al. (1971).

I.1.1 DIFFERENTIATION PRODUCT RULE

$$\frac{d(fg)}{dx} = f\frac{dg}{dx} + g\frac{df}{dx} \tag{I.1}$$

Example: differentiate the product xe^{ikx}

$$\frac{d(xe^{ikx})}{dx} = x(ik)e^{ikx} + e^{ikx} = e^{ikx}(1 + ikx)$$

I.1.2 Differentiation Quotient Rule

$$\frac{d(f/g)}{dx} = g^{-2}\left(g\frac{df}{dx} - f\frac{dg}{dx}\right) \tag{I.2}$$

I.1.3 Differentiation Power Rule

If n is an integer

$$\frac{d(f^n)}{dx} = nf^{n-1}\frac{df}{dx} \tag{I.3}$$

Example: differentiate $(x^2 + 1)^2$

$$\frac{d(x^2 + 1)^2}{dx} = 4x(x^2 + 1)$$

I.1.4 Differentiation via the Chain Rule

If y and x are functions of t

$$\frac{dy}{dt} = \frac{dy}{dx}\frac{dx}{dt} \tag{I.4}$$

Example: differentiate the function $y = e^{t^2+2t+1}$. Set $y = e^x$ and $x = t^2 + 2t + 1$. Then apply the chain rule

$$\frac{dy}{dt} = e^x(2t+2) = e^{t^2+2t+1}(2t+2)$$

I.1.5 Integration by Parts

$$\int f\ dg = fg - \int g\ df \tag{I.5}$$

Example: integrate by parts $\int xe^{ikx}\,dx$. Set $f = x$, $df = dx$, $dg = e^{ikx}dx$, and $g = e^{ikx}/ik$.

Then apply Equation (I.5)

$$\int xe^{ikx}\,dx = \frac{x}{ik}e^{ikx} - \int \frac{e^{ikx}}{ik}dx = \frac{e^{ikx}}{ik}\left(x - \frac{1}{ik}\right) + C$$

where C is a constant. Differentiation of $F(x) = (e^{ikx}/ik)\left(x - (1/ik)\right) + C$, using the product rule, leads back to xe^{ikx}.

REFERENCE

Flanders, H., Korfhage, R. R., and Price, J. J. (1970). *Calculus*, Academic, New York.

Appendix J
Poincare's Space

J.1 POINCARÉ'S SPACE

A useful tool in polarization notation is derived from *Poicarés sphere* (Poicaré, 1892).

This sphere, depicted in Figure J.1, has three axes 1, 2, and 3. Axis 2 is analogous to the usual Cartesian axis x, axis 3 is analogous to the usual Cartesian axis y, and axis 1 is analogous to the usual Cartesian axis z, that is

$$1 \rightarrow z$$

$$2 \rightarrow x$$

$$3 \rightarrow y$$

Adopting the notation of Robson (1974), the radius of the sphere is denoted by I. The angular displacement in the $1-2$ plane is 2ψ and the angular displacement between

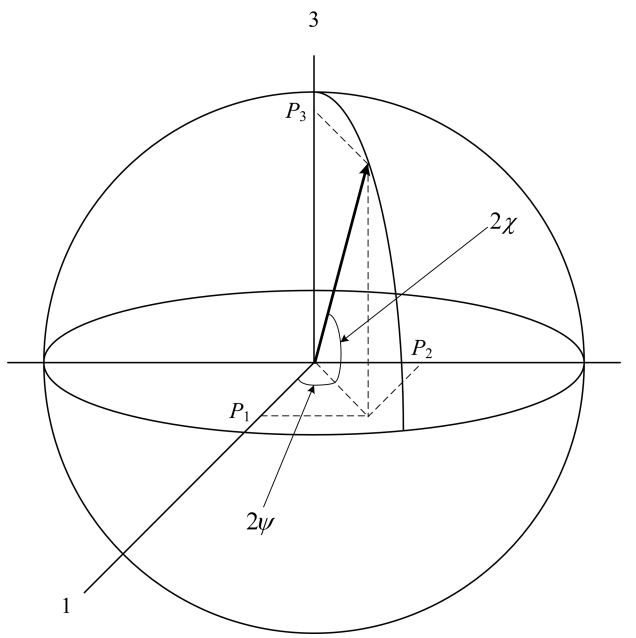

FIGURE J.1 Poicare's sphere.

the $1-2$ plane and the 3 axis is denoted by 2χ. In this system, the points P_1, P_2, P_3 are given by

$$P_1 = I\cos 2\chi \cos 2\psi \tag{J.1}$$

$$P_2 = I\cos 2\chi \sin 2\psi \tag{J.2}$$

$$P_3 = I\sin 2\chi \tag{J.3}$$

These are known as the *Stoke's parameters*. In addition to Poicarés sphere, the polarization space described here is also known as Bloch's sphere (Pelliccia et al., 2003).

REFERENCES

Pelliccia, D., Schettini, V., Sciarrino, F., Sias, C., and De Martini, F. (2003). Contextual realization of the universal quantum cloning machine and of the universal-NOT gate by quantum-injected optical parametric amplification. *Phys. Rev. A*. **68**, 042306.

Poicaré, H. (1892). *Théorie Mathematique de la Lumiere*, Vol. 2, Corré, Paris.

Robson, B. A. (1974). *The Theory of Polarization Phenomena*, Clarendon, Oxford, U.K.

Appendix K
Physical Constants and Optical Quantities

K.1 FUNDAMENTAL PHYSICAL CONSTANTS

Physical constants useful in optics are listed in Table K.1. The values of these constants are those listed by the National Institute of Science and Technology (NIST) available at the time of publication.

The format and context of the tables included here are adapted from Duarte (2003).

TABLE K.1
Fundamental Physical Constants

Name	Symbol	Value	Units
Boltzmann's constant	k_B	$1.3806488 \times 10^{-23}$	JK^{-1}
Elementary charge	e	$1.602176634 \times 10^{-19}$	C
Newtonian constant of gravitation	G	6.67384×10^{-11}	$m^3kg^{-1}s^{-2}$
Magnetic constant[a,b]	μ_0	$4\pi \times 10^{-7}$	Hm^{-1}
Electric constant[c]	ε_0	$8.854187817 \times 10^{-12}$	Fm^{-1}
Planck's constant	h	$6.62607015 \times 10^{-34}$	Js
Speed of light in vacuum	c	2.99792458×10^{8}	ms^{-1}

[a] Also known as permeability of vacuum.
[b] $\pi = 3.14159265$.
[c] Also known as permittivity of vacuum.

K.2 CONVERSION QUANTITIES

Conversion quantities often used in optics are listed in Table K.2. The conversion values for the electron volt and the atomic mass unit are listed by NIST at the time of publication.

TABLE K.2
Conversion Quantities

Name	Symbol	Value	Units
Electron volt	eV	$1.602176565 \times 10^{-19}$	J
Atomic mass unit	u	$1.660538921 \times 10^{-27}$	kg
Frequency	ν		$\mathrm{Hz} = \mathrm{s}^{-1}$
Light year	ly	$9.45425496 \times 10^{15}$	m
Linewidth	$\Delta\nu = c/\Delta x$		Hz
Linewidth	$\Delta\lambda = \lambda^2/\Delta x$		m
Wavelength	$\lambda = c/\nu$		m
Wavenumber	$k = 2\pi/\lambda$		m^{-1}
1 reciprocal cm	$1\,\mathrm{cm}^{-1}$	2.99792458×10^{1}	GHz

K.3 UNITS OF OPTICAL QUANTITIES

Units of optical quantities used throughout this book are listed in Table K.3.

TABLE K.3
Units of Optical Quantities

Name	Symbol	Units[a]
Angular dispersion	$\nabla_\lambda \phi$	m^{-1}
Angular frequency	$\omega = 2\pi\nu$	Hz
Beam divergence	$\Delta\theta$	rad
Beam magnification	m	Dimensionless
Beam waist	w	m
Cross section	σ	m^2
Diffraction limited $\Delta\theta$	$\Delta\theta = \lambda/\pi w$	rad
Energy	E	J
Frequency	ν	Hz
Intensity	I	$\mathrm{Js}^{-1}\mathrm{m}^{-2}$
Laser linewidth	$\Delta\nu$	Hz
Laser linewidth	$\Delta\lambda$	m
Probability amplitude	$\lvert\psi\rangle$	Dimensionless
Probability	$\lvert\psi\rangle\lvert\psi\rangle^*$	Dimensionless

(*Continued*)

TABLE K.3 (*Continued*)
Units of Optical Quantities

Name	Symbol	Units[a]
Power	P	$W = Js^{-1}$
Rayleigh length	$L_{\mathcal{R}} = (\pi w^2/\lambda)$	m
Refractive index	n	Dimensionless
Time	t	s
Wavelength	λ	m
Wavenumber	$k = 2\pi/\lambda = \omega/c$	m^{-1}

[a] Quantities like I and σ are also used in cgs units.

REFERENCE

Duarte, F. J. (2003). *Tunable Laser Optics*, Elsevier-Academic, New York.

Index